COMPARATIVE OSTEOLOGY

A LABORATORY AND FIELD GUIDE OF COMMON NORTH AMERICAN ANIMALS

BRADLEY ADAMS AND PAM CRABTREE

AP

Comparative Osteology

The views or opinions expressed in this book are solely those of the author and do not necessarily represent those of the City of New York.

Please visit our **Companion Web site**, where you can magnify and zoom into images to see specific skeletal landmarks and features which will assist with species and bone identification.

http://booksite.academicpress.com/9780123884374

Comparative Osteology

A Laboratory and Field Guide of Common North American Animals

Bradley Adams
Forensic Anthropology Department
Office of Chief Medical Examiner
New York, New York, USA

Pam Crabtree
Department of Anthropology
Center for the Study of Human Origins
New York University
New York, New York, USA

ELSEVIER

AMSTERDAM • BOSTON • HEIDELBERG • LONDON • NEW YORK • OXFORD
PARIS • SAN DIEGO • SAN FRANCISCO • SINGAPORE • SYDNEY • TOKYO
Academic Press is an imprint of Elsevier

Academic Press is an imprint of Elsevier
The Boulevard, Langford Lane, Kidlington, Oxford, OX5 1GB, UK
225 Wyman Street, Waltham, MA 02451, USA

First published 2012

Notices
Knowledge and best practice in this field are constantly changing. As new research and experience broaden our understanding, changes in research methods, professional practices, or medical treatment may become necessary.

Practitioners and researchers must always rely on their own experience and knowledge in evaluating and using any information, methods, compounds, or experiments described herein. In using such information or methods they should be mindful of their own safety and the safety of others, including parties for whom they have a professional responsibility.

To the fullest extent of the law, neither the Publisher nor the authors, contributors, or editors, assume any liability for any injury and/or damage to persons or property as a matter of products liability, negligence or otherwise, or from any use or operation of any methods, products, instructions, or ideas contained in the material herein.

British Library Cataloguing-in-Publication Data
A catalogue record for this book is available from the British Library

Library of Congress Control Number: 2011931789

ISBN: 978-0-12-388437-4

Printed and bound in China

12 13 14 15 10 9 8 7 6 5 4 3 2 1

Contents

CHAPTER 1

Introduction, Scope of Book, and Credits

Regardless of the context (forensic or archaeological), the correct identification of human and non-human remains is a very serious issue in osteological analyses. While the difference between various species is often very striking, it can also be quite subtle (Figures 1-01 and 1-02). Case studies and textbooks have highlighted similarities between some species, for example the hand and foot bones (metacarpals and metatarsals) of the human hand and the bear paw, in the forensic realm (Byers 2005; Owsley and Mann 1990; Stewart 1979; Ubelaker 1989). These comparisons between the human and bear are also presented in Chapter 10 of this book. Sometimes the morphological similarities between species are quite unusual and counterintuitive. For example, there is a remarkable correspondence between the adult human clavicle and the adult alligator femur (Figure 1-03).

The goal of this book is to create a comprehensive photographic guide for use by experienced archaeologists and forensic scientists to distinguish human remains from a range of common animal species. The first part of the atlas (Chapters 2–6) focuses on specific skeletal elements including crania, humeri, radii/ulnae, femora, and tibiae. The next 17 chapters (7–23) are organized by species. Chapter 7 includes selected elements pertaining to humans (*Homo sapiens*), both newborn human bones and adult bones. For the following chapters, the non-human species have been photographed alongside their human counterparts to allow easy comparison. The larger mammal species are compared to an adult human skeleton, while the smaller mammal, bird, and reptile species are compared to a newborn human skeleton. We have chosen to photograph the Old World domesticates – cow (*Bos taurus* for cranial material and *Bos indicus* for postcranial material), sheep (*Ovis aries*), goat (*Capra hircus*), horse (*Equus caballus*), and pig (*Sus scrofa*) – since these animals are frequently found on historic archaeological sites in North America, and are commonly recovered from Neolithic and later sites in the eastern hemisphere. Furthermore, they are also common in modern contexts and could easily end up being submitted as a forensic case.

The atlas includes three domestic bird species; two of them, chicken (*Gallus gallus*) and duck (*Anas platyrhynchos*), were initially domesticated in the eastern hemisphere, while the third, turkey (*Meleagris gallopavo*), was first domesticated by Native Americans. We have also chosen to illustrate a range of North American wild mammals, including many that were frequently hunted by Native Americans in pre-Columbian and colonial times. These include black bear (*Ursus americanus*), white-tailed deer (*Odocoileus virginianus*), raccoon (*Procyon lotor*), and opossum (*Didelphis virginiana*). We have also included two species of rabbit.

Comparative Osteology. DOI: 10.1016/B978-0-12-388437-4.00001-6

Figure 1-01: Comparison of anterior/cranial views of left femora from a newborn human (A), chicken (B), and adult cat (C).

The smaller is the native wild rabbit or cotton-tail (*Sylvilagus carolinensis*), while the larger is a domestic rabbit (*Oryctolagus cunniculus*) that is of European origin. Commensal species are frequently found in historic-period archaeological sites, and we have illustrated two of the most common: dog (*Canis familiaris*) and cat (*Felis catus*). We have also included a chapter of miscellaneous photographs (Chapter 23). In this chapter various views are presented of infant and adult human skeletons, and of selected comparisons between human and red fox (*Vulpes vulpes*), bobcat (*Lynx rufus*), rat (*Rattus norvigecus*), and snapping turtle (*Chelydra serpentina*). The snapping turtle is the only reptile that is included as many of

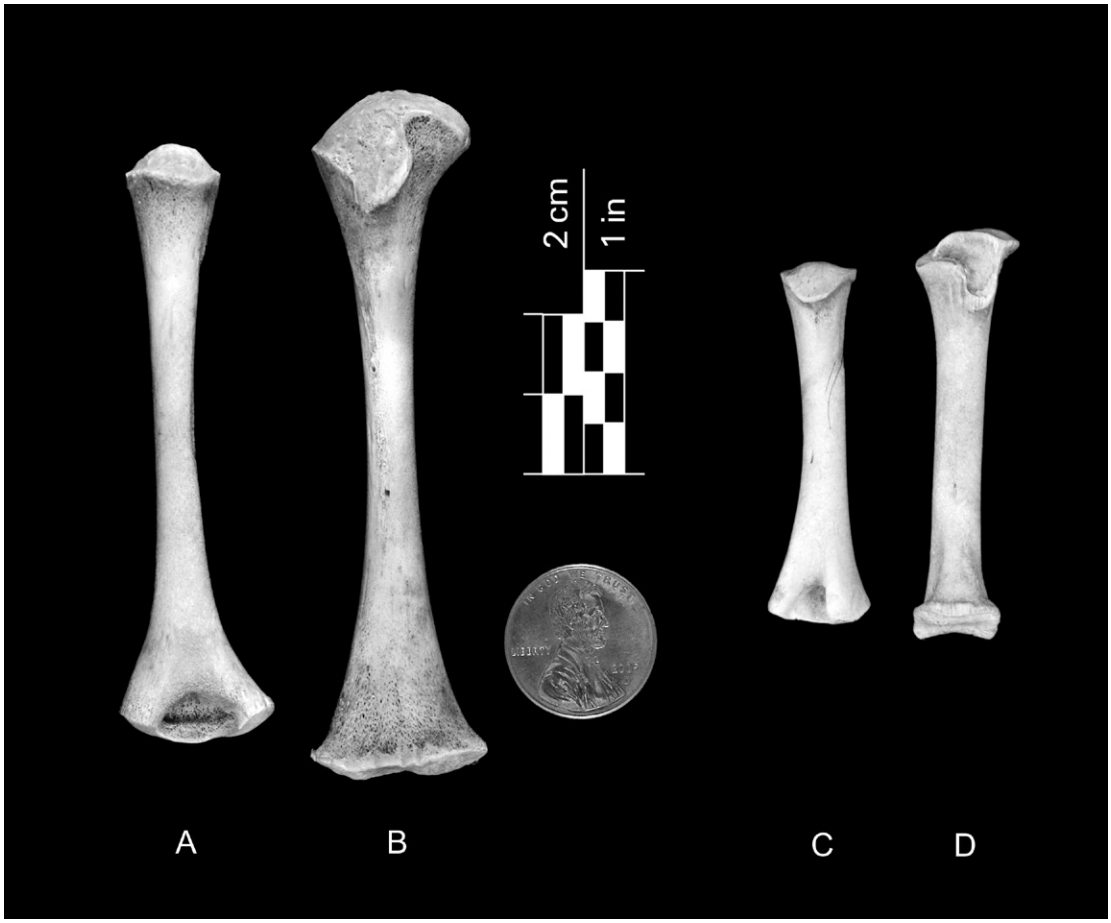

Figure 1-02: Posterior views of a newborn human left humerus (A) and femur (B) compared with caudal views of a fetal deer left humerus (C) and femur (D).

the bones are distinctive in shape and they are commonly recovered from North American archaeological sites.

Most archaeological faunal remains are the leftovers from prehistoric and historic meals. Many animal bones show traces of butchery that reveal the ways in which the carcass was dismembered. In this atlas we have illustrated a range of different butchery marks and techniques (Chapter 24), including both prehistoric cut marks made with stone tools and historic cut marks made with cleavers and saws. We have also included examples of sawn and butchered faunal bones, along with schematic diagrams of modern, commercial butchery patterns. Since bone was a common raw material throughout antiquity and up until the early twentieth century, we have also illustrated a number of examples of worked bone artifacts. Finally, knife cuts and saw marks in bone are not unique to non-human remains. There are numerous cases each year of intentional body mutilation using knives and/or saws.

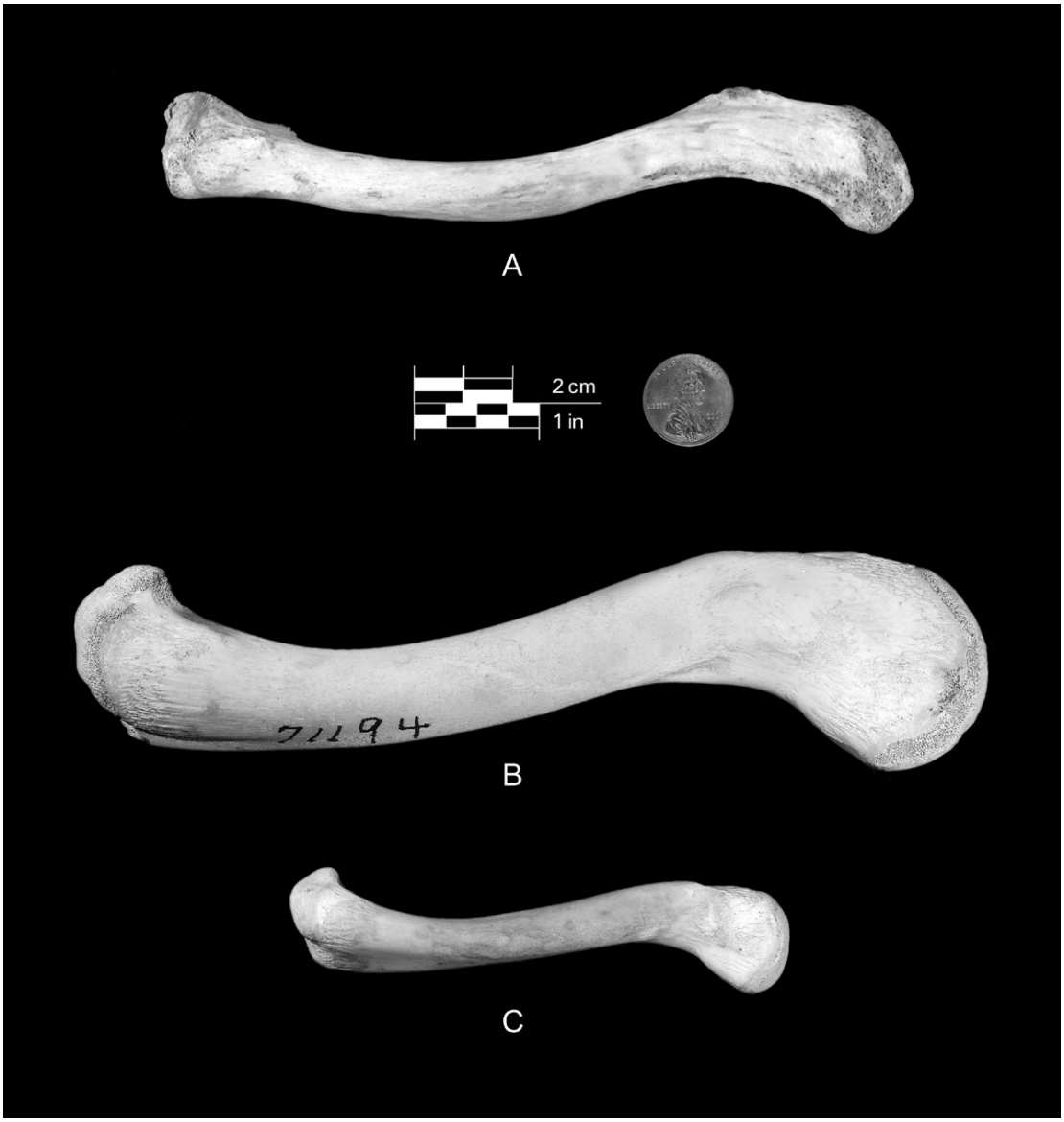

Figure 1-03: Comparison of an adult human left clavicle (A) with a crocodile's (*Crocodylus acutus*) right femur (B) and an alligator's (*Alligator mississippiensis*) right femur (C). Note the similar morphology of the human and non-human elements.

In cases of human dismemberment (usually implying sawing through bones) or disarticulation (usually implying separation between joints) it is quite possible that a badly decomposed or skeletonized human body portion may appear non-human to the untrained eye. A forensic example of postmortem human dismemberment is presented in Chapter 24 to show the similarity of tool mark evidence in human and non-human remains.

The ability to differentiate between human and non-human bones, both complete and fragmentary, is dependent on the training of the analyst and the available reference and/or comparative material. It is truly a skill that requires years of training and experience and is not something that can be gleaned entirely from books. There is no substitute for coursework and training in osteology with actual skeletal material in order to appreciate the range of variation within all animal species. An experienced osteologist should always be consulted for confirmation of element type and species if there is any doubt.

Archaeological Context

Animal bones have played critical roles in archaeological interpretation for more than 150 years of scientific endeavor. The discovery of the bones of extinct animals in association with simple chipped stone tools in sites in France and Britain helped to establish the antiquity of the human presence in Europe and to overthrow the traditional 6000-year biblical chronology for human life on earth. Faunal remains have also played a crucial role in the reconstruction of early human subsistence practices, in the study of animal domestication in both the eastern hemisphere and the Americas, and in the analysis of the ways in which historic cities were provisioned with food. Large numbers of animal bones are often recovered from archaeological sites, and these bones can be used to study past hunting practices, animal husbandry patterns, and diet. In order to use animal bones in archaeological interpretation, zooarchaeologists (archaeologists who specialize in the study of faunal remains) must be able to identify the bones, determine sex and age at death when possible, and examine the bones for evidence of butchery marks and traces of bone working.

While archaeologists expect to find human remains in cemeteries, human bones are often found in other contexts. For example, two adult human burials and the remains of several infants were unexpectedly recovered from the habitation area of the early Anglo-Saxon village site of West Stow in eastern England (West 1985: 58–59). This was the case even though the settlement site was associated with a nearby contemporary cemetery. In another example, at the late Neolithic site of Hougang near Anyang in China, burials of infants in pits or urns were associated with house construction activities (Chang 1986: 270). In short, zooarchaeologists and physical anthropologists must be able to confidently identify both animal bones and human remains in order to accurately interpret past cultures.

The first step in the analysis of animal bones recovered from archaeological sites is the careful identification of both body part and animal species. Precise identification requires a good

comparative collection of modern specimens whose species, sex, and age are well documented. However, a comparative collection must be supplemented by identification guides and atlases that can help the researcher distinguish between different species. Most zooarchaeological identification guides focus solely on non-human species (e.g., Brown and Gustafson 1979; Cornwall 1956; Gilbert 1990; Gilbert et al. 1981; Olsen 1964, 1968), even though human remains are commonly found in archaeological sites. Exceptions to this are Schmid (1972) and Hillson (1995) who illustrate human bones, but there is no comparison with subadult human bones, and France (2009) which includes photographs of both human and non-human skeletal remains.

Forensic Context

It is equally important for forensic scientists working with human skeletal remains to be able to differentiate between human and non-human bones. In the modern forensic context, it is quite common for non-human bones to be mistaken for human remains and end up in the medical examiner's or coroner's system. It is of obvious importance that they are correctly identified, or the consequences could be substantial. It is usually the role of a forensic anthropologist to make this assessment of "human versus non-human" and generate the appropriate report. In most forensic scenarios, once a determination of non-human is made it is seldom of investigative significance to correctly identify the species. There are numerous skeletal anatomy books dedicated to human osteology (e.g., Bass 2005; Brothwell 1981; Schaefer, et al. 2009; Scheuer and Black 2000; Steele and Bramblett 1988; White 2000; White and Folkens 2005). Some guides and textbooks on human osteology and forensic anthropology do include sections on differentiating between human and non-human remains (e.g., Bass 2005; Byers 2010; Ubelaker 1989) but these are more cursory discussions.

When attempting to differentiate between human and non-human skeletal remains, fragmentation only compounds the problem. If fragmentation is so extreme that gross identification of human versus non-human bone is not possible, microscopic (i.e., histological) techniques can be employed (e.g., Cattaneo, et al. 2009; Hillier and Bell 2007; Mulhern and Ubelaker 2001). Under magnification, the shape of the bone cells may be indicative of non-human bone, but this technique is not foolproof as some non-human animals (e.g., large dogs, bovines, and non-human primates) are nearly identical to humans microscopically. This atlas will only focus on the gross assessment of bones.

Book Terminology and Organization

In constructing this atlas, we have chosen to illustrate examples of both adult and juvenile animal bones in addition to both adult and newborn human skeletons. Other guides to the identification of birds and mammals from archaeological sites illustrate only adult bones. However, many animal bones recovered from archaeological sites and within the forensic context are the remains of juvenile animals. Farmers who keep cattle for milk, for example,

often slaughter excess male calves during their first year of life. In a meat-oriented economy, farmers frequently choose to slaughter adolescent animals, since these animals are nearly full-grown and continuing to feed animals beyond adolescence results in only limited increases in meat output. We have included illustrations of both adult and juvenile pigs, and we have illustrated both an adult sheep and an immature and an adult goat. We have also photographed examples of immature chickens, since most chickens consumed today are quite young.

In general, the animals in this atlas are presented in the order of their size, progressing from largest to smallest. In Chapters 7–22 the corresponding human and non-human elements are presented alongside each other in order to fully appreciate the variation in size and shape between them. To add a scaled perspective, a ruler (centimeters and inches) is present in each photograph along with a US penny. For consistency, all of the images depict left elements unless otherwise noted. When a right element was better preserved than its left counterpart, the image was reversed to show it as a left element. In most instances, the human bone is photographed on the left side of the image and is separated from the non-human counterpart by the scale and penny. Letters and arrows have been added to some images to highlight specific landmarks or skeletal elements.

Bipedalism (upright walking on two legs) is one of the most important developments in all of human evolution. However, as a result of bipedalism, many human bones are oriented in somewhat different ways to comparable bones in other mammals. In addition, the directional terms used to describe parts of the body differ somewhat between humans and other mammals (Figures 1-04 and 1-05). For example, in human osteology the term *anterior* is used to describe the front portion of a bone, while in quadrupeds the term *cranial* is used. Similarly, the back portion of the femur is described as *posterior* in humans, but it is described as *caudal* in other mammals. Different terms are also used for the lower portions of non-human limbs. For example, the surface of the forelimb (distal to the radius and ulna) that faces the ground is described as *palmar* (or *volar*), while the comparable surface in the hindlimb (distal to the tibia) is described as *plantar*. The opposite surfaces of the bone are described as *dorsal*. The terms *proximal*, *distal*, *medial*, and *lateral* are used to describe surfaces in both human and non-human bones. For humans, we have used the directional terms as described in Bass (2005). For other mammals, we have used the terms as defined in Evans and de Lahunta (1980) and Getty (1975). In describing bird bones, we have followed the terminology used by Cohen and Serjeantson (1996).

We have used the following notation for referring to adult dental formulae: upper incisors/lower incisors.upper canines/lower canines.upper premolars/lower premolars.upper molars/lower molars. For example, the adult human maxillary dentition includes 2 incisors on each side, 1 canine on each side, 2 premolars on each side, and 3 molars on each side. The mandibular dentition also includes 2 incisors, 1 canine, 2 premolars, and 3 molars on each side. The human dental formula is written as follows: 2/2.1/1.2/2.3/3.

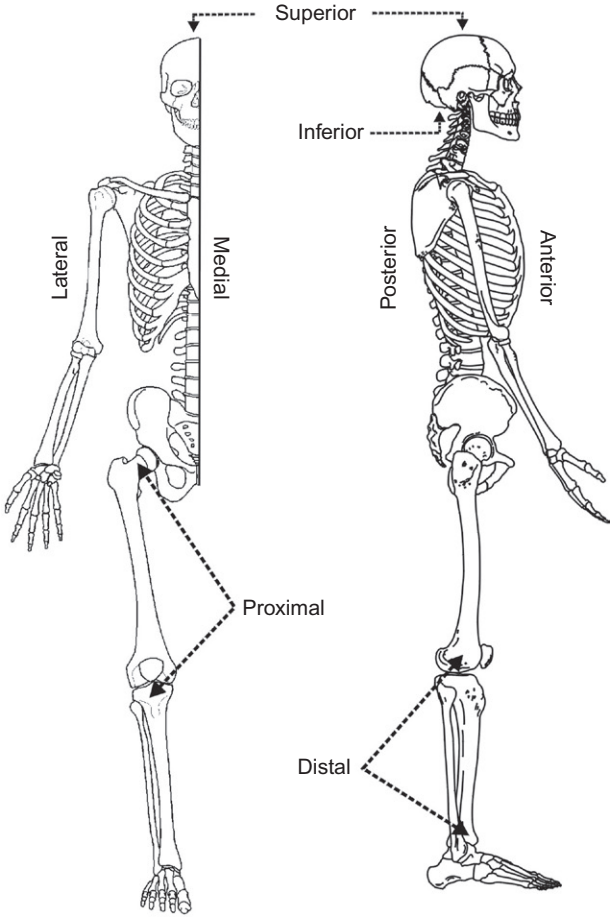

Figure 1-04: Schematic diagram of human skeleton in standard anatomical position (i.e., standing with arms at the side and palms forward so that no bones are crossing) labeled with anatomical terminology.

Background of the Specimens Included in this Book

Most of the non-human skeletons that are illustrated in this atlas come from the collections of the zooarchaeology laboratory in the Anthropology Department of New York University. The bear skeleton was borrowed from the Department of Mammology of the American Museum of Natural History. Some of the horse bones that are illustrated here are from a horse skeleton that was borrowed from the Museum Applied Science Center for Archaeology (MASCA) at the University of Pennsylvania Museum. The raccoon skeleton was borrowed from Susan Antón. The alligator and crocodile femora were provided by the Herpetology Department at the American Museum of Natural History and were photographed by Ilana Solomon and Tam Nguyen. The original photograph of the turkey skull was provided courtesy of the National

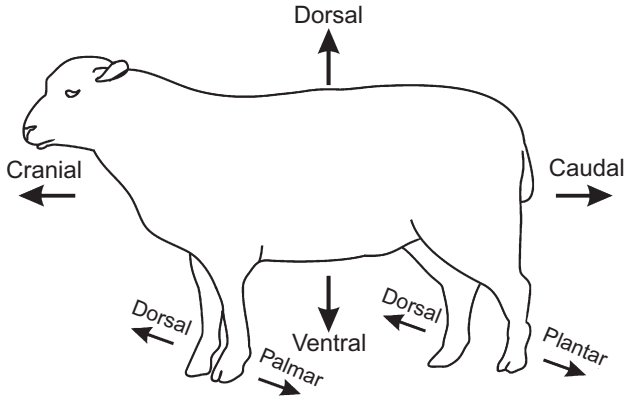

Figure 1-05: Schematic diagram labeled with the anatomical terminology used for faunal remains. For long bones the proper term for the forward-facing side of a bone in humans is "anterior," while in faunal remains the term "cranial" is used instead. For the back of a long bone, it is "posterior" in humans and "caudal" in faunal elements. The terms proximal, distal, medial, and lateral are used synonymously with both human and non-human elements.

Wild Turkey Federation, while Gina Santucci performed the artistic modifications to the photograph. Seth Brewington provided the photograph of the antler comb from Iceland. The horse metacarpus and metatarsus were borrowed from the Zooarchaeology Laboratory in the Anthropology Department at Hunter College. The human remains are from unidentified individuals that were analyzed at the Office of Chief Medical Examiner in New York City. We are grateful to everyone who loaned us specimens and assisted in this project.

Photographic Credits

Many of the original photographs used in this book were taken by Gina Santucci. Additional photographs were taken by Douglas Campana and Bradley Adams. Line drawings for the title pages of chapters 2–6 were created by Douglas Campana. The artistic images and layouts for the title pages of Chapters 7–23 were created by Gina Santucci.

This page intentionally left blank

CHAPTER 2

Crania

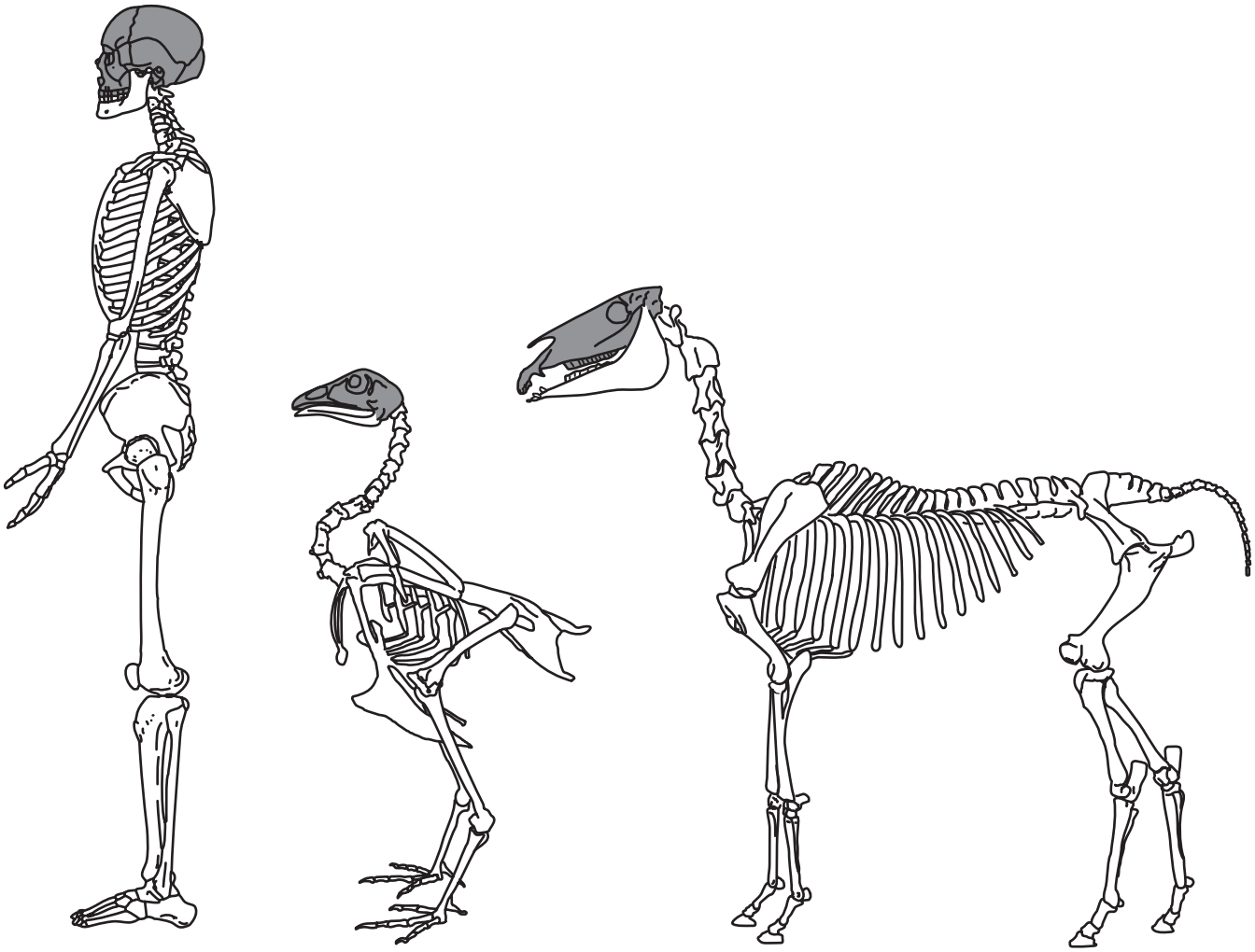

Comparative Osteology. DOI: 10.1016/B978-0-12-388437-4.00002-8

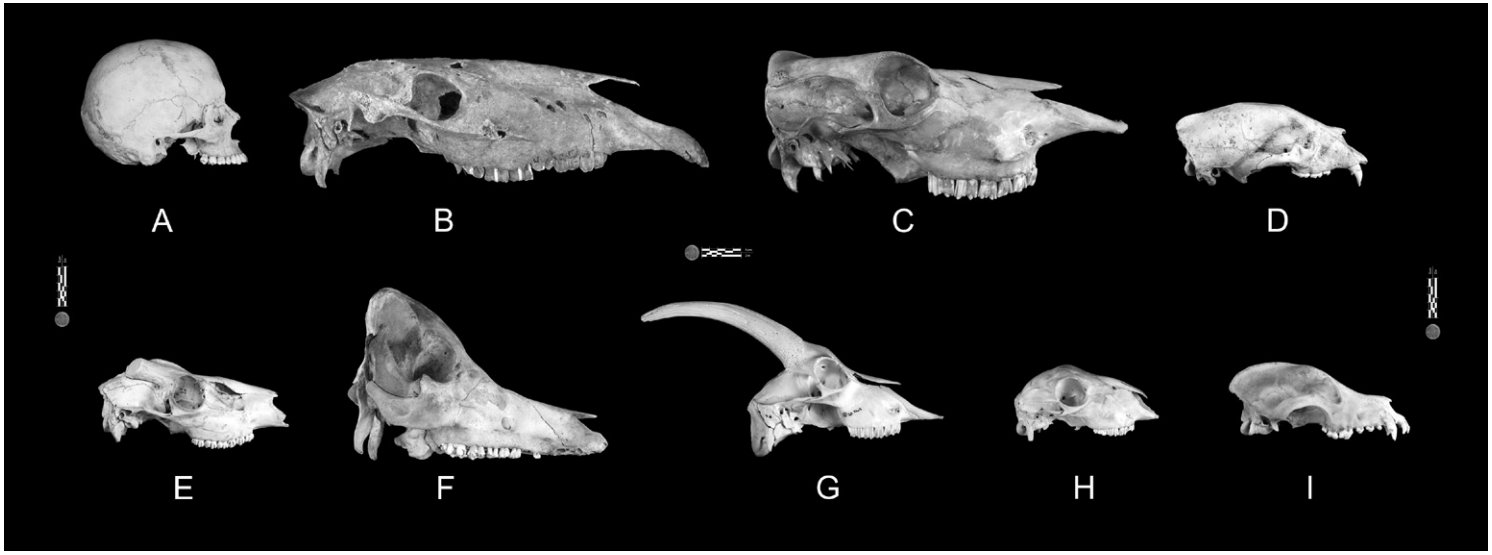

Figure 2-01: Crania showing the differences in scale between some of the larger animals (lateral right views). Pictured are: adult human (A), horse (B), cow (C), bear (D), white-tailed deer (E), pig (F), goat (G), sheep (H), and dog (I).

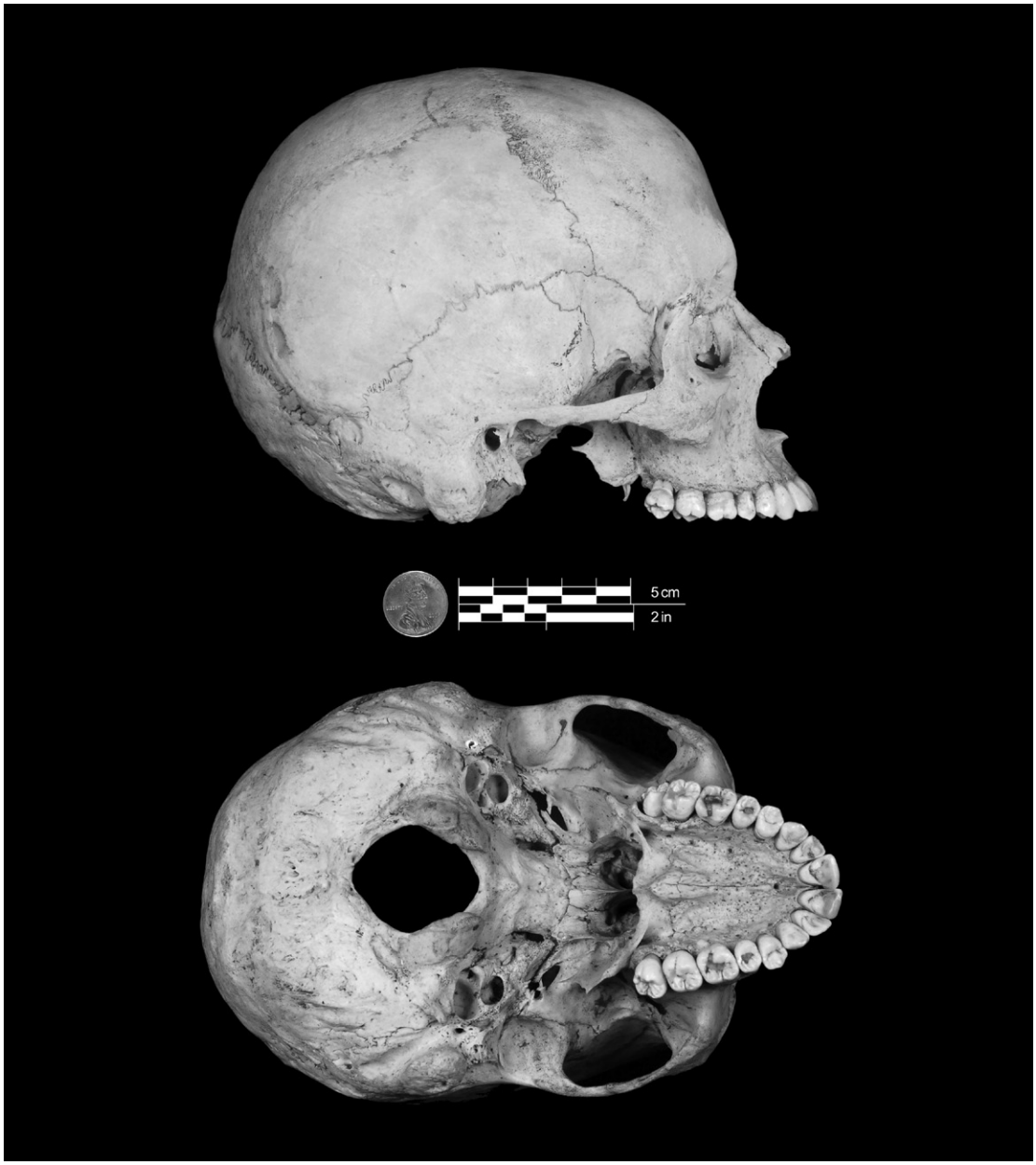

Figure 2-02: Adult human cranium: lateral right (top) and inferior (bottom) views.

Figure 2-03: Horse cranium: lateral right (top) and ventral (bottom) views. Note how the horse has upper incisors.

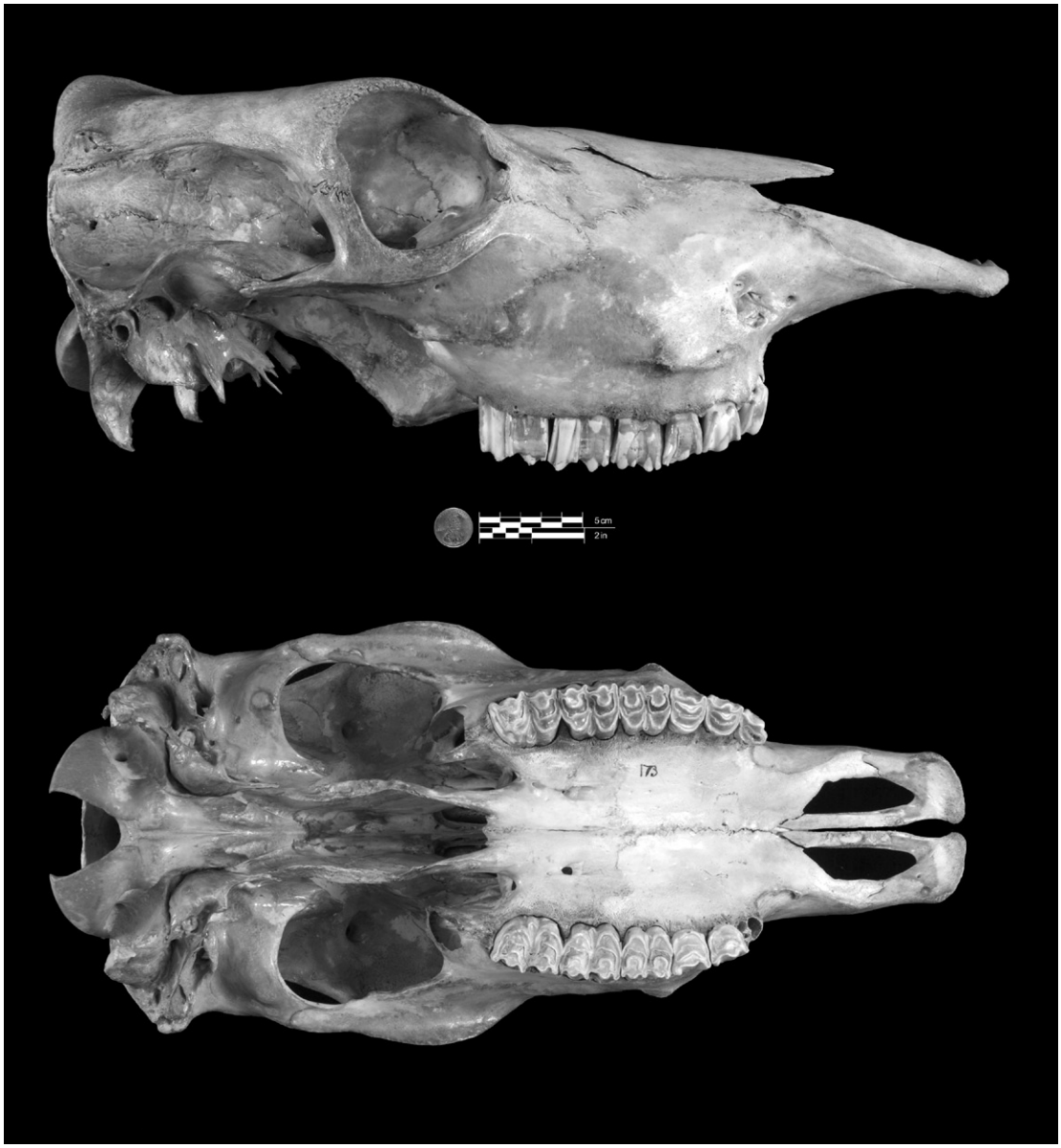

Figure 2-04: Cow cranium: lateral right (top) and ventral (bottom) views. Note how the cow lacks upper incisors.

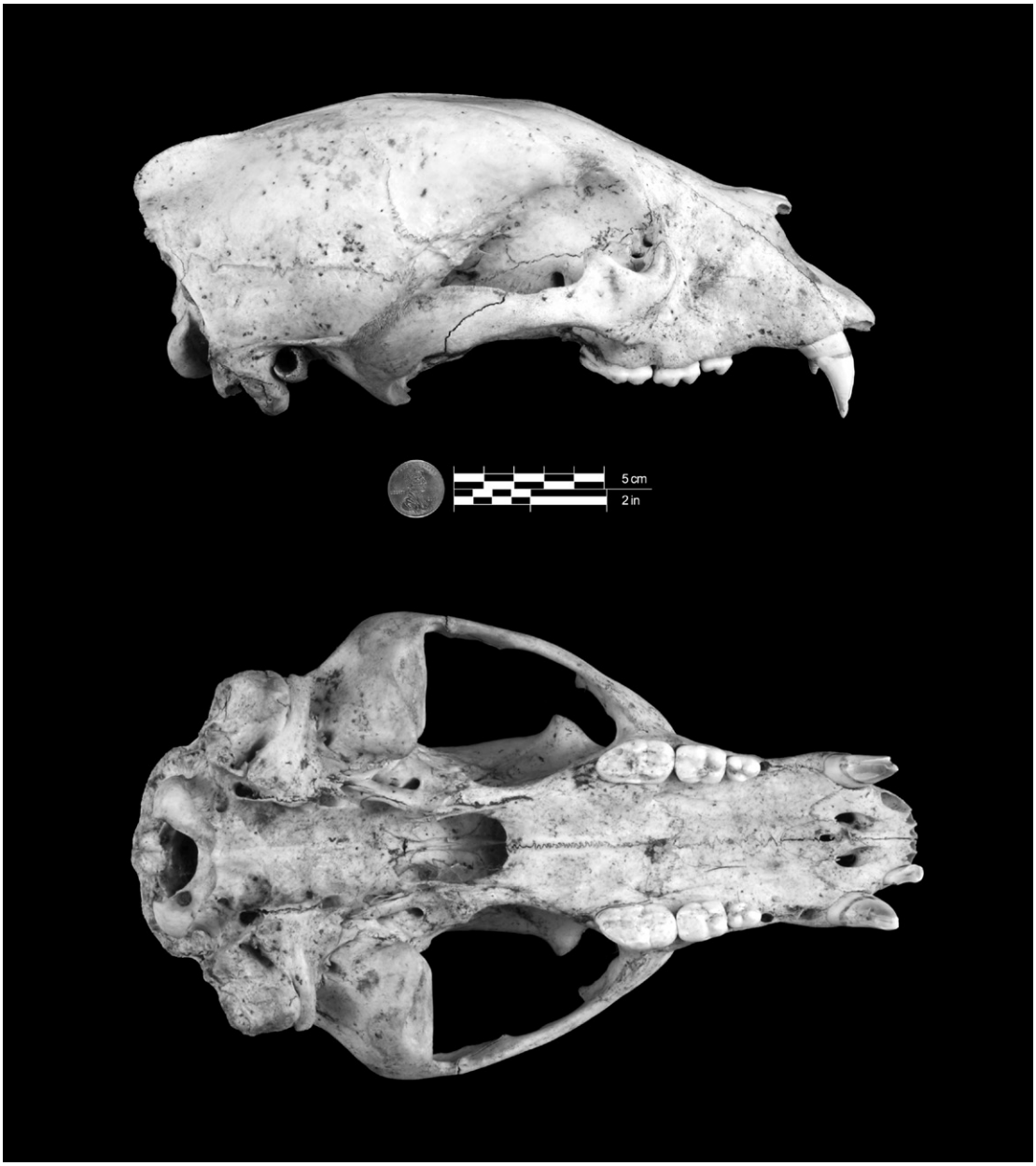

Figure 2-05: Bear cranium: lateral right (top) and ventral (bottom) views. Several premolars are missing antemortem (before death) and several incisors are missing postmortem (after death).

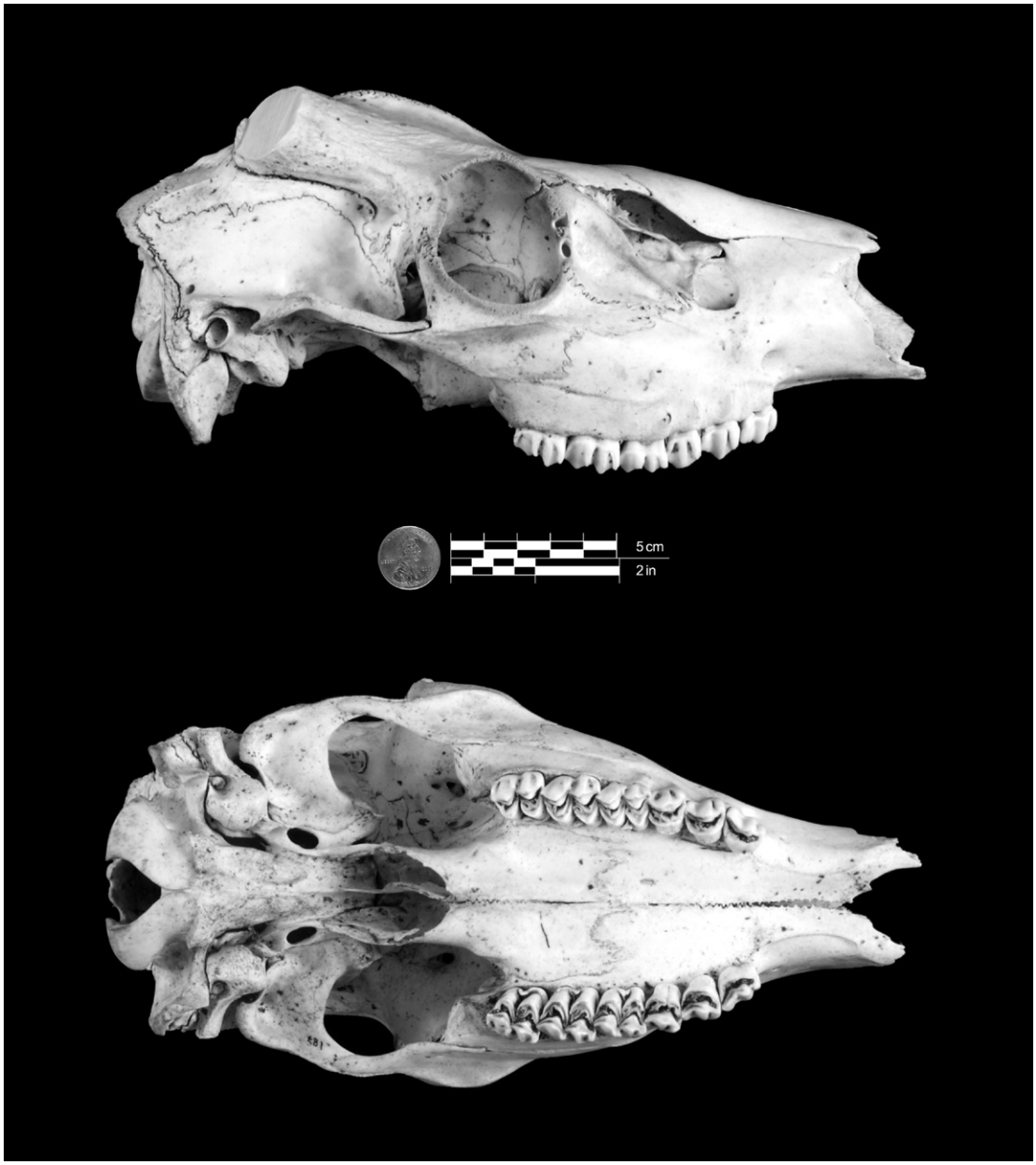

Figure 2-06: Male deer cranium: lateral right (top) and ventral (bottom) views; the deer's antlers have been sawn off. Note how the deer lacks upper incisors.

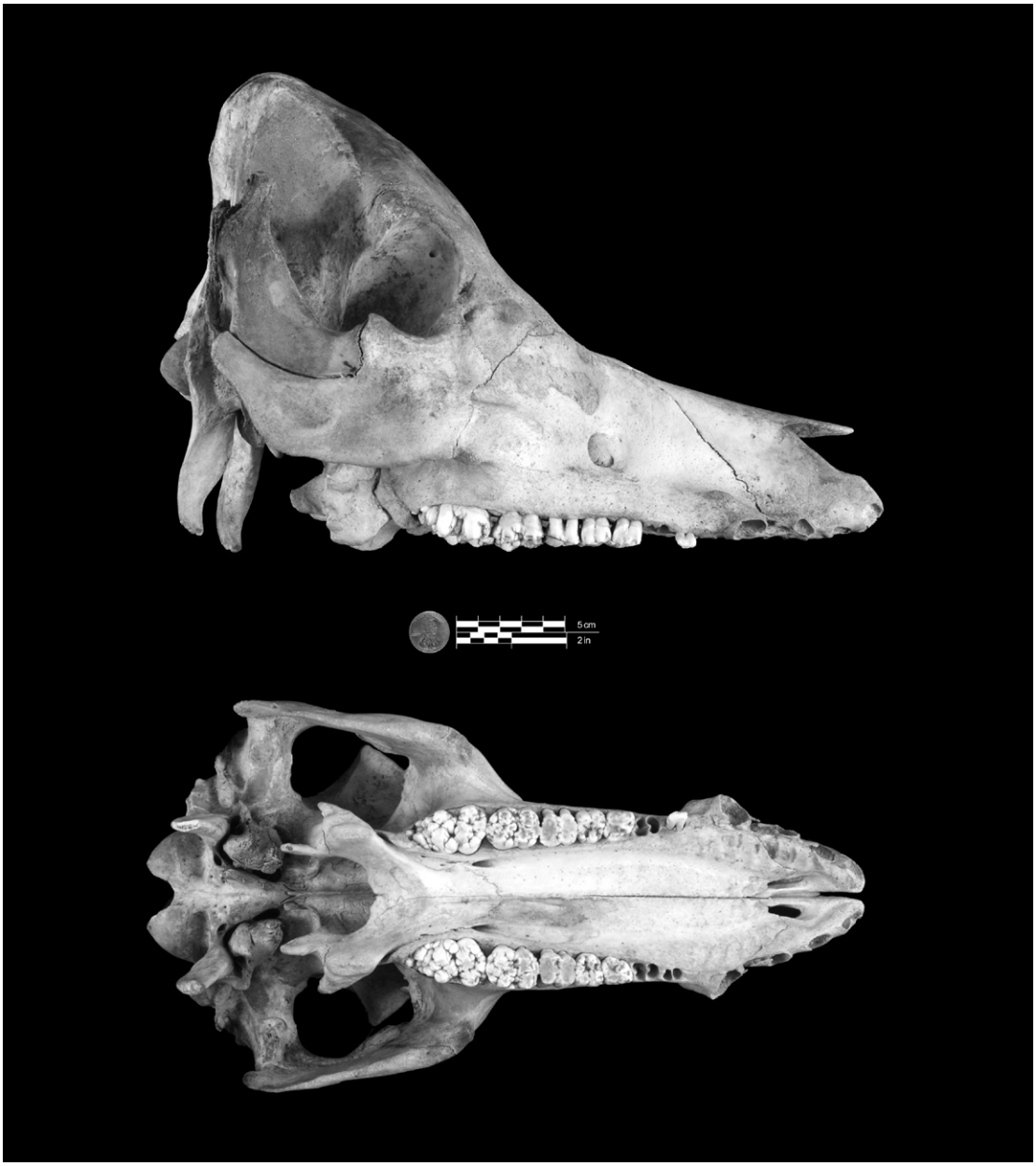

Figure 2-07: Pig cranium: lateral right (top) and ventral (bottom) views. Adult pigs often have large, curved canines. These canines are missing postmortem (after death) from this specimen, as are the incisors and several premolars.

Figure 2-08: Goat cranium: lateral right (top) and ventral (bottom) views. The goat's cranium has been sawn sagittally and the halves have been realigned in the ventral view. Note how the goat lacks upper incisors.

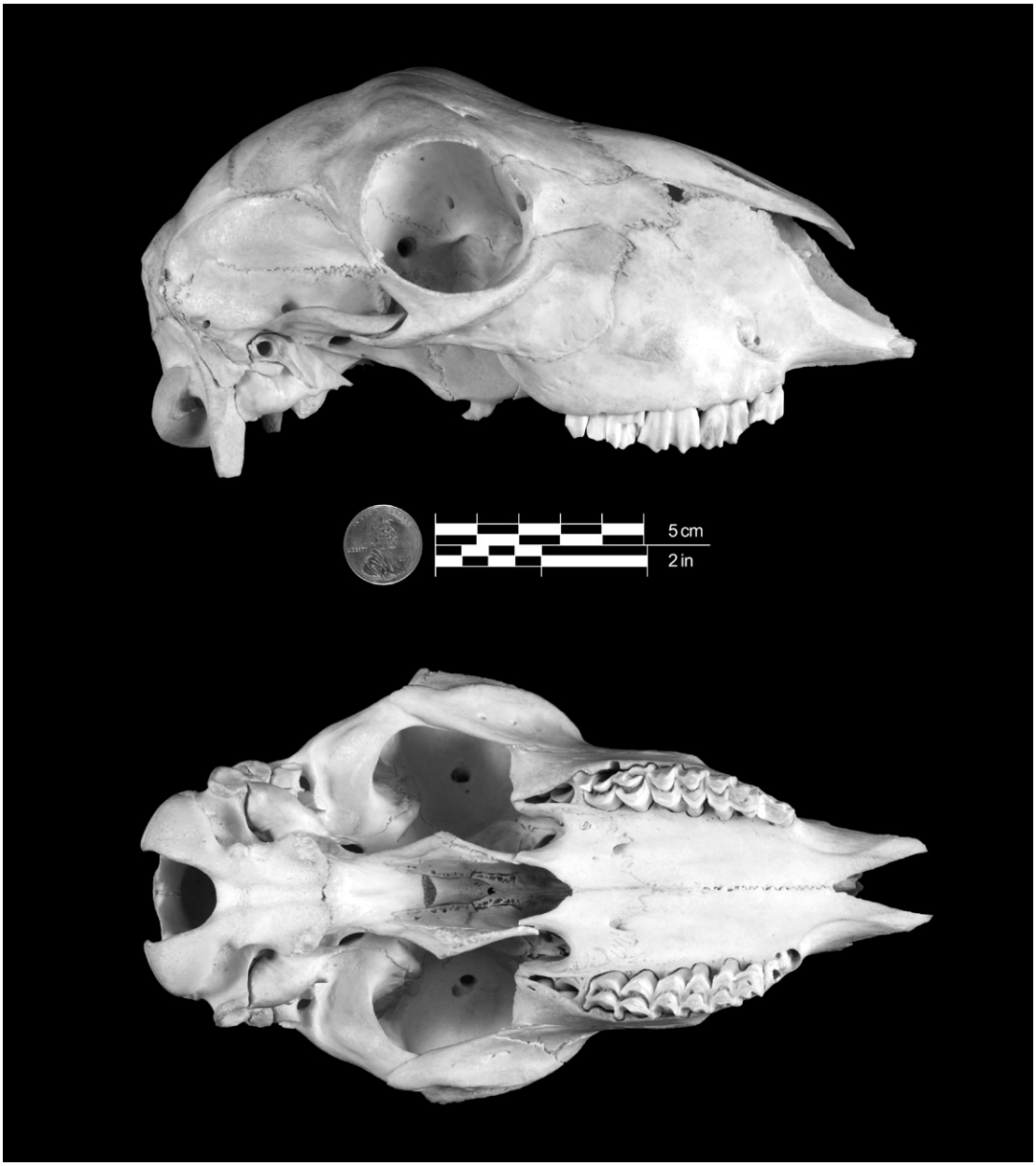

Figure 2-09: Sheep cranium: lateral right (top) and ventral (bottom) views. Note how the sheep lacks upper incisors.

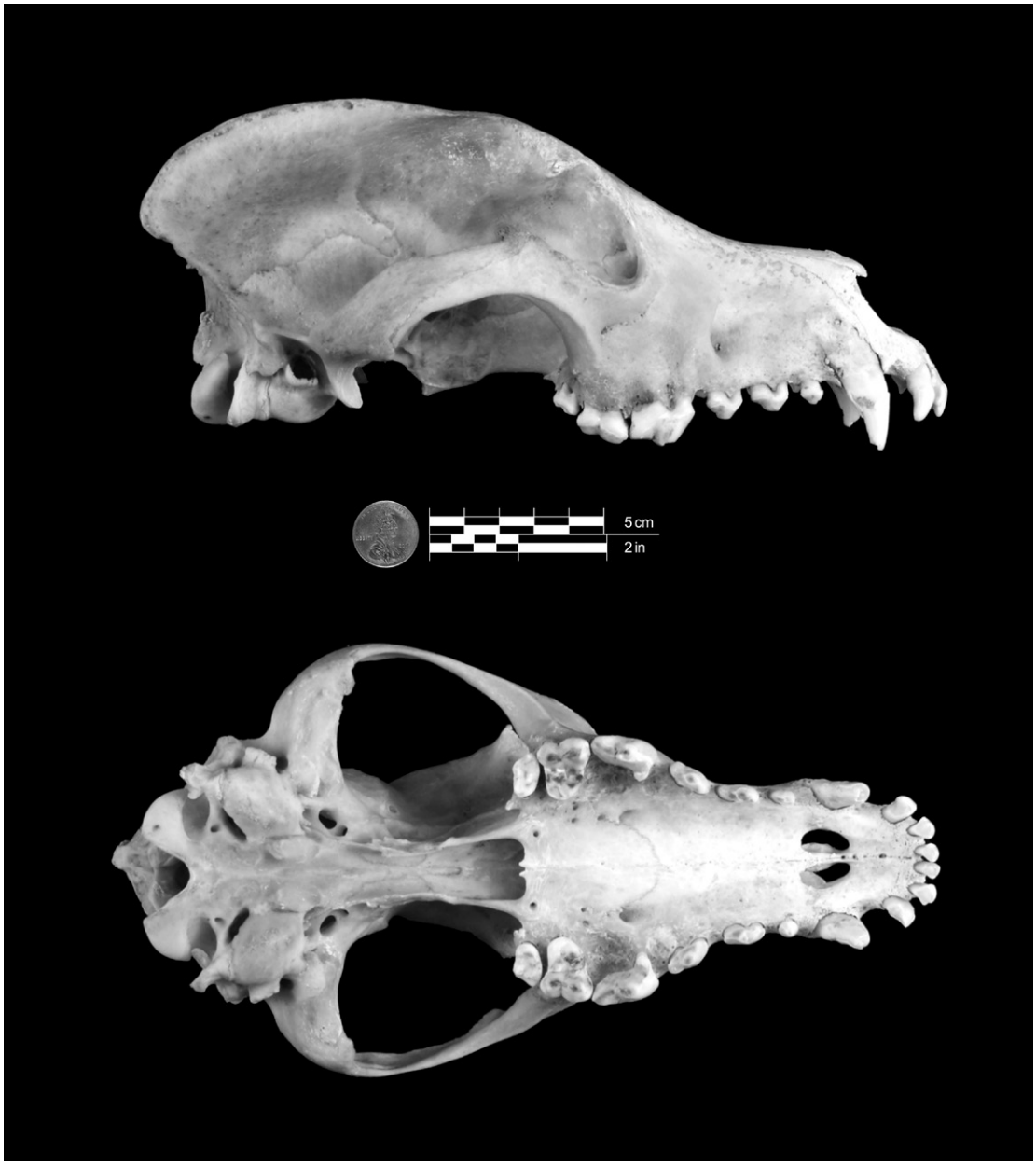

Figure 2-10: Dog cranium: lateral right (top) and ventral (bottom) views.

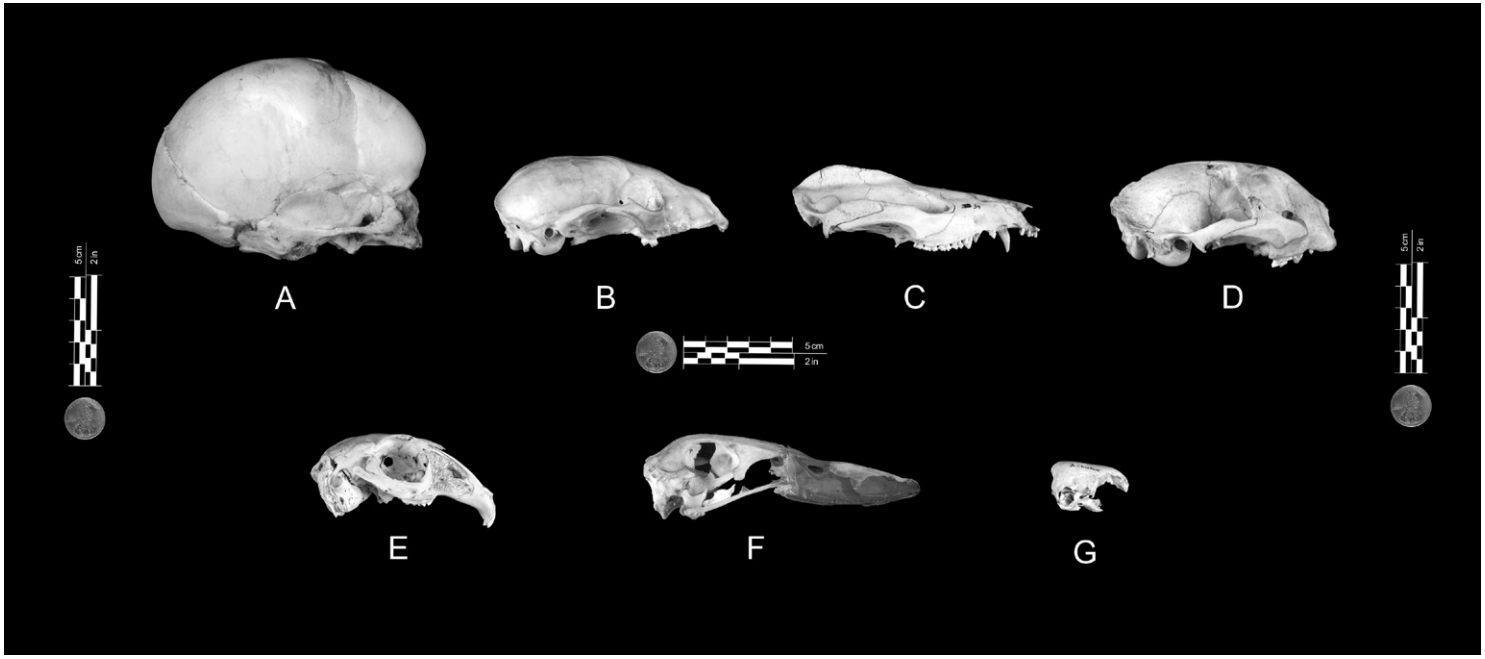

Figure 2-11: Crania showing the differences in scale between some of the smaller animals (lateral right views). Pictured are: newborn human (A), raccoon (B), opossum (C), cat (D), rabbit (E), duck (F), and chicken (G).

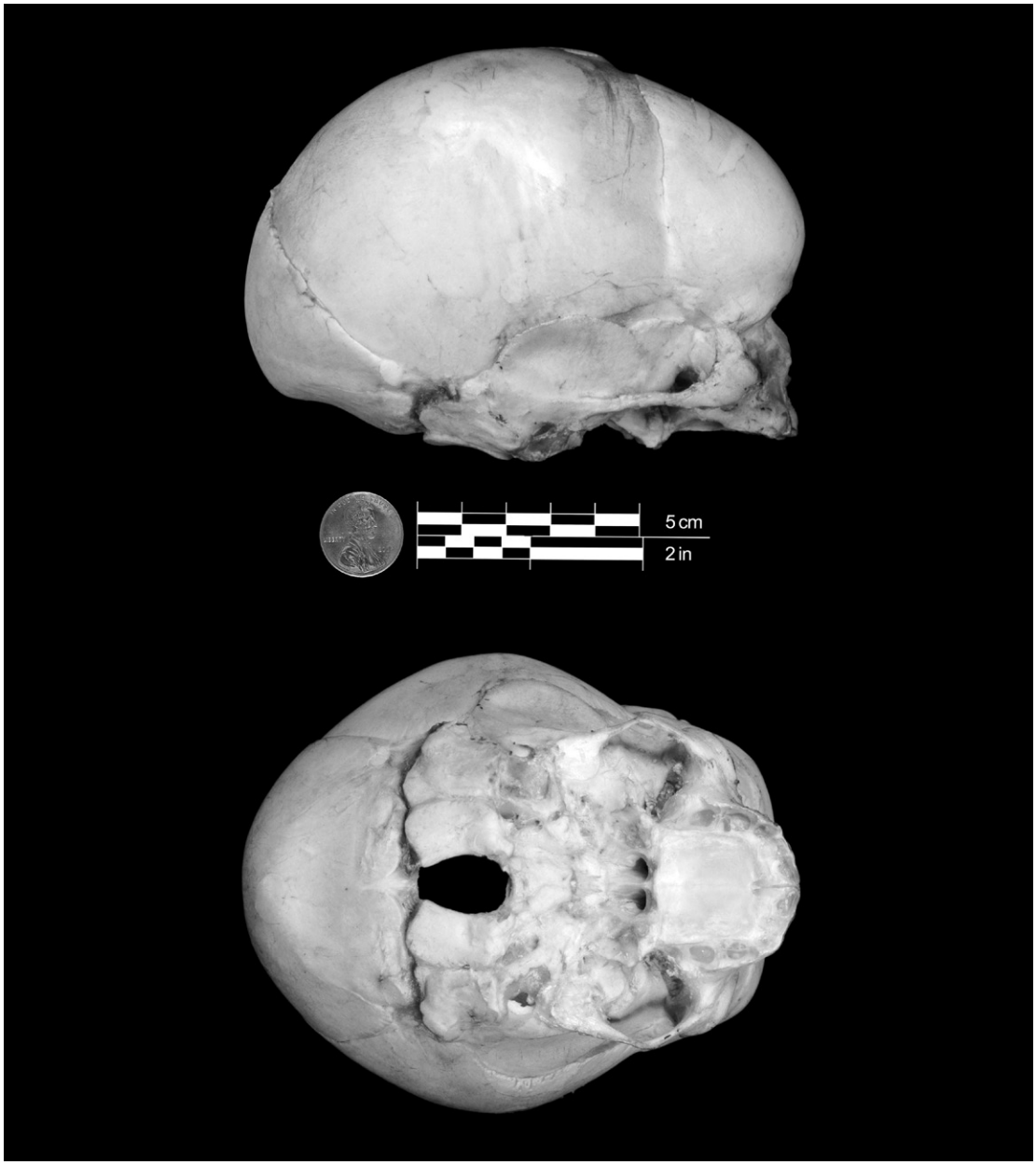

Figure 2-12: Newborn human cranium: lateral right (top) and inferior (bottom) views. In fetal, newborn, and infant remains the teeth are usually still forming and are unerupted. In very young individuals, the bones of the cranium will often be separate as opposed to articulated when skeletonized.

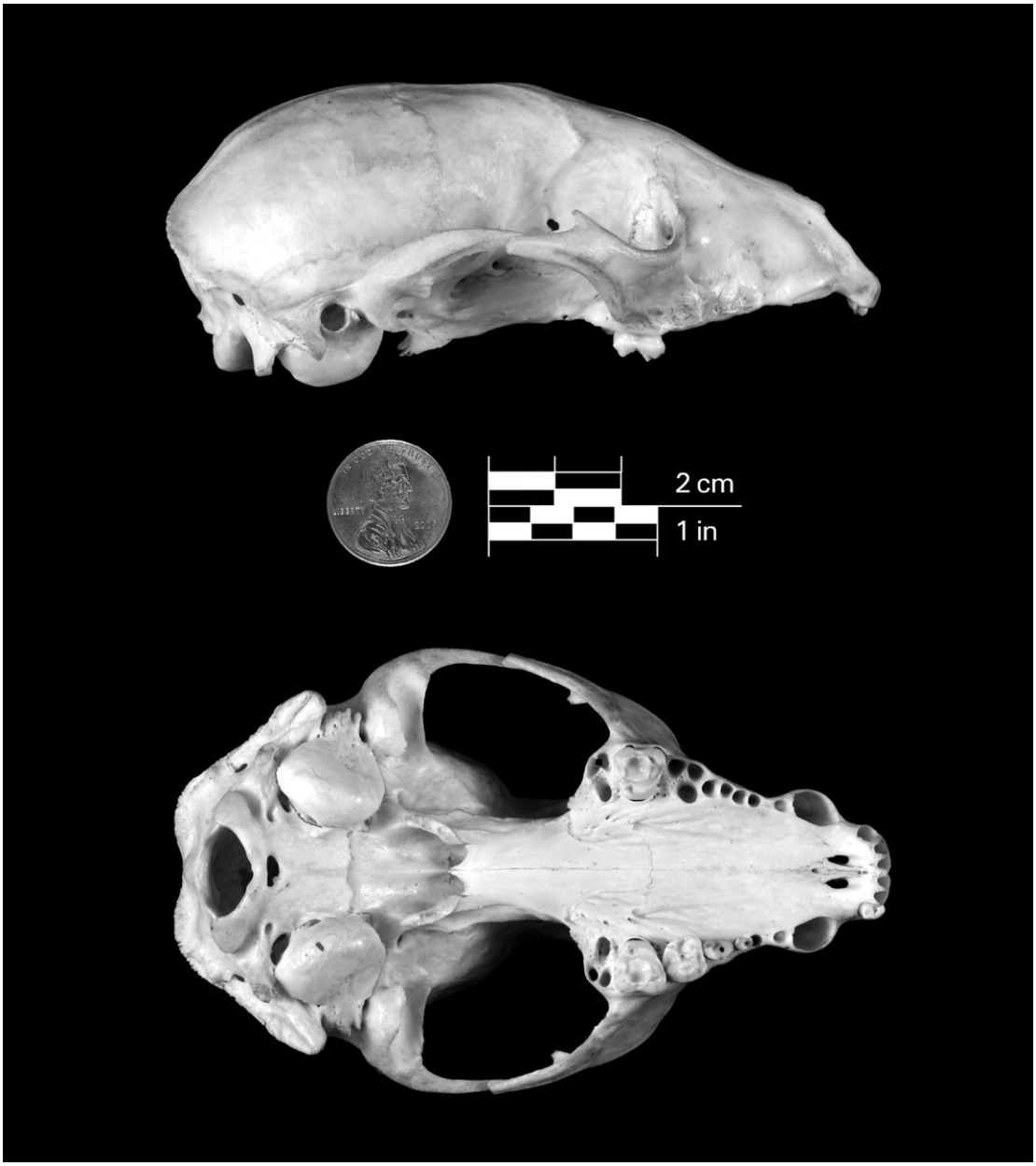

Figure 2-13: Raccoon cranium: lateral right (top) and ventral (bottom) views. Numerous teeth are missing postmortem (after death) from this specimen.

Figure 2-14: Opossum cranium: lateral right (top) and ventral (bottom) views. The opossum has a very distinctive dental pattern with five incisors on each side of the cranium. Several teeth are missing postmortem (after death) from this specimen.

Figure 2-15: Cat cranium: lateral right (top) and ventral (bottom) views. Numerous teeth are missing postmortem (after death) from this specimen.

Figure 2-16: Rabbit cranium: lateral right (top) and ventral (bottom) views.

Figure 2-17: Duck cranium: lateral right (top) and ventral (bottom) views. Some of the fragile bones of the cranium are damaged and missing from this specimen.

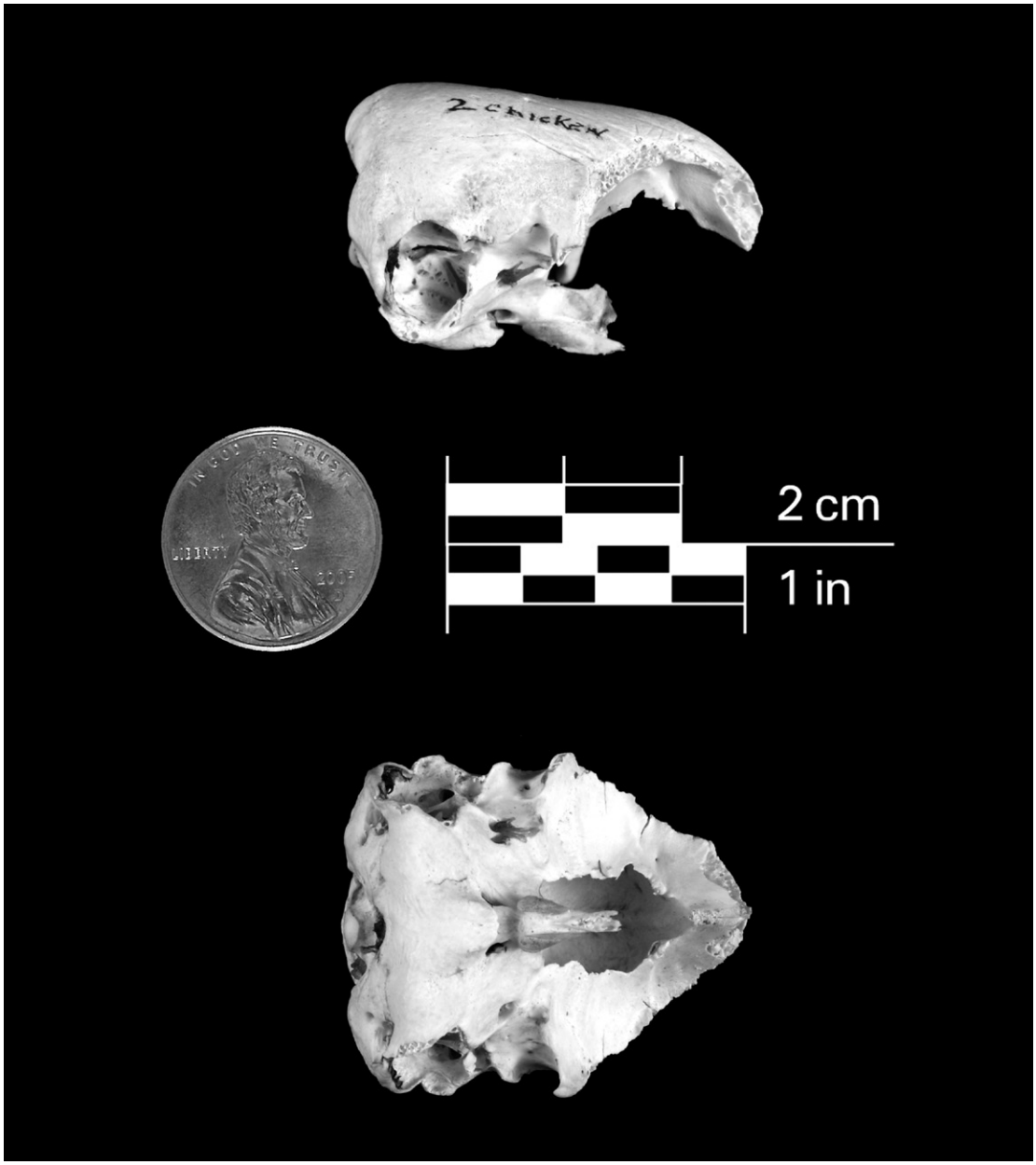

Figure 2-18: Chicken cranium (without beak): lateral right (top) and ventral (bottom) views.

This page intentionally left blank

CHAPTER 3

Humeri

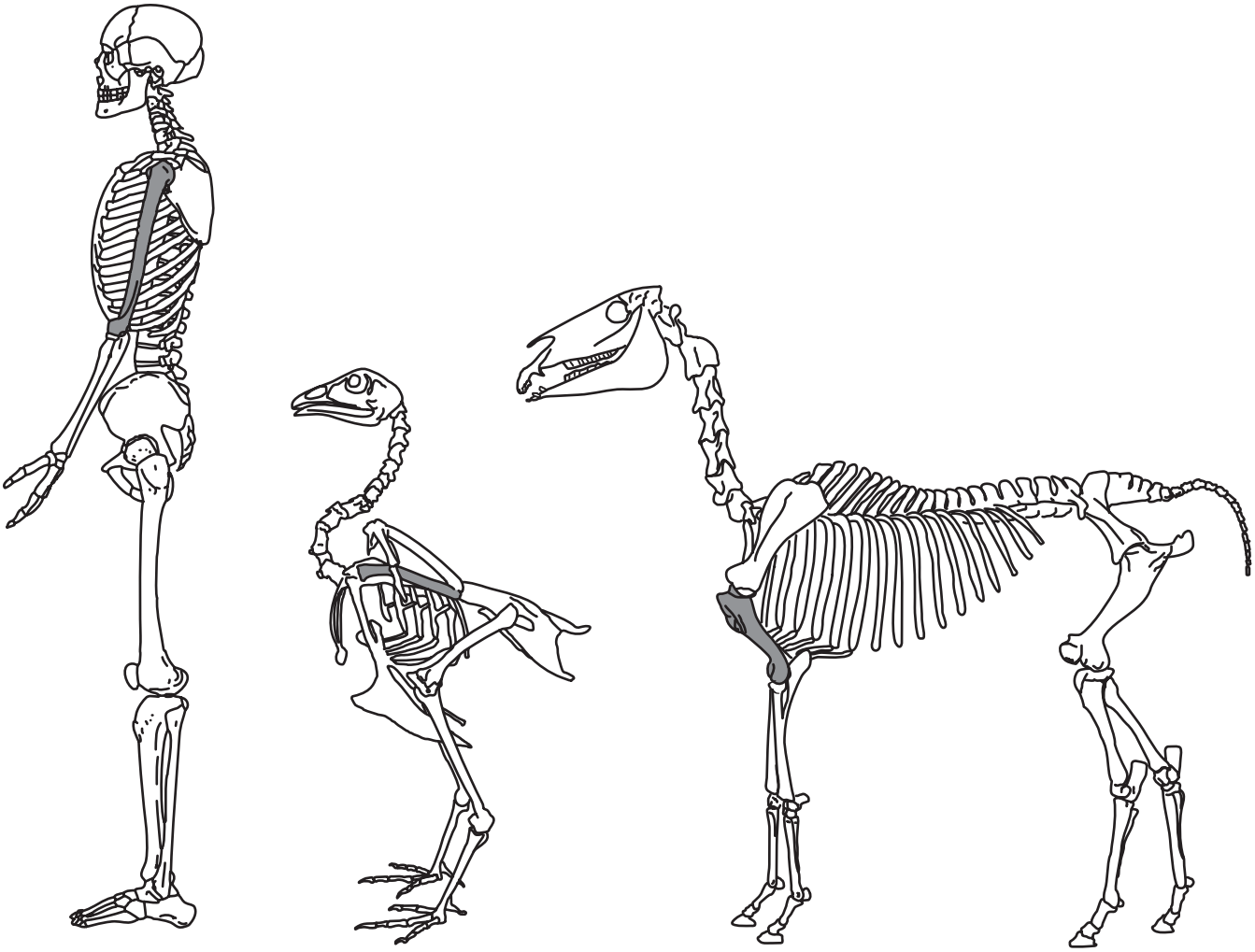

Comparative Osteology. DOI: 10.1016/B978-0-12-388437-4.00003-X

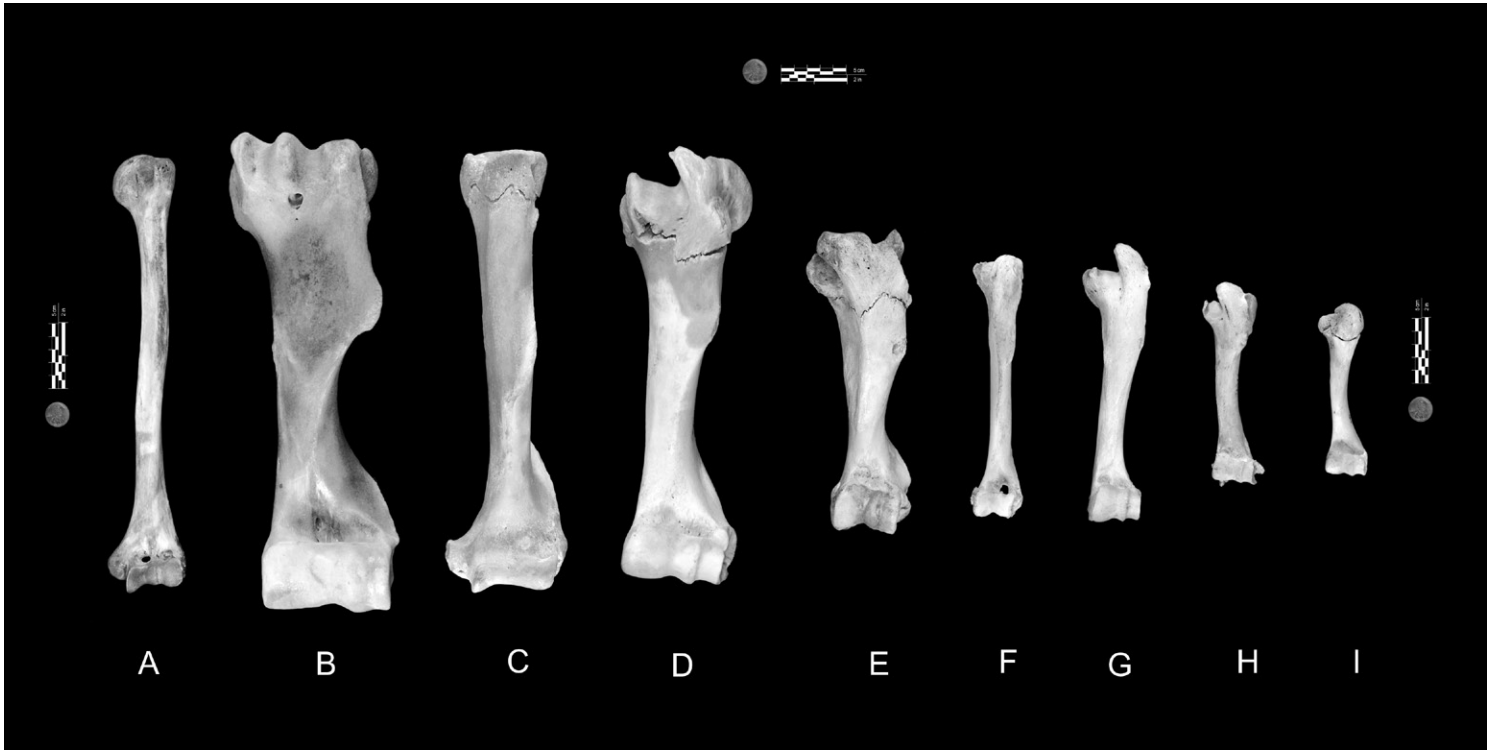

Figure 3-01: Left humeri showing the differences in scale between some of the larger animals. Pictured are the anterior view of an adult human (A) and cranial views of a horse (B), bear (C), cow (D), pig (E), dog (F), white-tailed deer (G), sheep (H), and juvenile goat (I).

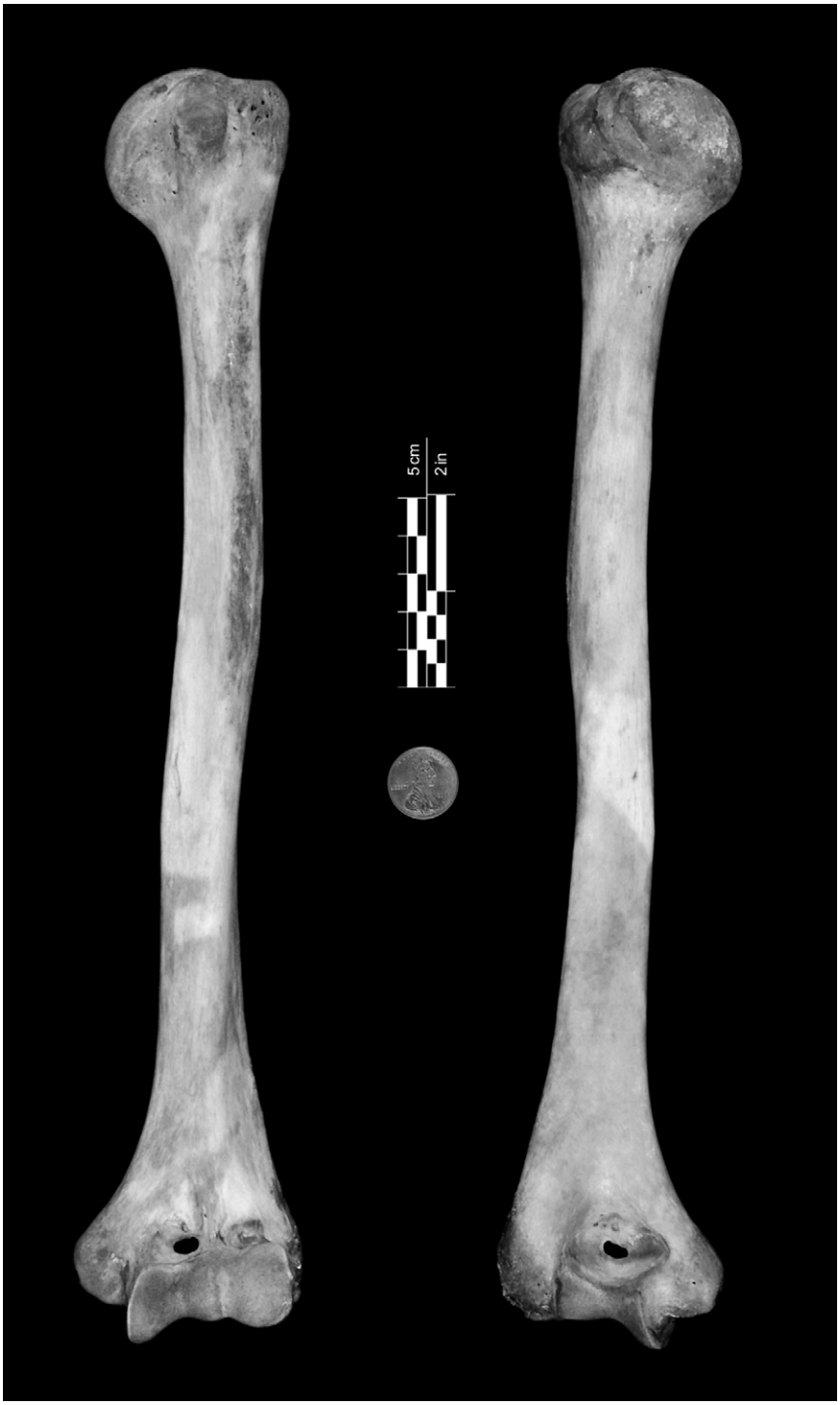

Figure 3-02: Adult human left humerus: anterior and posterior views.

Figure 3-03: Horse left humerus: cranial and caudal views.

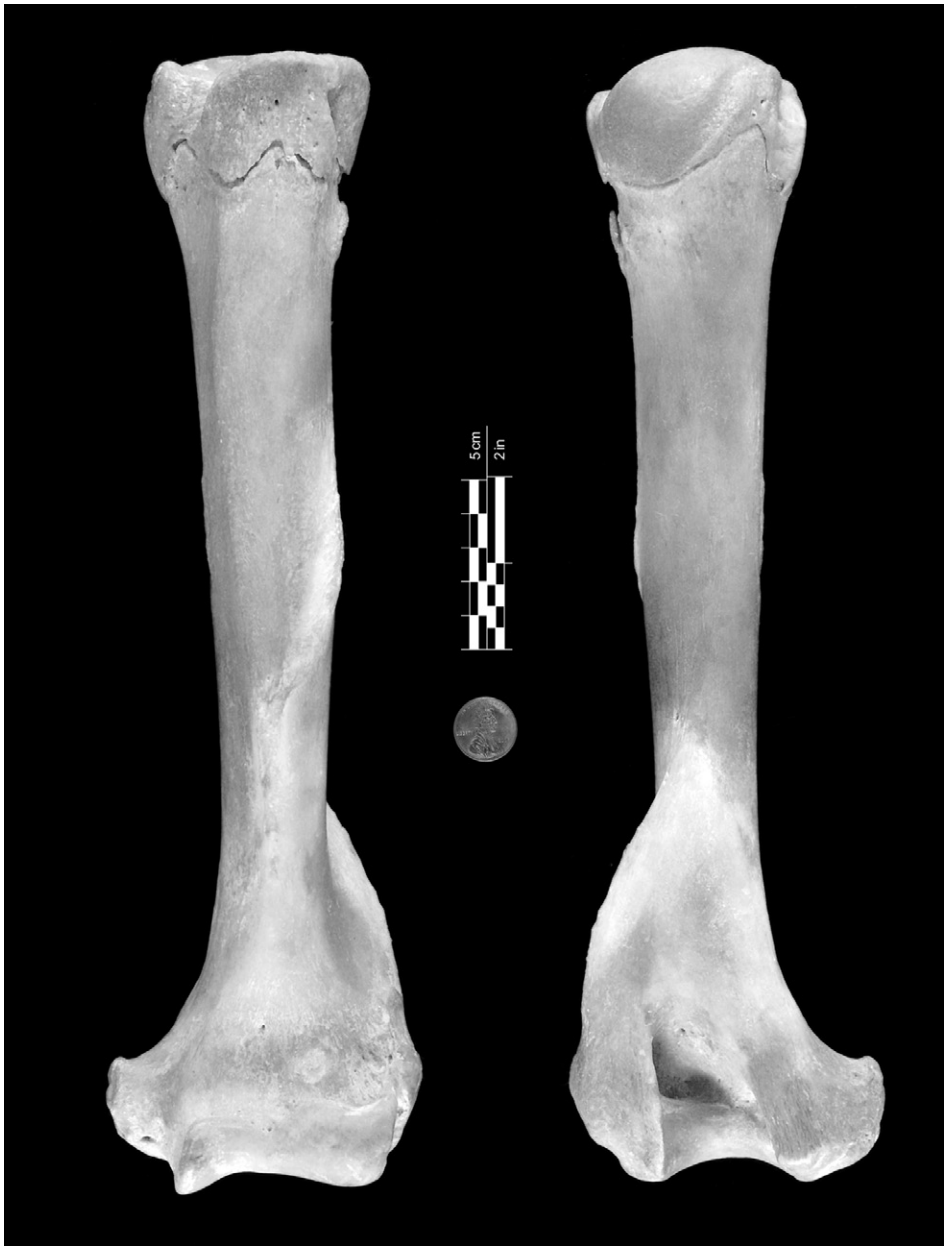

Figure 3-04: Bear left humerus: cranial and caudal views. Note how the fusion line is still visible at the proximal epiphysis.

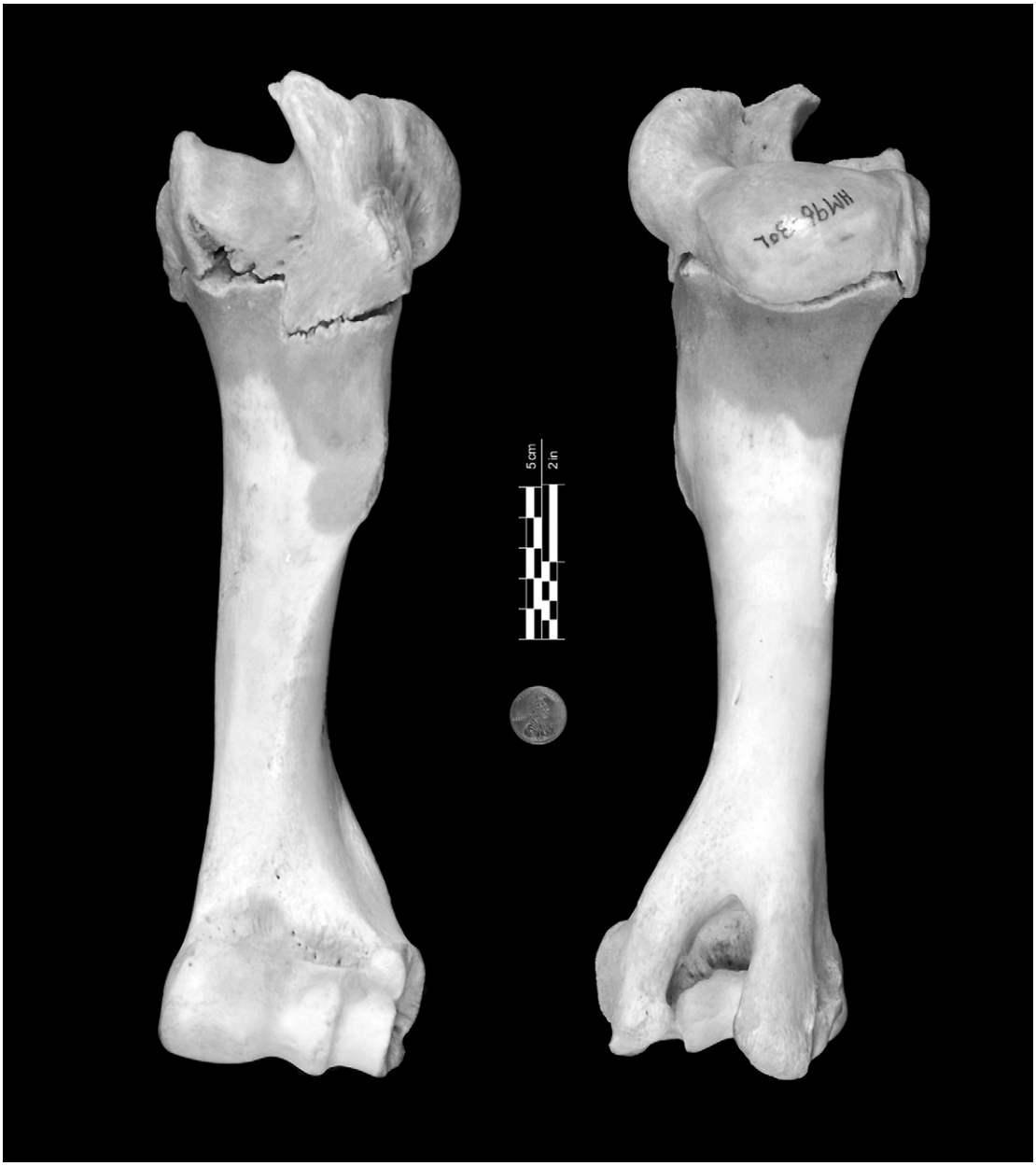

Figure 3-05: Cow left humerus: cranial and caudal views. Note how the fusion line is still visible at the proximal epiphysis.

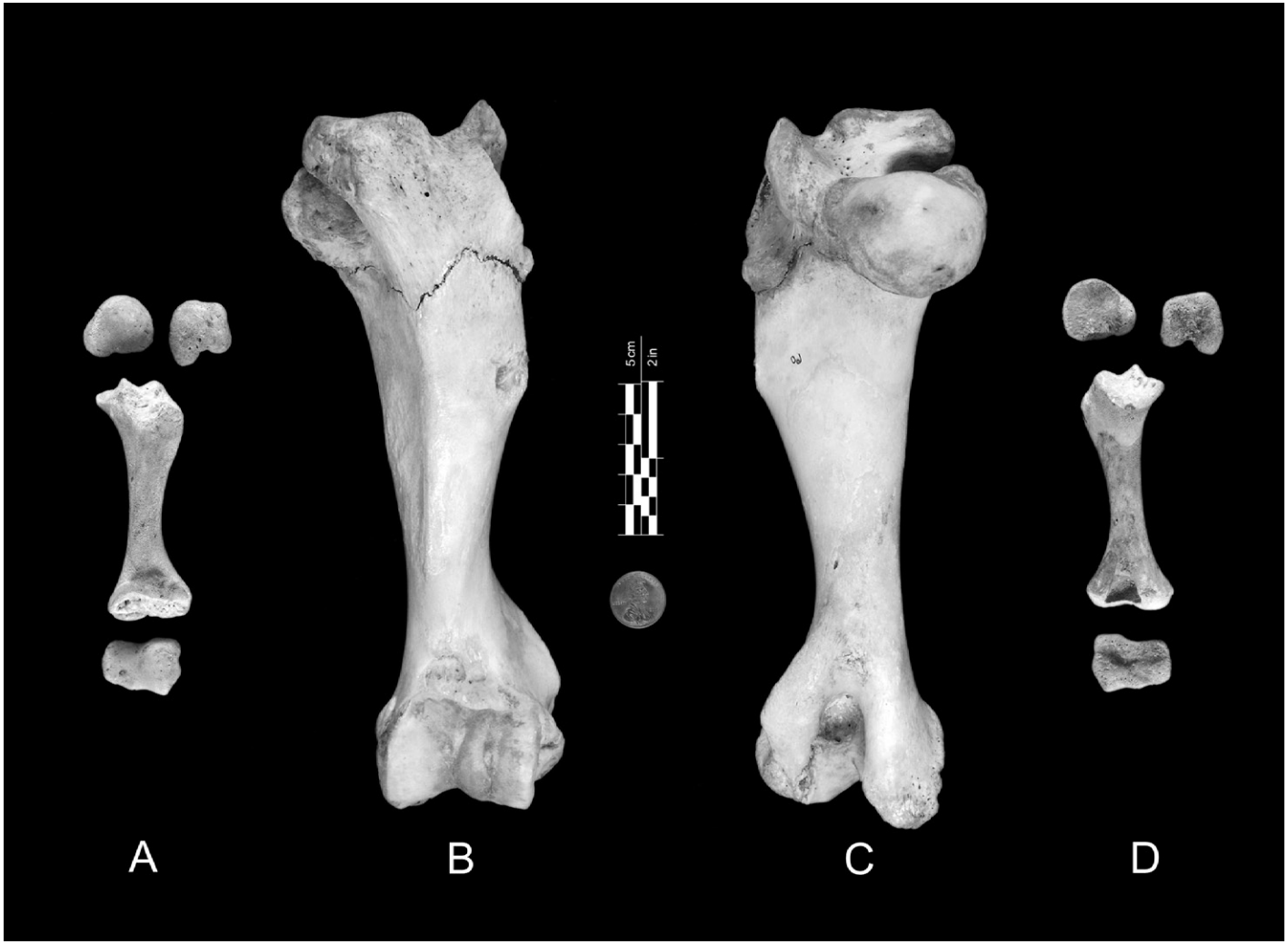

Figure 3-06: Juvenile pig (A and D) and adult pig (B and C) left humeri: cranial and caudal views. The separate epiphyses are pictured with the juvenile pig. The fusion line is still visible at the proximal epiphysis of the adult pig.

Figure 3-07: Dog left humerus: cranial and caudal views.

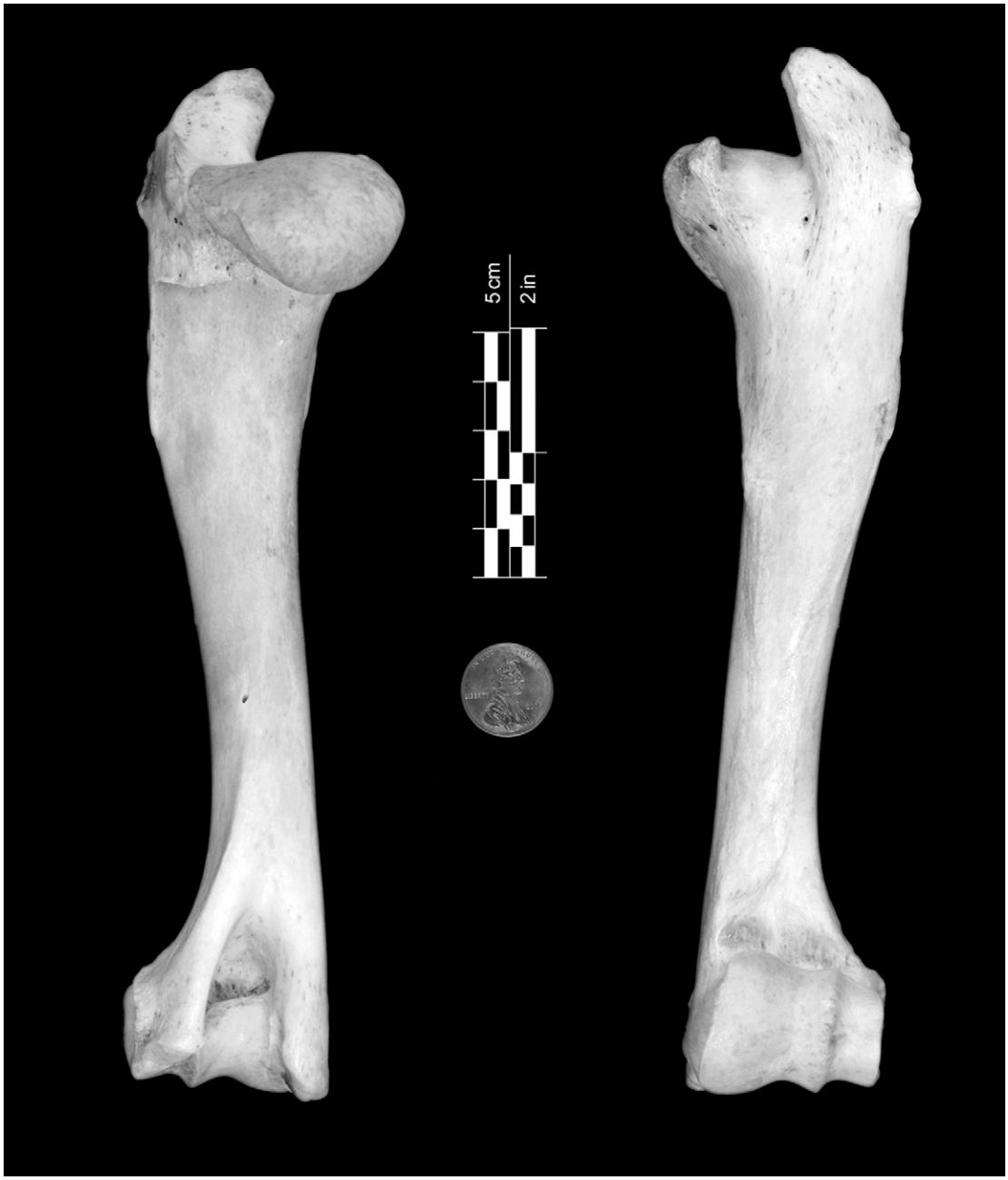

Figure 3-08: White-tailed deer left humerus: cranial and caudal views.

Figure 3-09: Sheep left humerus: cranial and caudal views. Degenerative changes associated with "penning elbow" are present on the distal end.

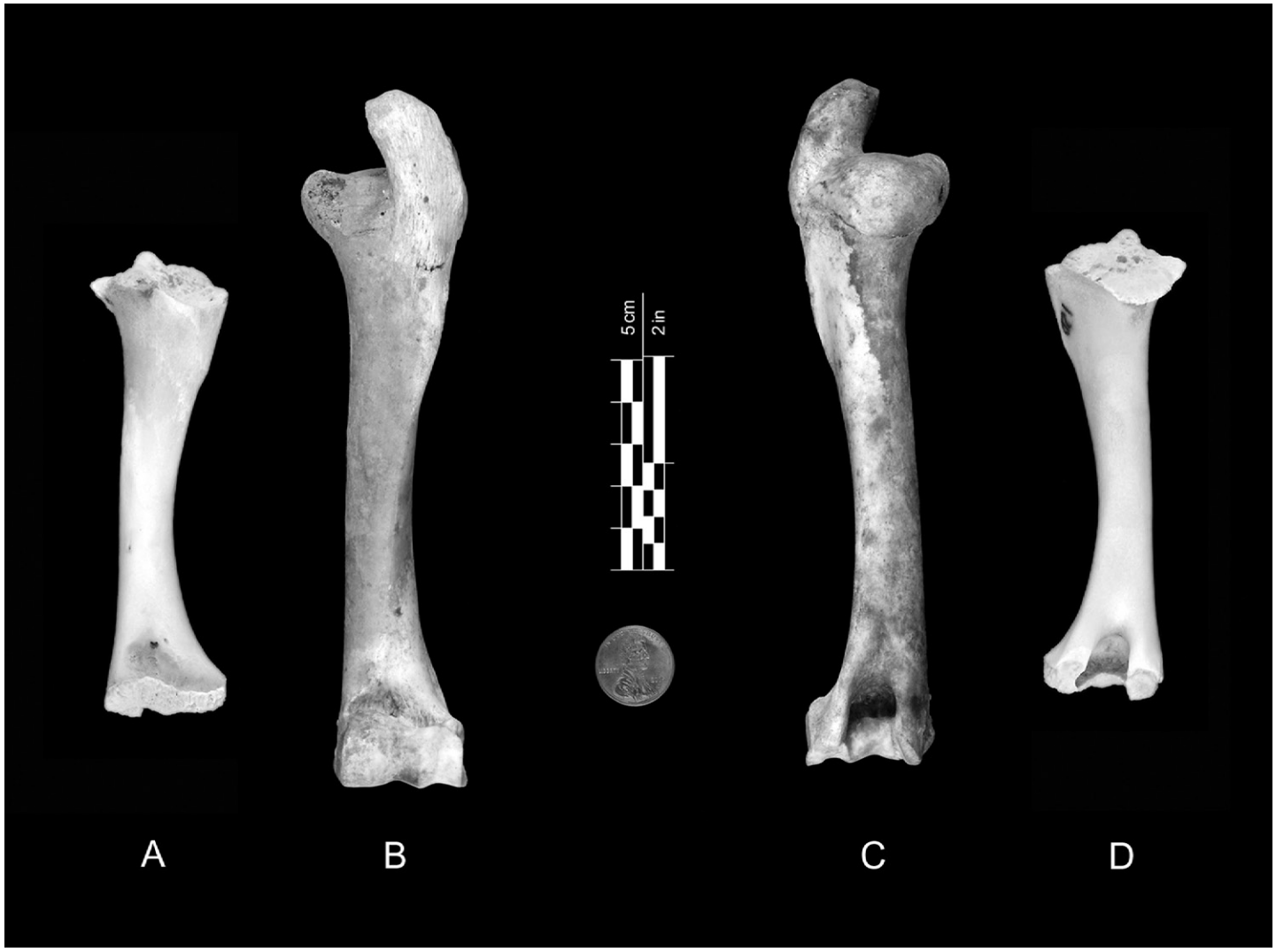

Figure 3-10: Juvenile (without epiphyses) goat (A and D) and adult goat (B and C) left humeri: cranial and caudal views.

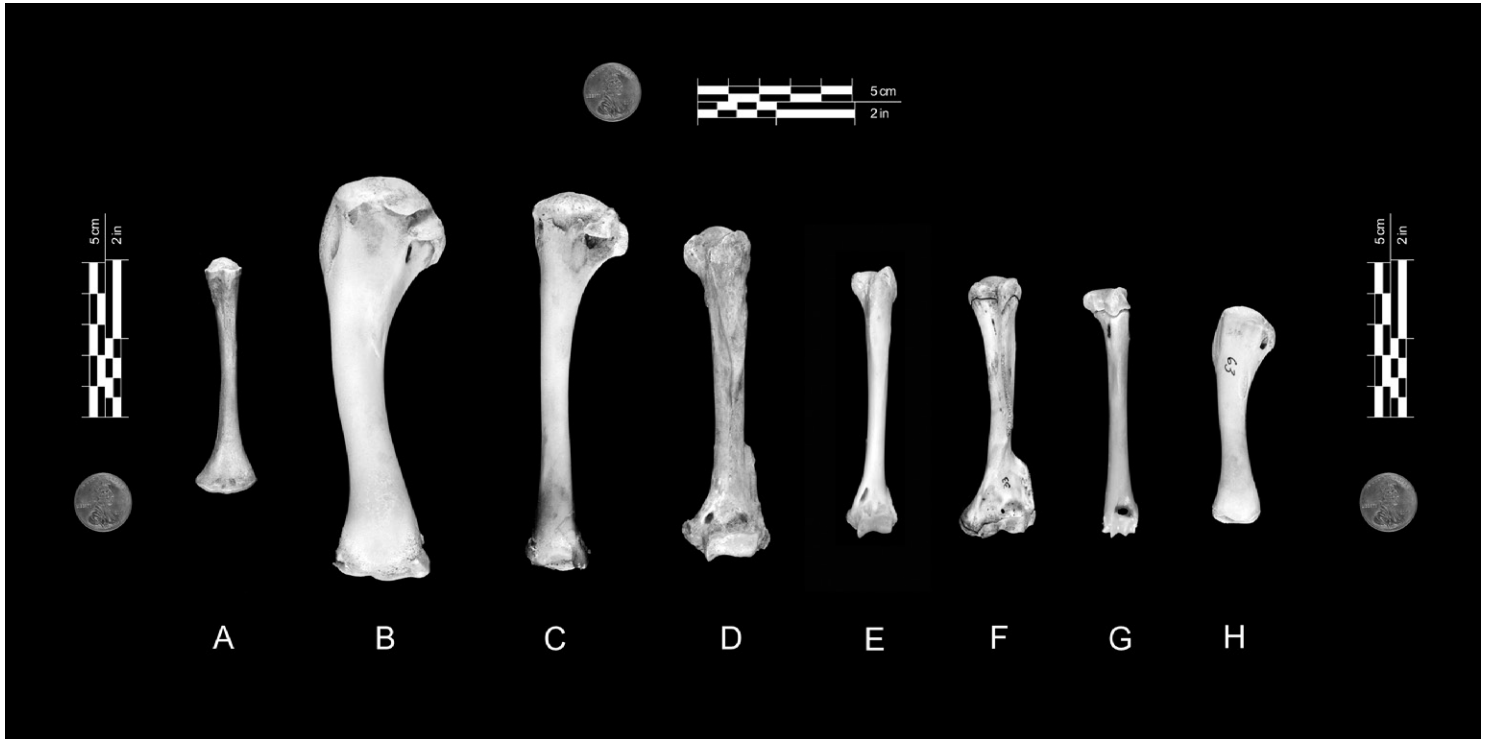

Figure 3-11: Left humeri showing the differences in scale between some of the smaller animals. Pictured are the anterior view of a newborn human (A) and cranial views of a turkey (B), duck (C), raccoon (D), cat (E), opossum (F), rabbit (G), and chicken (H).

Figure 3-12: Newborn human left humerus: anterior and posterior views.

Figure 3-13: Turkey left humerus: cranial and caudal views.

Figure 3-14: Duck left humerus: cranial and caudal views.

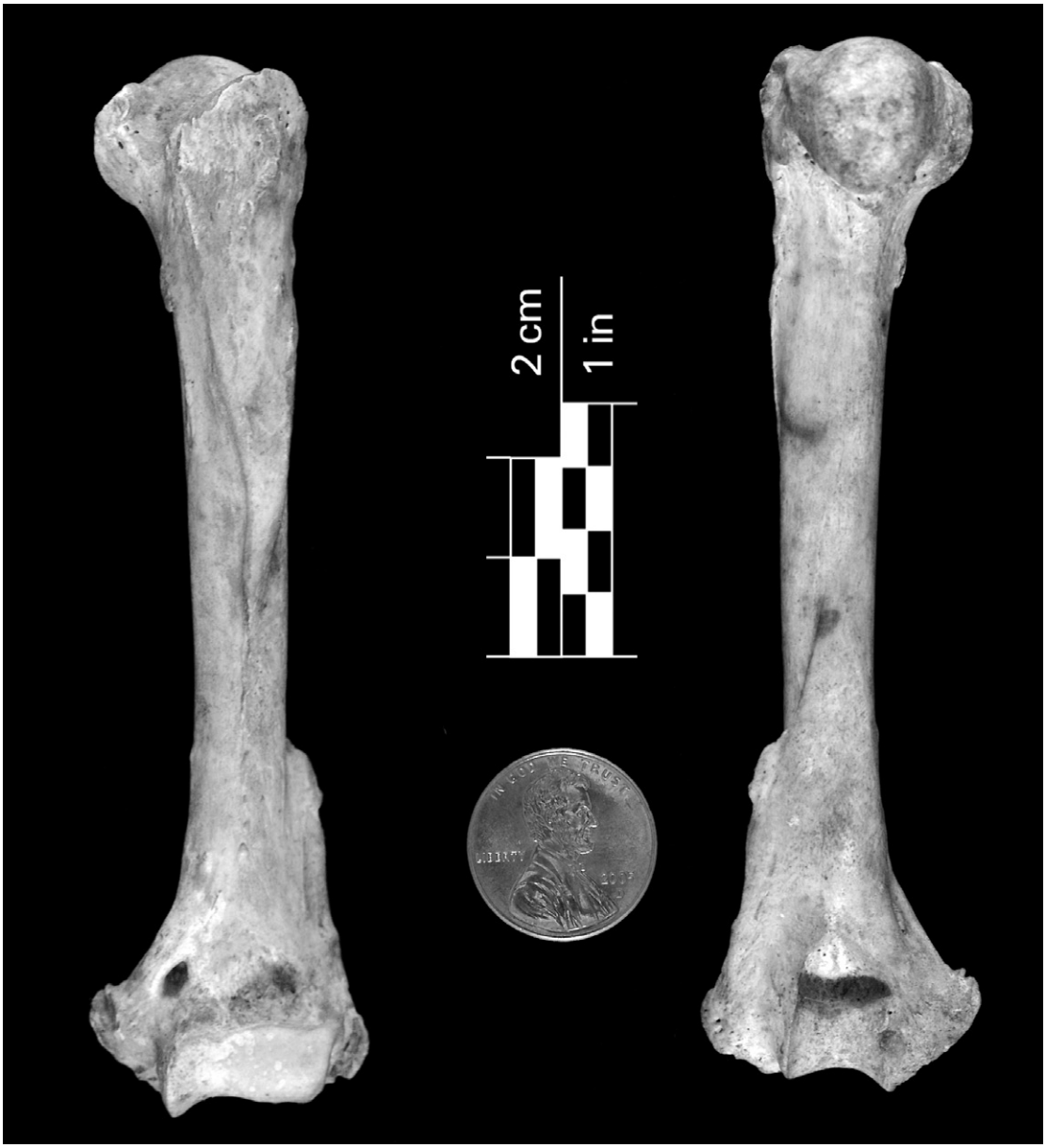

Figure 3-15: Raccoon left humerus: cranial and caudal views.

Figure 3-16: Cat left humerus: cranial and caudal views.

Figure 3-17: Opossum left humerus: cranial and caudal views. Note how the fusion line is still visible at the proximal and distal epiphyses.

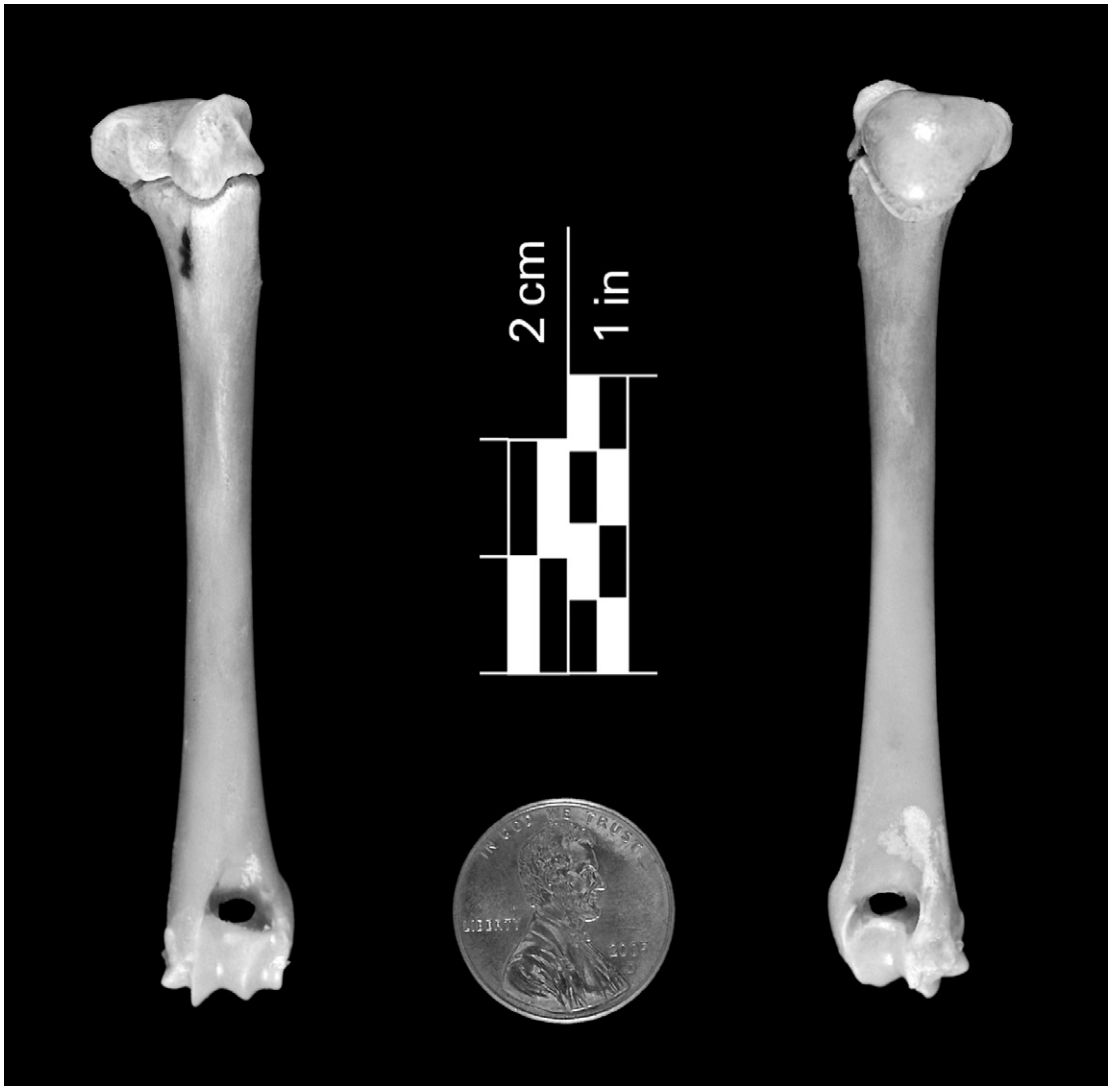

Figure 3-18: Rabbit left humerus: cranial and caudal views. Note how the fusion line is still visible at the proximal epiphysis.

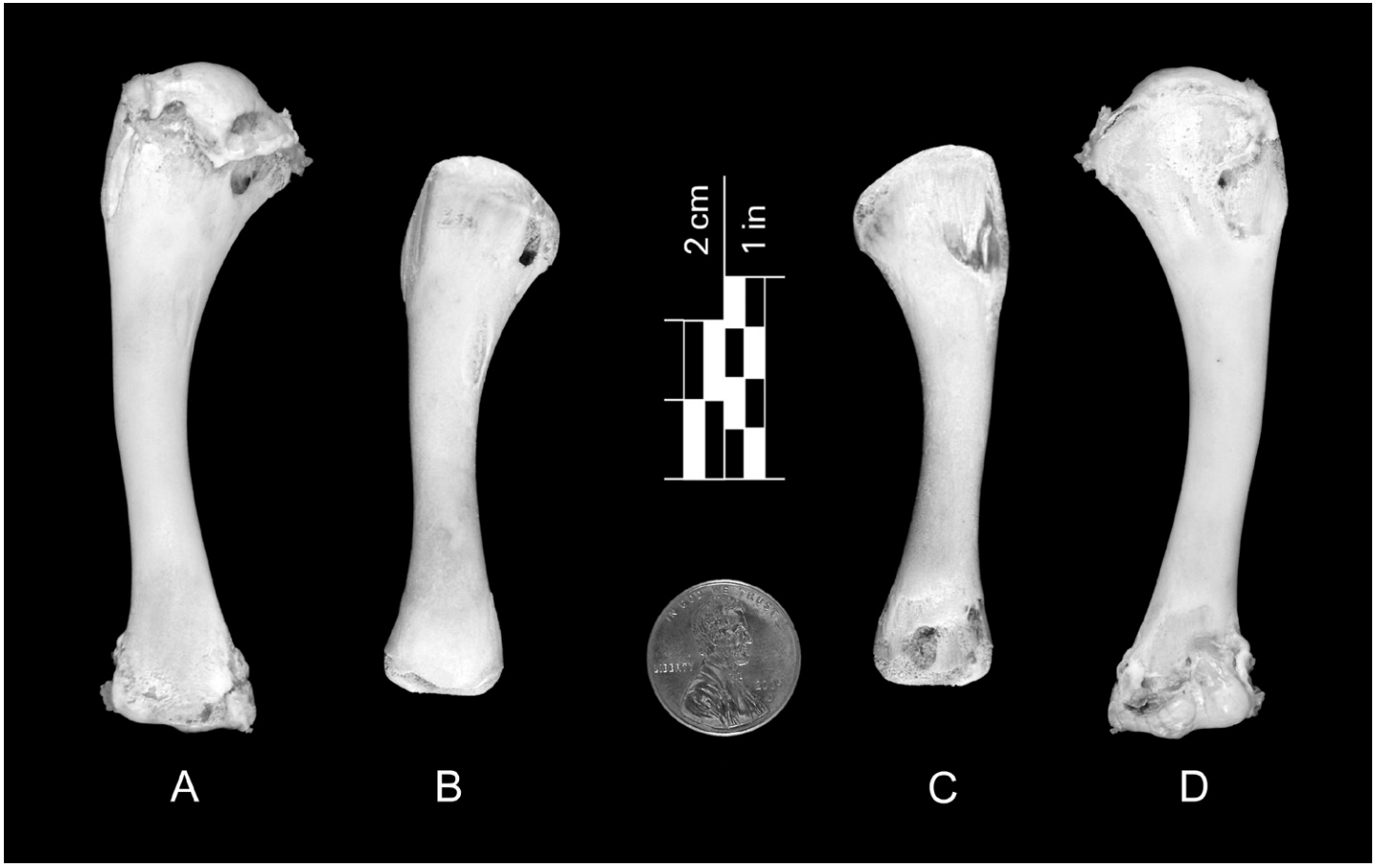

Figure 3-19: Chicken left humerus: cranial (A and B) and caudal (C and D) views. The smaller bone represents a younger chicken.

CHAPTER 4

Radii and Ulnae

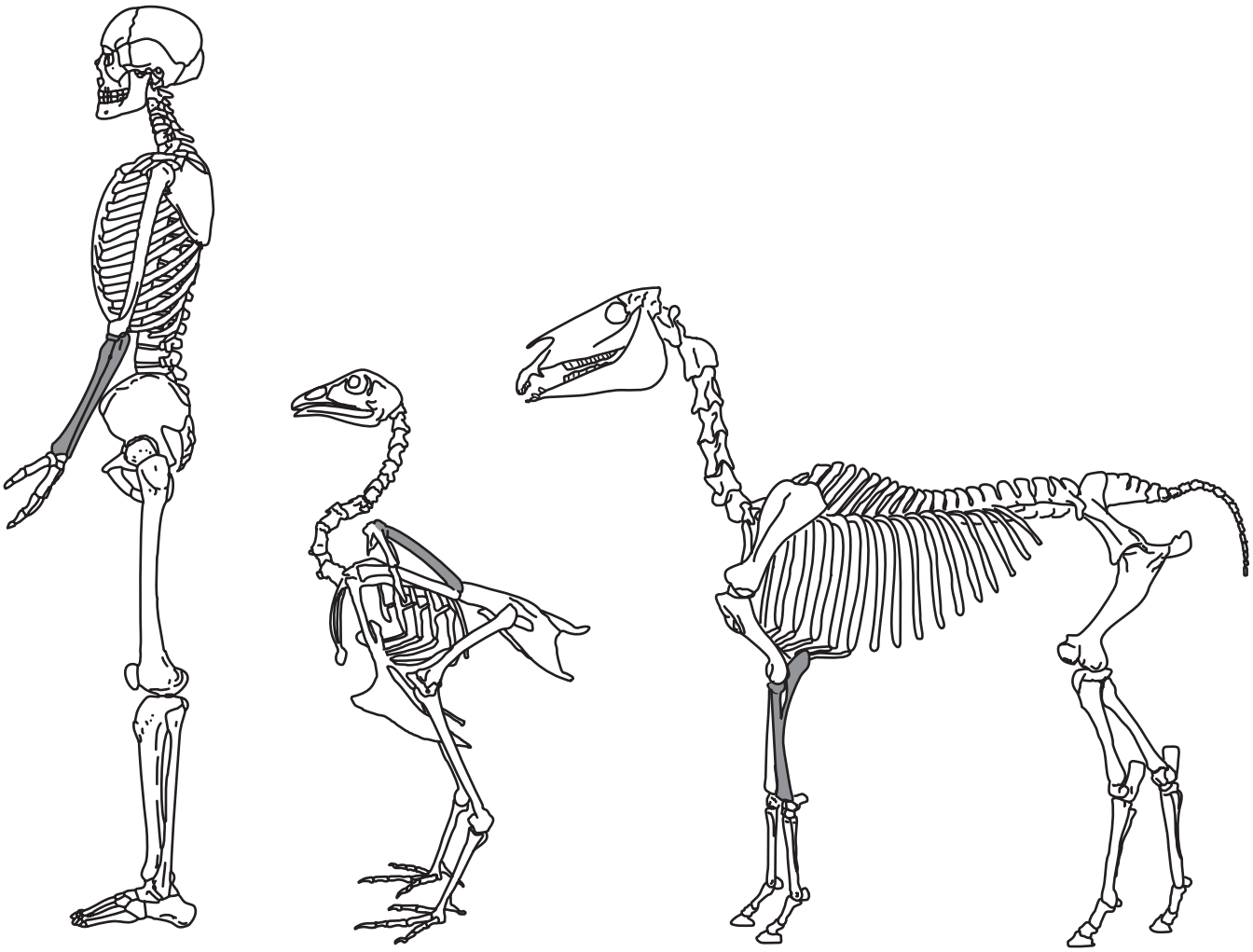

Comparative Osteology. DOI: 10.1016/B978-0-12-388437-4.00004-1

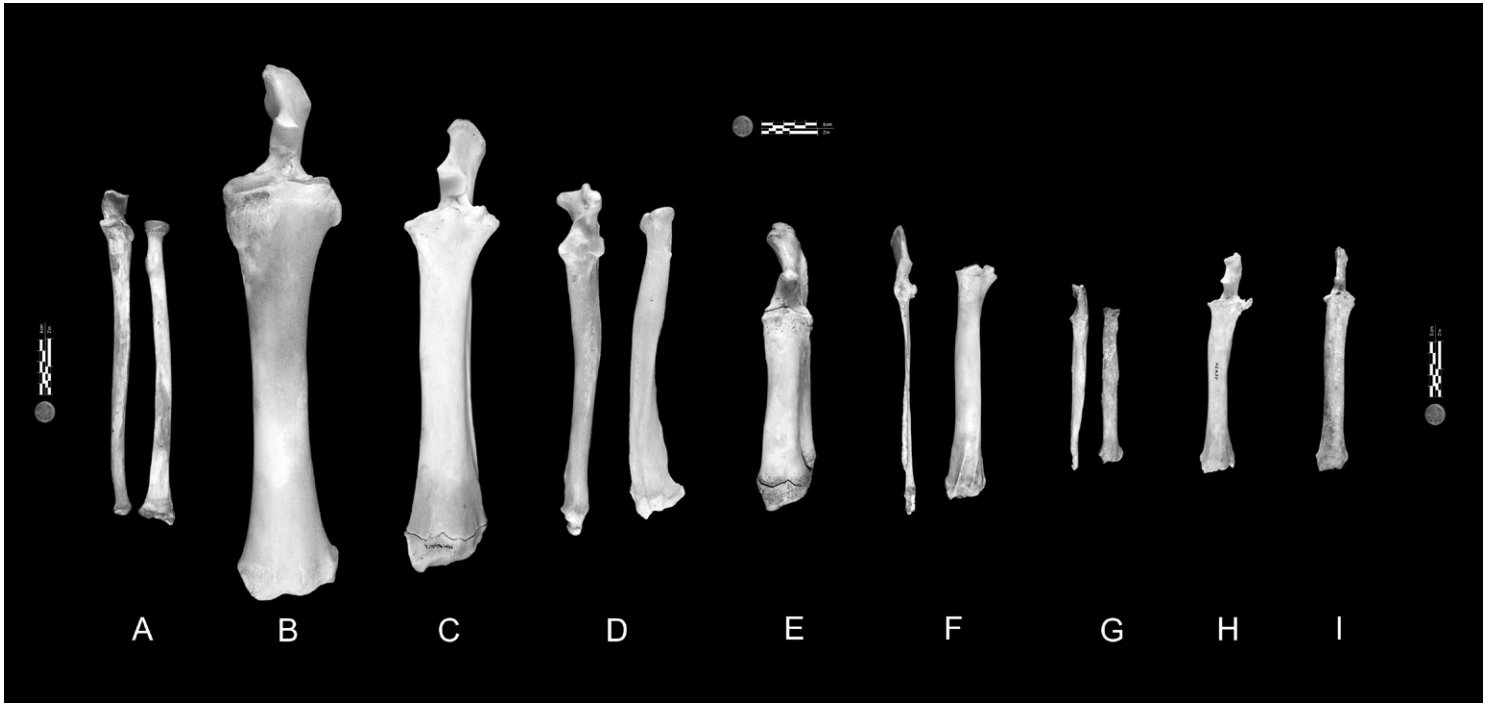

Figure 4-01: Left ulnae and radii showing the differences in scale between some of the larger animals. Pictured are the anterior view of an adult human (A) and the cranial views of a horse (B), cow (C), bear (D), pig (E), white-tailed deer (F), dog (G), adult sheep (H), and goat (I). Note that the human radius is oriented somewhat differently from the non-human radii. The human skeleton is oriented with the palms facing forward so that the radius and ulna do not cross. Quadrupedal mammals are oriented with the paws facing downward.

Figure 4-02: Adult human left ulna and radius: anterior and posterior views

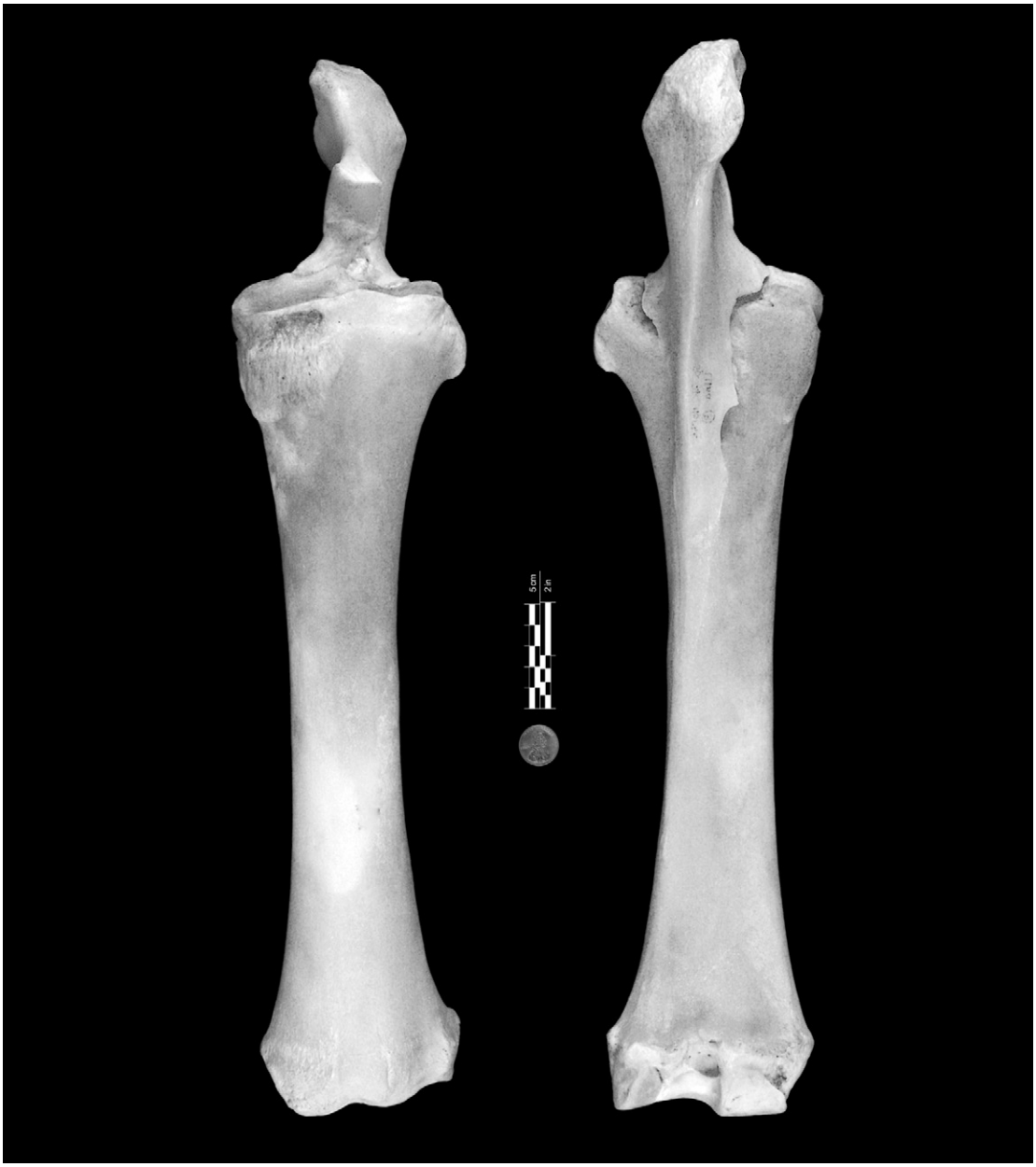

Figure 4-03: Horse left ulna and radius: cranial and caudal views.

Figure 4-04: Cow left ulna and radius: cranial and caudal views. The proximal epiphysis of the ulna is unfused. The fusion line is also still visible at the distal epiphysis.

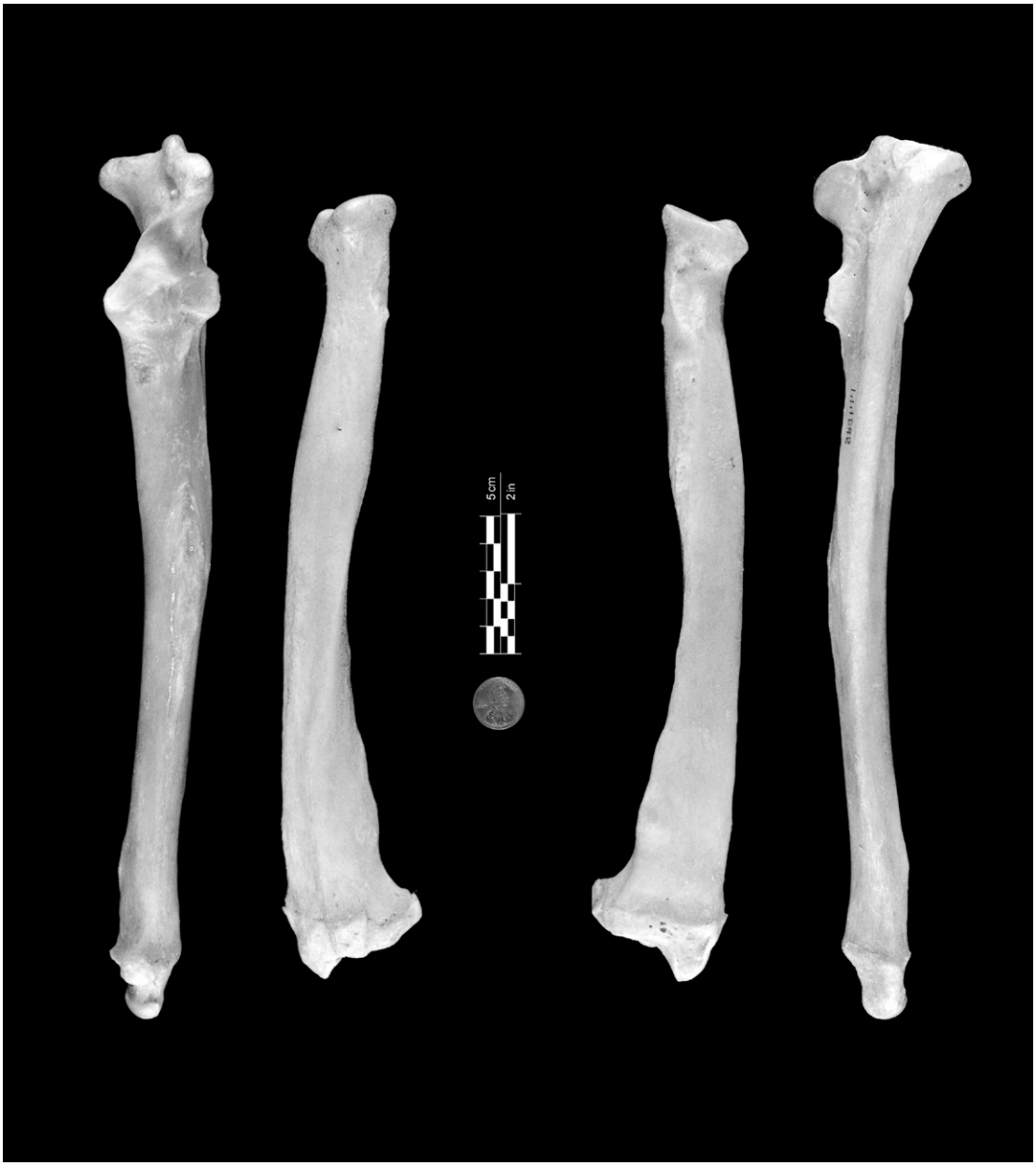

Figure 4-05: Bear left ulna and radius: cranial and caudal views.

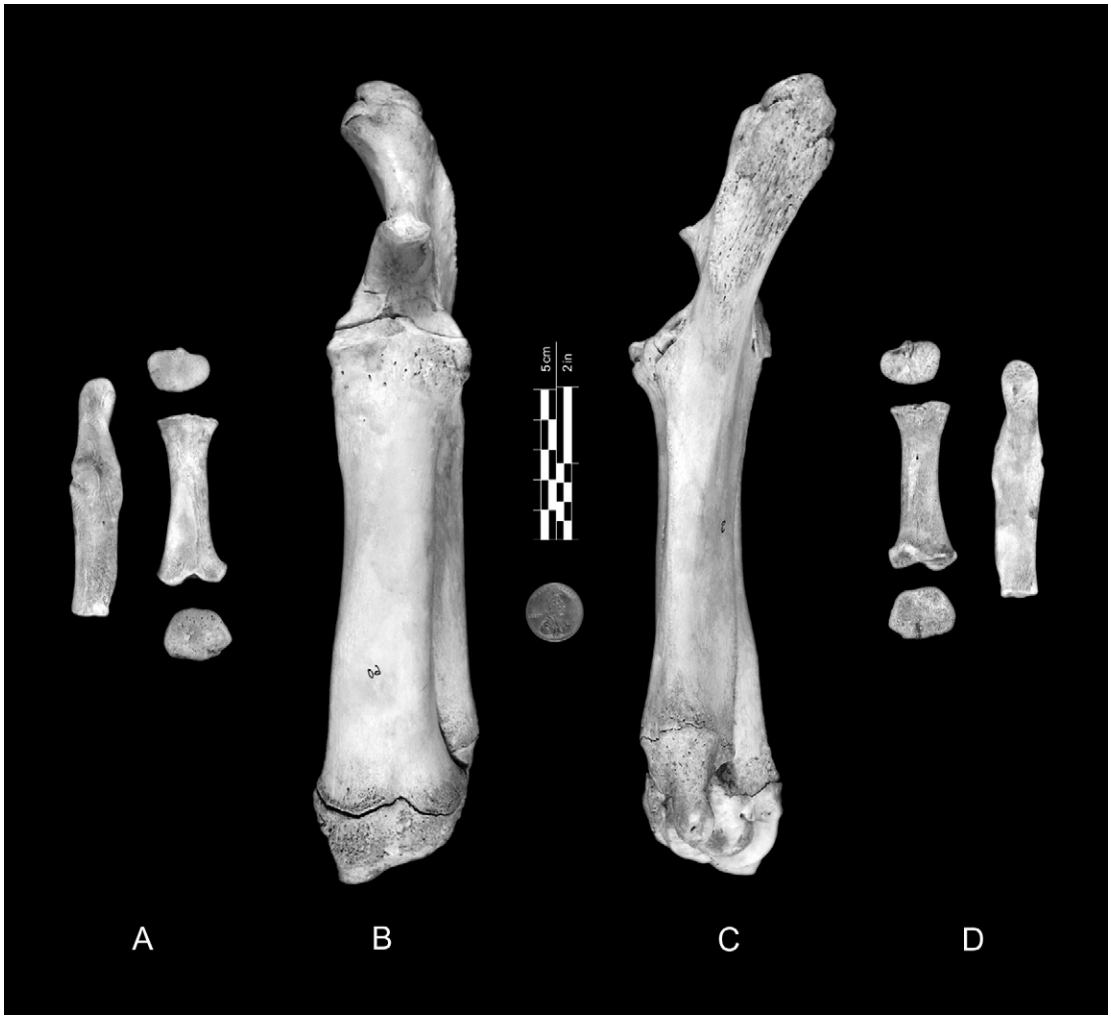

Figure 4-06: Juvenile pig (A and D) and adult pig (B and C) left ulnae and radii: cranial and caudal views. Note how the ulna and radius are separate elements in the juvenile, whereas they are often fused together in the adult. The separate epiphyses of the juvenile pig are pictured. Also, the fusion line is still visible at the distal end of the adult pig.

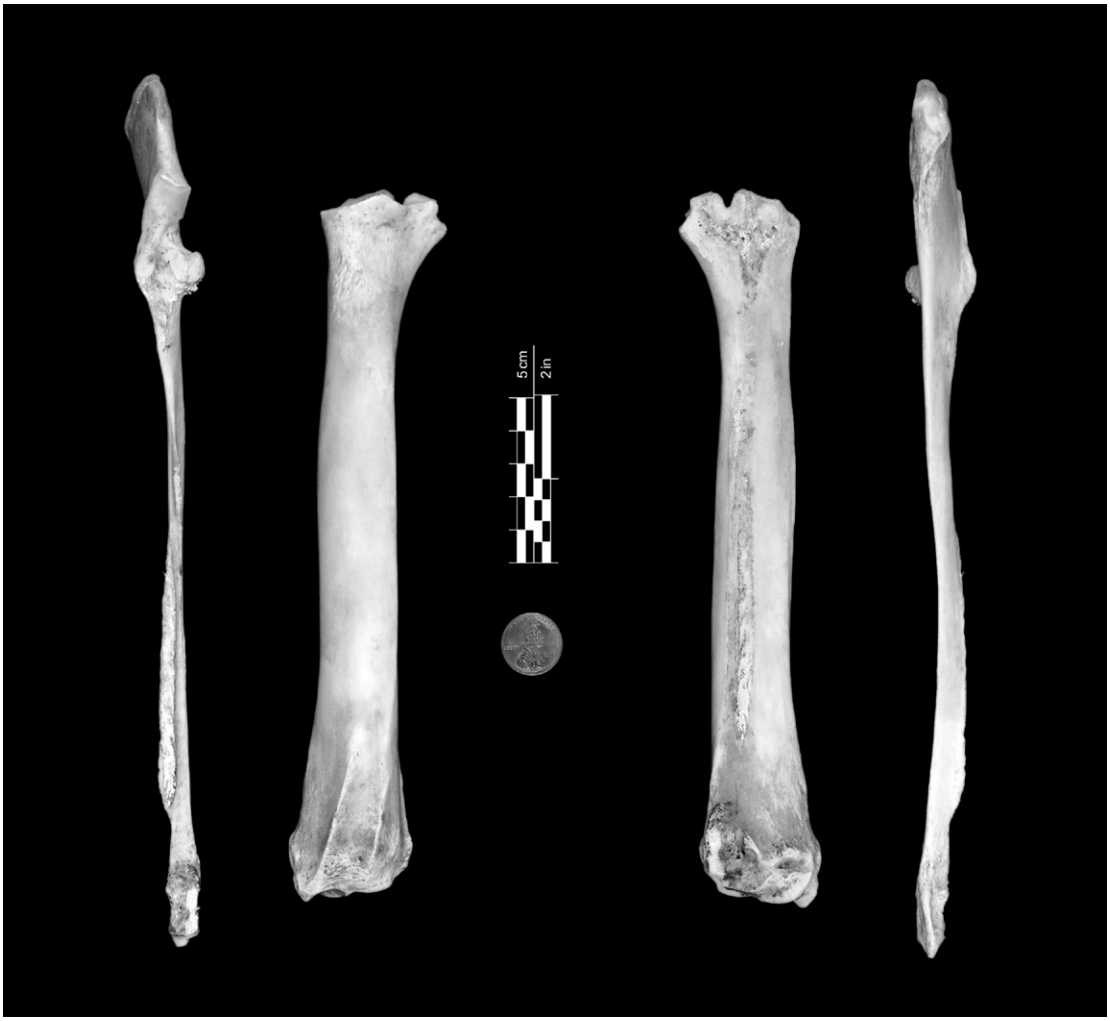

Figure 4-07: White-tailed deer left ulna and radius: cranial and caudal views.

Figure 4-08: Dog left ulna and radius: cranial and caudal views.

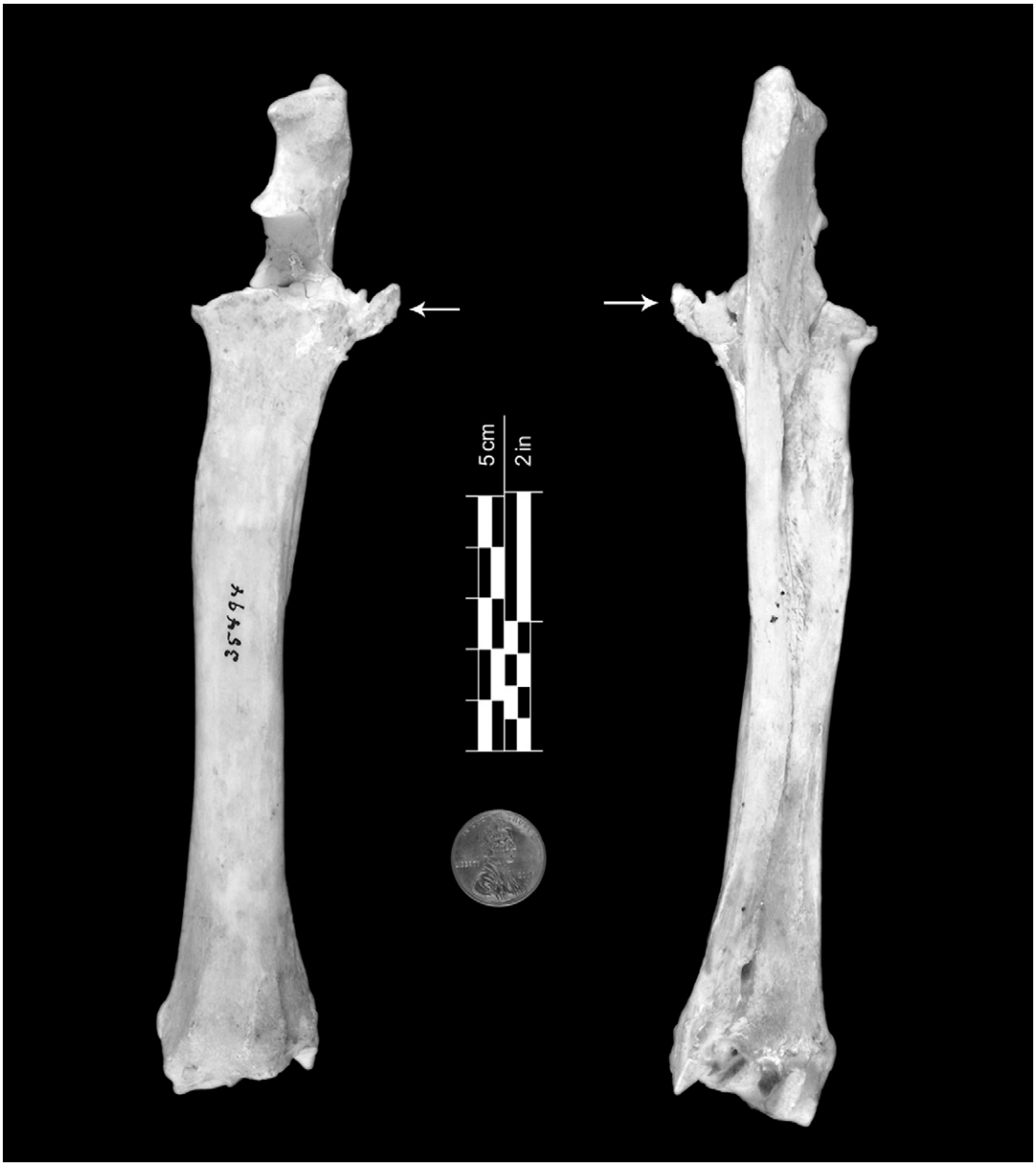

Figure 4-09: Sheep left ulna and radius: cranial and caudal views. Note the pathology, sometimes termed "penning elbow," that is visible on the lateral portion of the proximal radius of this elderly sheep (arrows).

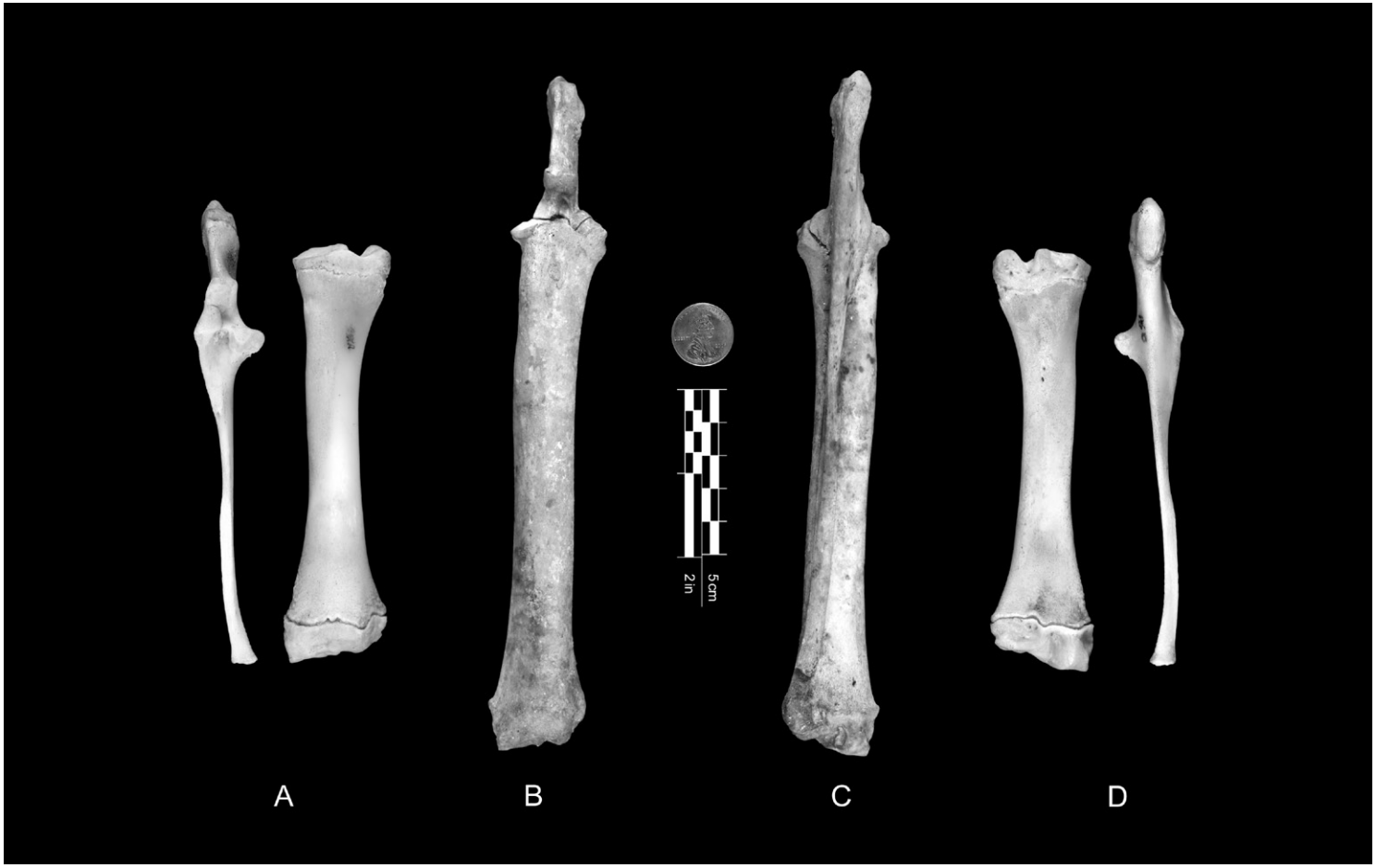

Figure 4-10: Juvenile goat (A and D) and adult goat (B and C) left ulnae and radii: cranial and caudal views. Note how the ulna and radius are separate elements in the juvenile, whereas they are fused together in the adult.

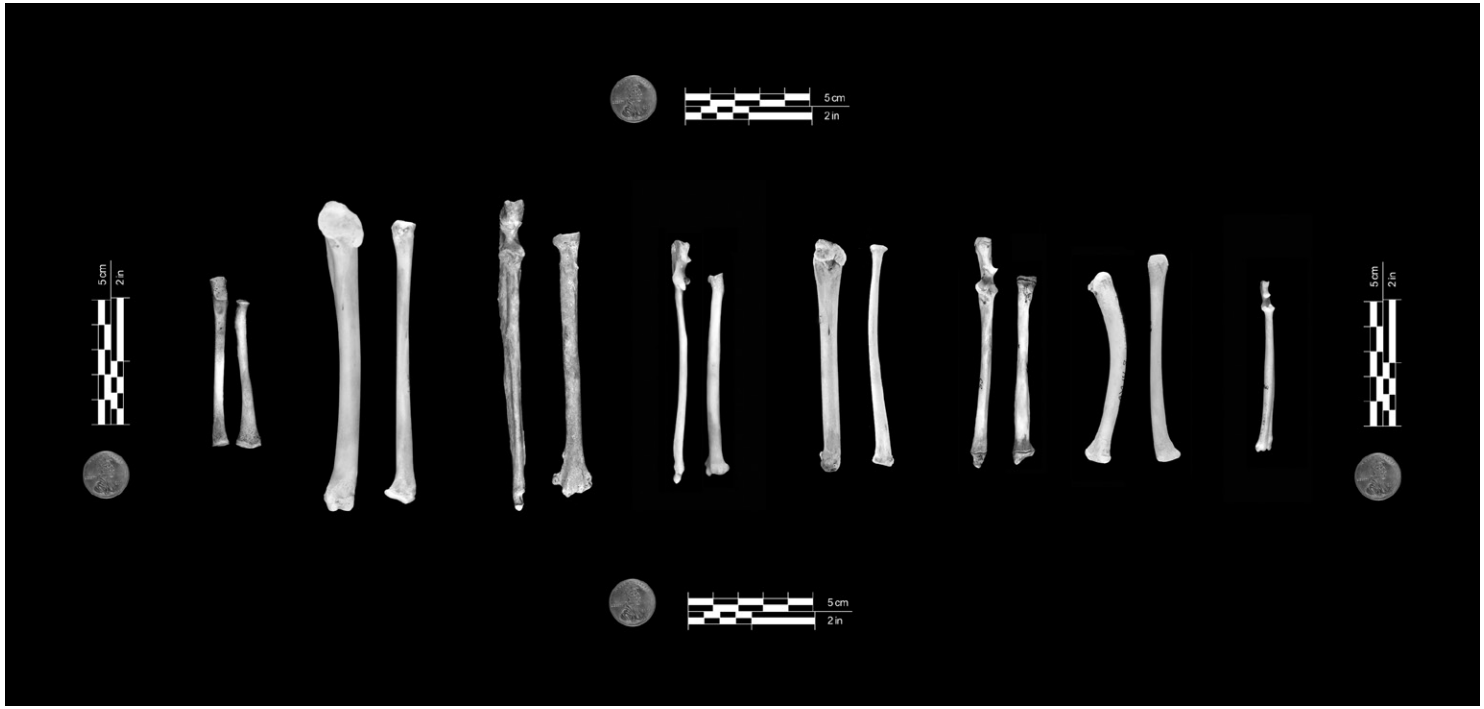

Figure 4-11: Left ulnae and radii showing the differences in scale between some of the smaller animals. Pictured are the anterior view of a newborn human (A) and cranial views of a turkey (B), raccoon (C), cat (D), duck (E), opossum (F), chicken (G, the ulna is in lateral view), and rabbit (H).

Figure 4-12: Newborn human ulna and radius: anterior and posterior views.

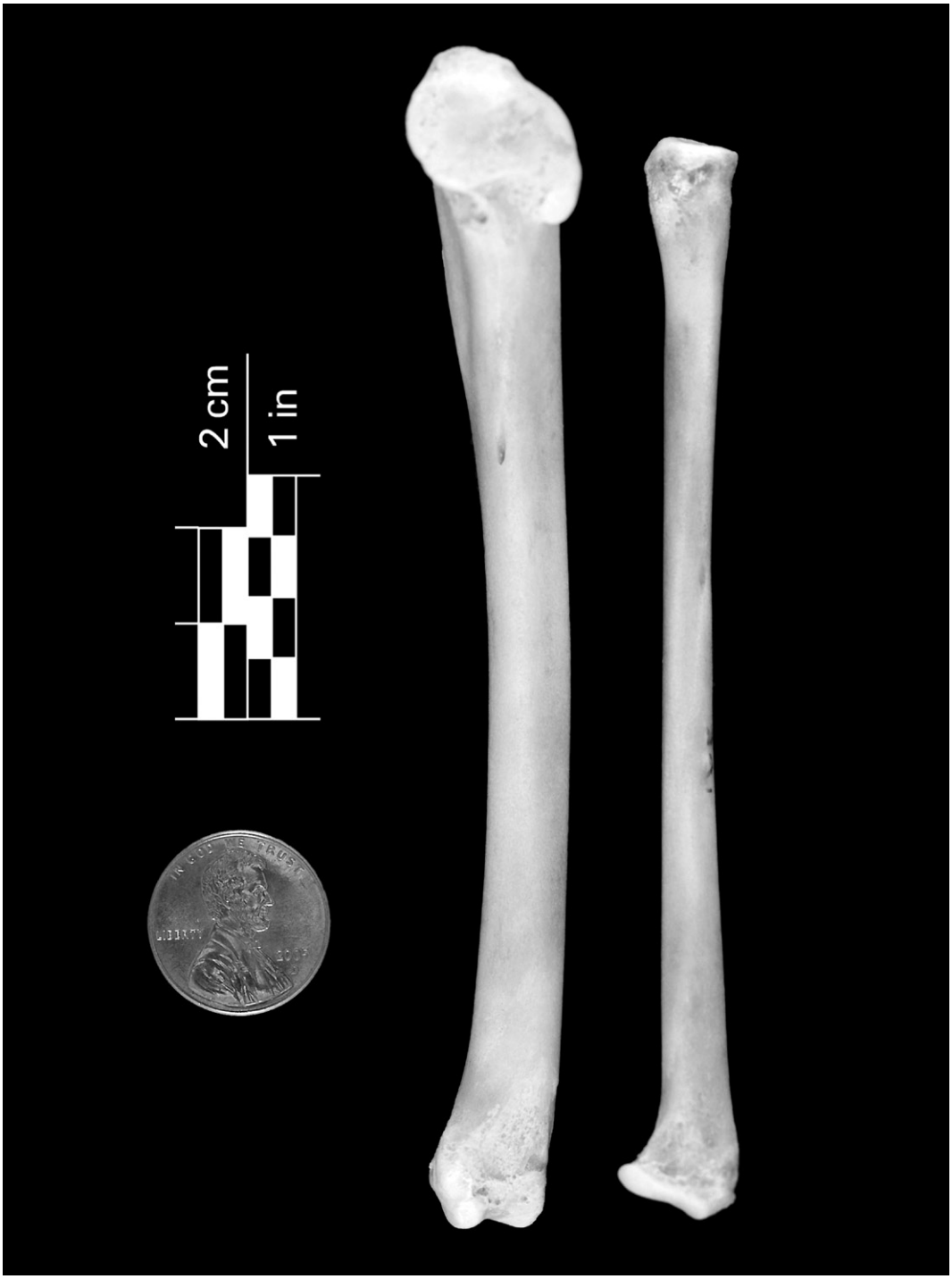

Figure 4-13: Turkey left ulna and radius: cranial view.

Figure 4-14: Raccoon left ulna and radius: cranial and caudal views.

Figure 4-15: Cat left ulna and radius: cranial and caudal views.

Figure 4-16: Duck left ulna and radius: cranial view.

Figure 4-17: Opossum left ulna and radius: cranial and caudal views. Note how the fusion lines are still visible at the proximal and distal epiphyses.

Figure 4-18: Chicken left ulna (lateral view) and radius (cranial view).

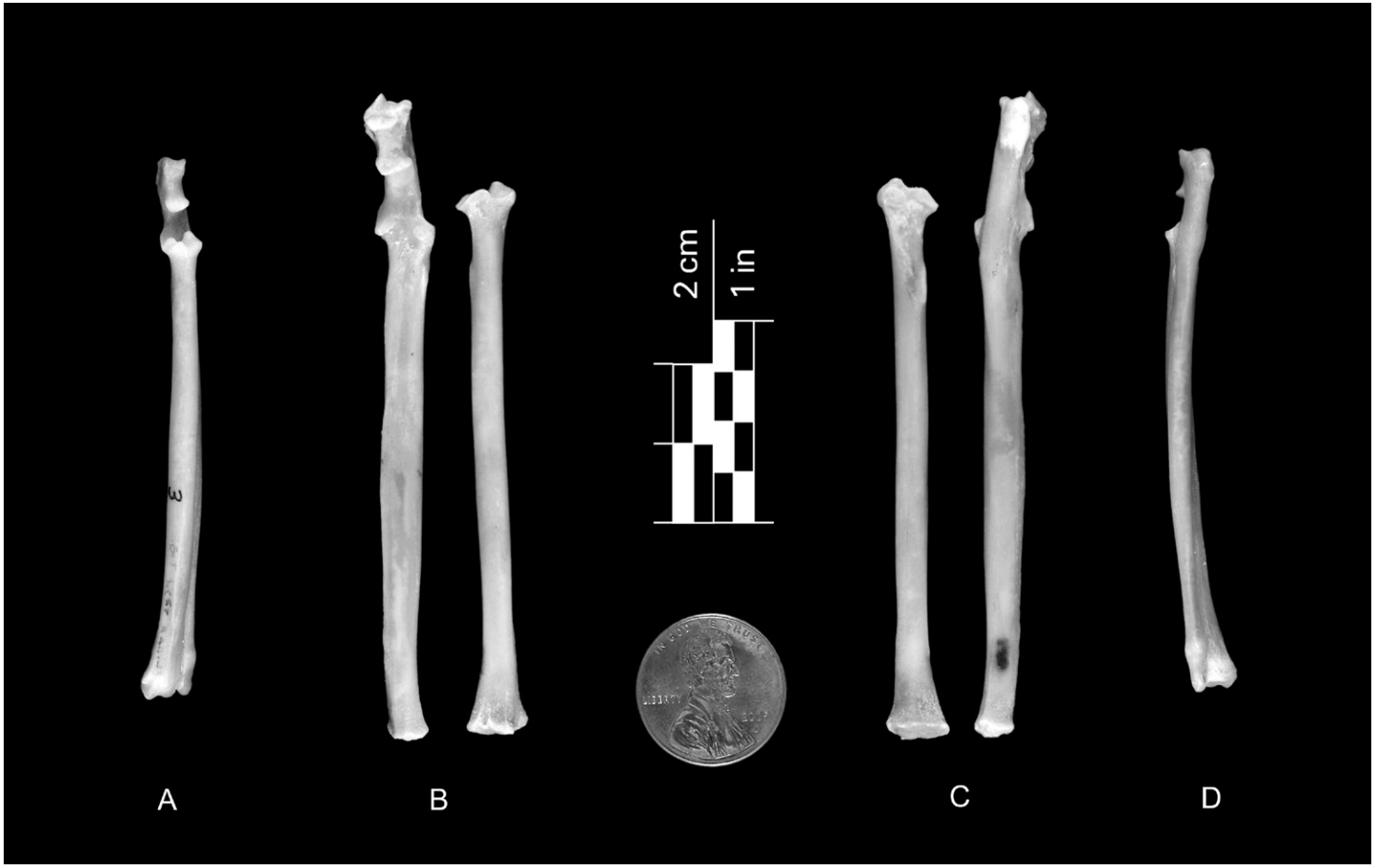

Figure 4-19: Rabbit (*Sylvilagus*) left ulna and radius (A, cranial view, fused); rabbit (*Oryctolagus*) left ulna and radius (B, cranial views, unfused); rabbit (*Oryctolagus*) left radius and ulna (C, caudal views, unfused); rabbit (*Sylvilagus*) left radius and ulna (D, caudal view, fused).

CHAPTER 5

Femora

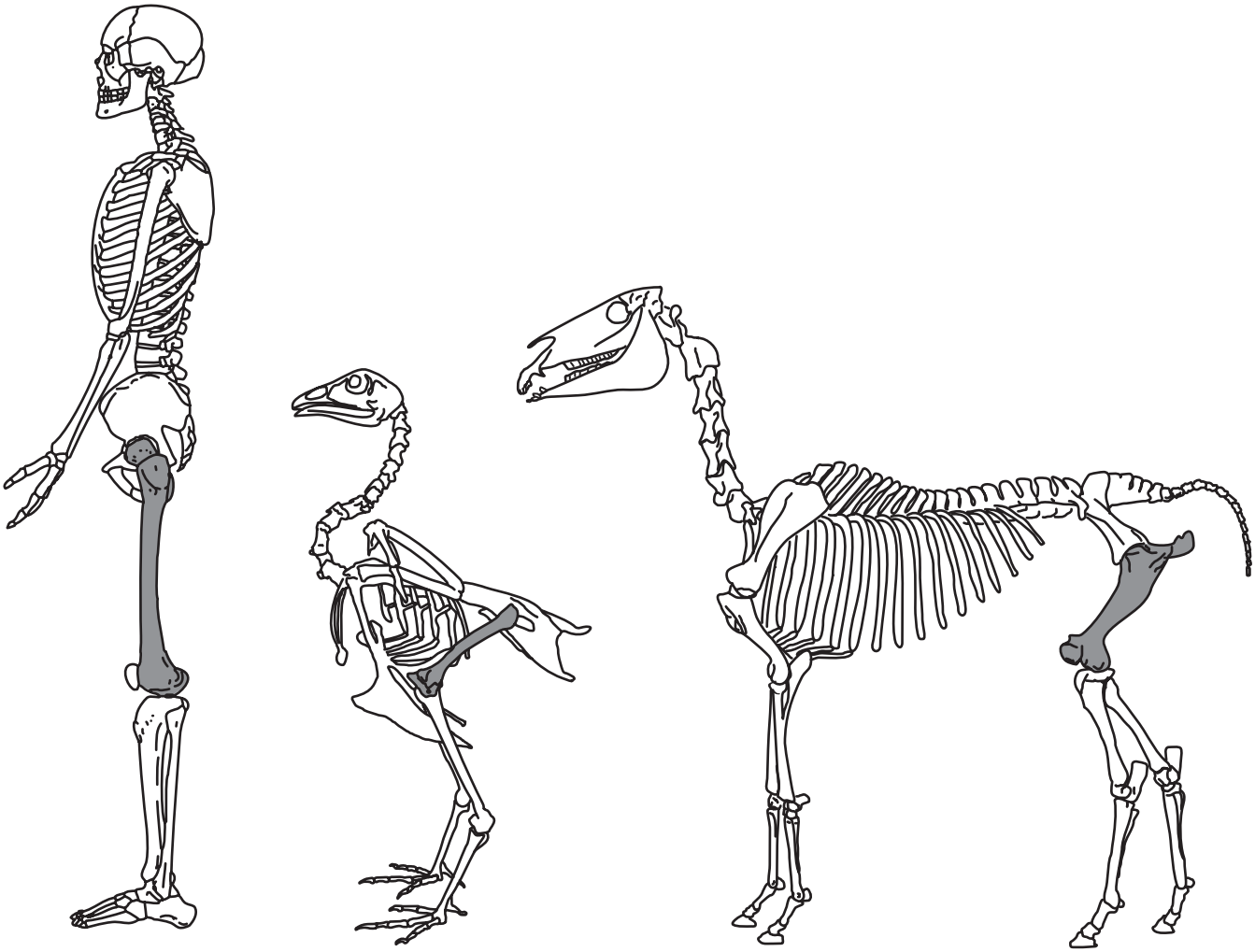

Comparative Osteology. DOI: 10.1016/B978-0-12-388437-4.00005-3

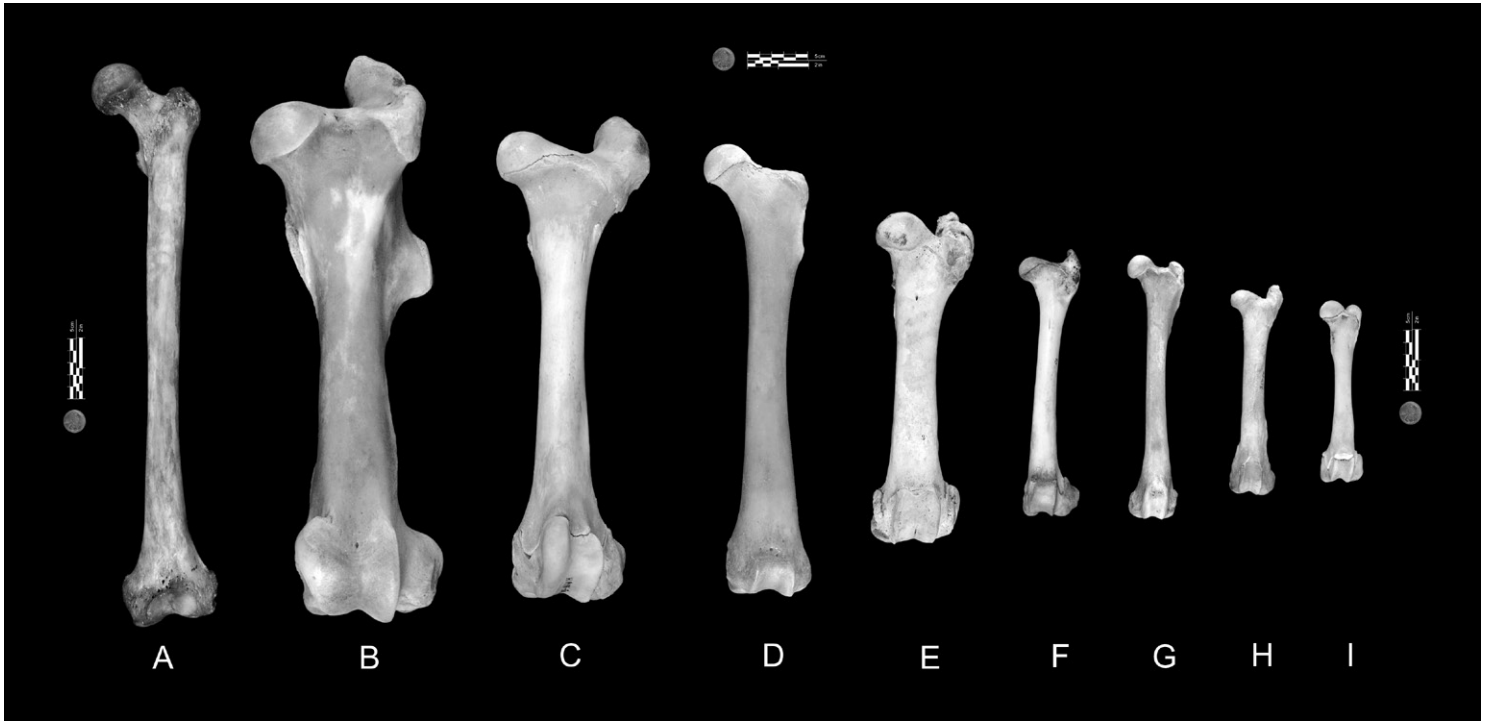

Figure 5-01: Left femora showing the differences in scale between some of the larger animals. Pictured are the anterior view of an adult human (A) and the cranial views of a horse (B), cow (C), bear (D), pig (E), white-tailed deer (F), dog (G), sheep (H), and juvenile goat (I).

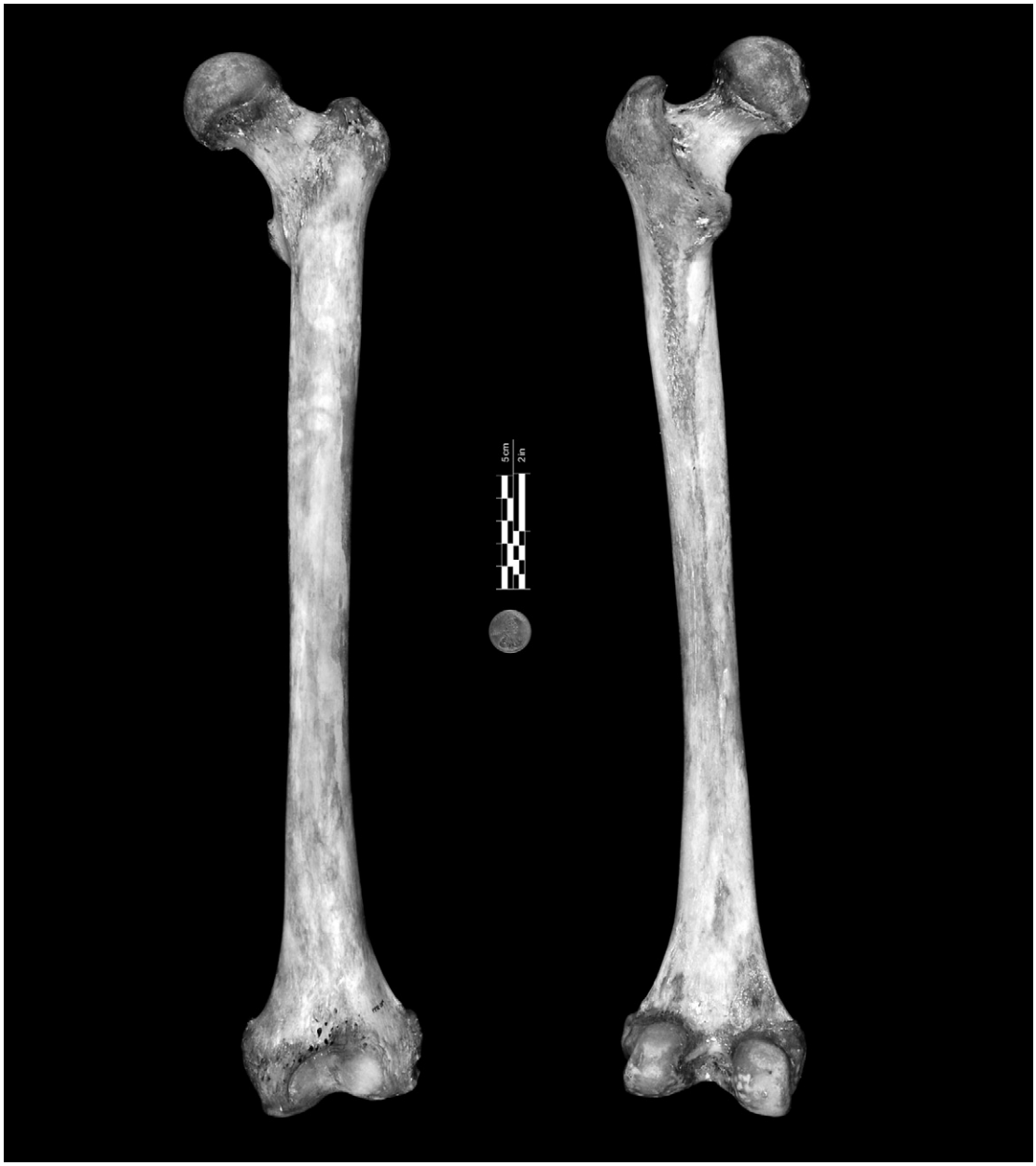

Figure 5-02: Adult human left femur: anterior and posterior views.

Figure 5-03: Horse left femur: cranial and caudal views.

Figure 5-04: Cow left femur: cranial and caudal views. Note how the fusion lines are still visible at the proximal and distal epiphyses.

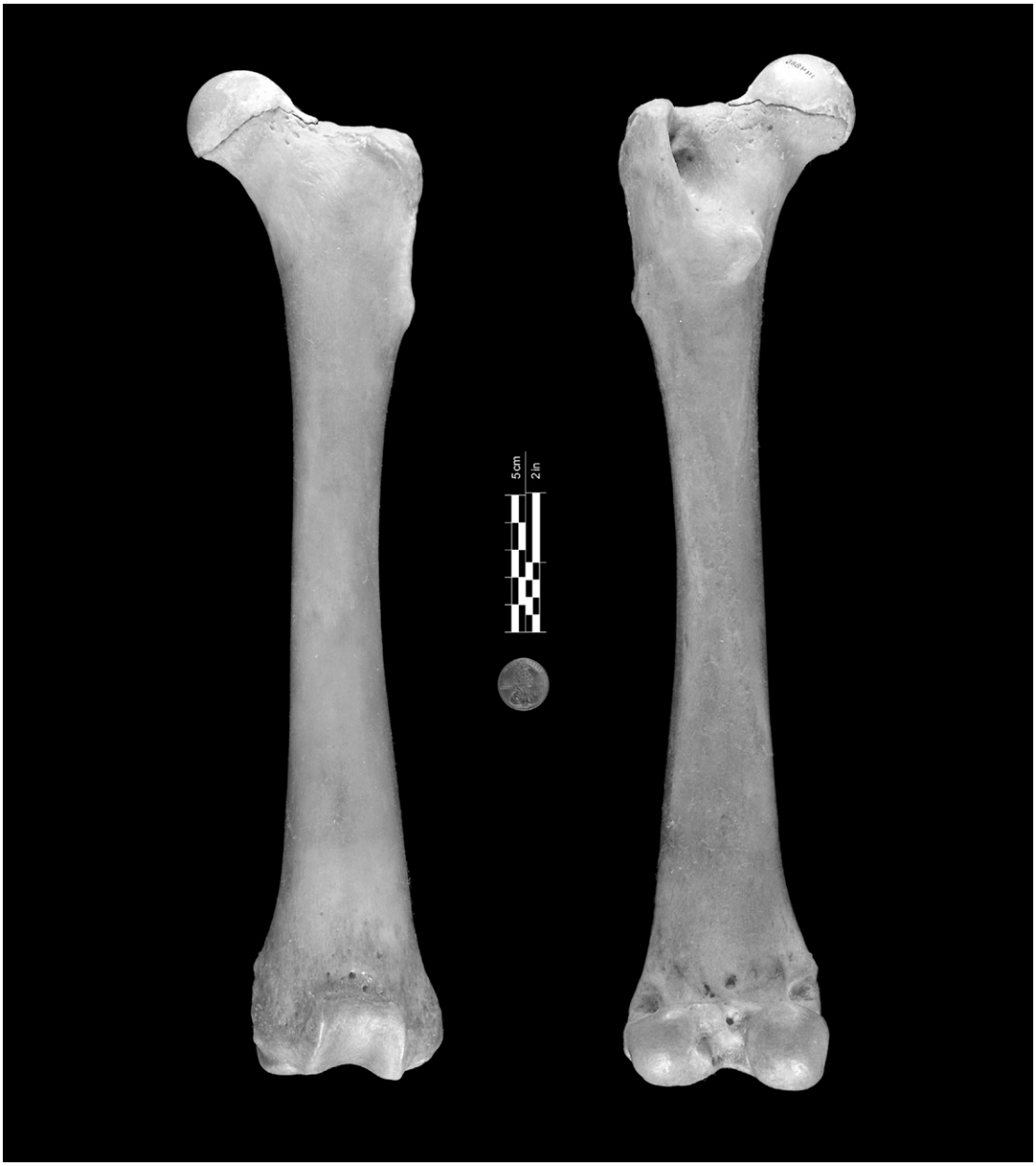

Figure 5-05: Bear left femur: cranial and caudal views. Note how the fusion line is still visible at the proximal epiphysis.

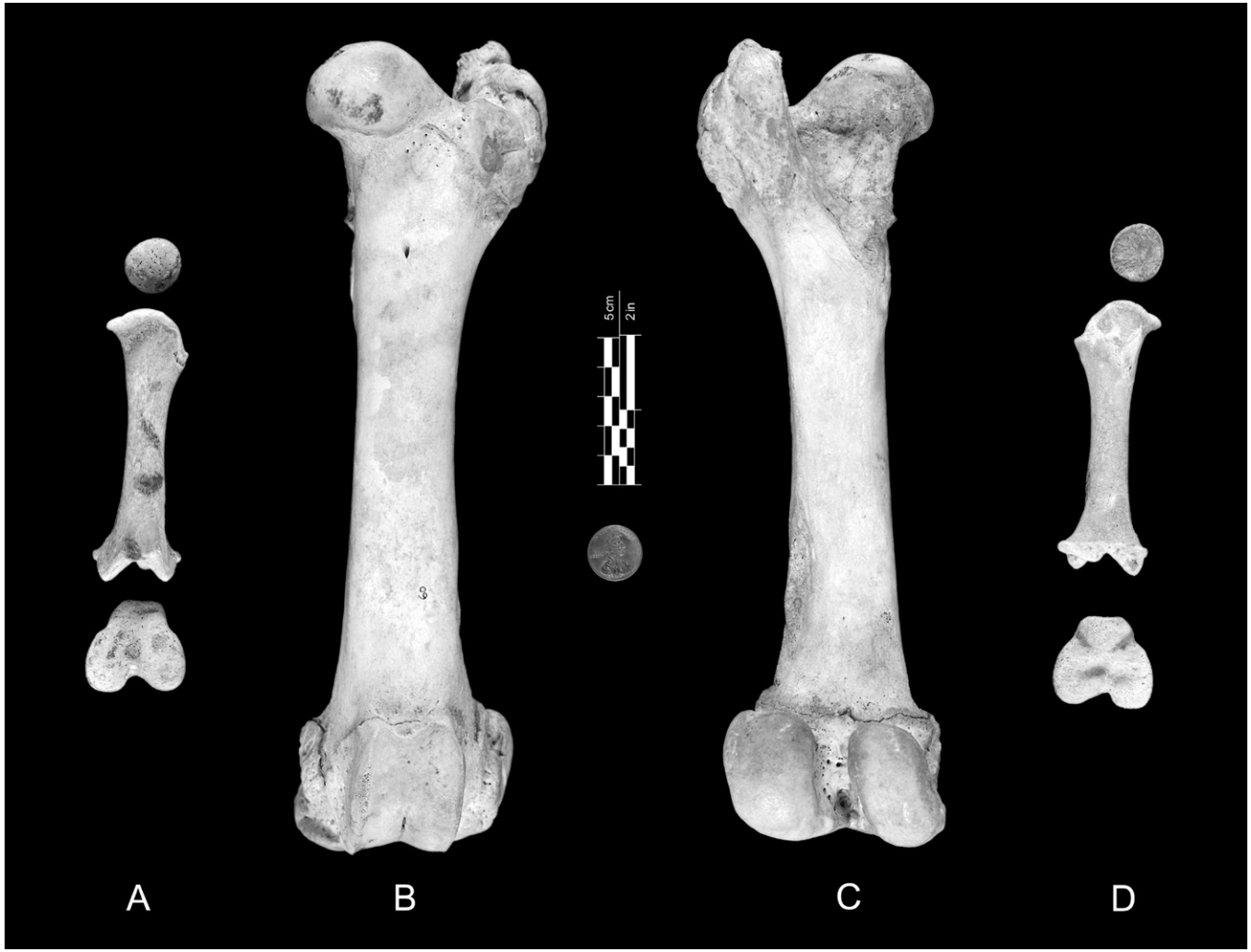

Figure 5-06: Juvenile pig (A and D) and adult pig (B and C) left femora: cranial and caudal views. The separate epiphyses are pictured with the juvenile pig.

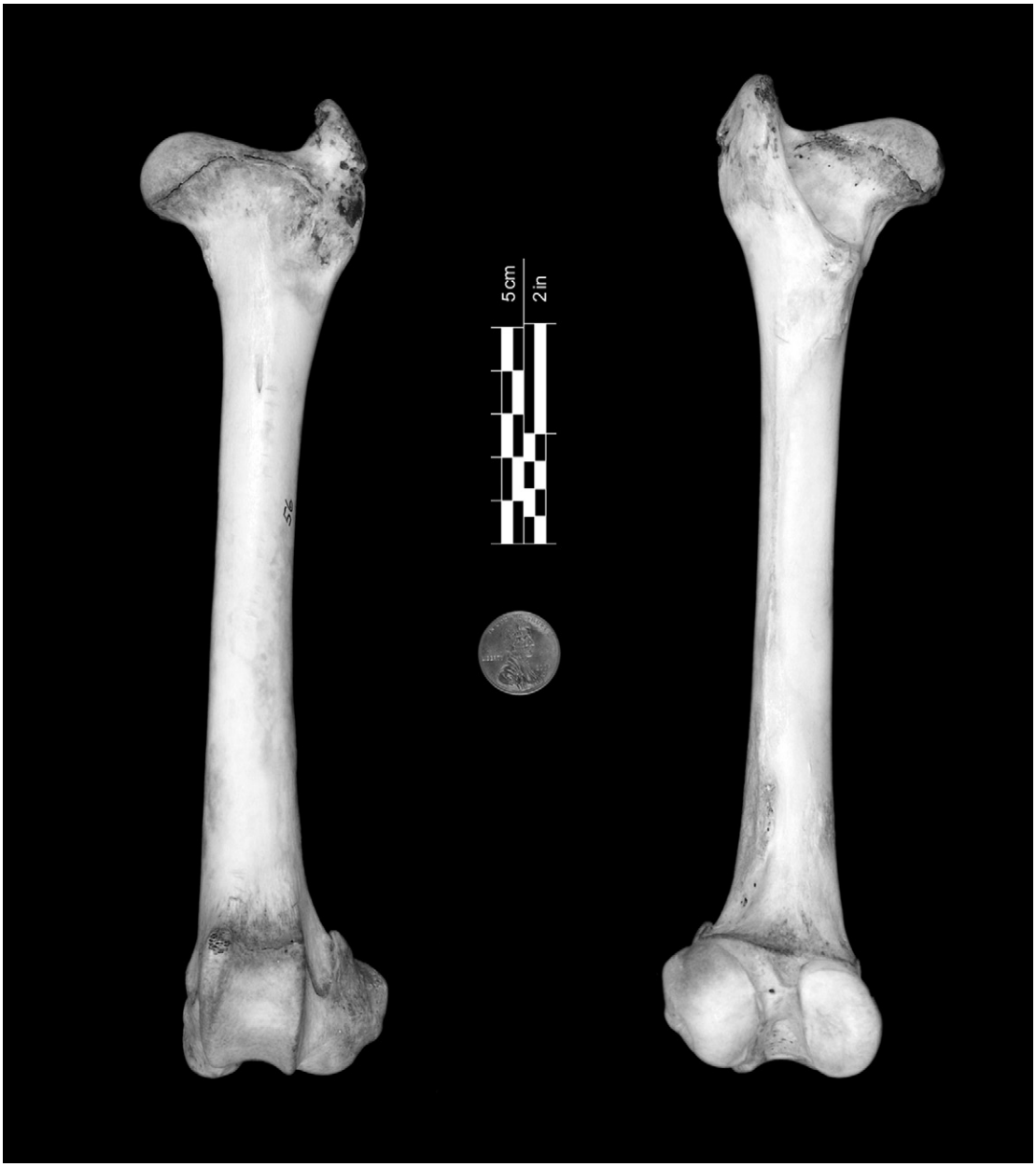

Figure 5-07: White-tailed deer left femur: cranial and caudal views.

Figure 5-08: Dog left femur: cranial and caudal views.

Figure 5-09: Sheep left femur: cranial and caudal views.

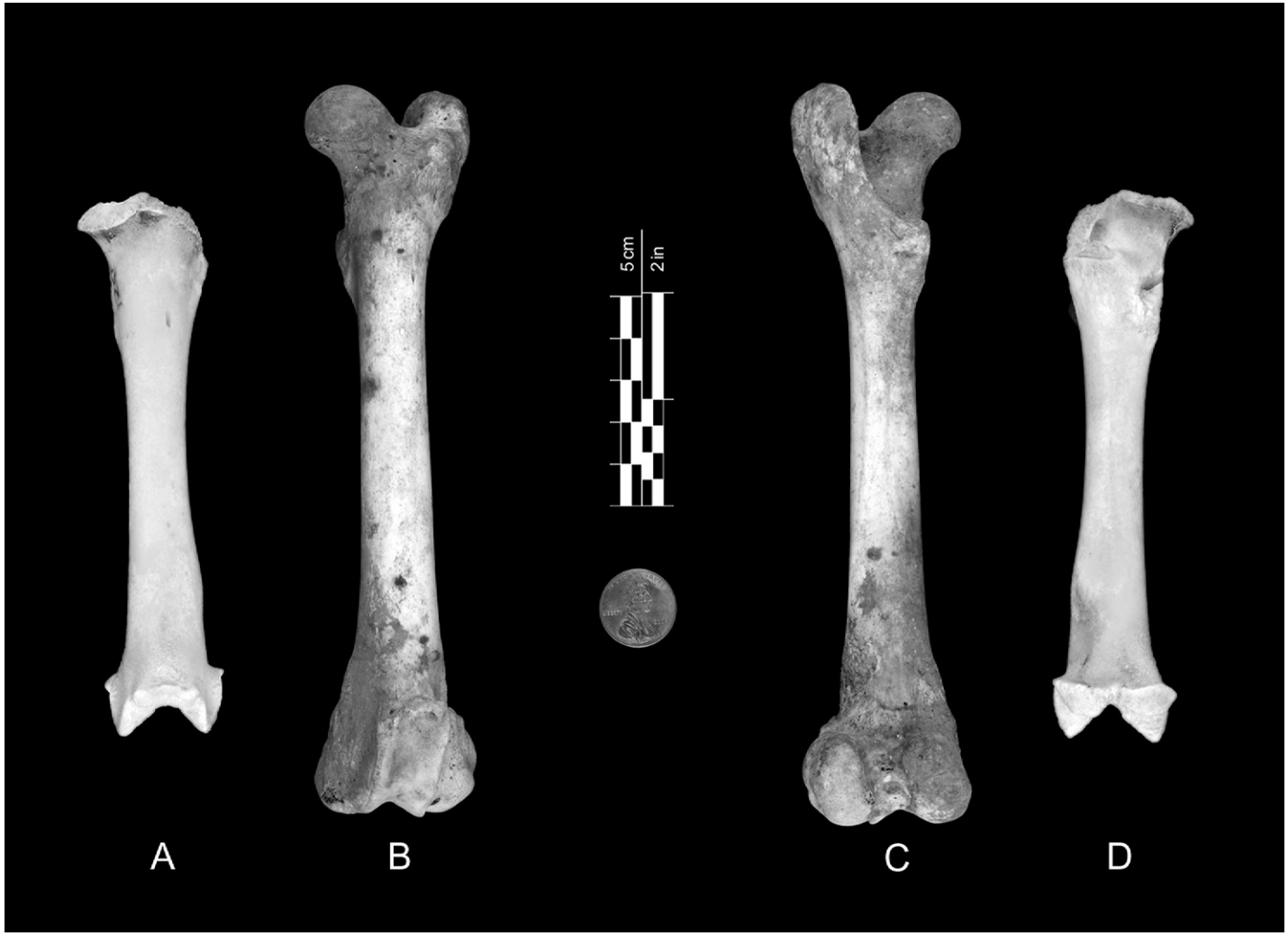

Figure 5-10: Juvenile goat without epiphyses (A and D) and adult goat (B and C) left femora: cranial and caudal views.

Figure 5-11: Left femora showing the differences in scale between some of the smaller animals. Pictured is the anterior view of a newborn human (A) and cranial views of a raccoon (B), turkey (C), cat (D), rabbit (E), opossum (F), chicken (G), and duck (H).

Figure 5-12: Newborn human left femur: cranial and caudal views.

Figure 5-13: Raccoon left femur: cranial and caudal views.

Figure 5-14: Turkey left femur: cranial and caudal views.

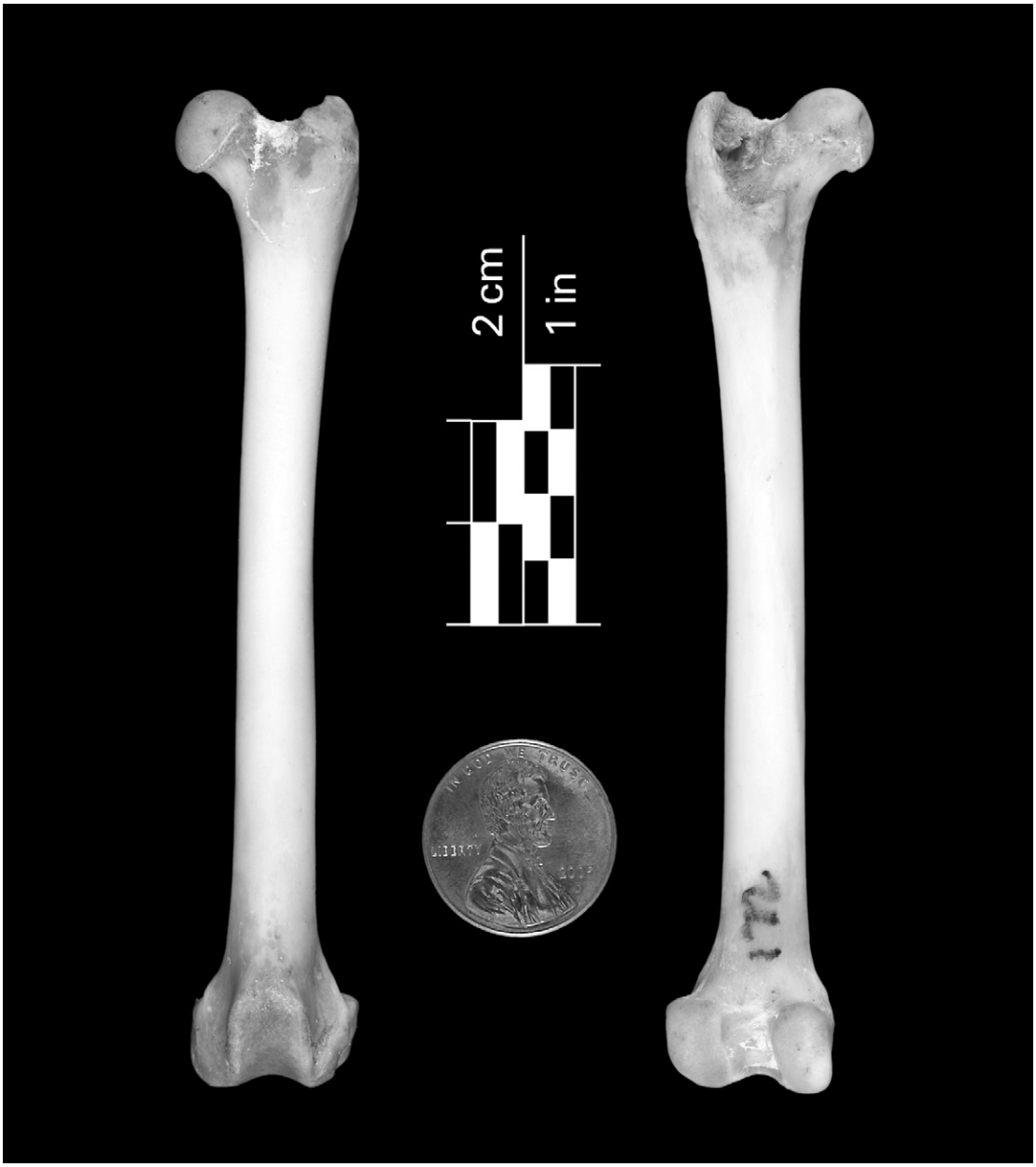

Figure 5-15: Cat left femur: cranial and caudal views.

Figure 5-16: Rabbit left femur: cranial and caudal views. Note how the fusion lines are still visible at the proximal and distal epiphyses.

Figure 5-17: Opossum left femur: cranial and caudal views. Note how the fusion lines are still visible at the proximal and distal epiphyses.

Figure 5-18: Adult (A and D) and juvenile (B and C) chicken femora: cranial and Caudal views.

Figure 5-19: Duck left femur: cranial and caudal views.

CHAPTER 6

Tibiae

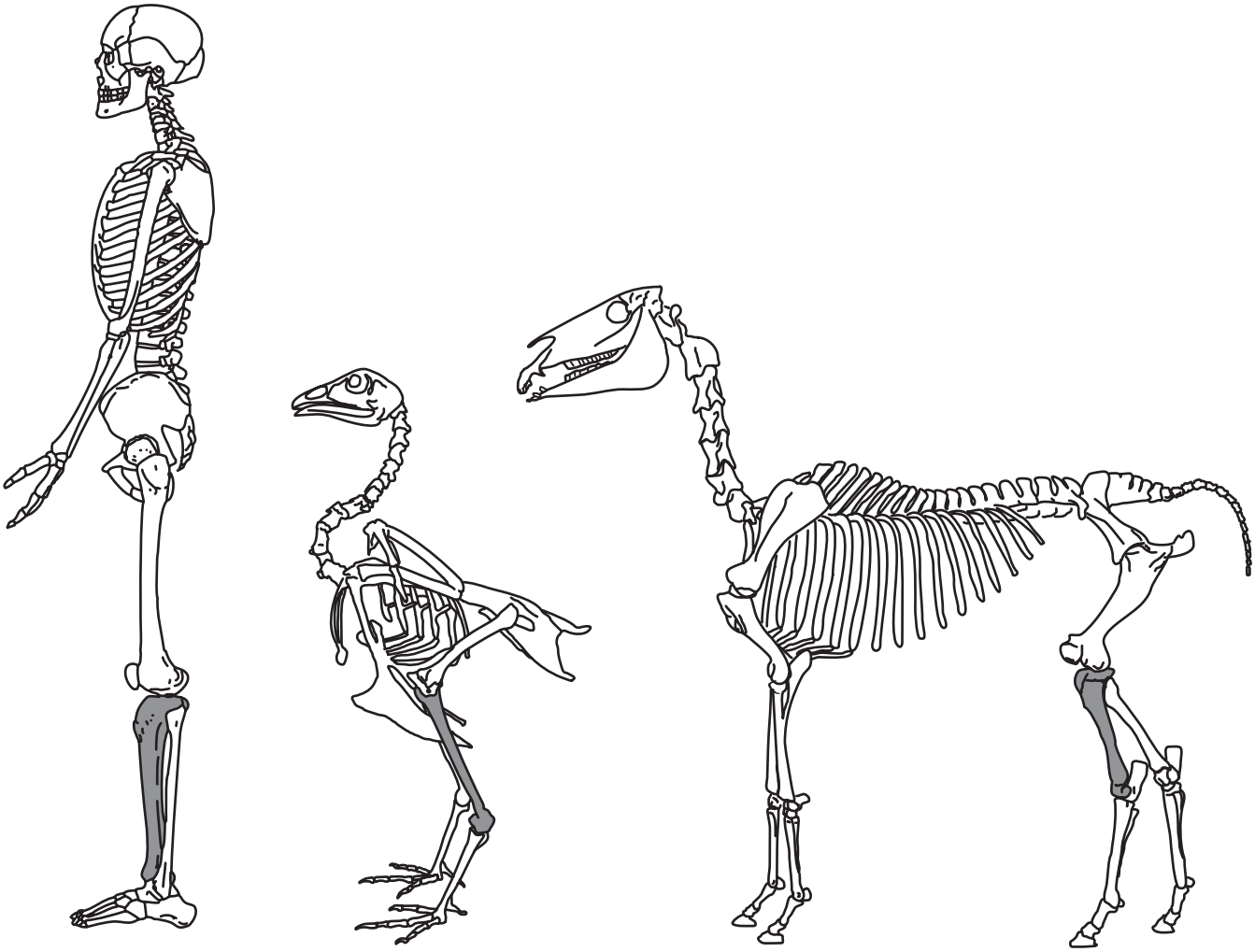

Comparative Osteology. DOI: 10.1016/B978-0-12-388437-4.00006-5

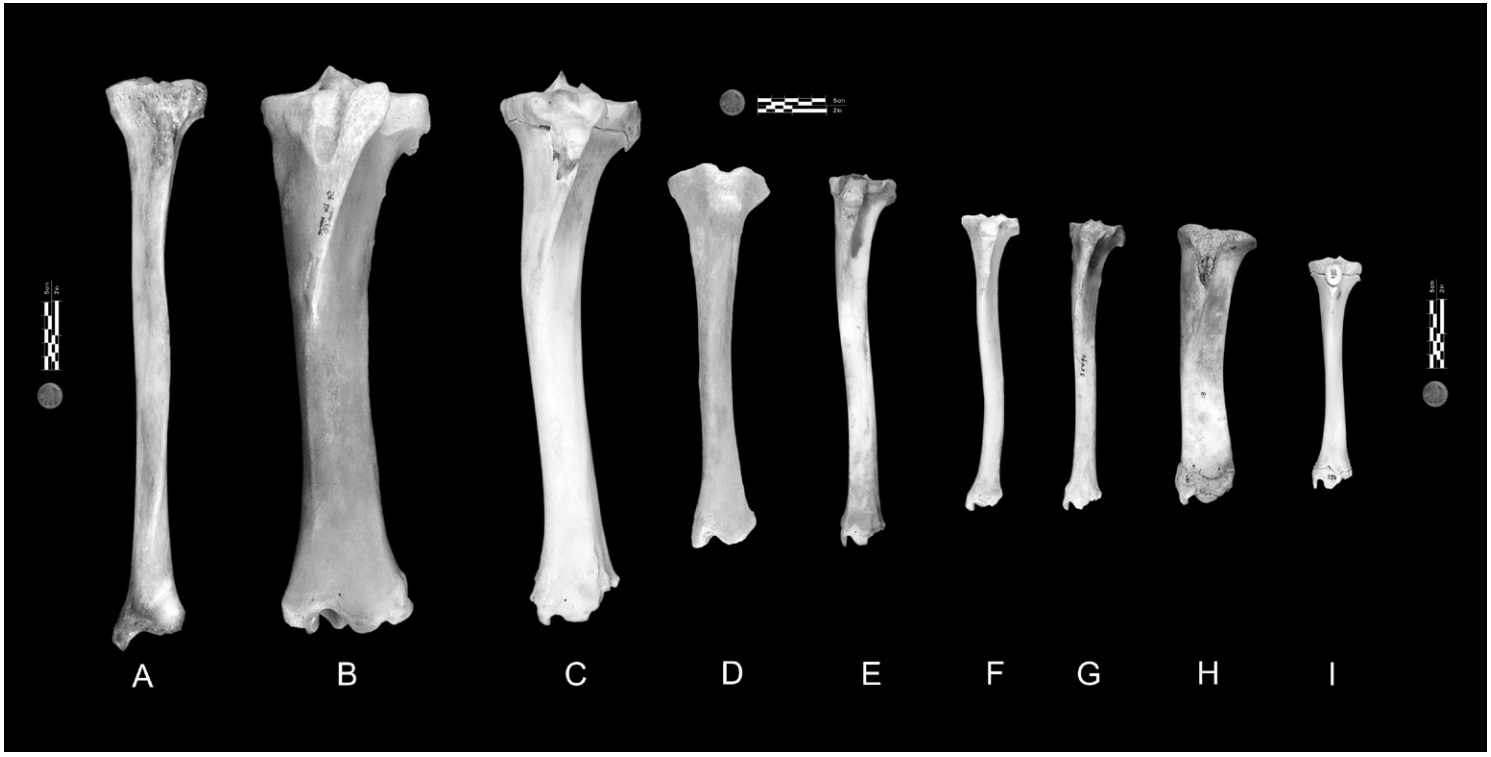

Figure 6-01: Left tibiae showing the differences in scale between some of the larger animals. Pictured are the anterior view of an adult human (A) and the cranial views of a horse (B), cow (C), bear (D), white-tailed deer (E), dog (F), sheep (G), pig (H), and juvenile goat (I).

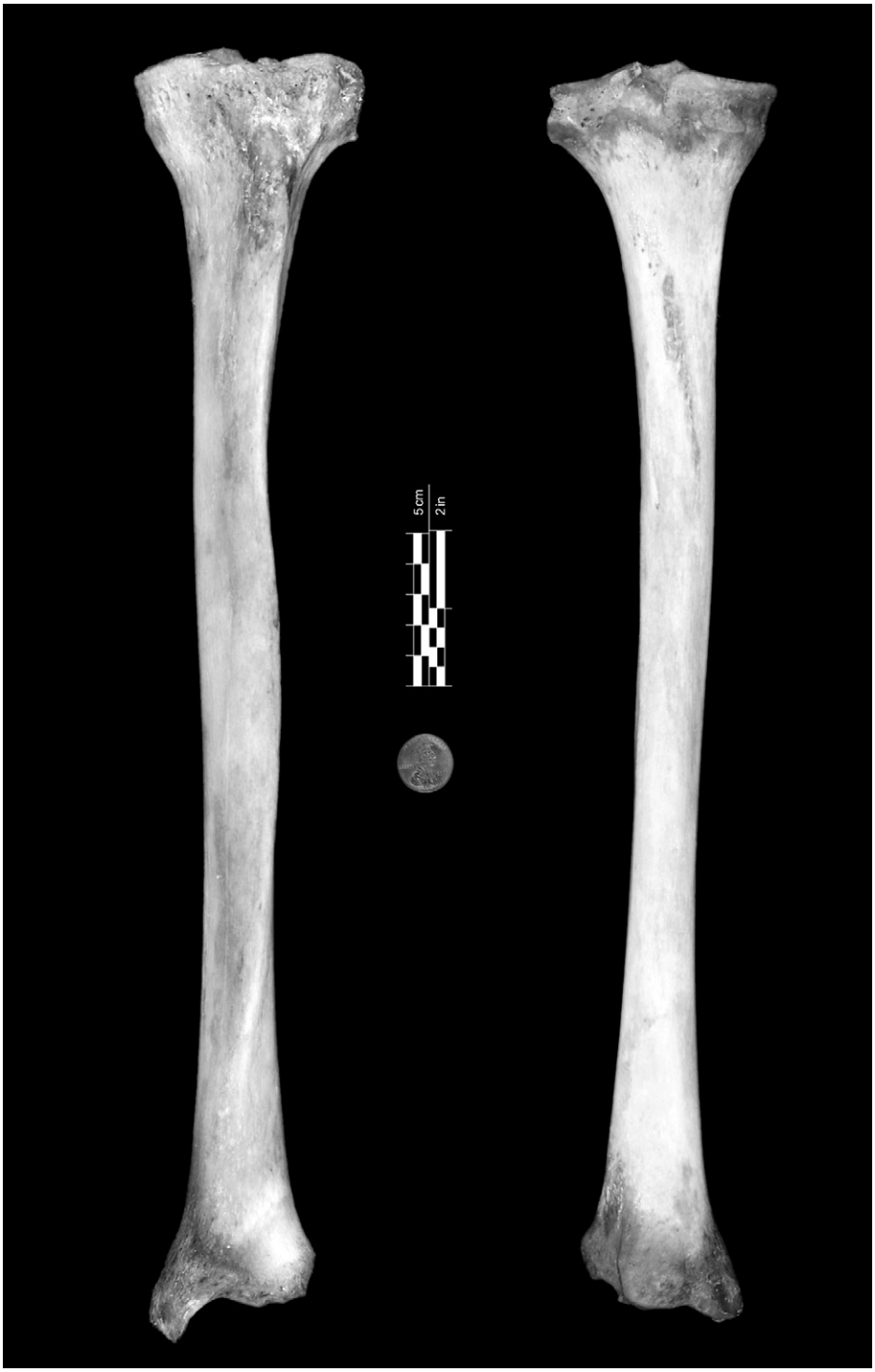

Figure 6-02: Adult human left tibia: anterior and posterior views.

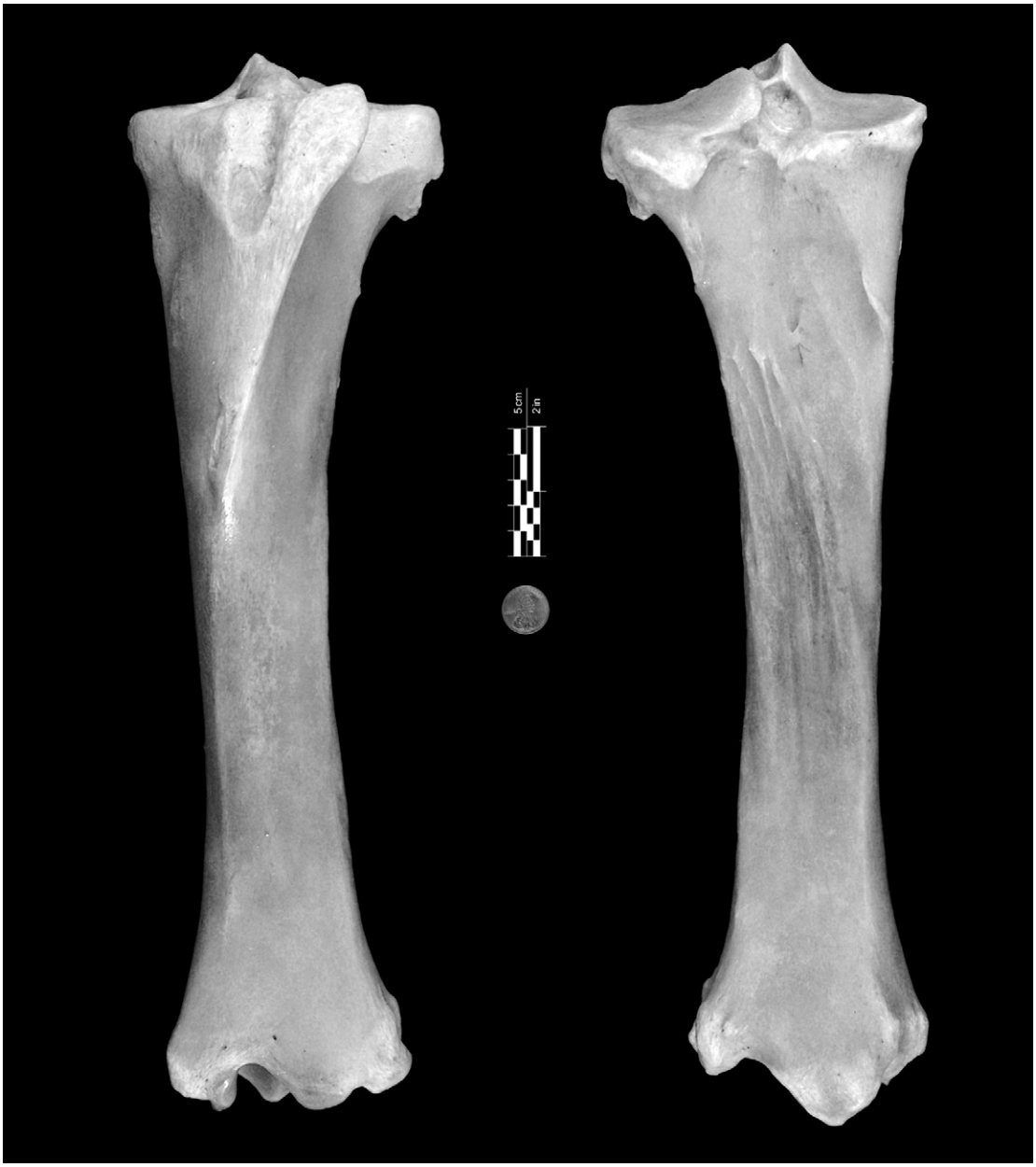

Figure 6-03: Horse left tibia: cranial and caudal views.

Figure 6-04: Cow left tibia: cranial and caudal views. Note how the fusion line is still visible at the proximal epiphysis.

Figure 6-05: Bear left tibia: cranial and caudal views.

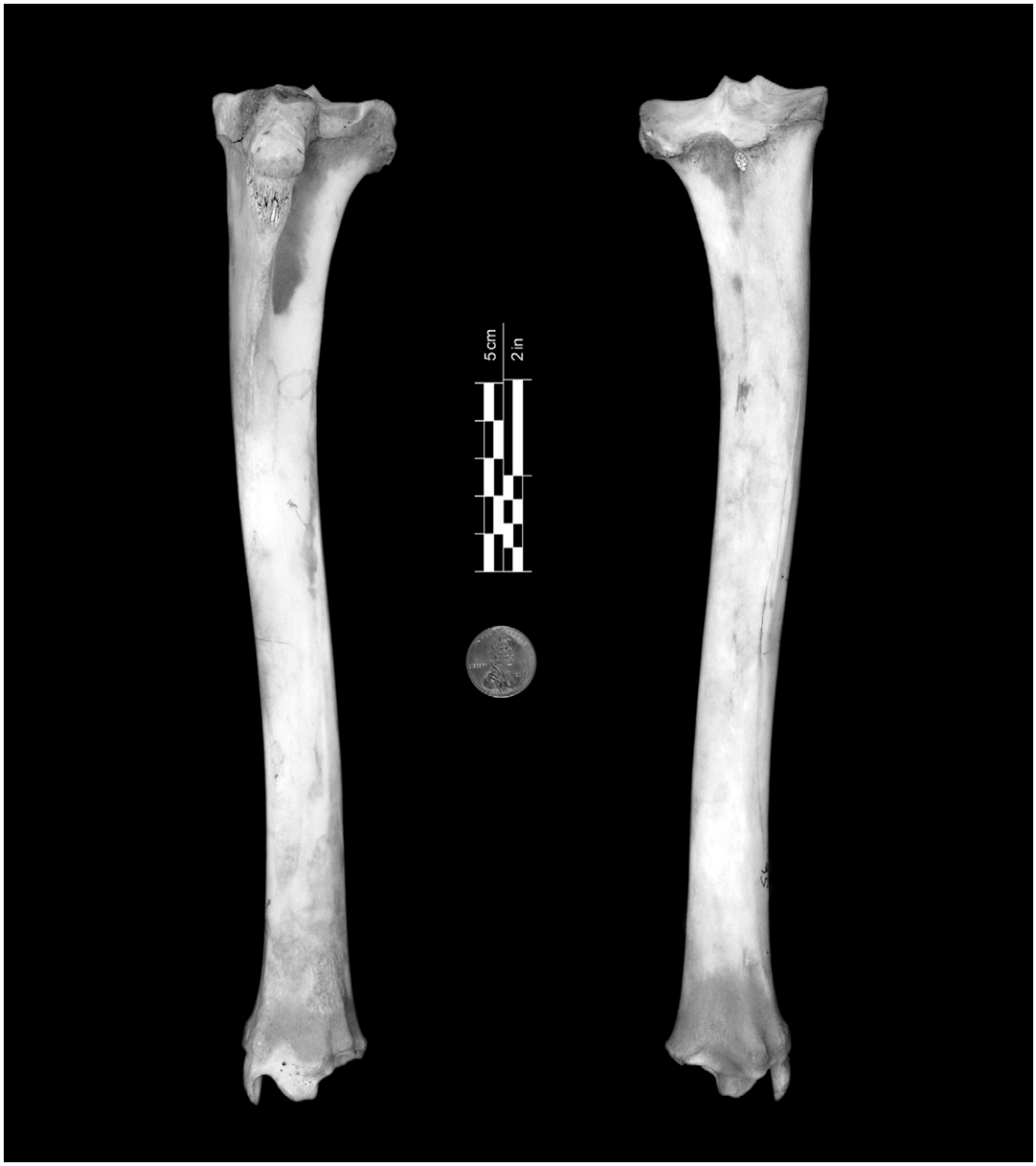

Figure 6-06: Deer left tibia: cranial and caudal views.

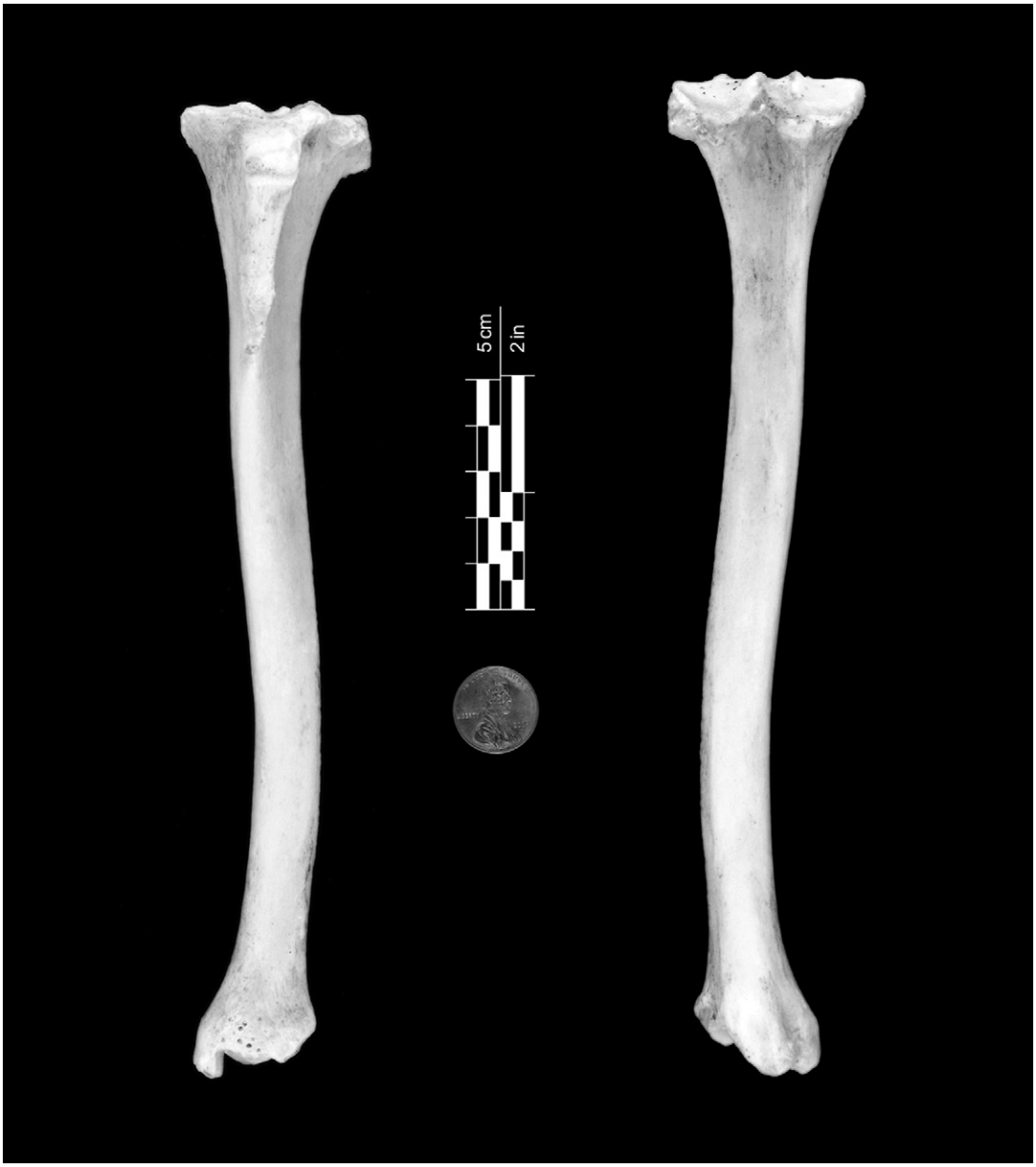

Figure 6-07: Dog left tibia: cranial and caudal views.

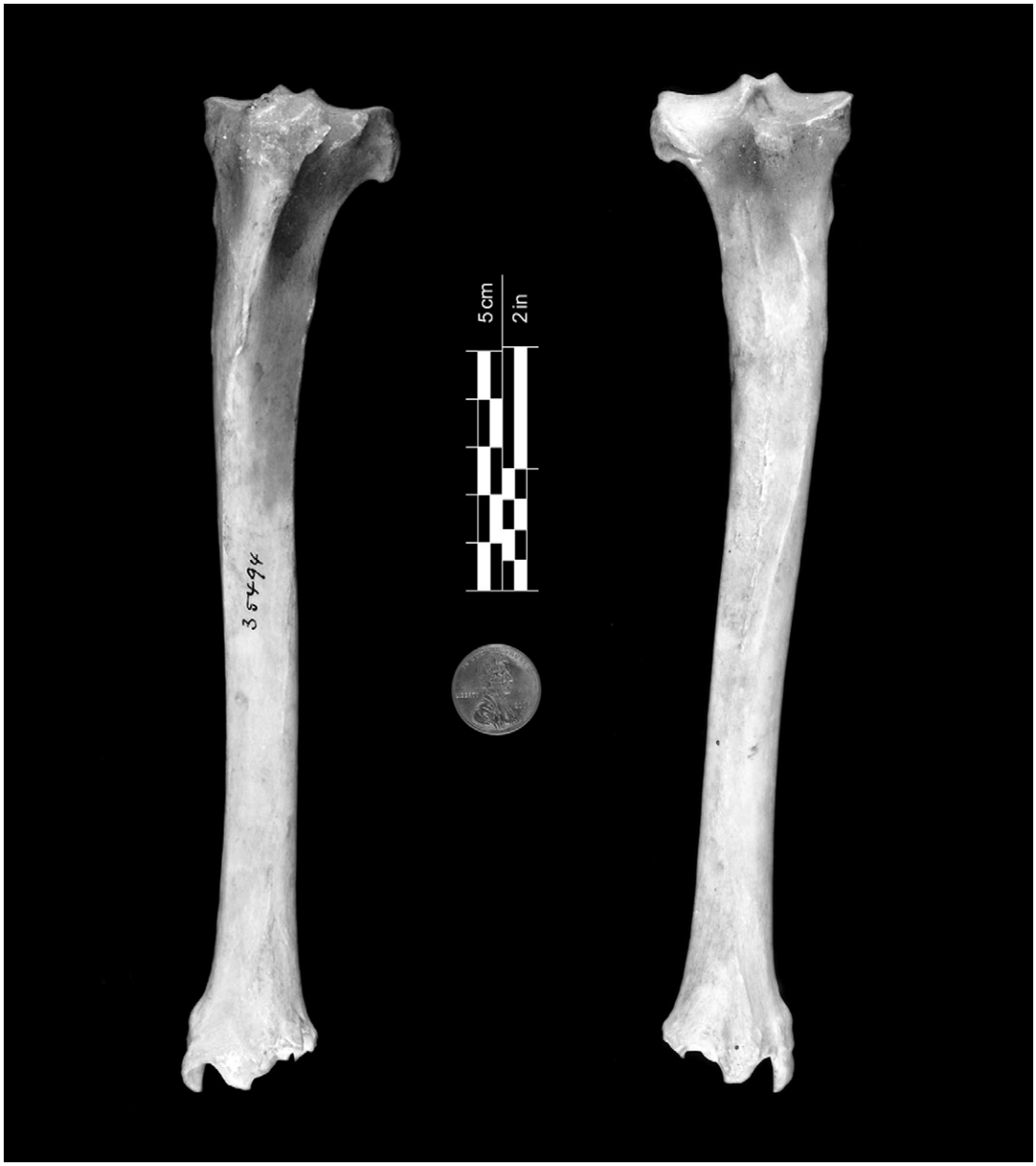

Figure 6-08: Sheep left tibia: cranial and caudal views.

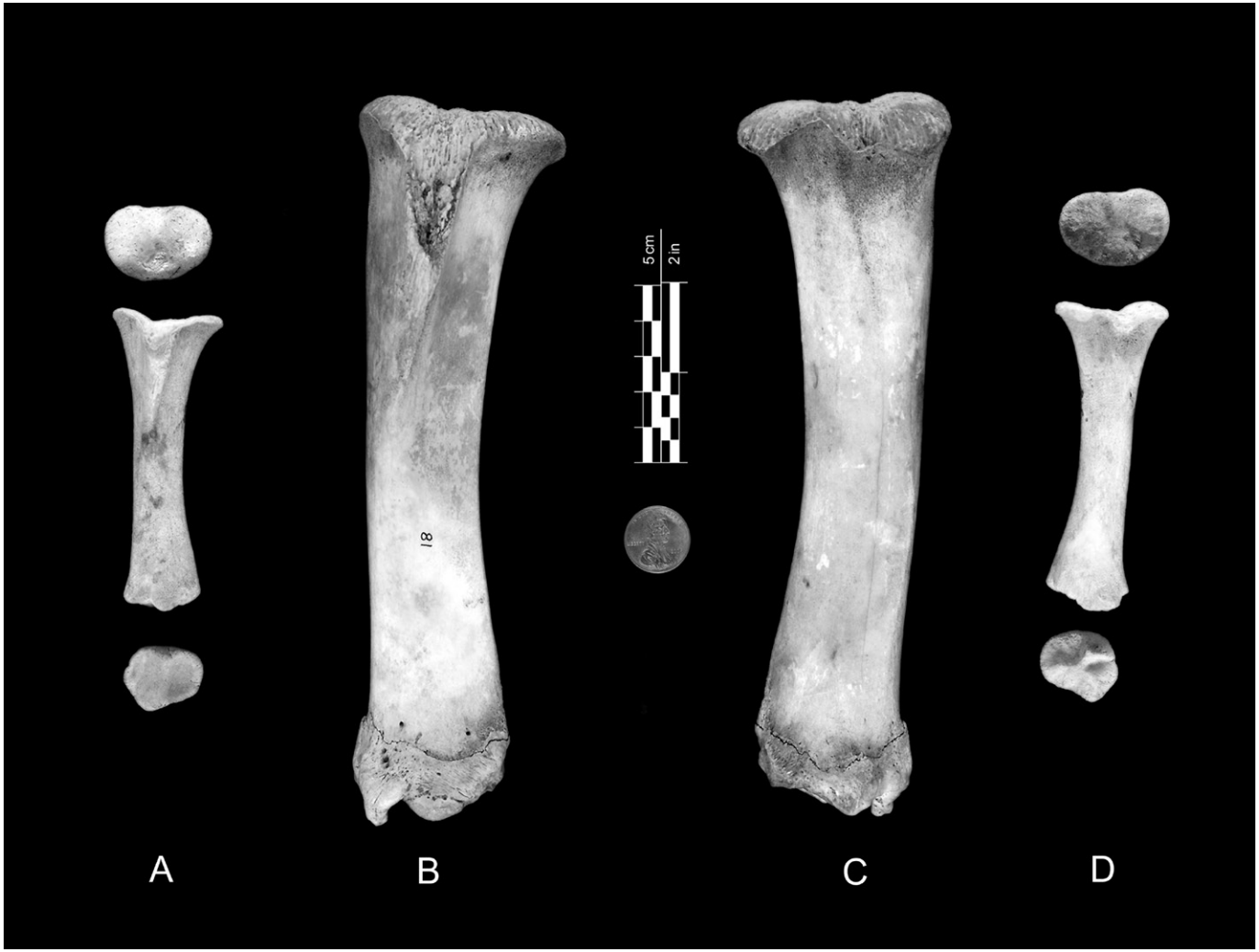

Figure 6-09: Juvenile pig (A and D) and more mature pig (B and C) left tibiae: cranial and caudal views. The larger tibia is missing its proximal epiphysis.

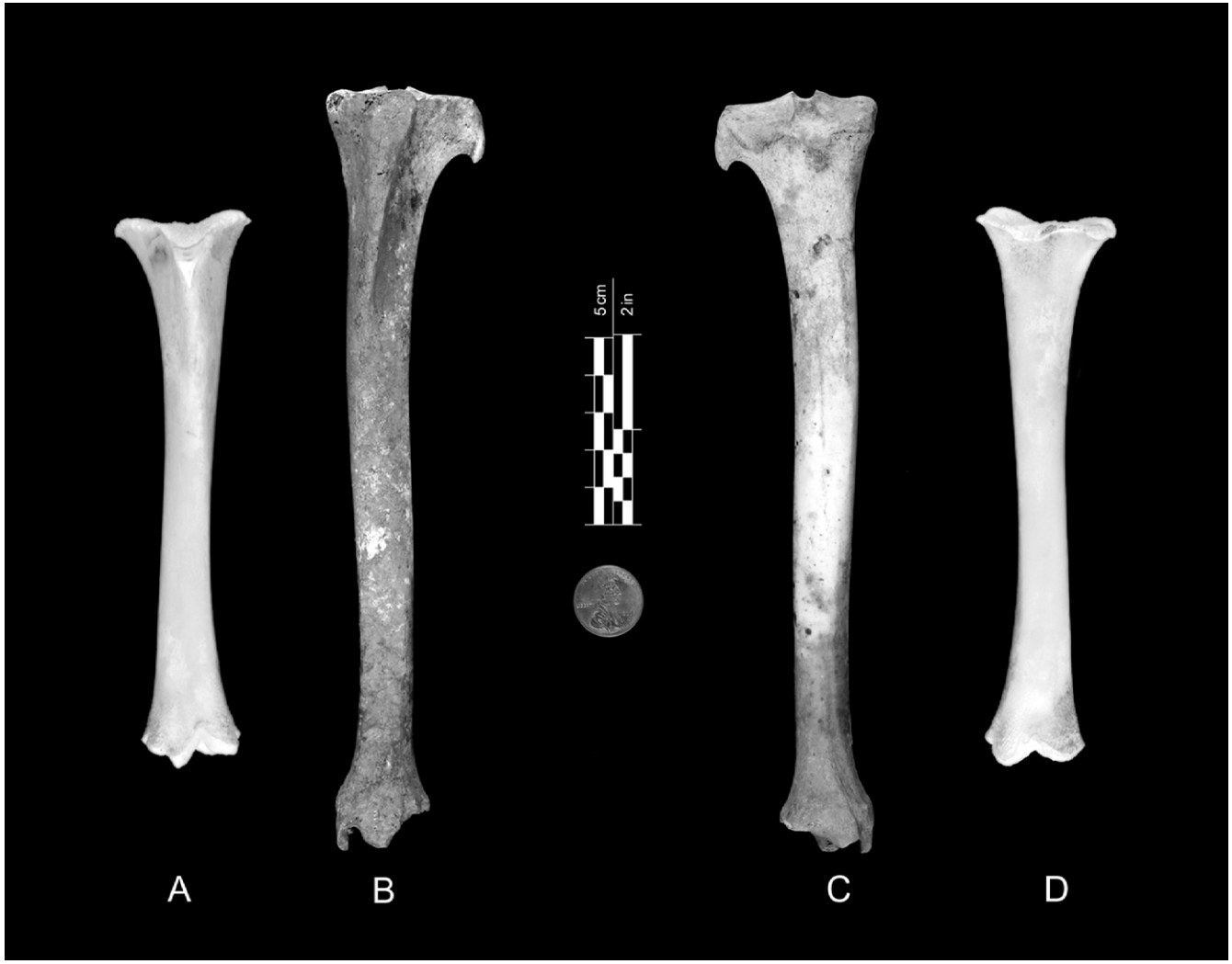

Figure 6-10: Juvenile goat without epiphyses (A and D) and adult goat (B and C) left tibiae: cranial and caudal views.

Figure 6-11: Left tibiae showing the differences in scale between some of the smaller animals. Pictured are the anterior view of a newborn human tibia (A) and cranial views of the tibiotarsus of a turkey (B), tibiotarsus of a chicken (C), tibiotarsus of a duck (D), tibia of a raccoon (E), tibia of a cat (F), tibia and fibula of a rabbit (G), and tibia of an opossum (H).

Figure 6-12: Newborn human left tibia: anterior and posterior views.

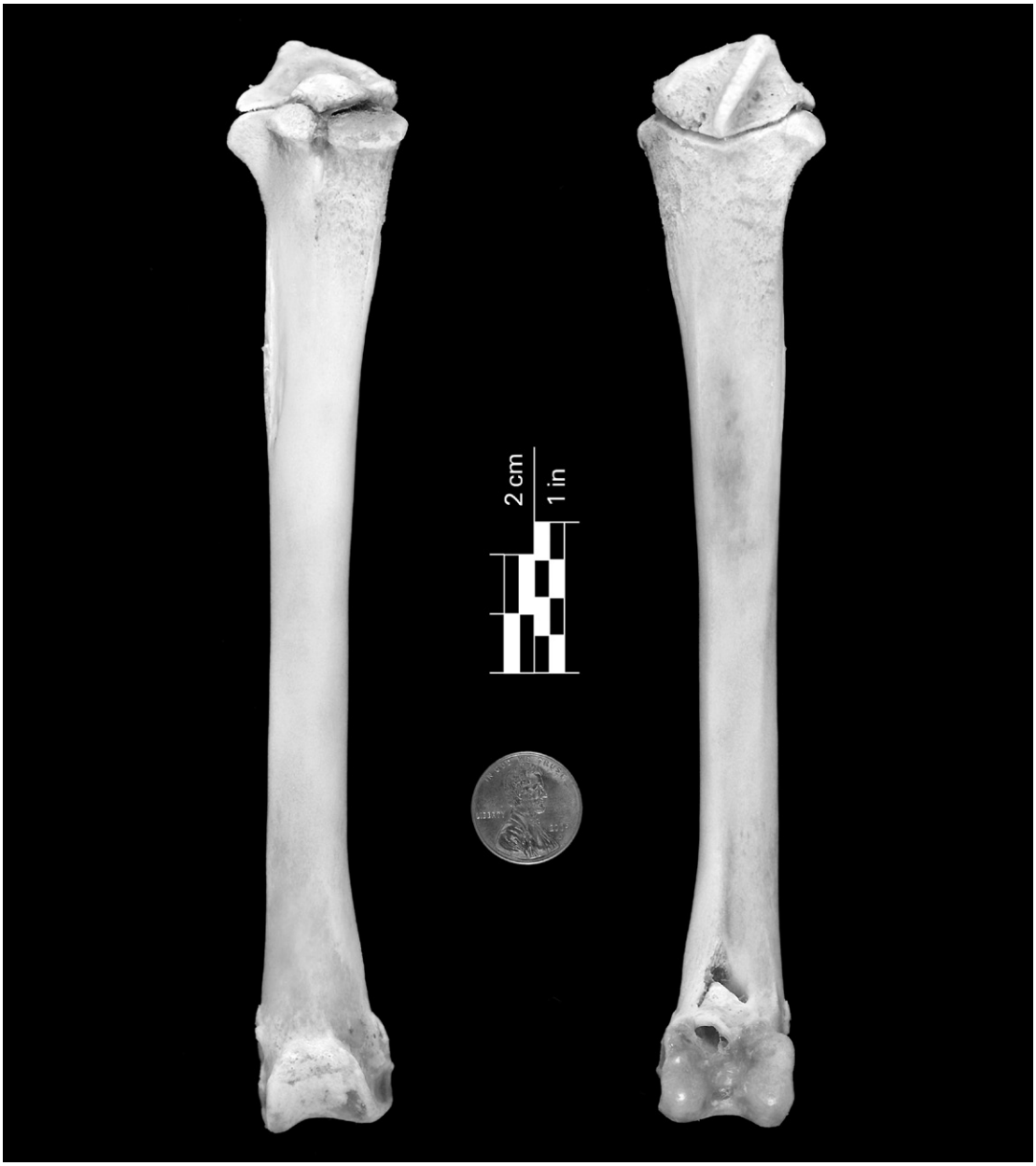

Figure 6-13: Turkey left tibiotarsus: cranial and caudal views.

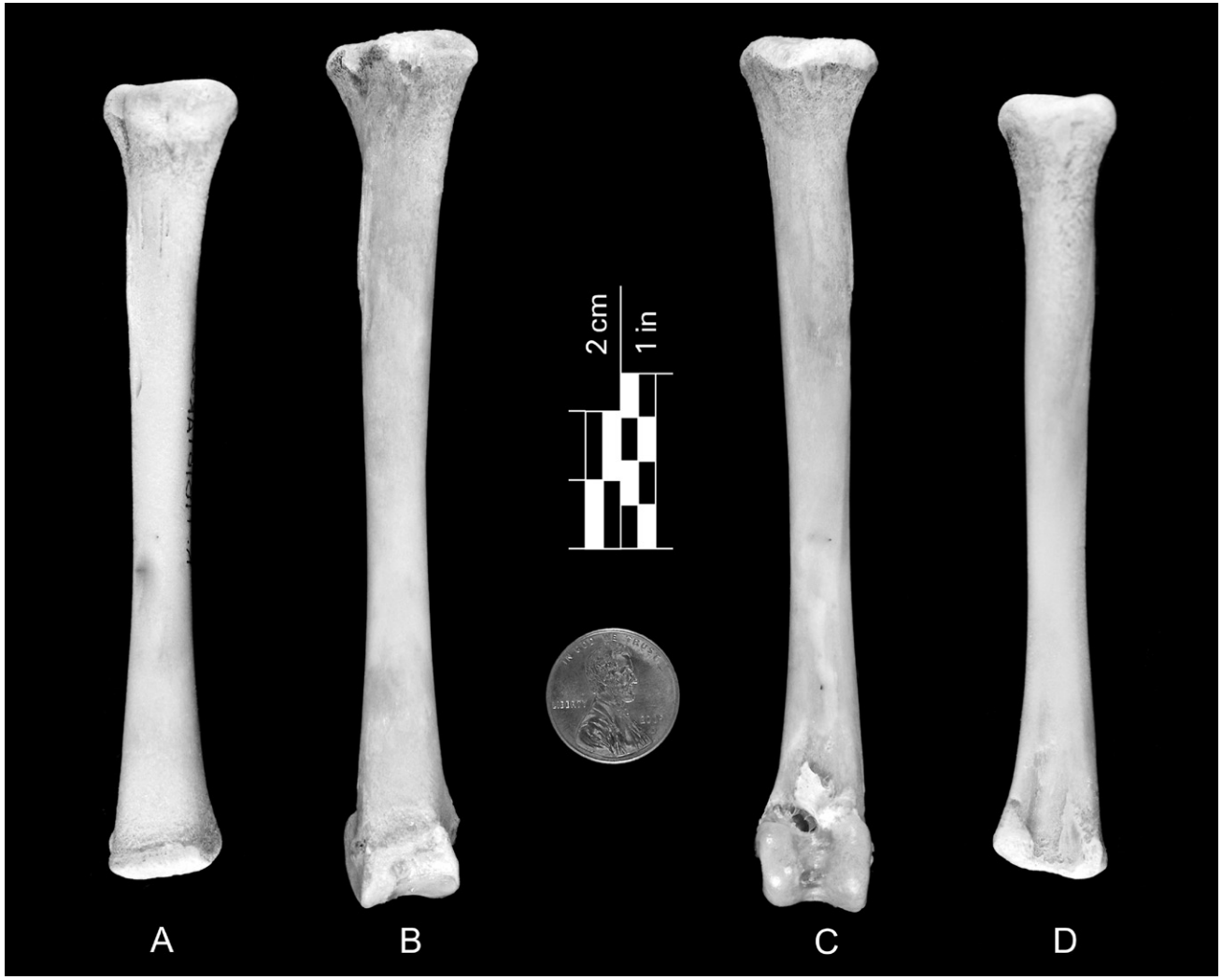

Figure 6-14: Chicken left tibiotarsi: cranial (A and B) and caudal (C and D) views. The smaller element is from a younger chicken.

Figure 6-15: Duck left tibiotarsus: cranial and caudal views.

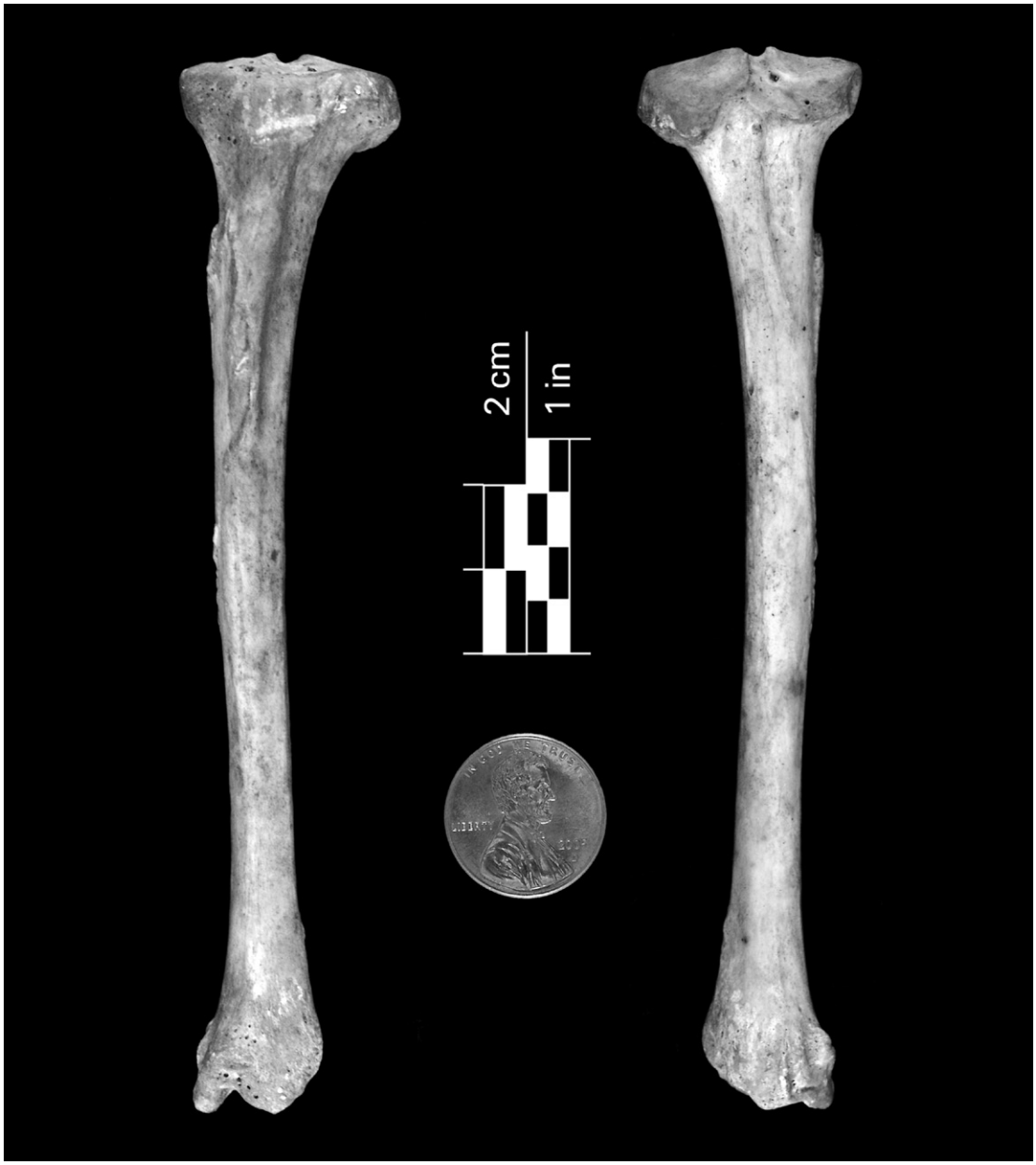

Figure 6-16: Raccoon left tibia: cranial and caudal views.

Figure 6-17: Cat left tibia: cranial and caudal views.

Figure 6-18: Rabbit left tibiae: cranial and caudal views. Note how the rabbit's fibula is fused to the tibia. The fusion line is still visible at the proximal epiphysis.

Figure 6-19: Opossum left tibia: cranial and caudal views. Note how the fusion lines are still visible at the proximal and distal epiphyses.

CHAPTER 7

Human (Homo sapiens)

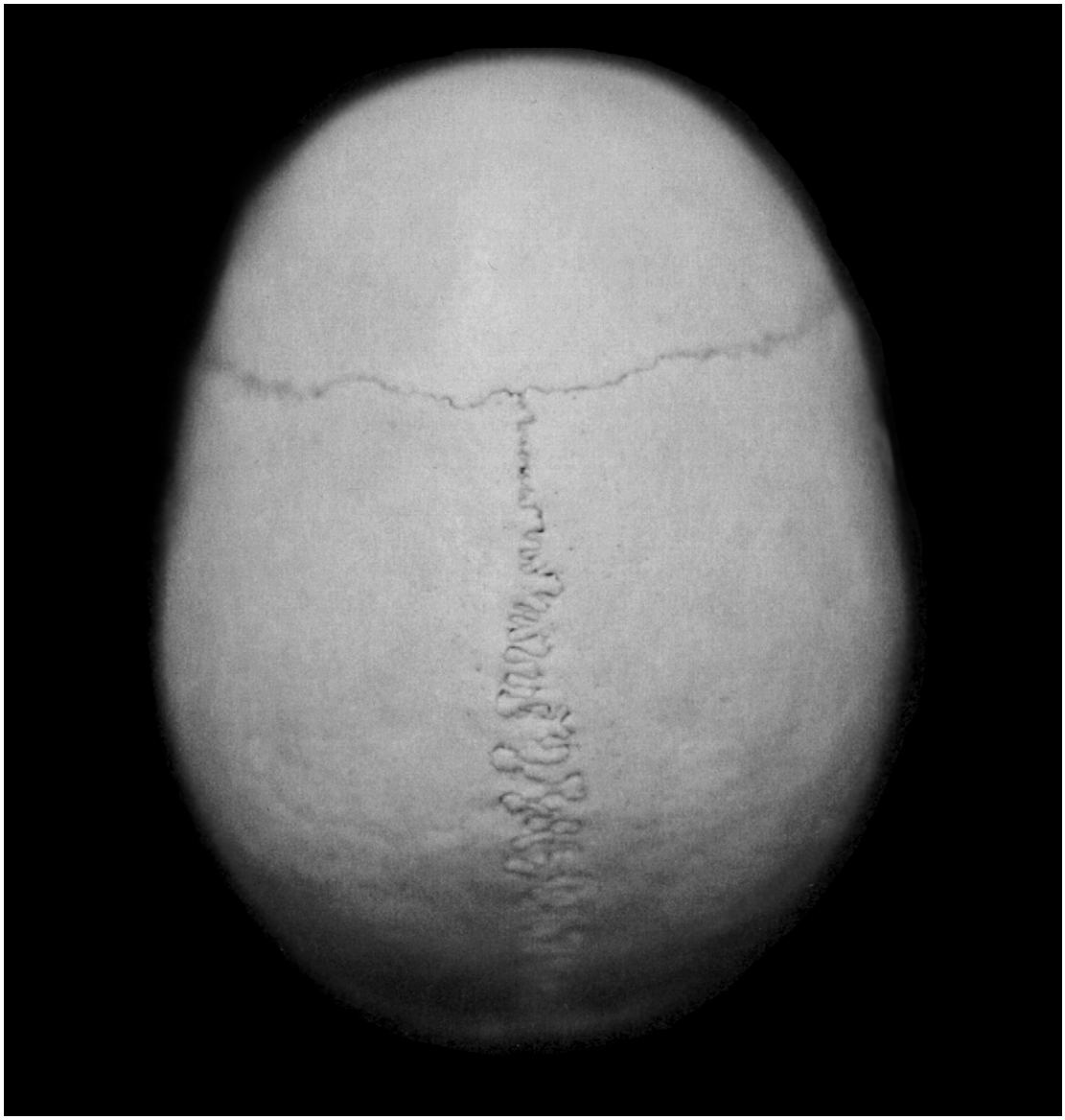

Comparative Osteology. DOI: 10.1016/B978-0-12-388437-4.00007-7

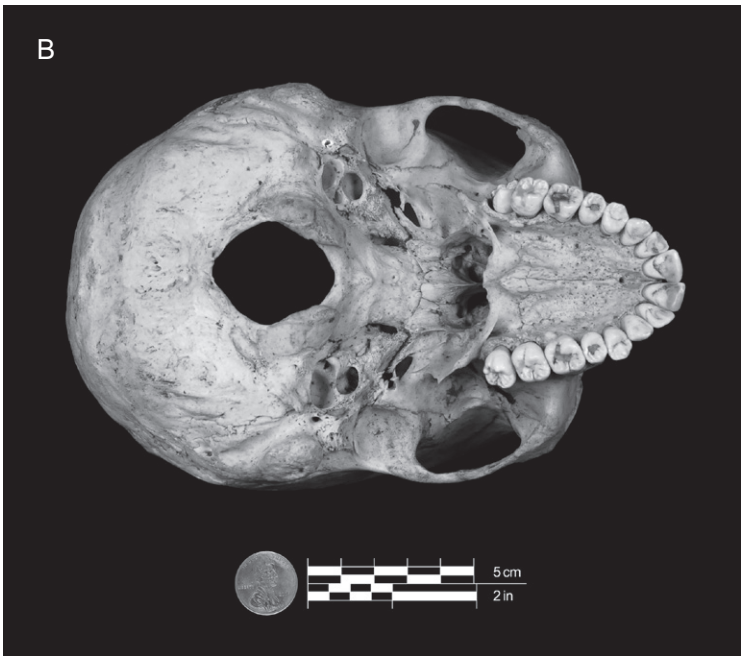

Figure 7-01: Adult human cranium (A) lateral view, right side; (B) inferior view. The adult human maxillary dentition includes 2 incisors, 1 canine, 2 premolars, and 3 molars on each side of the body. The mandibular dentition also includes 2 incisors, 1 canine, 2 premolars, and 3 molars on each side of the body. The human dental formula is written as follows: 2/2.1/1.2/2.3/3, listing the number of upper and lower incisors, canines, premolars, and molars of each side of the body.

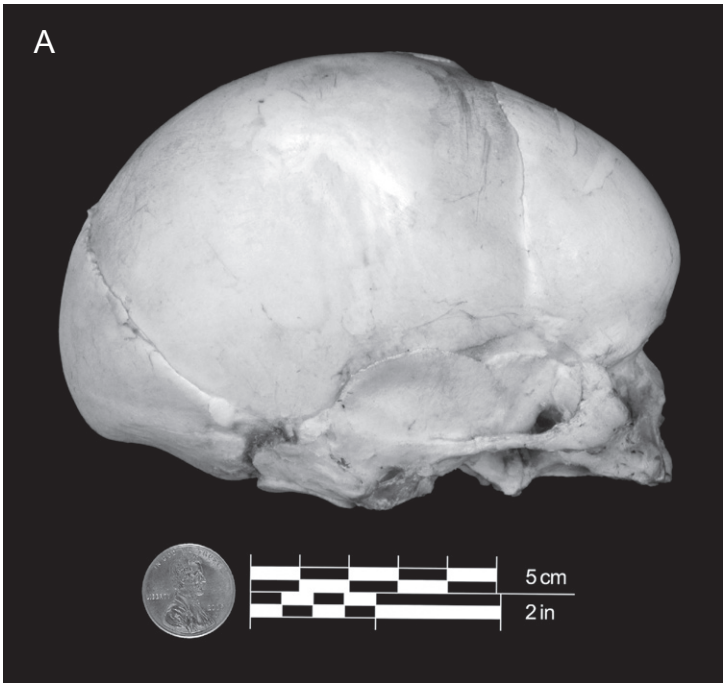

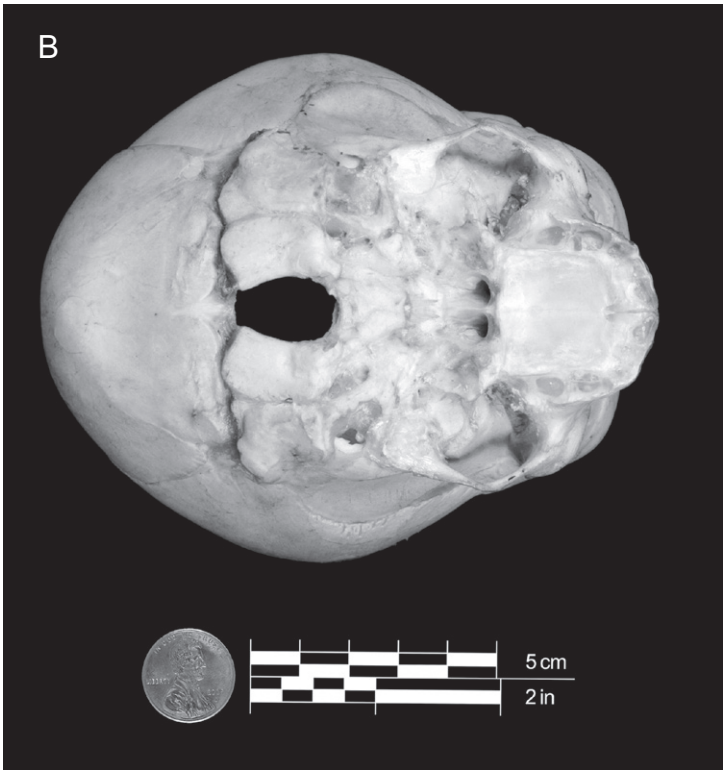

Figure 7-02: Newborn human cranium (A) lateral right view; (B) inferior view. At this age the teeth are still forming in the crypts but are unerupted.

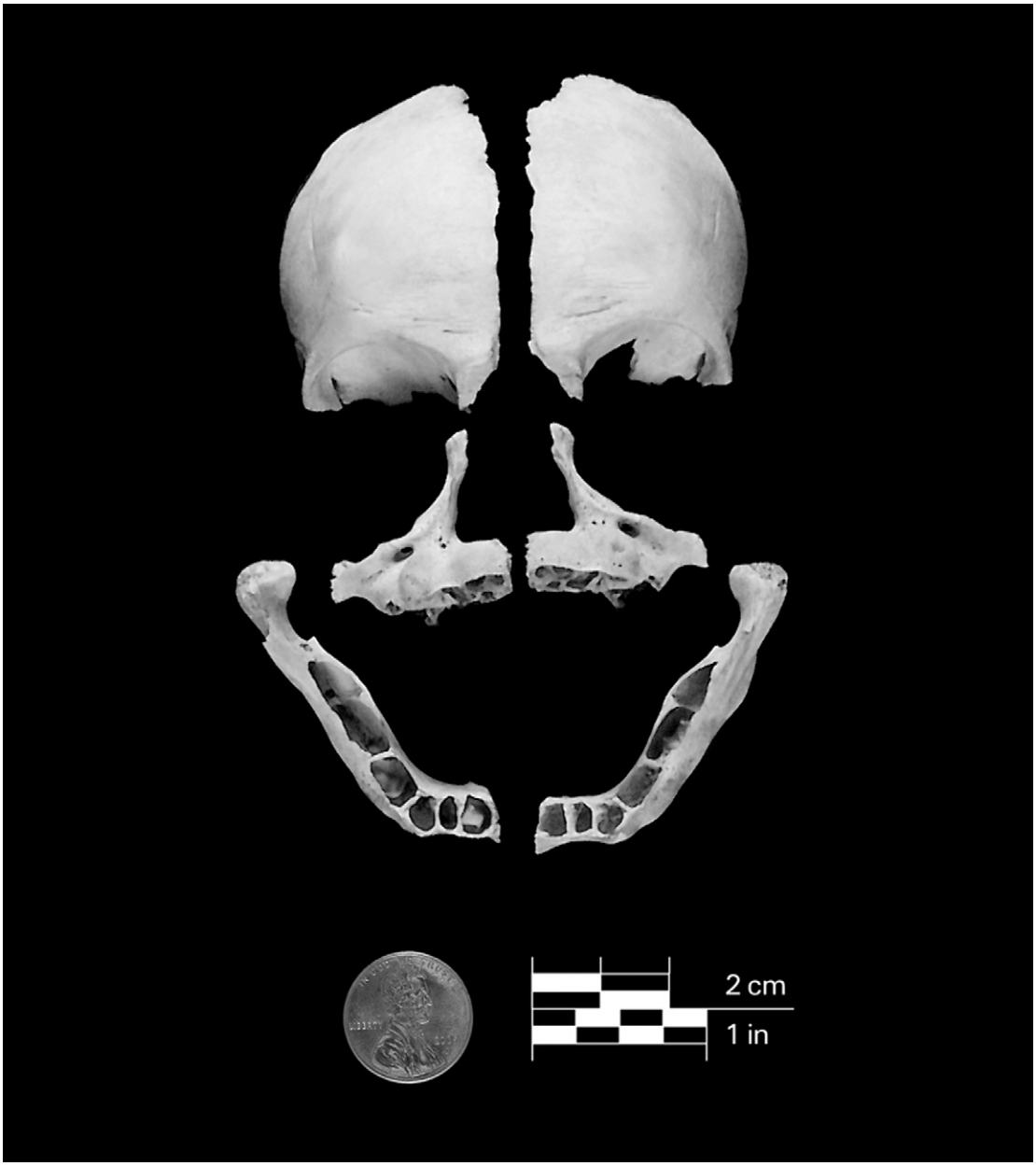

Figure 7-03: Selected newborn cranial bones (frontals and maxillae) and mandible. Note how the bones of the skull in infants are still separate and have not fused. Some unerupted/forming teeth are visible within the sockets.

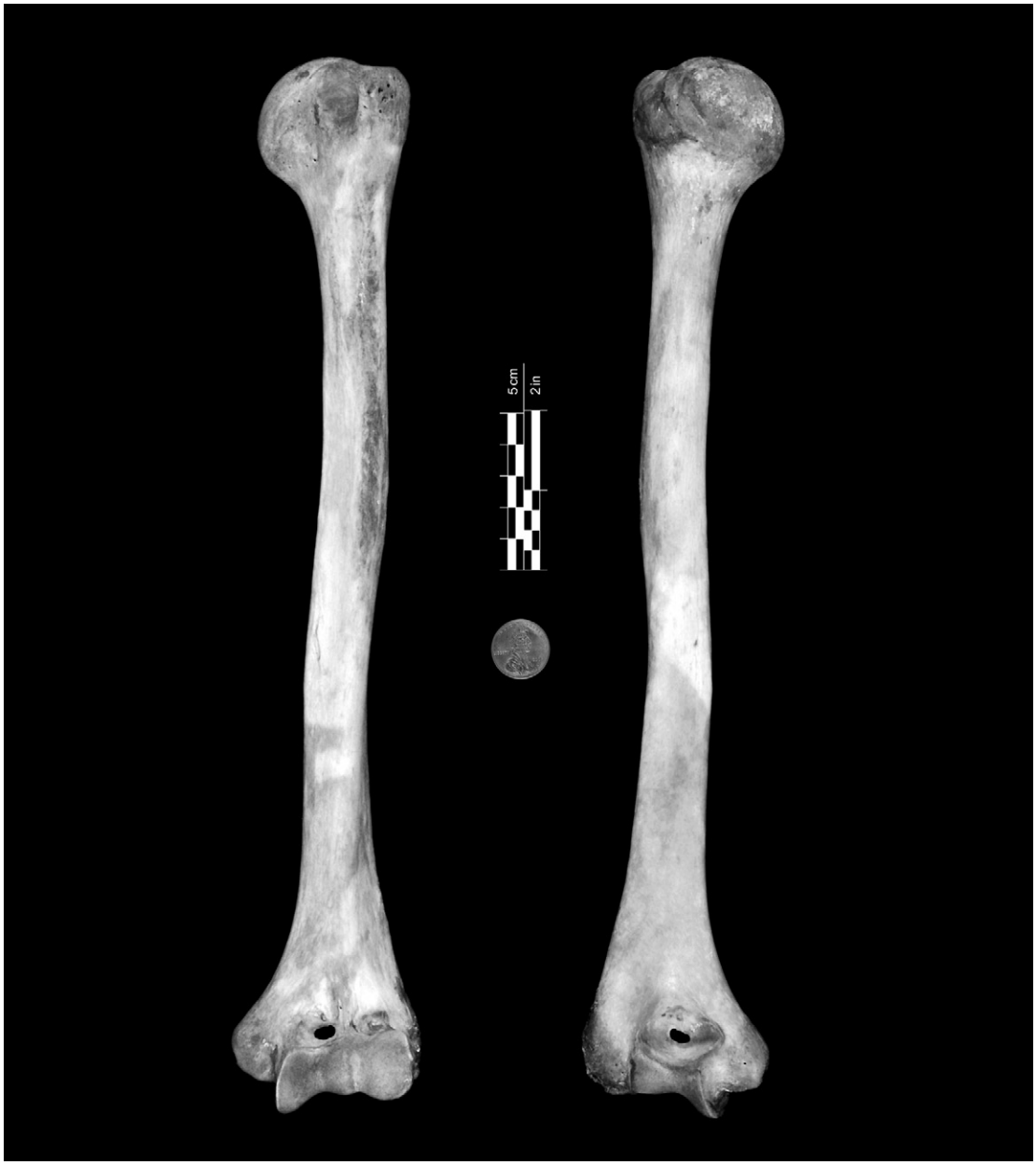

Figure 7-04: Adult human left humerus (anterior and posterior views).

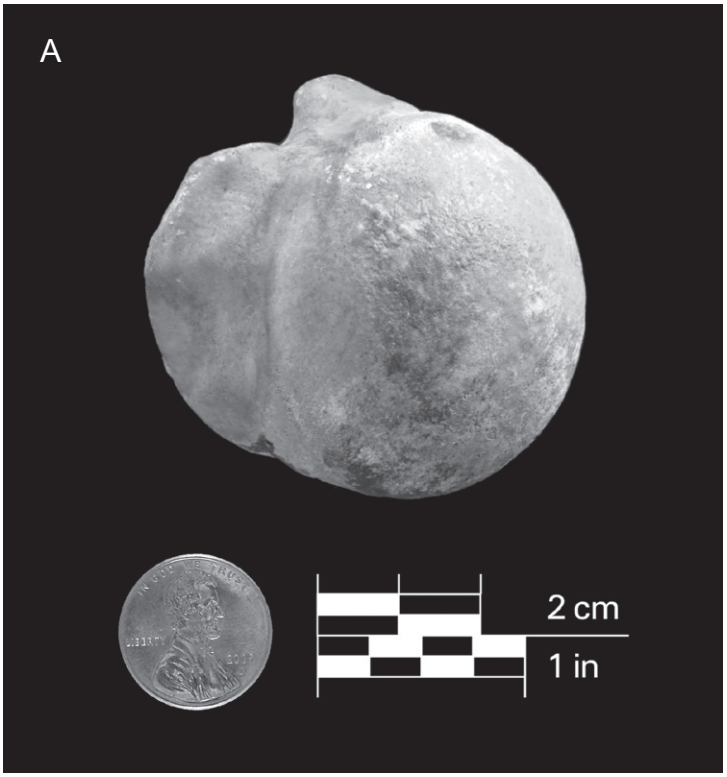

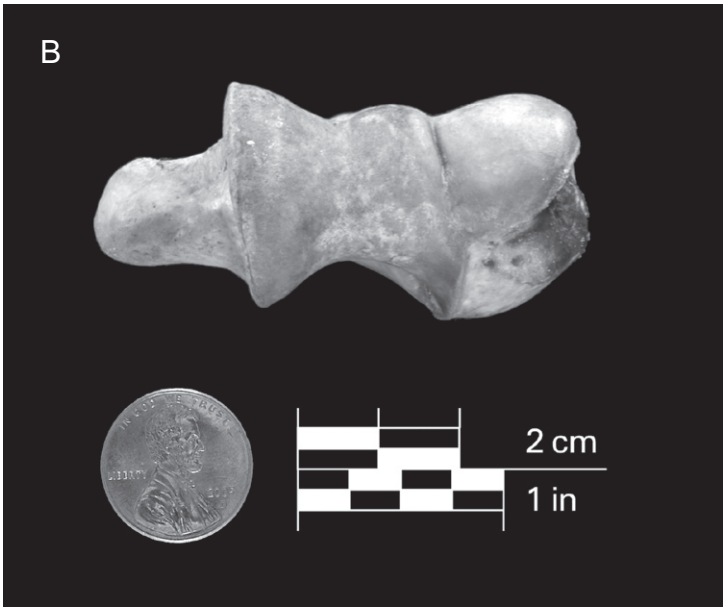

Figure 7-05: Adult human left humerus (A) humeral head, superior view; (B) distal end, inferior view.

Figure 7-06: Newborn human left humerus (anterior and posterior views).

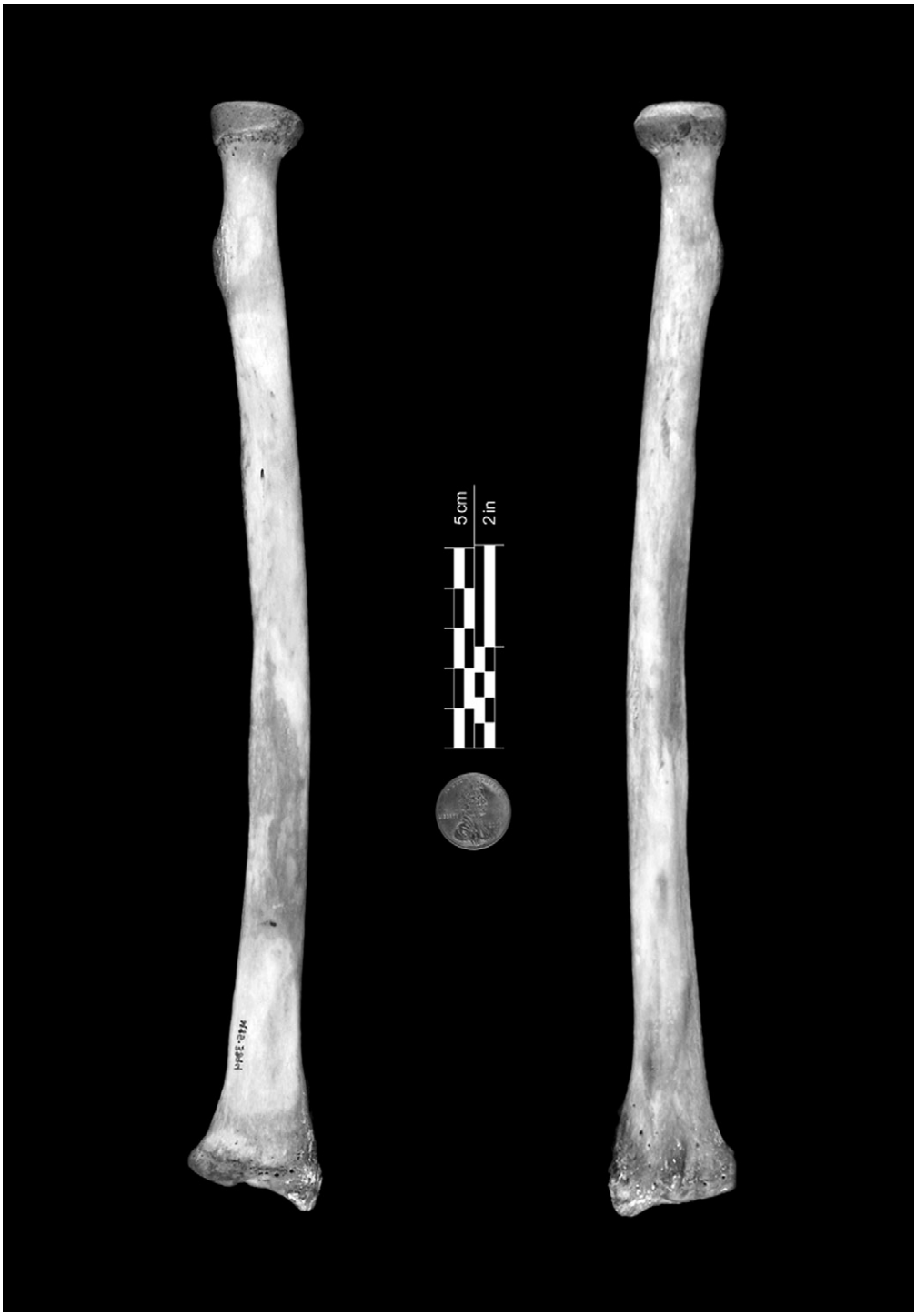

Figure 7-07: Adult human left radius (anterior and posterior views).

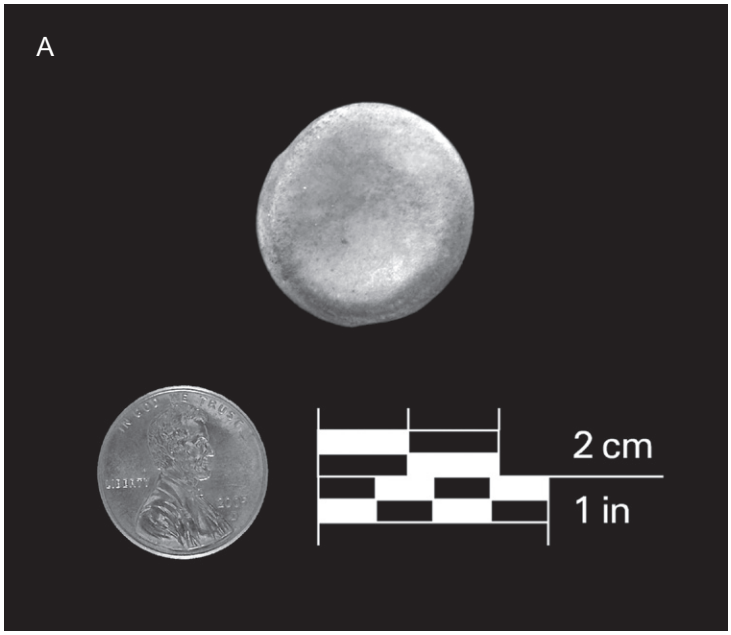

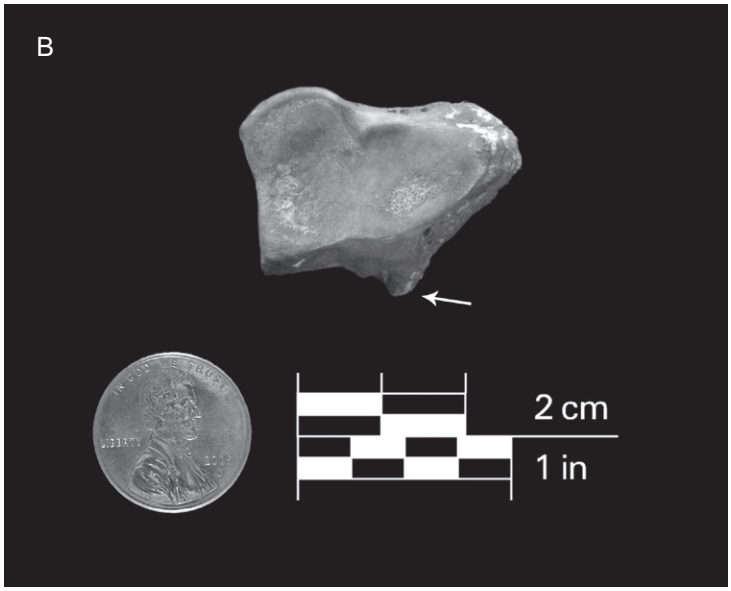

Figure 7-08: Adult human left radius (A) radial head, superior view. Note the circularity of this epiphysis; (B) distal end, inferior view. Note the raised tubercles that are present on the posterior surface (arrow).

Figure 7-09: Newborn human left radius (anterior and posterior views).

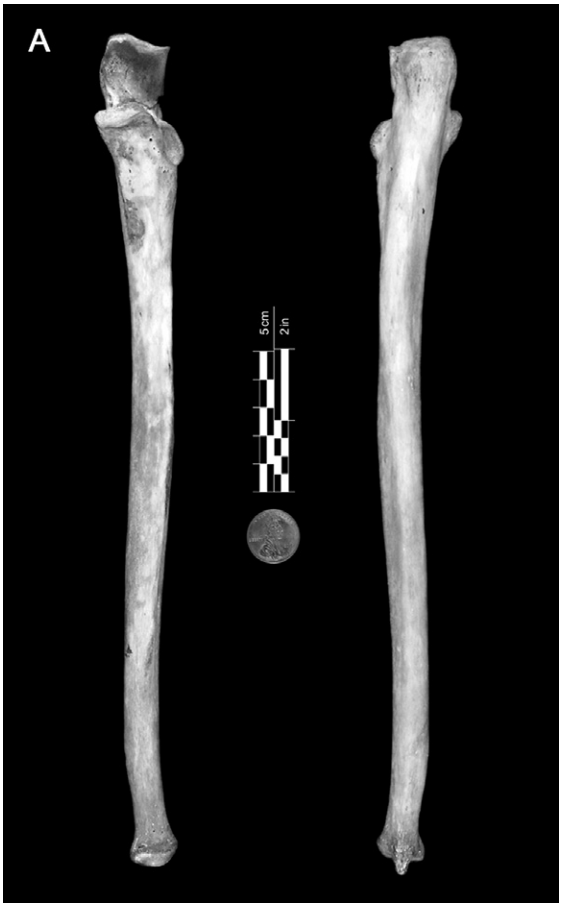

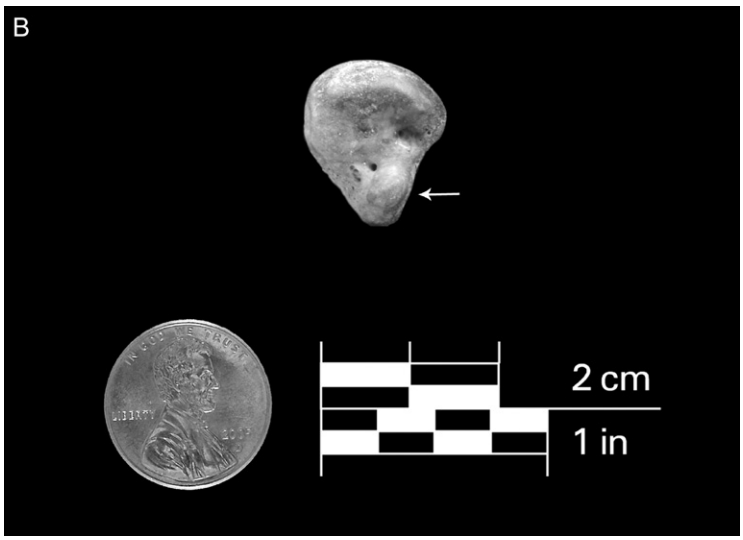

Figure 7-10: Adult human left ulna (A) anterior and posterior views; (B) distal end, inferior view. Note how this epiphysis is teardrop shaped and includes a styloid process (arrow).

Figure 7-11: Newborn human left ulna (anterior and posterior views).

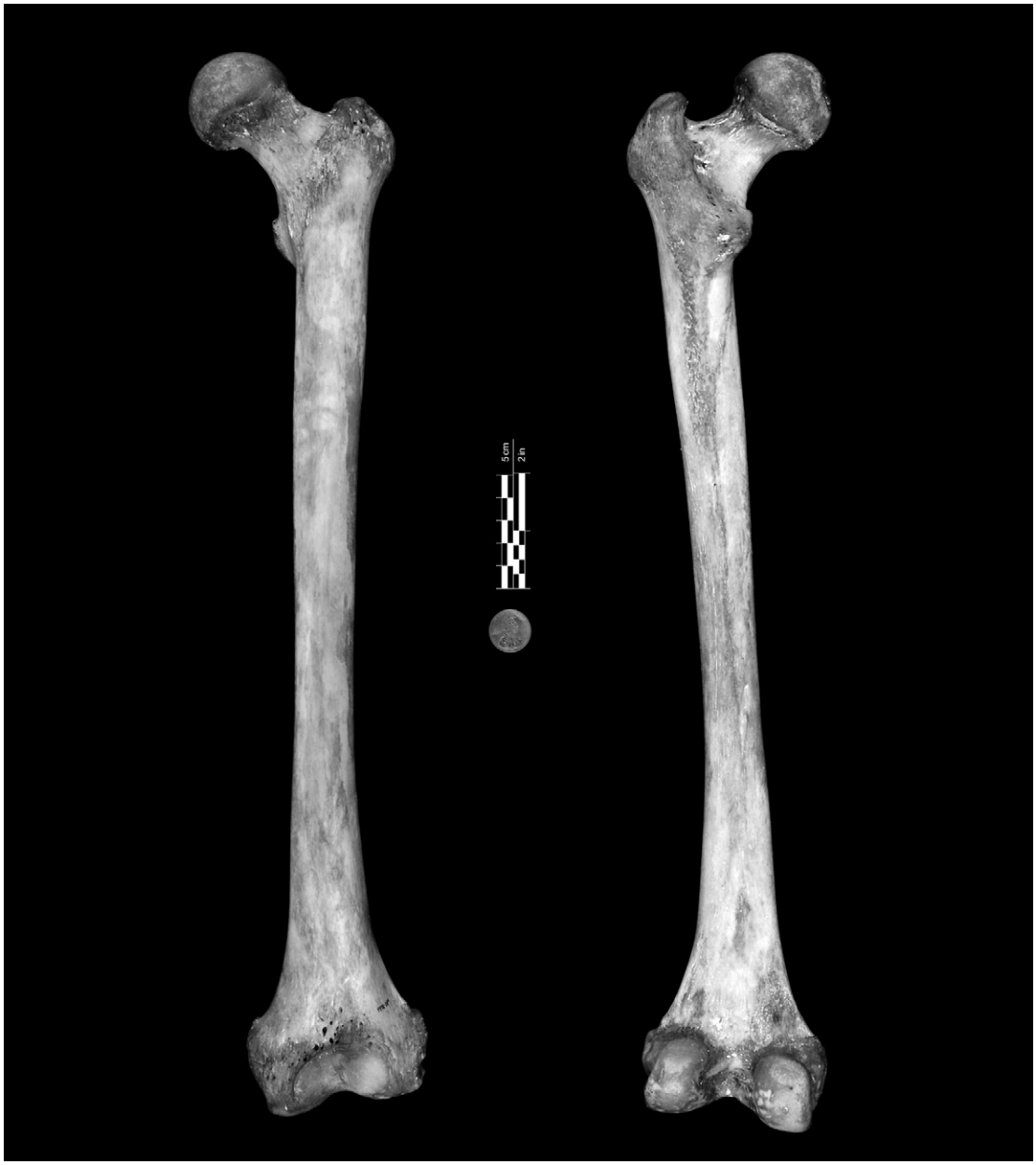

Figure 7-12: Adult human left femur (anterior and posterior views). The distal condyles of the human femur show a distinctive asymmetry that is a result of "kneeing in," or bringing the knees under the body, which occurs, because in humans the hips are widely spaced but the knees are much closer to the center of the body. This is also referred to as the valgus knee.

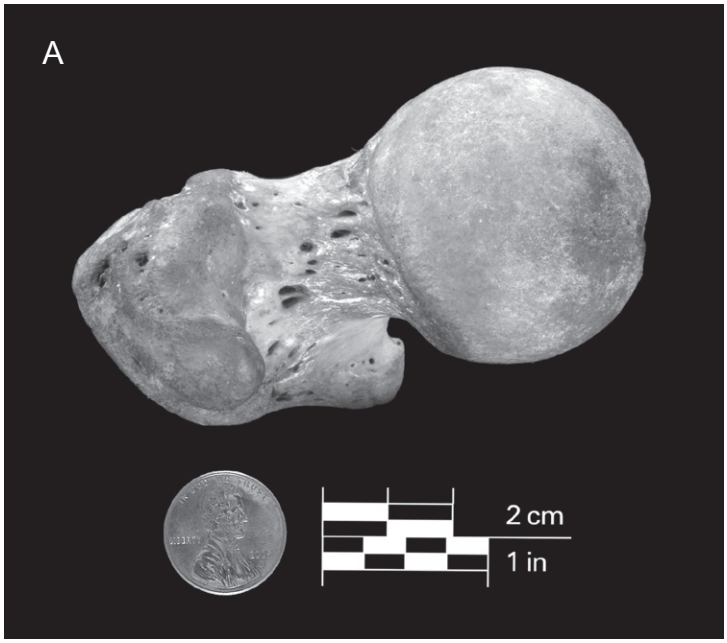

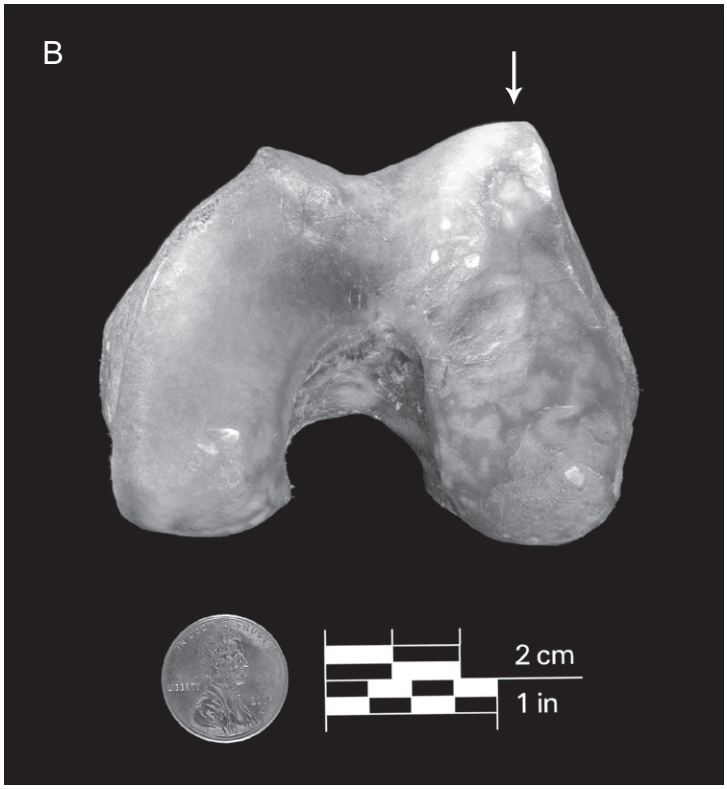

Figure 7-13: Adult human left femur (A) femoral head, greater trochanter, and lesser trochanter, superior view; (B) distal end, inferior view. Note how the articular surface is higher on the lateral surface (arrow).

Figure 7-14: Newborn human left femur (anterior and posterior views).

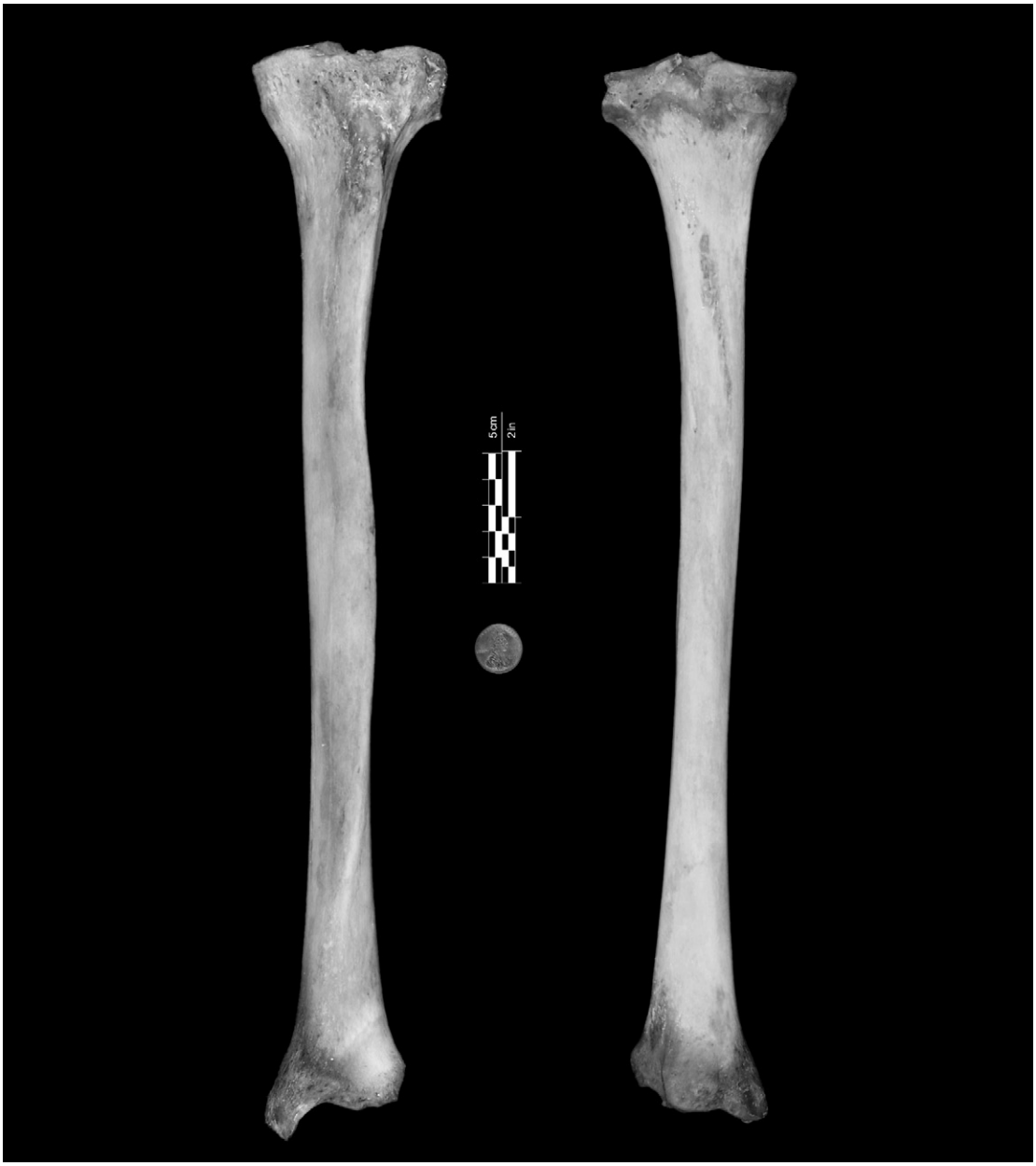

Figure 7-15: Adult human left tibia (anterior and posterior views).

Figure 7-16: Adult human left tibia (medial and lateral views).

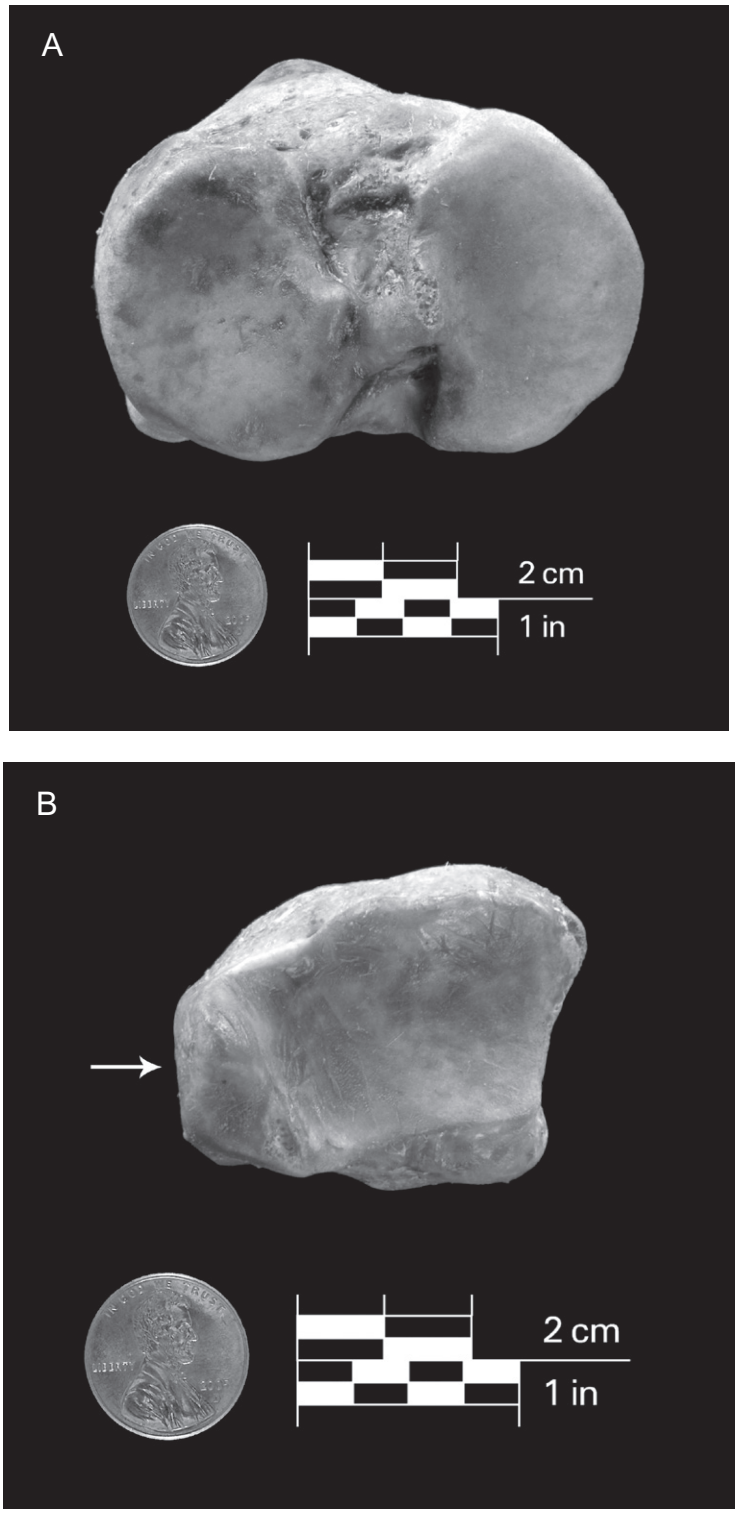

Figure 7-17: Adult human left tibia (A) proximal epiphysis, superior view; (B) distal epiphysis, inferior view. Note the location of the medial malleolus (arrow).

Figure 7-18: Newborn human left tibia (anterior and posterior views).

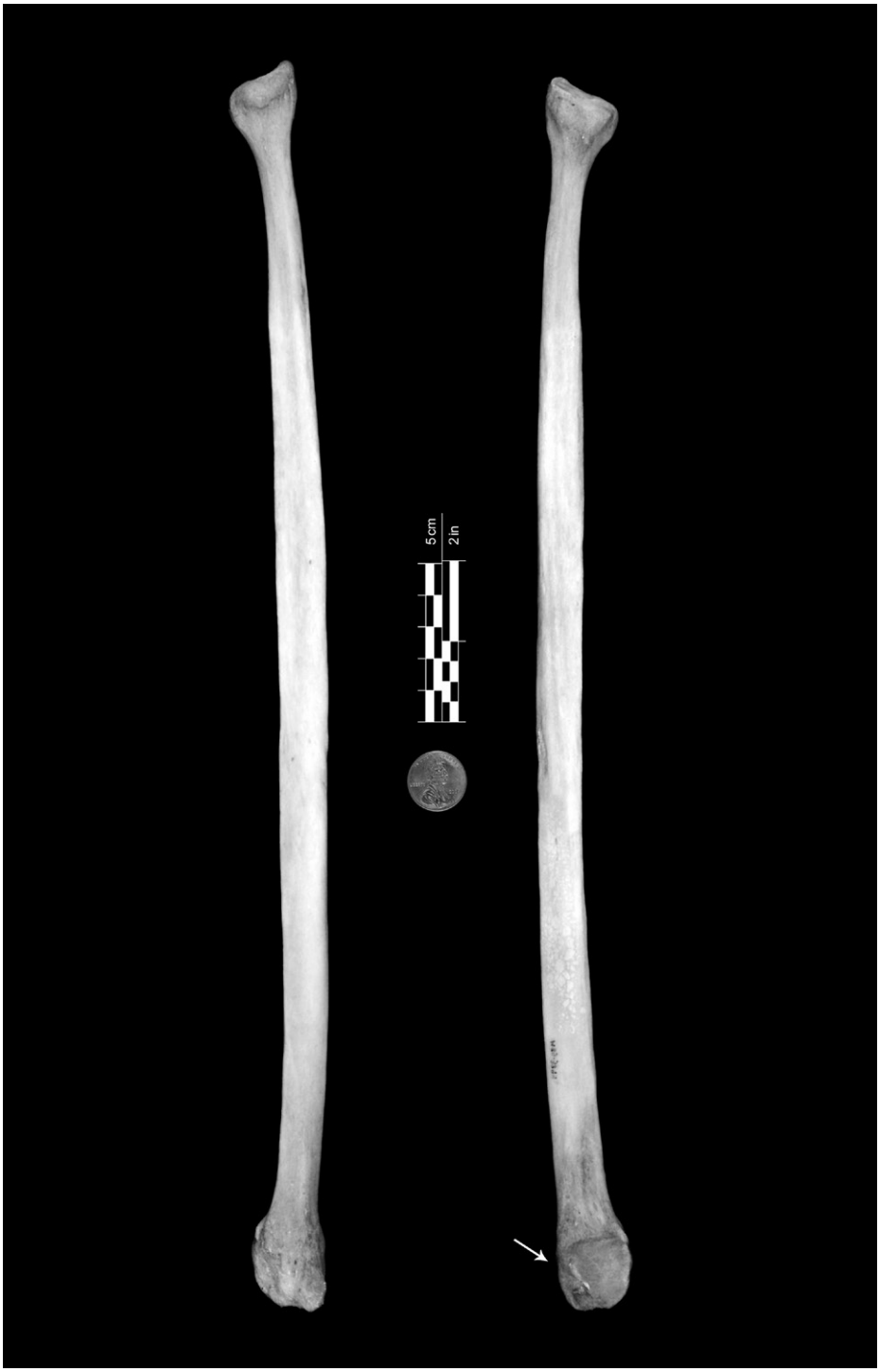

Figure 7-19: Adult human left fibula (lateral and medial views). A distinct groove (arrow) is located on the posterior aspect of the articular surface of the distal epiphysis.

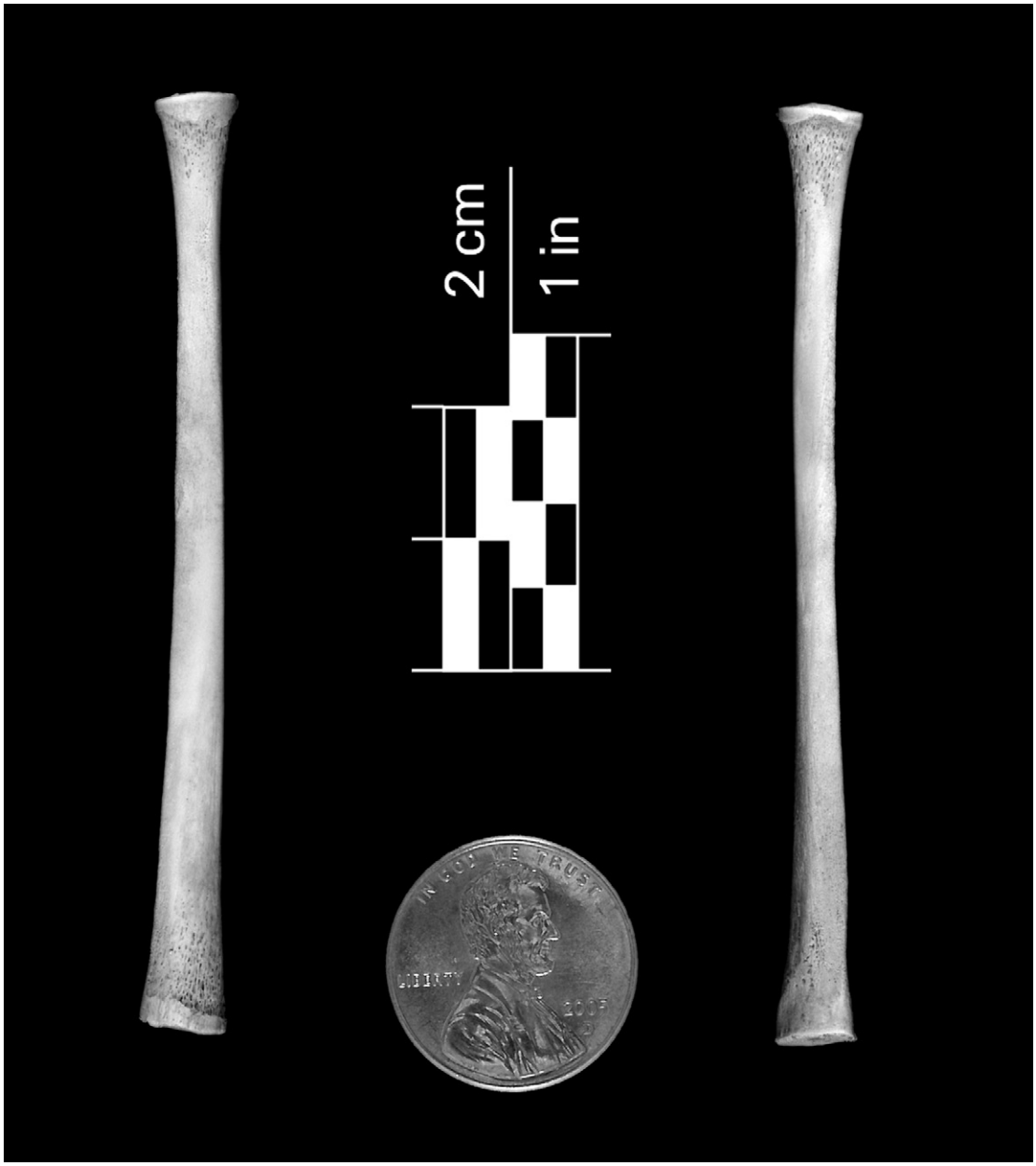

Figure 7-20: Newborn human left fibula (lateral and medial views).

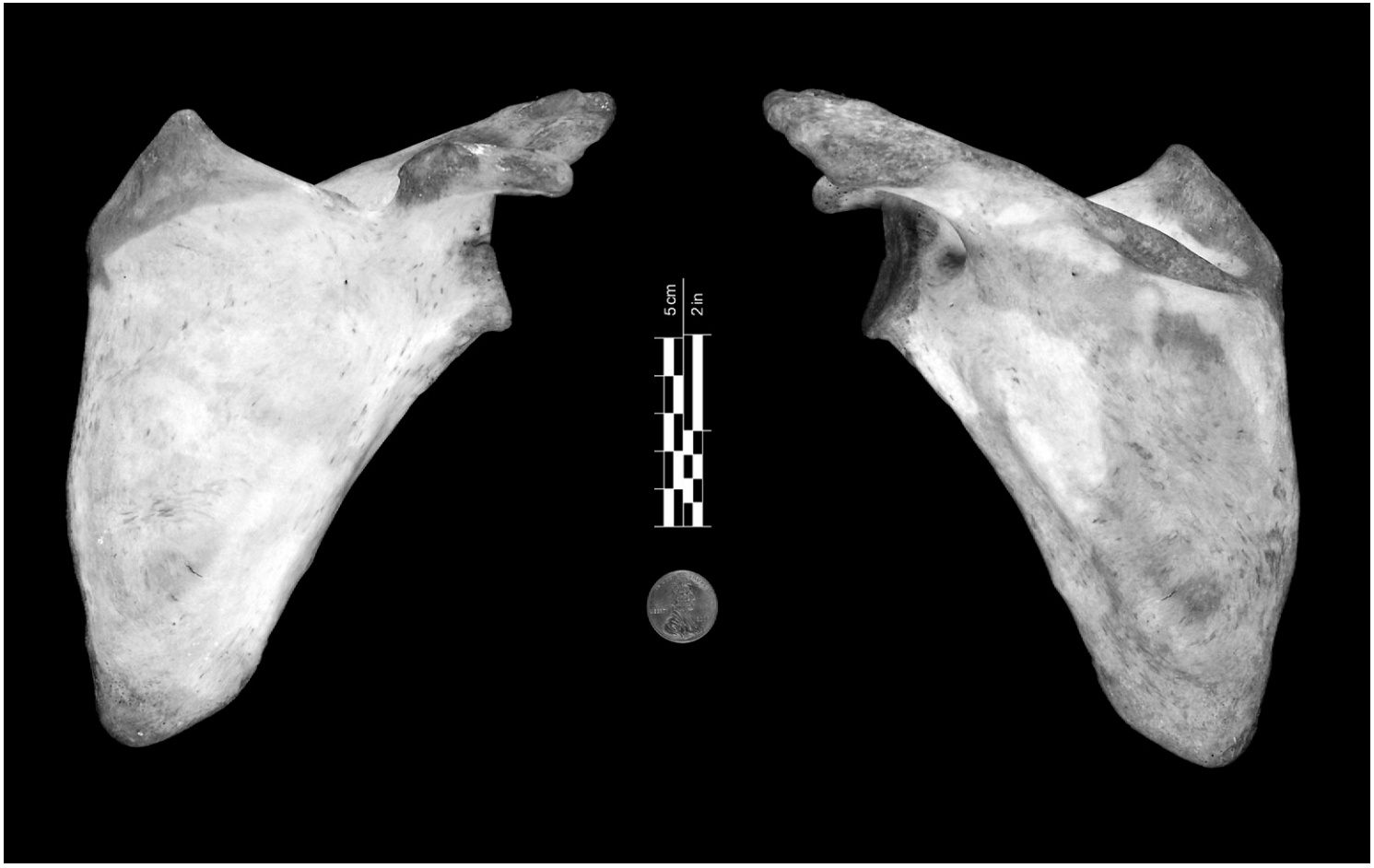

Figure 7-21: Adult human left scapula (anterior and posterior views).

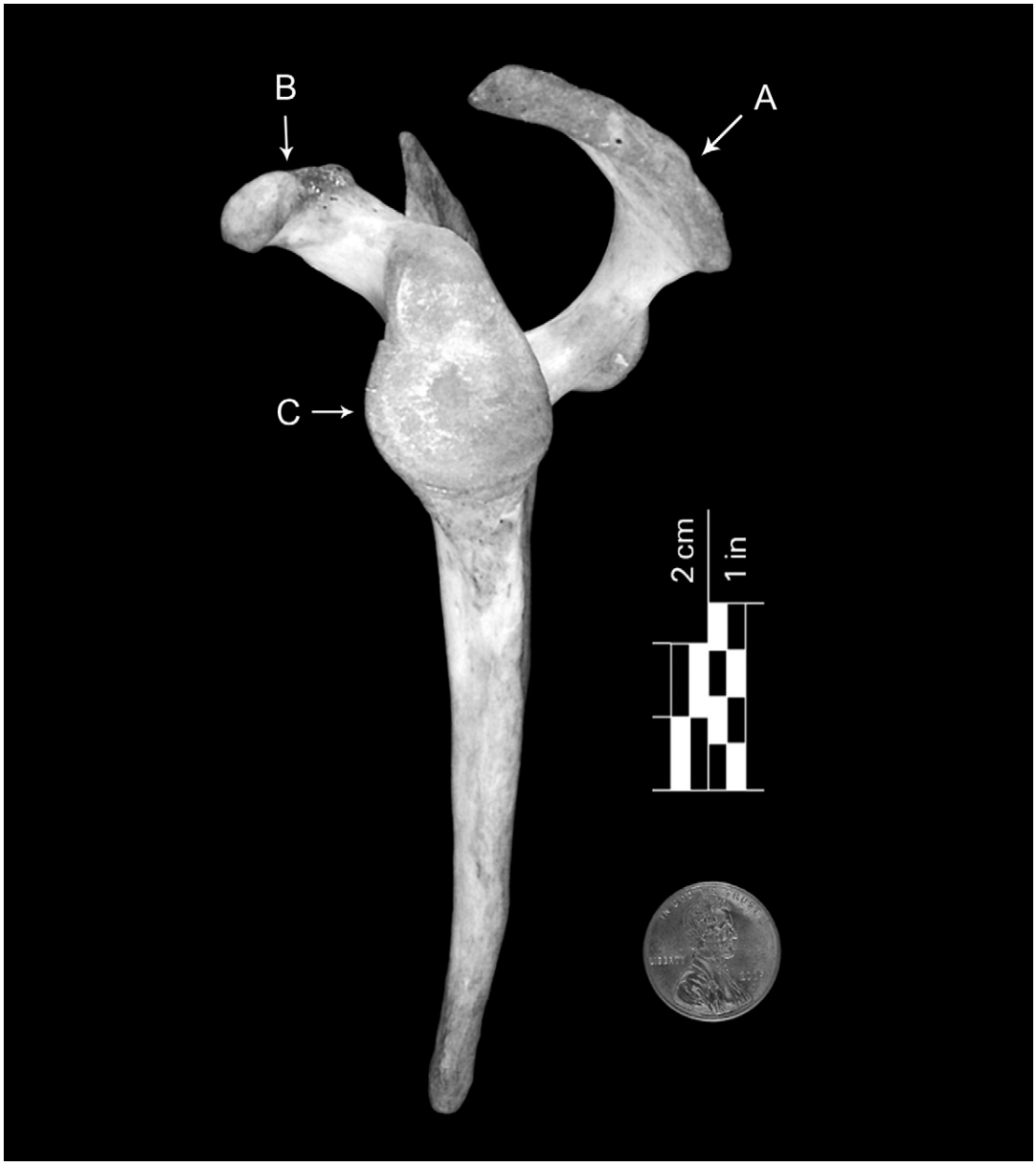

Figure 7-22: Adult human left scapula (lateral view), showing acromion process (A), coracoid process (B), and glenoid cavity (C) associated with the shoulder joint.

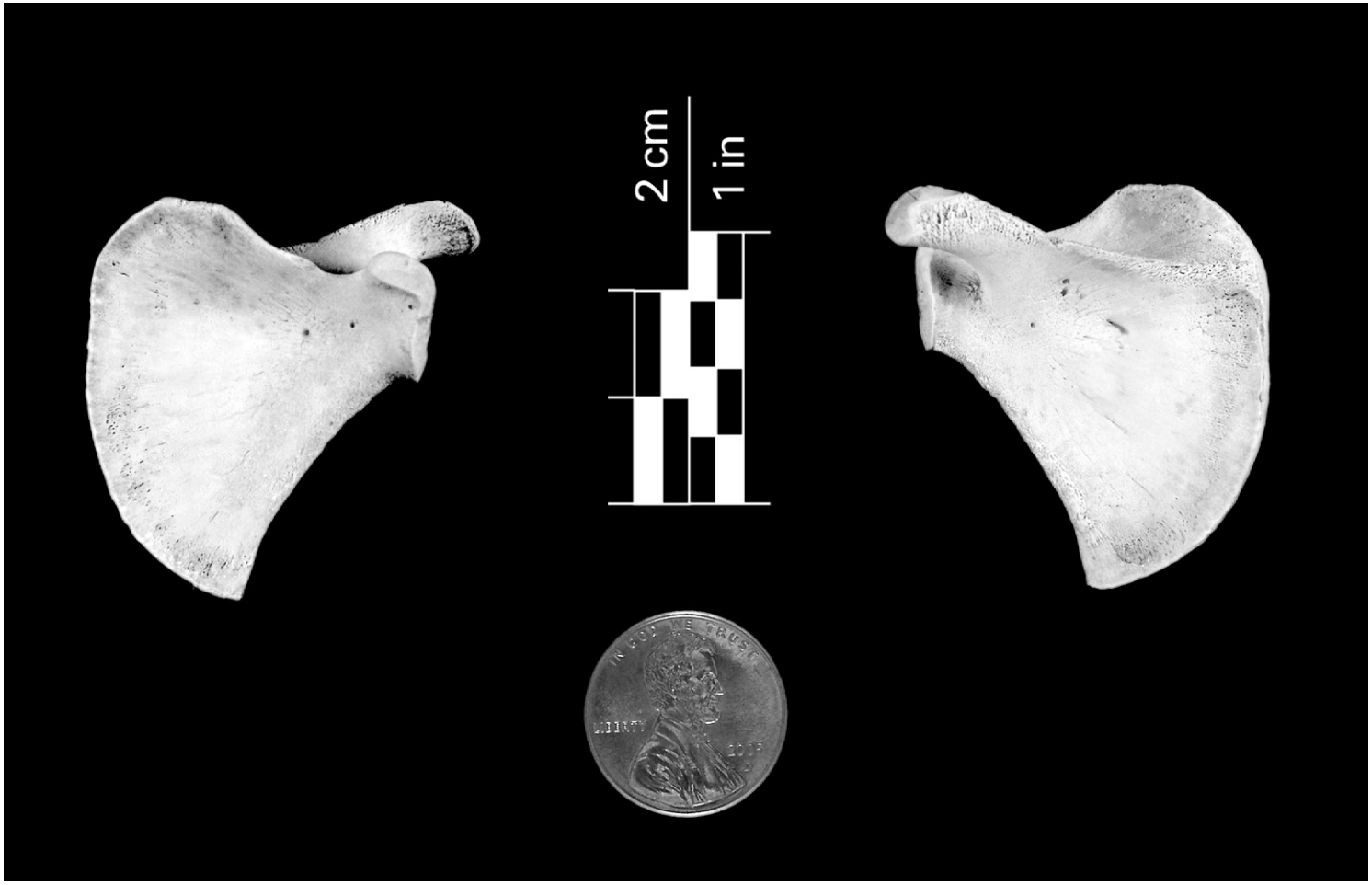

Figure 7-23: Juvenile human left scapula (anterior and posterior views).

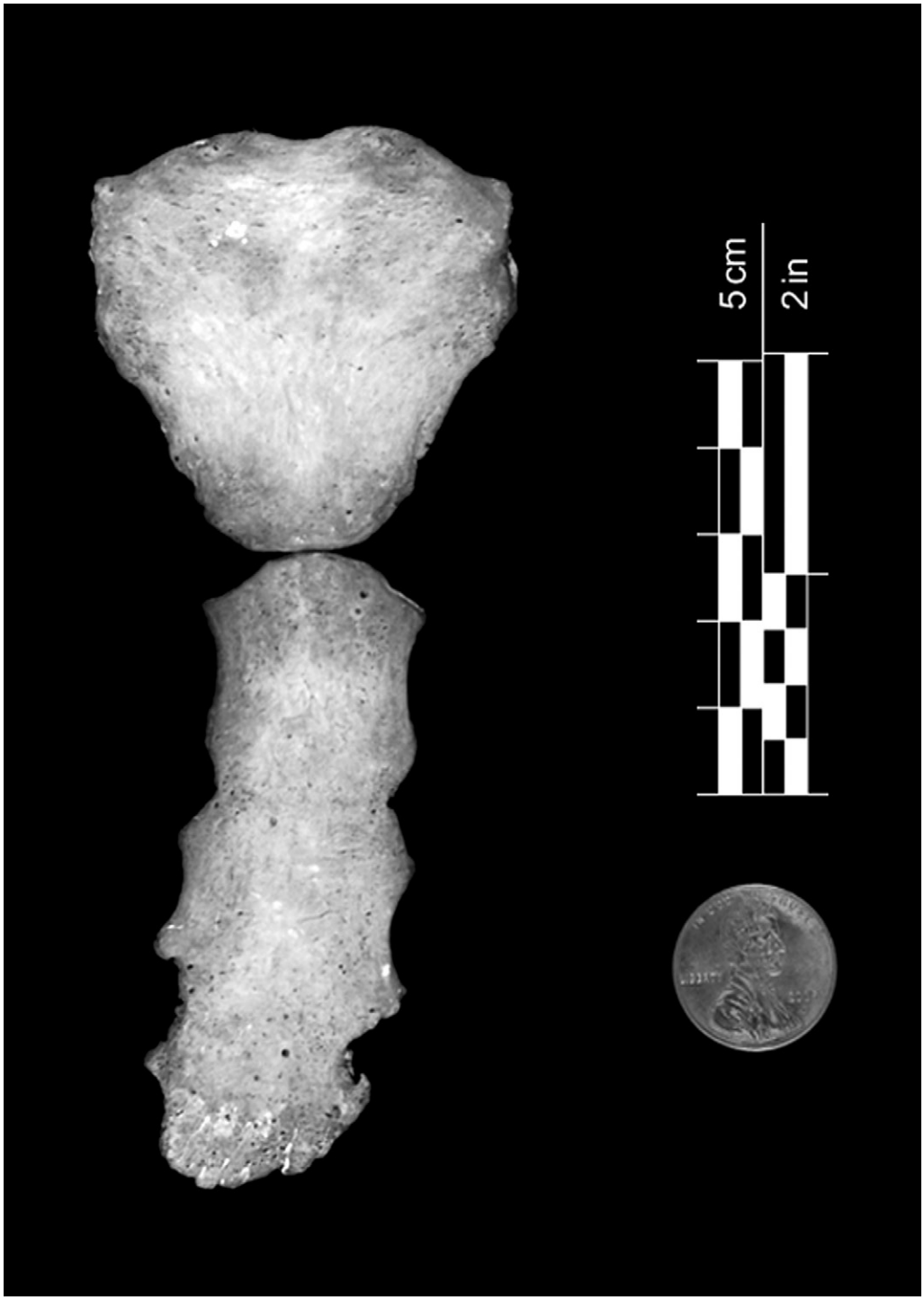

Figure 7-24: Adult human sternum (anterior view).

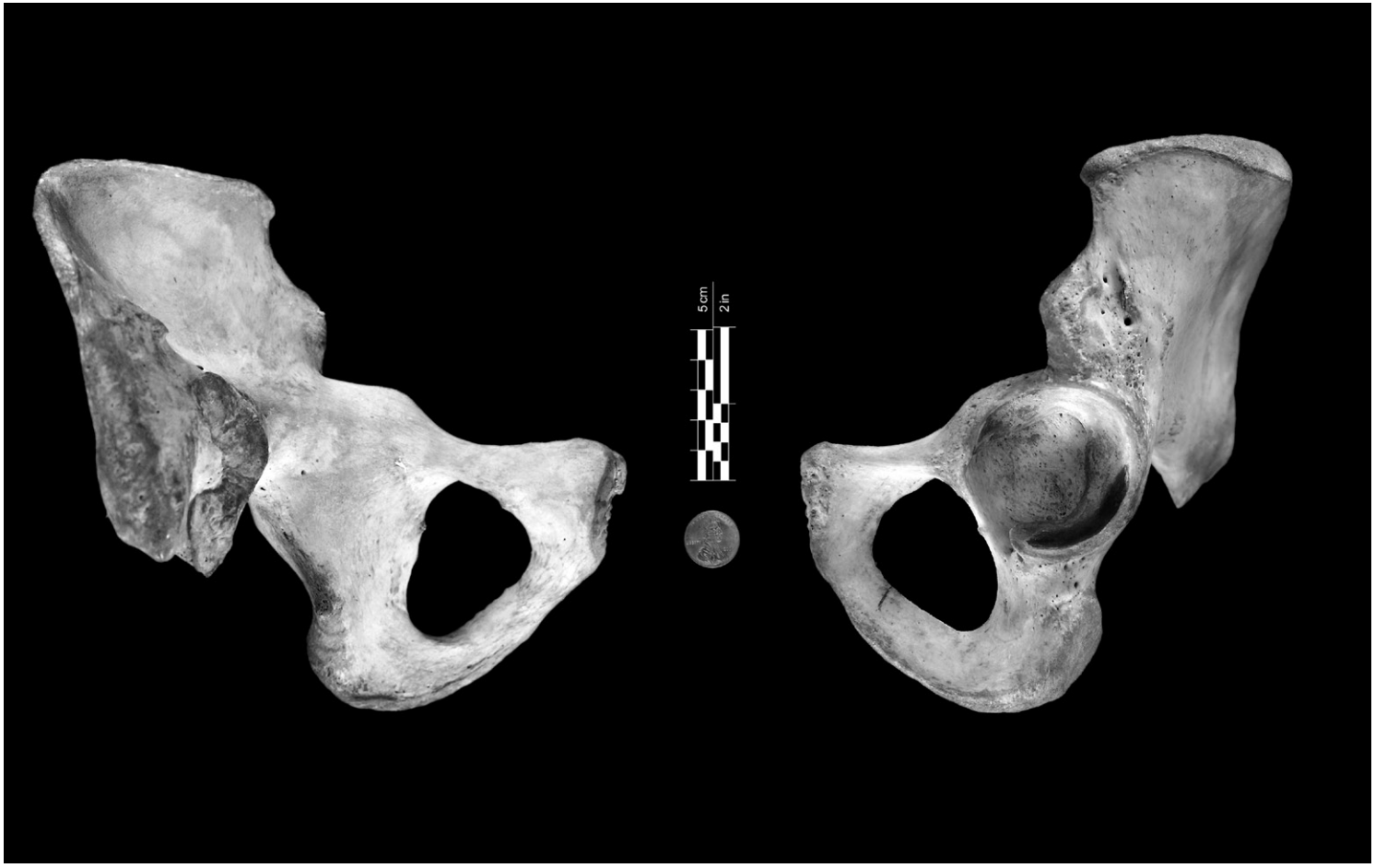

Figure 7-25: Adult human left innominate (medial and lateral views).

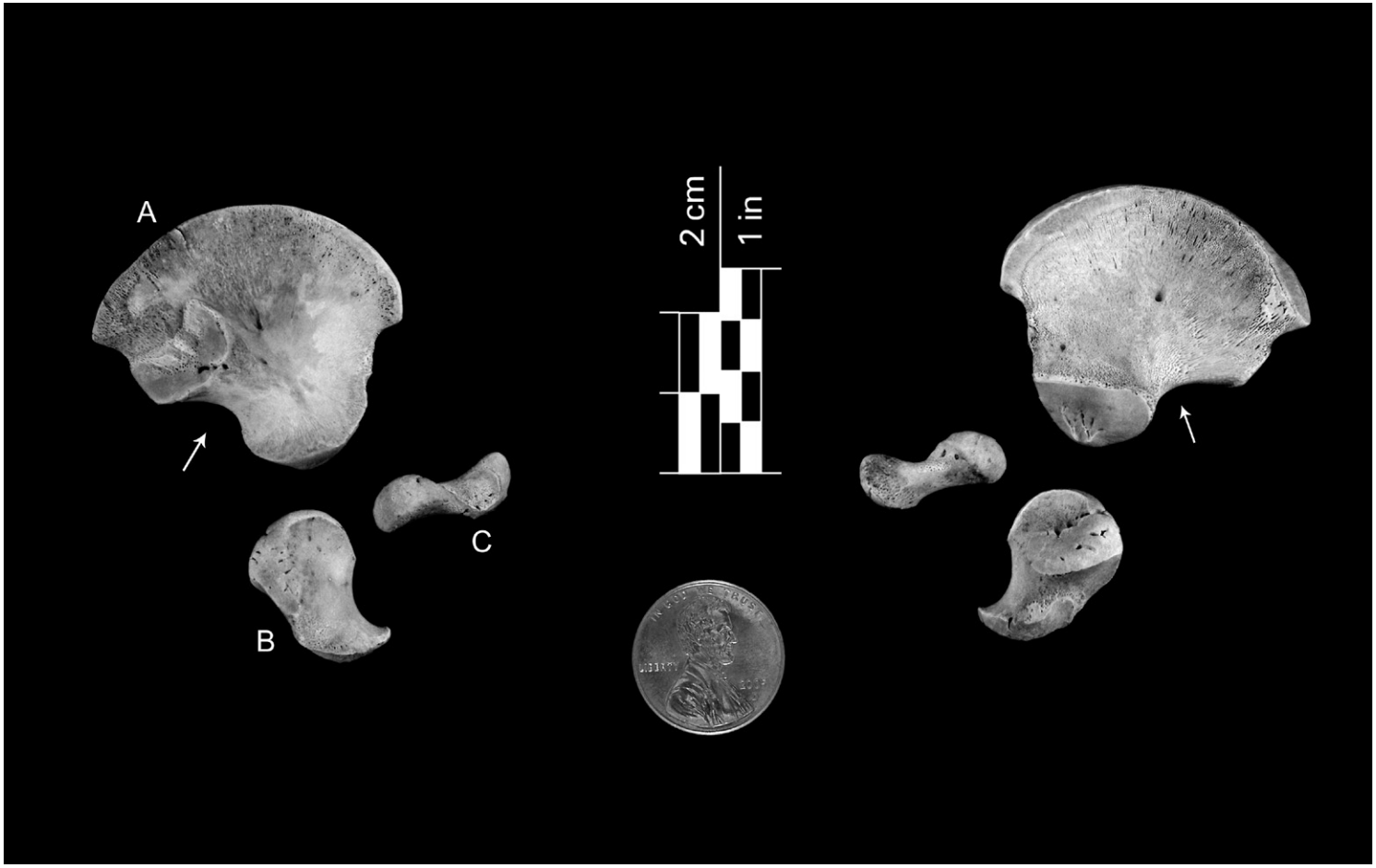

Figure 7-26: Juvenile human left innominate (medial and lateral views). Note how the ilium (A), ischium (B), and pubis (C) are separate and have not yet fused. The arrows mark the location of the sciatic notch.

Figure 7-27: Adult human sacrum (anterior and posterior views).

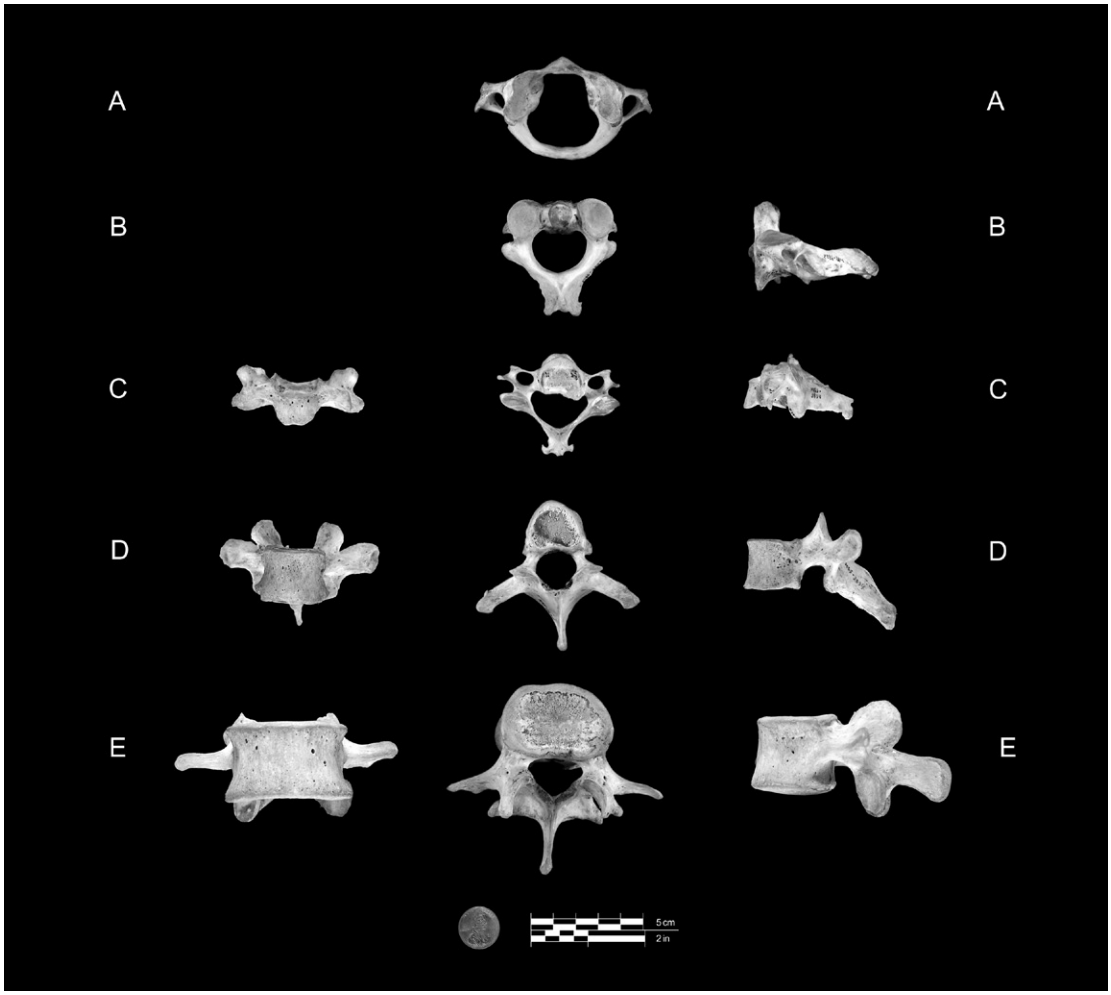

Figure 7-28: Adult human vertebrae: atlas (A), axis (B), and examples of typical cervical (C), thoracic (D), and lumbar (E) vertebrae. Images on the left are anterior, middle are superior, and right are lateral.

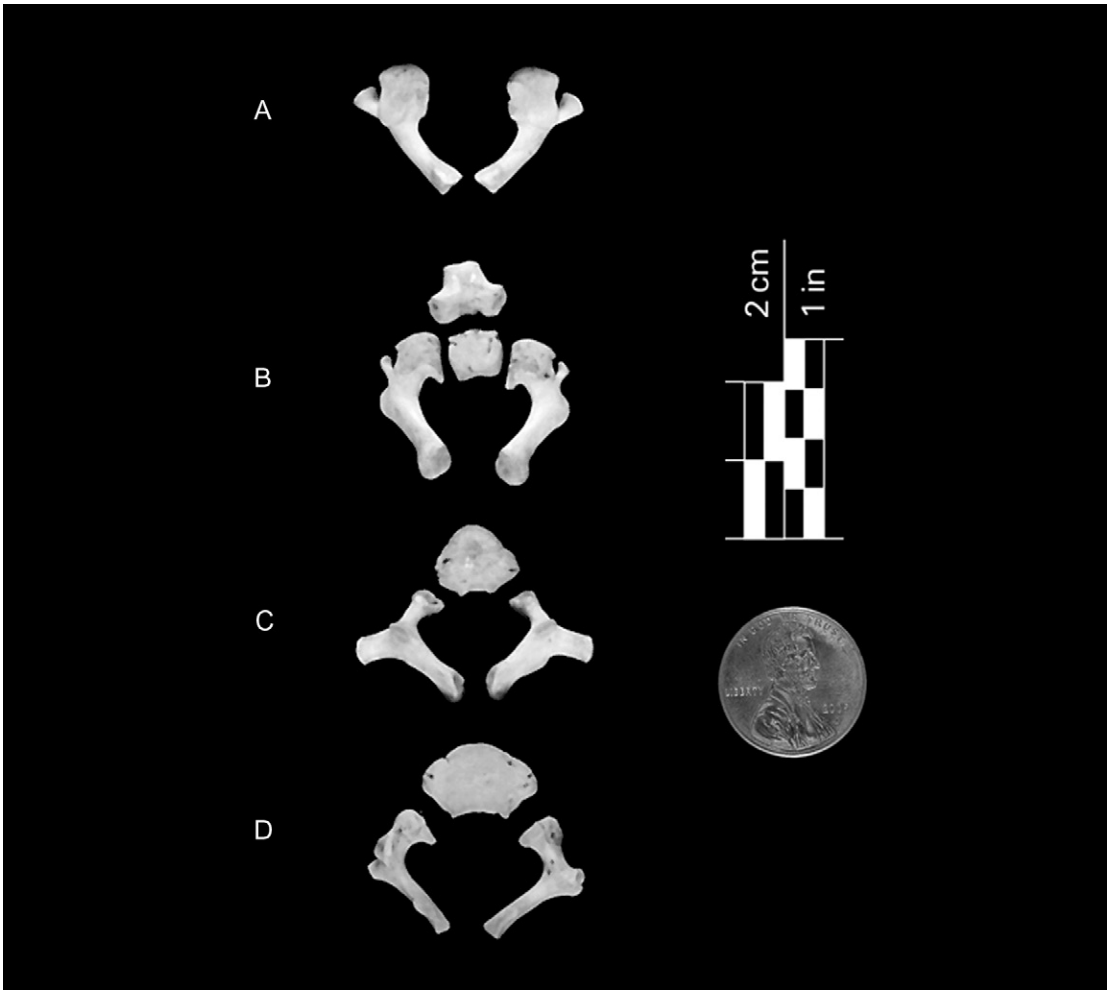

Figure 7-29: Newborn human vertebrae: atlas (A), axis (B), and examples of thoracic (C) and lumbar (D) vertebrae. Note how the centra are not yet fused to the vertebral/neural arches.

Figure 7-30: Human left metacarpals (anterior views). Each metacarpal is numbered corresponding to its anatomical location (e.g., "1" is the first metacarpal). The distal ends of the bones are pictured at the top of the photograph.

Figure 7-31: Human left metatarsals (superior views). Each metatarsal is numbered corresponding to its anatomical location (e.g., "5" is the fifth metatarsal). The distal ends of the bones are pictured at the top of the photograph.

Figure 7-32: Adult human left talus and calcaneus (superior views).

This page intentionally left blank

CHAPTER 8

Horse (Equus caballus)

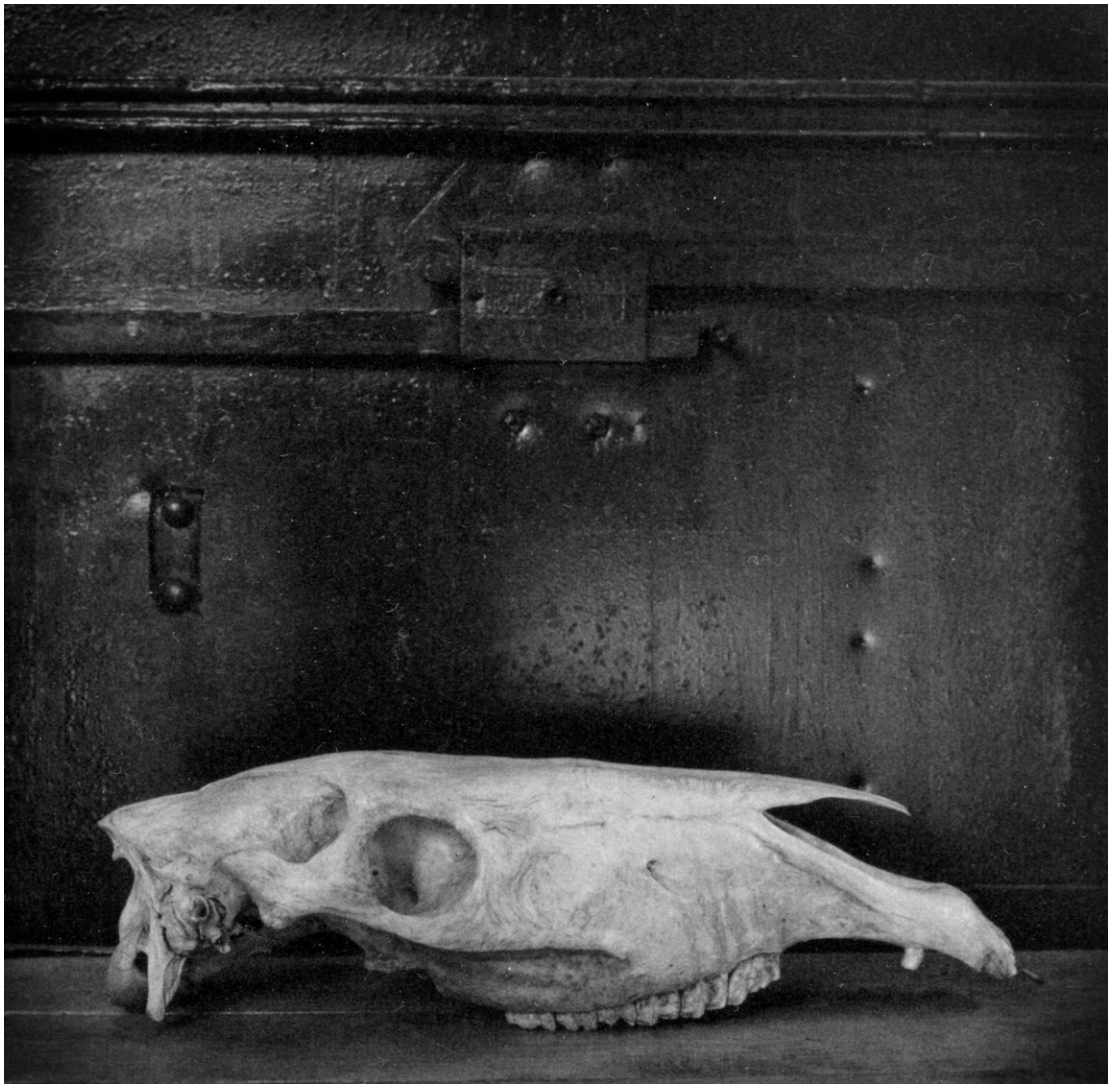

Comparative Osteology. DOI: 10.1016/B978-0-12-388437-4.00008-9

Figure 8-01: Horse cranium (A) lateral view, right side; (B) ventral view. The horse's dental formula is 3/3.0-1/0-1.3/3.3/3. Canines are usually seen only in males. Wear on horse incisors can be used as an indication of age.

Figure 8-02: A human left humerus (anterior view) is compared to a horse's left humerus (cranial view). The proximal end of the horse's humerus includes an intermediate tubercle (arrow), which is not seen on the human humerus.

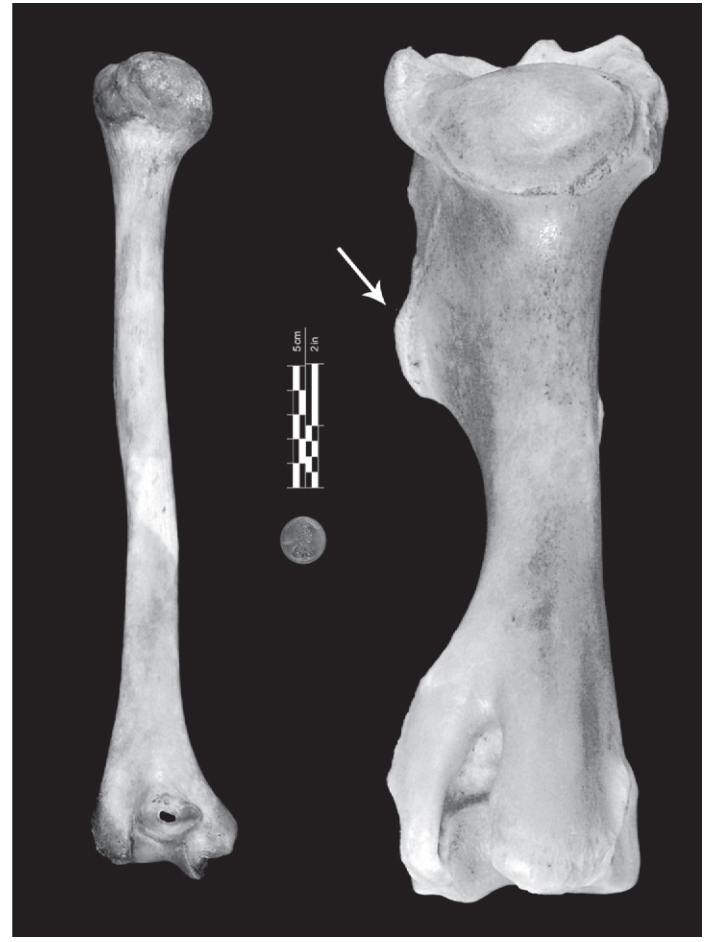

Figure 8-03: A human left humerus (posterior view) is compared to a horse's left humerus (caudal view). The shaft of the horse's humerus has a large deltoid tuberosity (arrow).

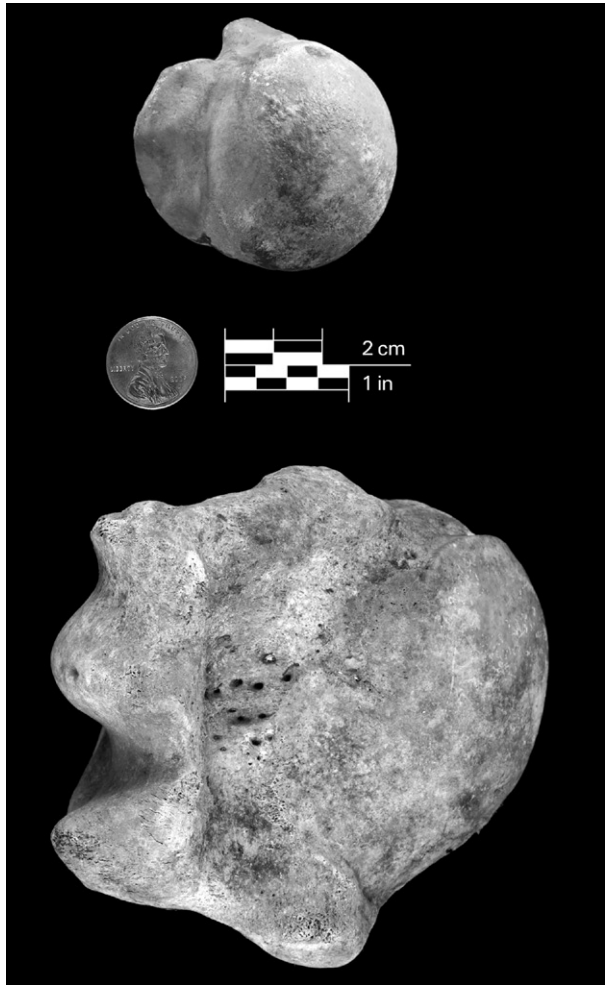

Figure 8-04: An adult human proximal humerus (superior view) is compared to a horse's proximal humerus (dorsal view).

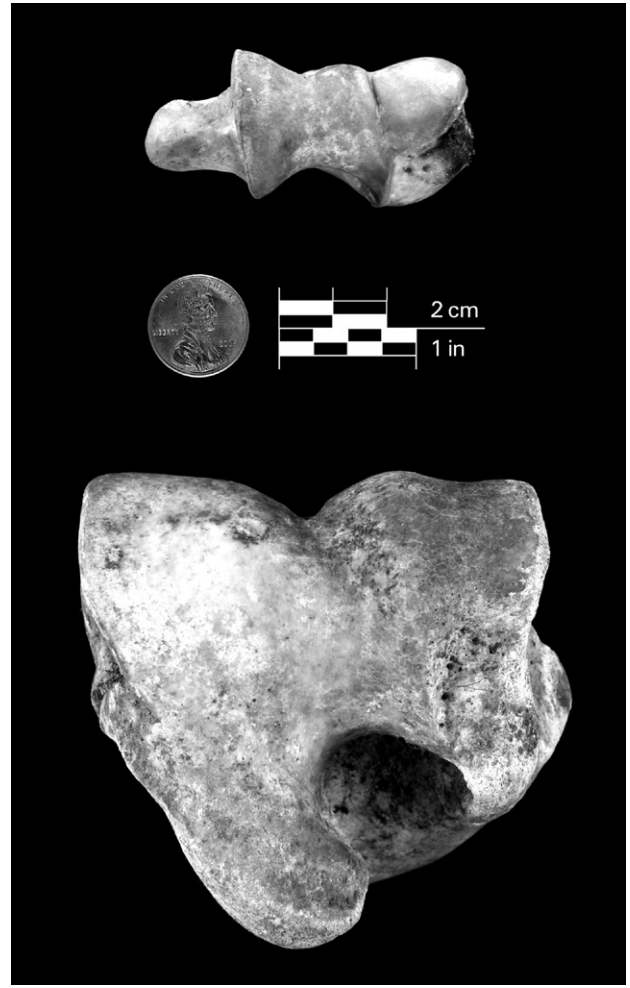

Figure 8-05: An adult human distal humerus (inferior view) is compared to a horse's distal humerus (ventral view). The horse's barrel-shaped trochlea and the olecranon fossa are visible in this view.

Figure 8-06: A human left radius and ulna (anterior views) are compared to a horse's radius and ulna (cranial view). Note the large olecranon process on the horse's ulna (arrow).

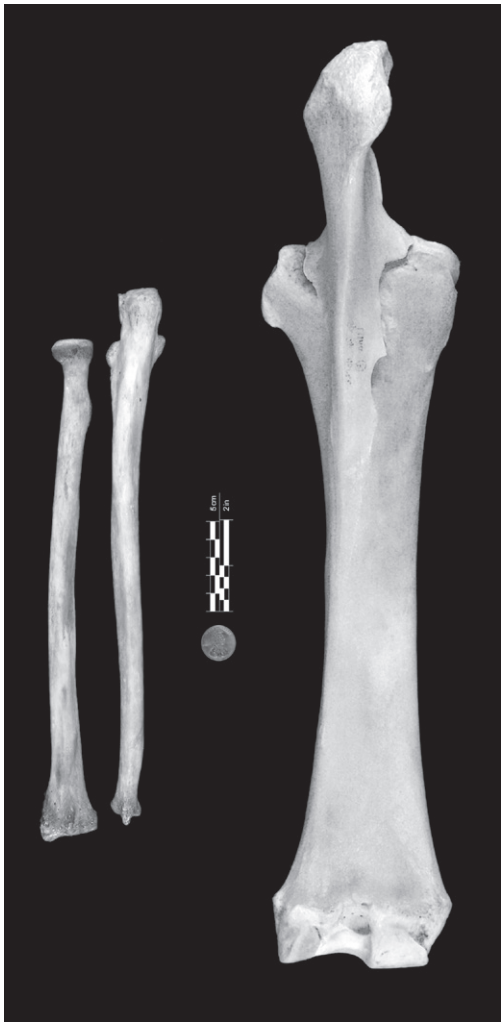

Figure 8-07: A human left radius and ulna (posterior views) are compared to a horse's radius and ulna (caudal view). The horse's ulna is partially fused to the radius in adults.

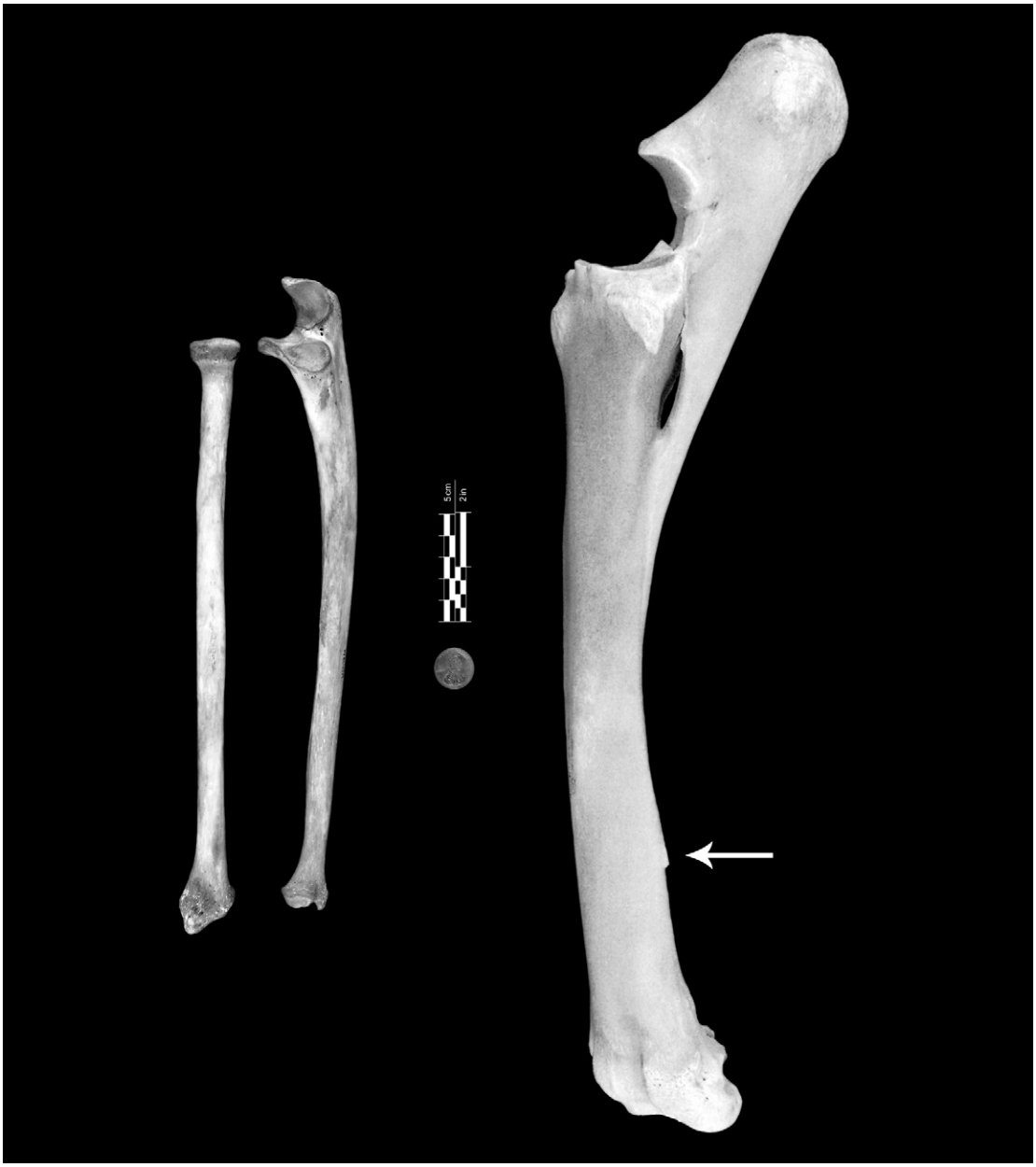

Figure 8-08: A human left radius and ulna (lateral views) are compared to a horse's radius and ulna (lateral view). Note that the horse's ulna tapers to a point about two thirds of the way down the shaft of the radius (arrow).

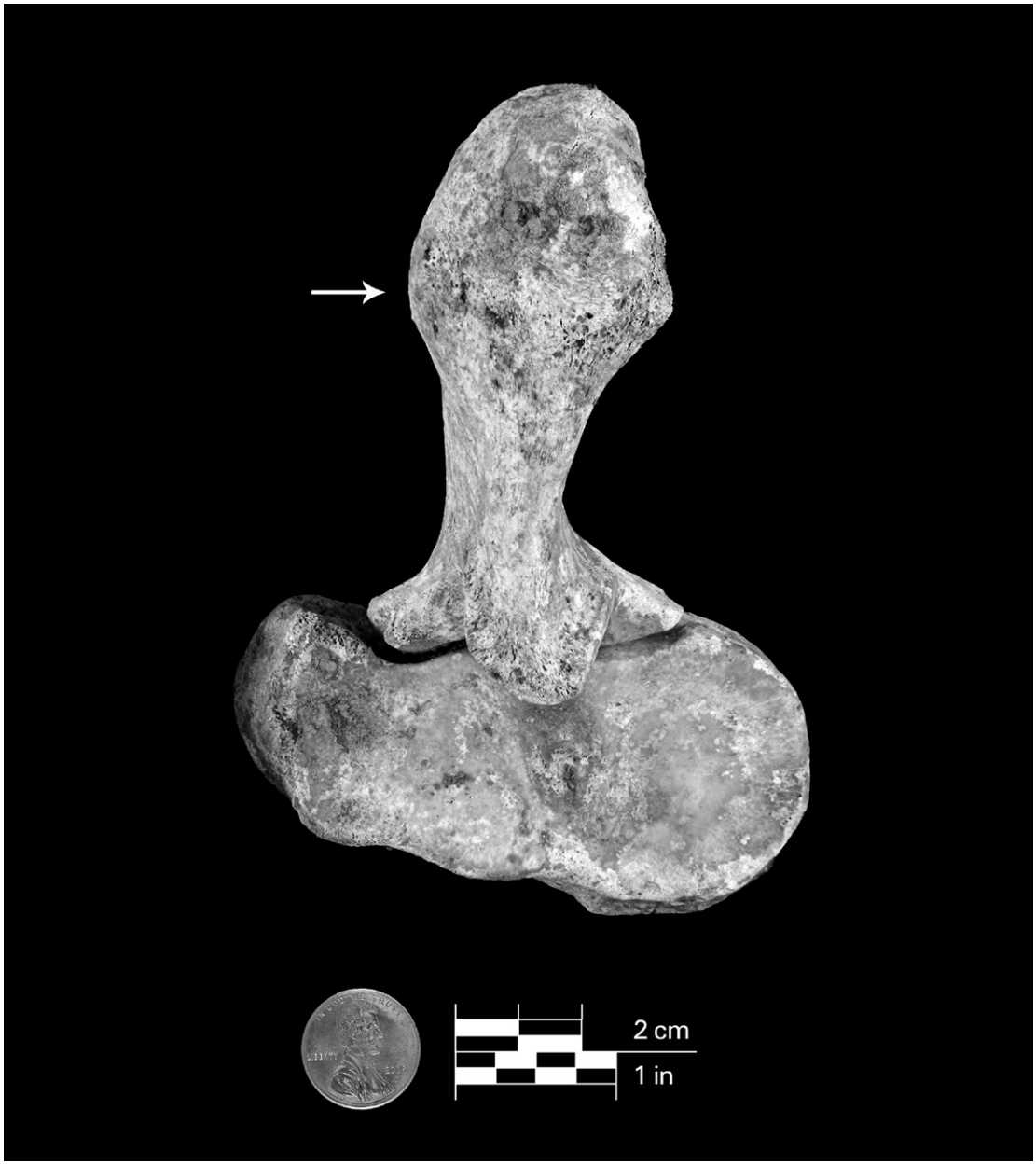

Figure 8-09: Horse proximal radius and ulna (left side, dorsal view). The olecranon process of the proximal ulna (arrow) is visible in this view.

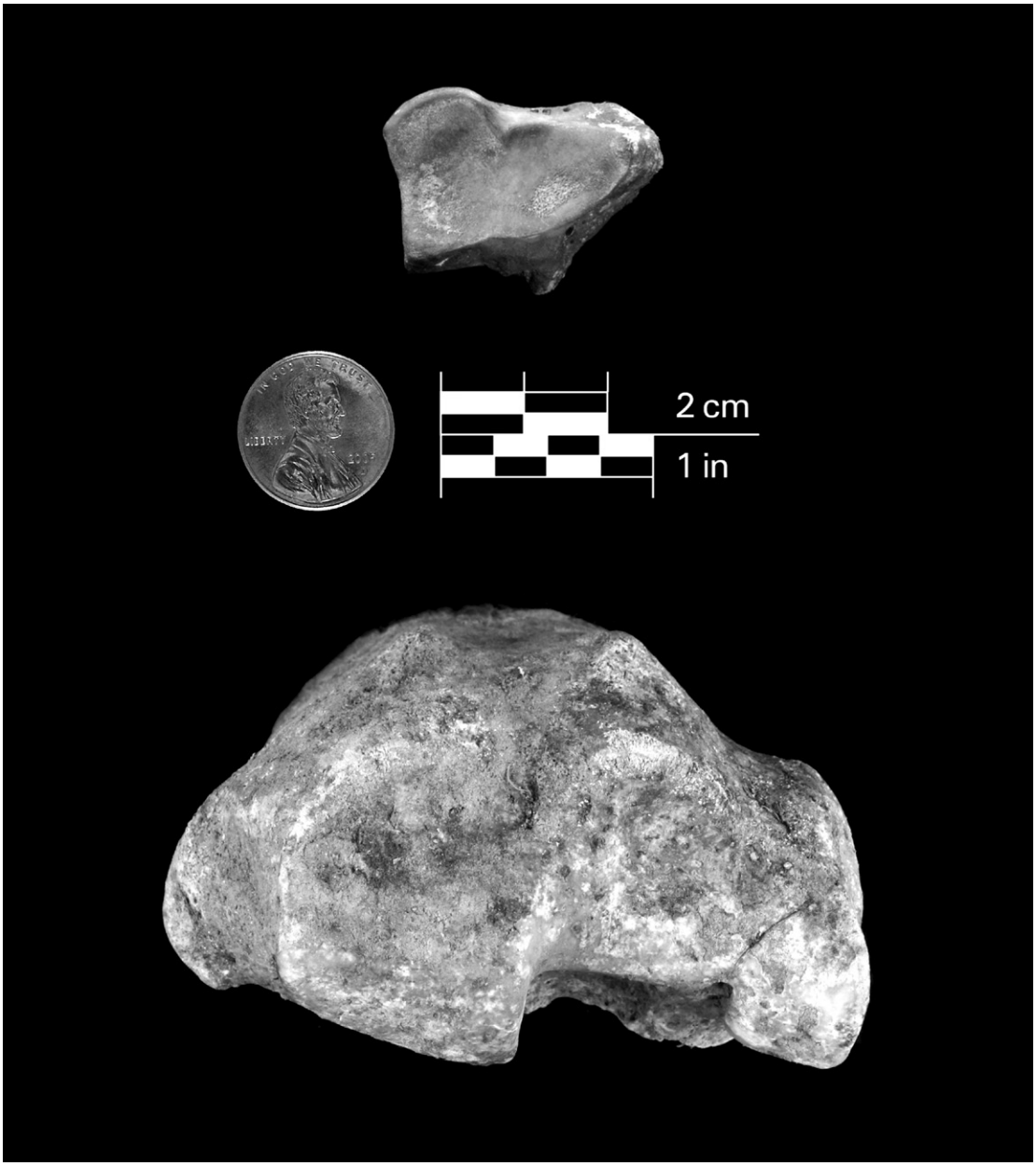

Figure 8-10: A human left distal radius (inferior view) is compared to a horse's left distal radius (ventral view). The articular facets for the horse's first carpal row are visible in this view.

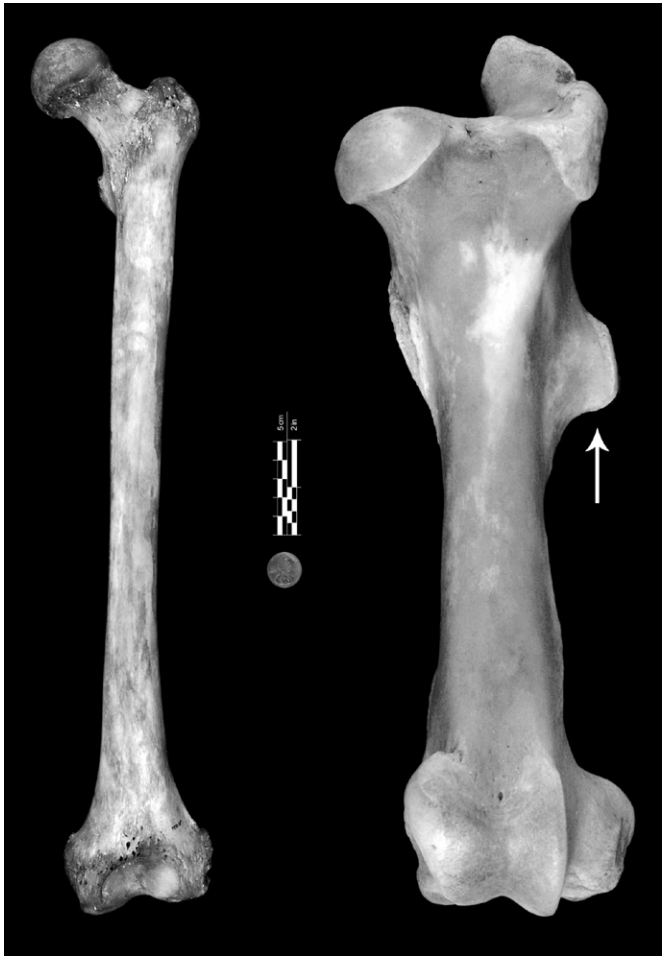

Figure 8-11: A human left femur (anterior view) is compared to a horse's left femur (cranial view). The horse's femur shows a well-developed third trochanter (arrow).

Figure 8-12: A human left femur (posterior view) is compared to a horse's left femur (caudal view).

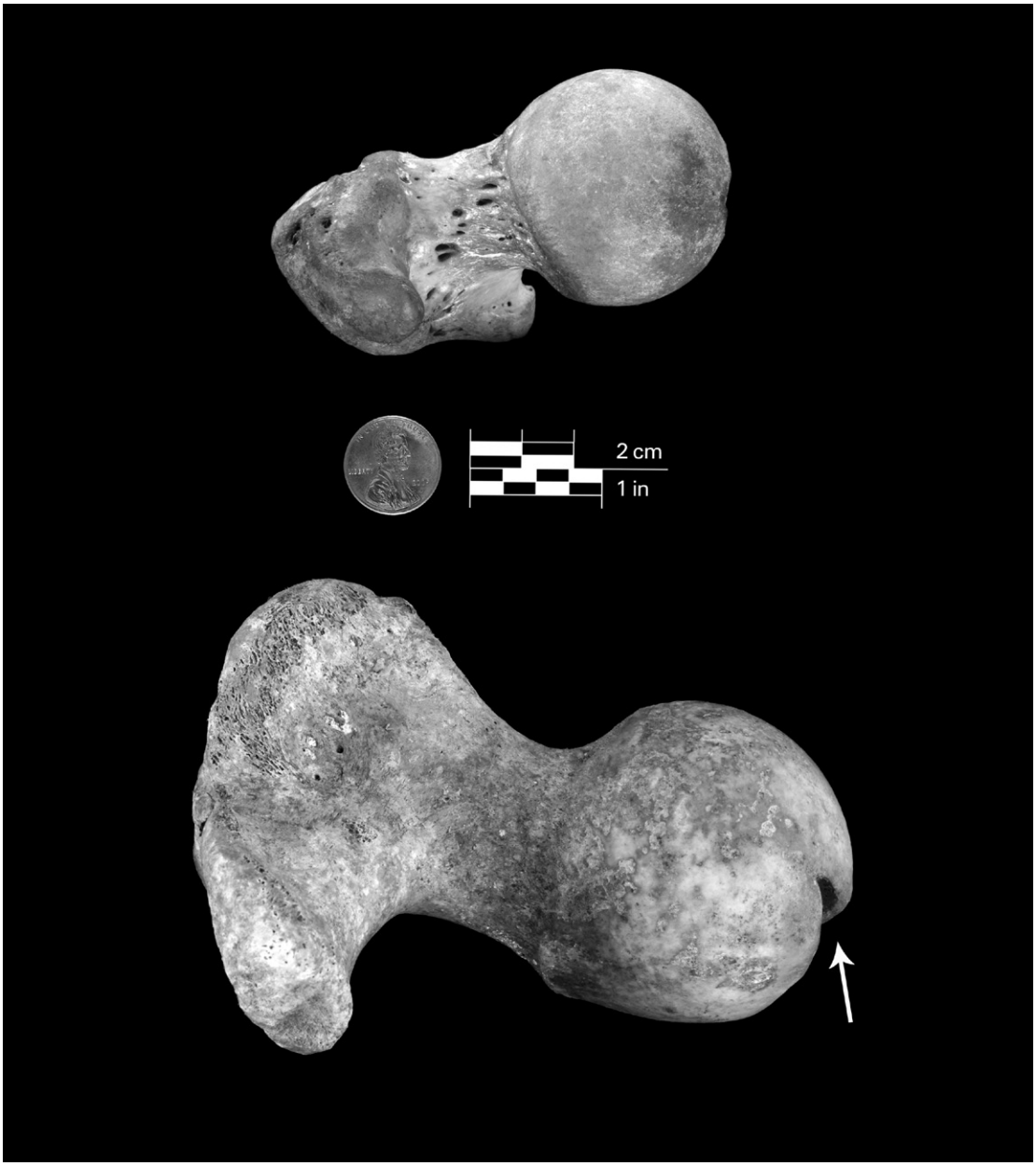

Figure 8-13: A human left proximal femur (superior view) is compared to a horse's left proximal femur (dorsal view). The head and the greater trochanter are visible in this view. The arrow points to the large, V-shaped fovea capitis that is distinctive in horses.

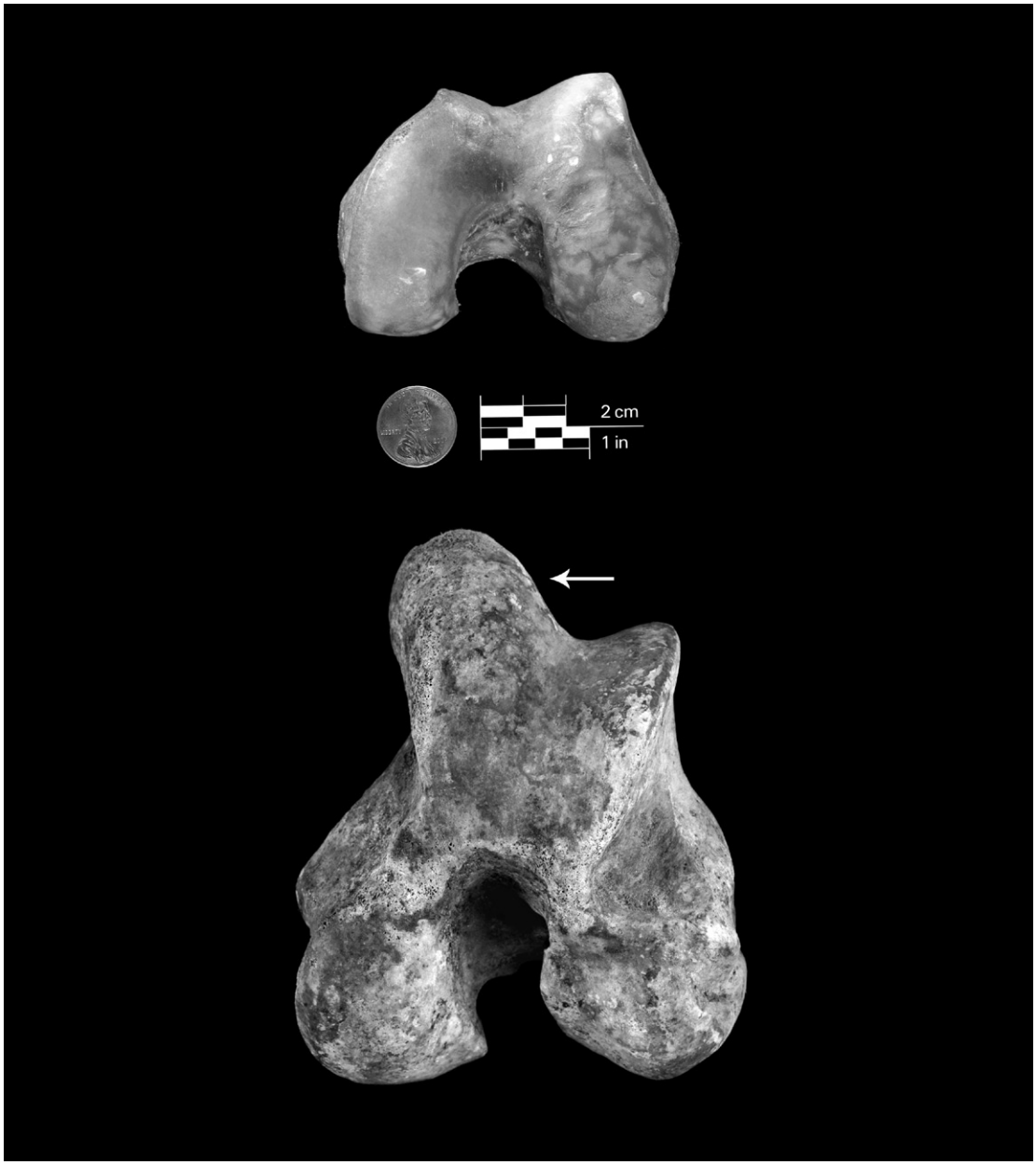

Figure 8-14: A human left distal femur (inferior view) is compared to a horse's left distal femur (ventral view). The distal condyles and the trochlea (patellar surface) are visible in this view. Note the enlarged medial portion of the horse's trochlea (arrow). This can be used to distinguish the horse femur from the cow femur.

Figure 8-15: A human left tibia (anterior view) is compared to a horse's left tibia (cranial view). The horse distal tibia includes both a medial and a lateral malleolus. The lateral malleolus is the evolutionary remnant of the distal fibula (arrow).

Figure 8-16: A human left tibia (posterior view) is compared to a horse's left tibia (caudal view).

Figure 8-17: A human left tibia (lateral view) is compared to a horse's left tibia (lateral view).

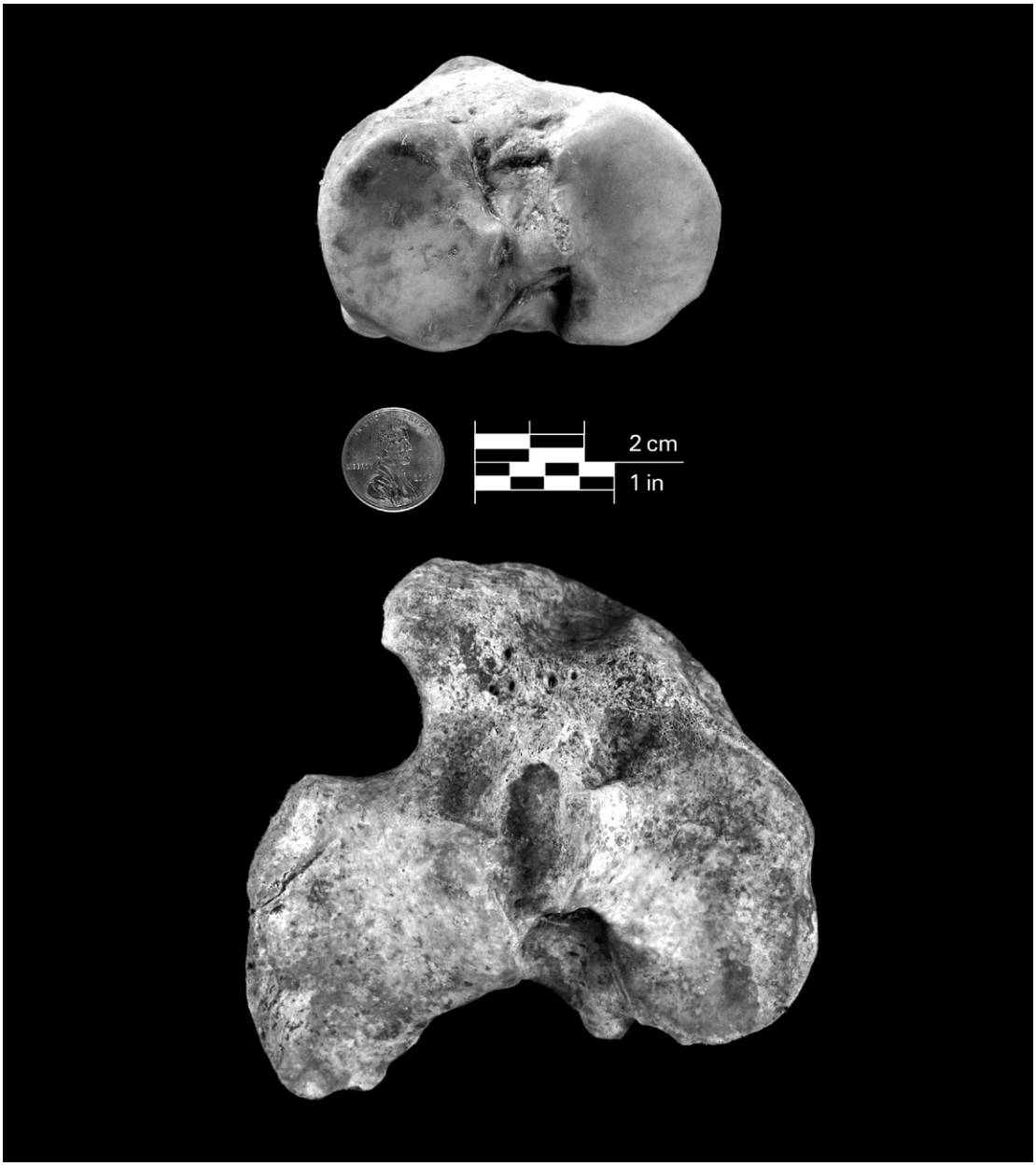

Figure 8-18: An adult human left proximal tibia (superior view) is compared to a horse's left proximal tibia (dorsal view). The two large facets for articulation with the condyles of the femur are visible in this view.

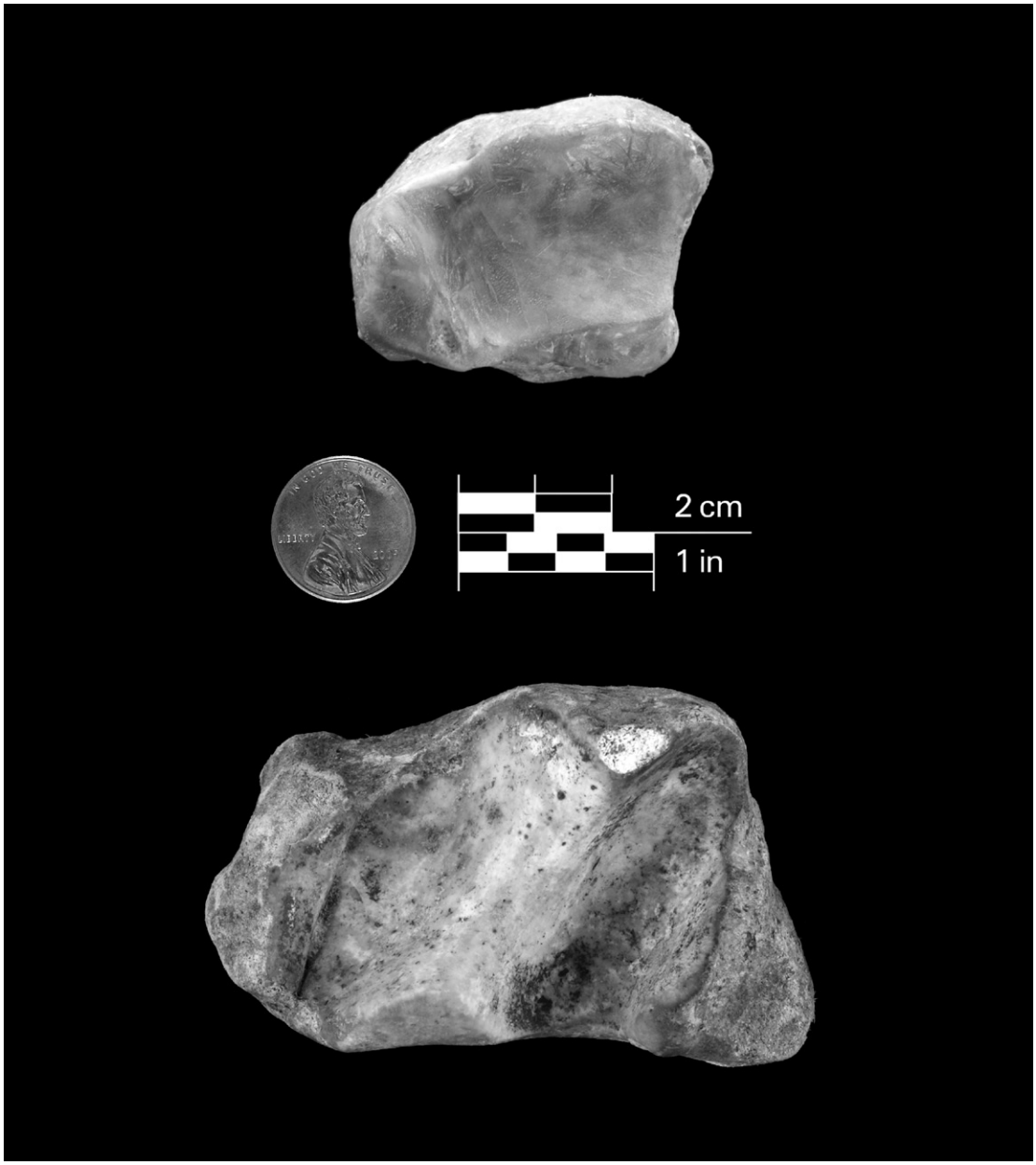

Figure 8-19: An adult human left distal tibia (inferior view) is compared to a horse's left distal tibia (ventral view). Note that in the horse the two facets for the articulation of the astragalus are oriented obliquely.

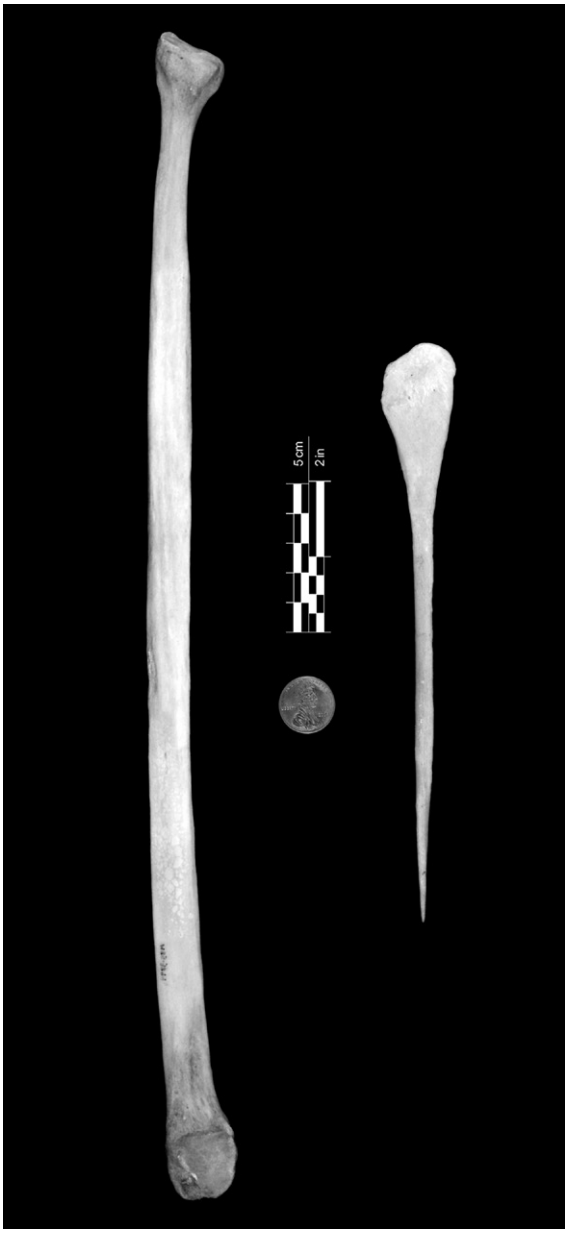

Figure 8-20: A human left fibula (medial view) is compared to a horse's left fibula (lateral view). The horse's fibula is greatly reduced. The rounded head is transversely flattened, and the shaft tapers to a point.

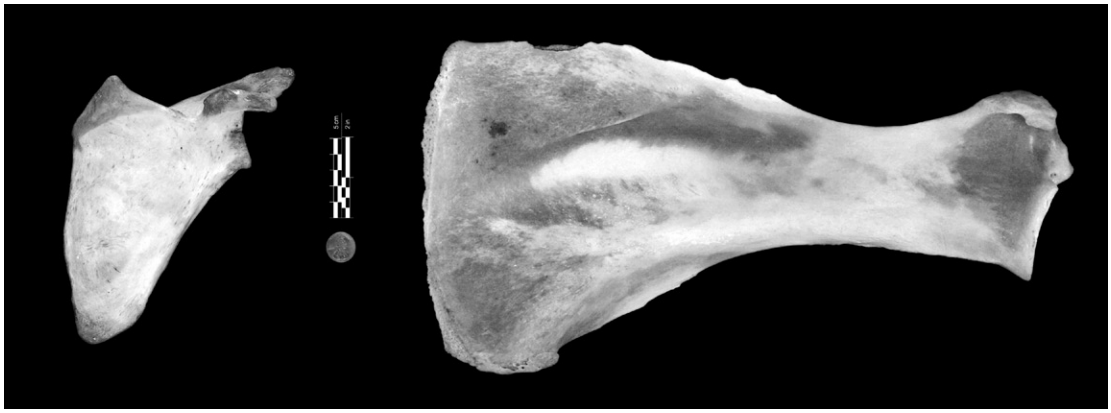

Figure 8-21: A human left scapula (anterior view) is compared to a horse's left scapula (medial view). Both scapulae are oriented as they would be in a human.

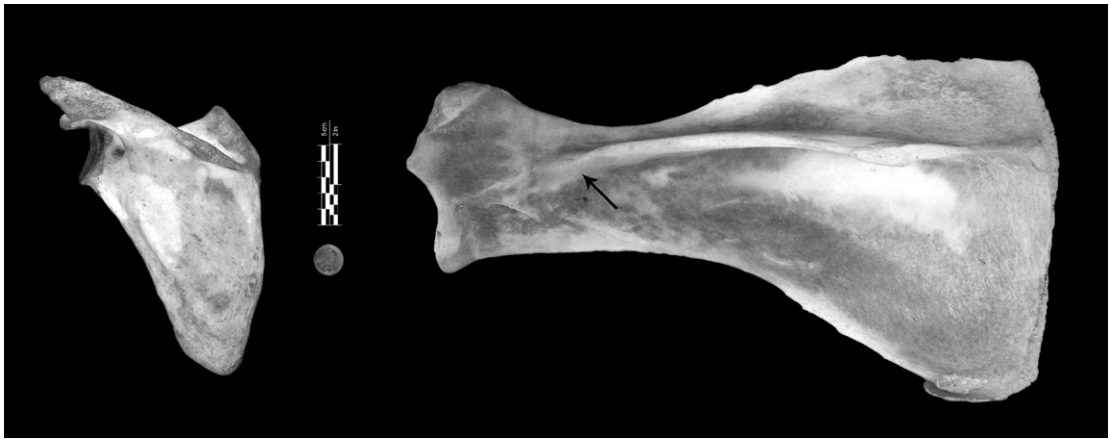

Figure 8-22: A human left scapula (posterior view) is compared to a horse's left scapula (lateral view). Note that the spine of the horse's scapula rises from the scapular neck (arrow).

Figure 8-23: The human and horse glenoid cavities are shown in this view.

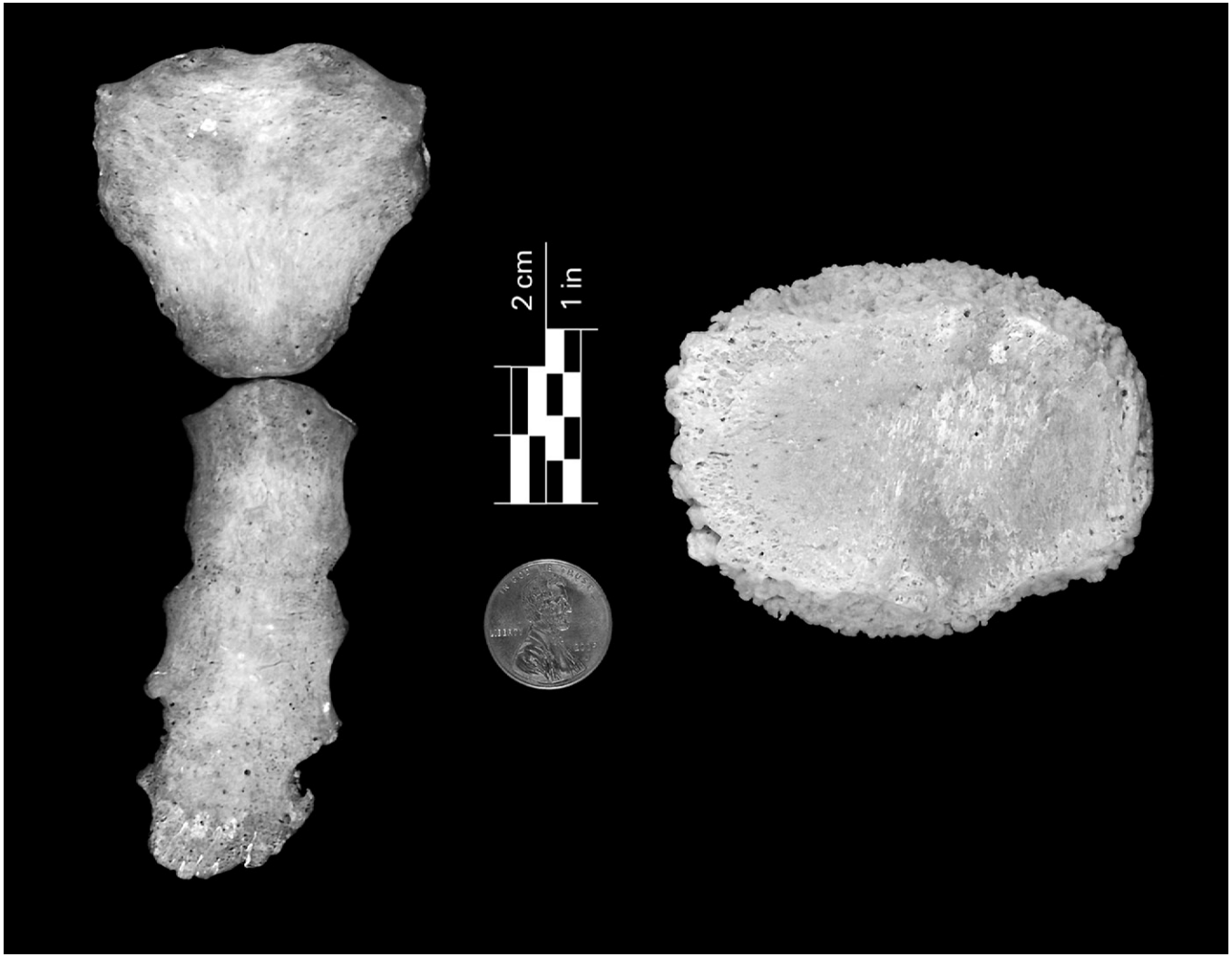

Figure 8-24: A human sternum (anterior view) is compared to one of the horse's sternabrae.

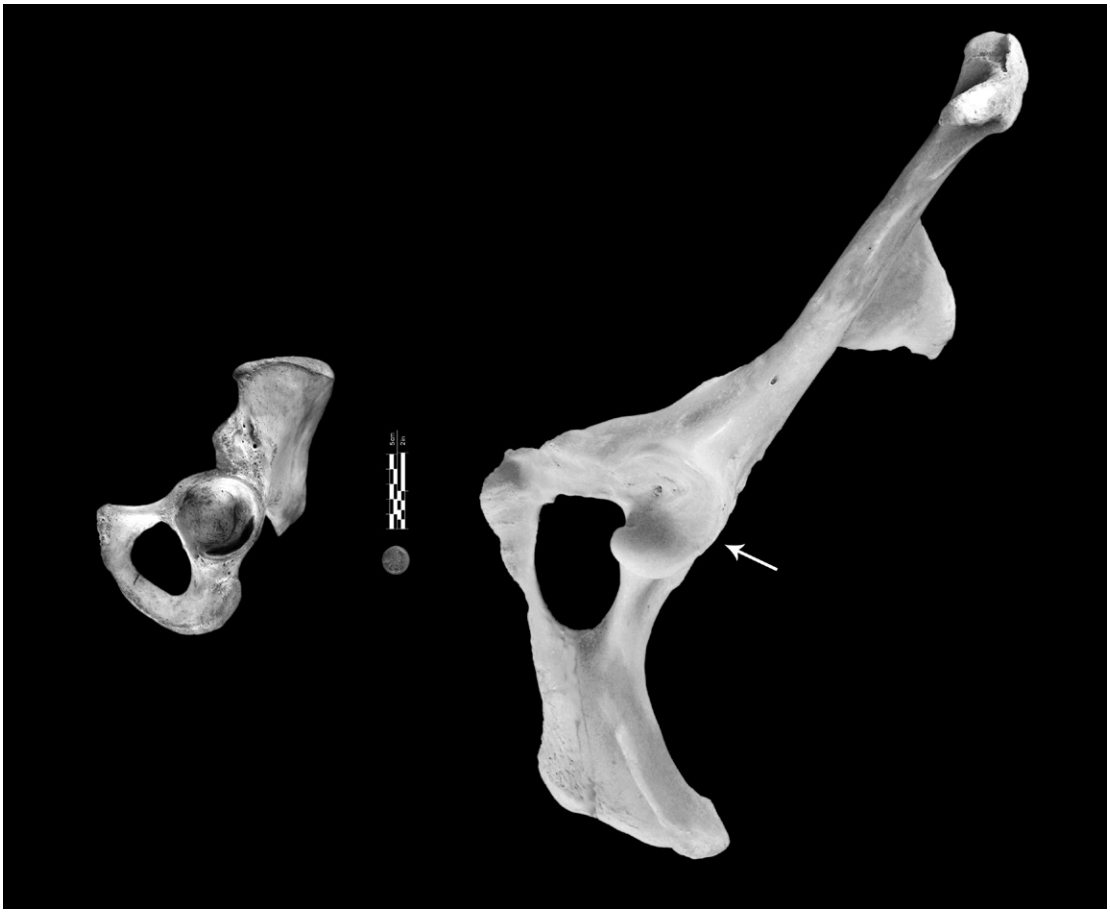

Figure 8-25: A human left innominate (lateral view) is compared to a horse's left innominate (lateral view). The articular surface on the horse's acetabulum is crescent shaped (arrow).

Figure 8-26: A human left innominate (posterior view) is compared to a horse's left innominate (dorsal view).

Figure 8-27: A human axis (C2) is compared to a horse's axis (C2). Both views are lateral. The cervical vertebrae generally reflect the length of the animal's neck. Note how much longer the horse's axis is compared to the human axis.

Figure 8-28: Three caudal, or tail, vertebrae of a horse (dorsal views). While the numbers may vary, most horses have about 18 caudal vertebrae. These bones can sometimes be confused with human phalanges.

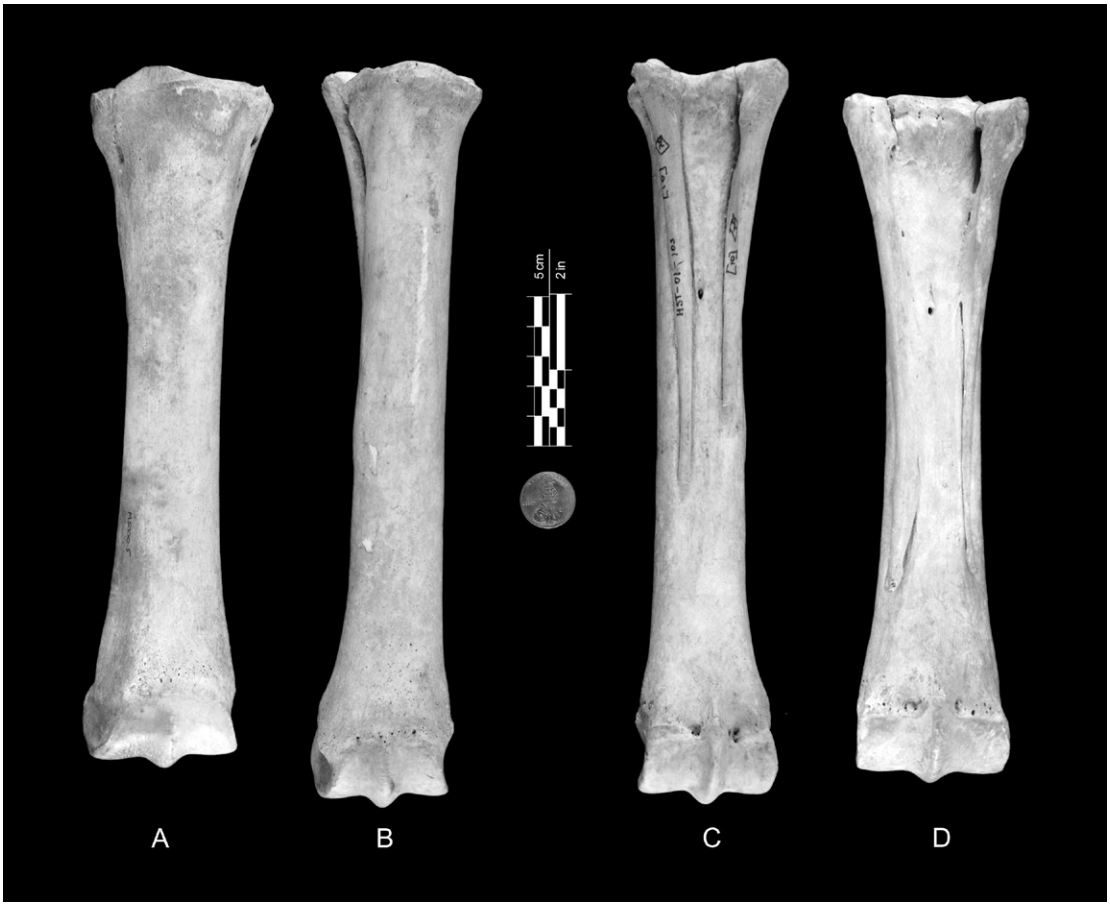

Figure 8-29: Horse metacarpus and metatarsus, left sides. Dorsal view of a metacarpus (A), dorsal view of a metatarsus (B), plantar view of a metatarsus (C), and volar view of a metacarpus (D). The horse has a single main metacarpus (third metacarpal) and metatarsus (third metatarsal). The remnants of the second and fourth metacarpals and second and fourth metatarsals can be seen in the volar/plantar views (shown on the right). These "splint bones" (lateral metapodia) taper to a point more than half way down the shaft of the main metapodial.

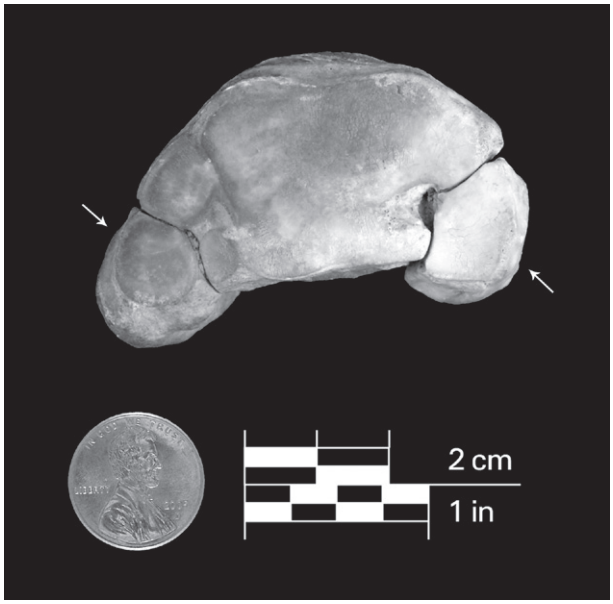

Figure 8-30: Horse proximal metacarpus (left side, dorsal view). The proximal end of the main (third) metacarpus is visible in the center. On either side are the small proximal ends of the second and fourth metacarpi (arrows).

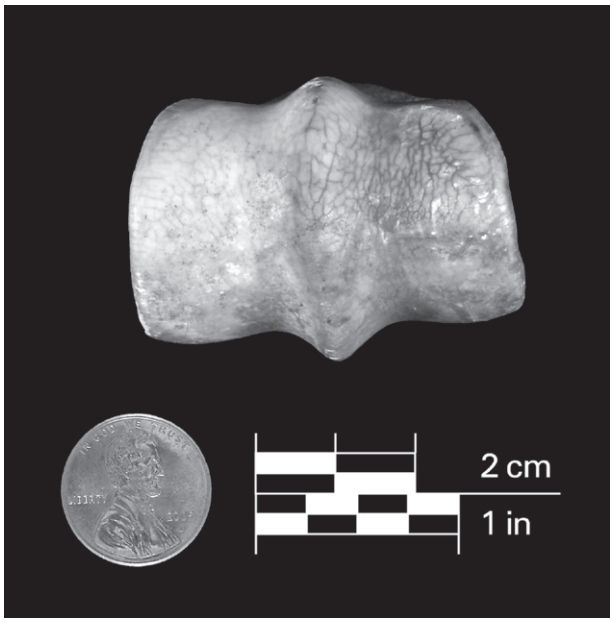

Figure 8-31: Horse distal metacarpus (left side, ventral view). In the horse, each distal metacarpus articulates with a single proximal/first phalanx.

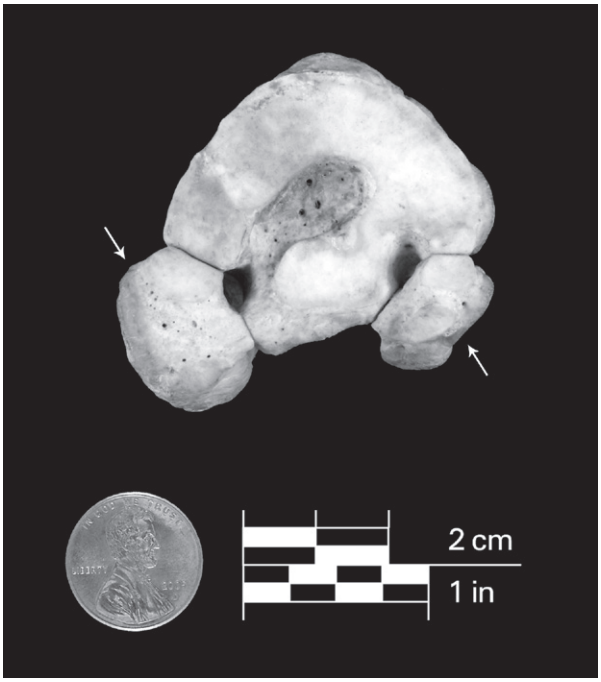

Figure 8-32: Horse proximal metatarsus (left side, dorsal view). The large third metatarsus is flanked by the smaller second and fourth metatarsi (arrows). While the horse's proximal metacarpus is D-shaped, the proximal metatarsus is more circular in shape.

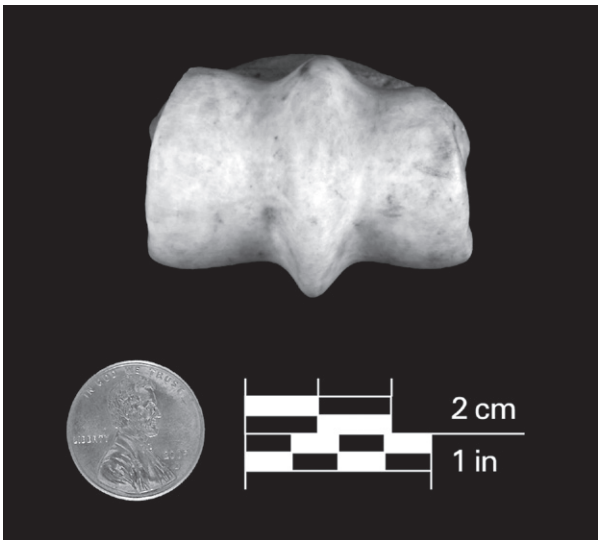

Figure 8-33: Horse distal metatarsus (left side, ventral view). In the horse, each distal metatarsus articulates with a single proximal/first phalanx.

CHAPTER 9

Cow (Bos taurus *and* Bos indicus)

Comparative Osteology. DOI: 10.1016/B978-0-12-388437-4.00009-0

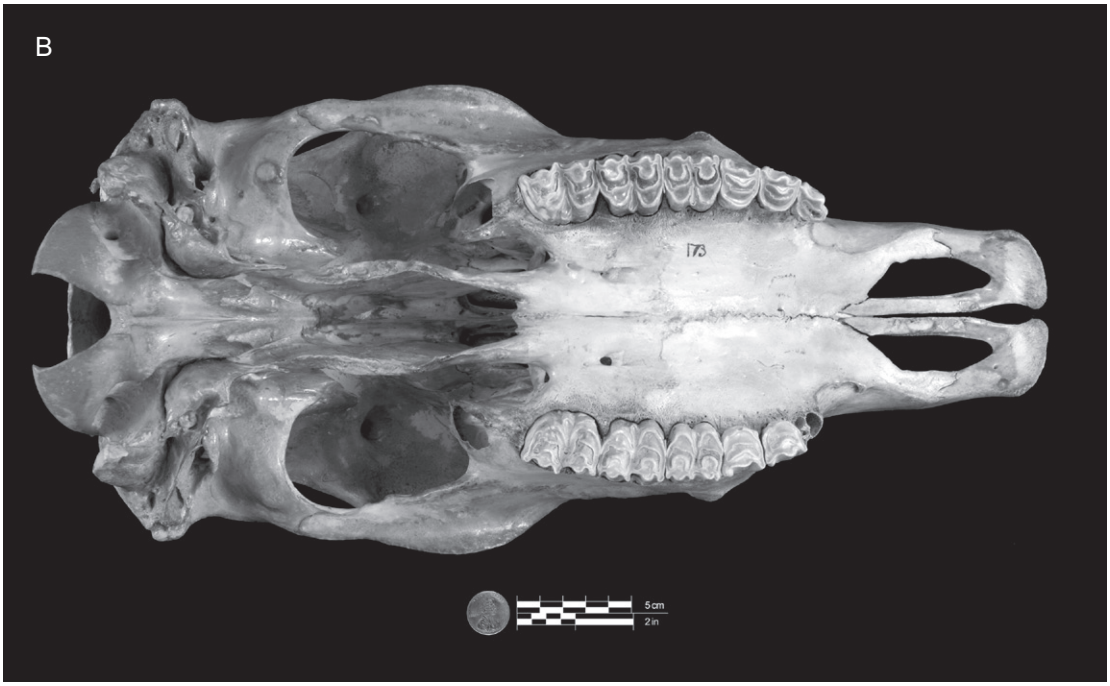

Figure 9-01: Cow cranium (A) lateral view, right side; (B) ventral view. The cow has no upper incisors or canines. The cow's dental formula is 0/3.0/1.3/3.3/3.

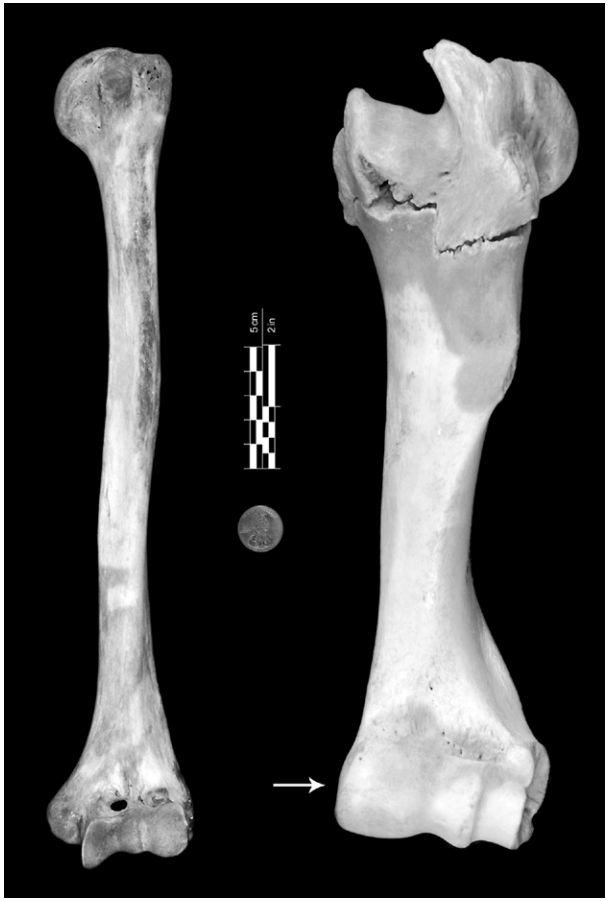

Figure 9-02: A human left humerus (anterior view) is compared to a cow's left humerus (cranial view). On the proximal end, the greater and lesser tubercles are far more well developed in the cow than they are in the human. On the distal end, the cow has a barrel-shaped trochlea (arrow).

Figure 9-03: A human left humerus (posterior view) is compared to a cow's left humerus (caudal view). Note that the cow's humerus has a particularly deep olecranon fossa (arrow) when compared to the human example.

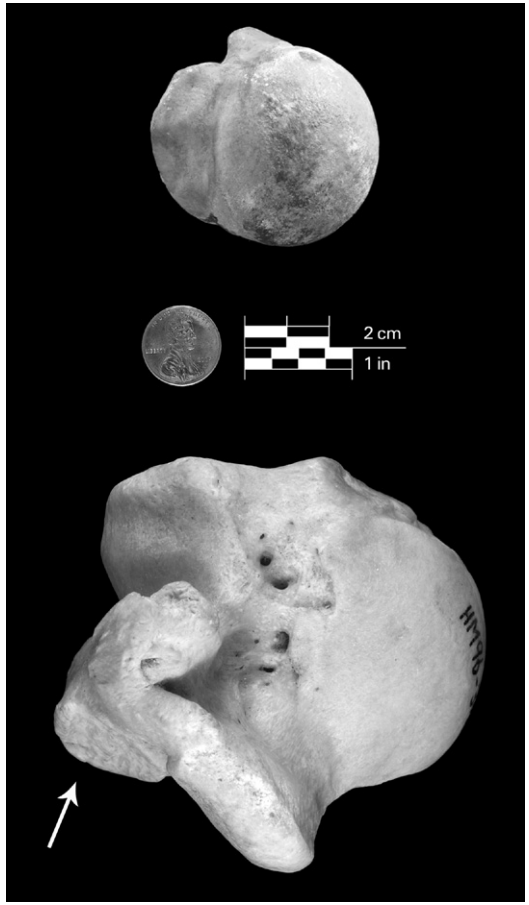

Figure 9-04: Proximal views of a human and a cow's left humerus. The head of the humerus and the greater and lesser tubercles are visible in this superior view. The arrow points to the deltoid tuberosity on the cow's humerus (dorsal view).

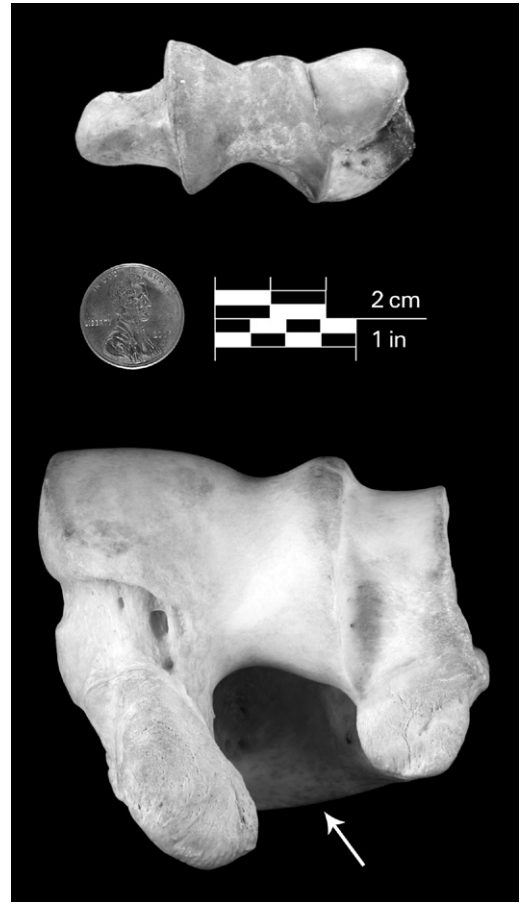

Figure 9-05: Distal ends of a human (inferior view) and a cow's (ventral view) left humerus. The cow's trochlea is barrel shaped, and the deep olecranon fossa is visible on the caudal surface (arrow).

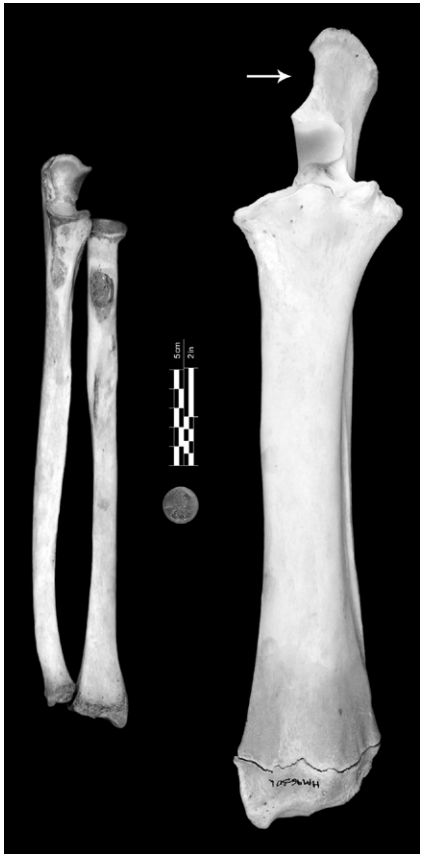

Figure 9-06: A human left radius and ulna (anterior views) are compared to a cow's left radius and ulna (cranial view). The human radius and ulna are roughly equal in size. With the exception of the large olecranon process (arrow), the cow's ulna is greatly reduced.

Figure 9-07: A human left radius and ulna (posterior views) are compared to a cow's left radius and ulna (caudal view). Note that the cow's ulna is fused to the lateral side of the radius shaft.

Figure 9-08: A human left radius and ulna (lateral views) are compared to a cow's left radius and ulna (lateral views). The shaft of the cow's ulna is quite slender. In adult animals, it is usually fused to the caudal surface of the radius.

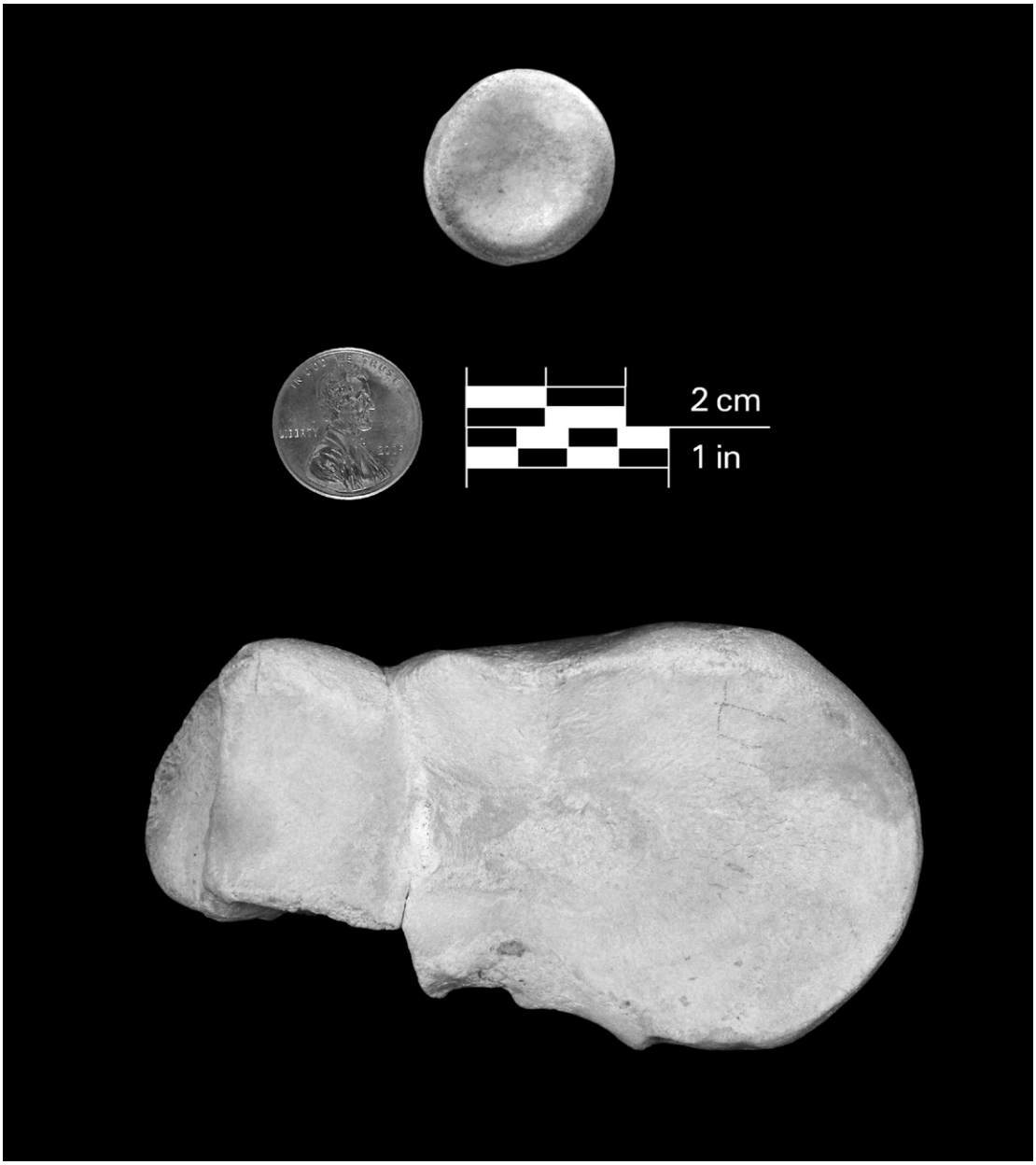

Figure 9-09: An adult human proximal radius (superior view) is compared to a cow's proximal radius (dorsal view). The human radius has a distinct circular shape, while the cow's is more elongated and broad and has a slightly concave articular surface.

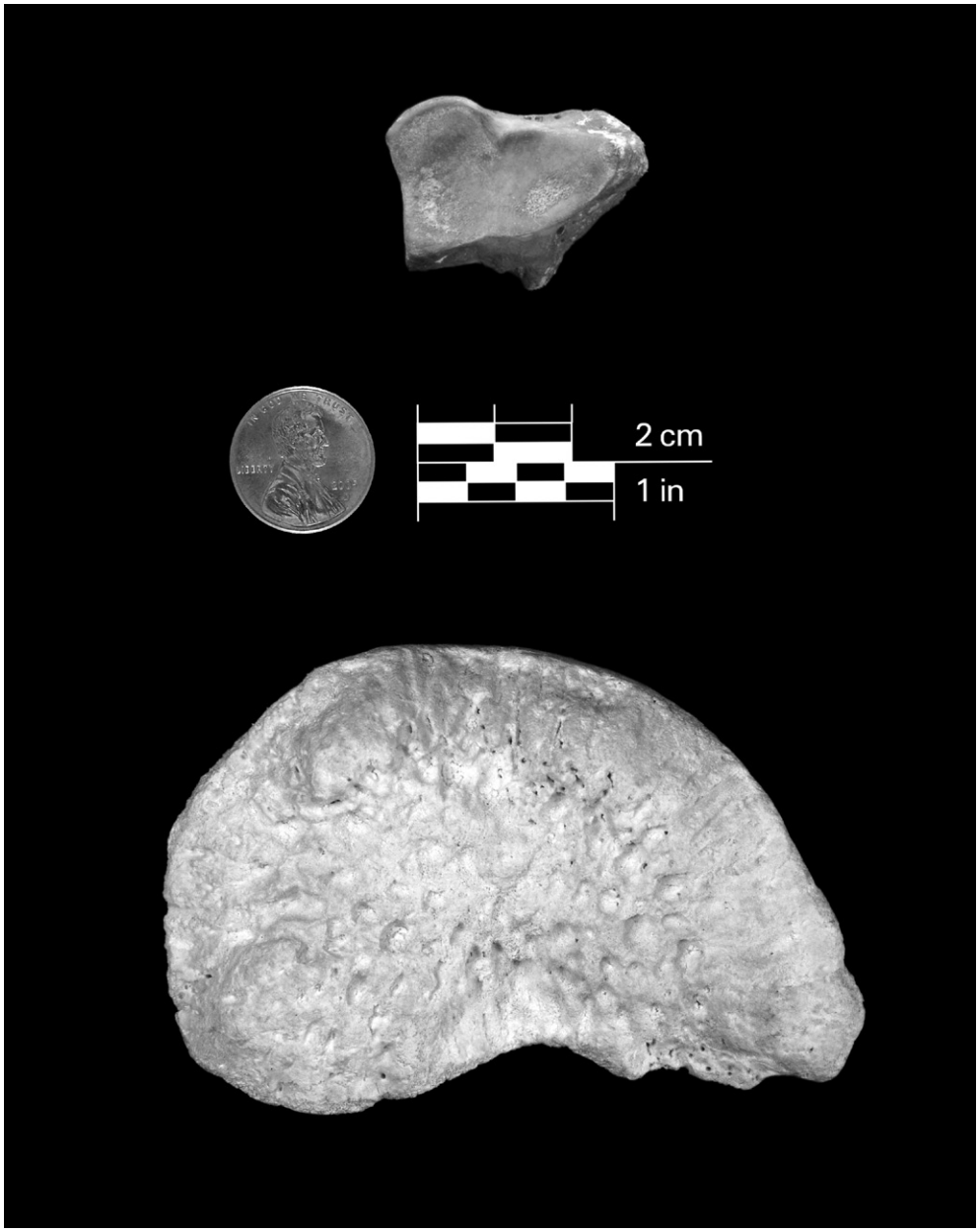

Figure 9-10: An adult human distal radius (inferior view) is compared to a cow's unfused distal radius (ventral view). Note that the cow's radius is broadly D-shaped in cross-section. The undulating and pitted character of the cow's metaphysis is distinctive of immature animals lacking the epiphyses. The distal radius does not fuse in a cow until about 3.5–4 years of age (Silver 1969: 285). Castration can also delay fusion.

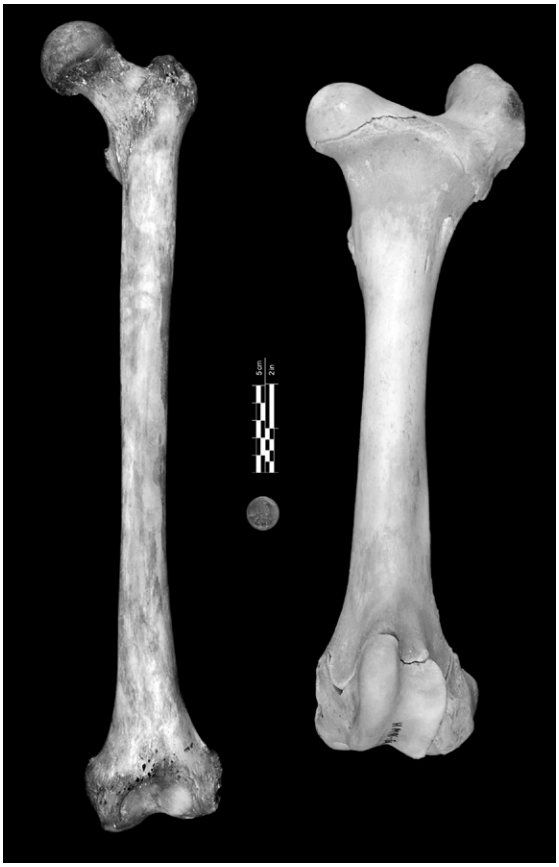

Figure 9-11: A human left femur (anterior view) is compared to a cow's left femur (cranial view). The cow skeleton illustrated here is a 6–7-year-old ox, or male castrate. While the distal epiphysis usually fuses by about 3.5–4 years of age (Silver 1969: 286), castration has delayed epiphyseal fusion in this specimen. The greatest length of the human femur extends from the head to the distal condyles; in the cow the greatest length extends from the greater trochanter to the condyles.

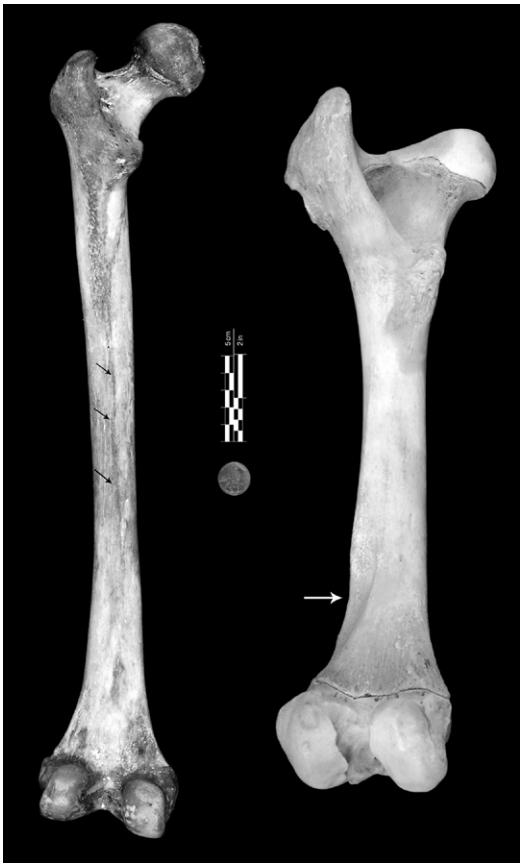

Figure 9-12: A human left femur (posterior view) is compared to a cow's left femur (caudal view). The human femur includes a linea aspera, which appears as a projecting ridge for the muscle attachment (black arrows). This is a unique human feature that is not seen in other mammals as it is an area of attachment for the muscles used in bipedalism. The cow's femur includes a supercondular fossa that can be seen on the lateral portion of the shaft (white arrow).

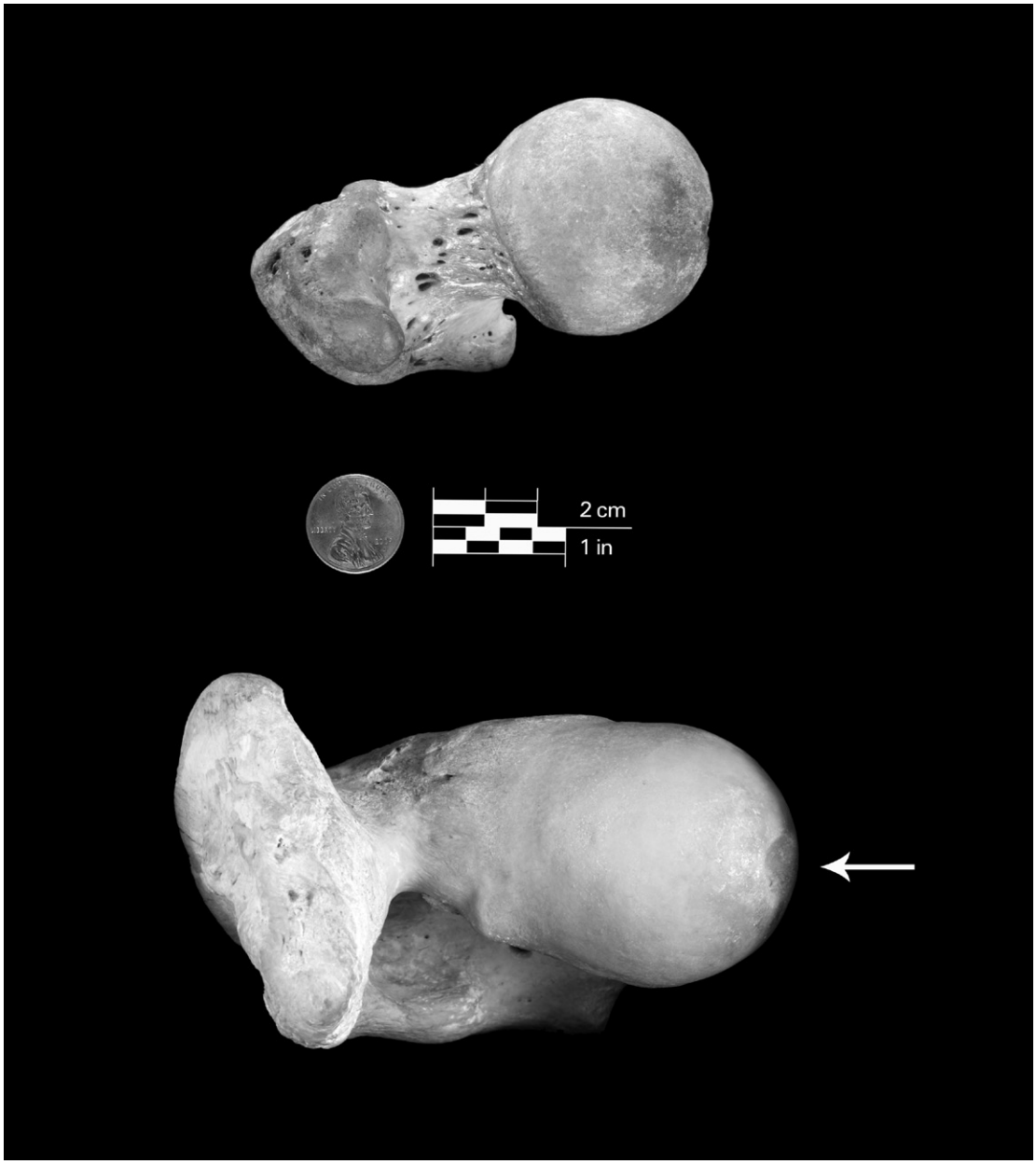

Figure 9-13: A human left proximal femur (superior view) is compared to a cow's left proximal femur (dorsal view). The head of the femur and the greater trochanter are visible in this view of the cow femur. The arrow points to the cow's small, round fovea capitis.

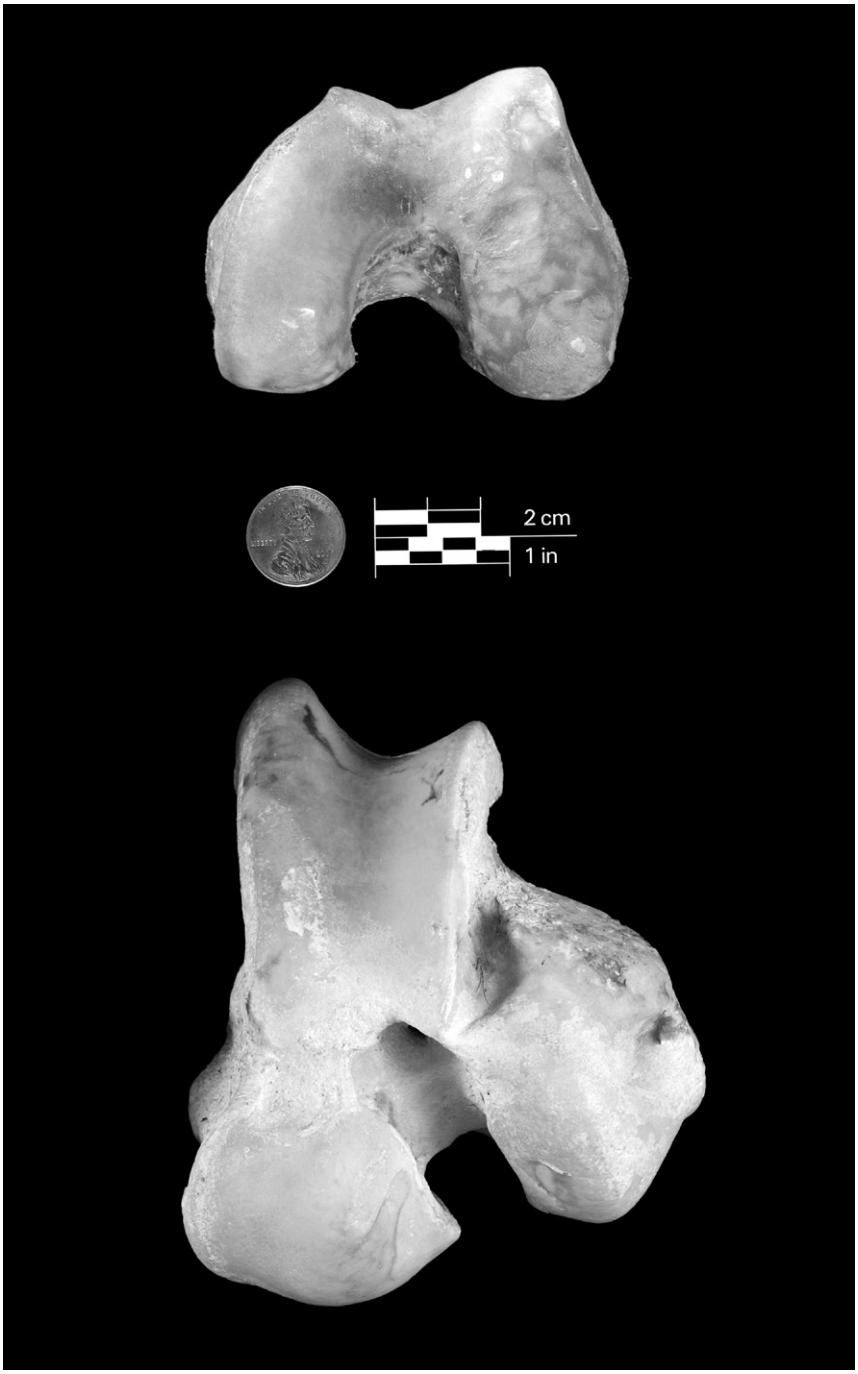

Figure 9-14: A human left distal femur (inferior view) is compared to a cow's left distal femur (ventral view). The two condyles and the trochlea (for articulation with the patella) are visible in both specimens in this view.

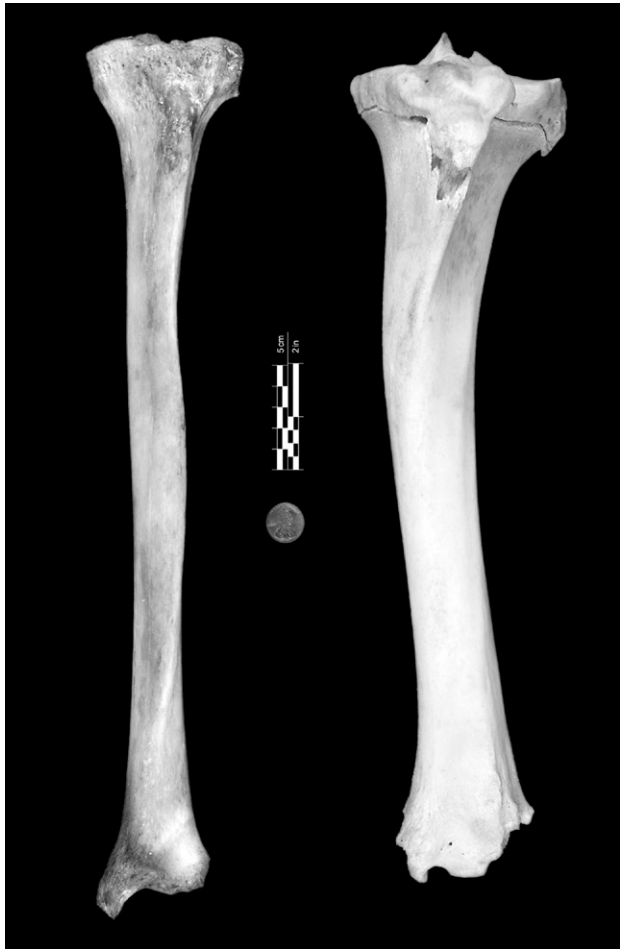

Figure 9-15: A human left tibia (anterior view) is compared to a cow's left tibia (cranial view). The shaft of the cow's tibia is significantly more robust.

Figure 9-16: A human left tibia (posterior view) is compared to a cow's tibia (caudal view).

Figure 9-17: A human left proximal tibia (superior view) is compared to a cow's left proximal tibia (dorsal view). The two large facets articulate with the distal femur.

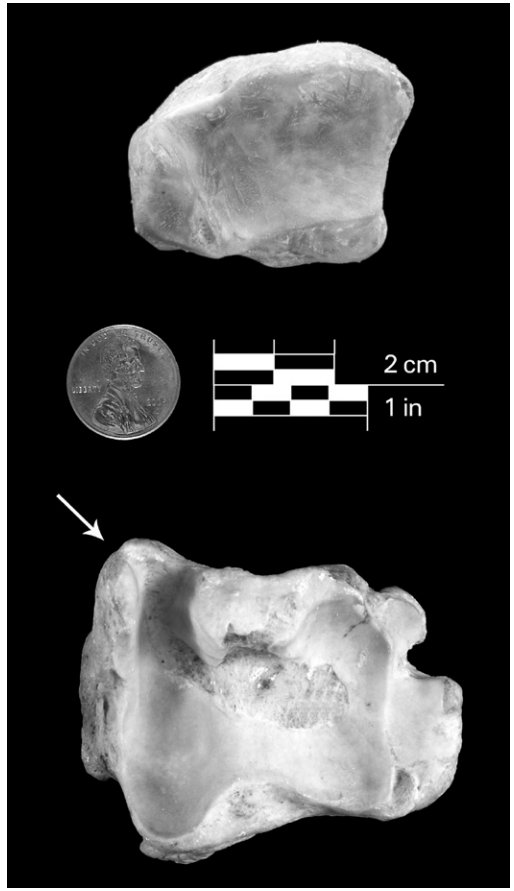

Figure 9-18: A human left distal tibia (inferior view) is compared to a cow's left distal tibia (ventral view). The two large parallel grooves seen on the cow's distal tibia are articular surfaces for the astragalus. The two small facets on the lateral side articulate with the malleolus bone. It is all that remains of the distal fibula. The arrow points to the medial malleolus on the cranial portion of the bone.

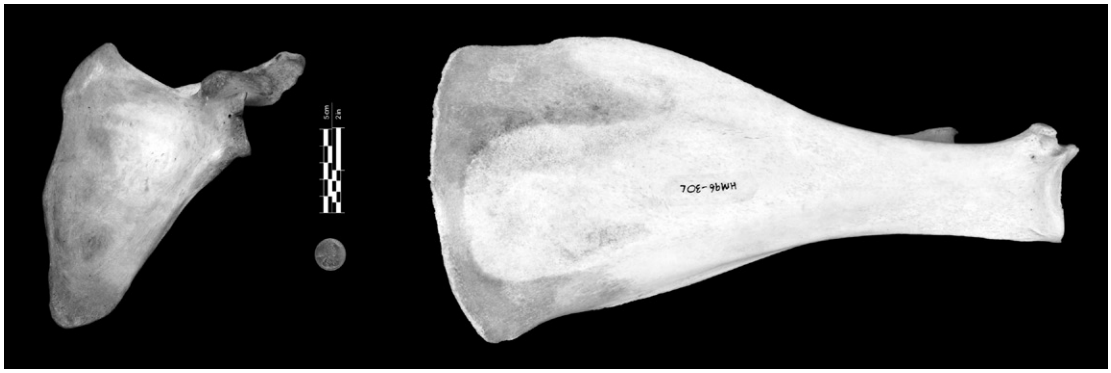

Figure 9-19: A human left scapula (anterior view) is compared to a cow's left scapula (medial view). Note that these bones are oriented as they would be in the human skeleton. Since the cow is a quadruped, the glenoid cavity forms the distal part of the bone. The blade of the cow's scapula is shaped like an elongated triangle.

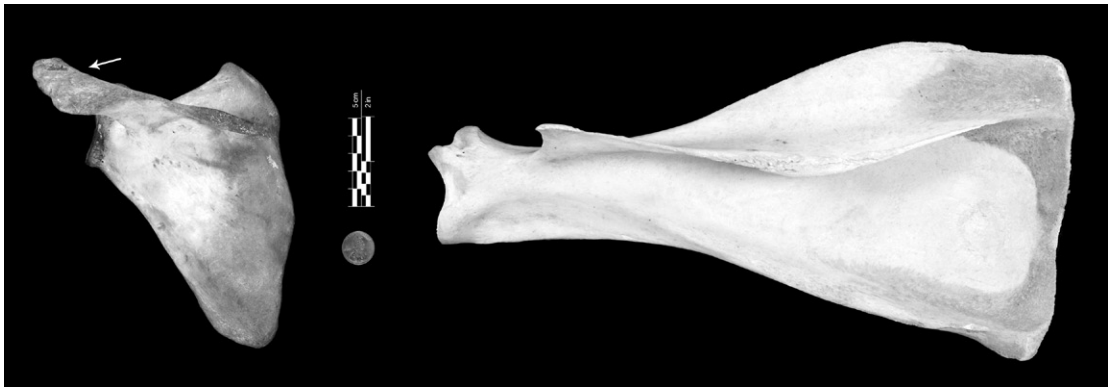

Figure 9-20: A human left scapula (posterior view) is compared to a cow's left scapula (lateral view). The acromion process is well developed in humans (arrow); it is very small in the cow and other ruminant artiodactyls. The greatest length of the cow's scapula (and the scapulas of most other mammals) extends from the glenoid cavity to the dorsal border (parallel to the scapular spine). This is not the case in humans, where the greatest length lies between the superior and inferior borders.

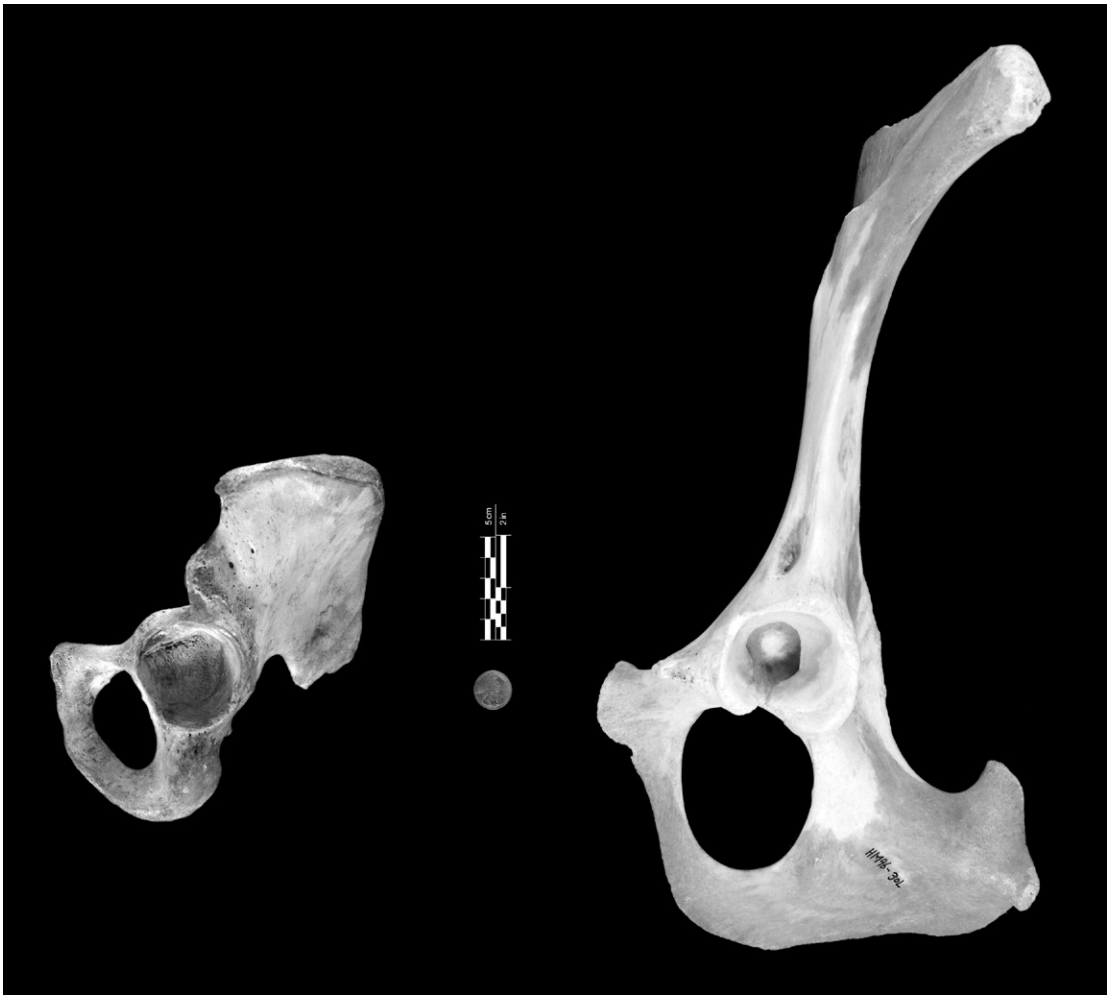

Figure 9-21: A human left innominate (lateral view) is compared to a cow's left innominate (lateral view).

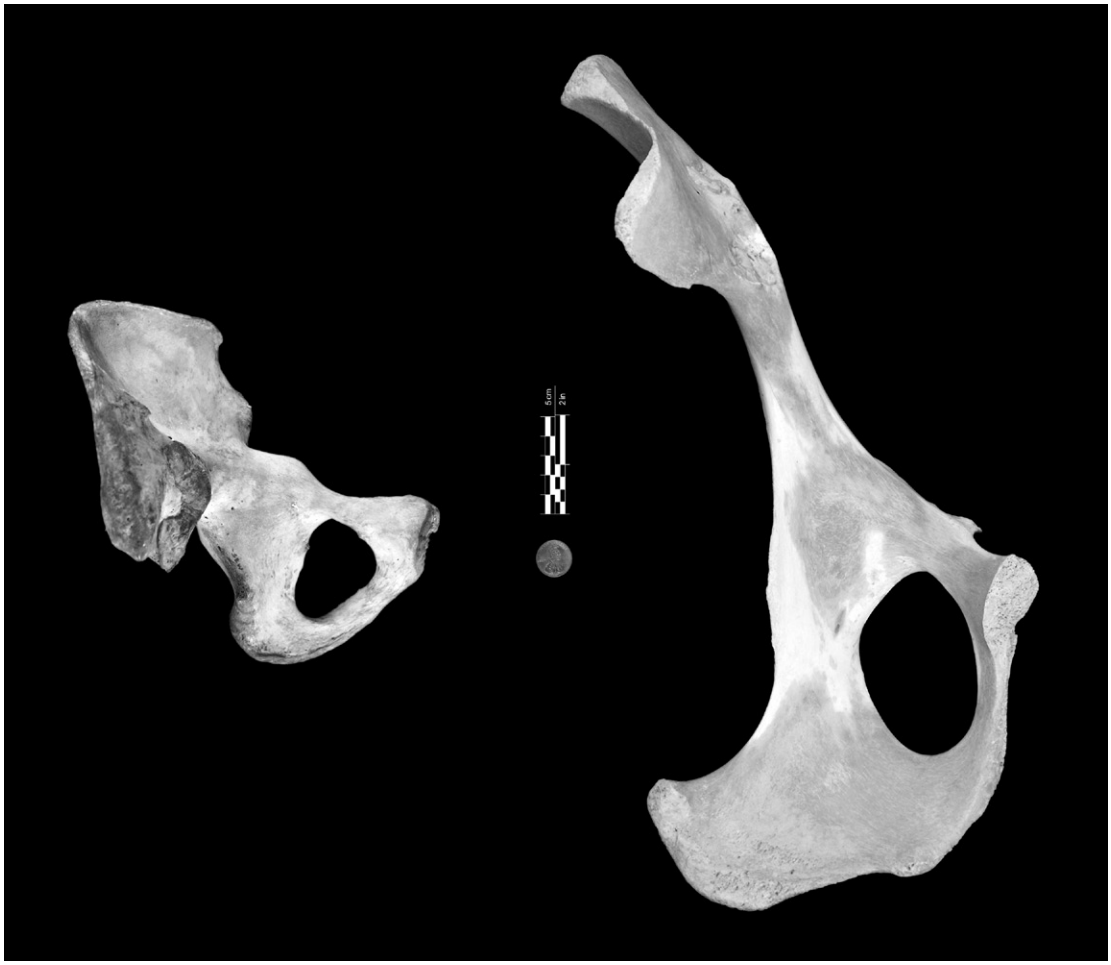

Figure 9-22: A human left innominate (medial view) is compared to a cow's left innominate (medial view).

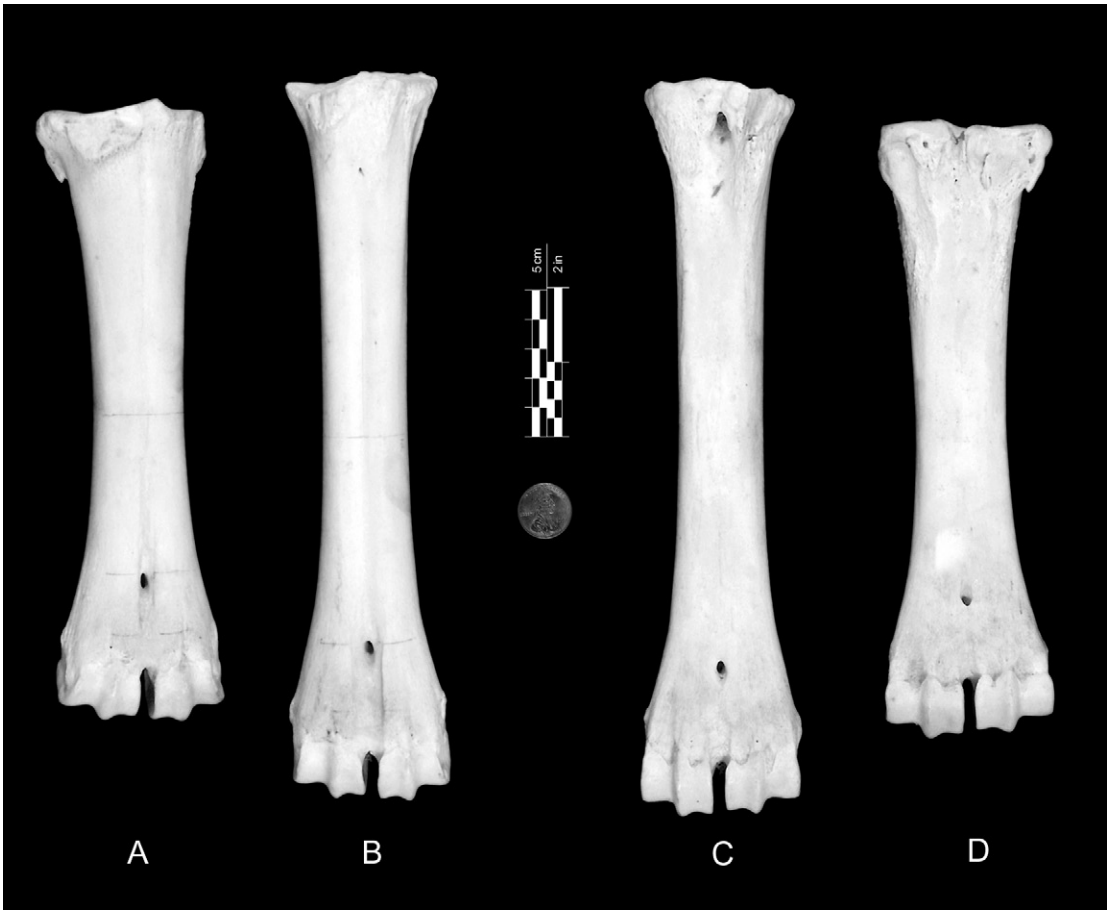

Figure 9-23: Cow metacarpus and metatarsus. The cow's left metacarpus (A, dorsal view), metatarsus (B, dorsal view), left metatarsus (C, plantar view), and left metacarpus (D, palmar (volar) view) are shown. These bones are formed through the fusion of the third and fourth metacarpals and metatarsals. Each of the two distal condyles articulates with a proximal/first phalanx.

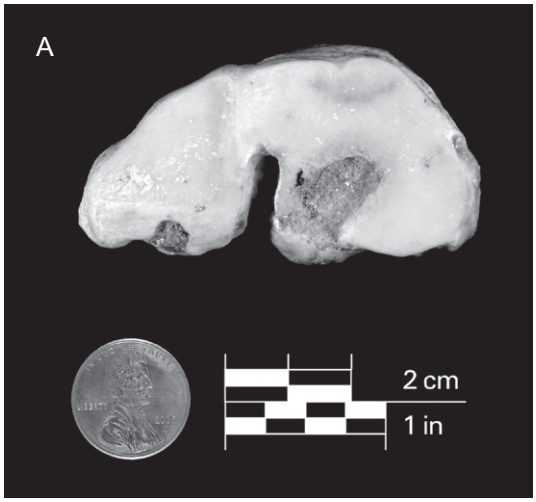

Figure 9-24a: Cow proximal metacarpus (left side, dorsal view). The proximal articular surface is D-shaped, and the larger articulation is located on the medial side.

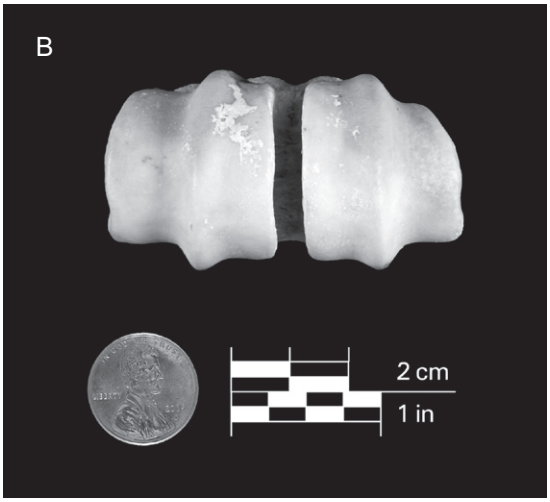

Figure 9-24b: Cow distal metacarpus (left side, volar view). Each distal metacarpus articulates with two proximal/first phalanges.

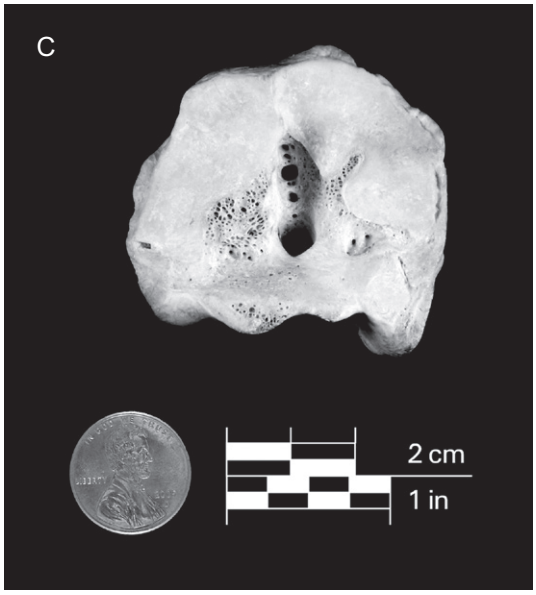

Figure 9-24c: Cow proximal metatarsal (left side, dorsal view). In comparison to the metacarpus, the proximal end is squarer in shape. The articular facets for the distal tarsal row are visible in this view.

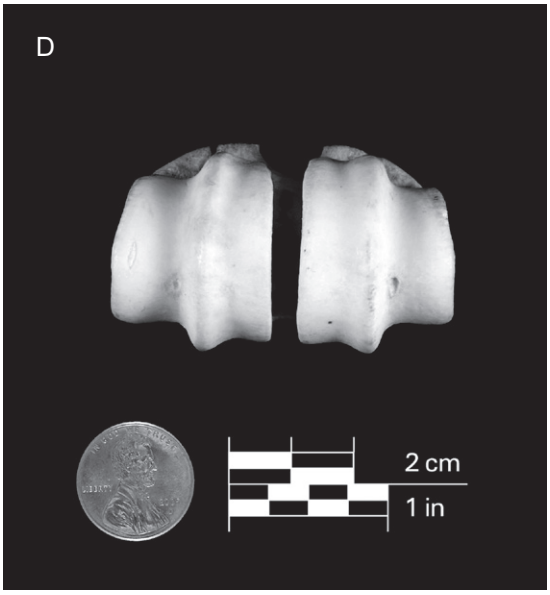

Figure 9-24d: Cow distal metatarsus (left side, plantar view). Each distal metatarsus articulates with two proximal/first phalanges.

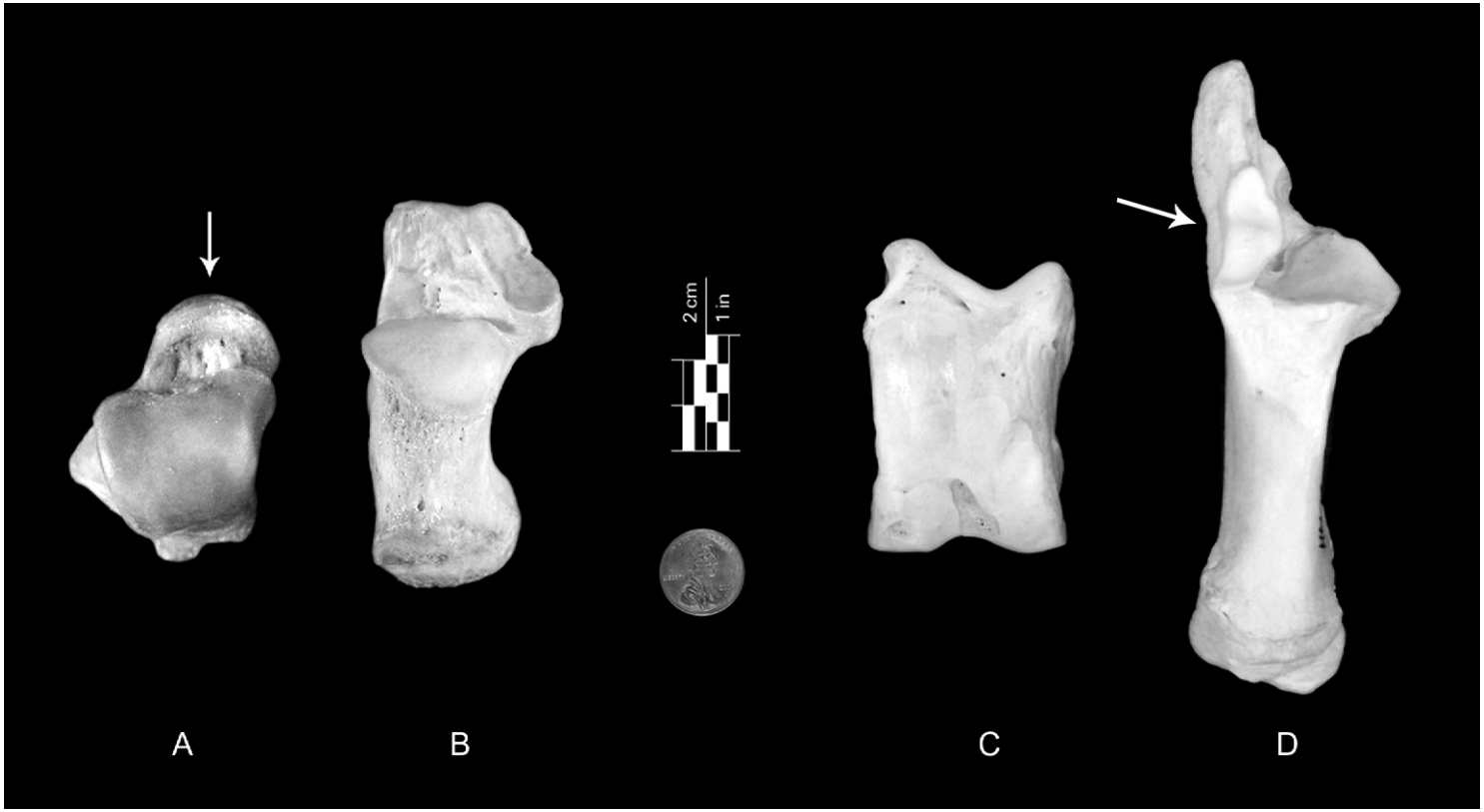

Figure 9-25: A human left talus (A, superior view) and calcaneus (B, superior view) compared to a cow's left astragalus (C, plantar view) and calcaneus (D, dorsal view). The human talus has a distinctive head (arrow), while the cow's astragalus has the "double pulley" form that is typical of all artiodactyls (even-toed ungulates). The cow's calcaneus is elongated and the dorsal surface includes an articular facet for the malleolus (arrow), a small tarsal bone that is the evolutionary remnant of the distal fibula. The cow does not have a separate fibula.

CHAPTER 10

Bear (Ursus americanus)

Comparative Osteology. DOI: 10.1016/B978-0-12-388437-4.00010-7

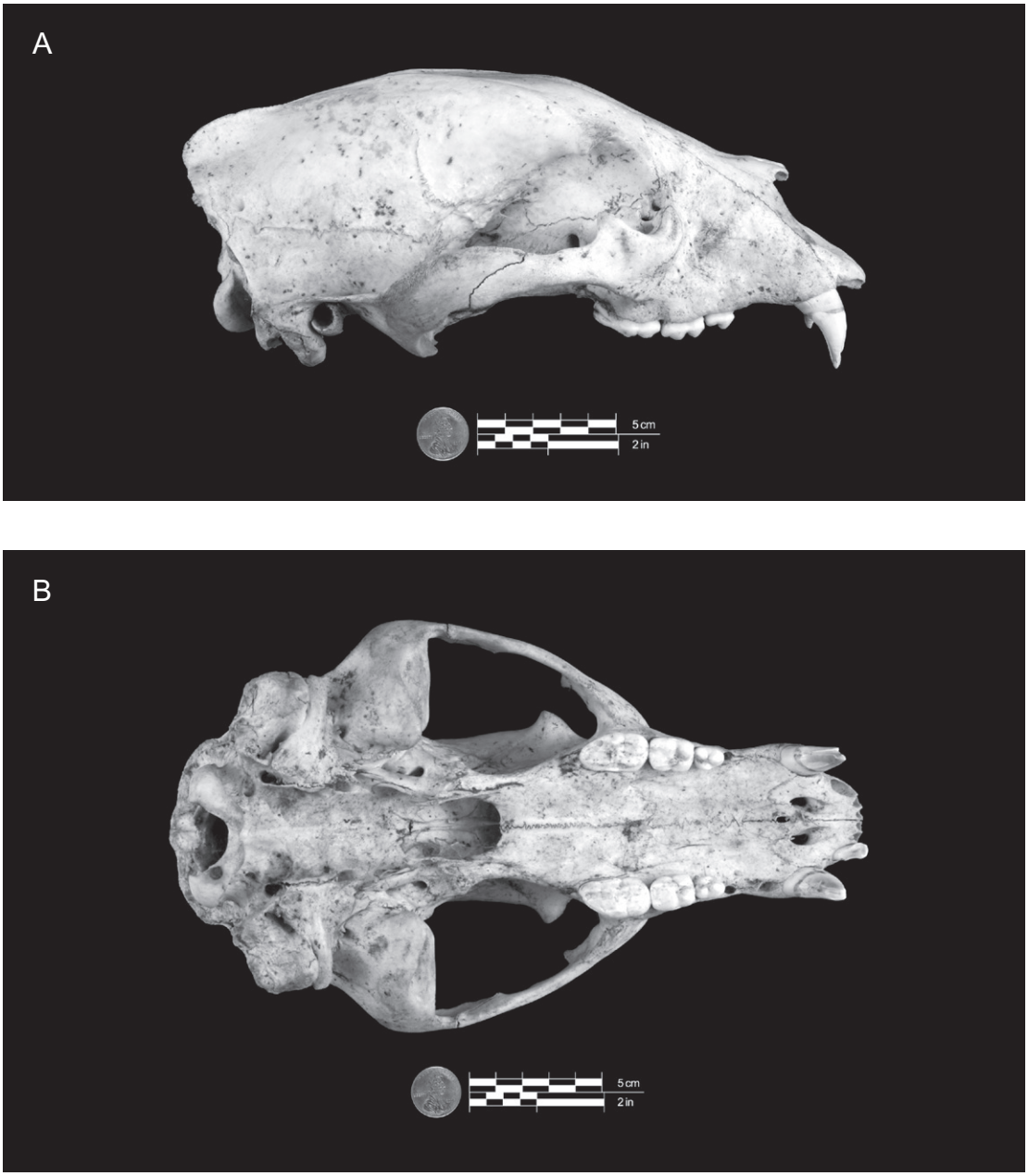

Figure 10-01: Bear cranium (A) lateral view, right side; (B) ventral view. The bear's dental formula is 3/3.1/1.2–4/2–4.2/3.

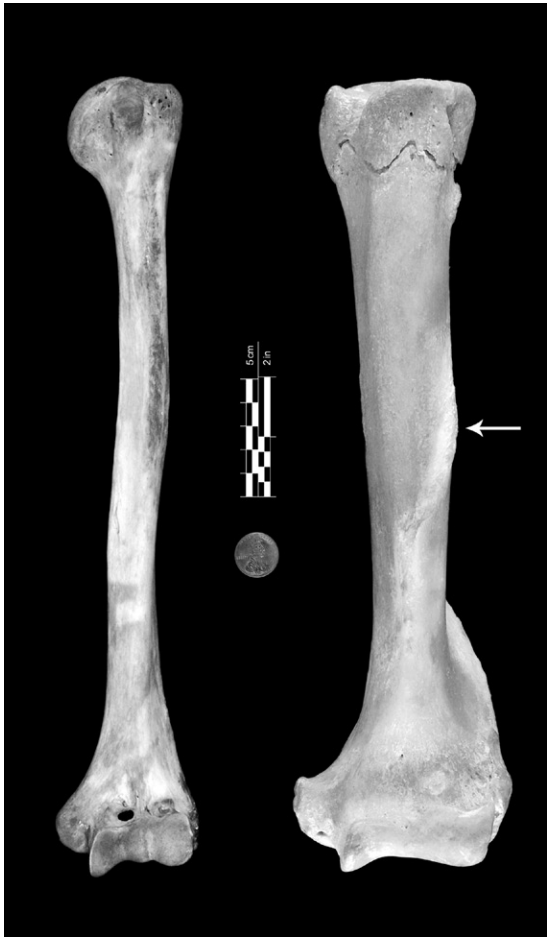

Figure 10-02: A human left humerus (anterior view) is compared to a bear's left humerus (cranial view). The lateral epicondylar crest (proximal to the lateral epicondyle) is well developed in the bear, as is the deltoid tuberosity (arrow).

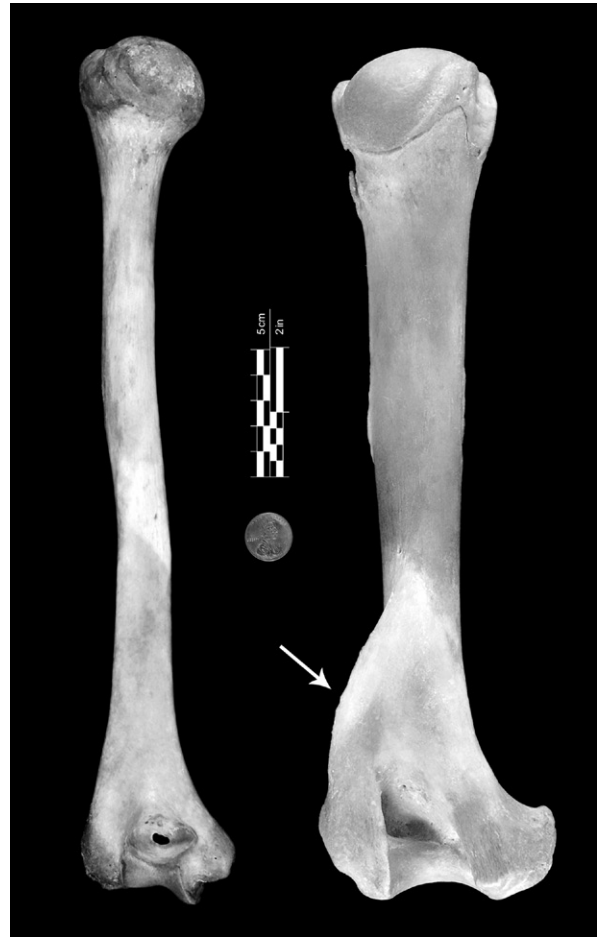

Figure 10-03: A human left humerus (posterior view) is compared to a bear's left humerus (caudal view). The arrow marks the well-developed epicondylar crest.

Figure 10-04: A human left radius (anterior view) is compared to a bear's left radius (cranial view). Human skeletons are oriented with the palms forward, so that the radius and ulna are not crossed. Quadrupedal animals are oriented with their paws facing the ground. This means that the proximal ulna is medial to the radius, while the distal ulna is on the lateral side.

Figure 10-05: A human left radius (posterior view) is compared to a bear's left radius (caudal view).

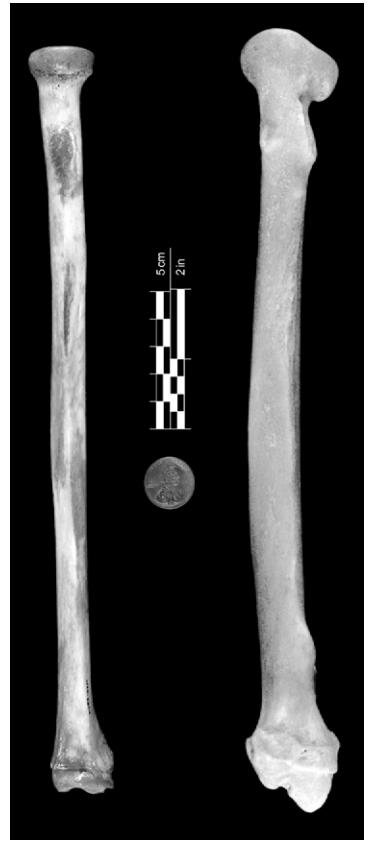

Figure 10-06: A human left radius (medial view) is compared to a bear's left radius (medial view).

Figure 10-07: A human left ulna (anterior view) is compared to a bear's left ulna (cranial view). Note that the bear's olecranon process (arrow) is larger and more well-developed.

Figure 10-08: A human left ulna (posterior view) is compared to a bear's left ulna (caudal view).

Figure 10-09: A human left ulna (lateral view) is compared to a bear's left ulna (lateral view).

Figure 10-10: A human left ulna (medial view) is compared to a bear's left ulna (medial view).

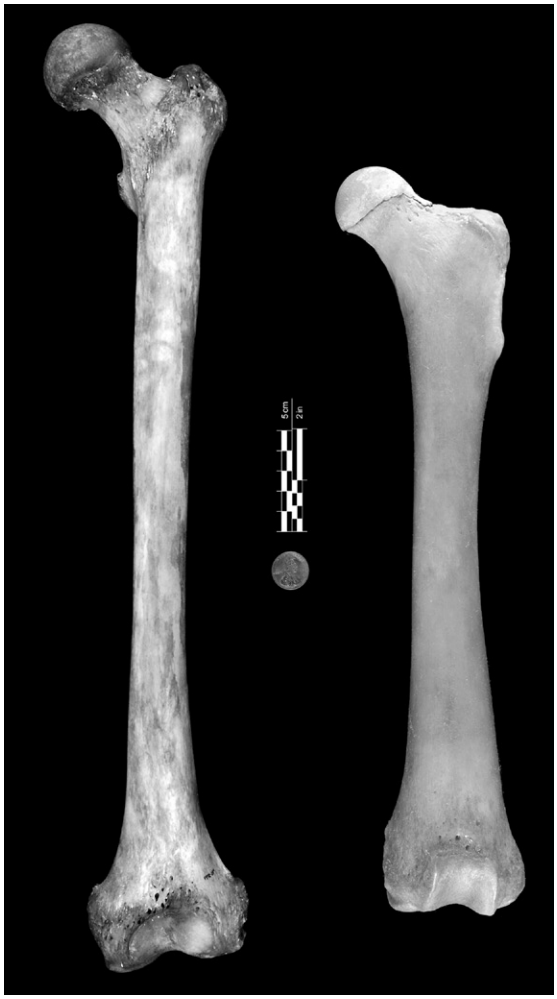

Figure 10-11: A human left femur (anterior view) is compared to a bear's left femur (cranial view). The distal condyles of the human femur show a distinctive asymmetry that is a result of "kneeing in," or bringing the knees under the body. This is also referred to as the valgus knee.

Figure 10-12: A human left femur (posterior view) is compared to a bear's left femur (caudal view). The human femur shows the distinctive linea aspera (arrows), which is not seen in quadrupeds.

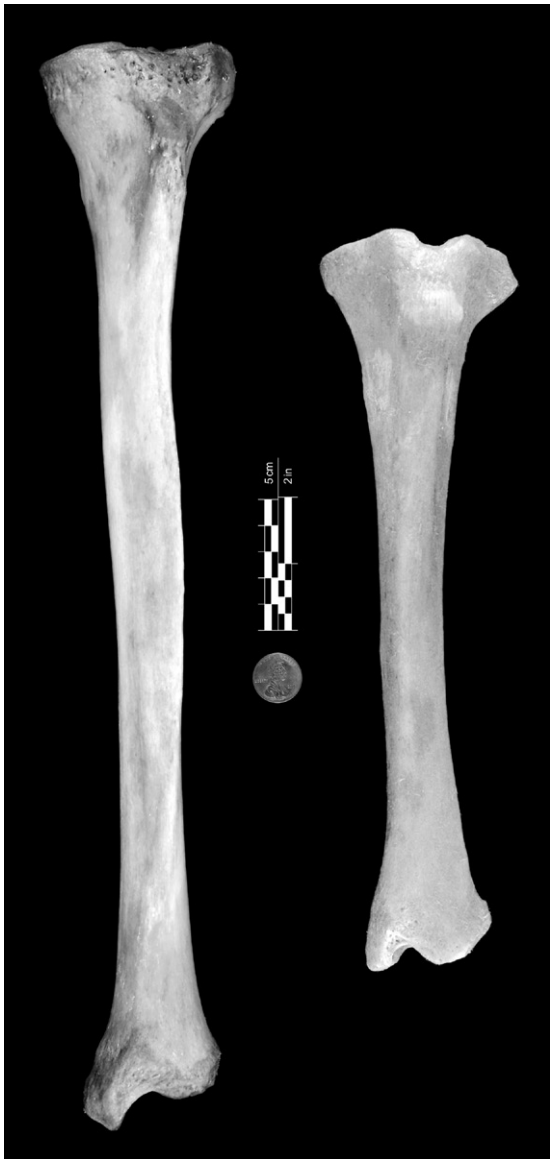

Figure 10-13: A human left tibia (anterior view) is compared to a bear's left tibia (cranial view).

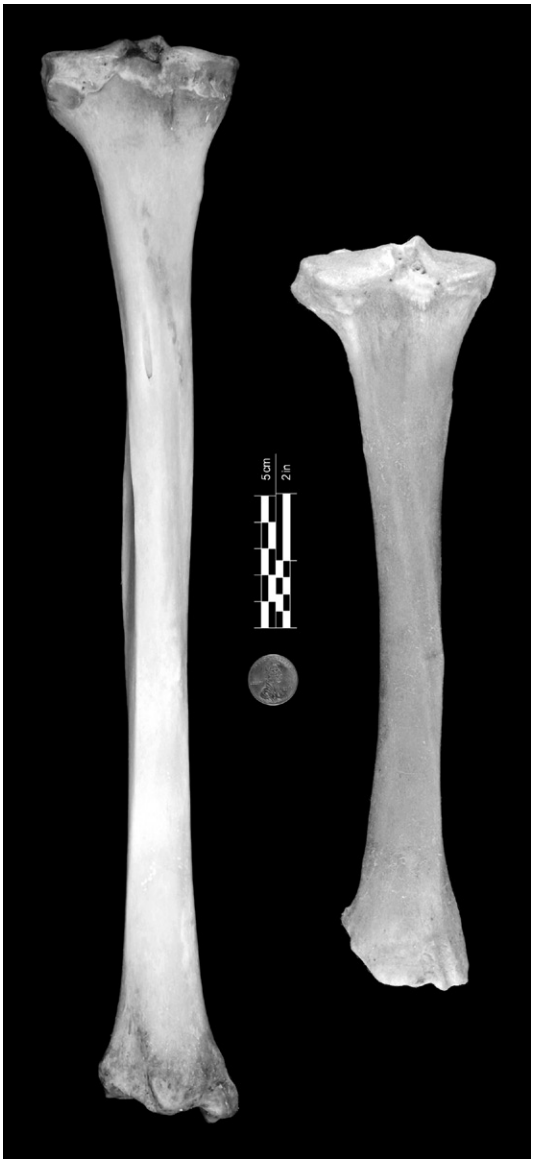

Figure 10-14: A human left tibia (posterior view) is compared to a bear's left tibia (caudal view).

Figure 10-15: A human left tibia (lateral view) is compared to a bear's left tibia (lateral view).

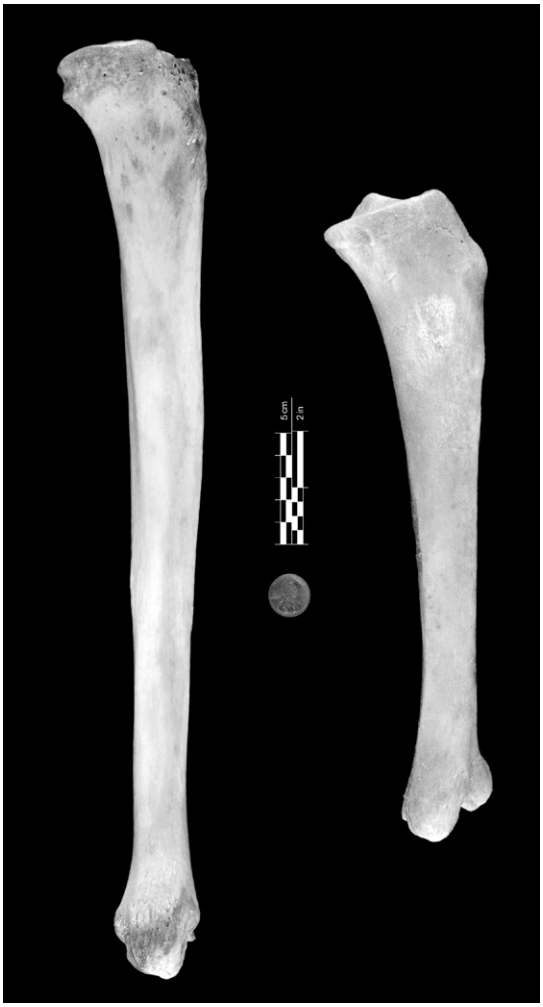

Figure 10-16: A human left tibia (medial view) is compared to a bear's left tibia (medial view).

Figure 10-17: A human left fibula (medial view) is compared to a bear's left fibula (medial view).

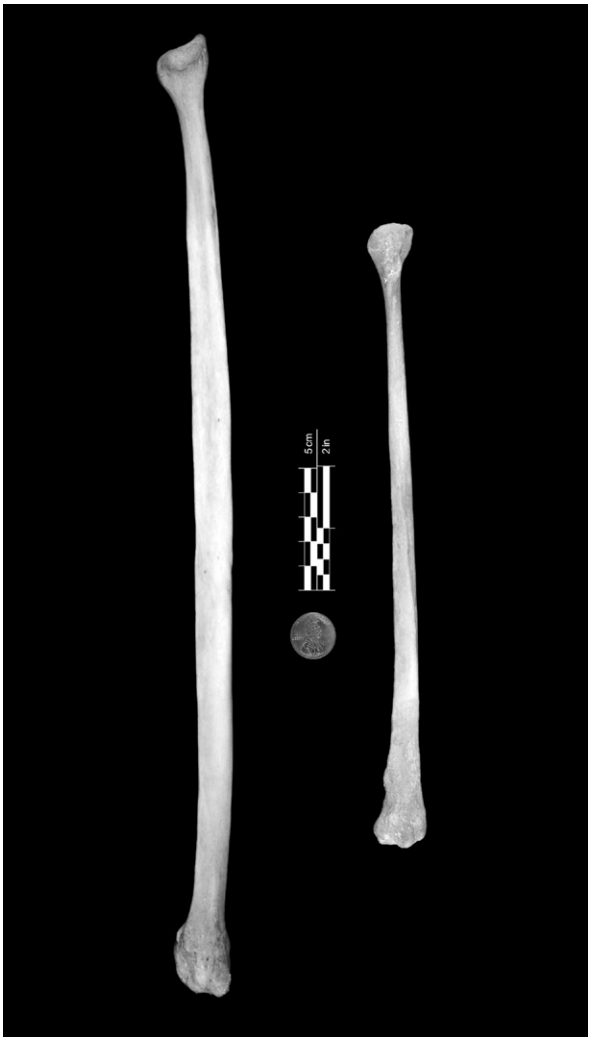

Figure 10-18: A human left fibula (lateral view) is compared to a bear's left fibula (lateral view).

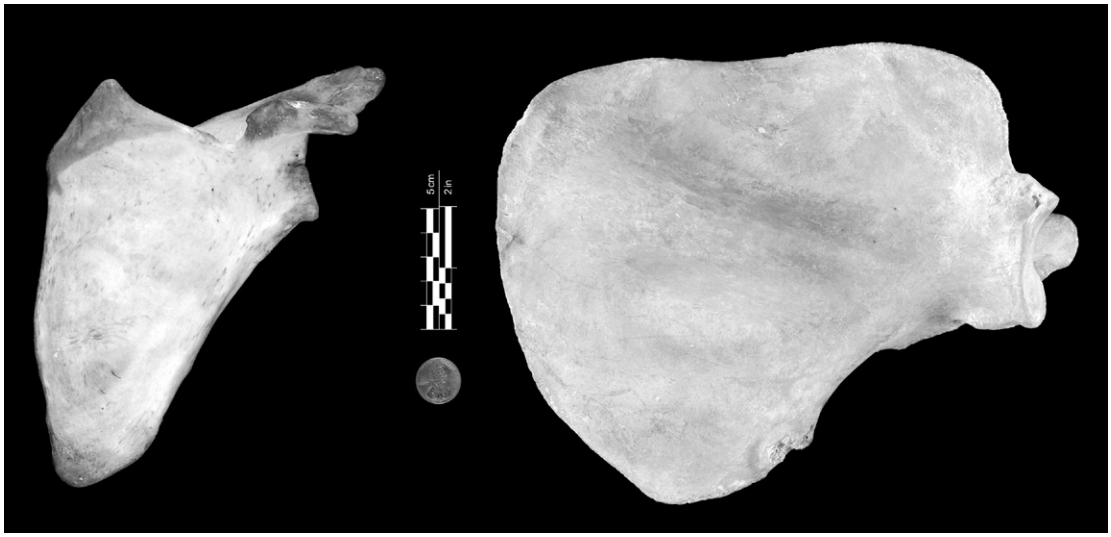

Figure 10-19: A human left scapula (anterior view) is compared to a bear's left scapula (medial view). Both scapulae are oriented as they would be in a human skeleton.

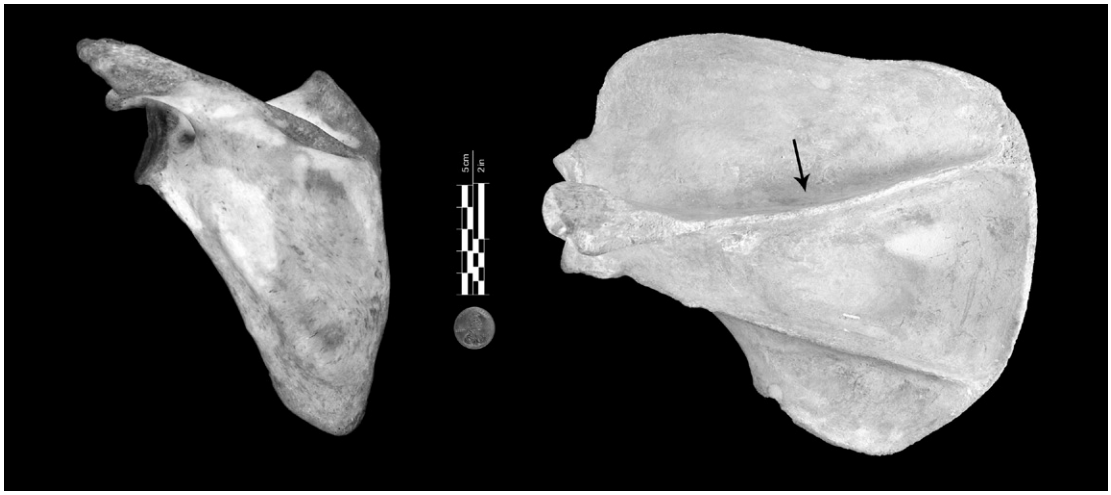

Figure 10-20: A human left scapula (posterior view) is compared to a bear's scapula (lateral view). The spine of the bear's scapula (arrow) divides the scapula into roughly equal halves. This feature is seen in many carnivores.

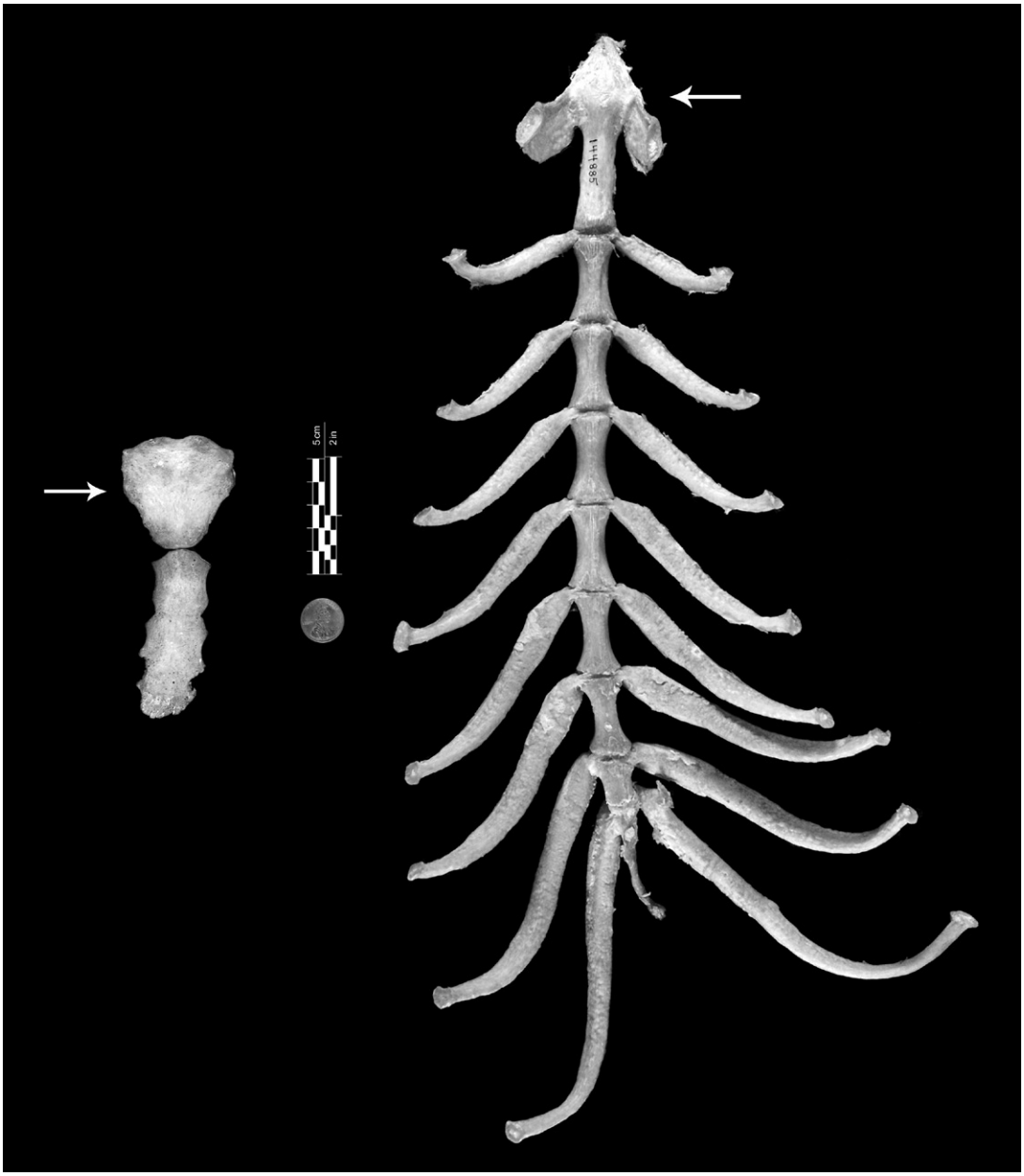

Figure 10-21: A human sternum is compared to a complete bear's sternum plus the associated cartilaginous ribs. Note the differences in the shape of the human and the bear's manubria (arrows).

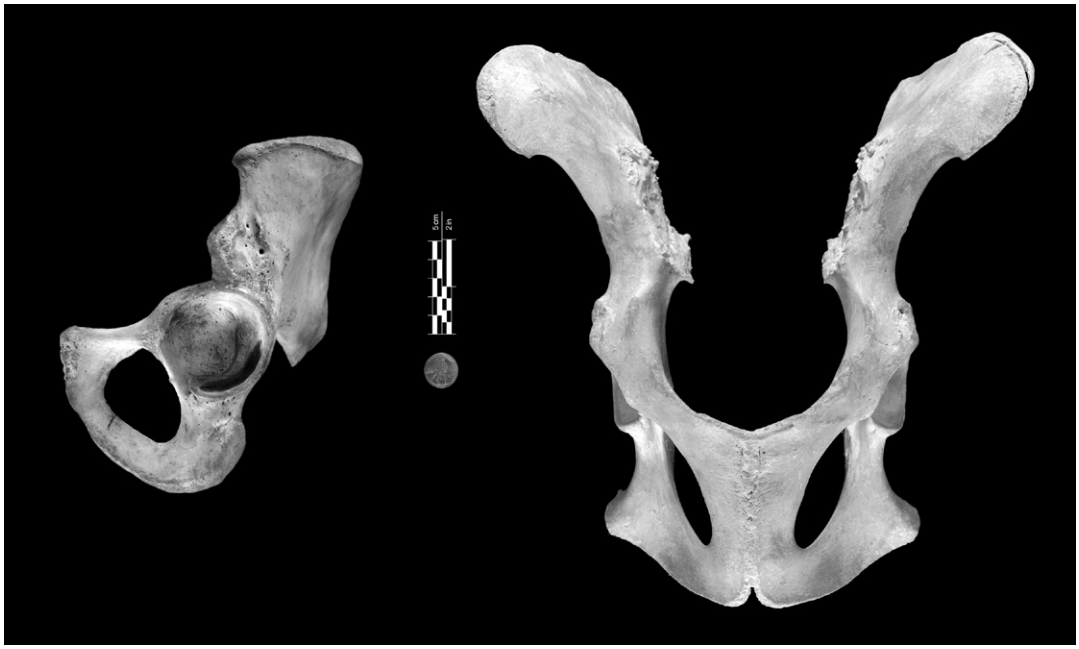

Figure 10-22: A human left innominate (lateral view) is compared to a bear's pelvis (ventral view). The broad ilium is typical of human pelves and is related to bipedalism. Quadrupeds have longer, narrower ilia.

Figure 10-23: A human left innominate (medial view) is compared to a bear's pelvis (dorsal view). The two bear innominates are fused along the pubic symphysis.

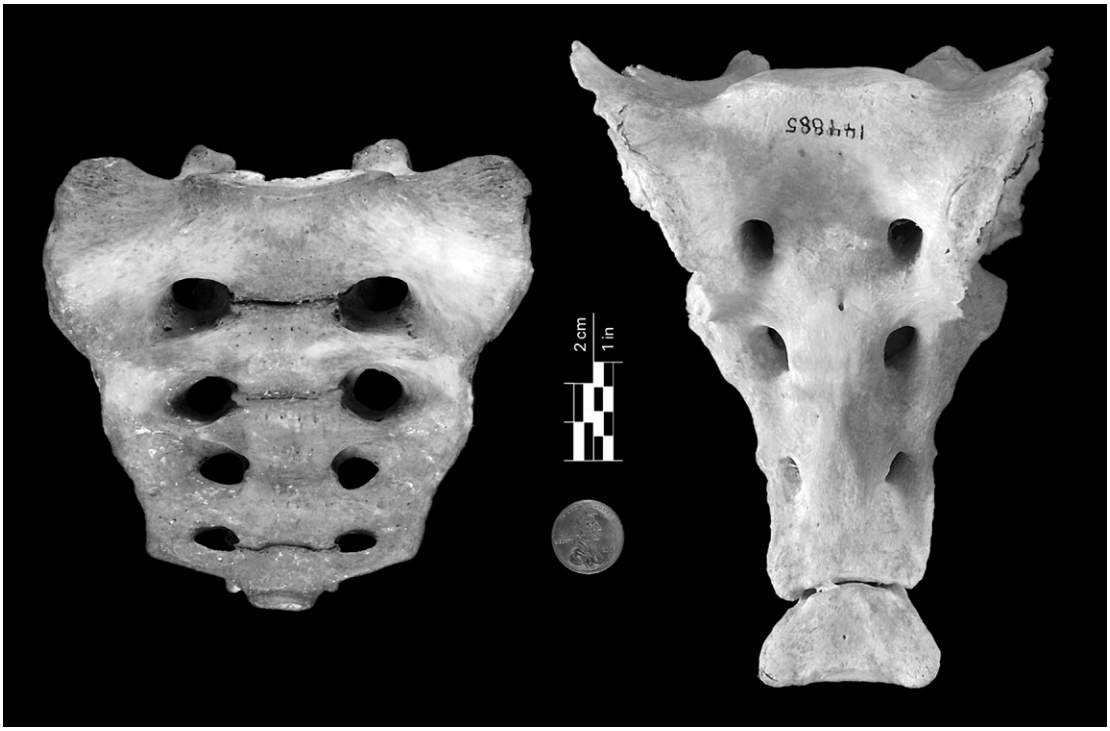

Figure 10-24: A human sacrum (anterior view) is compared to a bear's sacrum (ventral view).

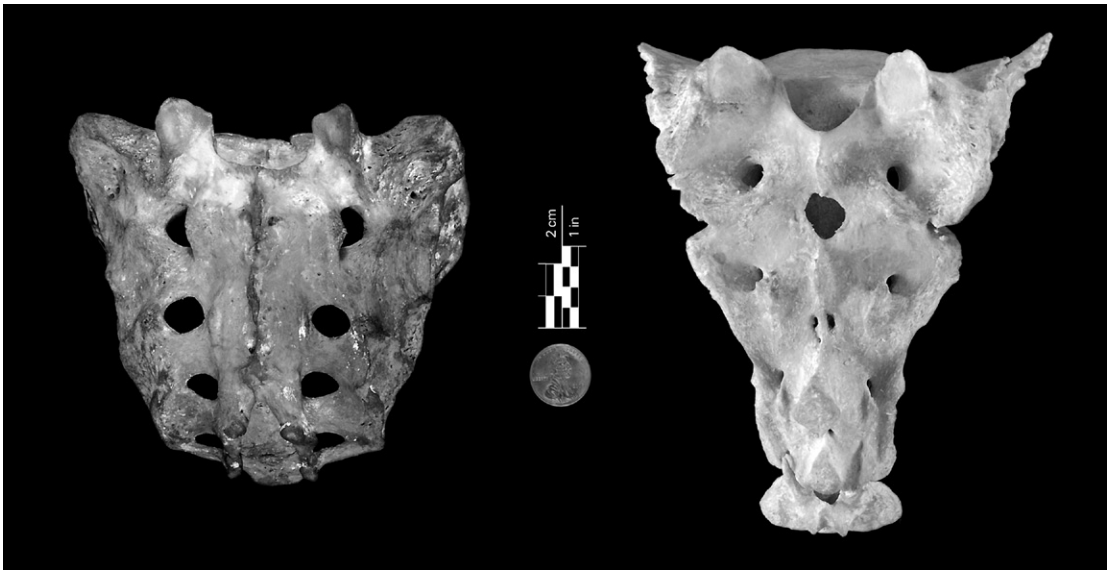

Figure 10-25: A human sacrum (posterior view) is compared to a bear's sacrum (dorsal view).

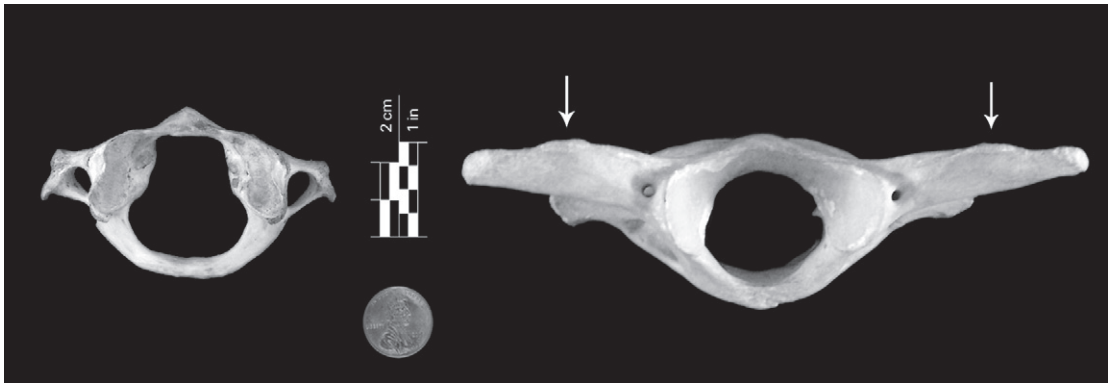

Figure 10-26: A human atlas (C1, superior view) is compared to a bear's atlas (C1, cranial view). Note the large wings (arrows) on the bear's atlas; these are typical of carnivores.

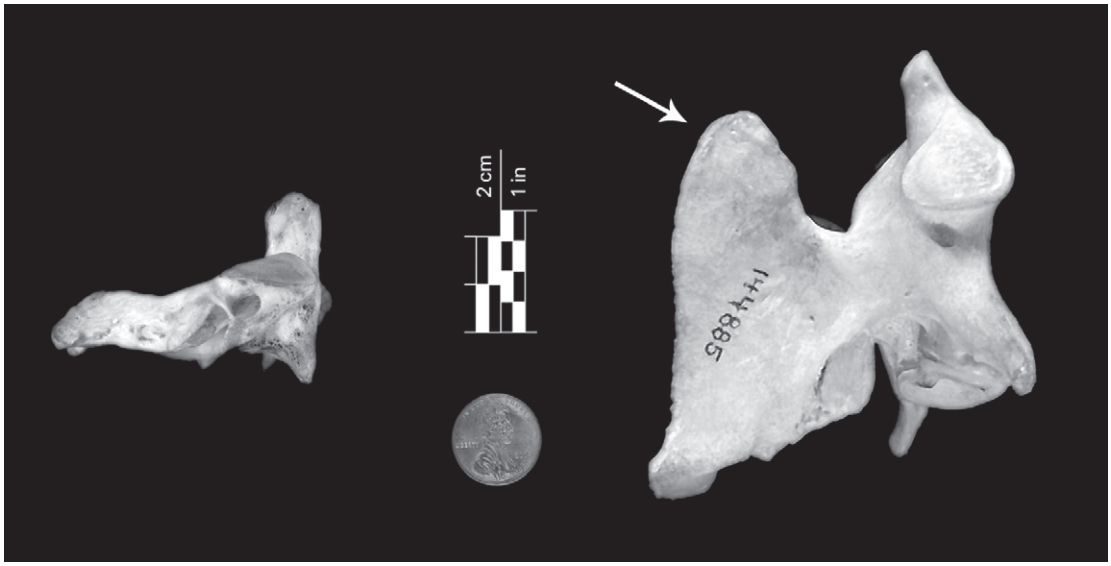

Figure 10-27: A human axis (C2, lateral view) is compared to a bear's atlas (C2, lateral view). The bear's atlas is much longer and includes a large spinous process (arrow).

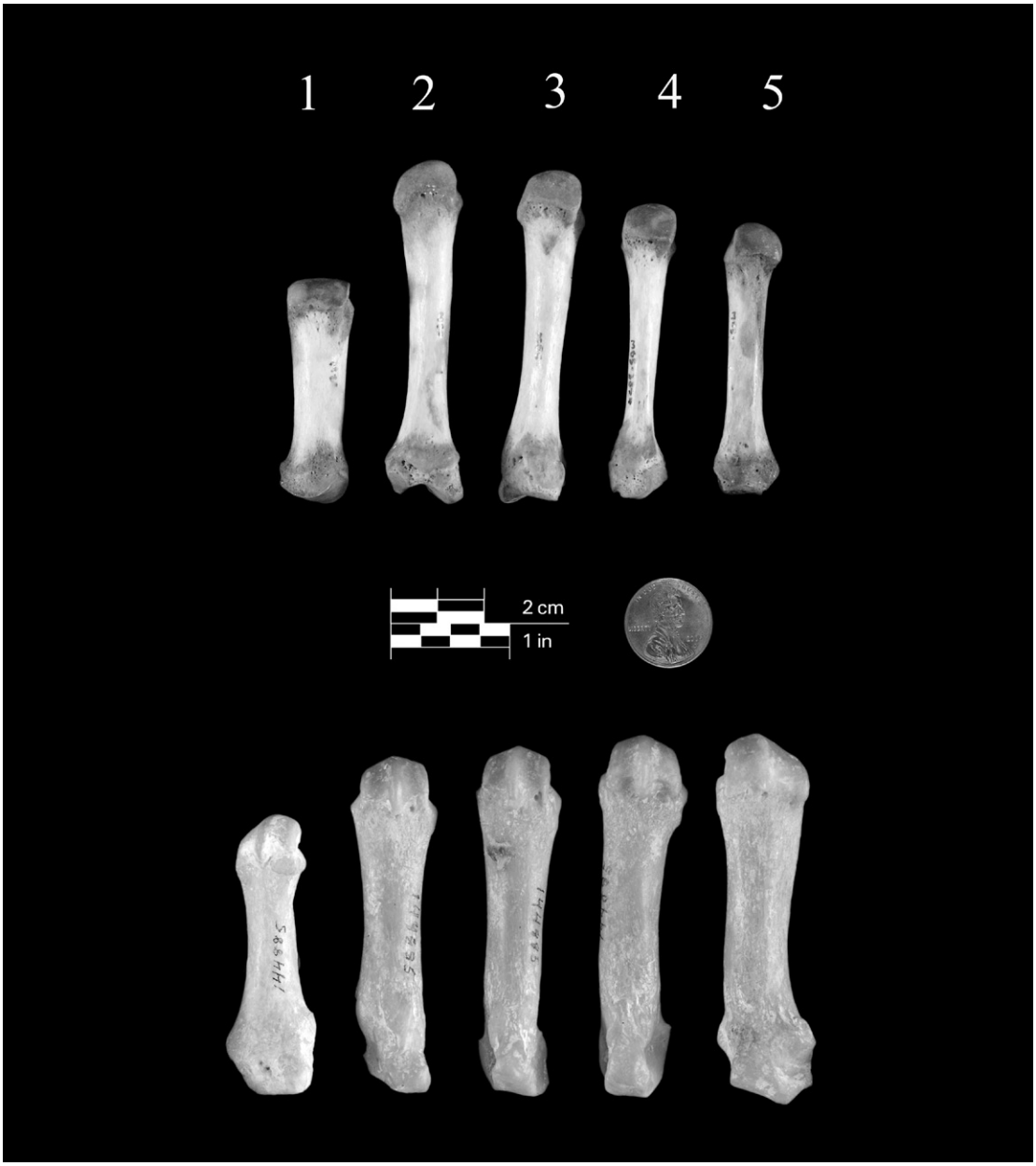

Figure 10-28: Human left metacarpals 1–5 (anterior view) are compared to a bear's left metacarpals (volar view). The similarity in size and shape between human and bear metacarpals is frequently noted. The distal ends of the bones are pictured at the top of the photograph.

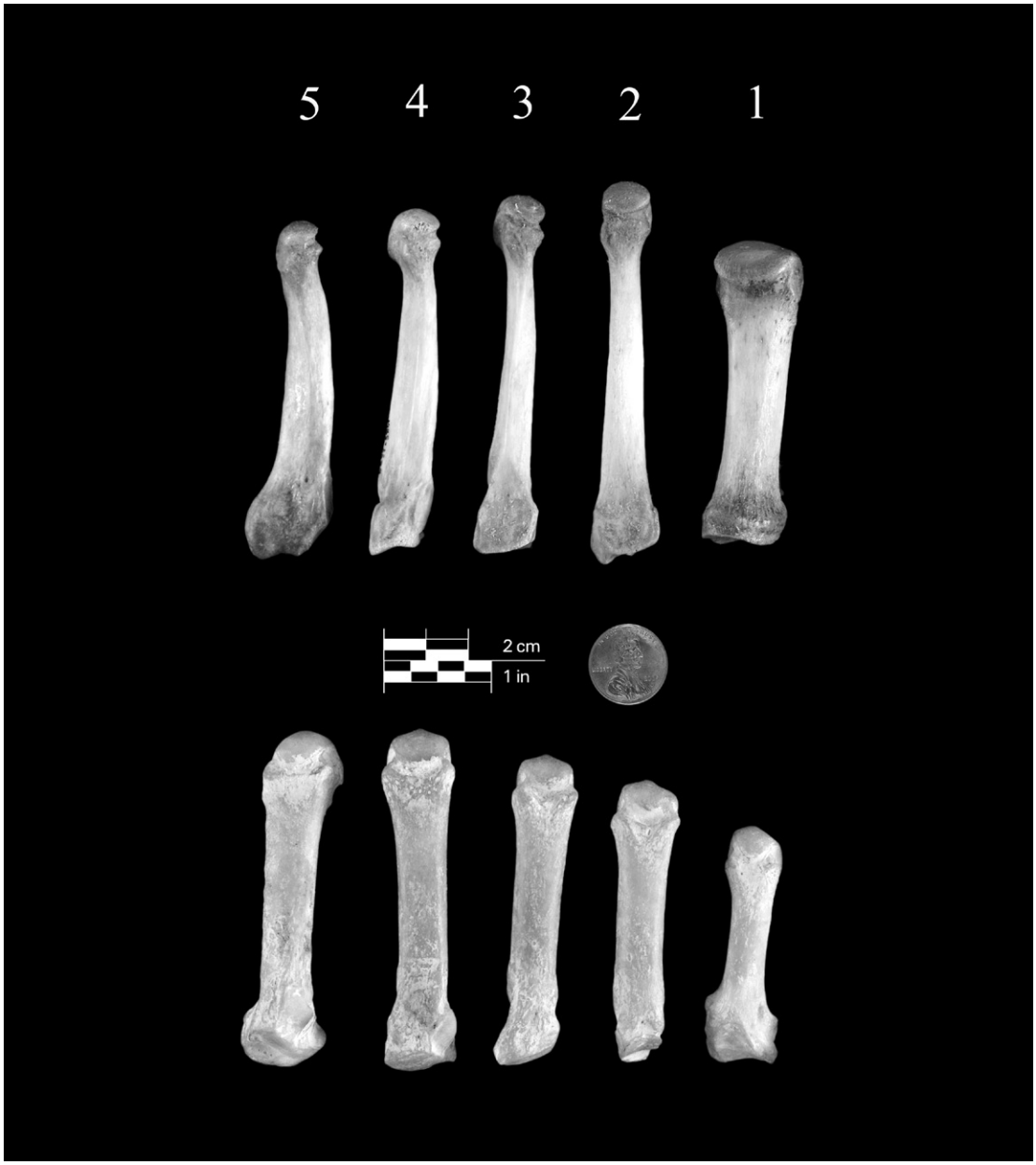

Figure 10-29: Human left metatarsals 1–5 (superior view) are compared to a bear's left metatarsals (dorsal view). The distal ends of the bones are pictured at the top of the photograph.

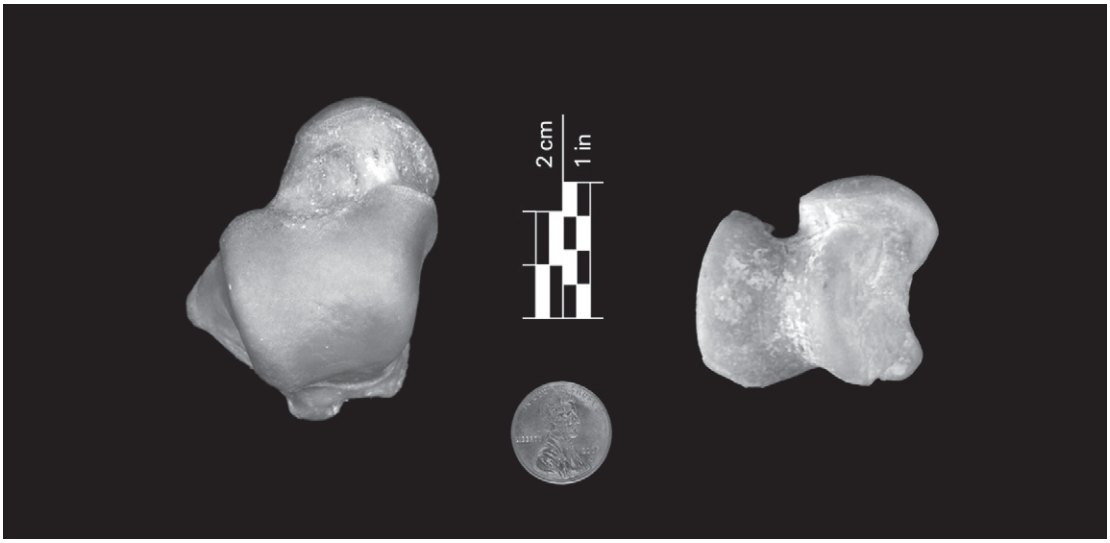

Figure 10-30: A human left talus (superior view) is compared to a bear's left astragalus (plantar view).

Figure 10-31: A human left calcaneus (superior view) is compared to a bear's left calcaneus (dorsal view). While these two bones are generally quite similar in form, note the differences in the shape of the sustentaculum tali (arrows).

CHAPTER 11

Deer (Odocoileus virginianus)

Comparative Osteology. DOI: 10.1016/B978-0-12-388437-4.00011-9

Figure 11-01: Male white-tailed deer cranium (A, lateral view, right side). In most deer species, the males have antlers while the females do not. The one exception is the reindeer; both male and female reindeer have antlers. Antlers differ from horns and are found only in cervids (e.g., deer and moose). (B, ventral view). The deer's dental formula is 0/3.0/1.3/3.3/3.

Figure 11-02: A human left humerus (anterior view) is compared to a deer's left humerus (cranial view). Note the height of the greater tubercle on the deer's proximal humerus (arrow).

Figure 11-03: A human left humerus (posterior view) is compared to a deer's left humerus (caudal view). Note the deeper olecranon fossa on the deer's distal humerus (arrow).

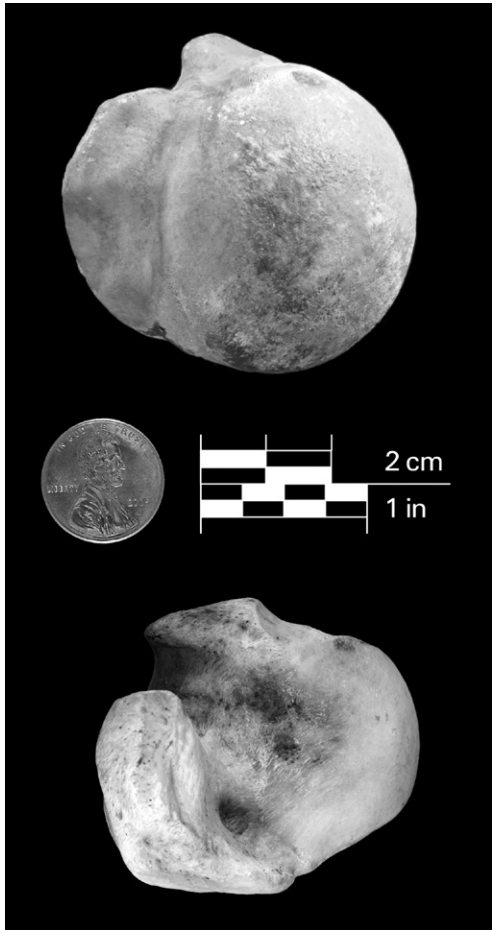

Figure 11-04: An adult human proximal humerus (superior view) is compared to a deer's proximal humerus (dorsal view). The greater and lesser tubercles and the head of the humerus are visible in this view.

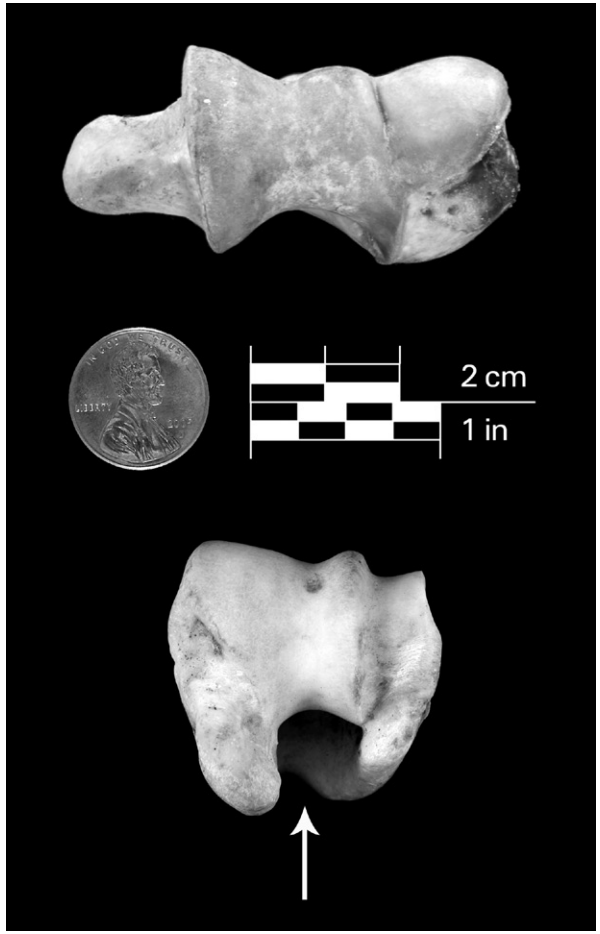

Figure 11-05: An adult human distal humerus (inferior view) is compared to a deer's distal humerus (ventral view). The deer has a very broad, barrel-shaped trochlea. The arrow points to the olecranon fossa.

Figure 11-06: A human left radius (anterior view) is compared to a deer's left radius (cranial view).

Figure 11-07: A human left radius (posterior view) is compared to a deer's left radius (caudal view). The human proximal radius has a distinct head and neck. The articulation with the ulna is visible on the lateral part of the caudal surface of the deer's radius (arrow).

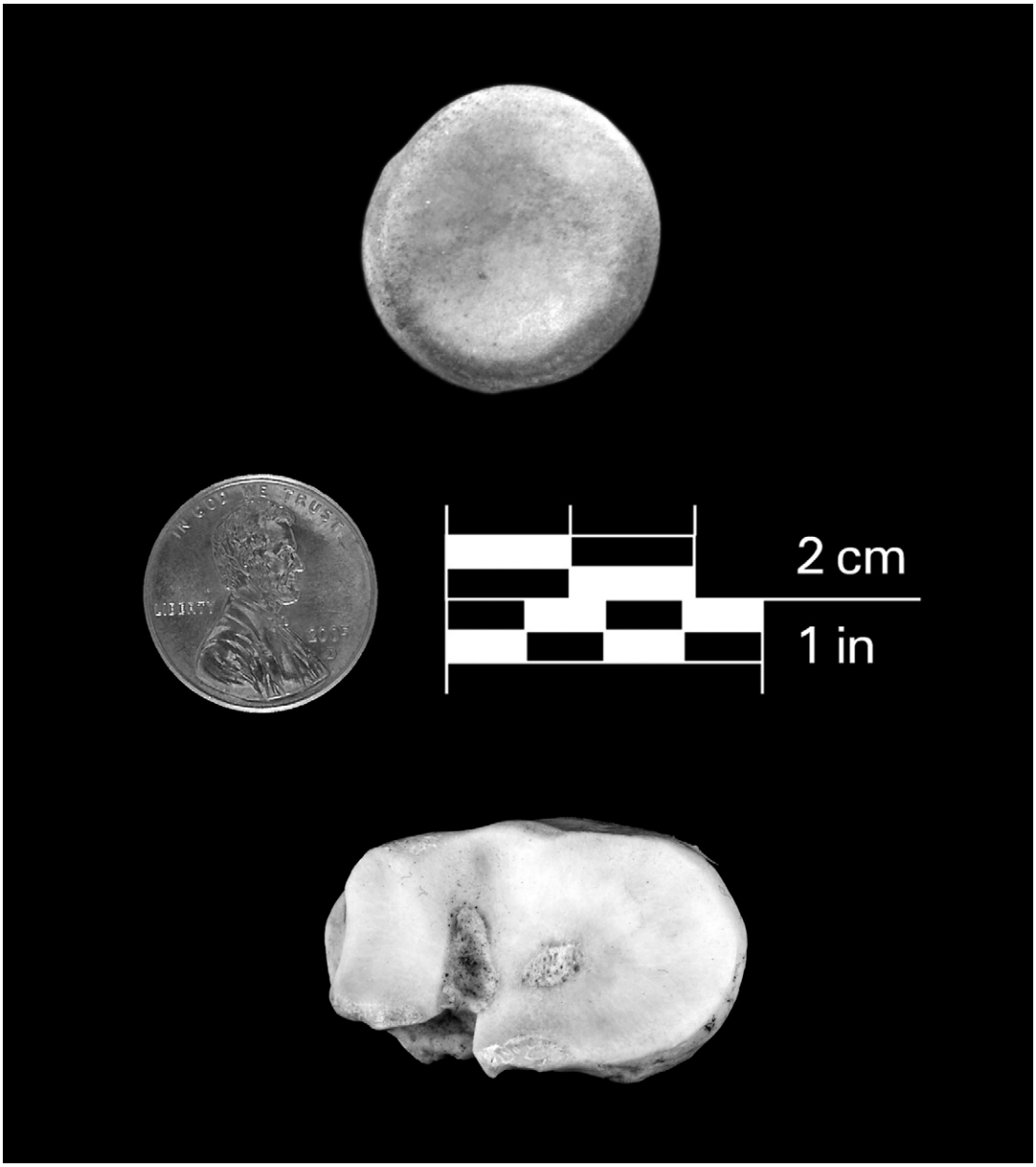

Figure 11-08: An adult human proximal radius (superior view) is compared to a deer's proximal radius (dorsal view). The deer's radius has a slightly concave articular surface.

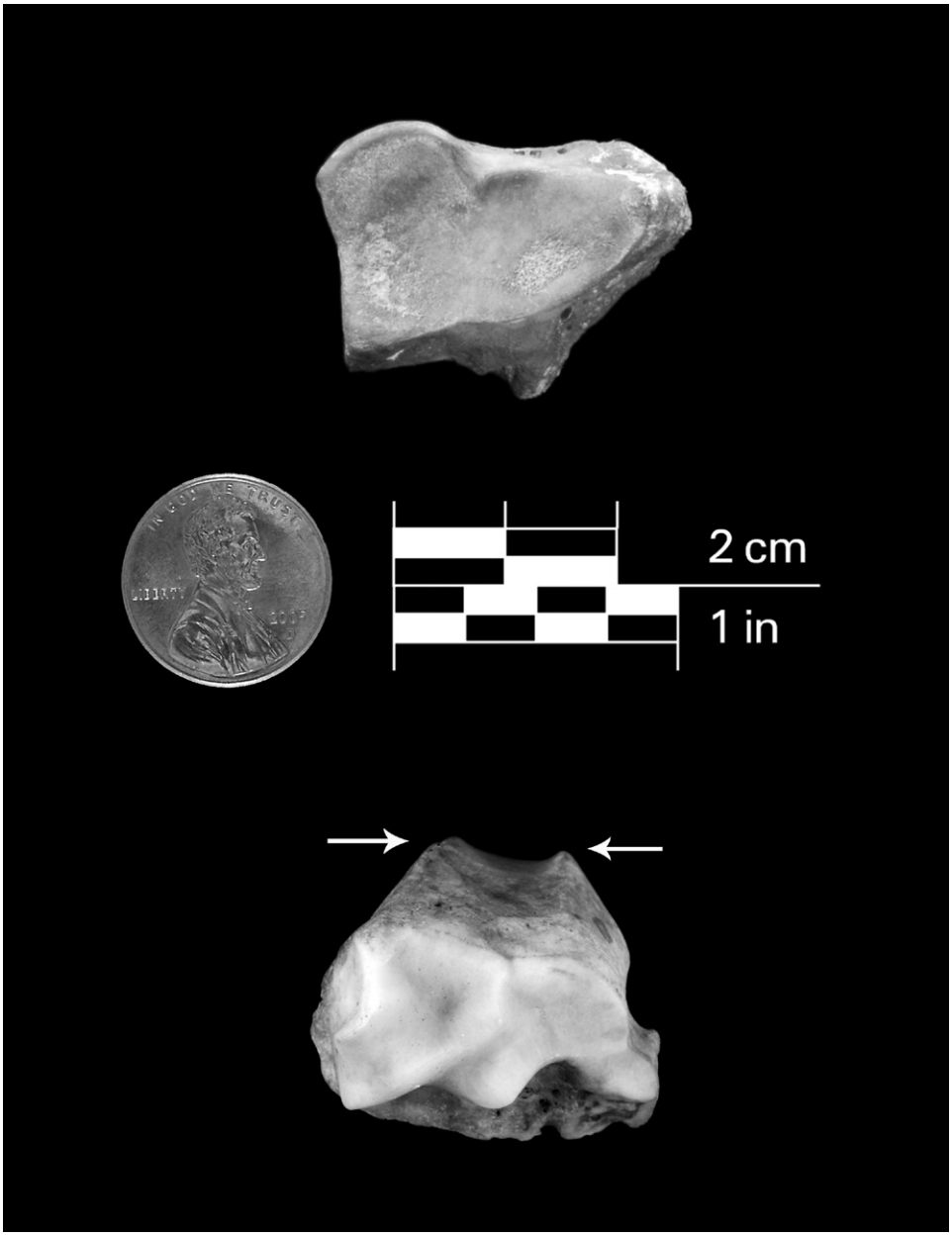

Figure 11-09: An adult human distal radius (inferior view) is compared to a deer's distal radius (ventral view). The facets visible on the deer's distal radius articulate with the first carpal row. The radial grooves (arrow) are more well marked in the cervids than they are in the bovids.

Figure 11-10: A human left ulna (anterior view) is compared to a deer's left ulna (cranial view). Note the slender shaft of the deer's ulna.

Figure 11-11: A human left ulna (posterior view) is compared to a deer's left ulna (caudal view).

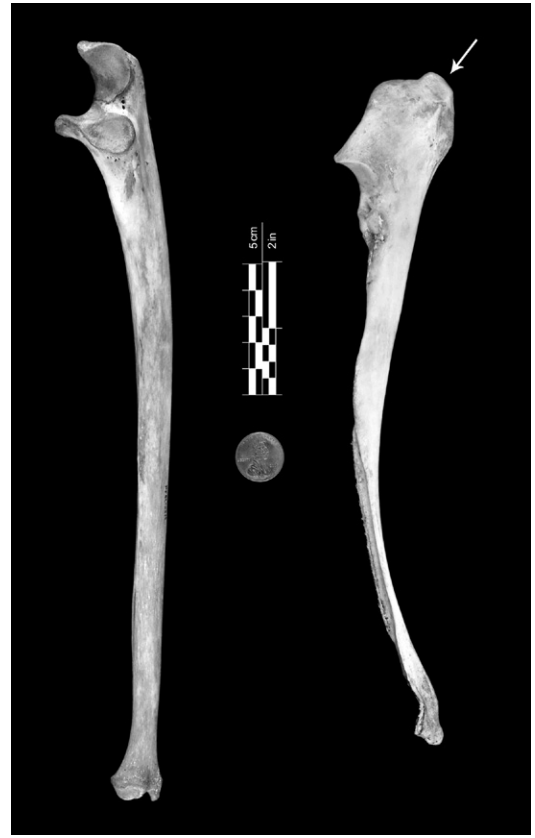

Figure 11-12: A human left ulna is compared to a deer's left ulna (both lateral views). Note the well-developed olecranon process on the deer's ulna (arrow).

Figure 11-13: A human left femur (anterior view) is compared to a deer's left femur (cranial view). Note the well-developed greater trochanter in the deer's femur (arrow).

Figure 11-14: A human left femur (posterior view) is compared to a deer's left femur (caudal view).

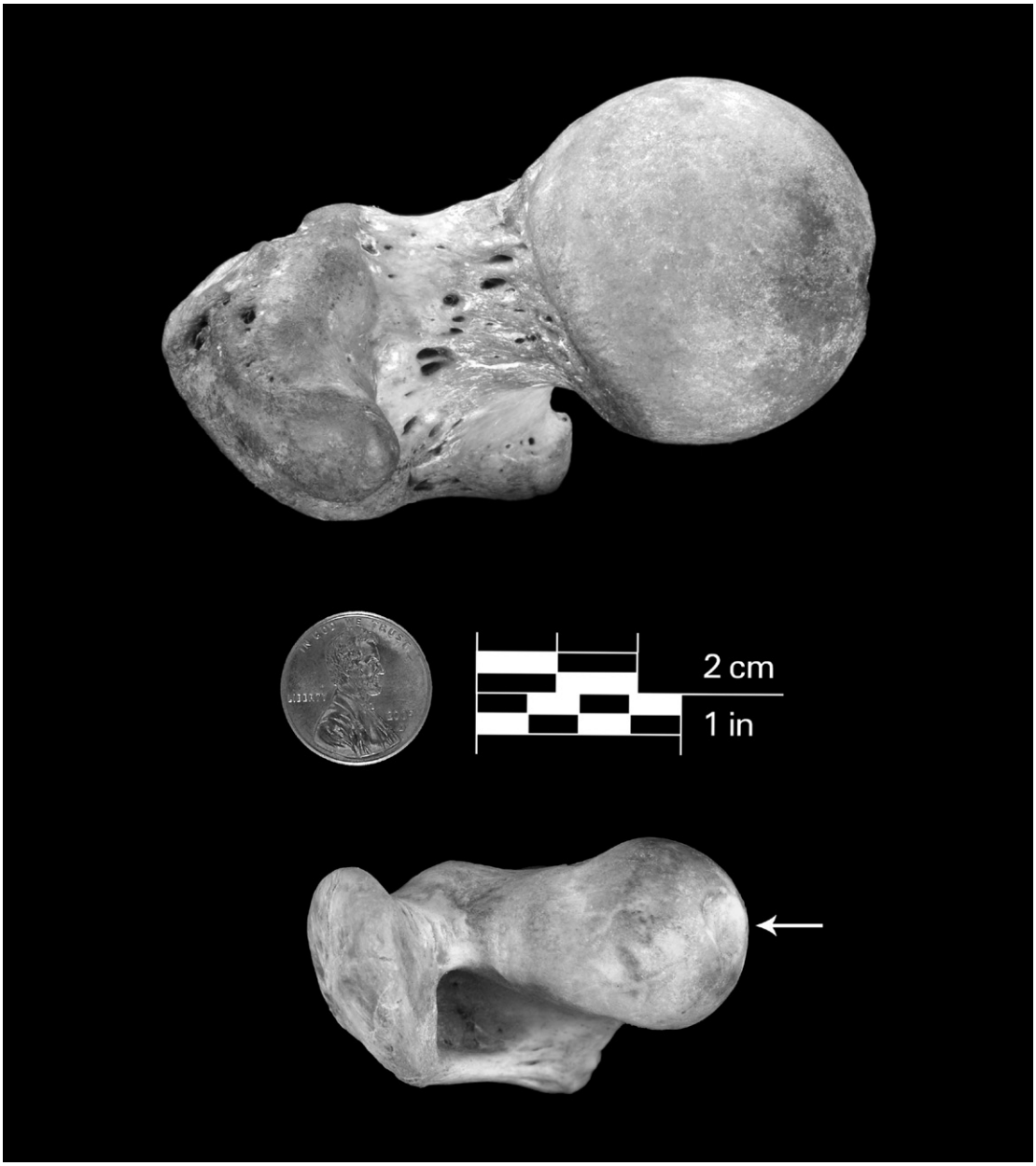

Figure 11-15: An adult human left proximal femur (superior view) is compared to a deer's left proximal femur (dorsal view). The greater trochanter, lesser trochanter, and head are visible in both specimens. The arrow points to the fovea capitis.

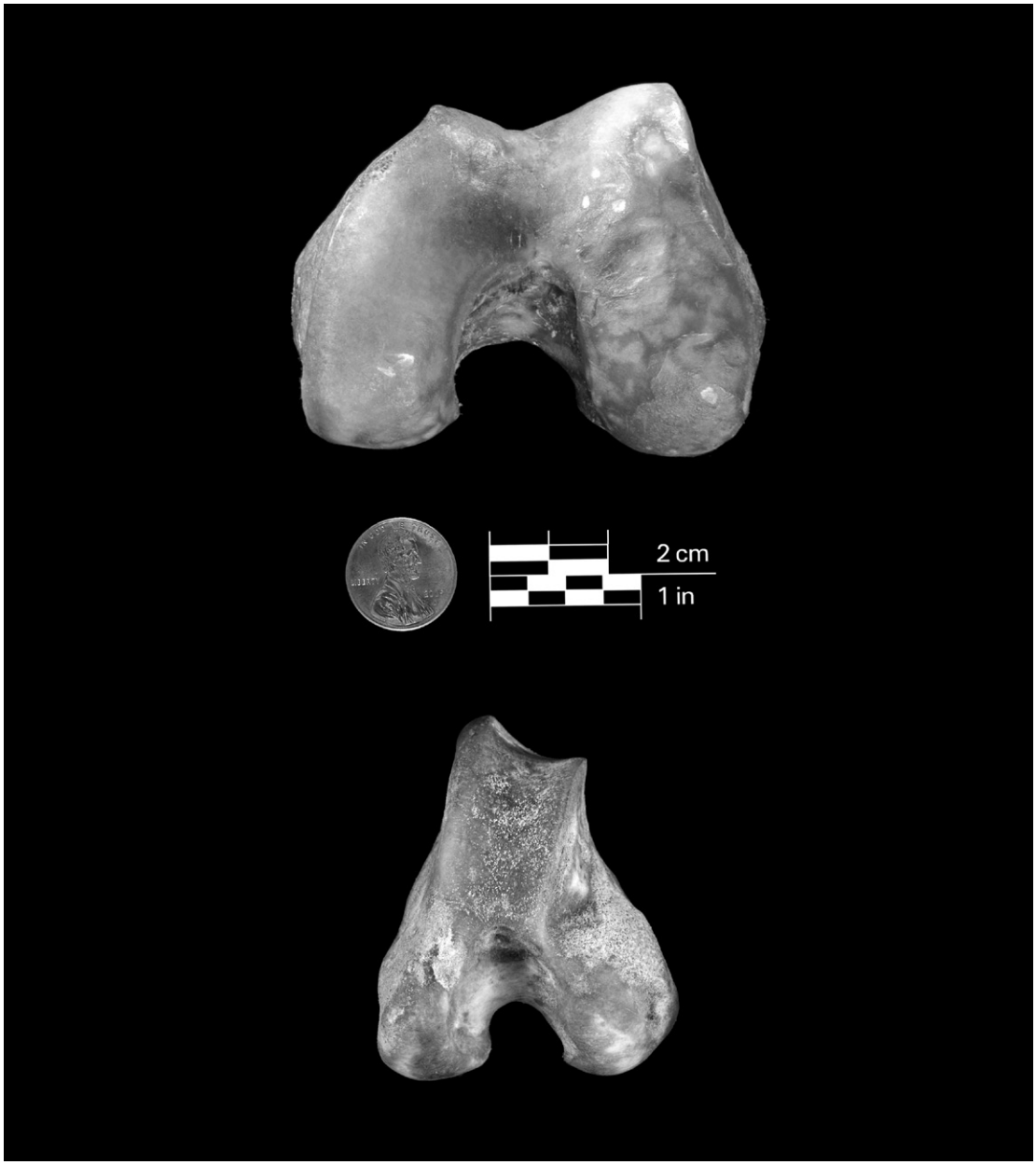

Figure 11-16: An adult human left distal femur (inferior view) is compared to a deer's left distal femur (ventral view). The two condyles and the trochlea for articulation with the patella are visible in this view.

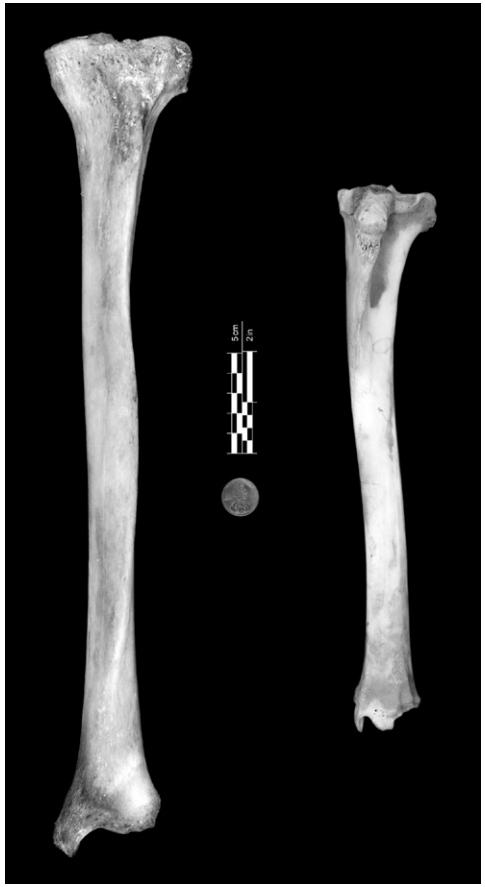

Figure 11-17: A human left tibia (anterior view) is compared to a deer's left tibia (cranial view).

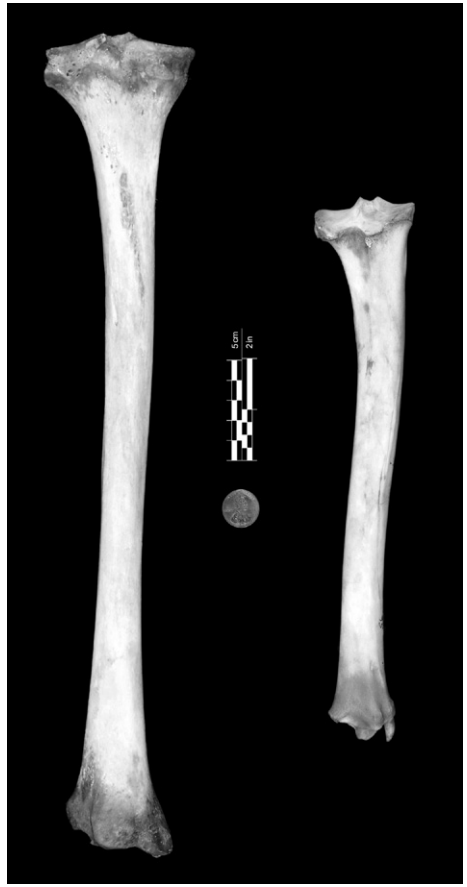

Figure 11-18: A human left tibia (posterior view) is compared to a deer's left tibia (caudal view).

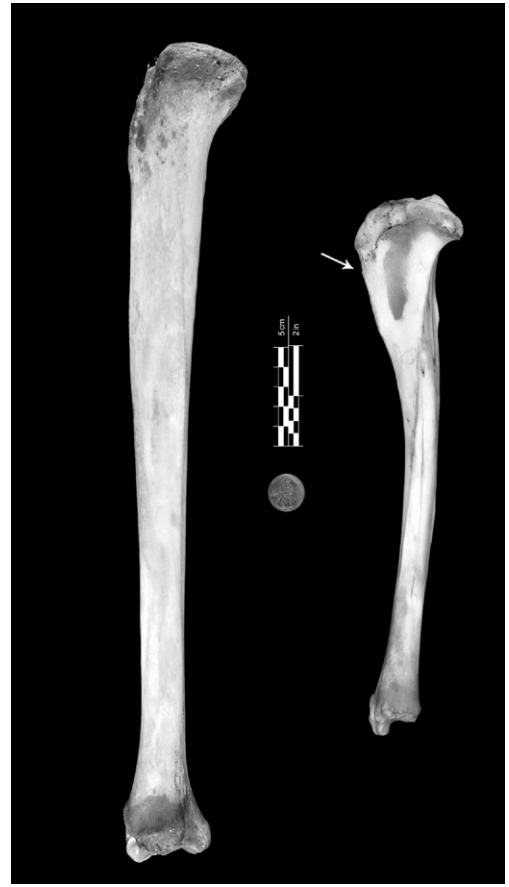

Figure 11-19: A human left tibia (lateral view) is compared to a deer's left tibia (lateral view). Note the well-developed tibial tuberosity on the deer's tibia (arrow).

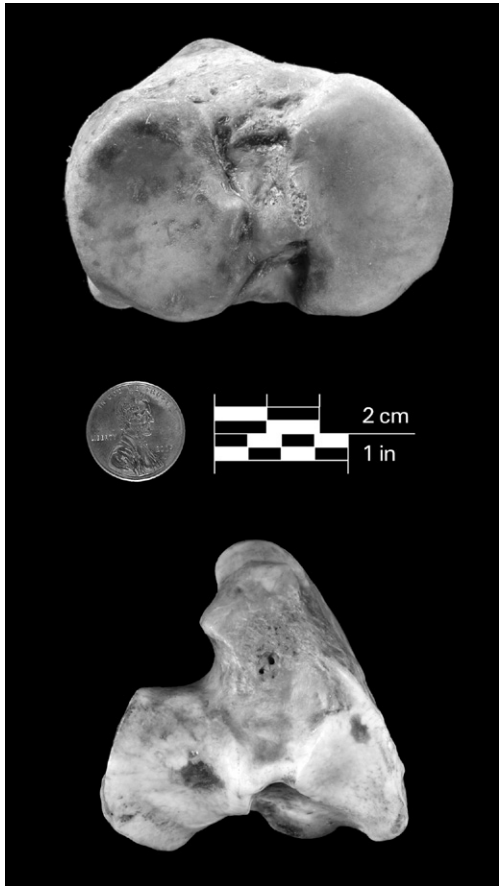

Figure 11-20: An adult human left proximal tibia (superior view) is compared to a deer's left proximal tibia (dorsal view). The facets that articulate with the distal condyles of the femur are visible in this view.

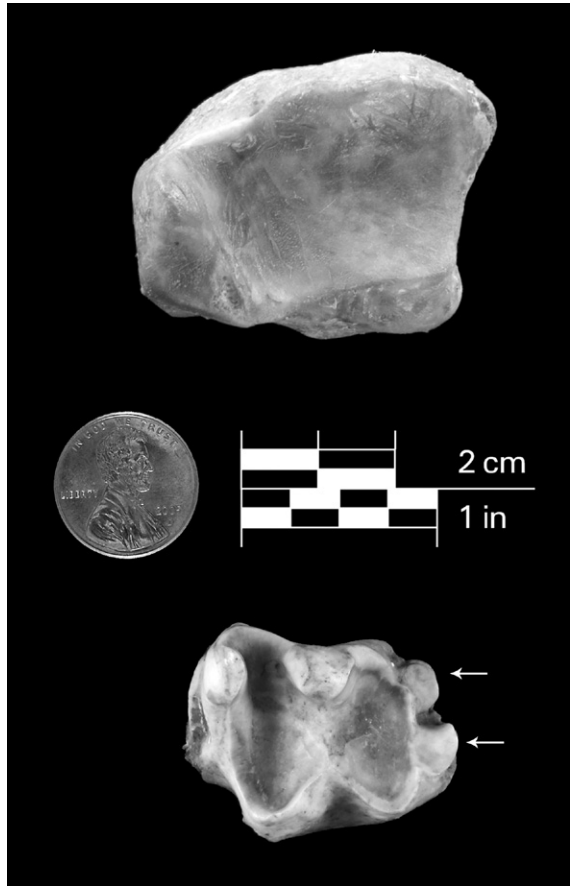

Figure 11-21: An adult human left distal tibia (inferior view) is compared to a deer's left distal tibia (ventral view). The two large parallel articular facets mark the articulation with the astragalus. The two small facets on the lateral side (arrows) mark the articulation with the malleolus, a small tarsal that is the remnant of the distal fibula.

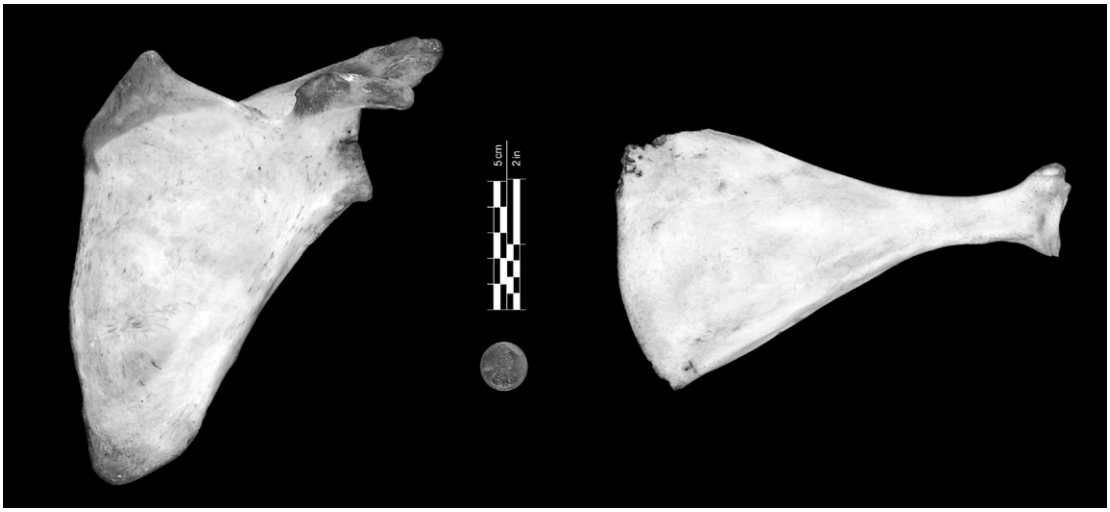

Figure 11-22: A human left scapula (anterior view) is compared to a deer's left scapula (medial view). Both bones are positioned as they would be in a human.

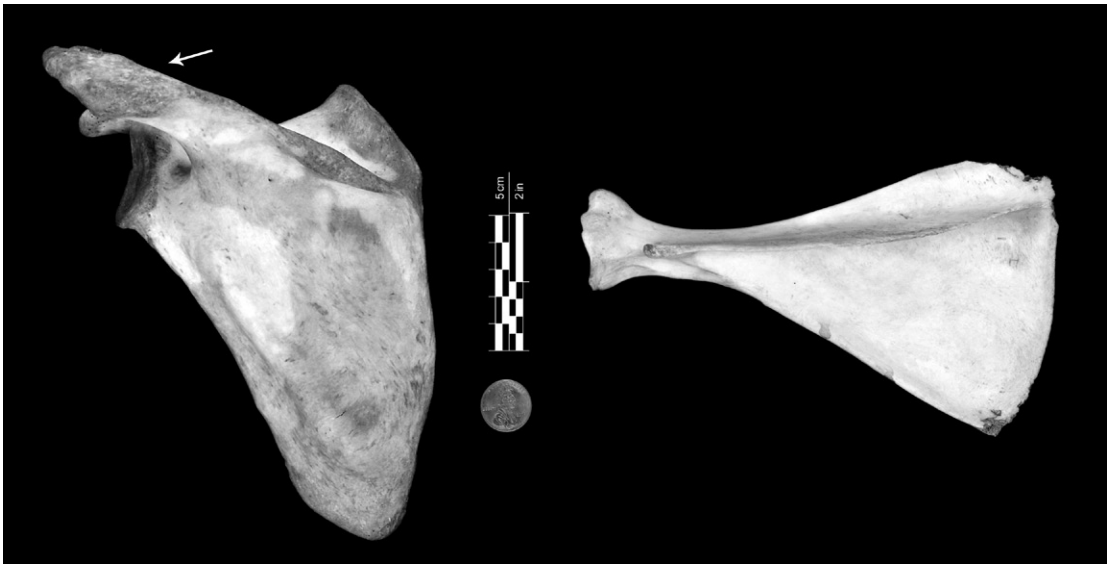

Figure 11-23: A human left scapula (posterior view) is compared to a deer's left scapula (lateral view). Note the large acromion process on the human scapula (arrow).

Figure 11-24: A human left scapula and a deer's left scapula are compared (glenoid views). Note that the deer's glenoid cavity is very round in shape. Those of the sheep and the goat tend to be somewhat more oval.

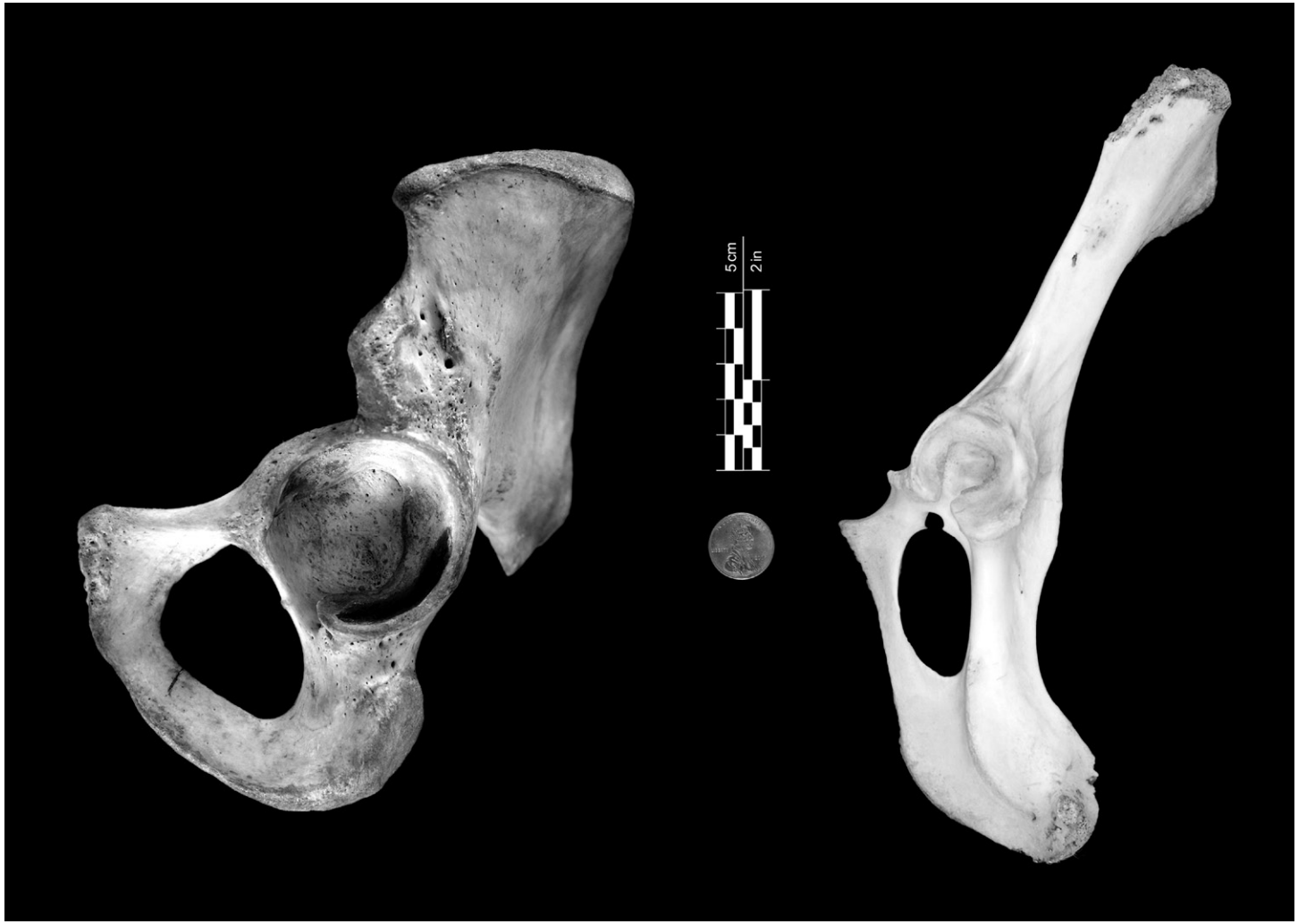

Figure 11-25: A human left innominate (lateral view) is compared to a deer's left innominate (lateral view).

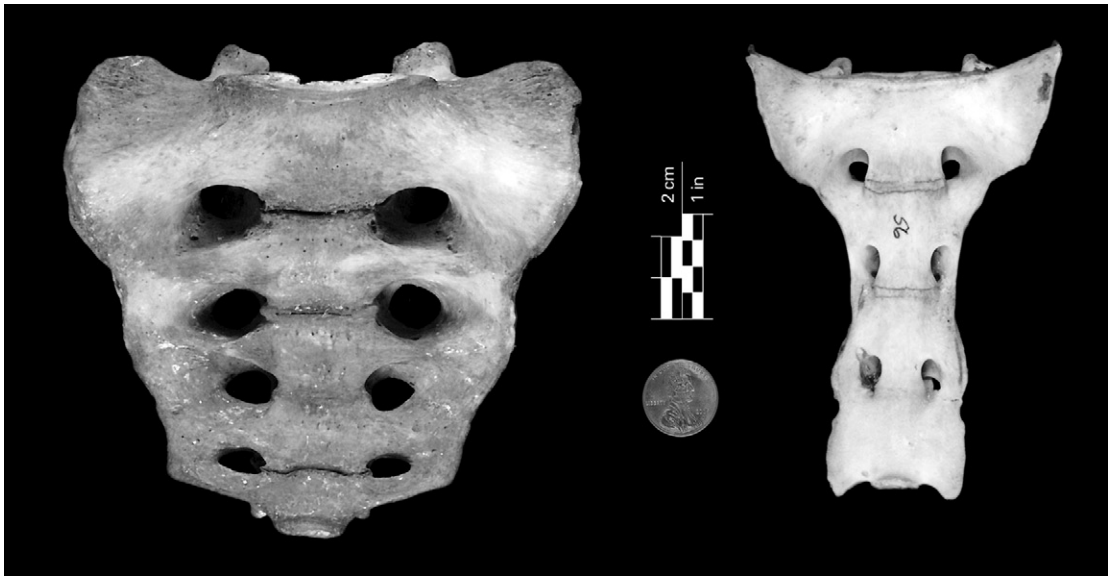

Figure 11-26: A human sacrum (anterior view) is compared to a deer's sacrum (ventral view). The wings of the deer's sacrum are wide in relation to the body.

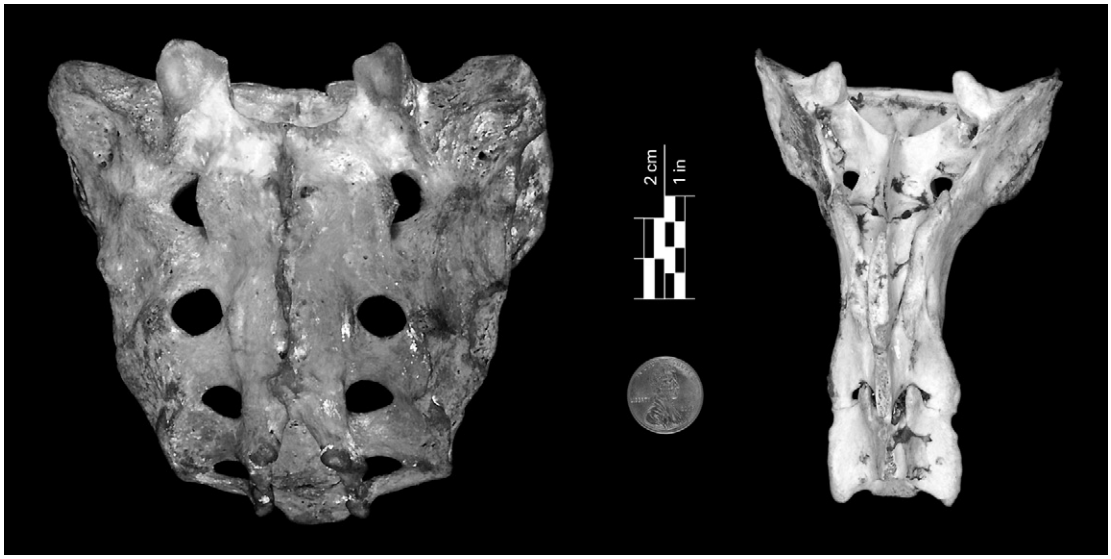

Figure 11-27: A human sacrum (posterior view) is compared to a deer's sacrum (dorsal view).

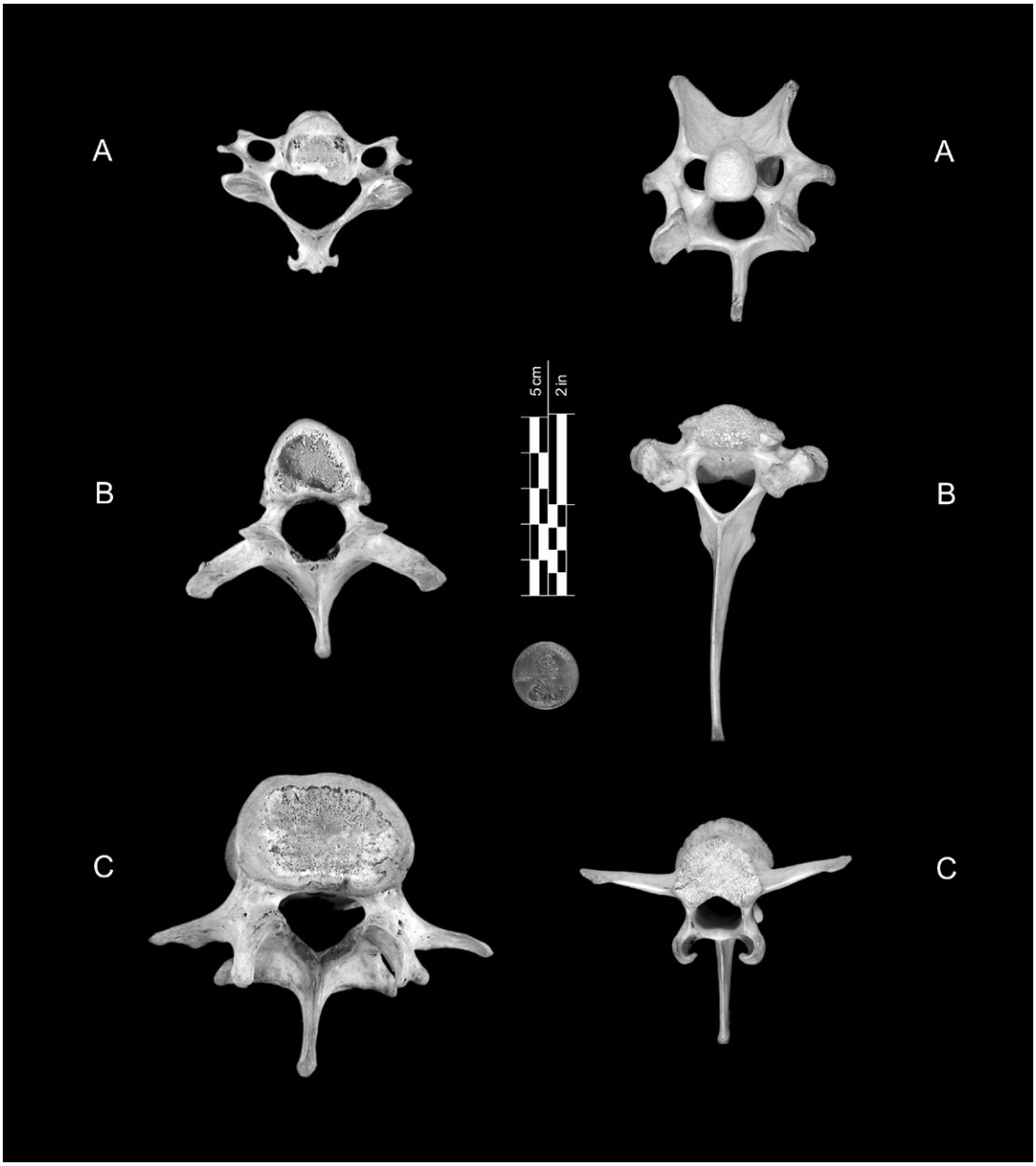

Figure 11-28: Superior views of typical human cervical (A, left), thoracic (B, left), and lumbar (C, left) vertebrae. Cranial views of typical white-tailed deer cervical (A, right), thoracic (B, right), and lumbar (C, right) vertebrae.

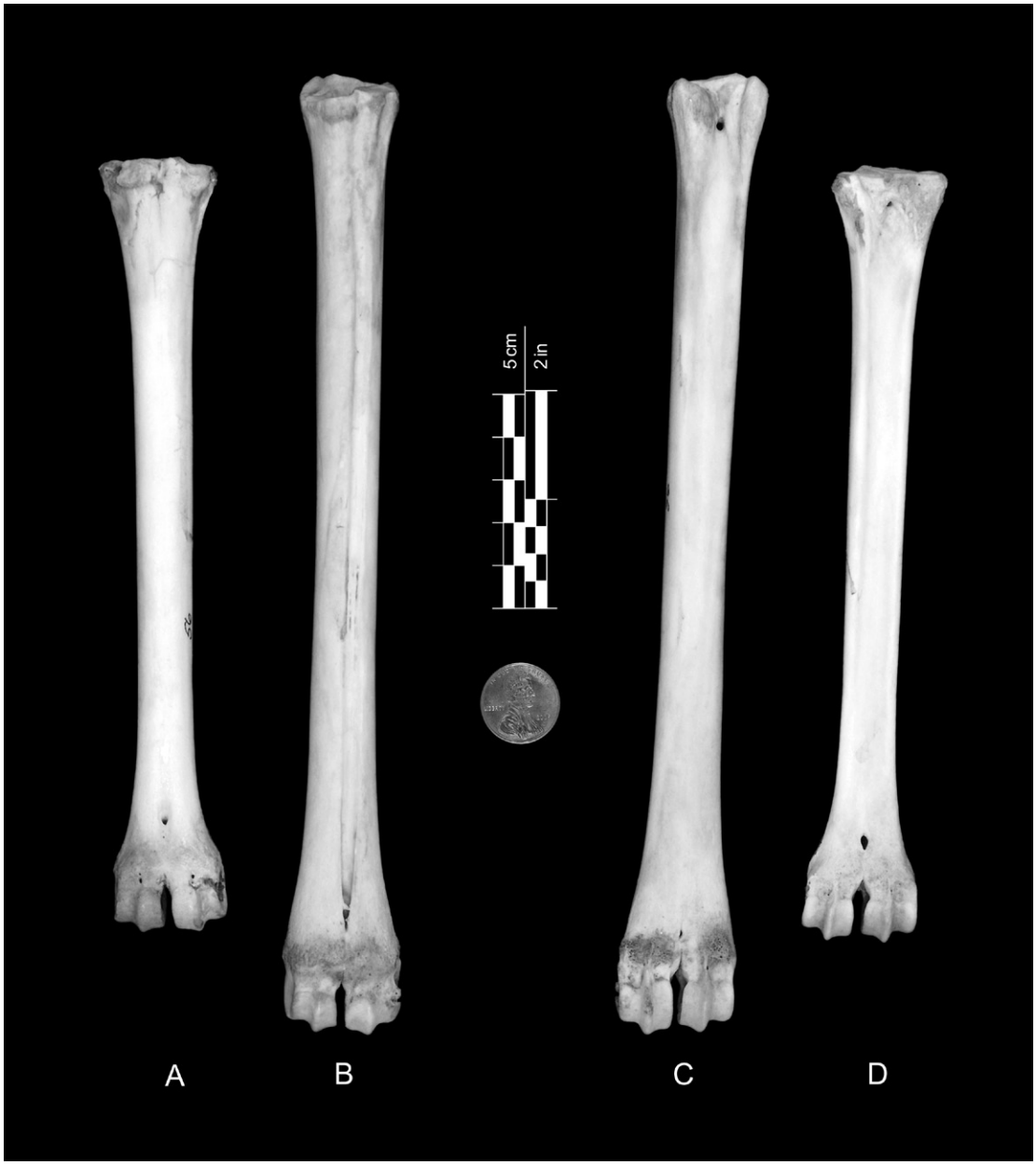

Figure 11-29: White-tailed deer metacarpus and metatarsus. The deer's left metacarpus (A, dorsal view), metatarsus (B, dorsal view), left metatarsus (C, plantar view), and the left metacarpus (D, palmar (volar) view). These metapodia are composed of the fused third and fourth metacarpals and metatarsals. The deer's metapodia have distinctive concave grooves along the plantar/volar surfaces that distinguish them from the metapodia of the bovids.

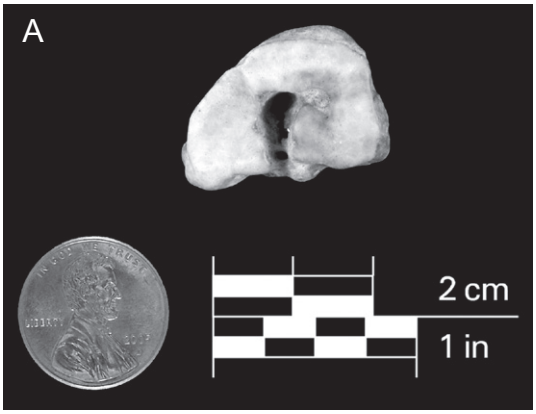

Figure 11-30a: Deer proximal metacarpus (left side, dorsal view). The articulation is D-shaped, with the larger articular facet on the medial side.

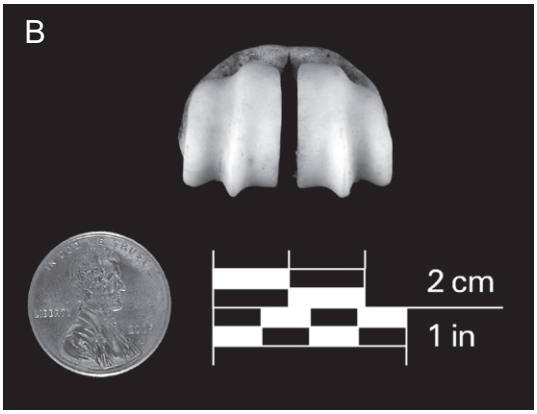

Figure 11-30b: Deer distal metacarpus (left side, volar view). The distal condyles articulate with two proximal/first phalanges.

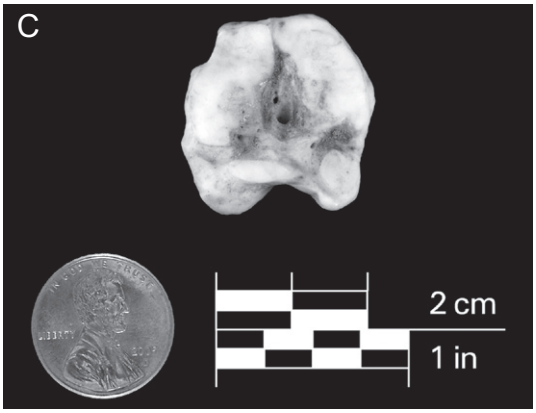

Figure 11-30c: Deer proximal metatarsus (left side, dorsal view).

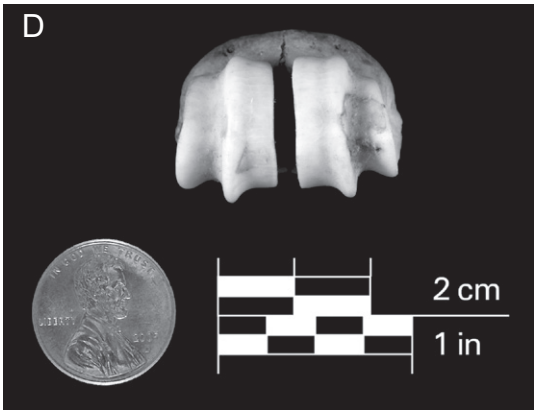

Figure 11-30d: Deer distal metatarsus (left side, plantar view). The distal condyles articulate with two proximal/first phalanges.

Figure 11-31: Human left talus (A, superior view) and calcaneus (B, superior view) are compared to a white-tailed deer's astragalus (C, plantar view) and left calcaneus (D, dorsal view). The deer's astragalus has the typical "double pulley" form that is characteristic of the artiodactyls. The dorsal calcaneus includes an articulation for the malleolus, a small tarsal that is the evolutionary remnant of the distal fibula.

This page intentionally left blank

CHAPTER 12

Pig (Sus scrofa)

Comparative Osteology. DOI: 10.1016/B978-0-12-388437-4.00012-0

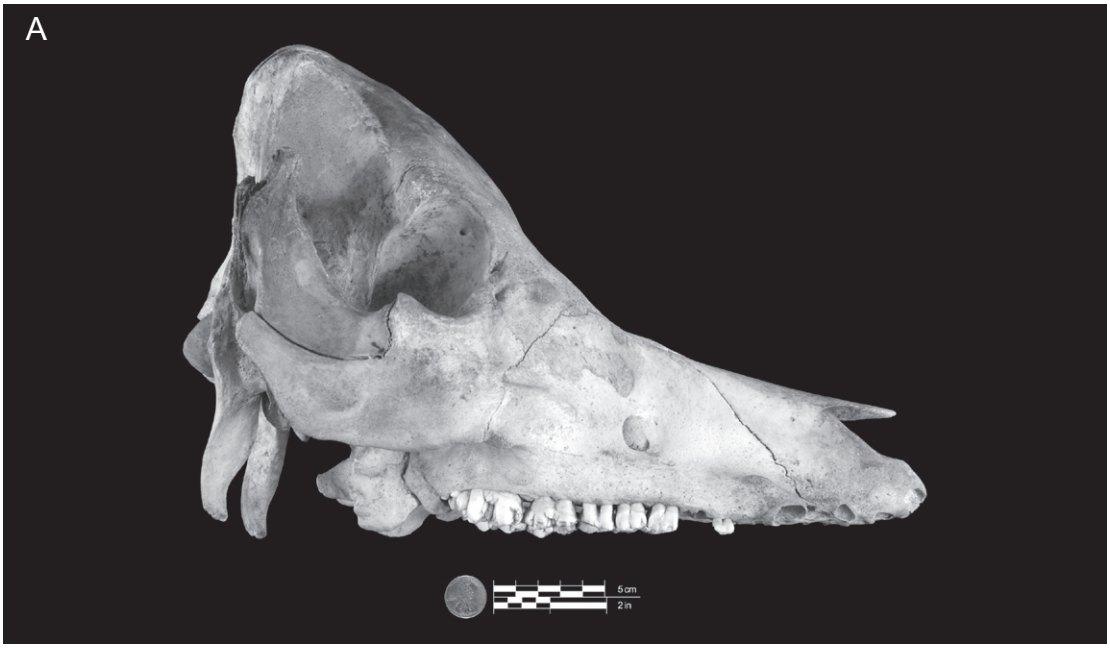

Figure 12-01: Pig cranium (A) lateral view, right side; (B) ventral view. The pig's dental formula is 3/3.1/1.4/4.3/3. Note that the incisors, canines, and some premolars were lost postmortem (after death) from this specimen.

Figure 12-02: A human left humerus (A, anterior view) is compared to adult (B) and juvenile (C) pig left humeri (cranial views). Note the large greater tubercle in the adult pig's proximal humerus (arrow). The unfused epiphyses of the juvenile pig are also shown.

Figure 12-03: A human left humerus (A, posterior view) is compared to adult (B) and juvenile (C) pig left humeri (caudal views). The unfused epiphyses of the juvenile pig are also shown.

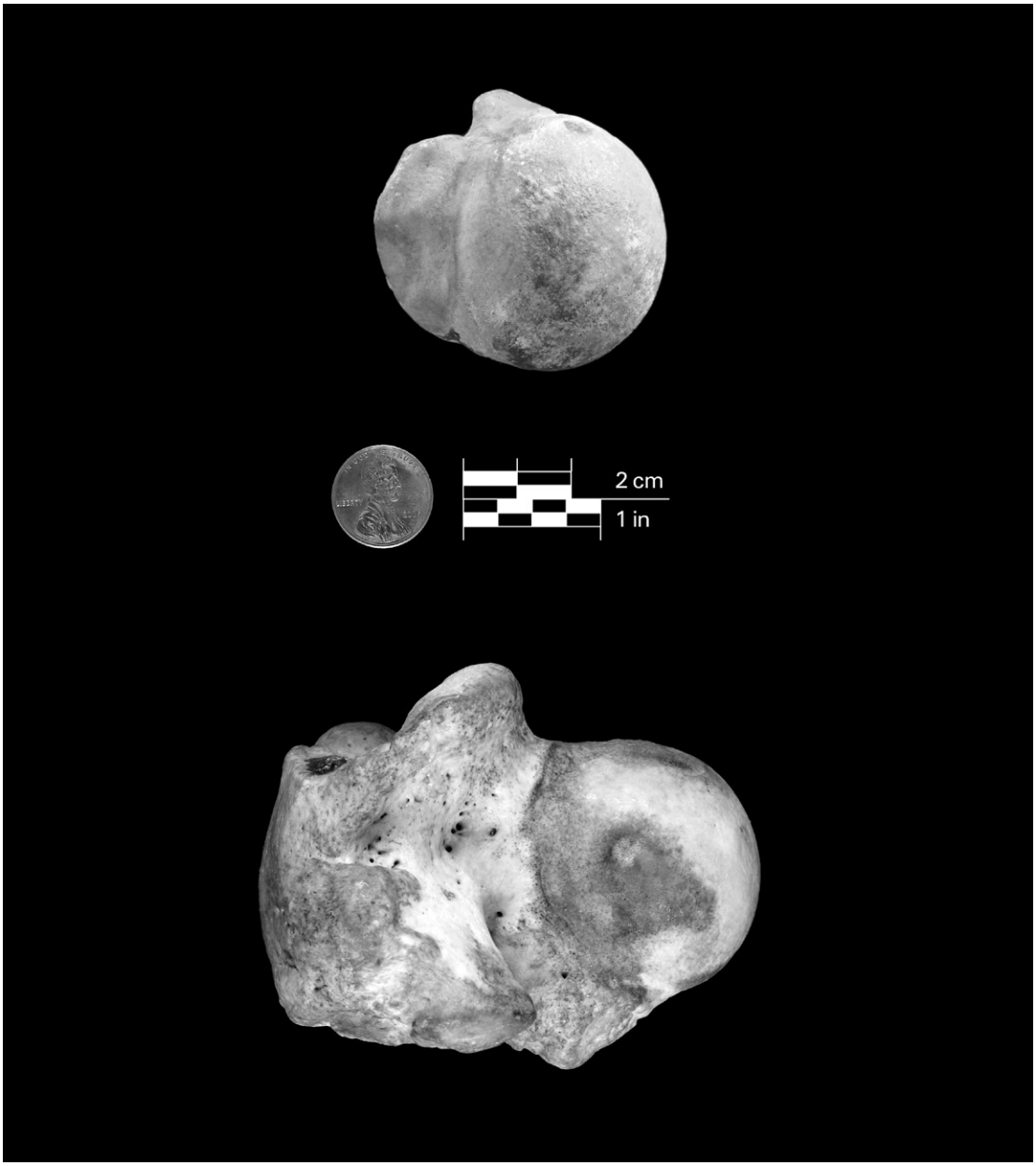

Figure 12-04: A human left proximal humerus (superior view) is compared to an adult pig's left proximal humerus (dorsal view). The head of the humerus and the pig's large tubercles are visible in this view.

Figure 12-05: A human left distal humerus (inferior view) is compared to a pig's left distal humerus (ventral view). The pig's trochlea and the olecranon fossa are visible in this view. The pig's distal humerus is one of the earliest fusing of all the pig limb bones. It fuses at about one year and is one of the elements that is commonly found in archaeological assemblages.

Figure 12-06: A human left radius and ulna (A, anterior views) are compared to adult (B) and juvenile (C) pig left radii and ulnae (cranial views). In the adult pig, the radius is often attached to the ulna. The unfused epiphyses of the juvenile pig's radius are also shown.

Figure 12-07: A human left radius and ulna (A, posterior views) are compared to adult (B) and juvenile (C) pig left radii and ulnae (caudal views). The unfused epiphyses of the juvenile pig's radius are also shown. In pigs, the ulna and radius are similar in size. The ulna is a much smaller bone in cattle, sheep, goats, and deer. In the horse, the distal ulna is completely absent.

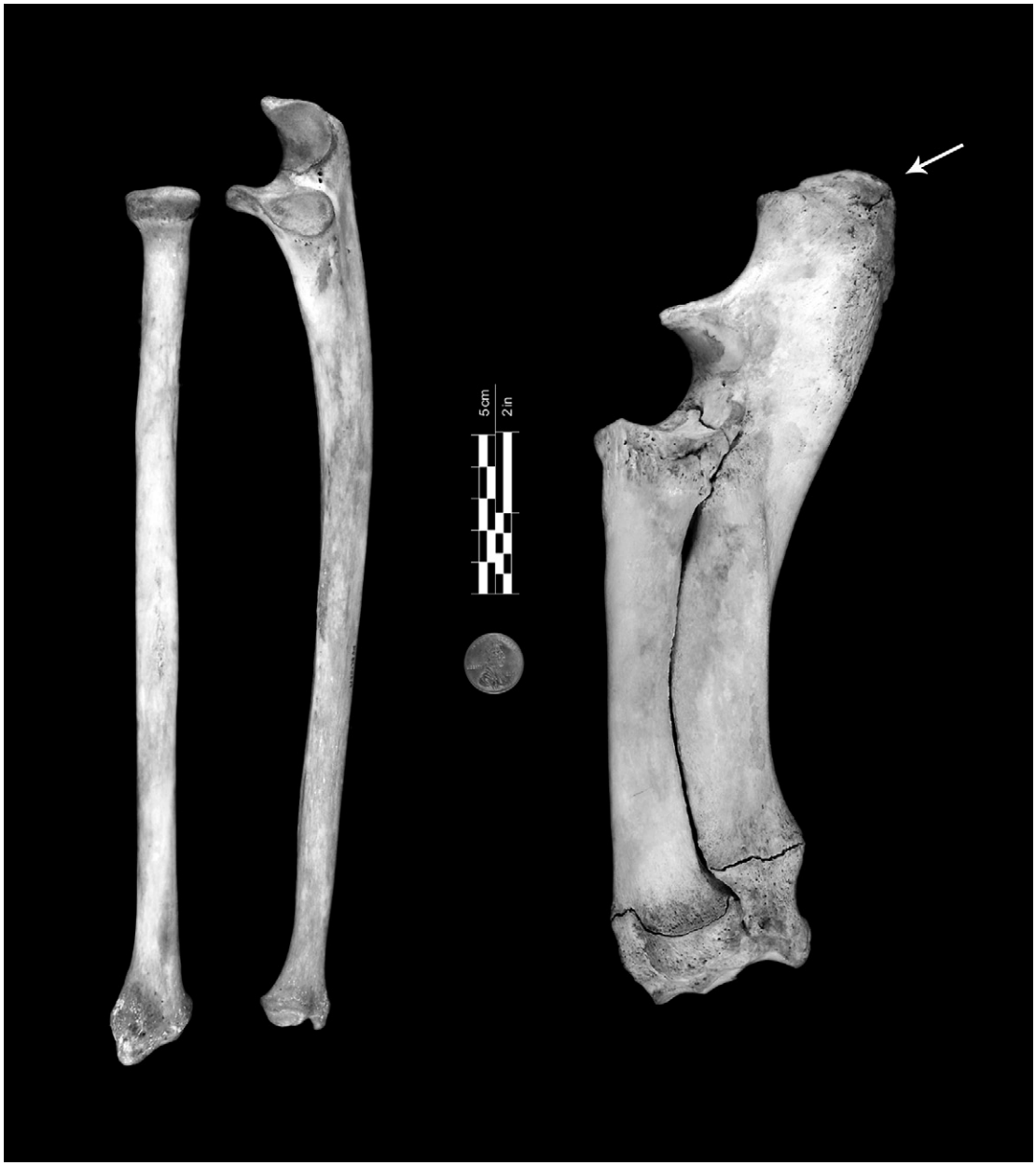

Figure 12-08: A human left radius and ulna (lateral views) are compared to an adult pig's left radius and ulna (lateral view). Note the large size of the pig's olecranon process (arrow).

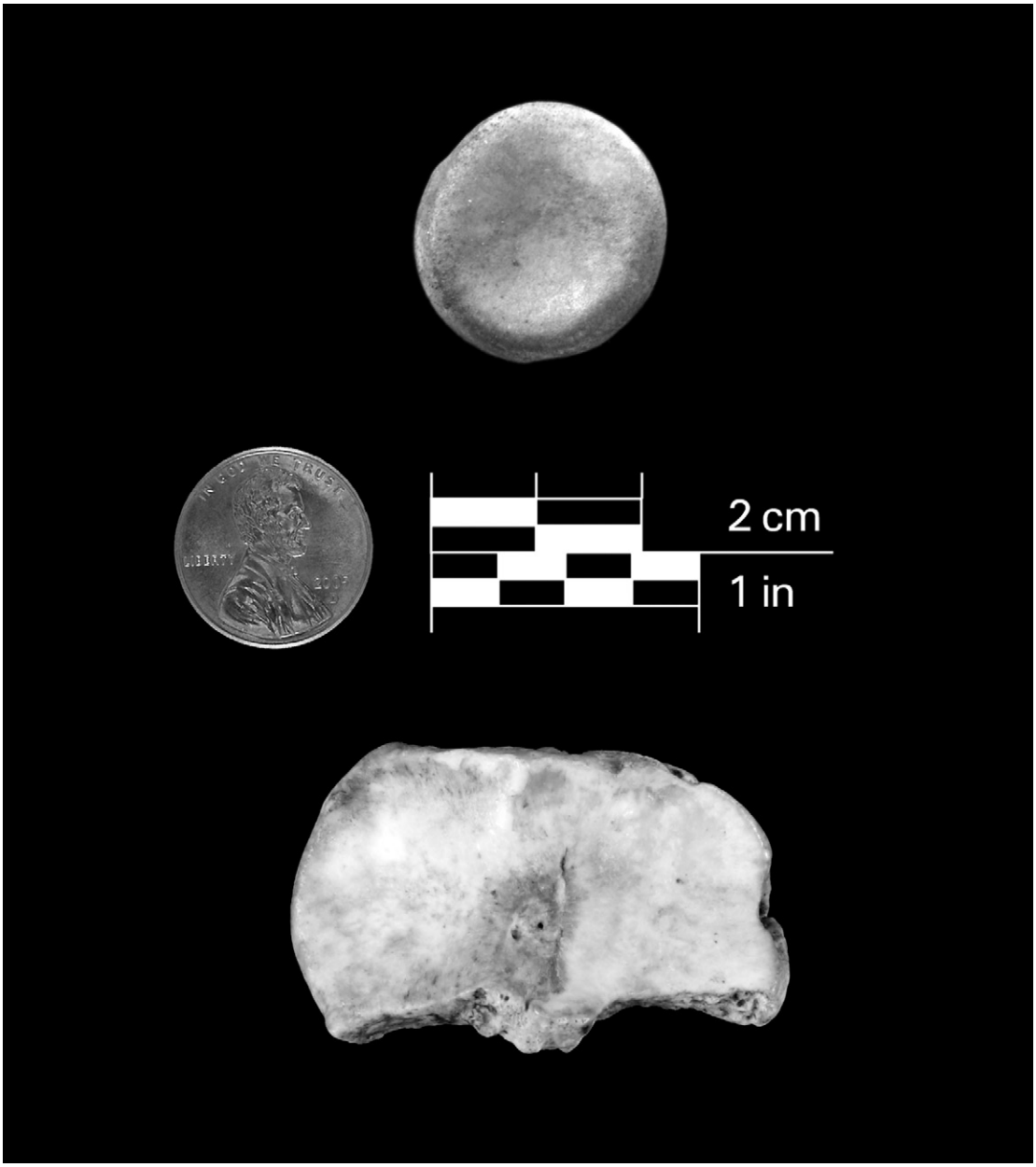

Figure 12-09: A human left proximal radius (superior view) is compared to a pig's left proximal radius (dorsal view). Most of the caudal surface of the pig's radius articulates with the large pig ulna. The surface that articulates with the distal humerus is visible in this view.

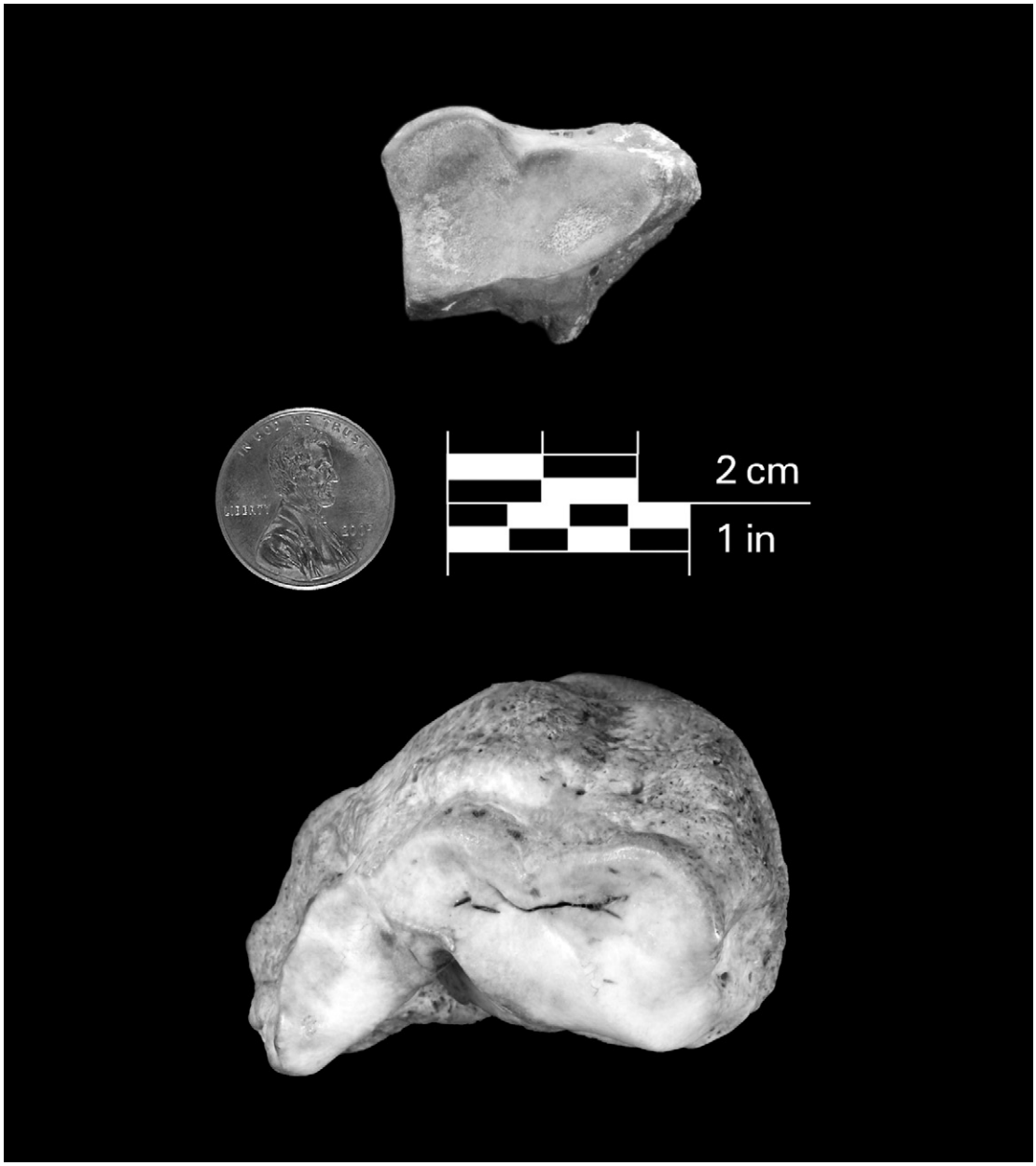

Figure 12-10: An adult human left distal radius (inferior view) is compared to a pig's left distal radius (ventral view). The articular facets for the first carpal row are visible in this view.

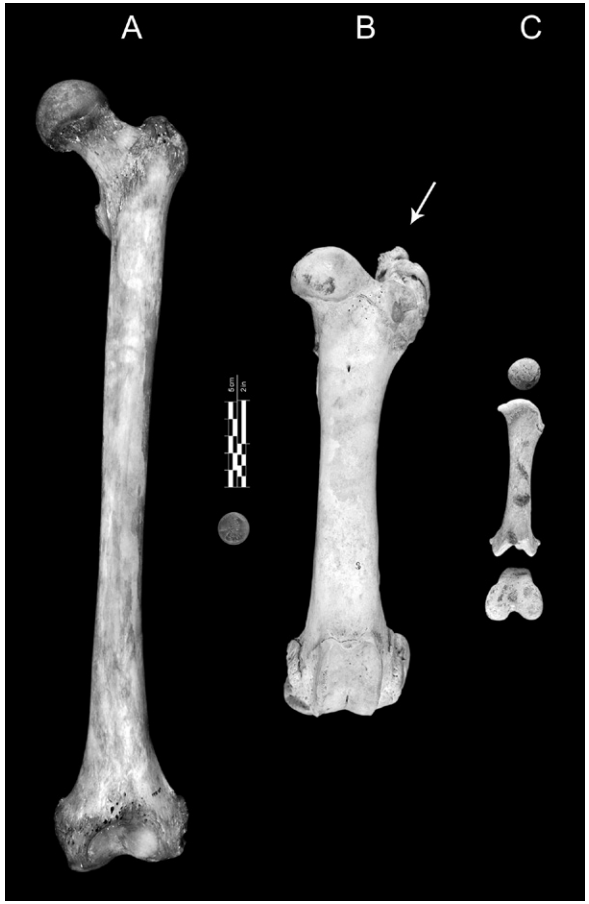

Figure 12-11: A human left femur (A, anterior view) is compared to adult (B) and juvenile (C) pig left femora (cranial views). Note the larger and more developed greater trochanter on the adult pig's femur (arrow). The unfused epiphyses of the juvenile pig are also shown.

Figure 12-12: A human left femur (A, posterior view) is compared to adult (B) and juvenile (C) pig left femora (caudal views). Note the presence of the linea aspera (arrows) on the human femur. The unfused epiphyses of the juvenile pig are also shown.

Figure 12-13: An adult human left distal femur (inferior view) is compared to a juvenile pig's left distal femur (ventral view). Note the distinctive notch on the lateral condyle of the pig (arrow).

Figure 12-14: A human left tibia (A, anterior view) is compared to adult (B) and juvenile (C) pig left tibiae (cranial views). Note that the proximal epiphysis of the large pig is unfused; this epiphysis fuses at about 3.5 years of age in the pig. The unfused epiphyses of the juvenile pig are pictured.

Figure 12-15: A human left tibia (A, posterior view) is compared to adult (B) and juvenile (C) pig left tibiae (caudal views). The unfused epiphyses of the juvenile pig are pictured.

Figure 12-16: A human left tibia (lateral view) is compared to an adult pig's left tibia (lateral view). Note that the proximal epiphysis of the pig is unfused.

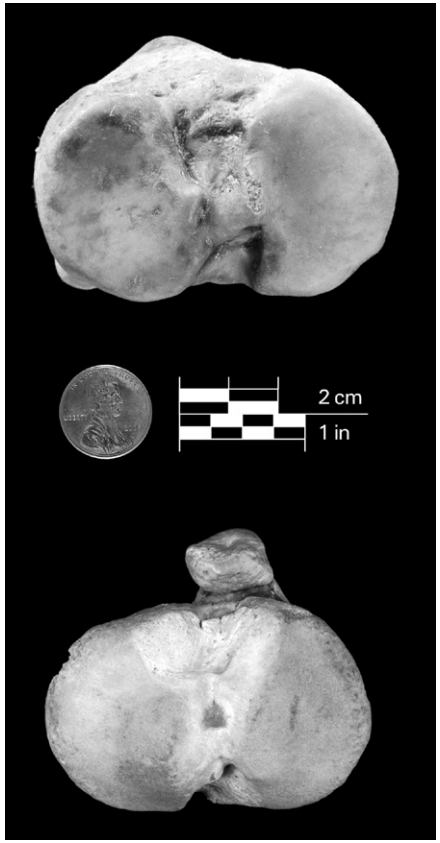

Figure 12-17: A human proximal tibia (superior view) is compared to a pig's proximal tibia (dorsal view). The patella is also pictured with the pig tibia.

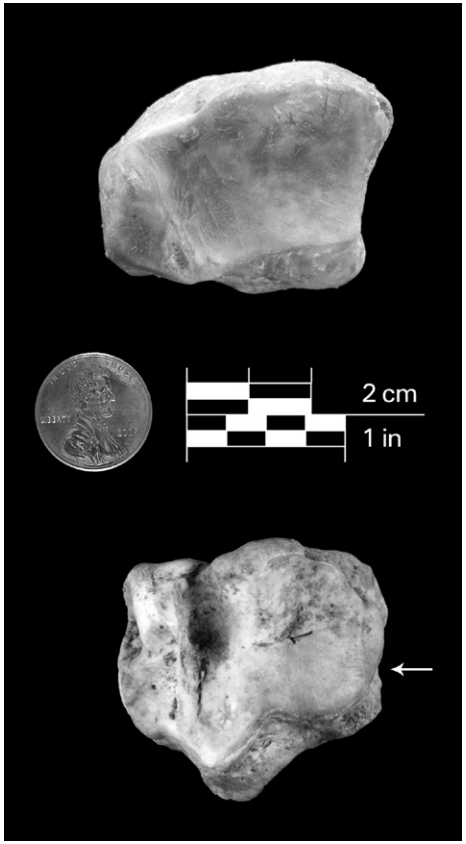

Figure 12-18: A human distal tibia (inferior view) is compared to a pig's distal tibia (ventral view). The malleolus and the two parallel grooves for the articulation of the astragalus are visible in this view. The arrow points to the small facet for articulation with the distal fibula on the lateral side of the bone.

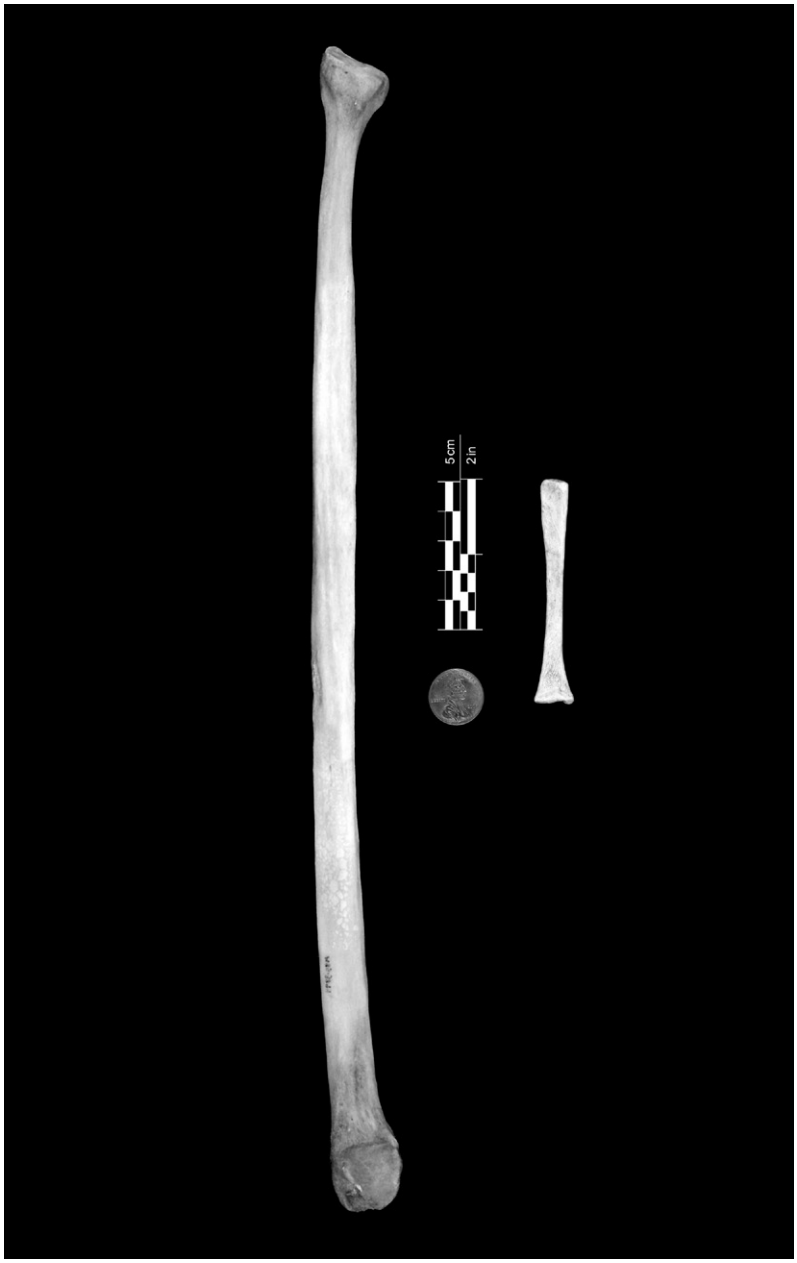

Figure 12-19: A human left fibula (medial view) is compared to a juvenile pig's left fibula (medial view).

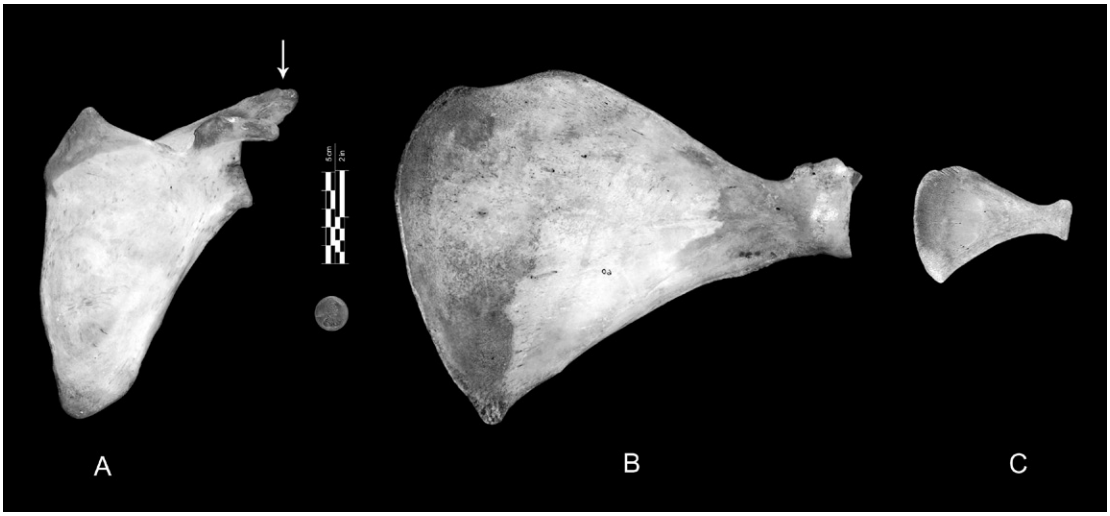

Figure 12-20: A human left scapula (A, anterior view) is compared to adult (B) and juvenile (C) pig left scapulae (medial views). Note that the large human acromion process is not entirely blocked by the body of the scapula and is visible in the anterior view (arrow).

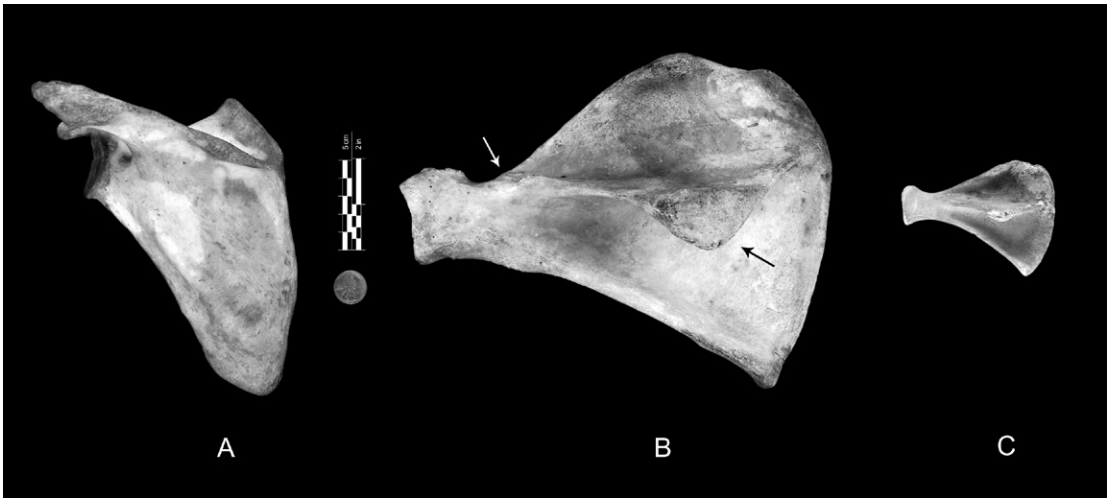

Figure 12-21: A human left scapula (A, posterior view) is compared to adult (B) and juvenile (C) pig left scapulae (lateral views). The pig's scapula has a large tuberosity of the spine (black arrow) but only a rudimentary acromion process (white arrow).

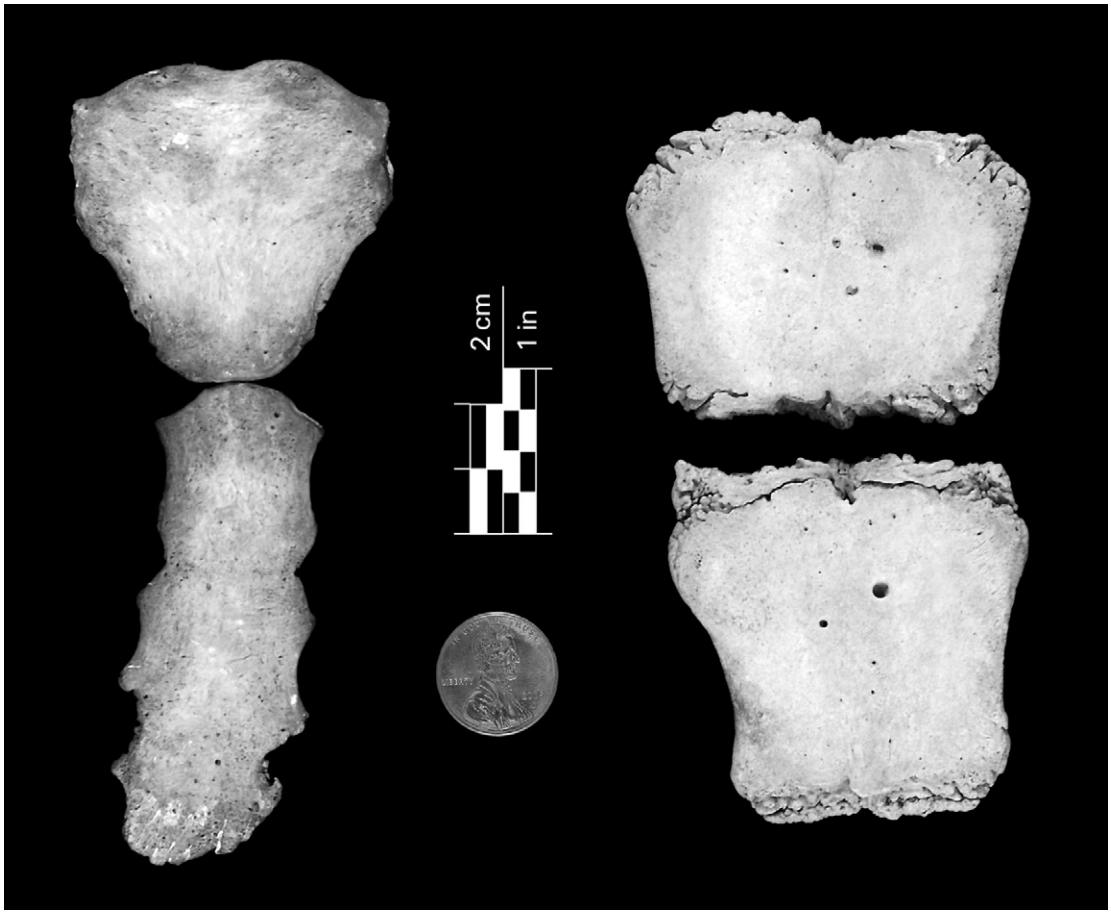

Figure 12-22: A human sternum (anterior view) is compared to two pig sternebrae.

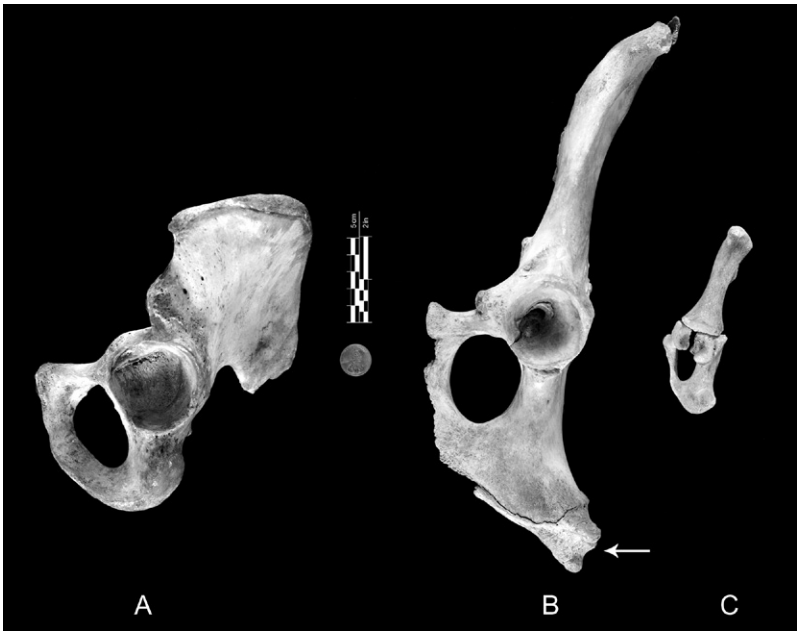

Figure 12-23: A human left innominate (lateral view) is compared to adult and juvenile pig left innominates (lateral views). Gaps in fusion of the pelvic bones are visible on the juvenile pig in the acetabulum. Note the large size of the ischial tuberosity on the adult pig's pelvis (arrow).

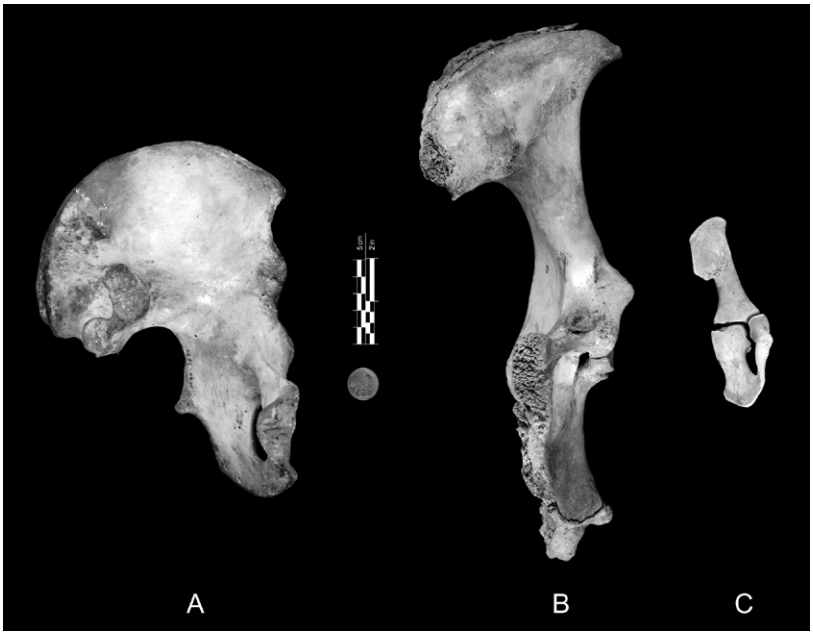

Figure 12-24: A human left innominate (A, medial view) is compared to adult (B) and juvenile (C) pig left innominates (medial views).

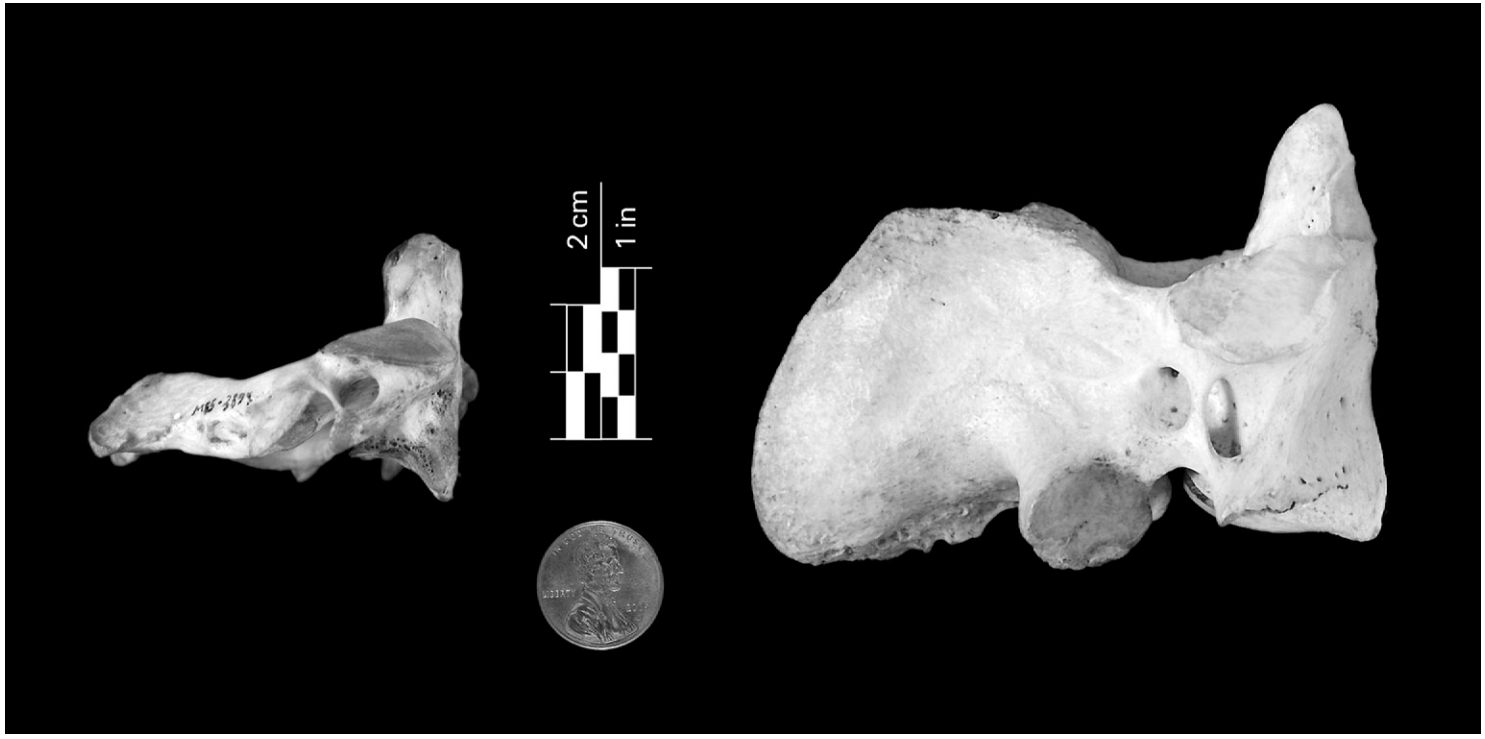

Figure 12-25: A human axis (C2) is compared with an adult pig's axis (C2). Both views are lateral.

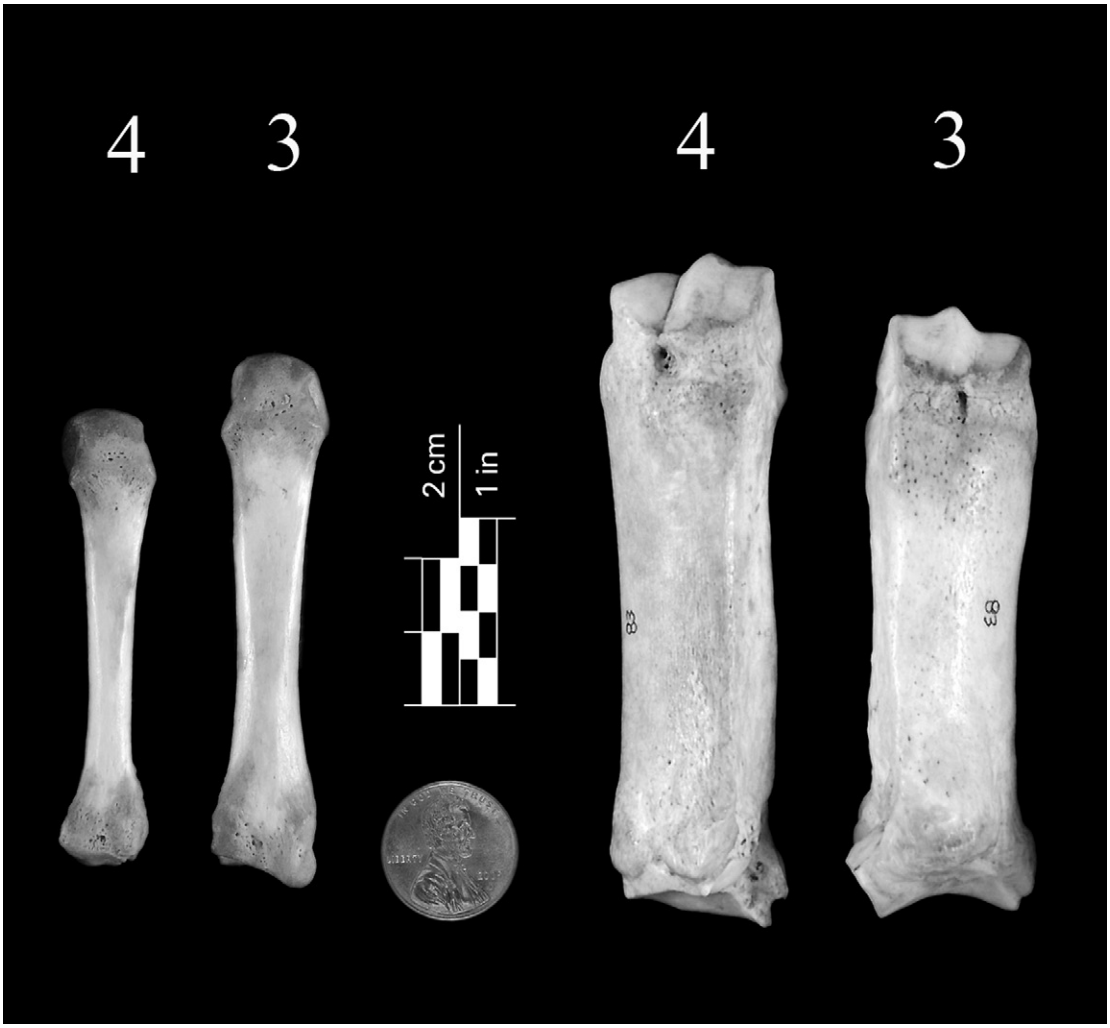

Figure 12-26: Human third and fourth left metacarpals (anterior views) are compared to adult pig left third and fourth metacarpals (dorsal views). The pig is an artiodactyl or even-toed ungulate. It has four metapodia (II–V present) on each foot. The third and fourth metapodia are larger central metapodia, while the second and fifth metapodia are smaller. The distal ends of the bones are pictured at the top of the photograph.

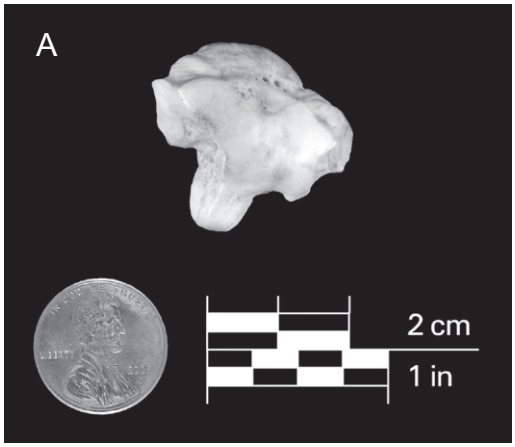

Figure 12-27a: Pig left third proximal metcarpal (dorsal view). The pig has four metacarpals on each forefoot. The third and fourth metacarpals are larger and located medially. The second and fifth metacarpals are smaller and located laterally.

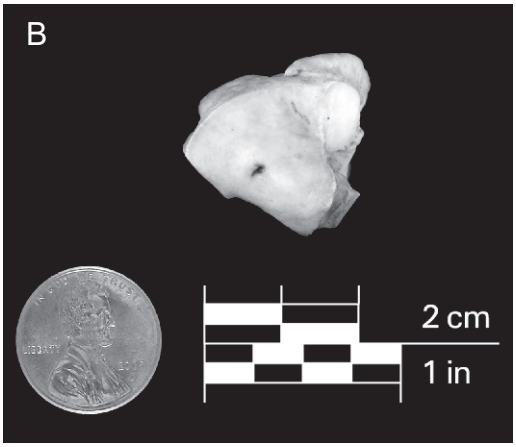

Figure 12-27b: Pig left fourth proximal metacarpal (dorsal view).

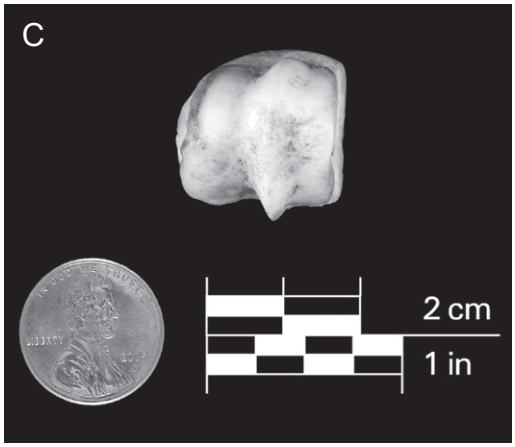

Figure 12-27c: Pig left third distal metacarpal (volar view).

Figure 12-28: Human third and fourth left metatarsals (superior views) are compared to adult pig left third and fourth metatarsals (dorsal views). Note that the distal epiphyses on the pig are unfused. The pig is an artiodactyl or even-toed ungulate. It has four metapodia (II–V present) on each foot. The third and fourth metapodia are larger central metapodia, while the second and fifth metapodia are smaller. The distal ends of the bones are pictured at the top of the photograph.

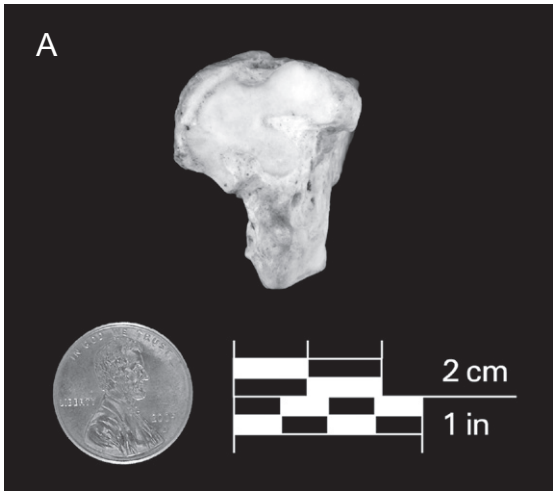

Figure 12-29a: Pig left third proximal metatarsal (dorsal view). The pig has four metacarpals on each forefoot. The third and fourth metacarpals are larger and located medially. The second and fifth metacarpals are smaller and located laterally.

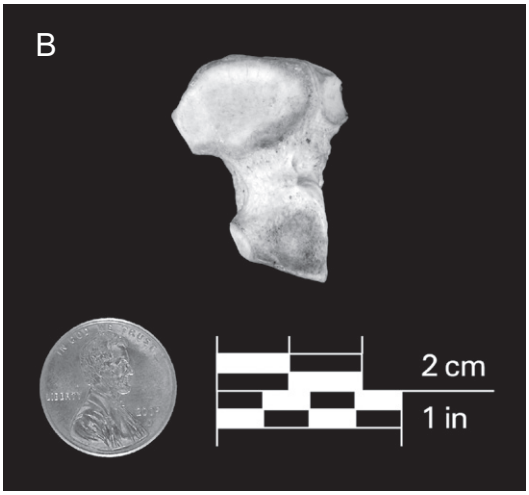

Figure 12-29b: Pig left fourth proximal metatarsal (dorsal view).

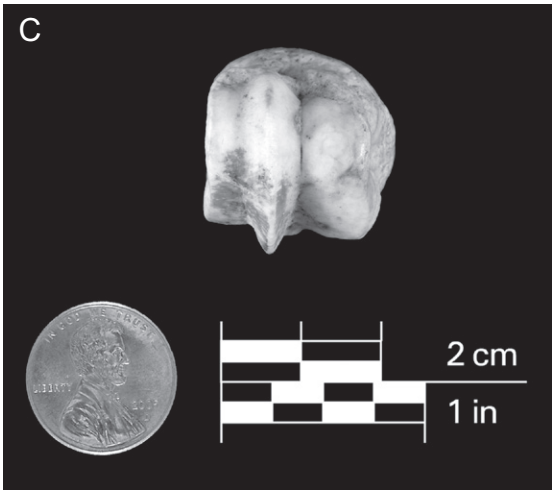

Figure 12-29c: Pig left third distal metatarsal (plantar view).

Figure 12-30: A human left talus (superior view) is compared to an adult pig's left astragalus (dorsal view). Note that the pig's astragalus has the "double pulley" form that is characteristic of the artiodactyls.

Figure 12-31: A human left calcaneus (A, superior view) is compared to adult (B) and juvenile (C) pig left calcanei (dorsal views).

CHAPTER 13

Goat (Capra hircus)

Comparative Osteology. DOI: 10.1016/B978-0-12-388437-4.00013-2

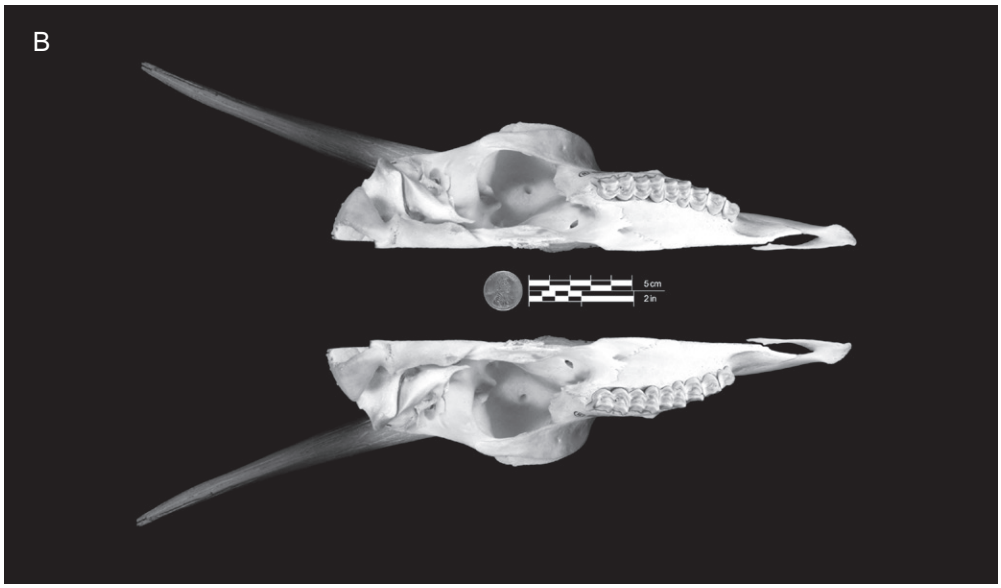

Figure 13-01: Goat cranium (A, lateral view, right side). The sheep and goat are closely related species, and fragmentary remains of the two taxa can be difficult to distinguish. Boessneck and colleagues (Boessneck 1969; Boessneck et al. 1964) present the most comprehensive guide to the osteological distinctions that are evident on the postcranial skeleton. (B, ventral view the cranium has been sagittally split). The goat's dental formula is 0/3.0/1.3/3.3/3. Since the publication of Boessneck's work, researchers have attempted to identify distinguishing features of the dentition of sheep and goats. Payne (1985) identifies several distinctions that can be seen on the deciduous dentition, while Halstead, et al. (2002) identify differences on the mandibles and mandibular teeth of adult sheep and goats. Zeder and Pilaar (2010) assess the reliability of the criteria used to distinguish mandibles and mandibular teeth, while Zeder and Lapham (2010) assess the reliability of the postcranial criteria.

Figure 13-02: A human left humerus (A, anterior view) is compared to a mature goat's left humerus (B, cranial view), an immature goat's left humerus with epiphyses (B, cranial view), and an immature goat's left humerus with epiphysis (C, cranial view). When compared to sheep, the greater tubercle is higher and narrower in goats. The nutrient foramen (arrows) is often located on the dorsal surface of the humeral shaft in goats.

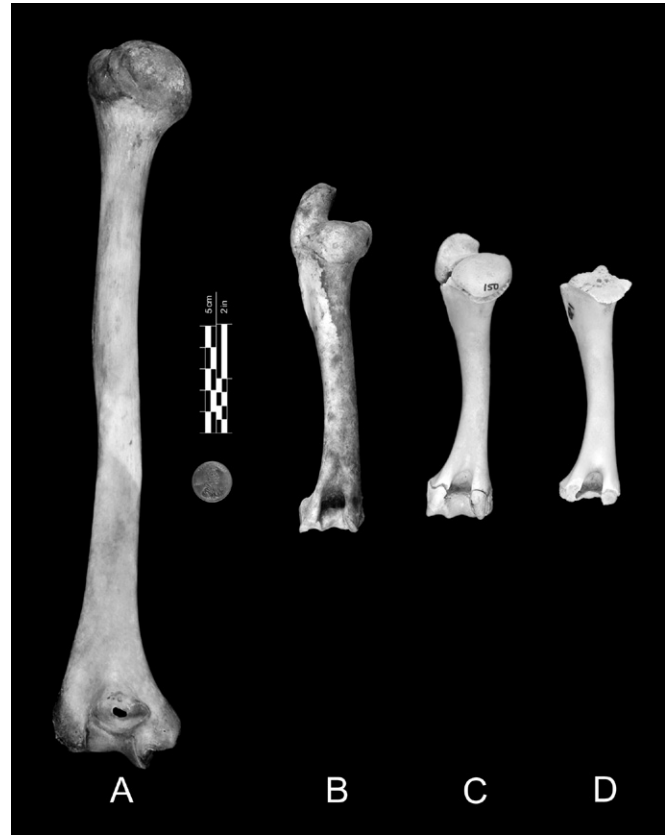

Figure 13-03: A human left humerus (A, posterior view) is compared to a mature goat's left humerus (B, caudal view), an immature goat's left humerus with epiphyses (C, caudal view), and an immature goat's left humerus without epiphyses (D, caudal view).

Figure 13-04: Adult goat left humerus (medial and lateral views). The arrow points to the lateral epicondyle.

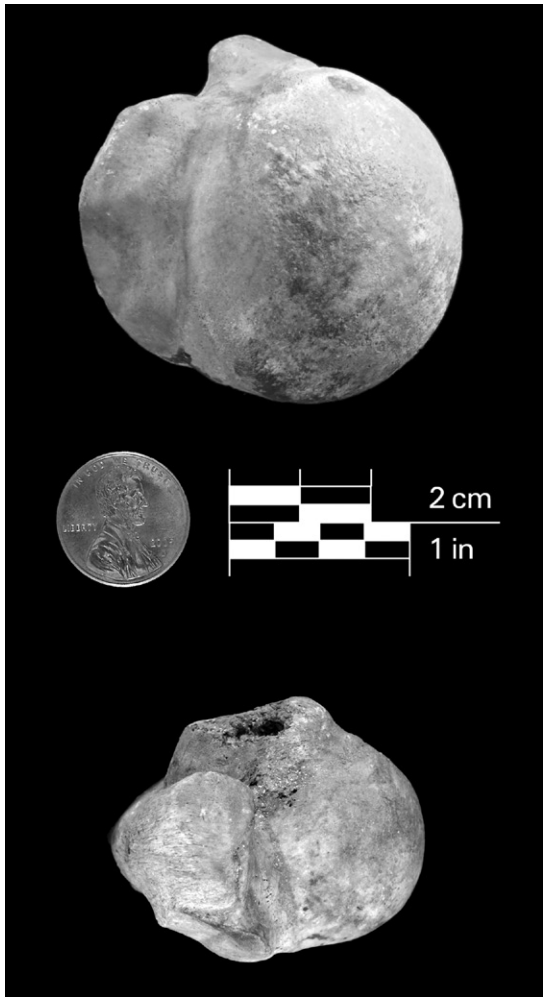

Figure 13-05: An adult human proximal humerus (superior view) is compared to an adult goat's proximal humerus (dorsal view).

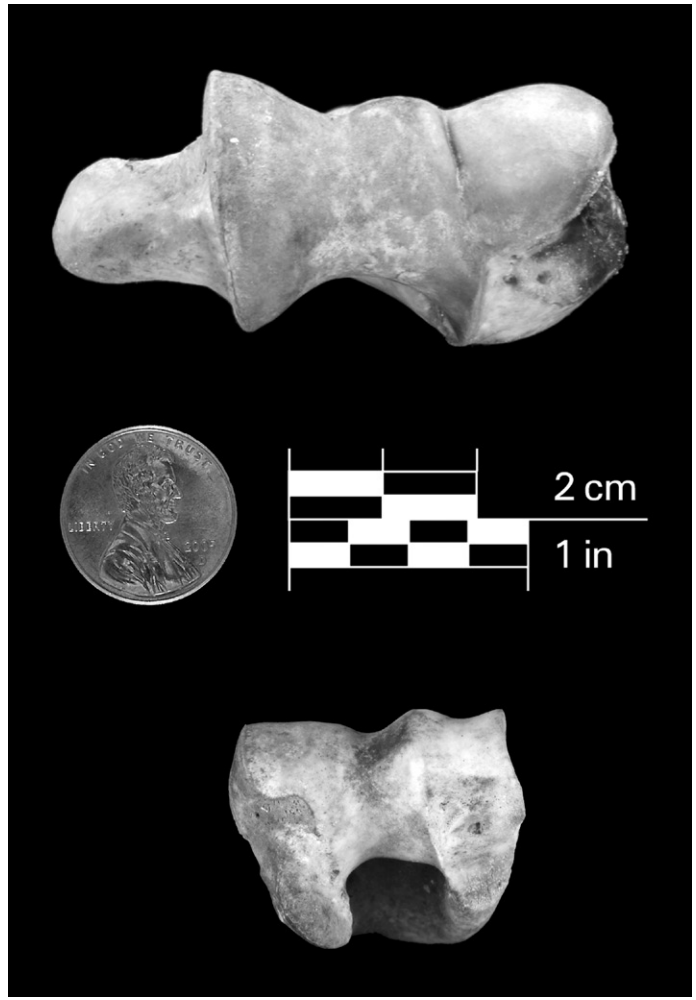

Figure 13-06: An adult human distal humerus (inferior view) is compared to an adult goat's distal humerus (ventral view). The goat's barrel-shaped trochlea is visible in this view.

Figure 13-07: A human left radius (A, anterior view) is compared to a goat's left radius (B, cranial view with epiphyses) and a goat's left radius without epiphyses (C, cranial view).

Figure 13-08: A human left radius (A, posterior view) is compared to a goat's left radius with epiphyses (B, caudal view) and a goat's left radius without epiphyses (C, caudal view).

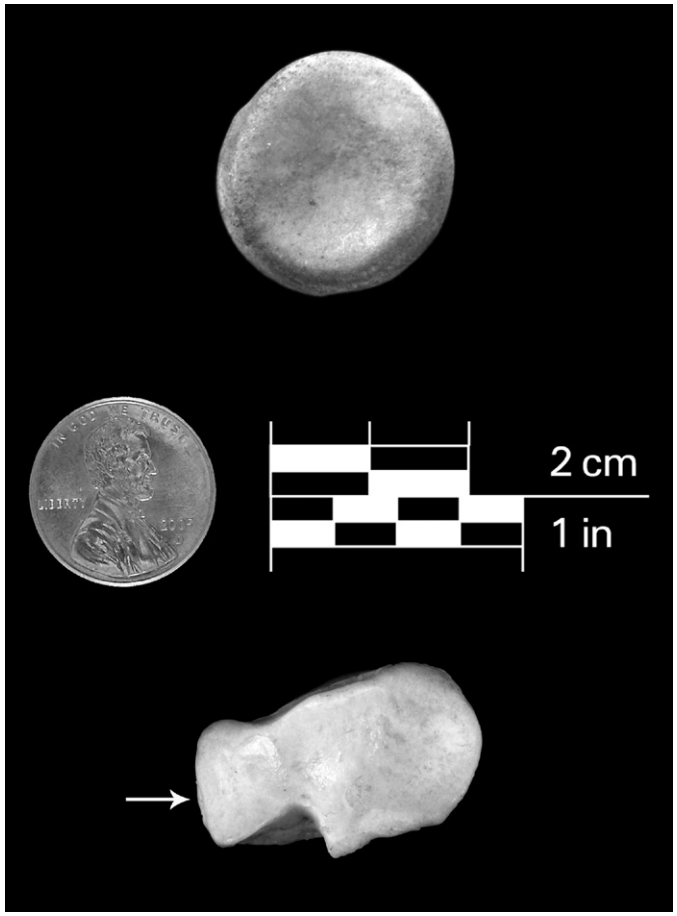

Figure 13-09: A human left proximal radius (superior view) is compared to a goat's left proximal radius (dorsal view). The articular surface is concave and lateral bicipetal tuberosity (arrow) is poorly developed in goats. Note the circular shape of the human proximal radius.

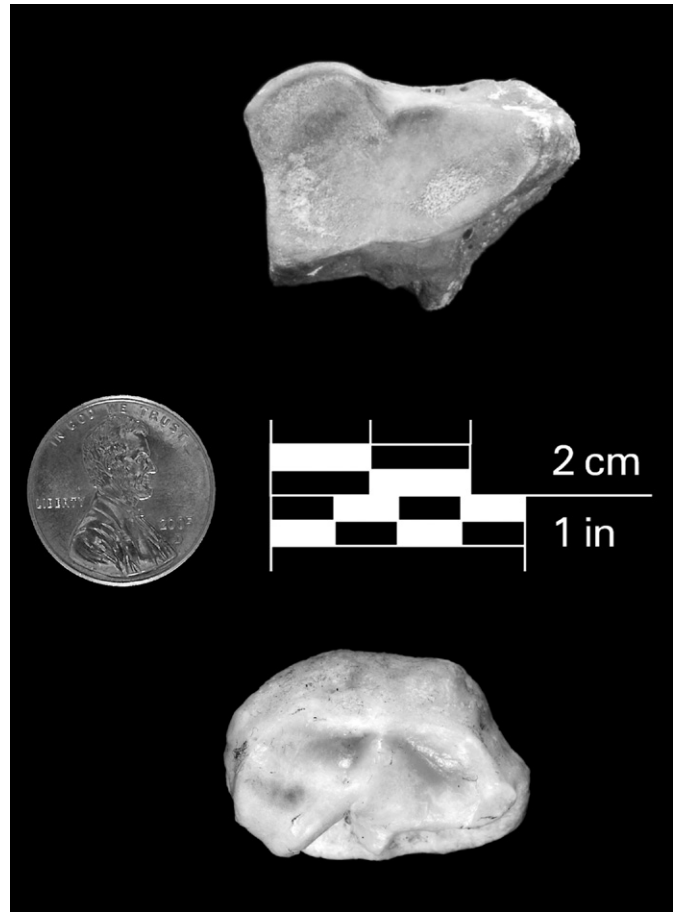

Figure 13-10: A human left distal radius (inferior view) is compared to a goat's left distal radius (ventral view). The articular facets for the first carpal row are visible in this view.

Figure 13-11: A human left ulna (anterior view) is compared to a goat's left ulna (cranial view).

Figure 13-12: A human left ulna (posterior view) is compared to a goat's left ulna (caudal view).

Figure 13-13: A human left ulna (lateral view) is compared to a goat's left ulna (lateral view).

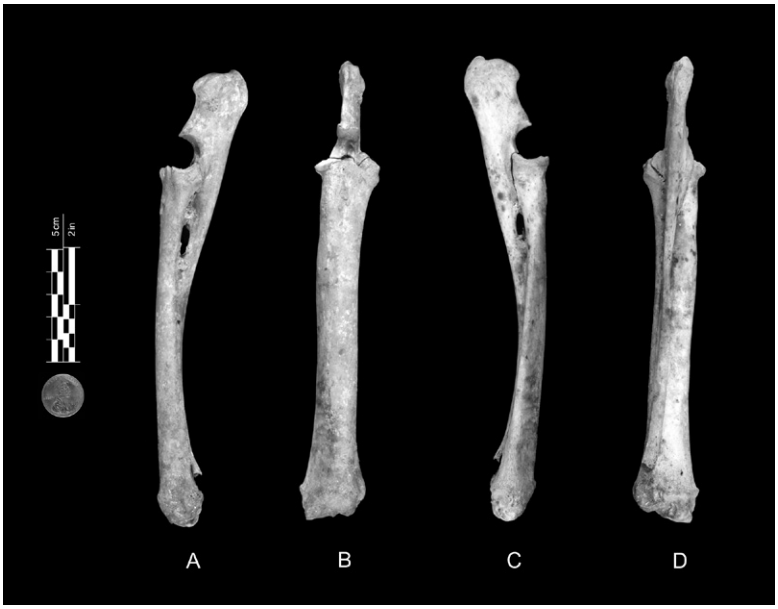

Figure 13-14: An adult goat's left radius and ulna in various views: lateral (A), cranial (B), medial (C), and caudal (D). The radius and ulna will often fuse together in older goats. In the caudal view, the slender shaft of the ulna extends along the lateral portion of the radius shaft.

Figure 13-15: An adult goat's radius and ulna (proximal views). Note that the ulnar articulation extends all the way to the lateral side of the proximal radius (arrow).

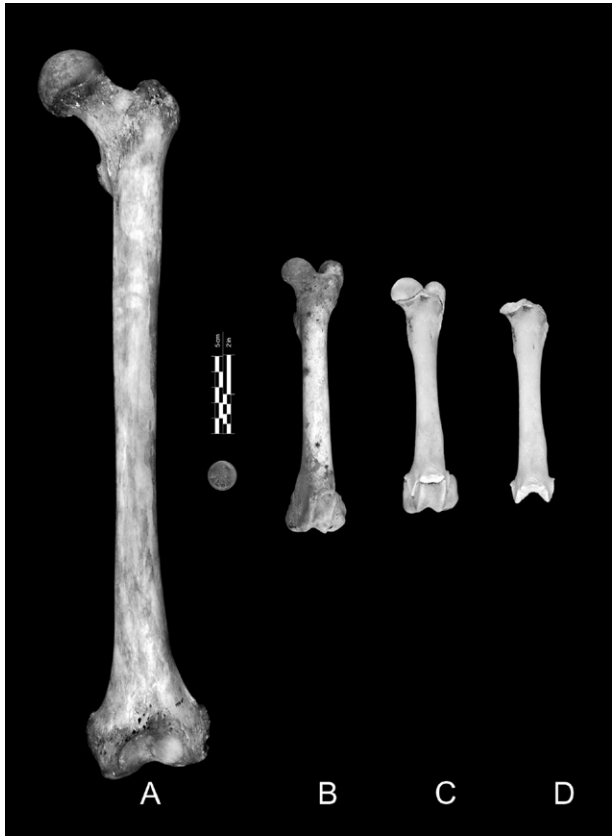

Figure 13-16: A human left femur (A, anterior view) is compared to an adult goat's left femur (B, cranial view), a juvenile goat's left femur with epiphyses (C, cranial view), and a juvenile goat's femur without epiphyses (D, cranial view).

Figure 13-17: A human left femur (A, posterior view) is compared to an adult goat's left femur (B, caudal view), a juvenile goat's left femur with epiphyses (C, caudal view), and a juvenile goat's femur without epiphyses (D, caudal view).

Figure 13-18: Adult goat femur (lateral and medial views). In the lateral view, the greater trochanter is visible on the proximal end (arrow). The supracondylar fossa is also visible on the distal end (arrow).

Figure 13-19: A human left proximal femur (superior view) is compared to an adult goat's left proximal femur (dorsal view). The head and the greater trochanter are visible on the proximal end. The head of the femur is generally more ball-shaped in goats than in sheep, and the greater trochanter is located somewhat closer to the head of the femur in goats.

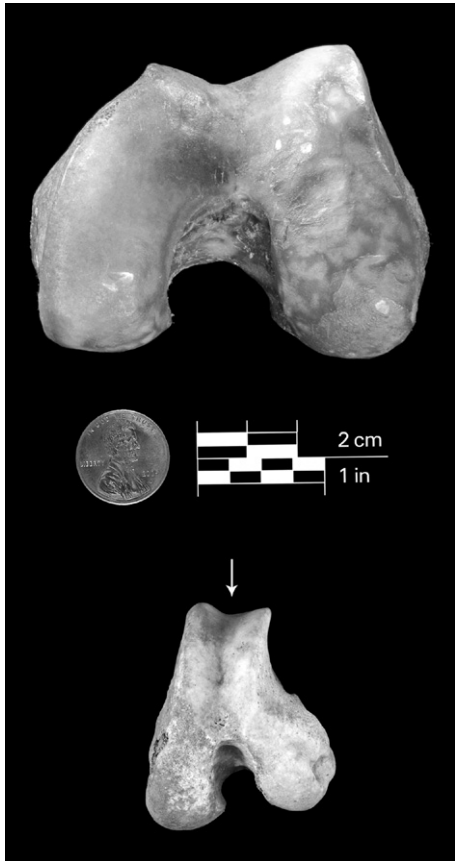

Figure 13-20: A human left distal femur (inferior view) is compared to an adult goat's left distal femur (ventral view). When viewed from this angle, the trochlea is slightly more V-shaped in goats than in sheep (arrow).

Figure 13-21: A human left tibia (A, anterior view) is compared to an adult goat's left tibia (B, cranial view), a juvenile goat's left tibia with epiphyses (C, cranial view), and a juvenile goat's tibia without epiphyses (D, cranial view). The arrow points to the remnant of the proximal fibula.

Figure 13-22: A human left tibia (A, posterior view) is compared to an adult goat's left tibia (B, caudal view), a juvenile goat's left tibia with epiphyses (C, caudal view), and a juvenile goat's tibia without epiphyses (D, caudal view).

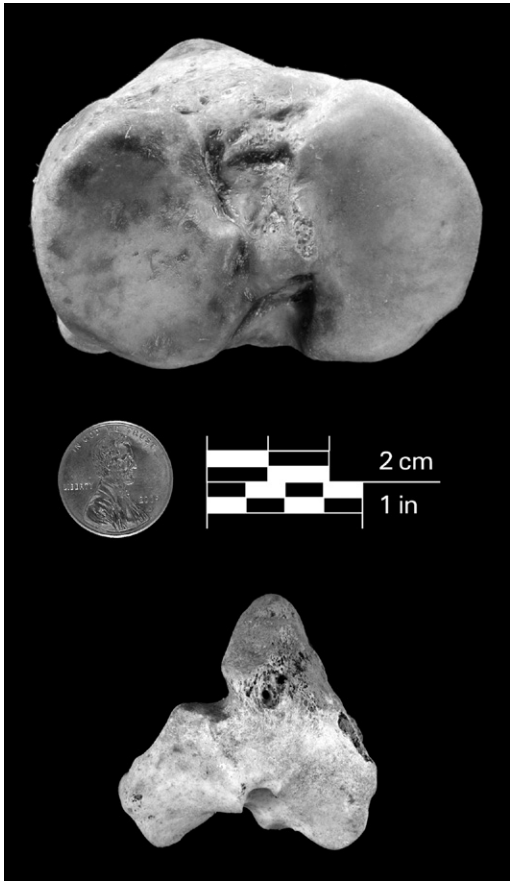

Figure 13-23: An adult human proximal tibia (superior view) is compared to a goat's proximal tibia (dorsal view).

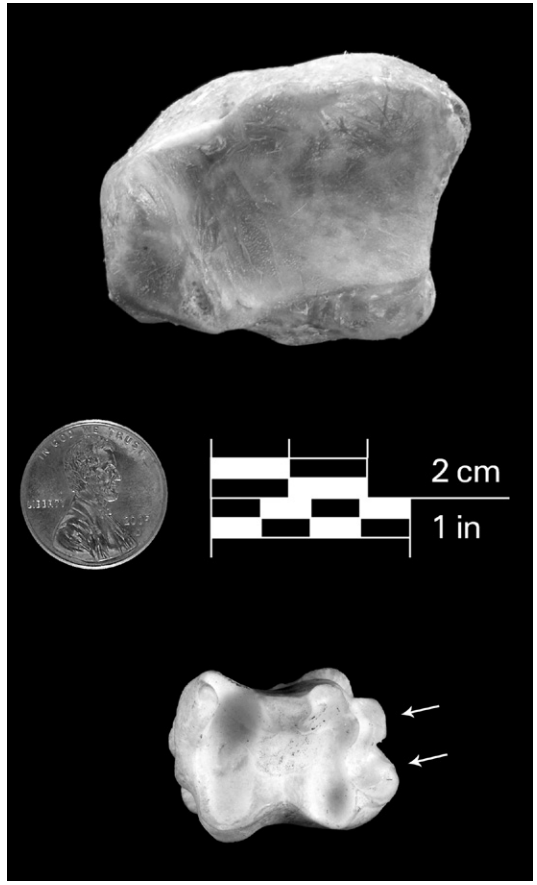

Figure 13-24: An adult human distal tibia (inferior view) is compared to a goat's distal tibia (ventral view). The large parallel facets for the articulation of the astragalus are visible in this view. The two small facets are for the articulation of the malleolus, a small tarsal that is the evolutionary remnant of the fibula, are visible on the lateral side (arrows).

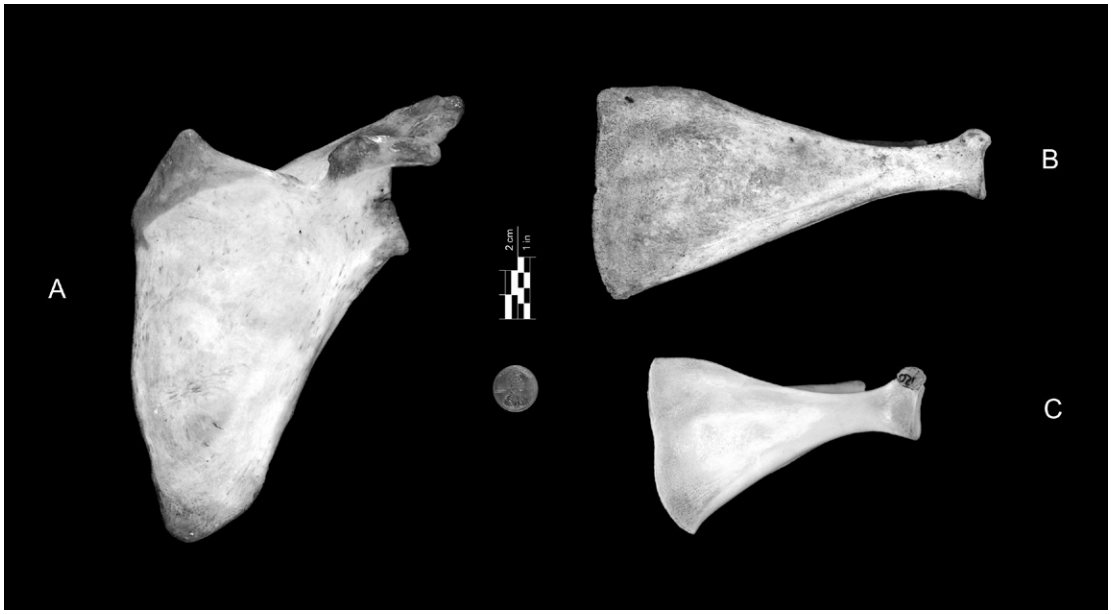

Figure 13-25: A human left scapula (A, anterior view) is compared to an adult goat's (B) and a juvenile goat's (C) left scapula (medial views).

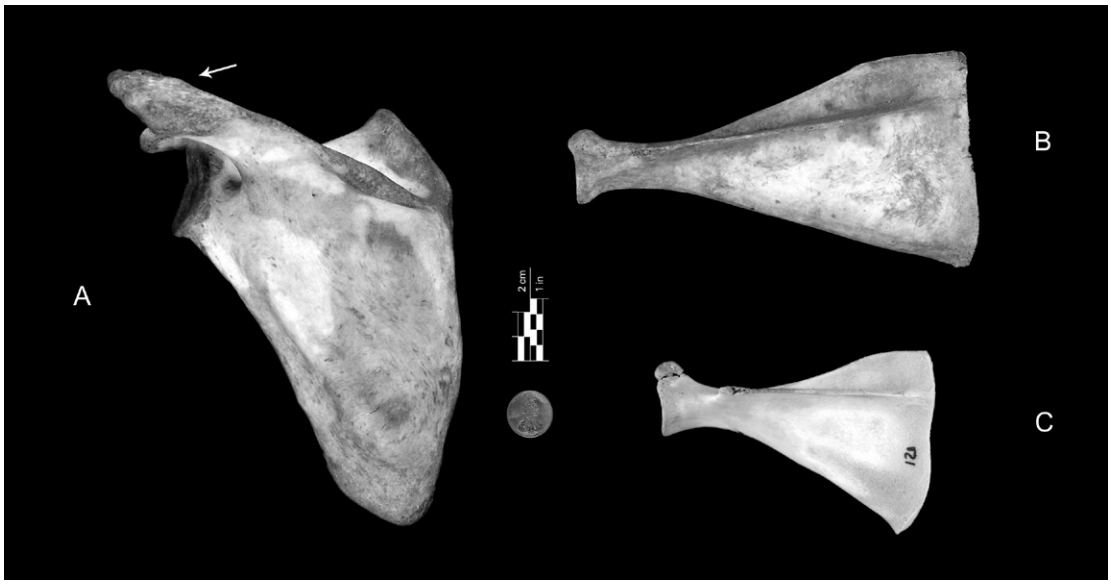

Figure 13-26: A human left scapula (A, posterior view) is compared to an adult goat's (B) and a juvenile goat's (C) left scapula (lateral view). Note the large acromion process on the human scapula (arrow). The blade of the goat's scapula is broadly triangular. The spine divides the blade into two unequal parts.

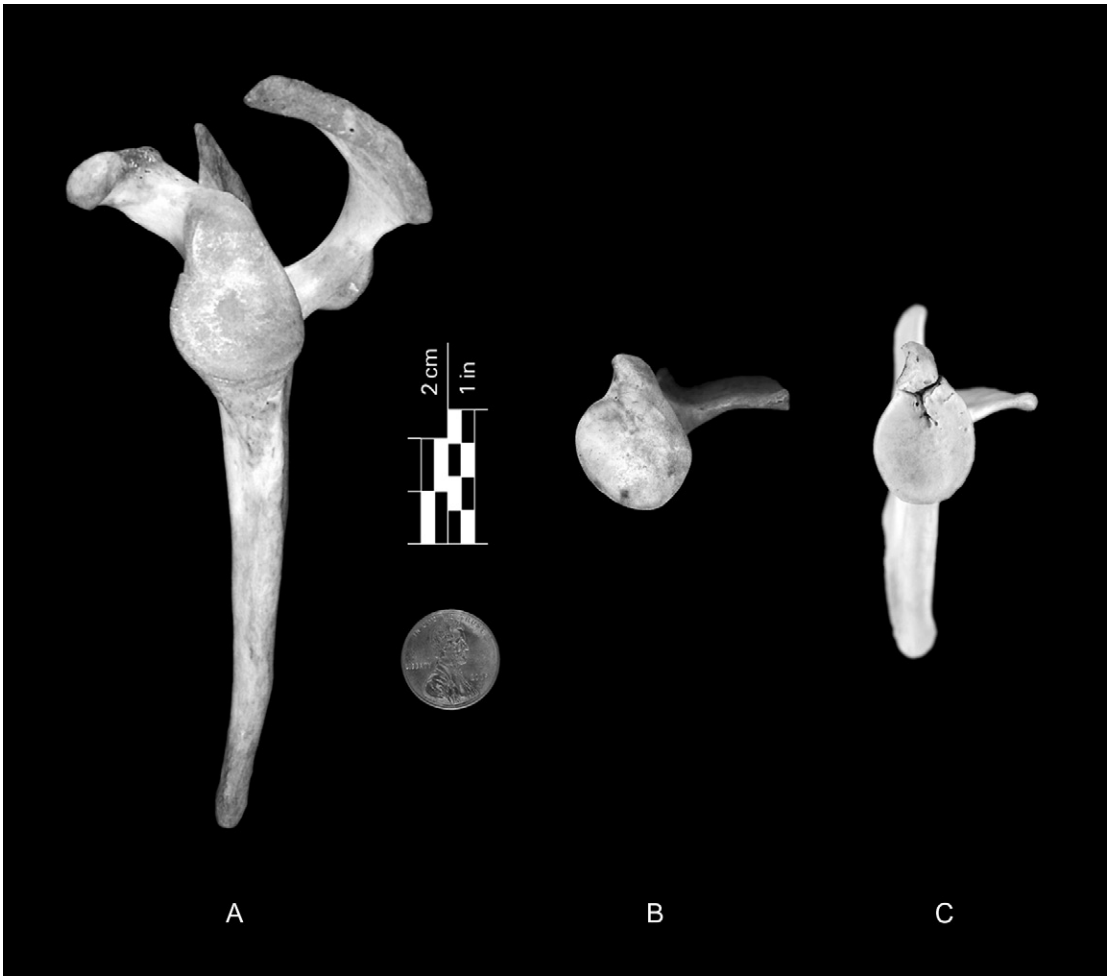

Figure 13-27: A human left scapula (A, lateral view) is compared to an adult goat's (B) and a juvenile goat's (C) left scapula (distal view). The glenoid cavity and the base of the spine are visible in this view. The goat's and sheep's glenoid cavities are generally more oval in shape, while the deer's is more rounded.

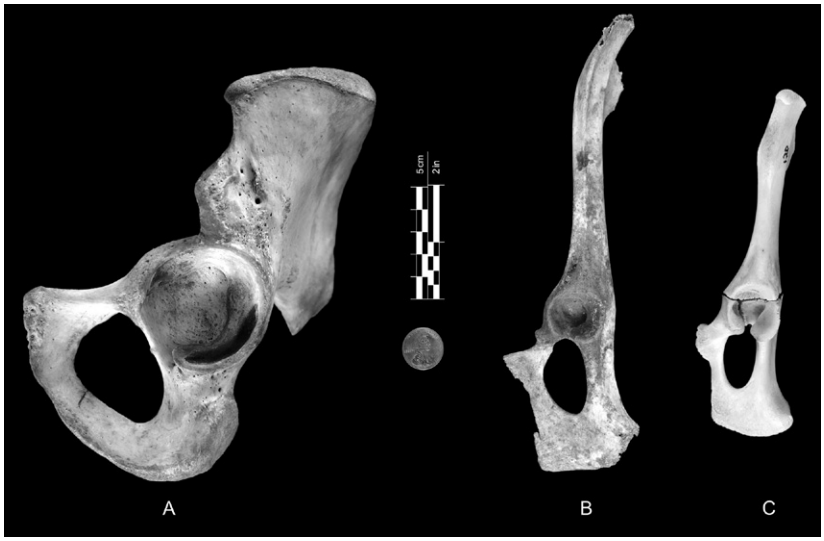

Figure 13-28: A human left innominate (A, lateral view) is compared to an adult goat's (B) and a juvenile goat's (C) left innominate (lateral view).

Figure 13-29: An adult goat's left innominate (medial and lateral views).

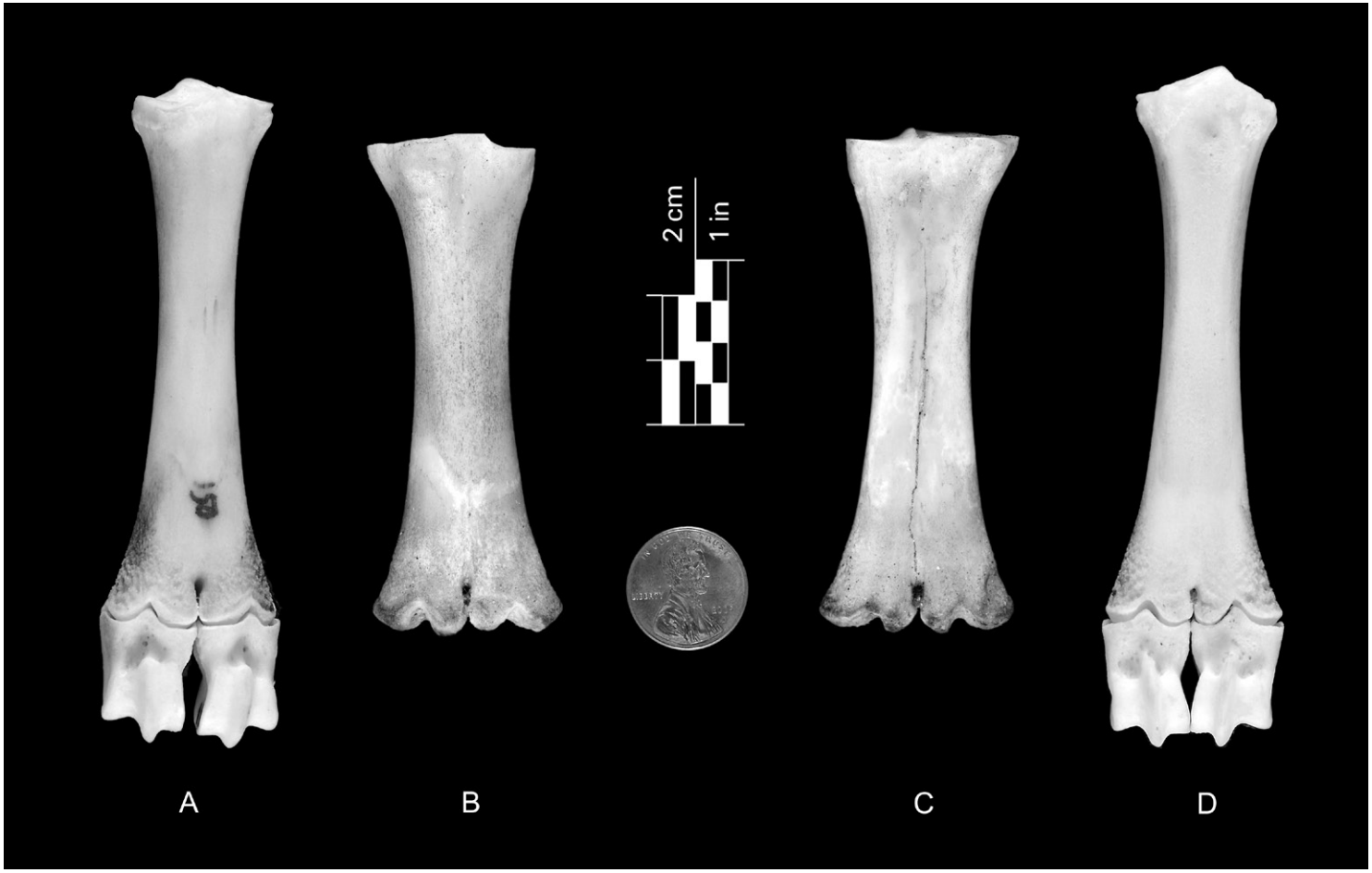

Figure 13-30: A goat's left metatarsus with epiphysis (A, dorsal view) and a goat's left metacarpus without epiphysis (B, dorsal view) are compared to a goat's left metacarpus without epiphysis (C, volar view) and a goat's left metatarsus with epiphysis (D, plantar view). The goat's metacarpus and metatarsus are composed of the fused third and fourth metacarpals and metatarsals.

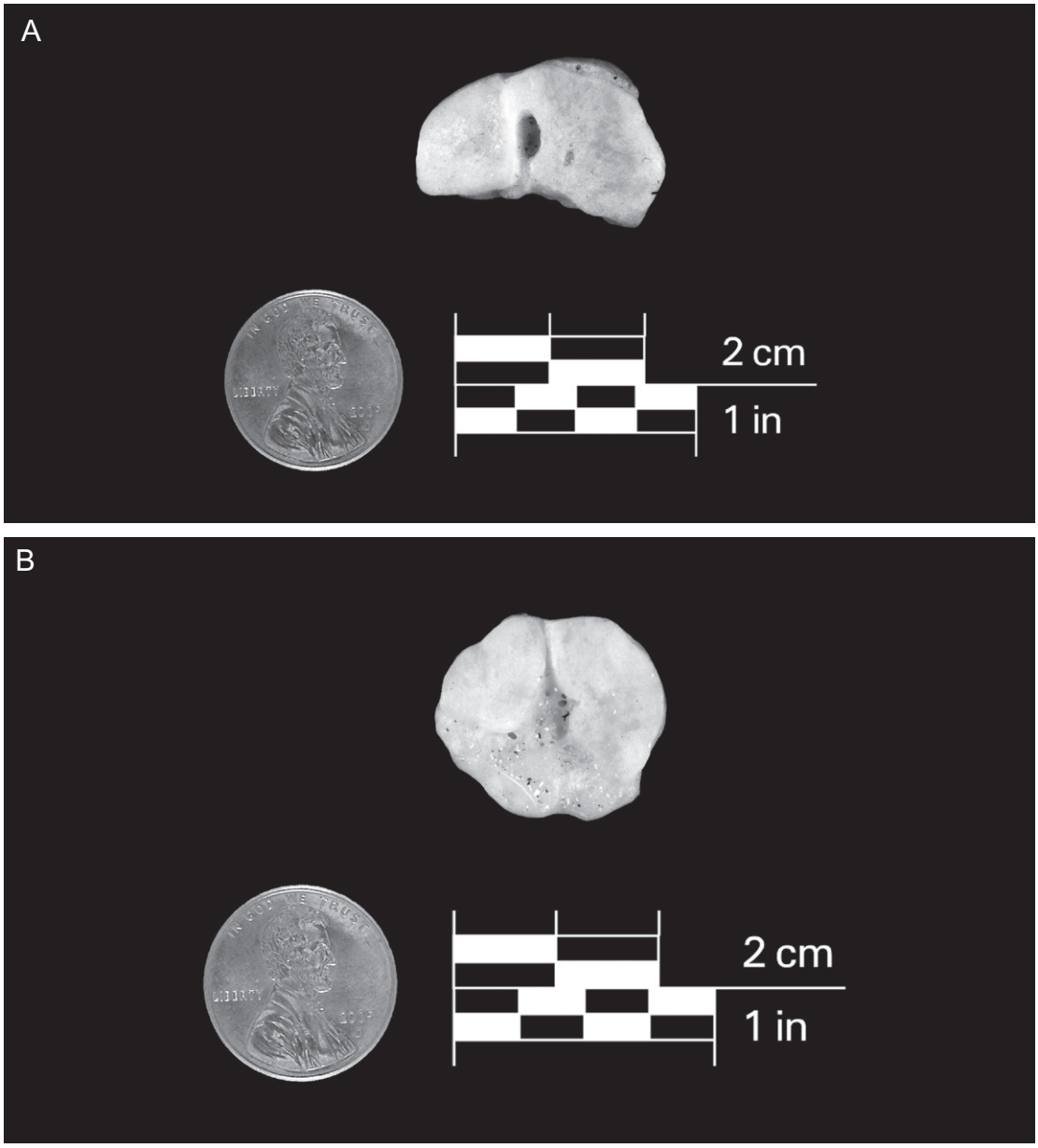

Figure 13-31: (A) Goat left proximal metacarpus (dorsal view). (B) Goat left proximal metatarsus (dorsal view). When compared to the D-shaped proximal metacarpus, the proximal metatarsus in goats is more circular in shape. The facets mark the articulation with the distal row of tarsals.

This page intentionally left blank

CHAPTER 14

Sheep (Ovis aries)

Comparative Osteology. DOI: 10.1016/B978-0-12-388437-4.00014-4

Figure 14-01: Horned sheep cranium (A, lateral view, right side). The horn core, the bony portion of the skull that underlies the horn, is visible in this view. Horns differ from antlers and are found in bovids (e.g., cattle, sheep, and goats). The horn itself is made of keratin and rarely survives in archaeological contexts. (B, ventral view, the left portion of the maxilla is missing). The sheep's dental formula is 0/3.0/1.3/3.3/3. The mandibular canine is incisiform and is followed by a long diastema.

Figure 14-02: (A) Polled (hornless) sheep cranium (lateral view, right side). Sheep and goat are closely related species, and fragmentary remains of the two taxa can be difficult to distinguish. Boessneck and colleagues (Boessneck 1969; Boessneck, et al. 1964) present the most comprehensive guide to the osteological distinctions that are evident on the postcranial skeleton. Since the publication of Boessneck's work, researchers have attempted to identify distinguishing features of the dentition of sheep and goats. Payne (1985) identifies several distinctions that can be seen on the deciduous dentition, while Halstead and Collins (2002) identify differences on the mandibles and mandibular teeth of adult sheep and goats. Zeder and Pilaar (2010) assess the reliability of the criteria used to distinguish mandibles and mandibular teeth, while Zeder and Lapham (2010) assess the reliability of the postcranial criteria. (B) Polled sheep cranium (ventral view). The sheep's third molars have not erupted but are visible in the crypts.

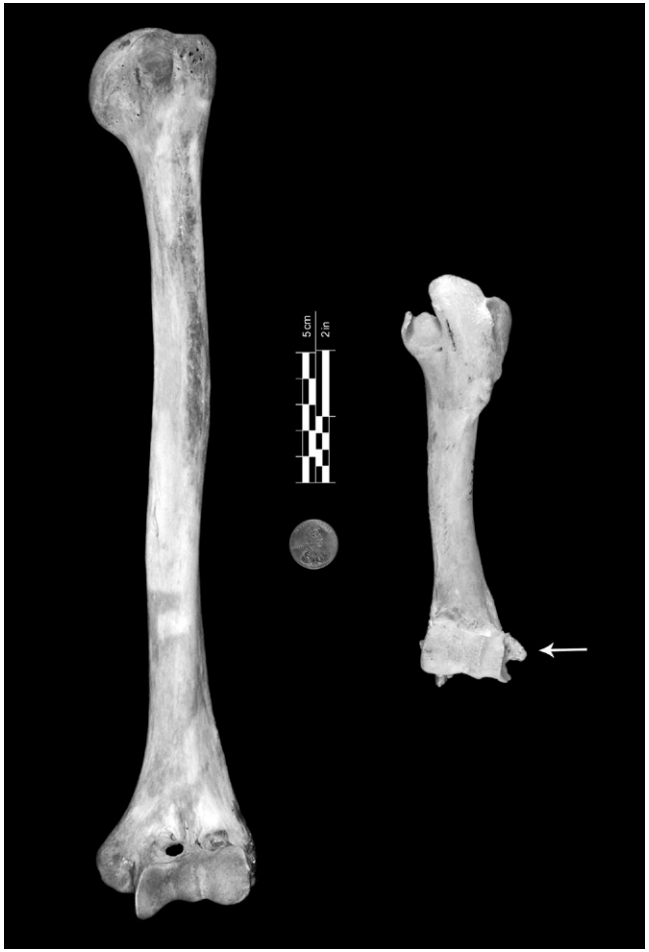

Figure 14-03: A human left humerus (anterior view) is compared to a sheep's left humerus (cranial view). A slight exostosis is apparent on the lateral epicondyle of the sheep's distal humerus (arrow). This is an example of "penning elbow," a pathological condition that is relatively common in domestic sheep and is caused by trauma to the joint area. Note also that the greater tubercle is more well developed in the sheep's humerus than it is in the human humerus.

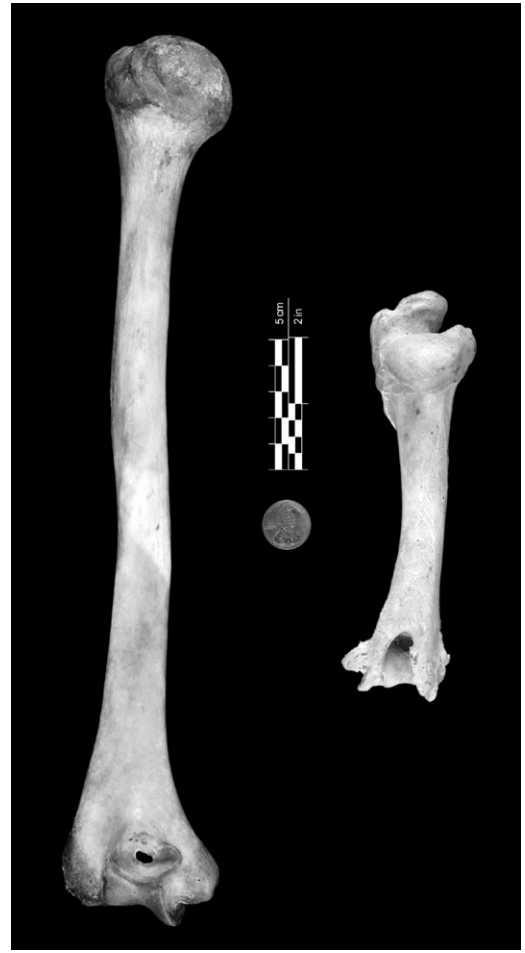

Figure 14-04: A human left humerus (posterior view) is compared to a sheep's left humerus (caudal view). Note that the overall morphology of the sheep's skeleton is quite similar to the cow's, but that the sheep is significantly smaller.

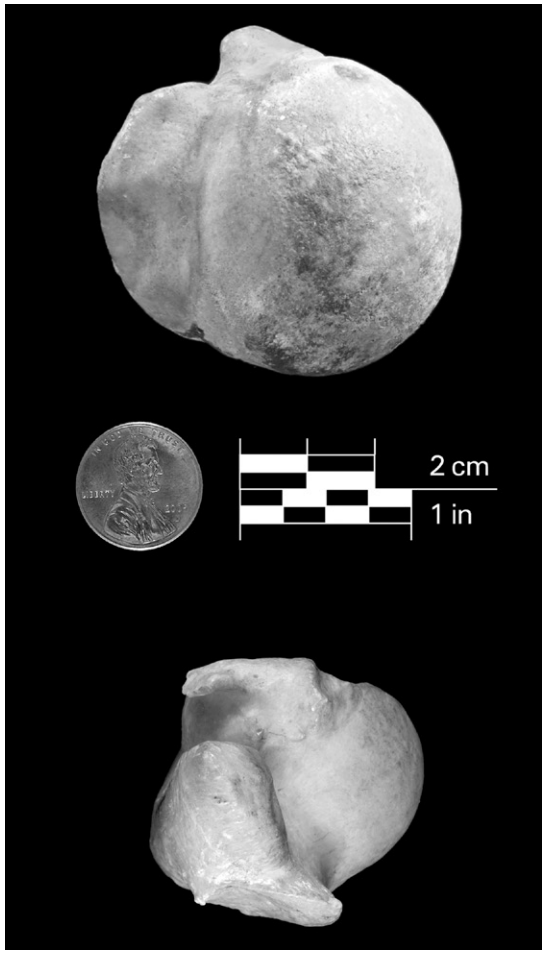

Figure 14-05: A human proximal humerus (superior view) is compared to a sheep's proximal humerus (dorsal) view. The head of the humerus and the tubercles are visible in this view.

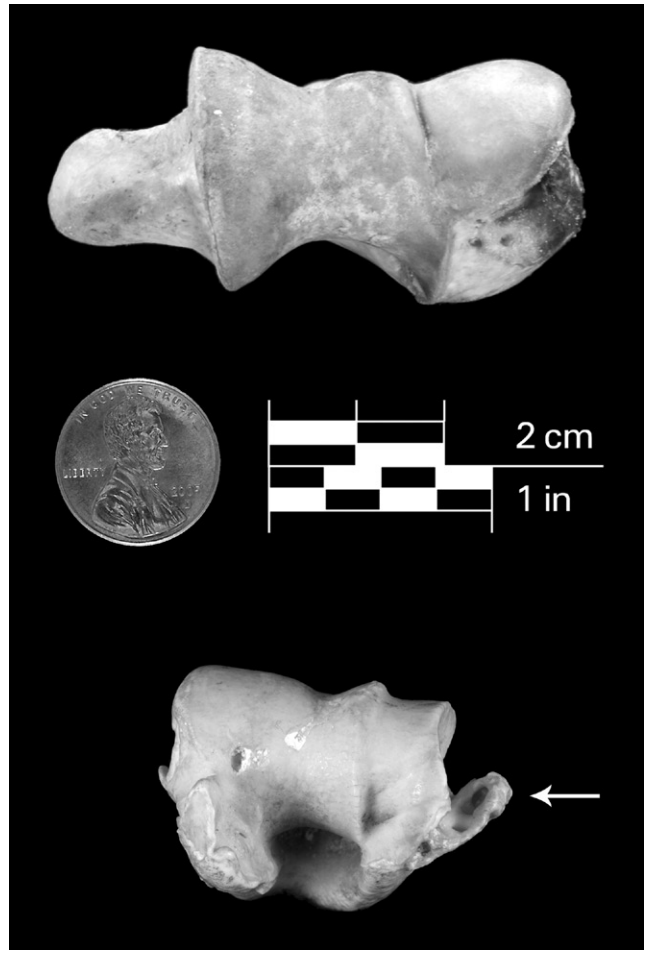

Figure 14-06: A human distal humerus (inferior view) is compared to a sheep's distal humerus (ventral view). Note the closer view of "penning elbow" (arrow).

Figure 14-07: A human left ulna and radius (anterior views) are compared to a sheep's left radius and ulna (cranial view). Note that the sheep's radius is large in relation to the ulna. In many older adult sheep the shaft of the radius is fused to the ulna.

Figure 14-08: A left human radius and ulna (posterior views) are compared to a sheep's left radius and ulna (caudal view). Note that the shaft of the sheep's ulna is fused to the caudal surface of the radius in this older individual. The exostosis associated with "penning elbow" can also be seen on the lateral side of the proximal radius (arrow).

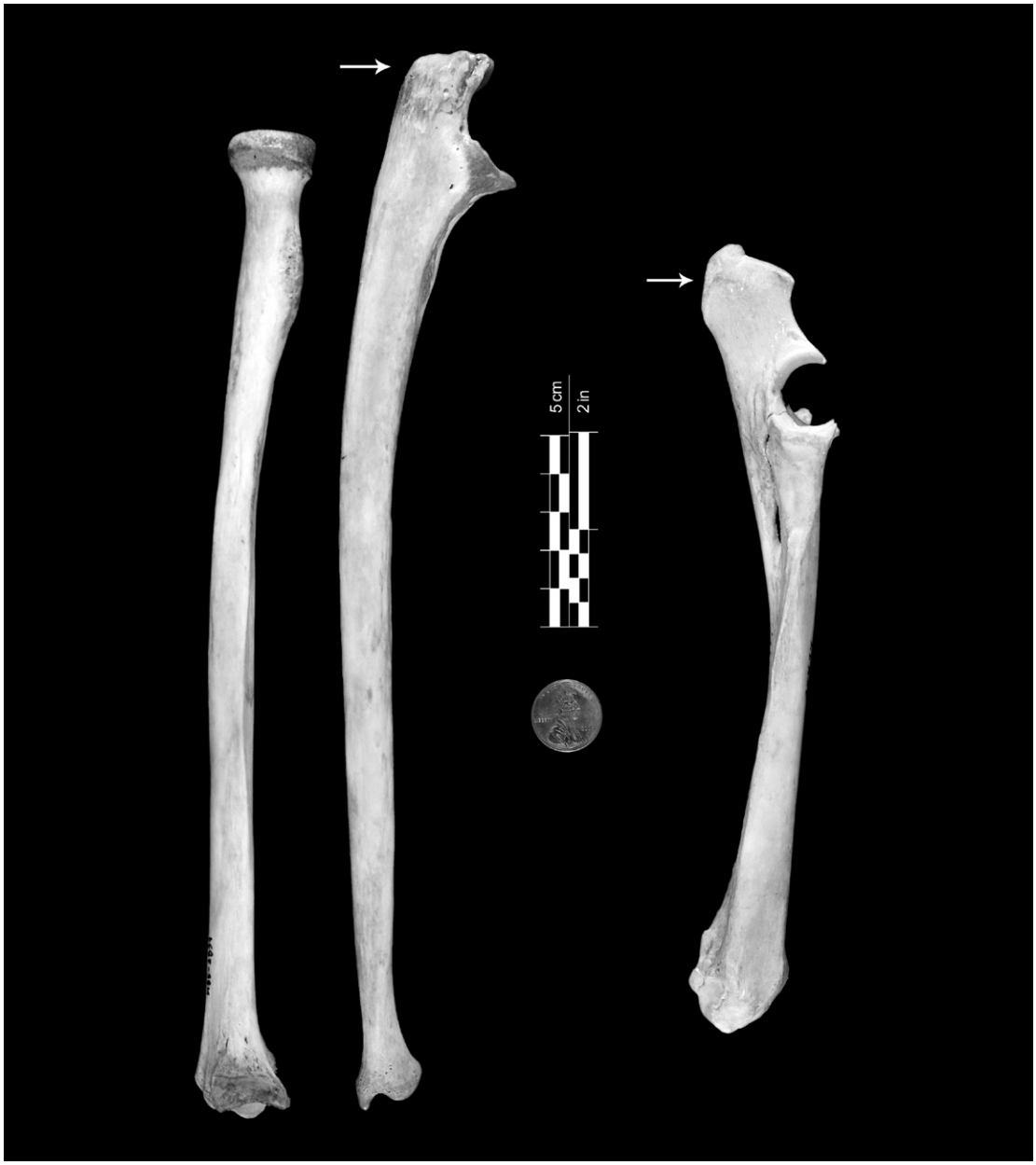

Figure 14-09: A human left radius and ulna (medial views) are compared to a sheep's left radius and ulna (medial view). Although the shaft of the sheep's ulna is very slender, the olecranon process is well developed compared to the human olecranon process (arrows).

Figure 14-10: Sheep radius and ulna (proximal end, dorsal view). The proximal ulna (olecranon process) is visible in this view.

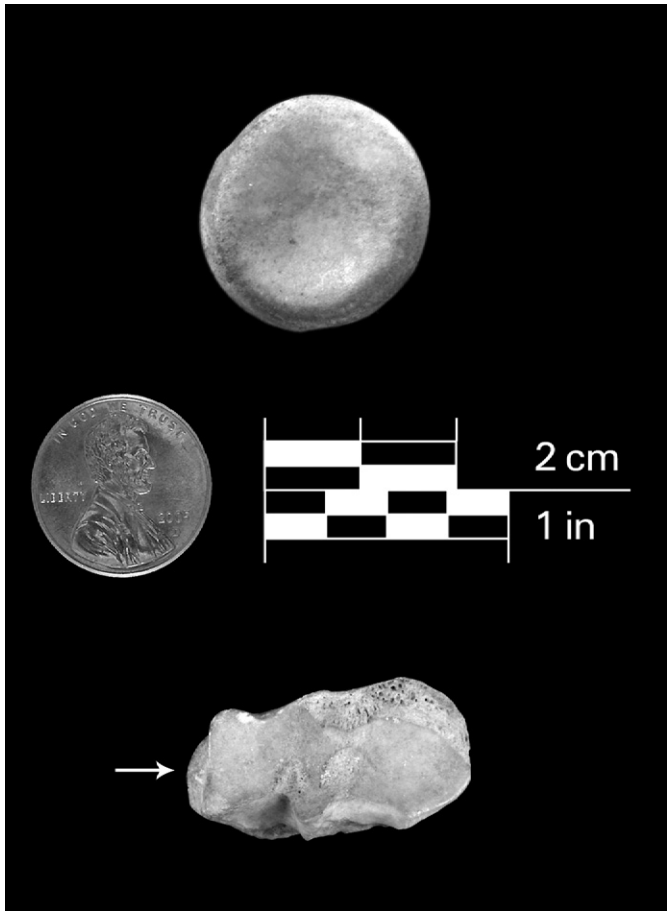

Figure 14-11: A human proximal radius (superior view) is compared to a sheep's proximal radius (dorsal view). Note that the lateral bicipital tuberosity (arrow) is more well developed in sheep than it is in goats.

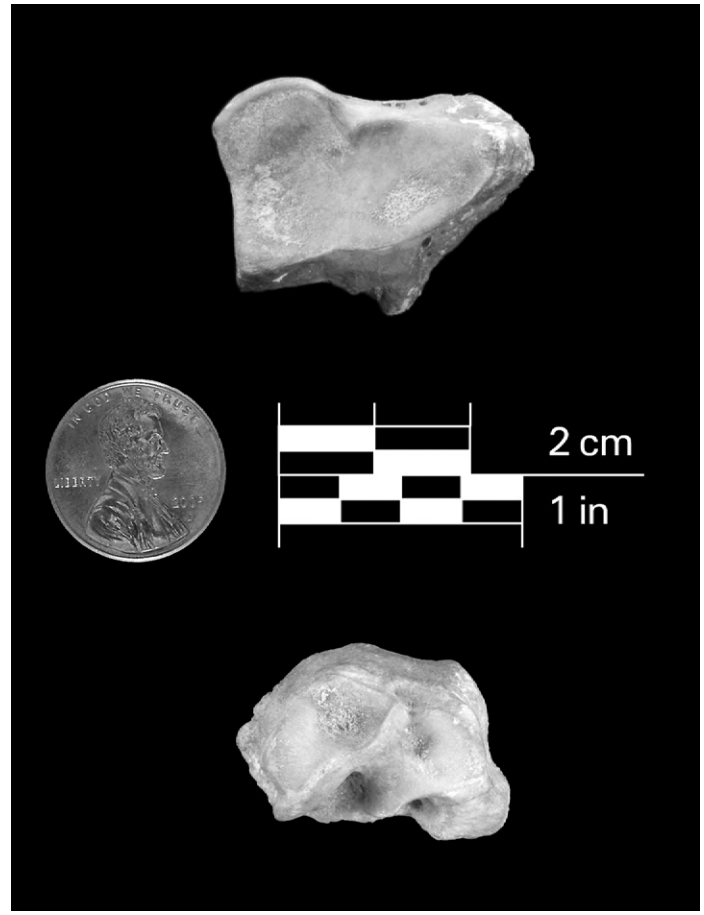

Figure 14-12: A human distal radius (inferior view) is compared to a sheep's distal radius (ventral view).

Figure 14-13: A human left femur (anterior view) is compared to a sheep's left femur (cranial view). The most proximal point of the human femur is the head, while the most proximal point on the sheep's femur is the greater trochanter. The sheep and goat are quite similar (both are members of the subfamily Caprinae), and the differences between their postcranial skeletons are quite subtle. The angle formed between the head and the greater trochanter is generally about 90 degrees in sheep, while the angle is acute in goats.

Figure 14-14: A human left femur (posterior view) is compared to a sheep's left femur (caudal view). The sheep's femur is marked by a supercondylar fossa on the lateral portion of the shaft (arrow). The linea aspera along the midline of the posterior femur shaft is a distinctively human feature.

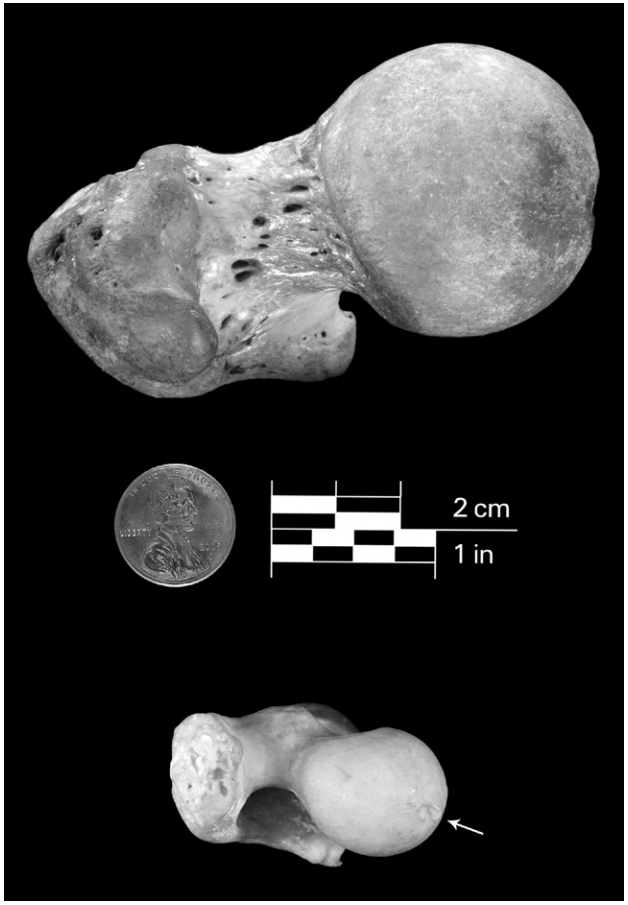

Figure 14-15: An adult human proximal left femur (superior view) is compared to a sheep's proximal left femur (cranial view). The sheep's femoral head, greater trochanter, and lesser trochanter are visible in this view. The arrow points to the small, circular fovea capitis.

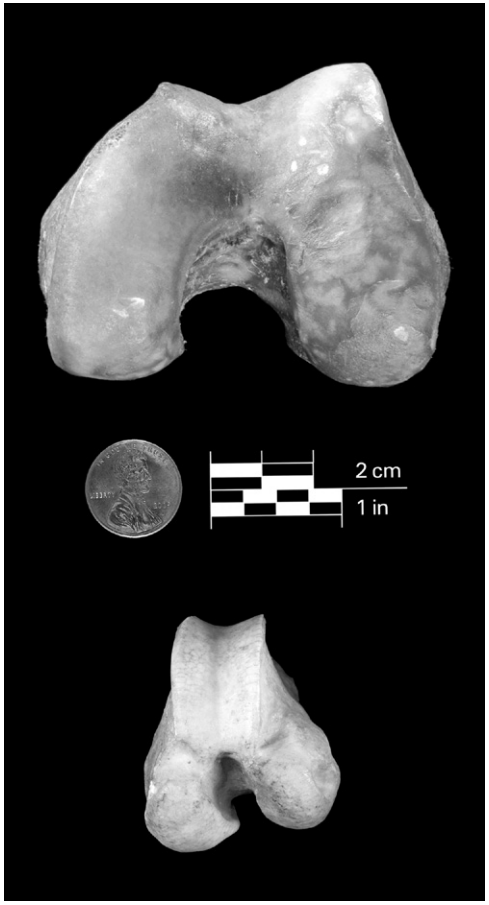

Figure 14-16: An adult human distal left femur (inferior view) is compared to a sheep's distal left femur (ventral view). The two condyles and the trochlea (for articulation with the patella) are visible in both specimens.

Figure 14-17: A human left tibia (anterior view) is compared to a sheep's left tibia (cranial view).

Figure 14-18: A human left tibia (posterior view) is compared to a sheep's left tibia (caudal view).

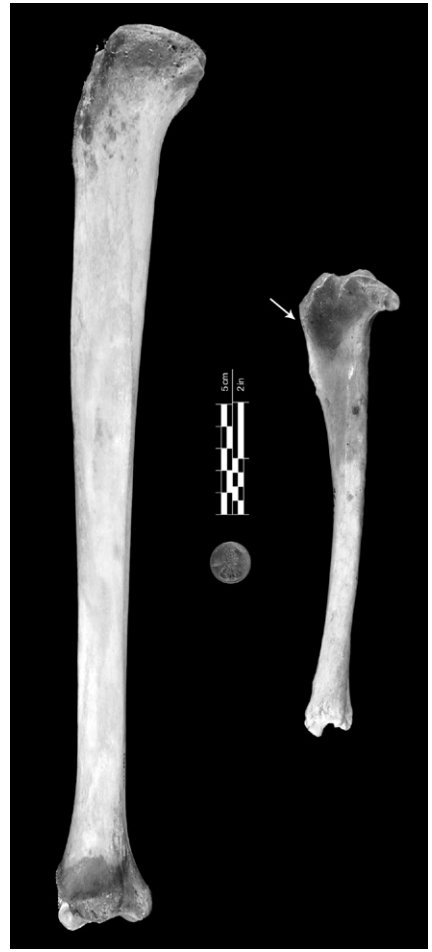

Figure 14-19: A human left tibia (lateral view) is compared to a sheep's left tibia (lateral view). Note that the tibial tuberosity and crest (arrow) are well developed in the sheep.

Figure 14-20: A human proximal left tibia (superior view) is compared to a proximal sheep's left tibia (cranial view). The facets for articulation with the distal condyles of the femur are visible in this view for both specimens. It is very difficult to distinguish sheep from goats based on the proximal tibia.

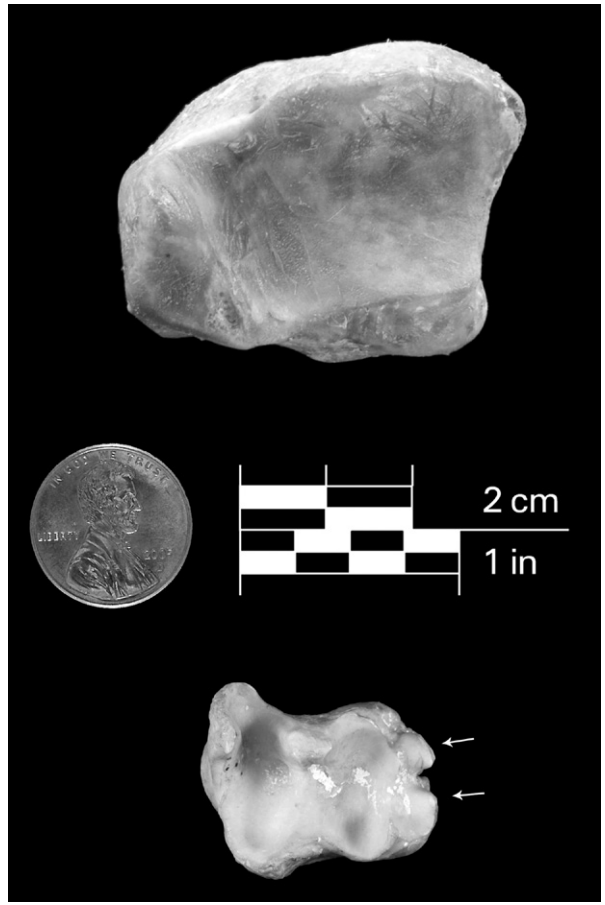

Figure 14-21: A human distal left tibia (inferior view) is compared to a sheep's distal left tibia (ventral view). The medial malleolus and articular facets for the tibia (parallel grooves) are visible in this view. The two small facets on the lateral surface (arrows) are for the articulation with the malleolus, a small tarsal that is the evolutionary remnant of the distal fibula.

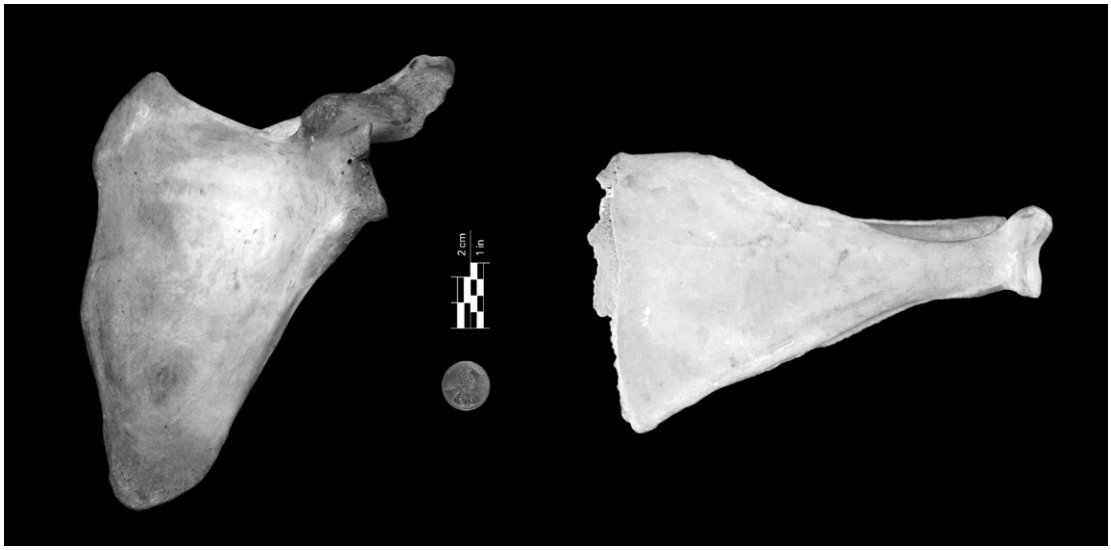

Figure 14-22: A human left scapula (anterior view) is compared with a sheep's left scapula (medial view). Both scapulae are oriented as they would be in a human skeleton. In comparison to the human scapula, the sheep's scapula is elongated.

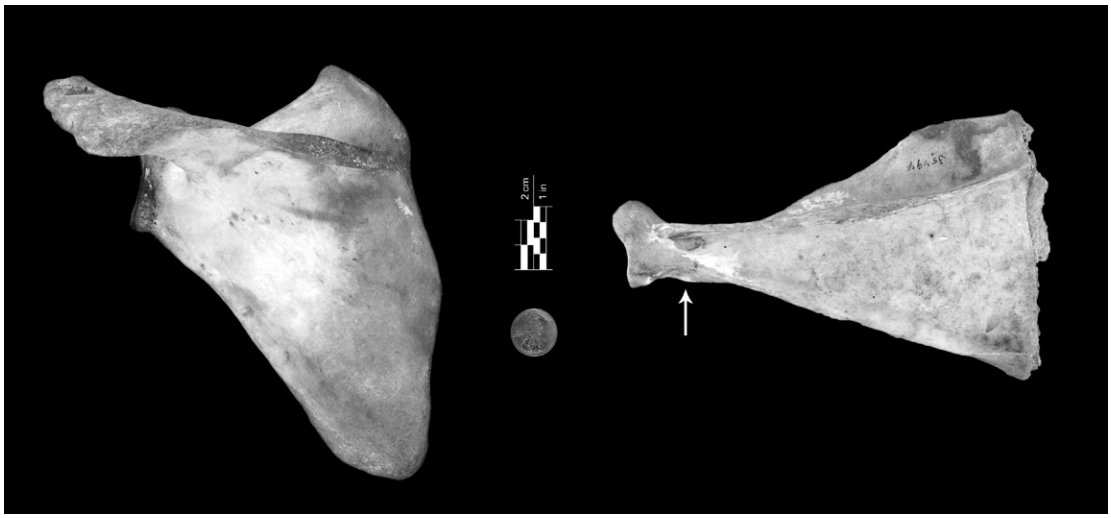

Figure 14-23: A human left scapula (posterior view) is compared to a sheep's left scapula (lateral view). The acromion process in the sheep is quite small, while it is quite large in the human. In addition, a small crest is visible on the caudal border of the neck of the sheep's scapula (arrow). The presence of this crest can be used to distinguish sheep from goats.

Figure 14-24: A human left innominate (lateral view) is compared to a sheep's left innominate (lateral view).

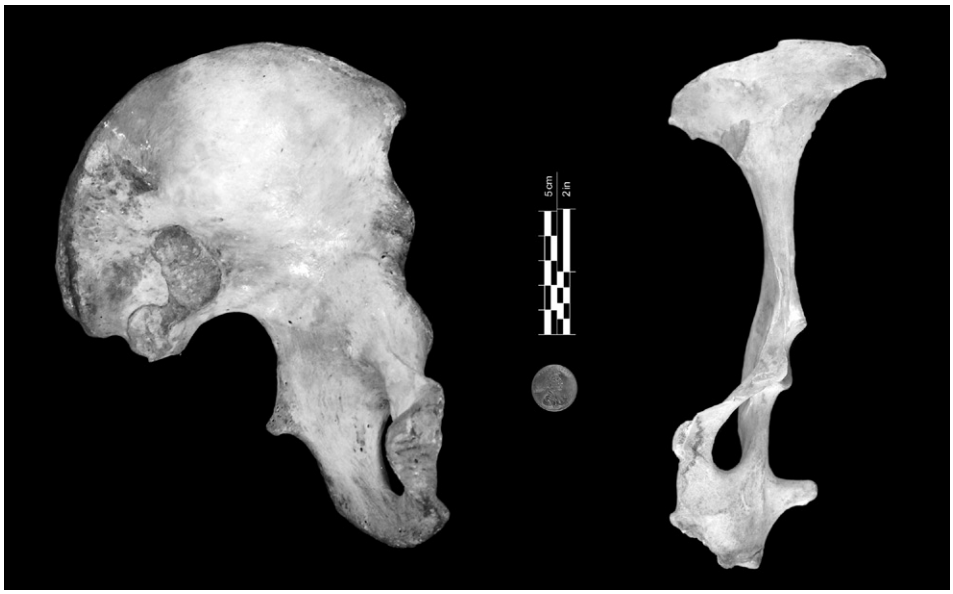

Figure 14-25: A human left innominate (medial view) is compared to a sheep's left innominate (ventral view). Note the sheep's elongated ilium.

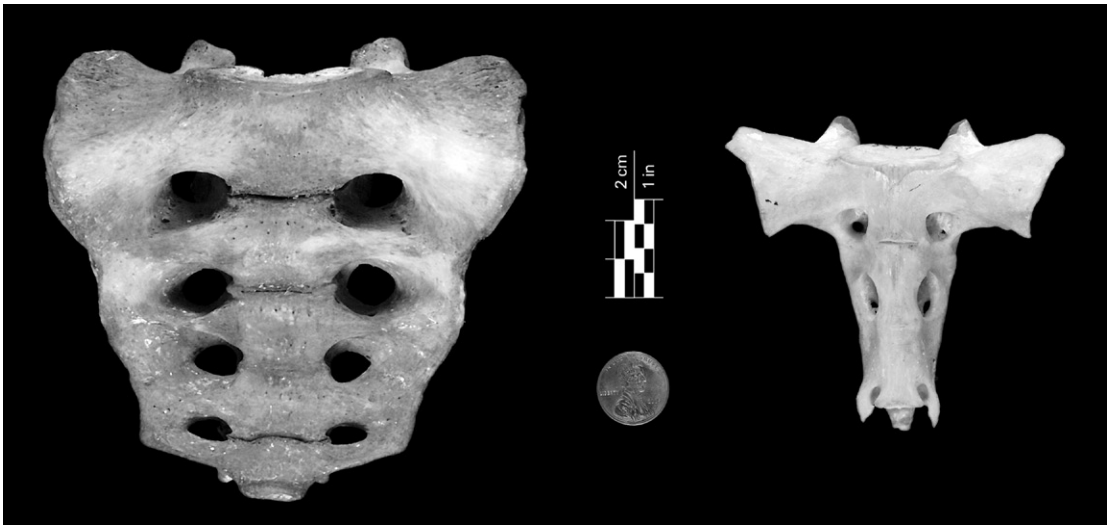

Figure 14-26: A human sacrum (anterior view) is compared to a sheep's sacrum (ventral view). The wings of the sheep's sacrum are quite wide, while the rest of the sacrum is relatively narrow.

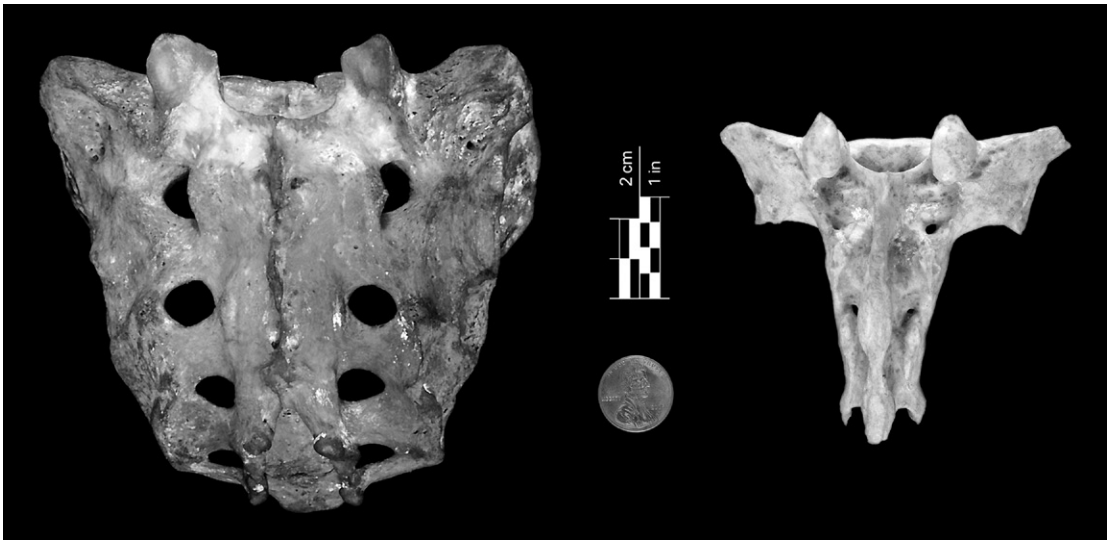

Figure 14-27: A human sacrum (posterior view) is compared to a sheep's sacrum (dorsal view).

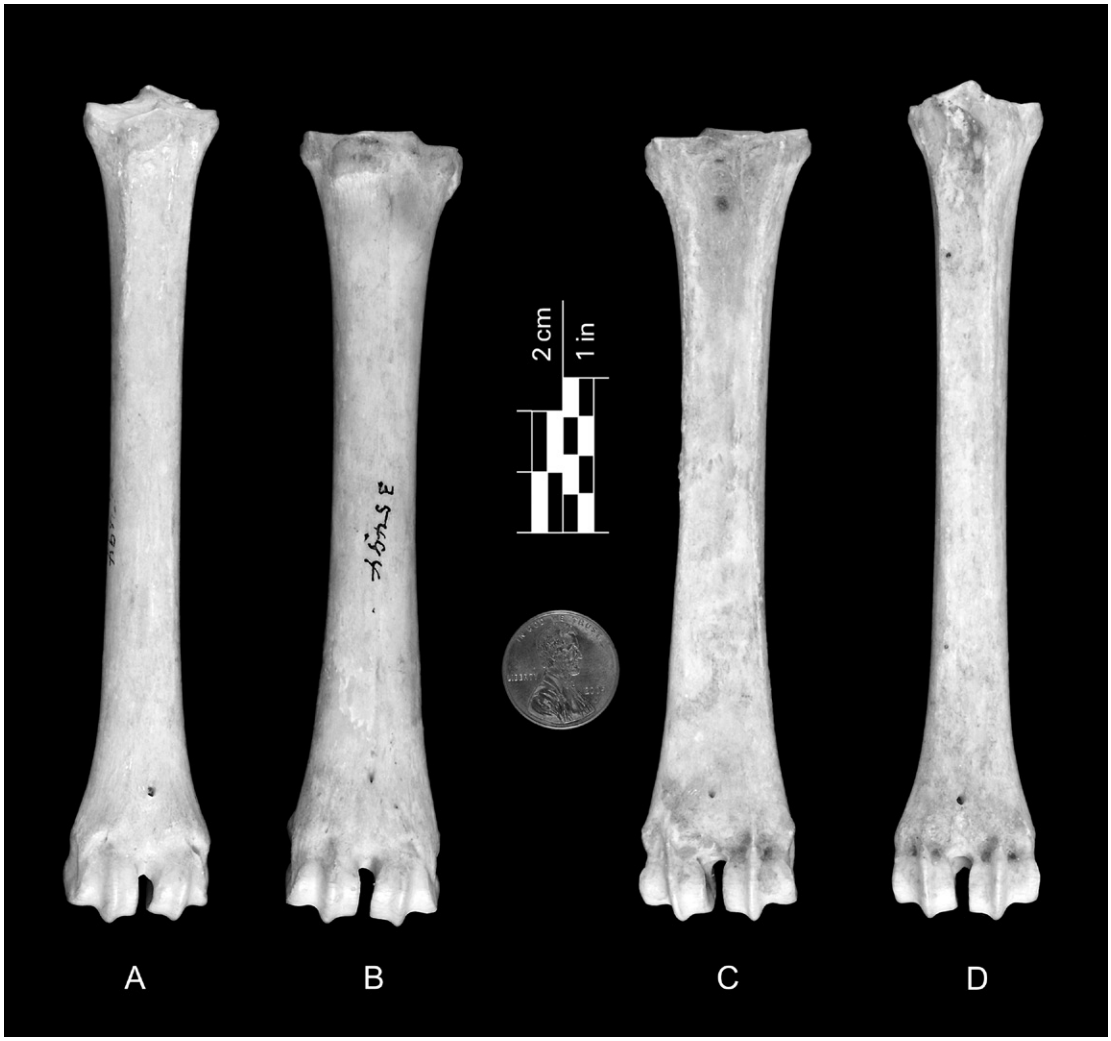

Figure 14-28: The sheep's left metatarsus (A, dorsal view) and metacarpus (B, dorsal view) are shown on the left. The sheep's metacarpus (C, palmar view) and metatarsus (D, plantar view) are shown on the right. The sheep's metapodia are composed of the fused third and fourth metacarpals and metatarsals.

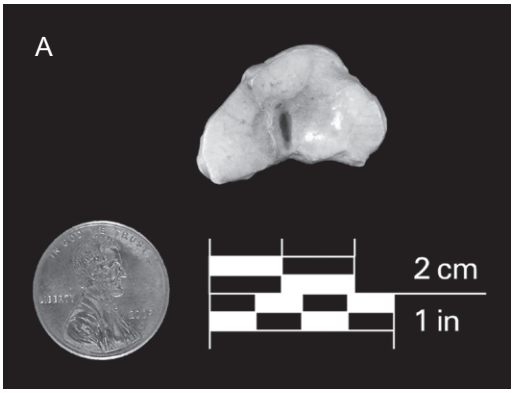

Figure 14-29a: Sheep proximal left metacarpal (dorsal view). The two large facets for the articulation of the distal carpal row, including the fused second and third carpals (larger medial facet) and the fourth carpal (smaller lateral facet), are visible in this view.

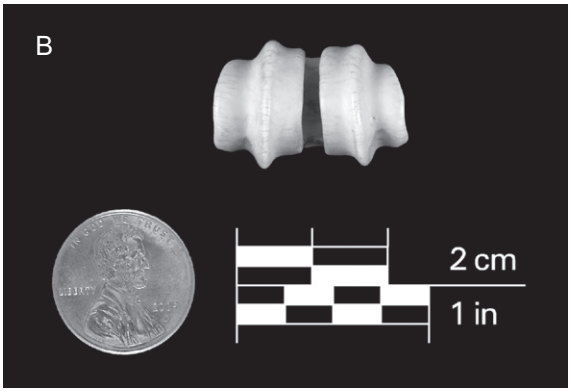

Figure 14-29b: Sheep distal left metacarpal (volar view).

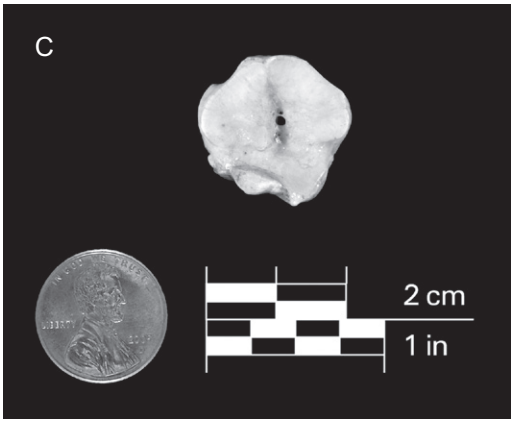

Figure 14-29c: Sheep proximal left metatarsal (dorsal view). This view shows the articular facets for the distal tarsal row. While the proximal metacarpus is D-shaped, the proximal metatarsus is roughly circular in outline.

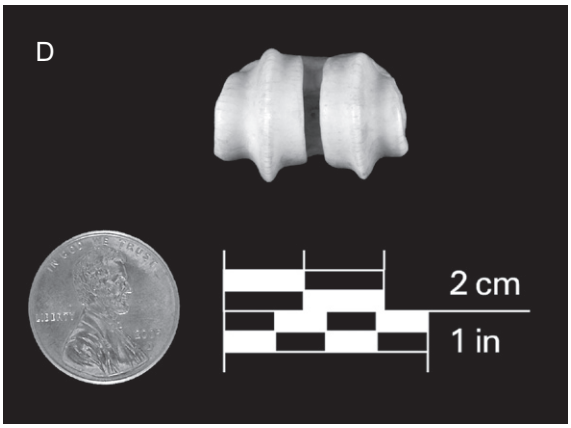

Figure 14-29d: Sheep distal left metatarsal (plantar view).

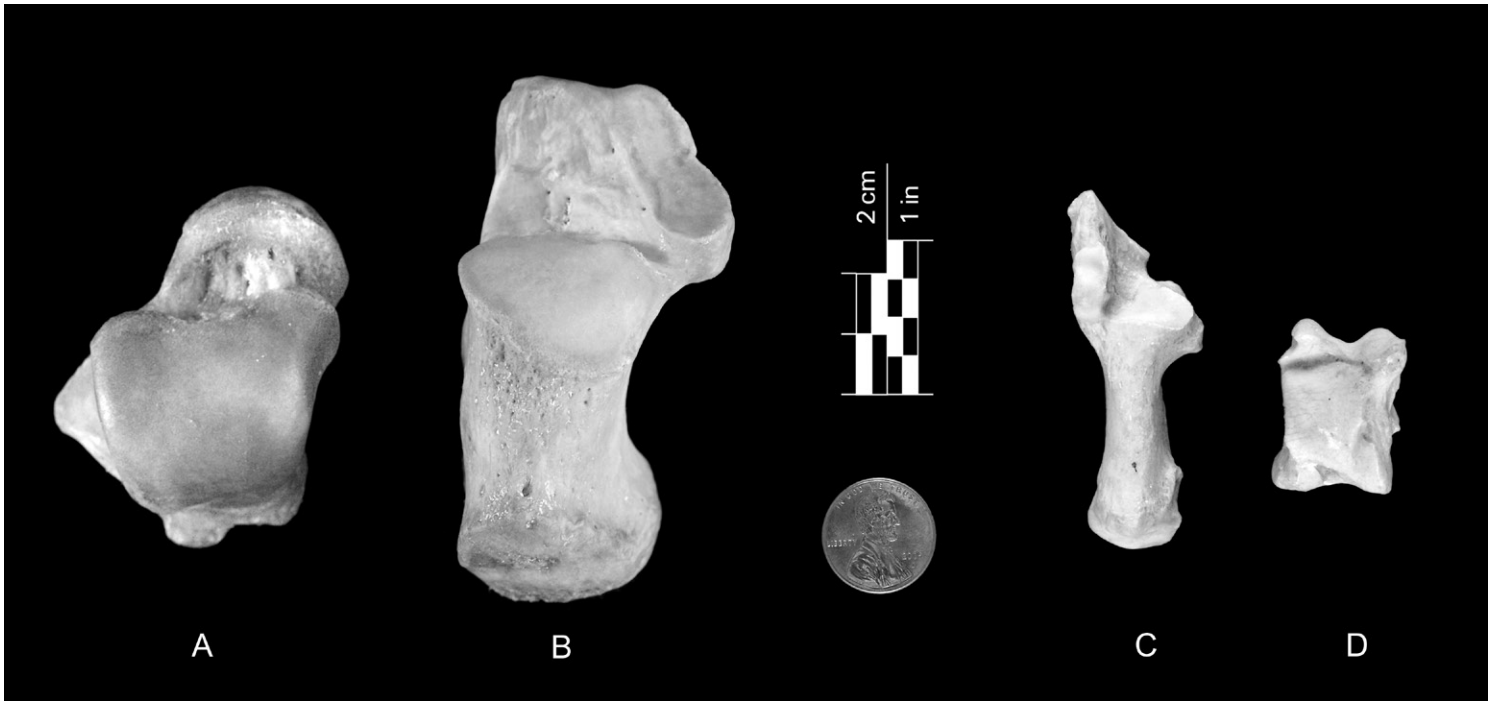

Figure 14-30: A human left talus (A, superior view) and calcaneus (B, superior view) are compared to a sheep's left calcaneus (C, dorsal view) and a sheep's left astragalus (D, plantar view). The sheep's astragalus has the "double pulley" form that is seen in all artiodactyls. The sheep's calcaneus is elongated and includes a dorsal articular facet for the malleolus (the evolutionary remnant of the distal fibula).

This page intentionally left blank

CHAPTER 15

Dog (Canis familiaris)

Comparative Osteology. DOI: 10.1016/B978-0-12-388437-4.00015-6

Figure 15-01: Dog cranium (lateral view, right side). The dental formula for the adult dog includes three incisors, one large canine, four premolars, and two molars on the maxilla, and three incisors, one canine, four premolars, and three molars on the mandible (not shown). In the carnivores, the large canines are used to seize and dispatch prey. The sectorial cheek teeth work like a pair of scissors to cut meat into pieces that are small enough to be swallowed. (B) Dog cranium (ventral view). The dog's dental formula is 3/3.1/1.4/4.2/3.

Figure 15-02: A human left humerus (anterior view) is compared to a dog's left humerus (cranial view). One of the features of the dog's humerus is that the radial fossa communicates with the olecranon fossa, producing a supratrochlear foramen (arrow). These foramina (also called septal apertures) are sometimes seen in humans. A small septal aperture is seen in this human specimen.

Figure 15-03: A human left humerus (posterior view) is compared to a dog's left humerus (caudal and medial views). When compared to the human head of the humerus, the head of the humerus in the dog is elongated sagittally.

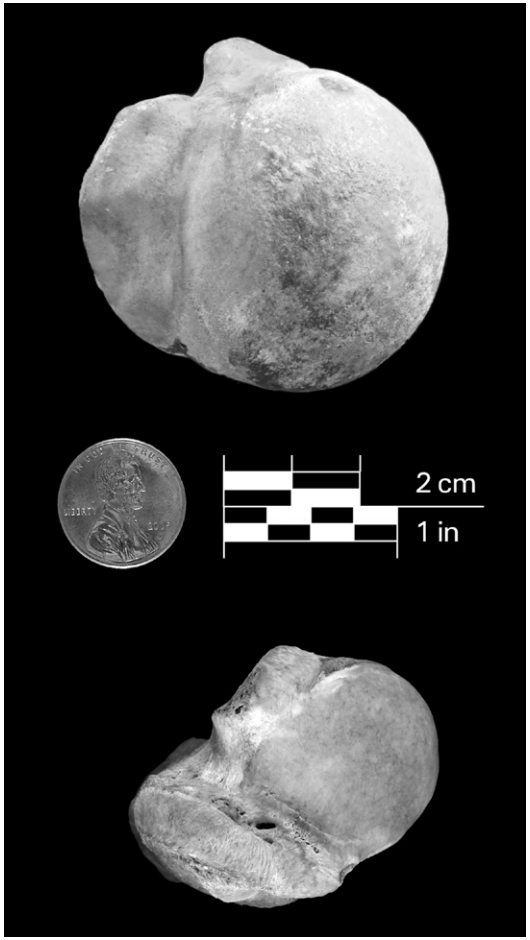

Figure 15-04: An adult human proximal humerus (superior view) is compared to a dog's proximal humerus (dorsal view). The greater tubercle, lesser tubercle, and head are visible in both specimens in this view.

Figure 15-05: An adult human distal humerus (inferior view) is compared to a dog's distal humerus (ventral view).

Figure 15-06: A human left radius (anterior view) is compared to a dog's left radius (cranial view). Both the human and the dog's radius have a distinctive head and neck. Note the elongated neck on the human radius (arrow).

Figure 15-07: A human left radius (posterior view) is compared to a dog's left radius caudal view).

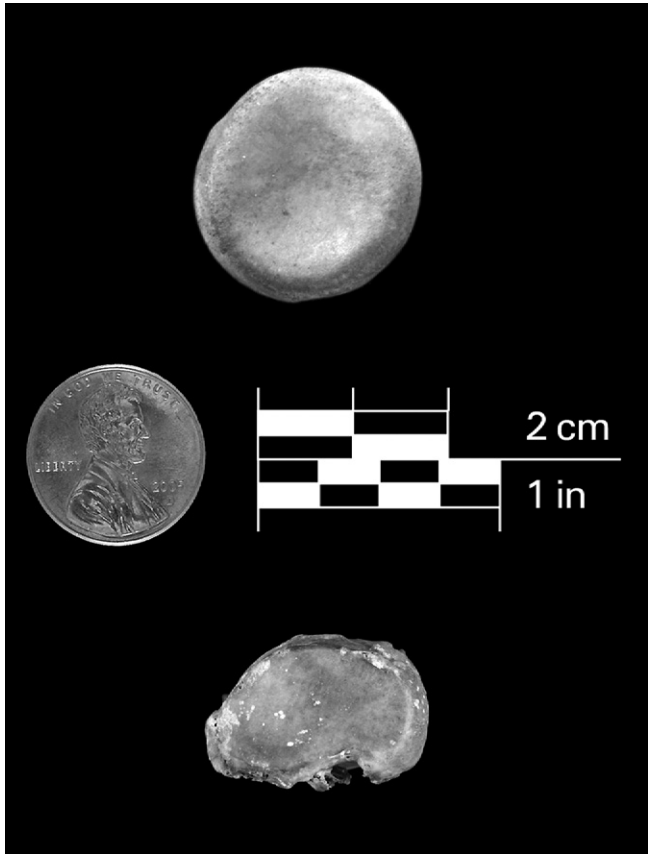

Figure 15-08: A human proximal radius (superior view) is compared to a dog's proximal radius (dorsal view).

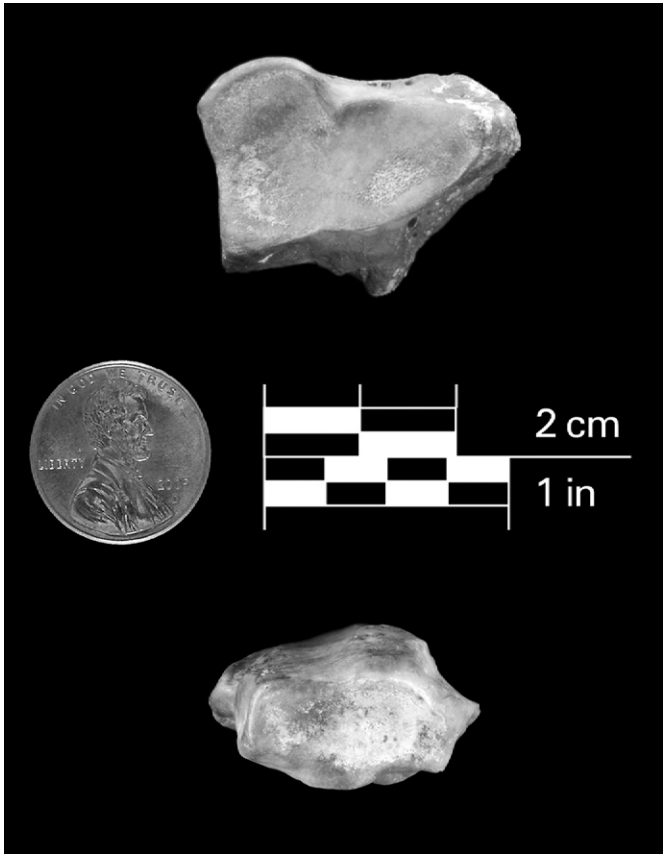

Figure 15-09: A human distal radius (inferior view) is compared to a dog's distal radius (ventral view).

Figure 15-10: A human left ulna (anterior view) is compared to a dog's left ulna (cranial view).

Figure 15-11: A human left ulna (posterior view) is compared to a dog's left ulna (caudal view).

Figure 15-12: A human left ulna (medial view) is compared to a dog's left ulna (medial view). The olecranon is larger and more well developed in the dog (arrow).

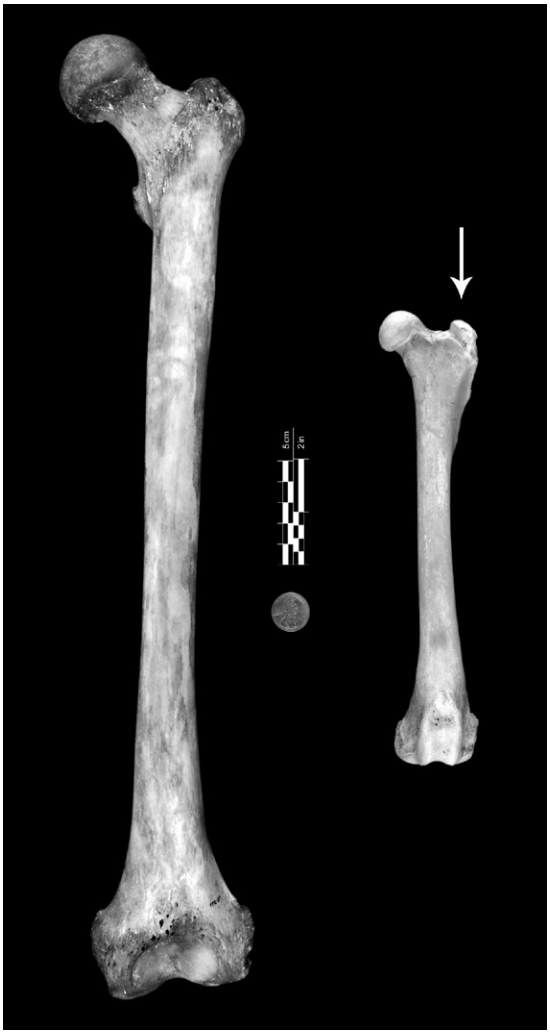

Figure 15-13: A human left femur (anterior view) is compared to a dog's left femur (cranial view). When compared to the human femur, the dog's greater trochanter is more well developed (arrow). The distal condyles of the human femur show a distinctive asymmetry while the distal femur of the dog is more even and symmetric.

Figure 15-14: A human left femur (posterior view) is compared to a dog's left femur (caudal view). Two small articular facets are visible on the dog's femur, just proximal to the distal condyles (arrows). These are the medial and lateral articular facets for two sesamoids that are located in the origin of the gastrocnemius muscle.

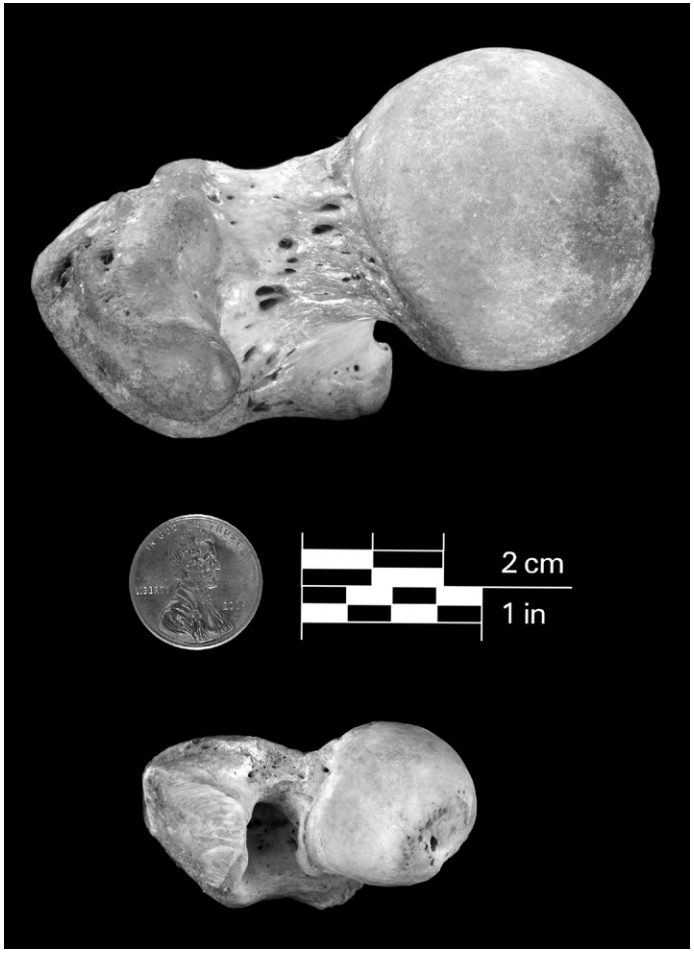

Figure 15-15: A human left proximal femur (superior view) is compared to a dog's left proximal femur (dorsal view).

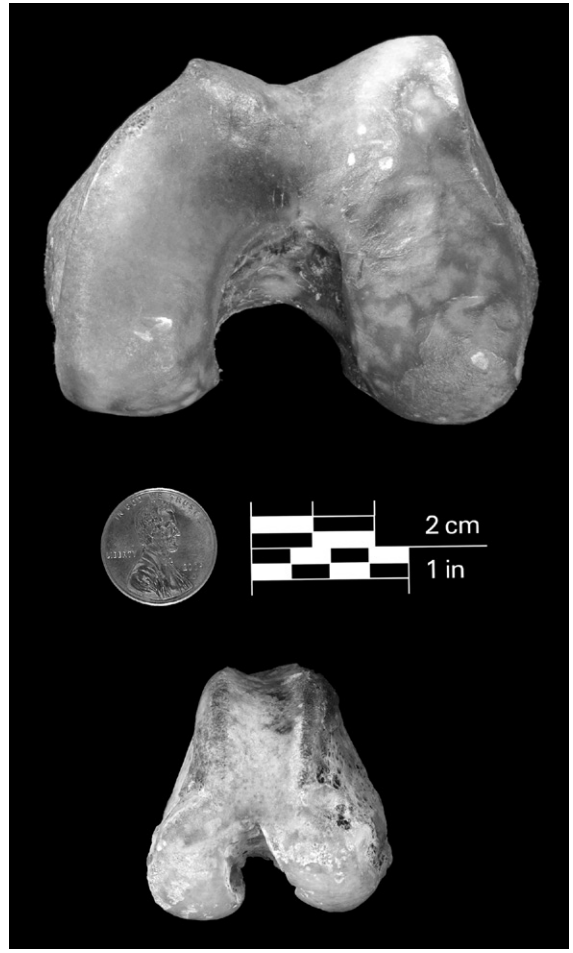

Figure 15-16: A human left distal femur (inferior view) is compared to a dog's left distal femur (ventral) view. The two distal condyles and the trochlea are visible in this view.

Figure 15-17: A human left tibia (anterior view) is compared to a dog's left tibia (cranial view).

Figure 15-18: A human left tibia (posterior view) is compared to a dog's left tibia (caudal view).

Figure 15-19: A human left tibia (lateral view) is compared to a dog's left tibia (lateral view). Although these two tibiae are broadly similar in form, the proximal tibia of the dog has a more well-developed tibial tuberosity (arrow).

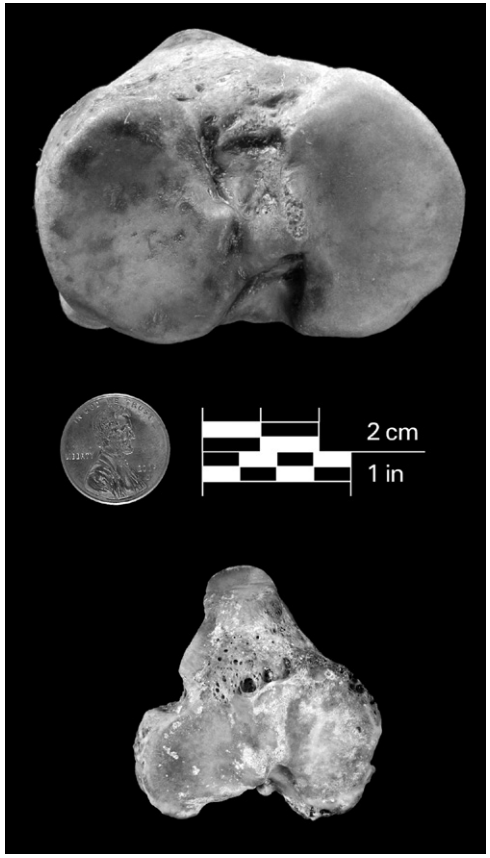

Figure 15-20: A human left proximal tibia (superior view) is compared to a dog's left proximal tibia (dorsal) view. The dog's tibia is elongated in the dorsal–plantar (anterior–posterior) direction when compared to the tibiae of the cow, sheep, goat, deer, and horse. The dog's tibia is relatively narrow mediolaterally.

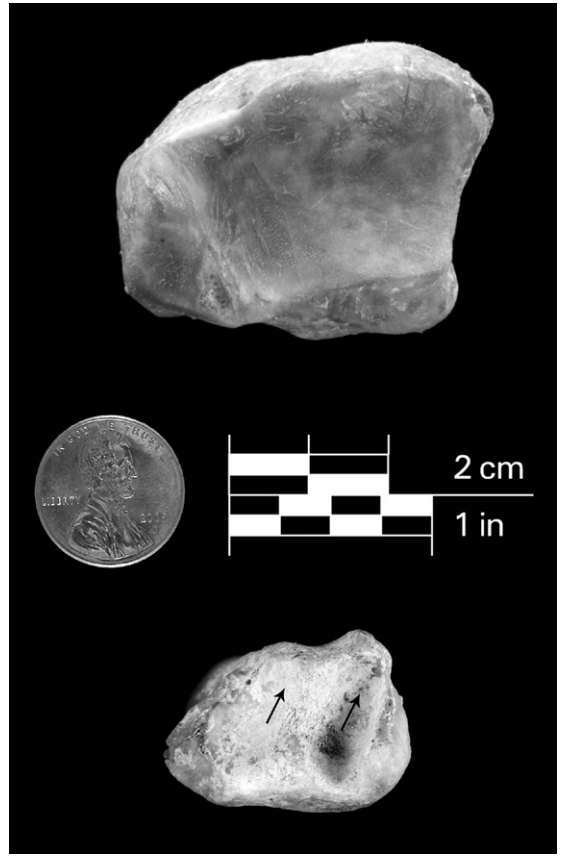

Figure 15-21: A human left distal tibia (inferior view) is compared to a dog's left distal tibia (ventral view). The two facets for the articulation of the talus (astragalus) are oriented obliquely (arrows), unlike those in the artiodactyls.

Figure 15-22: A human left fibula (lateral view) is compared to a dog's left fibula (lateral view). The body of the dog's fibula is quite slender.

Figure 15-23: A human left fibula (medial view) is compared to a dog's left fibula (medial view).

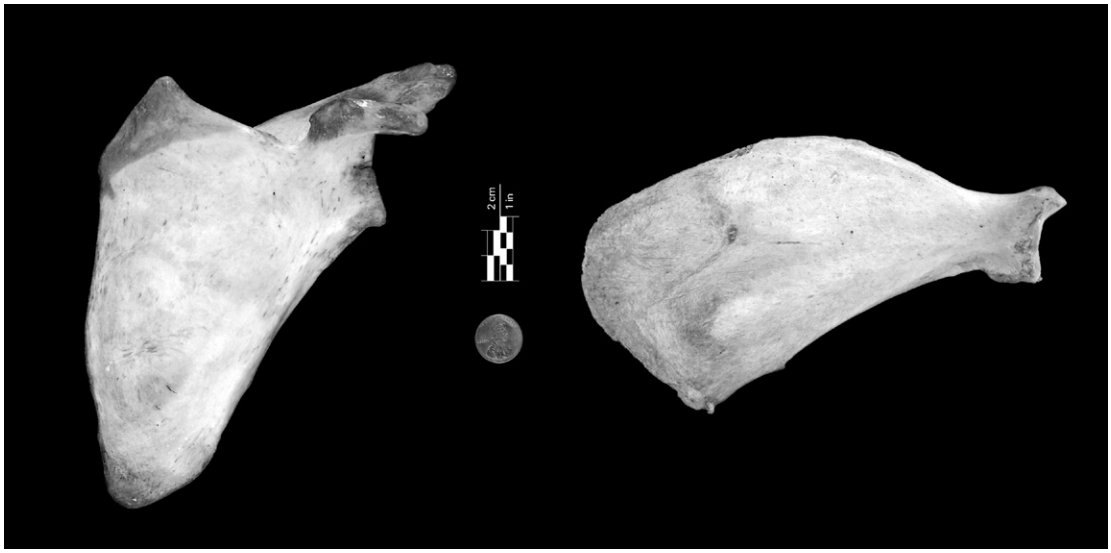

Figure 15-24: A human left scapula (anterior view) is compared to a dog's left scapula (medial view). Both bones are oriented as they would be in a human. Note that the dog's scapula is elongated.

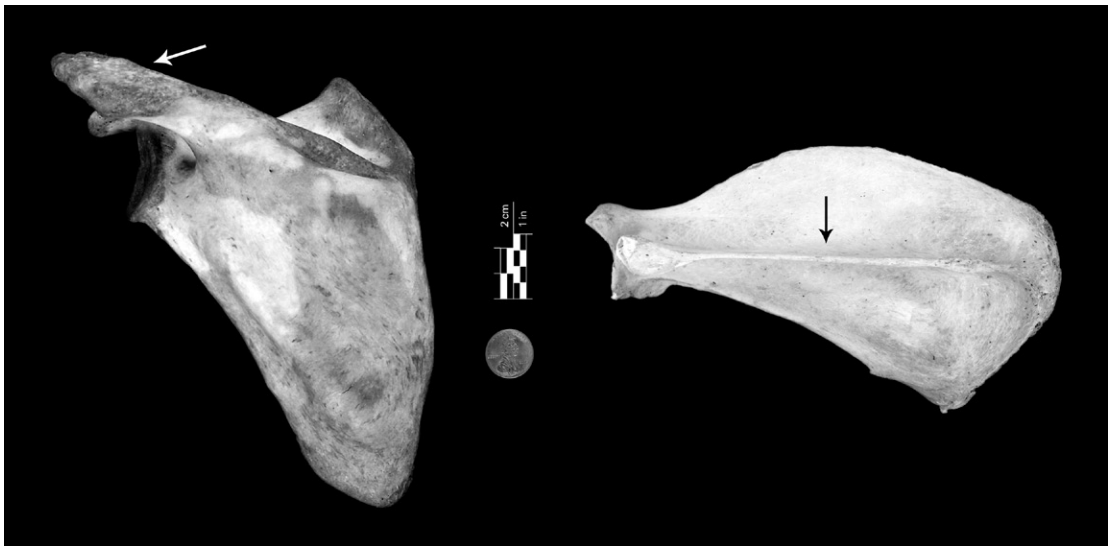

Figure 15-25: A human left scapula (posterior view) is compared to a dog's left scapula (lateral view). Note that the spine of the dog's scapula (black arrow) divides the scapula into two nearly equal halves. The human scapula's larger acromion process is visible in this view (white arrow).

Figure 15-26: A human left innominate (lateral view) is compared to a dog's pelvis (ventral view). The two dog innominates are fused at the pubic symphysis.

Figure 15-27: A human left innominate (medial view) is compared to a dog's pelvis (dorsal view).

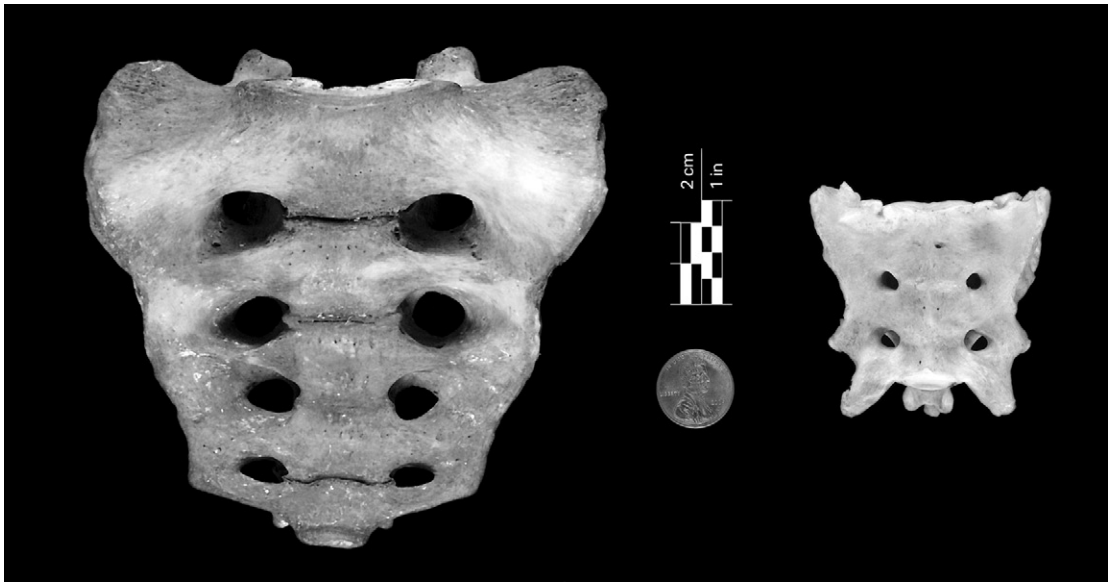

Figure 15-28: A human sacrum (anterior view) is compared to a dog's sacrum (ventral view). The dog's sacrum is usually composed of three fused vertebrae, while the human's is usually composed of five fused vertebrae.

Figure 15-29: A human sacrum (posterior view) is compared to a dog's sacrum (dorsal view).

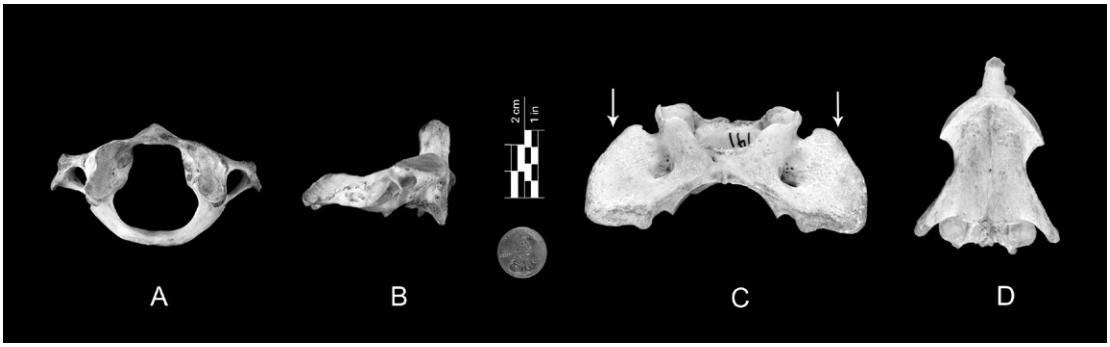

Figure 15-30: A superior view of a human atlas (A) and a lateral view of a human axis (B) are compared to ventral views of a dog's atlas (C) and axis (D). All mammals have seven cervical vertebrae and, in general, the lengths of these vertebrae reflect the length of the animal's neck. The dog's atlas and axis are clearly longer than the human's. The dog's atlas is marked by large transverse processes or wings (arrows).

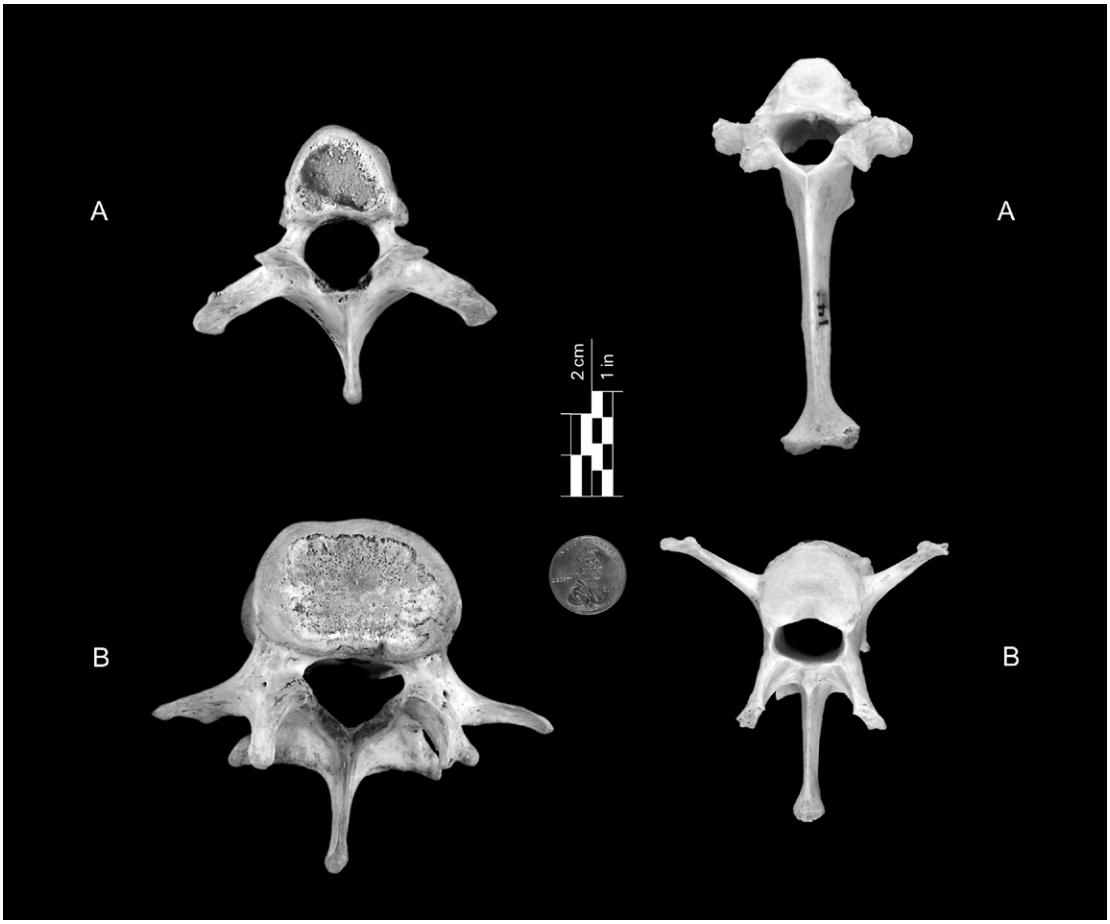

Figure 15-31: Superior views of typical thoracic (A, left) and lumbar (B, left) human vertebrae are compared to cranial views of typical thoracic (A, right) and lumbar (B, right) dog vertebrae.

CHAPTER 16

Raccoon (Procyon lotor)

Comparative Osteology. DOI: 10.1016/B978-0-12-388437-4.00016-8

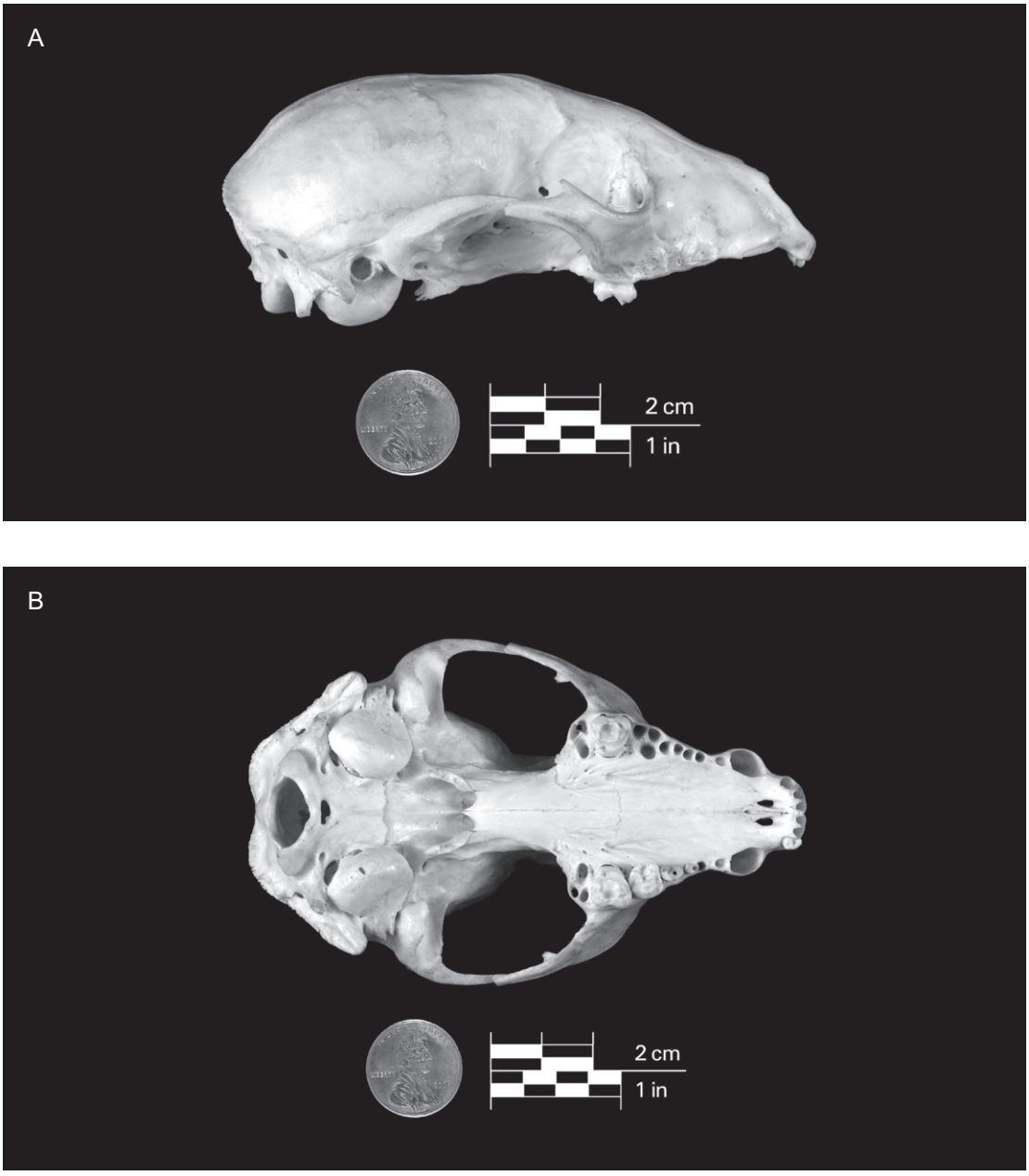

Figure 16-01: Raccoon cranium (A) lateral view, right side; (B) ventral view. The raccoon's dental formula is 3/3.1/1.4/4.2/2. Numerous teeth are missing postmorterm (after death) from this specimen.

Figure 16-02: A newborn human left humerus (anterior view) is compared to a raccoon's left humerus (cranial view). The raccoon, like the cat, has a supercondylar foramen (arrow). The raccoon has a more well-developed lateral epicondylar crest than the cat.

Figure 16-03: A newborn human left humerus (posterior view) is compared to a raccoon's left humerus (caudal view).

Figure 16-04: A newborn human left radius (anterior view) is compared to a raccoon's left radius (cranial view).

Figure 16-05: A newborn human left radius (posterior view) is compared to a raccoon's left radius (caudal view).

Figure 16-06: A newborn human left ulna (anterior view) is compared to a raccoon's left ulna (cranial view). Note that the distal end of the raccoon's ulna tapers to a small, blunt point, the styloid process (arrow).

Figure 16-07: A newborn human left ulna (posterior view) is compared to a raccoon's left ulna (caudal view).

Figure 16-08: A newborn human left ulna (lateral view) is compared to a raccoon's left ulna (lateral view).

Figure 16-09: A newborn human left femur (anterior view) is compared to a raccoon's left femur (cranial view). Note that the second trochanter on the raccoon femur is clearly visible distal to the head (arrow).

Figure 16-10: A newborn human left femur (posterior view) is compared to a raccoon's left femur (caudal view).

Figure 16-11: A newborn human left tibia (anterior view) is compared to a raccoon's left tibia (cranial view).

Figure 16-12: A newborn human left tibia (posterior view) is compared to a raccoon's left tibia (caudal view).

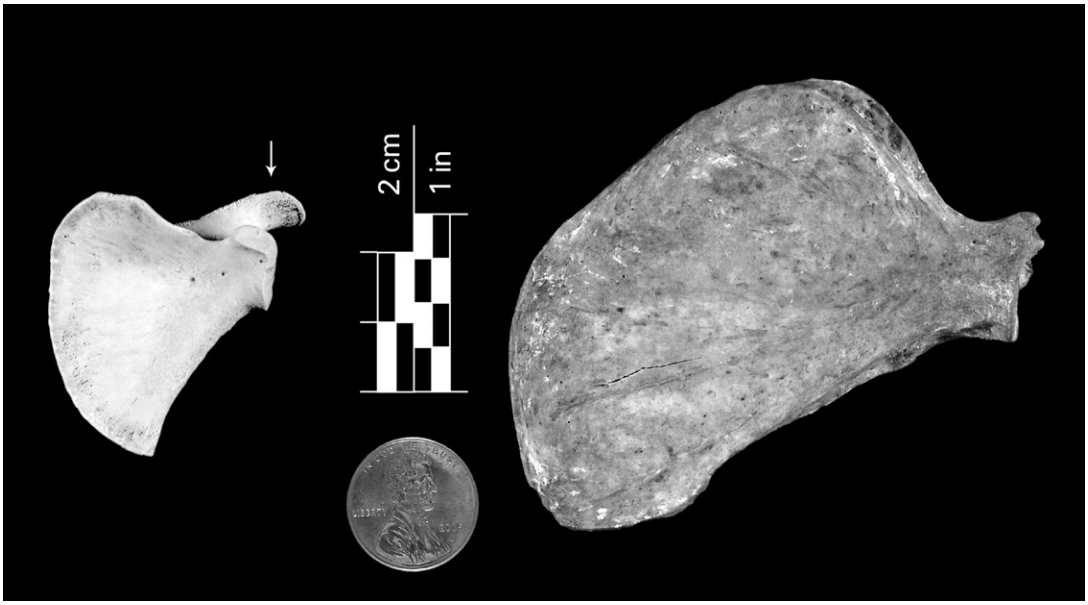

Figure 16-13: A newborn human left scapula (anterior view) is compared to a raccoon's left scapula (medial view). Both are oriented as they would be in a human skeleton. Although the shapes of the two scapulae are similar, the prominent acromion process (arrow) is visible from the anterior view of the human scapula but not that of the raccoon.

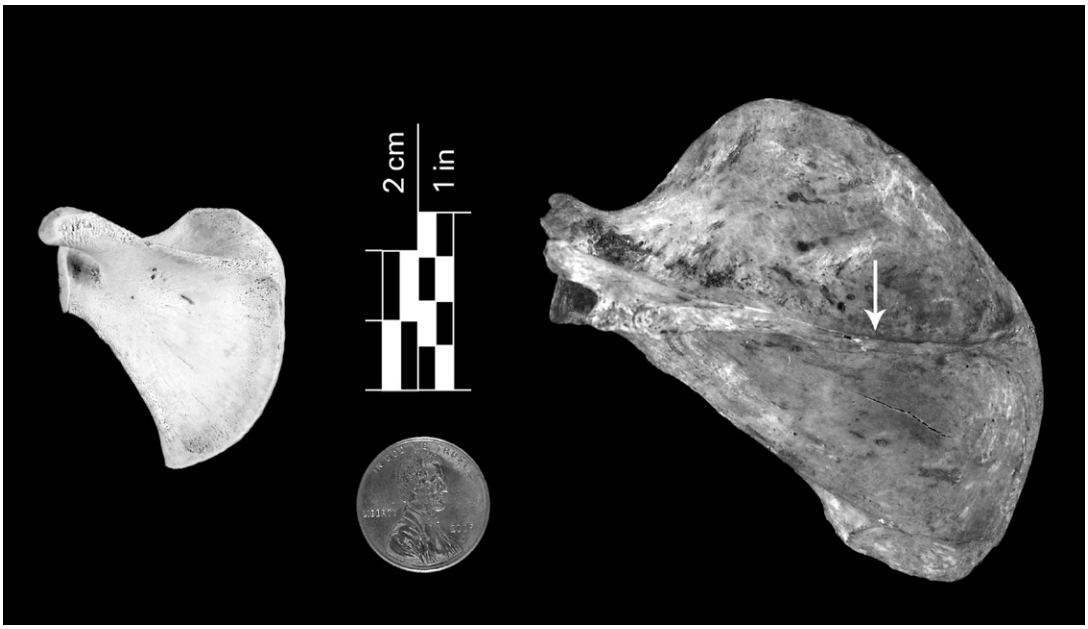

Figure 16-14: A newborn human left scapula (posterior view) is compared to a raccoon's left scapula (lateral view). The spine of the raccoon's scapula (arrow) divides the scapula neatly in half.

Figure 16-15: A newborn human left innominate (medial view) is compared to a complete raccoon's innominate (ventral view). The two halves of the raccoon's pelvis have fused along the pubic symphysis. Note the broad blade of the ilium on the human innominate (arrow).

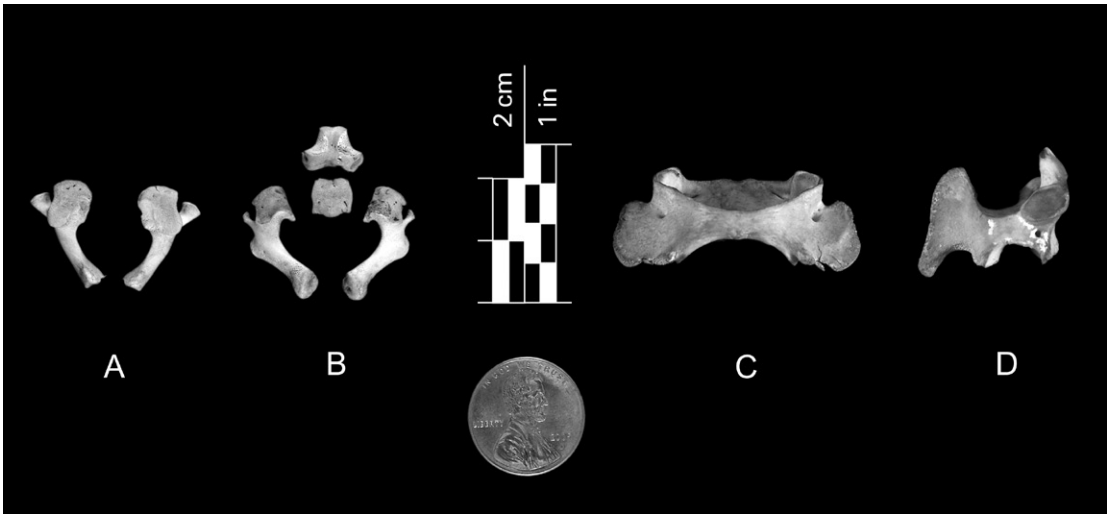

Figure 16-16: Superior views of a newborn human atlas (A) and axis (B) are compared to a raccoon's atlas (C, ventral view) and axis (D, lateral view).

Figure 16-17: A baculum (penis bone) from a male raccoon. The baculum is found in male carnivores, insectivores, bats, and non-human primates.

CHAPTER 17

Opossum (Didelphis virginiana)

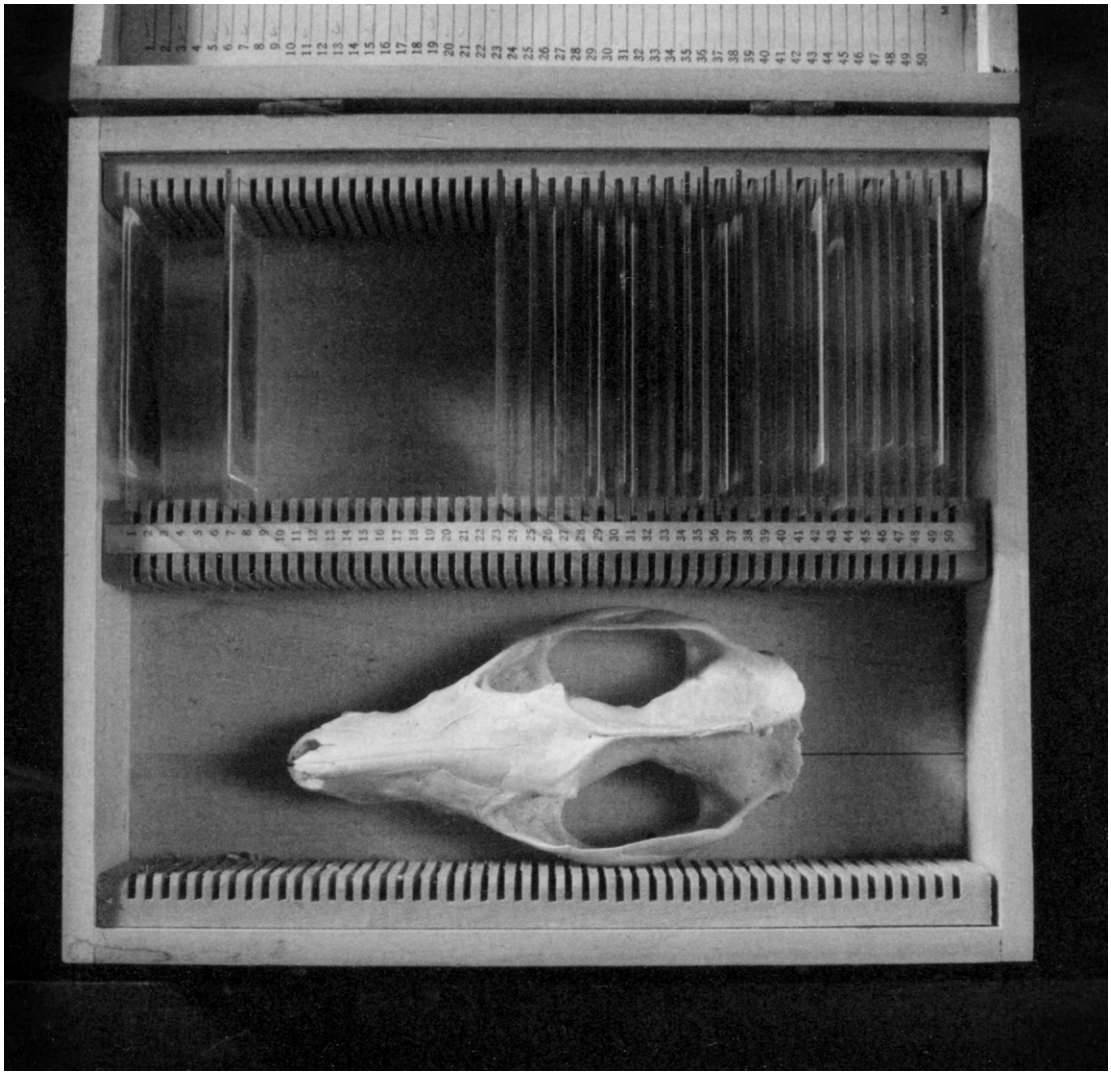

Comparative Osteology. DOI: 10.1016/B978-0-12-388437-4.00017-X

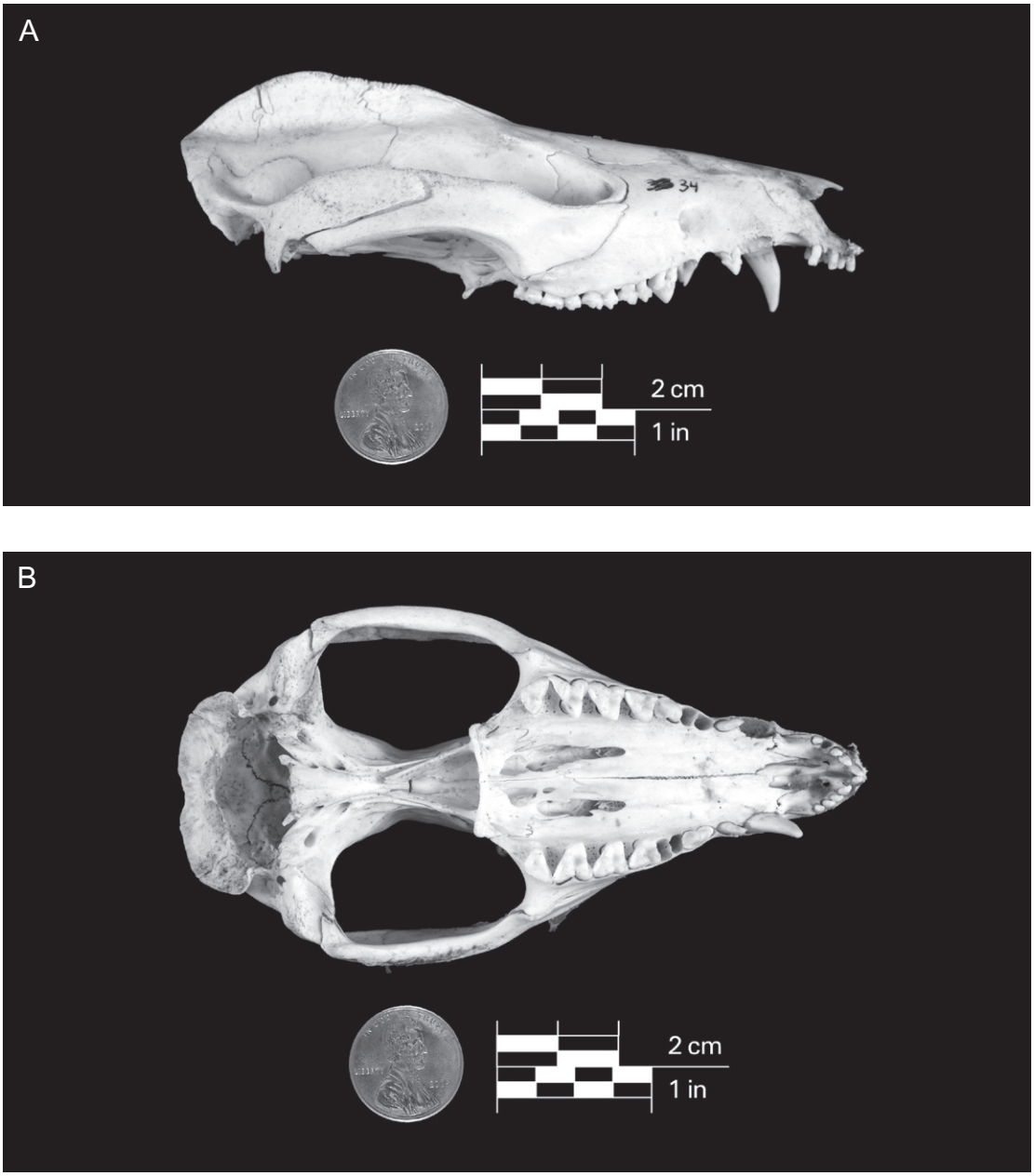

Figure 17-01: Opossum cranium (A) lateral view, right side; (B) ventral view. One canine and two premolars are missing postmortem (after death) from this specimen.

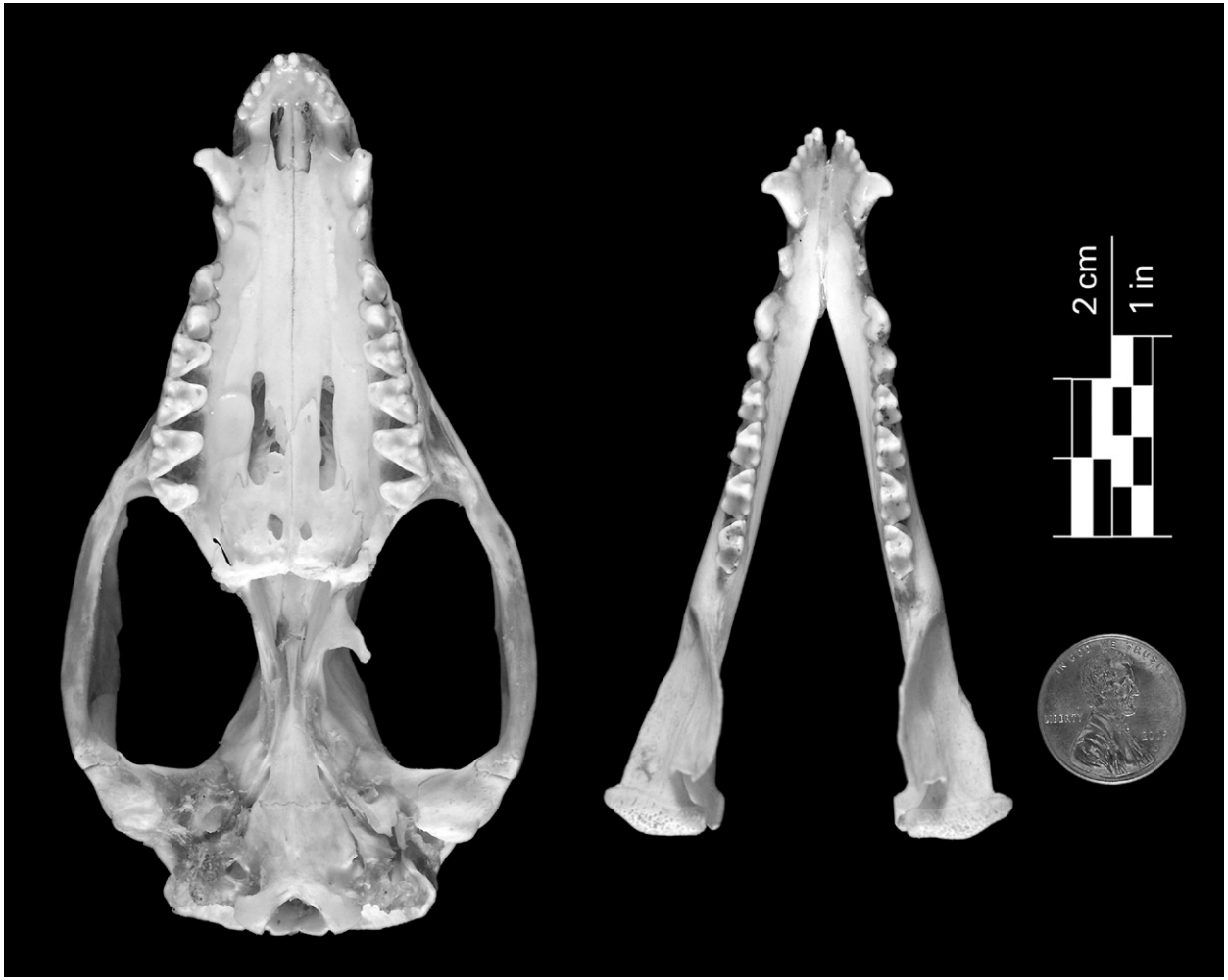

Figure 17-02: Opossum cranium (ventral view) and mandible (dorsal view). The opossum dental formula is 5/4.1/1.3/3.4/4. Note that opossums have different numbers of incisors in the upper and lower jaws. Opossums have more teeth than any other land mammal.

Figure 17-03: A newborn human left humerus (anterior view) is compared to an opossum's left humerus (cranial view). The possum humerus has a well-developed lateral epicondylar crest (arrow).

Figure 17-04: A newborn human left humerus (posterior view) is compared to an opossum's left humerus (caudal view).

Figure 17-05: An opossum's left humerus with epiphyses (cranial view) is compared to an opossum's left humerus without epiphyses (cranial view). This photo shows the size and shape differences that may be encountered within the same species.

Figure 17-06: A newborn human left radius (anterior view) is compared to an opossum's radius (cranial view).

Figure 17-07: A newborn human left radius (posterior view) is compared to an opossum's radius (caudal view).

Figure 17-08: A newborn human left ulna (anterior view) is compared to an opossum's left ulna (cranial view). Note the larger and more well-developed olecranon processes on the opossum's ulna.

Figure 17-09: A newborn human left ulna (posterior view) is compared to an adult opossum's left ulna (caudal view).

Figure 17-10: A newborn human left ulna (lateral view) is compared to an opossum's left ulna (lateral view).

Figure 17-11: A newborn human left femur (anterior view) is compared to an opossum's left femur (cranial view).

Figure 17-12: A newborn human left femur (posterior view) is compared to an opossum's left femur (caudal view).

Figure 17-13: A newborn human left tibia (anterior view) is compared to an opossum's left tibia (cranial view).

Figure 17-14: A newborn human left tibia (posterior view) is compared to an opossum's left tibia (caudal view).

Figure 17-15: A newborn human left fibula (medial view) is compared to an opossum's left fibula (medial view).

Figure 17-16: A newborn human left fibula (lateral view) is compared to an opossum's left fibula (lateral view).

Figure 17-17: A newborn human scapula (anterior view) is compared to an opossum's scapula (medial view). Both scapulae are oriented as they would be in a human skeleton. Note that the opossum's scapula is more elongated than the human scapula.

Figure 17-18: A newborn human scapula (posterior view) is compared to an opossum's scapula (lateral view). The spine of the opossum's scapula (arrow) divides the scapula into two equal halves.

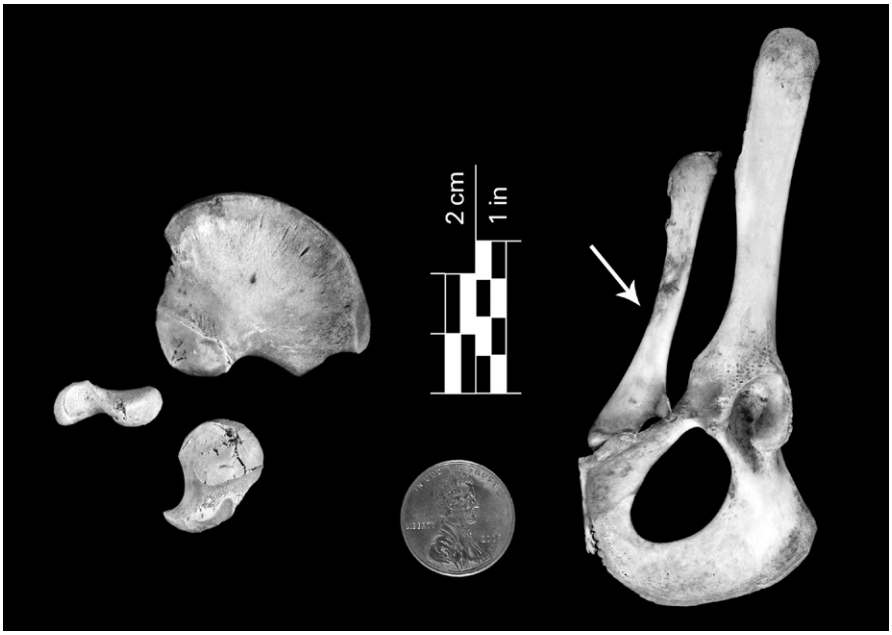

Figure 17-19: A newborn human left innominate (lateral view) is compared to an adult opossum's left innominate (lateral view). The epipubic bone can be seen on the opossum's innominate (arrow).

Figure 17-20: A newborn human left innominate (medial view) is compared to an adult opossum's left innominate (medial view). The female opossum's pelvis includes epipubic bones. These bones are found only in marsupials, and they serve to support the pouch.

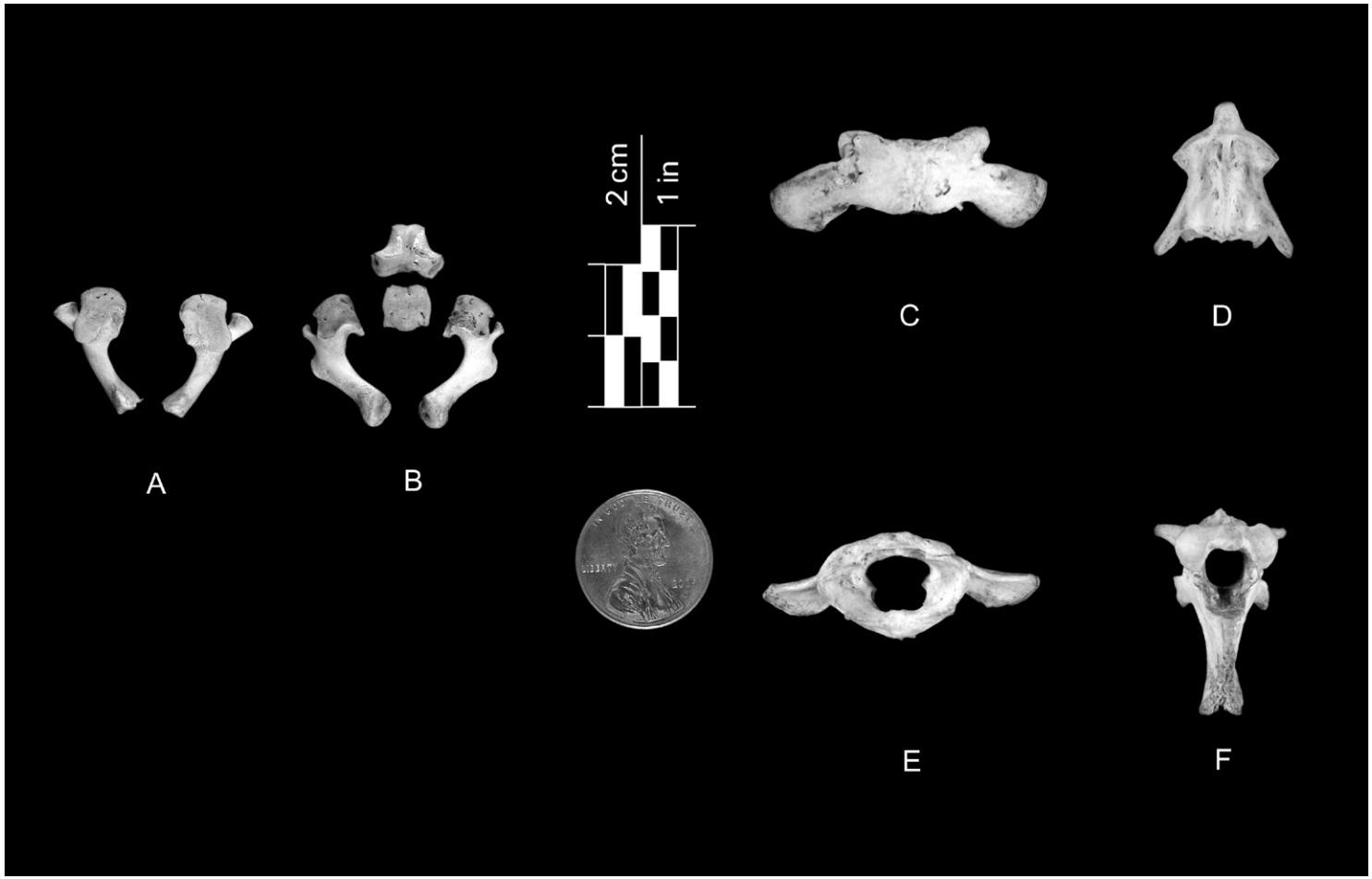

Figure 17-21: A newborn human atlas (A, superior view) and axis (B, superior view) are compared to an opossum's atlas (C, ventral view; E, cranial view) and axis (D, ventral view; F, cranial view).

This page intentionally left blank

CHAPTER 18

Cat (Felis catus)

Comparative Osteology. DOI: 10.1016/B978-0-12-388437-4.00018-1

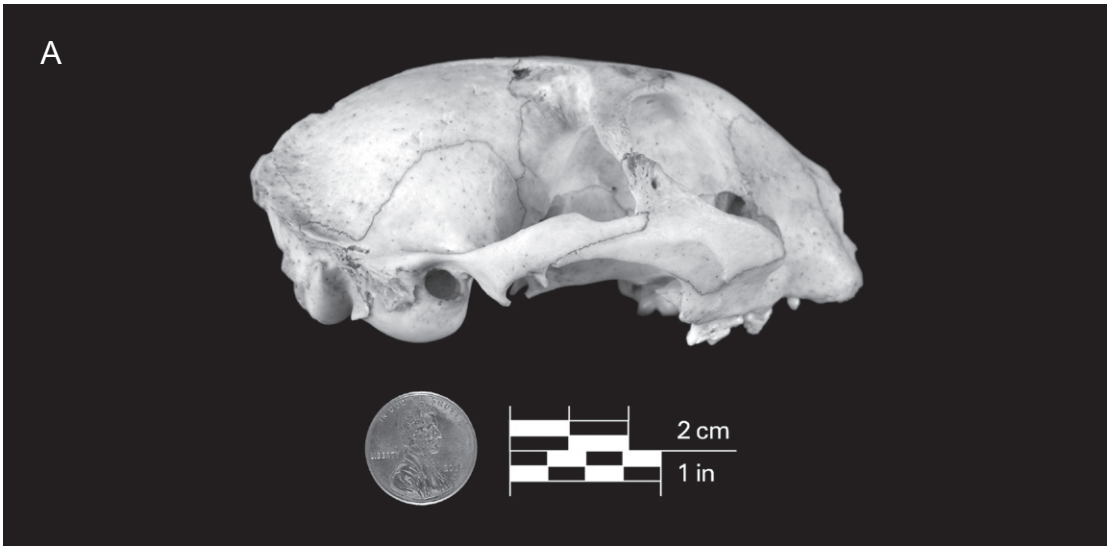

Figure 18-01: Cat cranium (A) lateral view, right side; (B) ventral view. The cat's dental formula is 3/3.1/1.3/2.1/1. The incisors and canines are missing postmortem (after death) from this specimen.

Figure 18-02: A newborn human left humerus (anterior view) is compared to a cat's left humerus (cranial view). The cat's humerus includes a supercondylar foramen on the distal portion of the shaft (arrow).

Figure 18-03: A newborn human left humerus (posterior view) is compared to a cat's left humerus (caudal view).

Figure 18-04: A newborn human left radius (anterior view) is compared to a cat's left radius (cranial view). Although the two bones are quite similar, the human radius has a longer neck (arrow).

Figure 18-05: A newborn human left radius (posterior view) is compared to a cat's left radius (caudal view).

Figure 18-06: A newborn human left ulna (anterior view) is compared to a cat's left ulna (cranial view). Note the larger and more well-developed olecranon process on the cat's ulna (arrow).

Figure 18-07: A newborn human left ulna (posterior view) is compared to a cat's left ulna (caudal view).

Figure 18-08: A newborn human left femur (anterior view) is compared to a cat's left femur (cranial view).

Figure 18-09: A newborn human left femur (posterior view) is compared to a cat's left femur (caudal view).

Figure 18-10: A newborn human left tibia (anterior view) is compared to a cat's left tibia (cranial view).

Figure 18-11: A newborn human left tibia (posterior view) is compared to a cat's left tibia (caudal view).

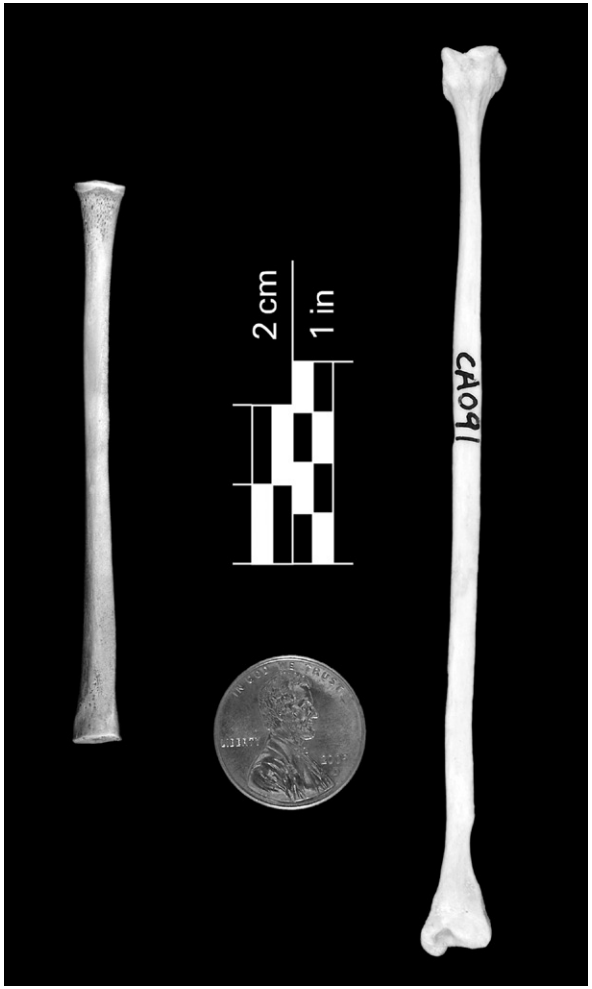

Figure 18-12: A newborn human left fibula (medial view) is compared to a cat's left fibula (medial view).

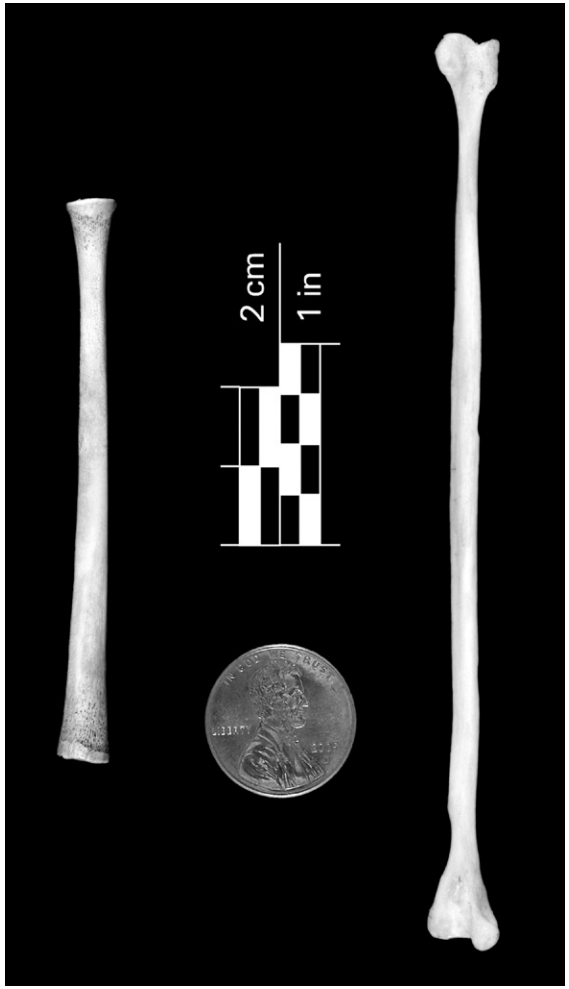

Figure 18-13: A newborn human left fibula (lateral view) is compared to a cat's left fibula (lateral view). The body of the cat's fibula is relatively slender.

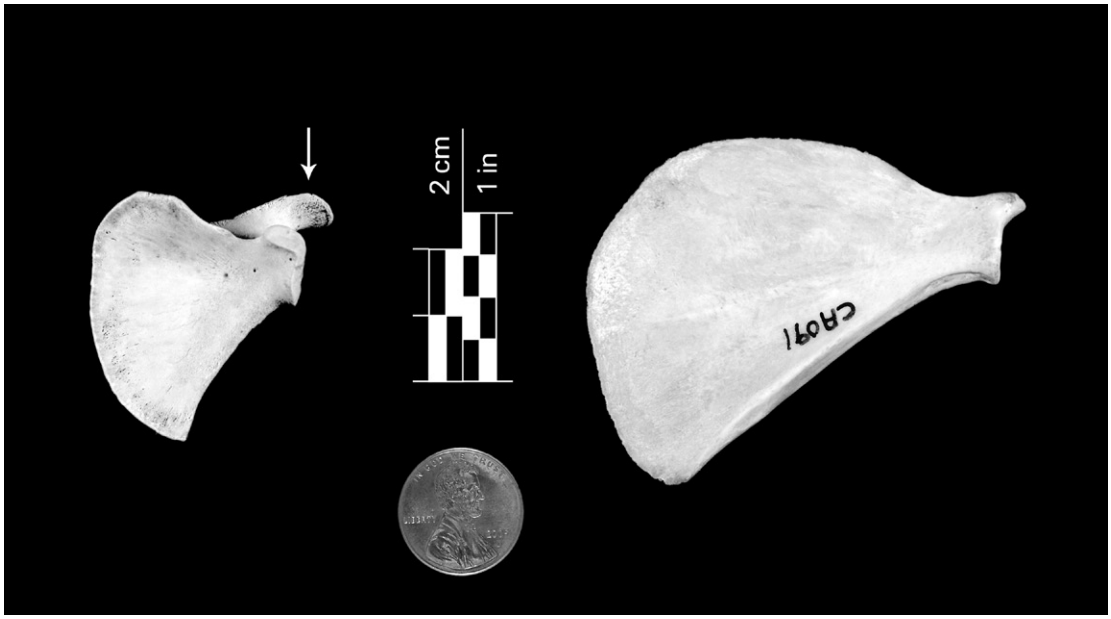

Figure 18-14: A newborn human left scapula (anterior view) is compared to a cat's left scapula (medial view). Both are oriented as they would be in a human. Note the presence of the prominent acromion process on the human scapula (arrow) that is visible from the anterior view.

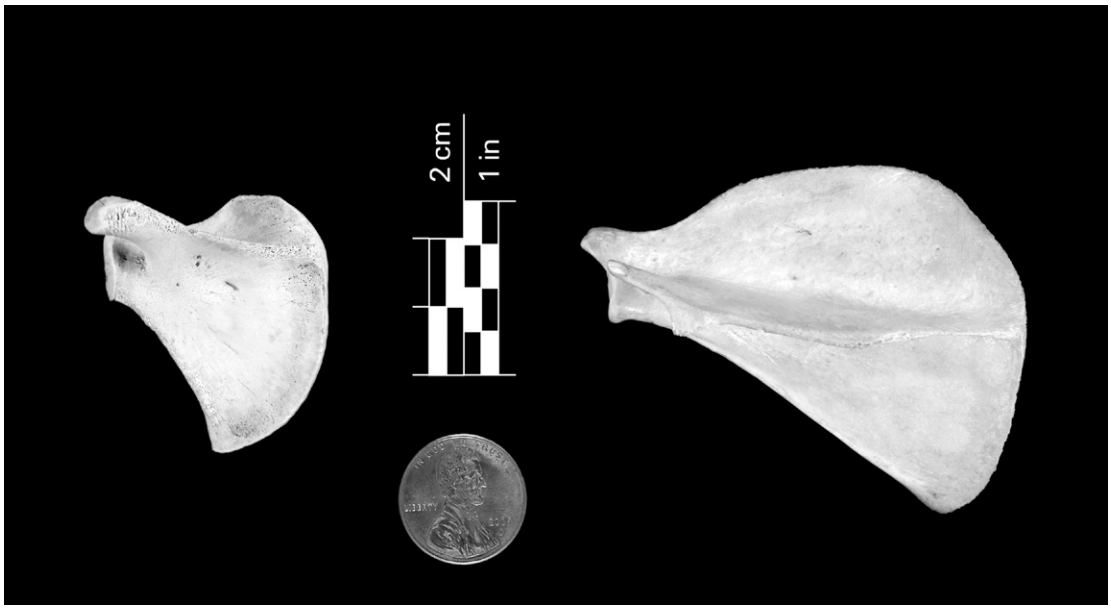

Figure 18-15: A newborn human left scapula (posterior view) is compared to a cat's left scapula (lateral view). The cat's scapula is longer than the human scapula.

Figure 18-16: A newborn human left innominate (A, lateral view) is compared to a cat's left innominate (B, lateral view) and a complete cat's pelvis (C, ventral view). Note that the blade of the ilium is much narrower in the cat than in the human.

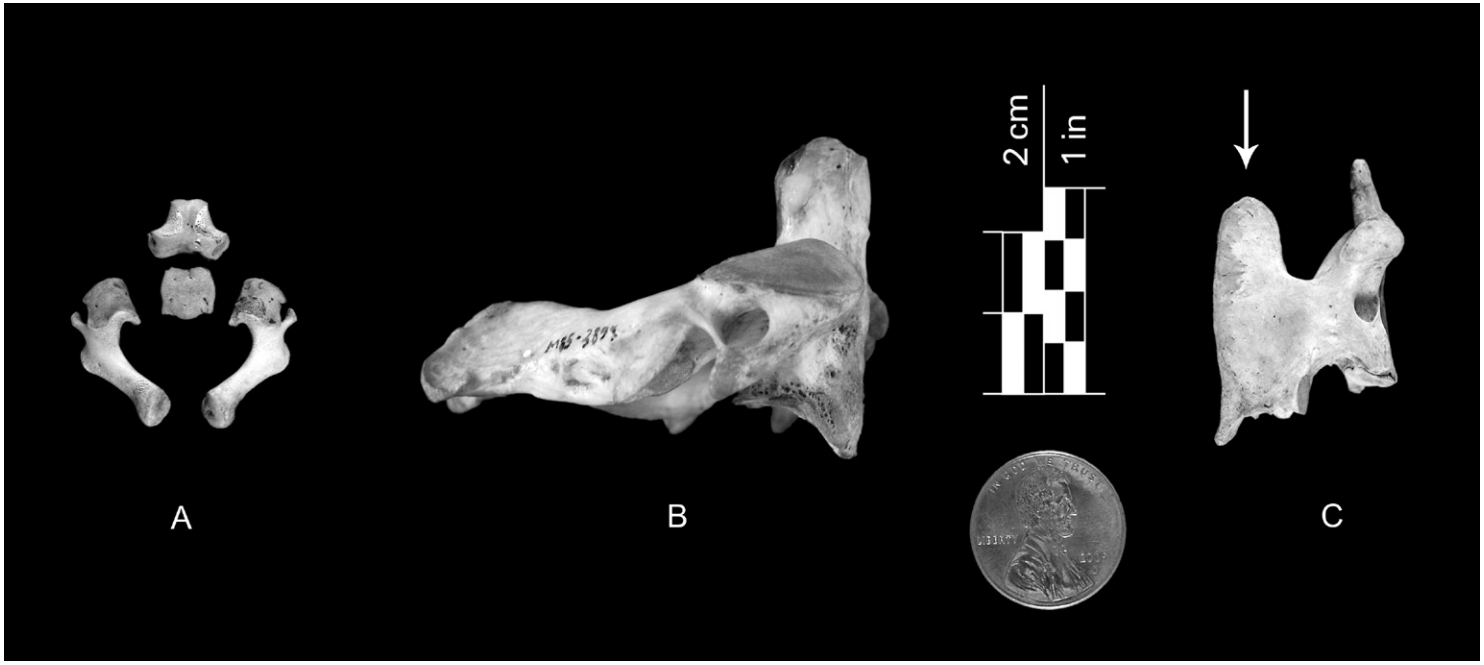

Figure 18-17: A newborn human axis (A, superior view) and an adult human axis (B, lateral view) are compared to a cat's axis (C, lateral view). Note the presence of the large spinous process on the cat's axis (arrow).

This page intentionally left blank

CHAPTER 19

Rabbit (Oryctolagus cunniculus *and* Sylvilagus carolinensis)

Comparative Osteology. DOI: 10.1016/B978-0-12-388437-4.00019-3

Figure 19-01: Rabbit cranium (A) lateral view, right side. All photographs in this chapter are domestic rabbits (*Oryctolagus cunniculus*) unless otherwise indicated. (B) ventral view. Rabbits are lagomorphs and have distinctive dental patterns. The rabbit dental formula is 2/1.0/0.3/2.3/3. The rabbit upper second incisor is a small peg tooth that is located directly behind the upper first incisor. The rabbit's teeth are open-rooted and continue to grow throughout the animal's lifetime.

Figure 19-02: A newborn human left humerus (anterior view) is compared to a rabbit's left humerus (cranial view). The rabbit's humerus sometimes has a supratrochlear foramen (arrow).

Figure 19-03: A newborn human left humerus (posterior view) is compared a rabbit's left humerus (caudal view).

Figure 19-04: A newborn human left radius and ulna (A, anterior views) are compared to an *Oryctolagus* left ulna and radius (B, cranial view, separate) and a *Sylvilagus* left radius and ulna (C, cranial view, fused). The human radius includes a distinctive head and neck, while the olecranon process is much larger on the rabbit's ulna.

Figure 19-05: A newborn human left radius and ulna (A, posterior views) are compared to an *Oryctolagus* left radius and ulna (B, caudal views, separate) and a *Sylvilagus* left radius and ulna (C, caudal view, fused). In the rabbit, the ulna crosses behind the radius and terminates on the lateral side of the carpus.

Figure 19-06: A newborn human left femur (anterior view) is compared to a rabbit's left femur (cranial view). Note that the rabbit femur has a small third trochanter (arrow), which is not seen in the human femur.

Figure 19-07: A newborn human left femur (posterior view) is compared to a rabbit's left femur (caudal view).

Figure 19-08: A newborn human left tibia and fibula (anterior views) are compared to a rabbit's left tibia and fibula (cranial view). The rabbit's fibula is fused to the shaft of the tibia.

Figure 19-09: A newborn human left tibia and fibula (posterior views) are compared to a rabbit's left tibia and fibula (caudal view).

Figure 19-10: A newborn human left scapula (anterior view) is compared to a rabbit's left scapula (medial view). Note the elongated shape of the rabbit's scapula.

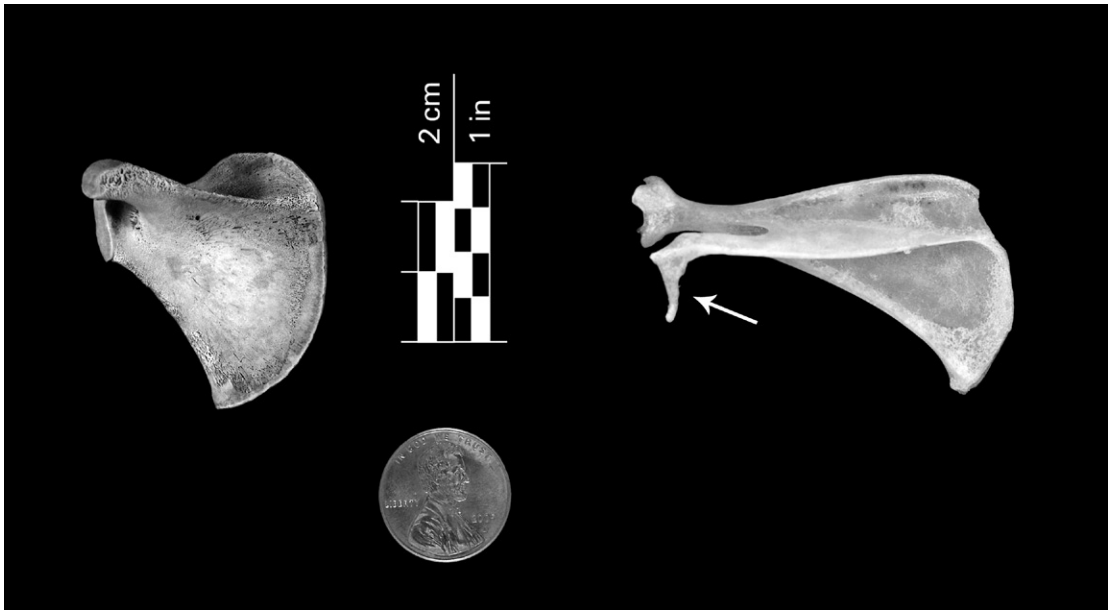

Figure 19-11: A newborn human left scapula (posterior view) is compared to a rabbit's left scapula (lateral view). The rabbit's scapula includes a metacromium that is not found on the human scapula. It is the small process that can be seen near the base of the spine (arrow).

Figure 19-12: A newborn human left innominate (lateral view) is compared to a rabbit's left innominate (lateral view).

Figure 19-13: A newborn human left innominate (medial view) is compared to a rabbit's left innominate (dorsal view).

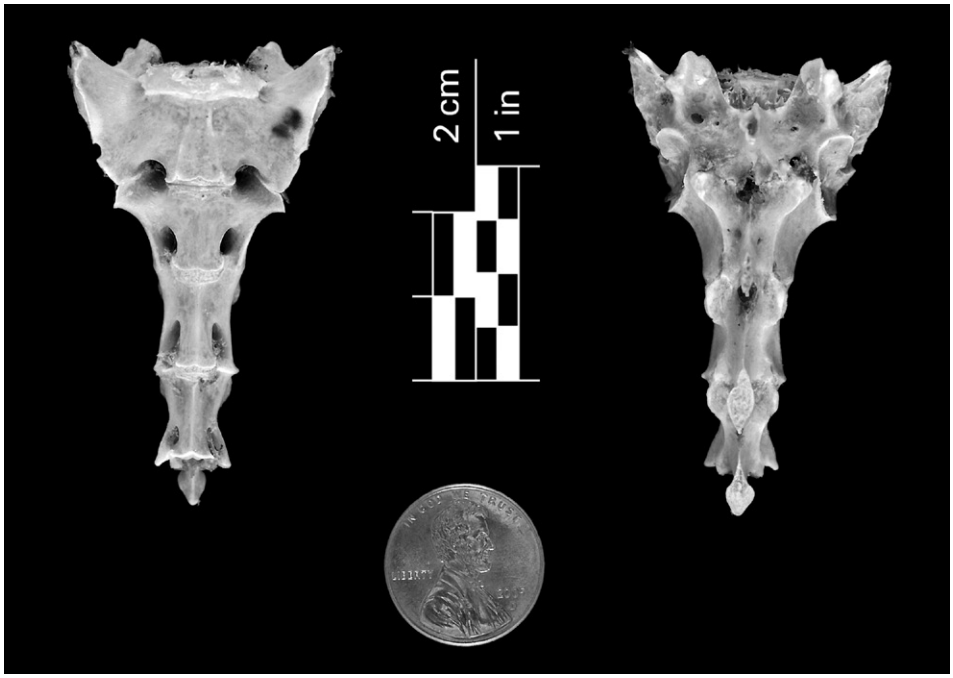

Figure 19-14: Rabbit sacrum (ventral and dorsal views).

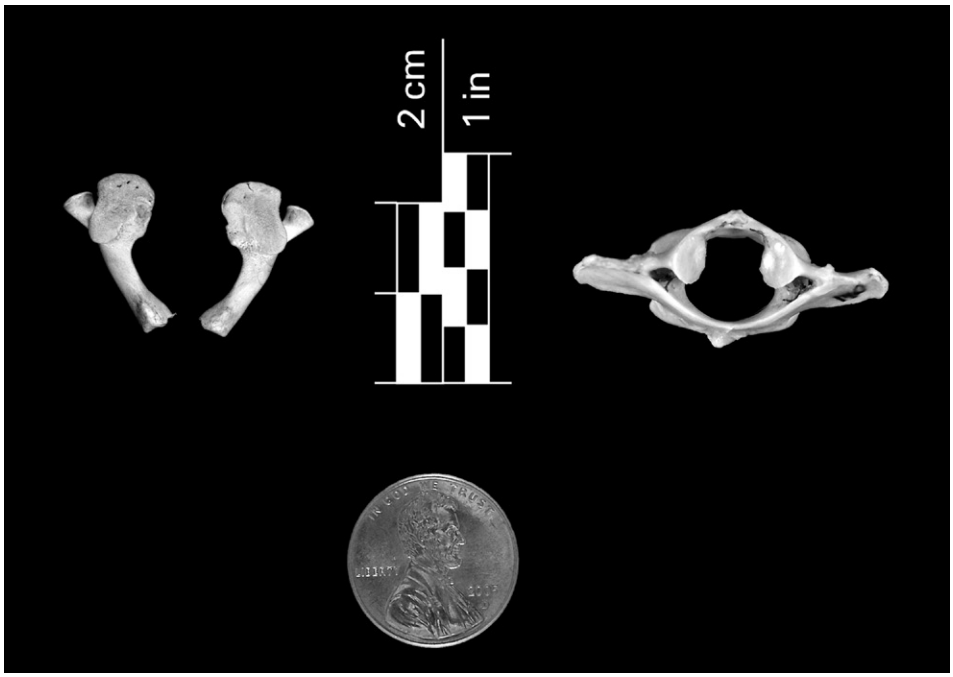

Figure 19-15: A newborn human atlas (superior view) is compared to a rabbit's atlas (cranial view).

This page intentionally left blank

CHAPTER 20

Turkey (Meleagris gallopavo)

Comparative Osteology. DOI: 10.1016/B978-0-12-388437-4.00020-X

Figure 20-01: A newborn human left humerus (anterior view) is compared to a turkey's left humerus (cranial view). Note the pneumatic fossa near the proximal end of the turkey's humerus (arrow). The pneumatic fossa allows for the invasion of the clavicular air sac, which pneumatizes the interior of the humerus. This lightens the skeleton, which is an adaptation for flight.

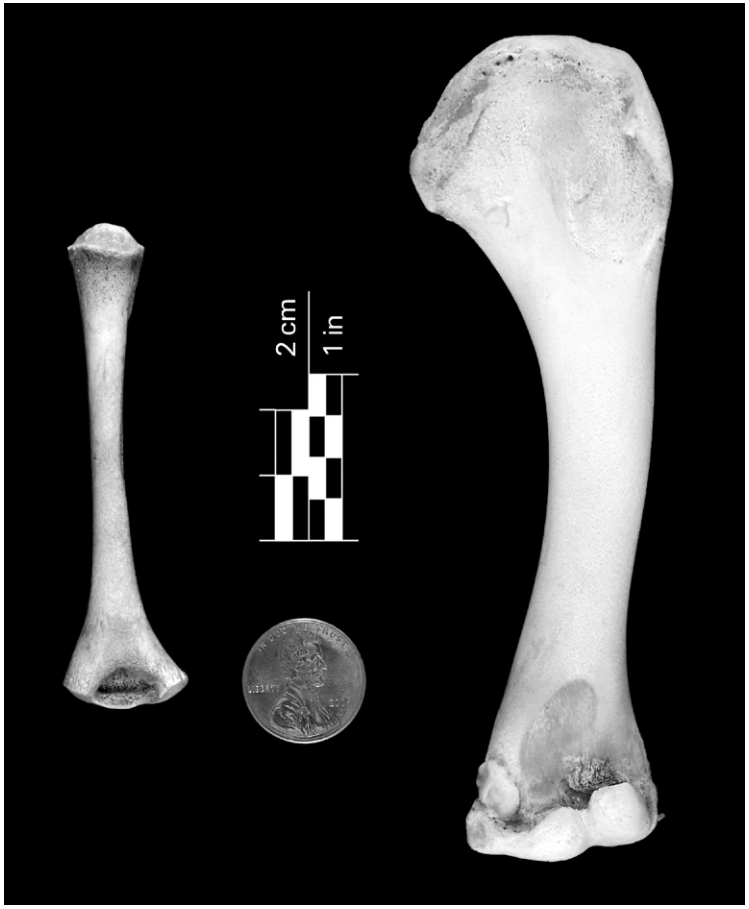

Figure 20-02: A newborn human left humerus (posterior view) is compared to a turkey's left humerus (caudal view).

Figure 20-03: A newborn human left radius (anterior view) is compared to a turkey's left radius (cranial view).

Figure 20-04: A newborn human left radius (posterior view) is compared to a turkey's left radius (caudal view).

Figure 20-05: A newborn human left ulna (anterior view) is compared to a turkey's left ulna (cranial view)

Figure 20-06: A newborn human left ulna (lateral view) is compared to a turkey's left ulna (lateral view).

Figure 20-07: A newborn human left femur (anterior view) is compared to a turkey's left femur (cranial view).

Figure 20-08: A newborn human left femur (posterior view) is compared to a turkey's left femur (caudal view).

Figure 20-09: A newborn human left tibia (anterior view) is compared to a turkey's left tibiotarsus (cranial view).

Figure 20-10: A newborn human left tibia (posterior view) is compared to a turkey's left tibiotarsus (caudal view).

Figure 20-11: A newborn human left fibula (medial view) is compared to a turkey's left fibula (medial view).

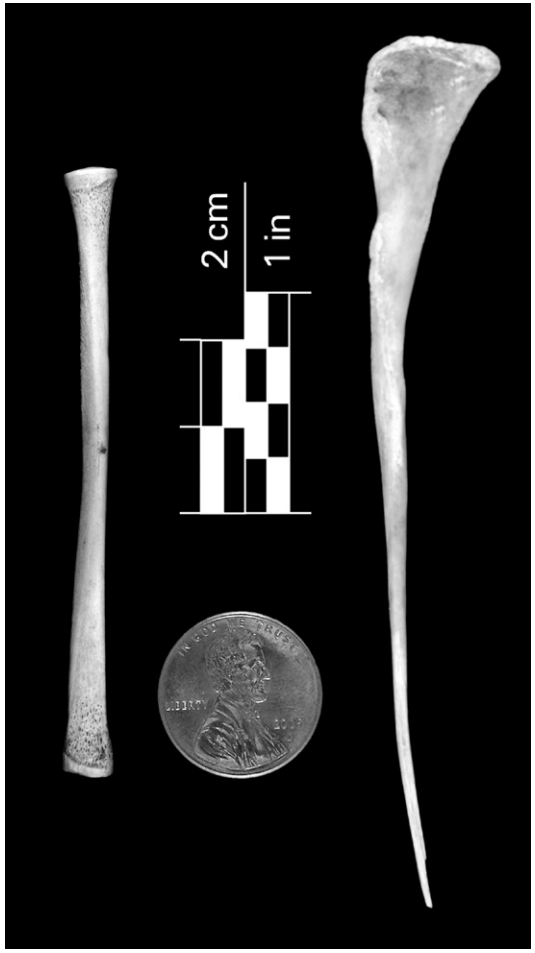

Figure 20-12: A newborn human left fibula (lateral view) is compared to a turkey's left fibula (lateral view).

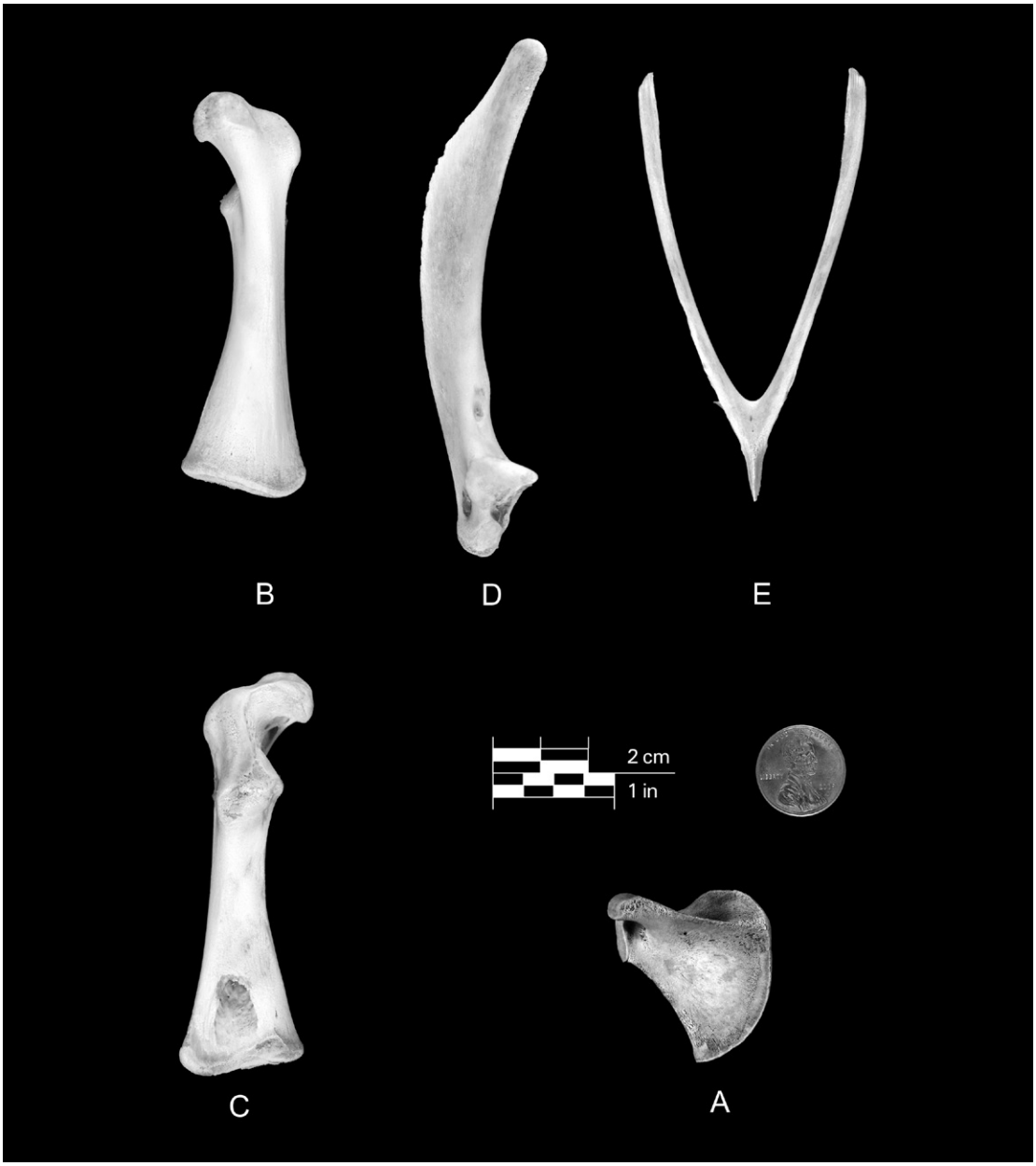

Figure 20-13: A newborn human left scapula (A, posterior view) is compared to the pectoral girdle of the turkey. The bird pectoral girdle includes three elements: the coracoid, the scapula, and the furcula (wishbone). A turkey's left coracoid (B, ventral view; C dorsal view), a turkey's scapula (D, costal view), and a turkey's furcula (E) are pictured.

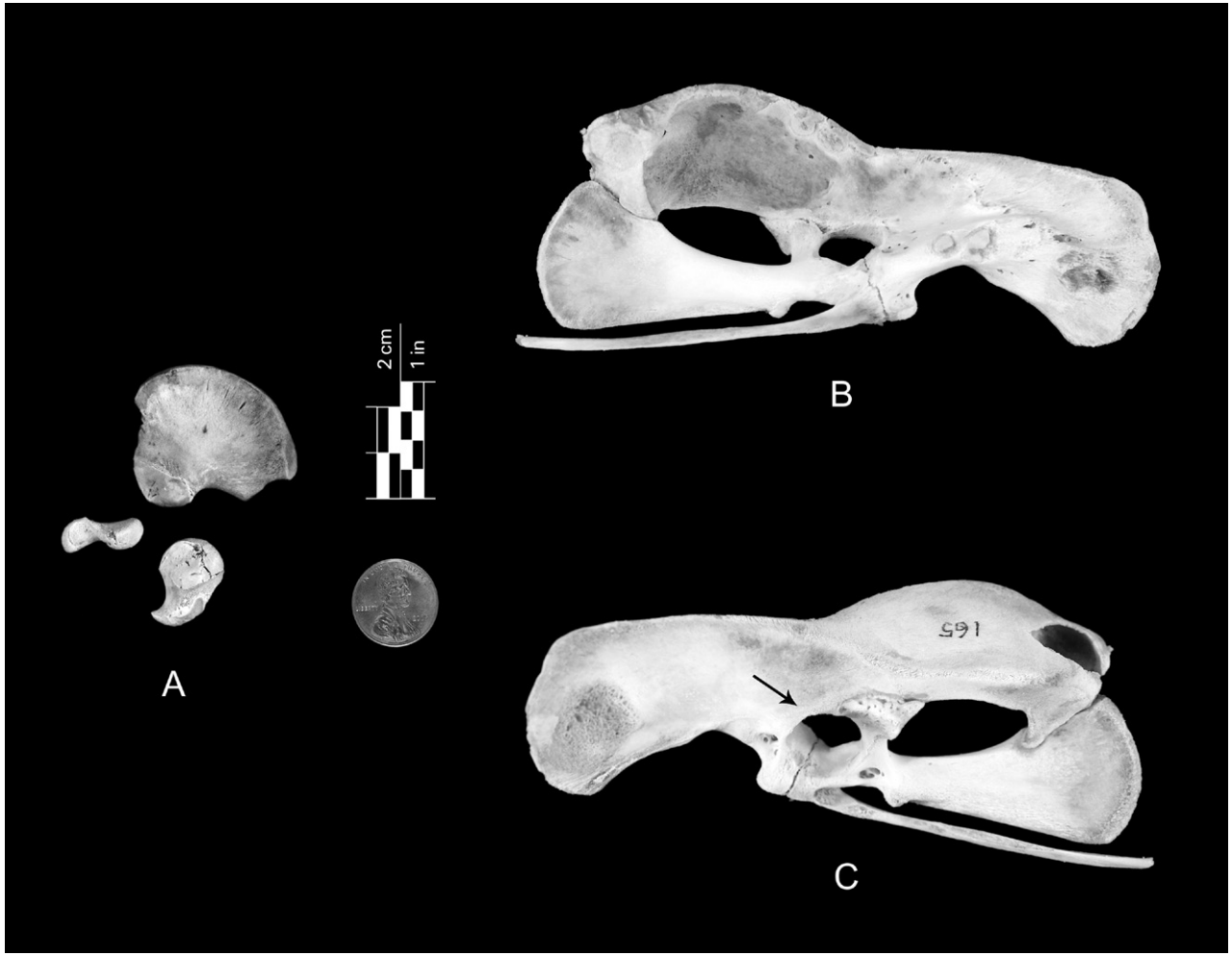

Figure 20-14: A newborn human left innominate (A, lateral view) is compared to a turkey's left pelvis (B, medial view; C, lateral view). Note that the turkey's acetabulum is perforated (arrow).

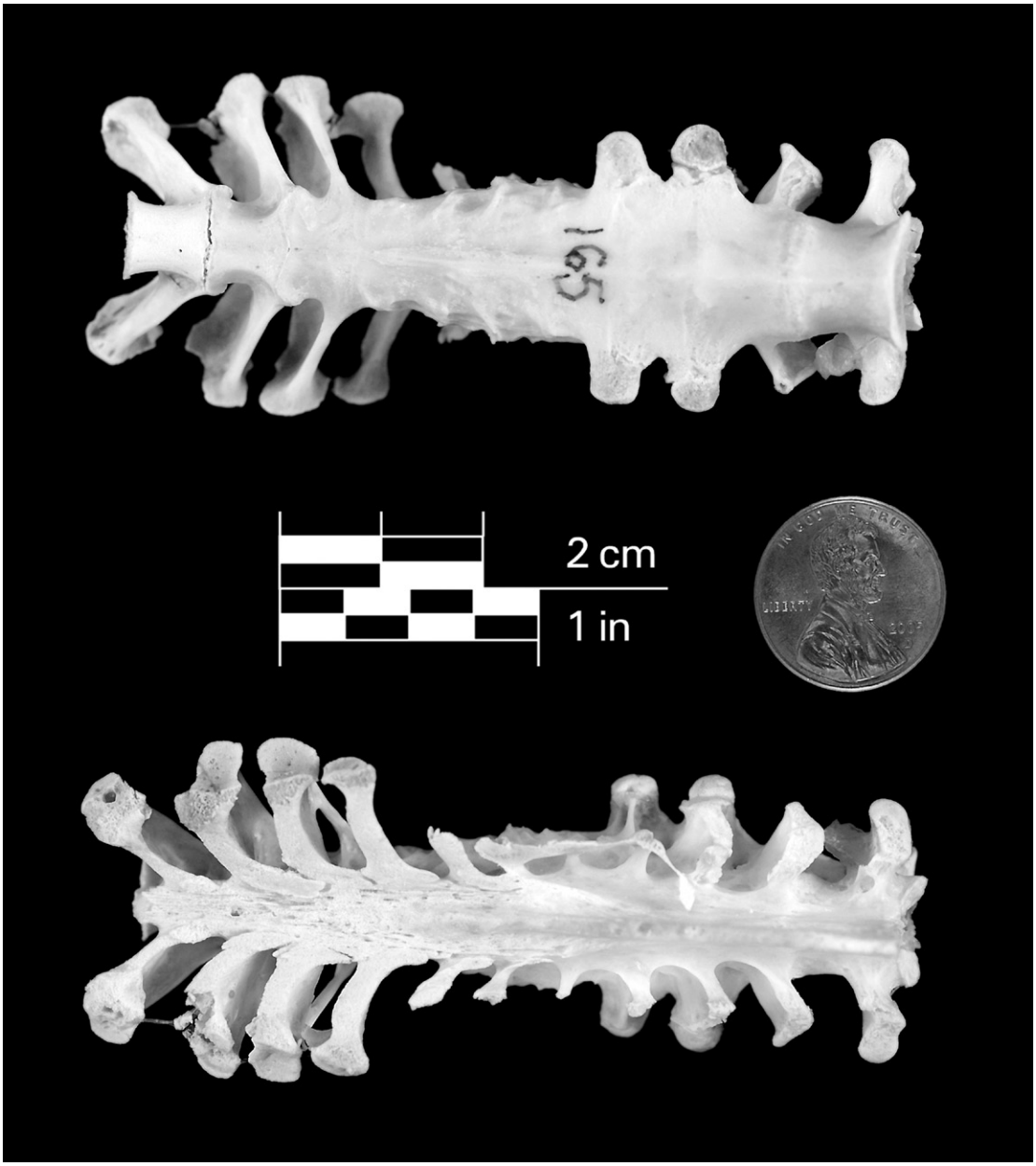

Figure 20-15: Turkey synsacrum (ventral and dorsal views).

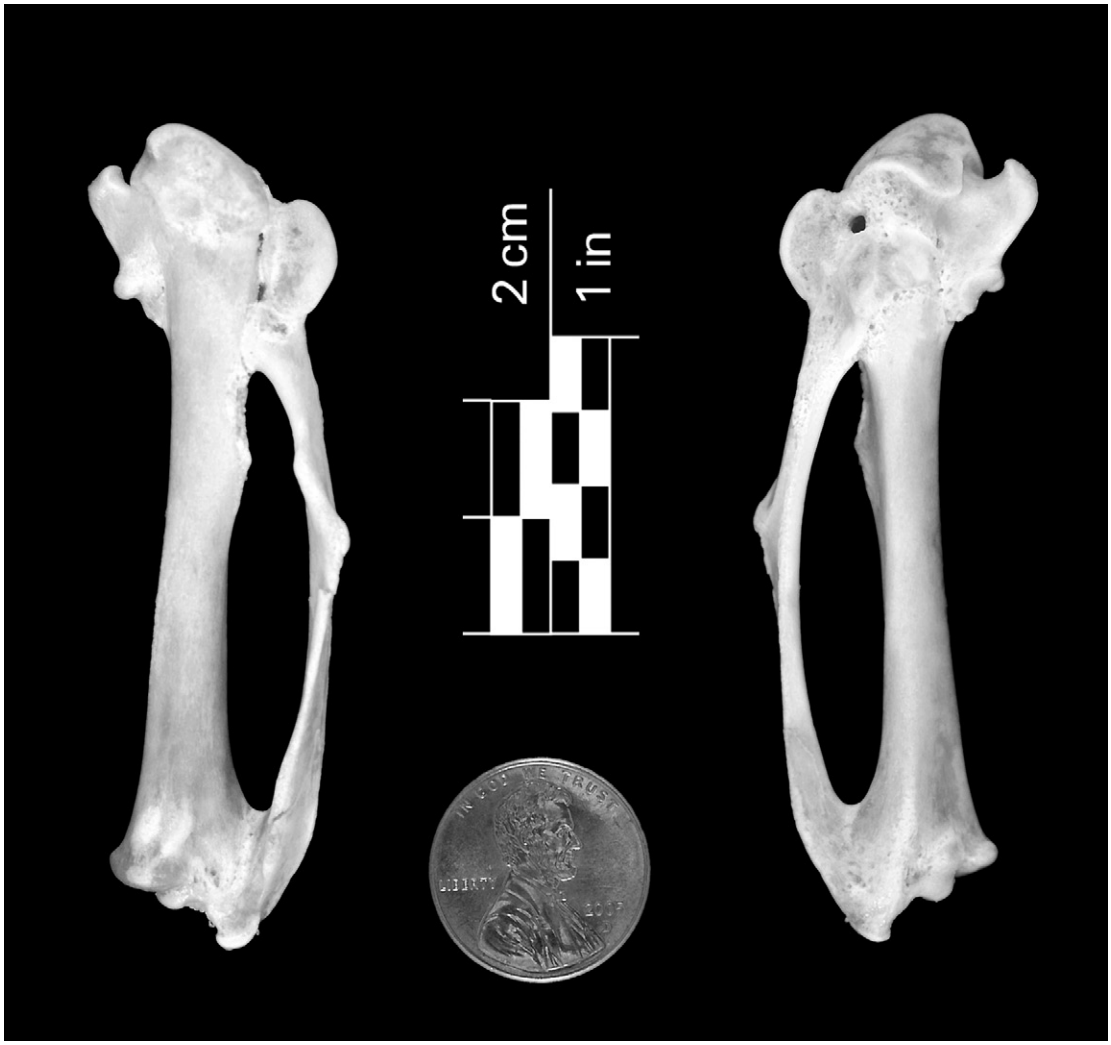

Figure 20-16: Turkey left carpometacarpus (dorsal and ventral views). The bone is made up of three fused elements: the second, third, and fourth metacarpals.

This page intentionally left blank

CHAPTER 21

Duck (Anas platyrhynchos)

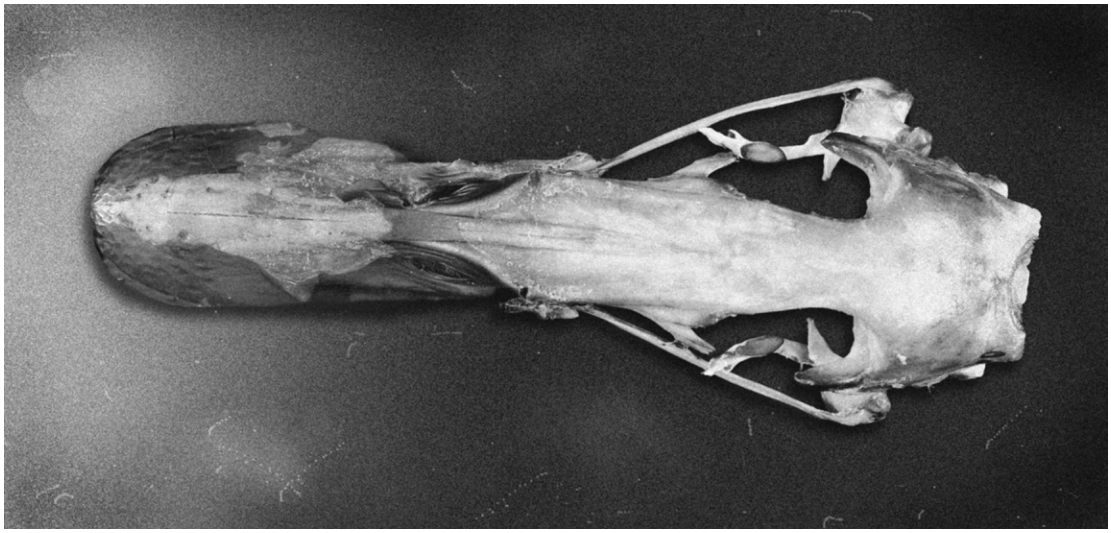

Comparative Osteology. DOI: 10.1016/B978-0-12-388437-4.00021-1

Figure 21-01: Duck cranium (A) lateral view, right side. (B) ventral view.

Figure 21-02: A newborn human left humerus (anterior view) is compared to a duck's left humerus (cranial view). Note the pneumatic fossa near the proximal end of the duck's humerus (arrow). This is an adaptation for flight.

Figure 21-03: A newborn human left humerus (posterior view) is compared to a duck's left humerus (caudal view).

Figure 21-04: A newborn human left radius (anterior view) is compared to a duck's left radius (cranial view).

Figure 21-05: A newborn human left radius (posterior view) is compared to a duck's left radius (caudal view).

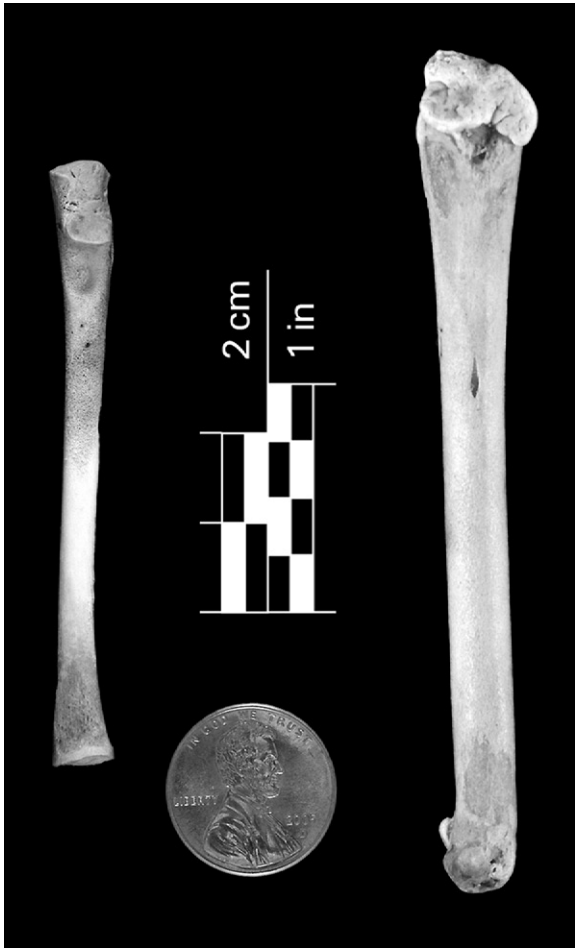

Figure 21-06: A newborn human left ulna (anterior view) is compared with a duck's left ulna (cranial view).

Figure 21-07: A newborn human left ulna (lateral view) is compared to a duck's left ulna (caudal view).

Figure 21-08: A newborn human left femur (anterior view) is compared to a duck's left femur (cranial view).

Figure 21-09: A newborn human left femur (posterior view) is compared to a duck's left femur (caudal view).

Figure 21-10: A newborn human left tibia (anterior view) is compared to a duck's left tibiotarsus (cranial view).

Figure 21-11: A newborn human left tibia (posterior view) is compared to a duck's left tibiotarsus (caudal view).

Figure 21-12: A newborn human left fibula (medial view) is compared to a duck's left fibula (medial view).

Figure 21-13: A newborn human left fibula (lateral view) is compared to a duck's left fibula (lateral view).

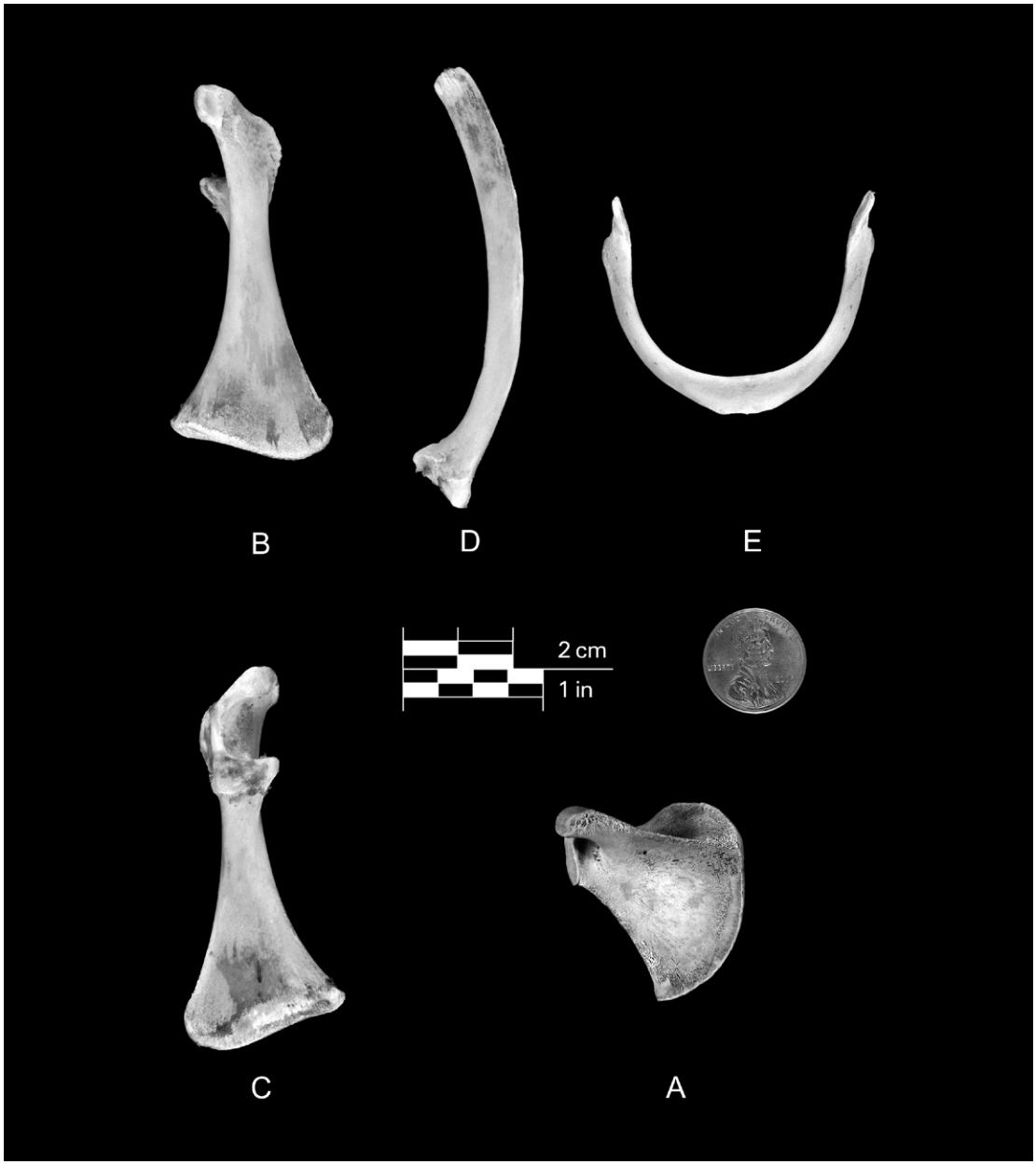

Figure 21-14: A newborn human left scapula (A, posterior view) is compared to the pectoral girdle of a duck. The bird pectoral girdle includes three elements: the coracoid, the scapula, and the furcula (wishbone). A duck's left coracoid (B, ventral view; C, dorsal view), a duck's scapula (C, costal view), and a duck's furcula (E) are pictured.

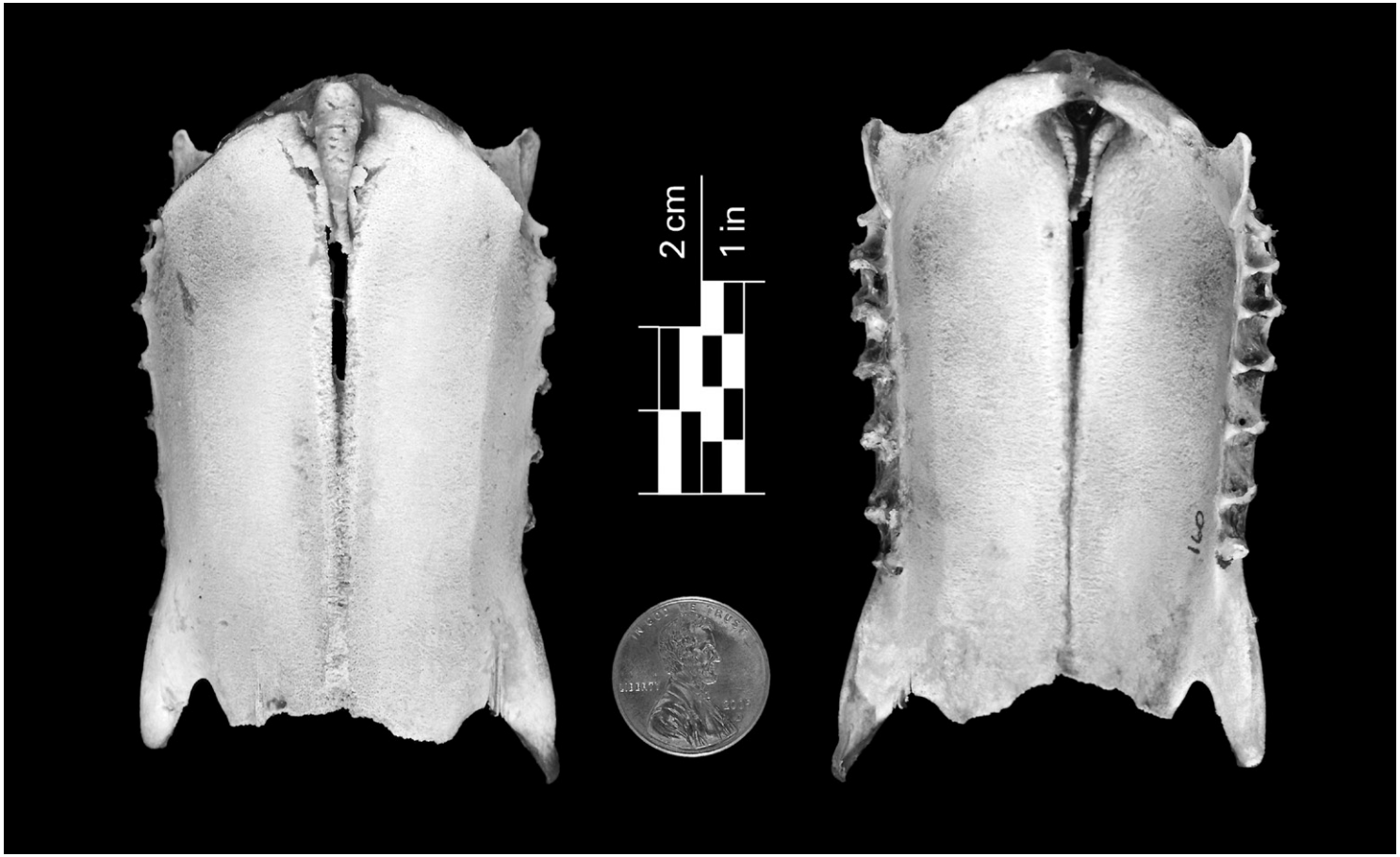

Figure 21-15: Ventral and dorsal views of the duck's sternum. The keel of the sternum is enlarged and serves as an area of origin for the major muscles of flight.

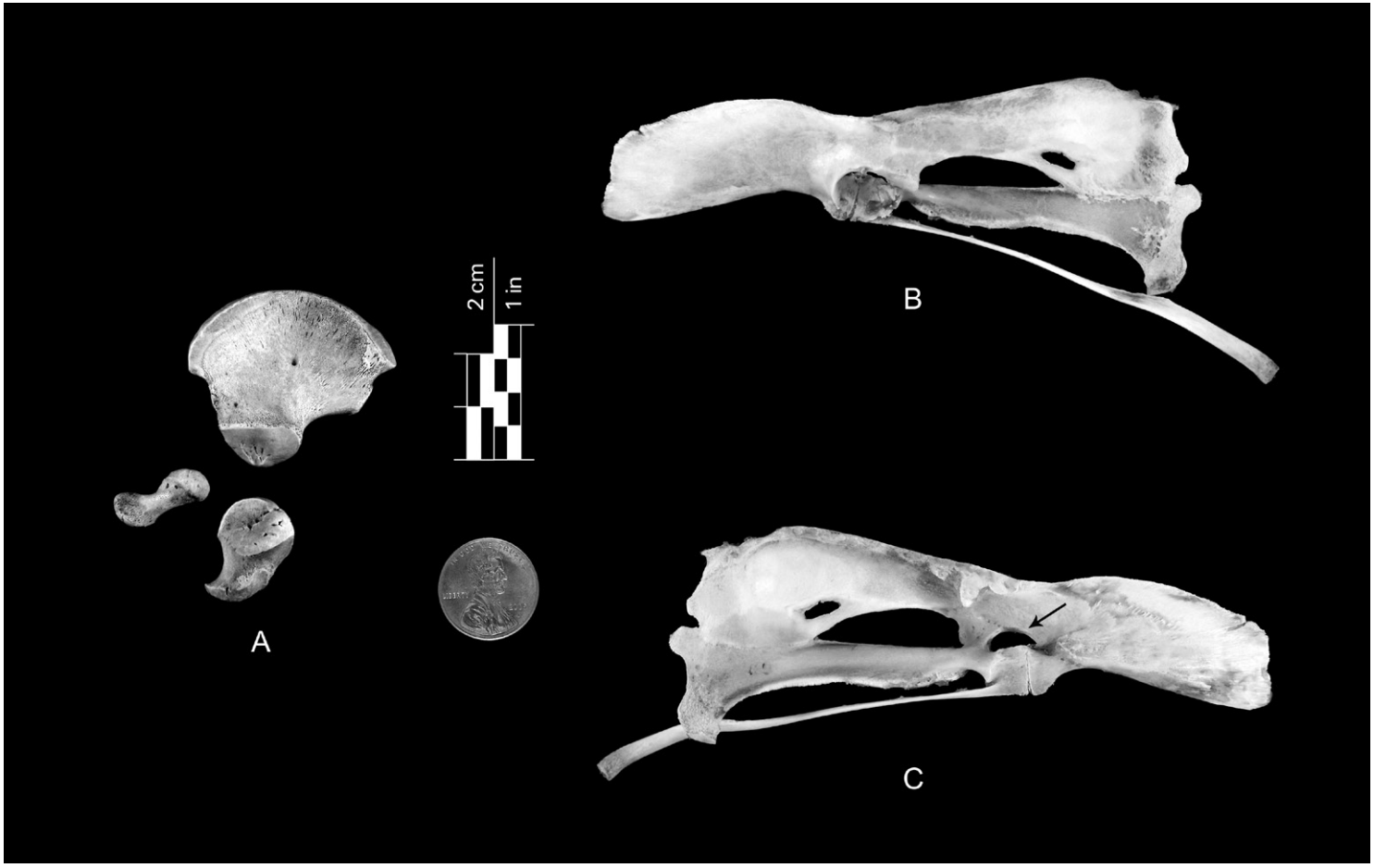

Figure 21-16: A newborn human left innominate (A, lateral view) is compared to a duck's left pelvis (B, lateral view; C, medial view). Note that the duck's acetabulum is perforated (arrow).

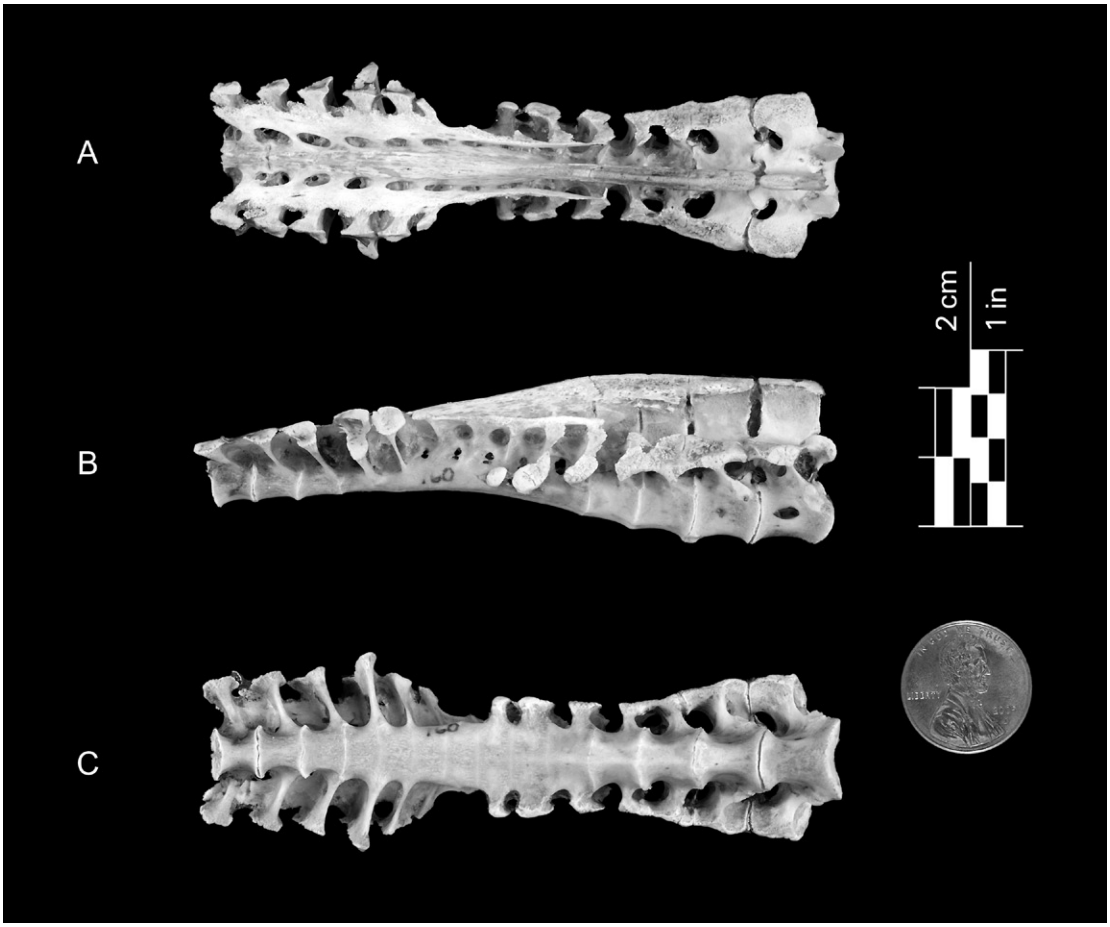

Figure 21-17: Dorsal (A), lateral (B), and ventral (C) views of the duck's synsacrum. In birds, the synsacrum is a made up of the fused lumbar and sacral vertebrae.

Figure 21-18: The duck's left carpometacarpus (dorsal and ventral views).

Figure 21-19: The duck's left tarsometatarsus (dorsal and plantar views). This bone is composed of the fused distal tarsal bones along with three metatarsals.

This page intentionally left blank

CHAPTER 22

Chicken (Gallus gallus)

Comparative Osteology. DOI: 10.1016/B978-0-12-388437-4.00022-3

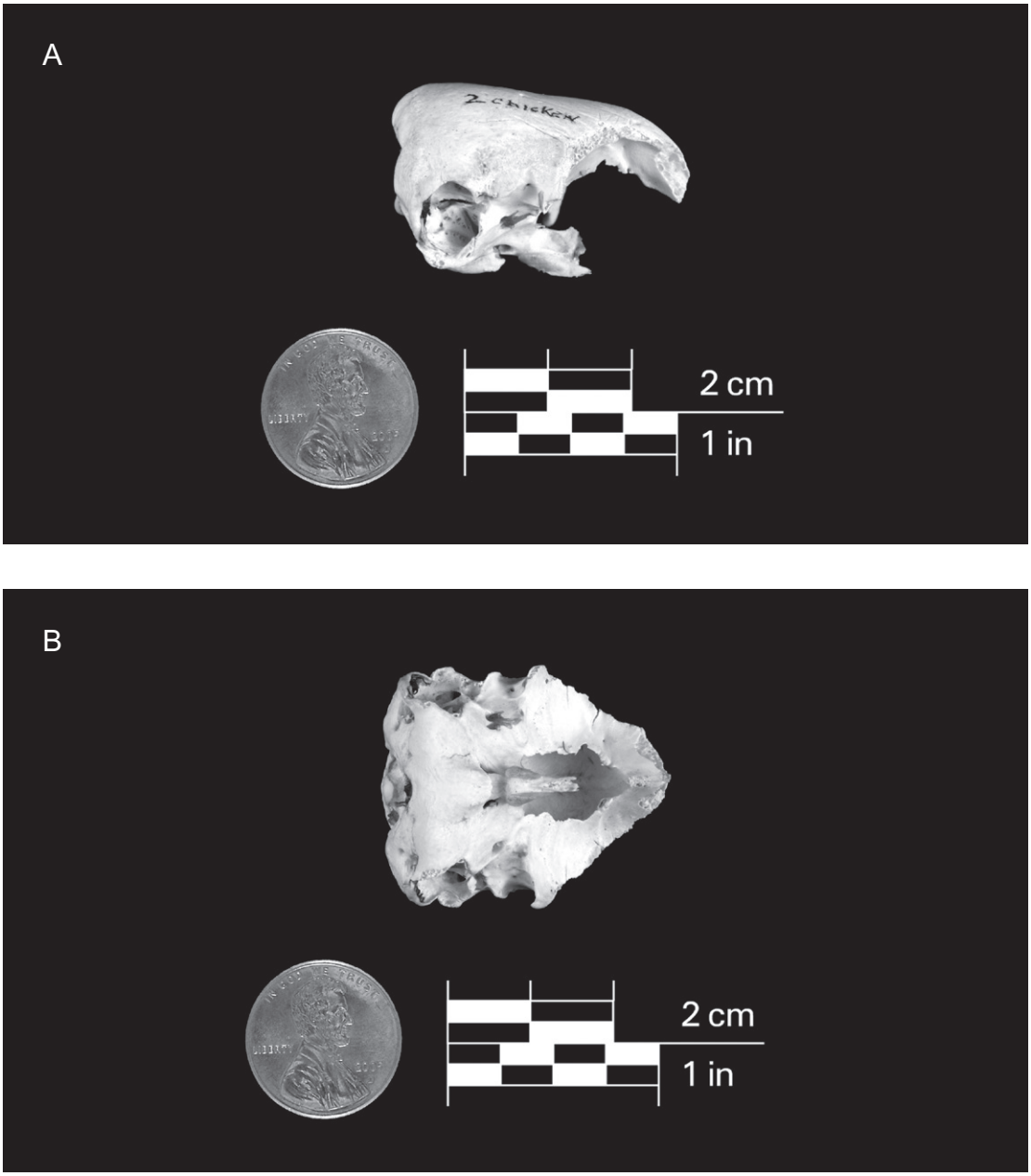

Figure 22-01: Chicken skull (no beak) (A) lateral view, right side; (B) ventral view.

Figure 22-02: A newborn human left humerus (A, anterior view) is compared to two chicken left humeri (B and C, cranial views). The smaller element is from a younger chicken.

Figure 22-03: A newborn human left humerus (A, posterior view) is compared to two chicken left humeri (B and C, caudal views).

Figure 22-04: A newborn human left radius (A, anterior view) is compared to two chicken left radii (B and C, cranial views). The smaller element is from a younger chicken.

Figure 22-05: A newborn human left radius (A, posterior view) is compared to two chicken left radii (B and C, caudal views).

Figure 22-06: A newborn human left ulna (A, lateral view) is compared to two chicken left ulnae (B and C, lateral views). The smaller element is from a younger chicken.

Figure 22-07: A newborn human left femur (A, anterior view) is compared to two chicken left femora (B and C, cranial views). The smaller element is from a younger chicken.

Figure 22-08: A newborn human left femur (A, posterior view) is compared to two chicken femora (B and C, caudal views).

Figure 22-09: A newborn human left tibia (A, anterior view) is compared to two chicken left tibiotarsi (B and C, cranial views). The smaller element is from a younger chicken.

Figure 22-10: A newborn human left tibia (A, posterior view) is compared to two chicken left tibiotarsi (B and C, caudal views).

Figure 22-11: A newborn human left fibula (A, medial view) is compared to two chicken left fibulae (B and C, medial view). The smaller element is from a younger chicken.

Figure 22-12: A newborn human left fibula (A, lateral view) is compared to two chicken left fibulae (B and C, lateral view).

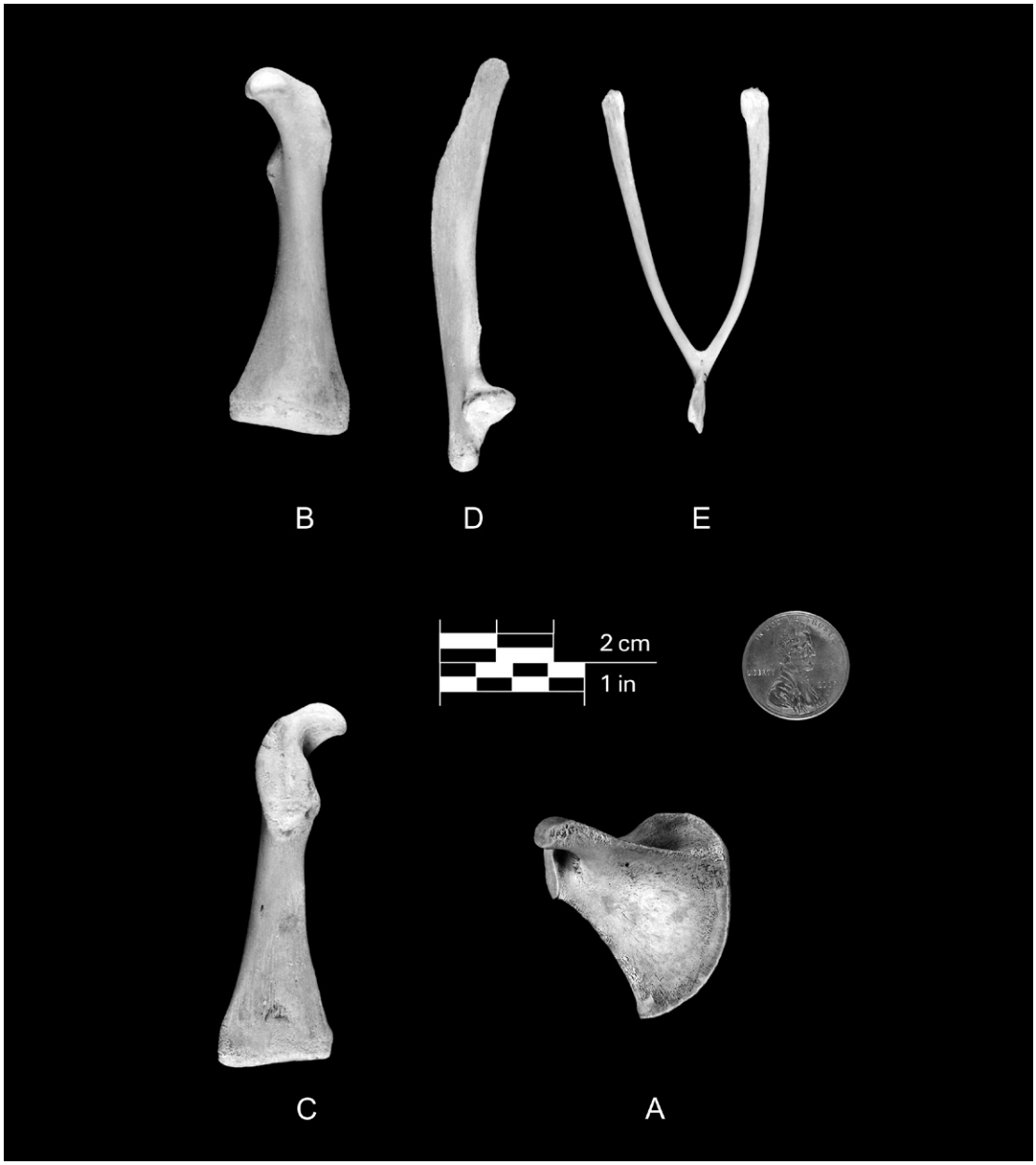

Figure 22-13: A newborn human scapula (A, posterior view) is compared to the pectoral girdle of a chicken. The bird pectoral girdle includes three elements: the coracoid, the scapula, and the furcula (wishbone). A chicken's left coracoid (B, ventral view; C, dorsal view), a chicken's scapula (D, costal view), and a chicken's furcula (E) are pictured.

Figure 22-14: Chicken sternum (ventral and lateral views). The keel on the sternum forms the origin for the muscles involved in flight.

Figure 22-15: A newborn human left innominate (lateral view) is compared to a chicken's left pelvis (lateral and medial views). Note that the chicken's acetabulum is perforated (arrow).

Figure 22-16: A chicken's left carpometacarpus (dorsal and ventral views).

Figure 22-17: A chicken's left tarsometatarsus (dorsal and plantar views). This bone is composed of the fused distal tarsal bones along with three metatarsals. Male chickens have a bony spur core on the midshaft of the tarsometatarsus. The spur occurs only rarely in females.

CHAPTER 23

Miscellaneous

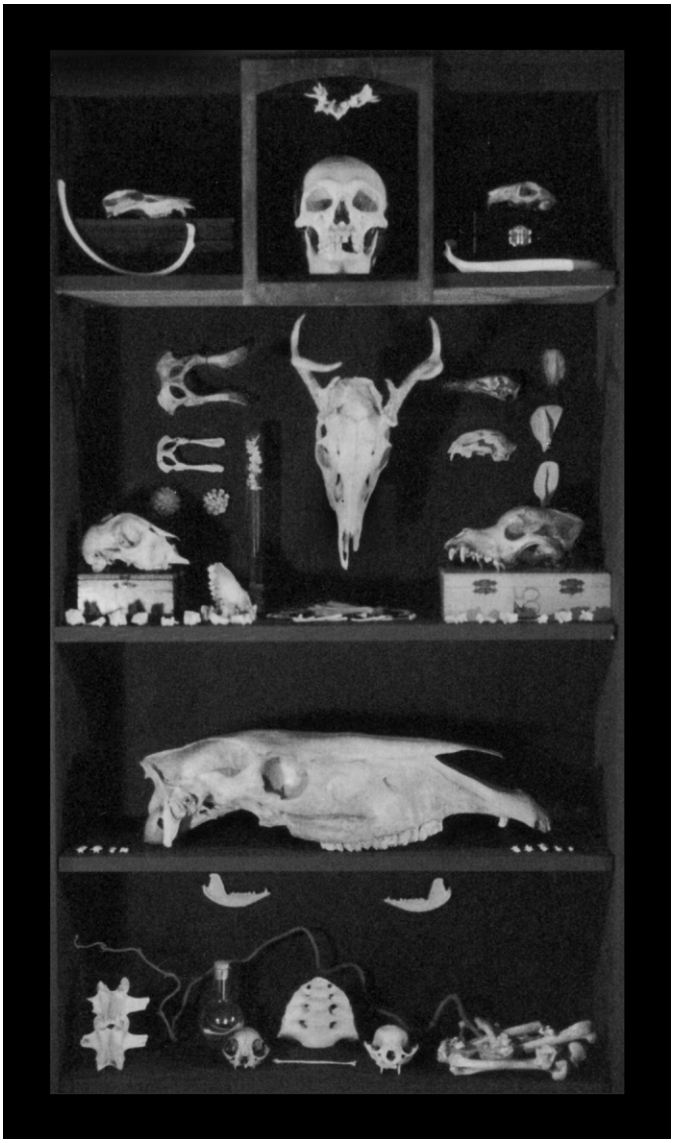

Comparative Osteology. DOI: 10.1016/B978-0-12-388437-4.00023-5

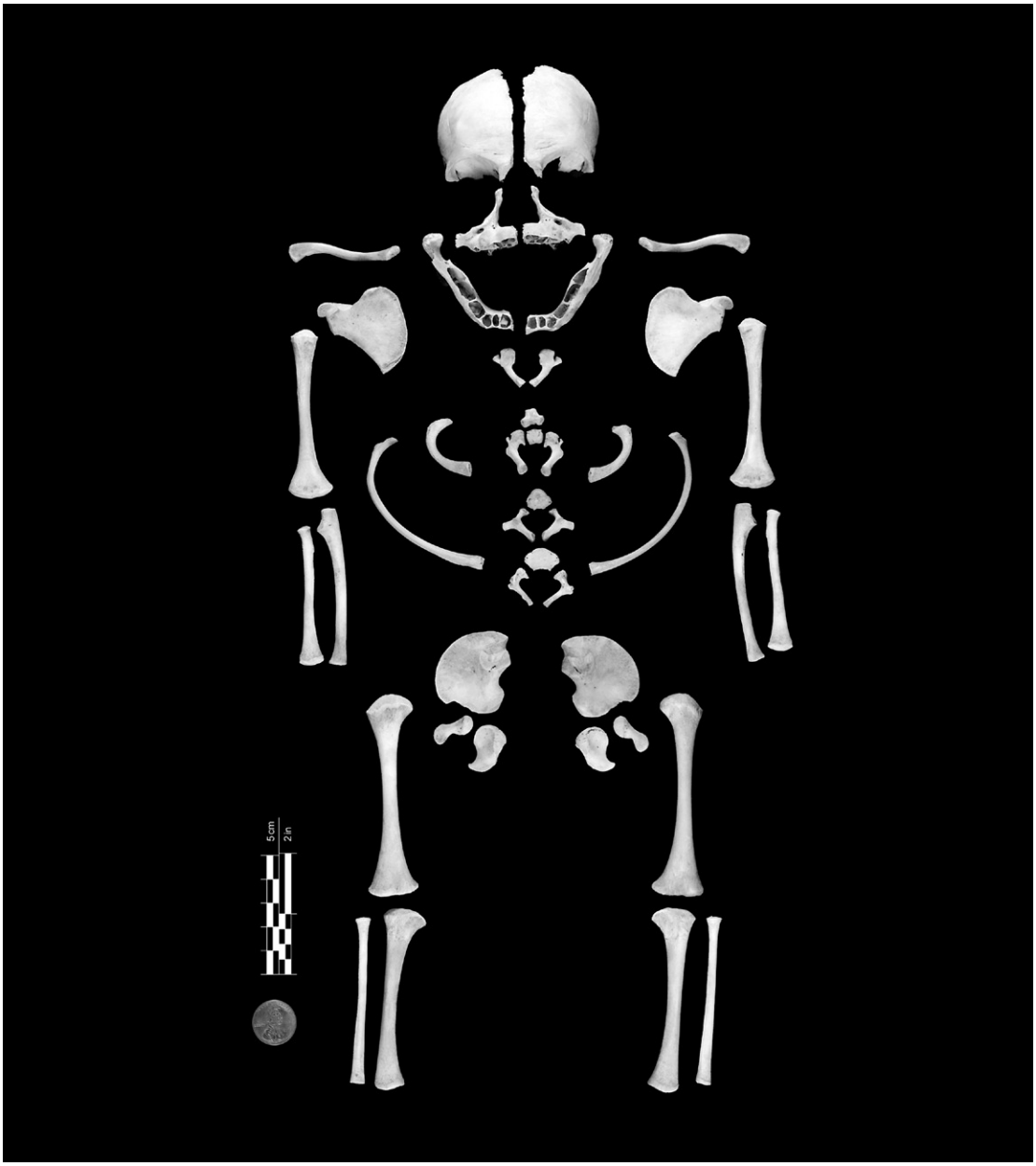

Figure 23-01: Major skeletal elements of a newborn human skeleton positioned in anatomical order (i.e., anterior view with hands at the side and palms forward).

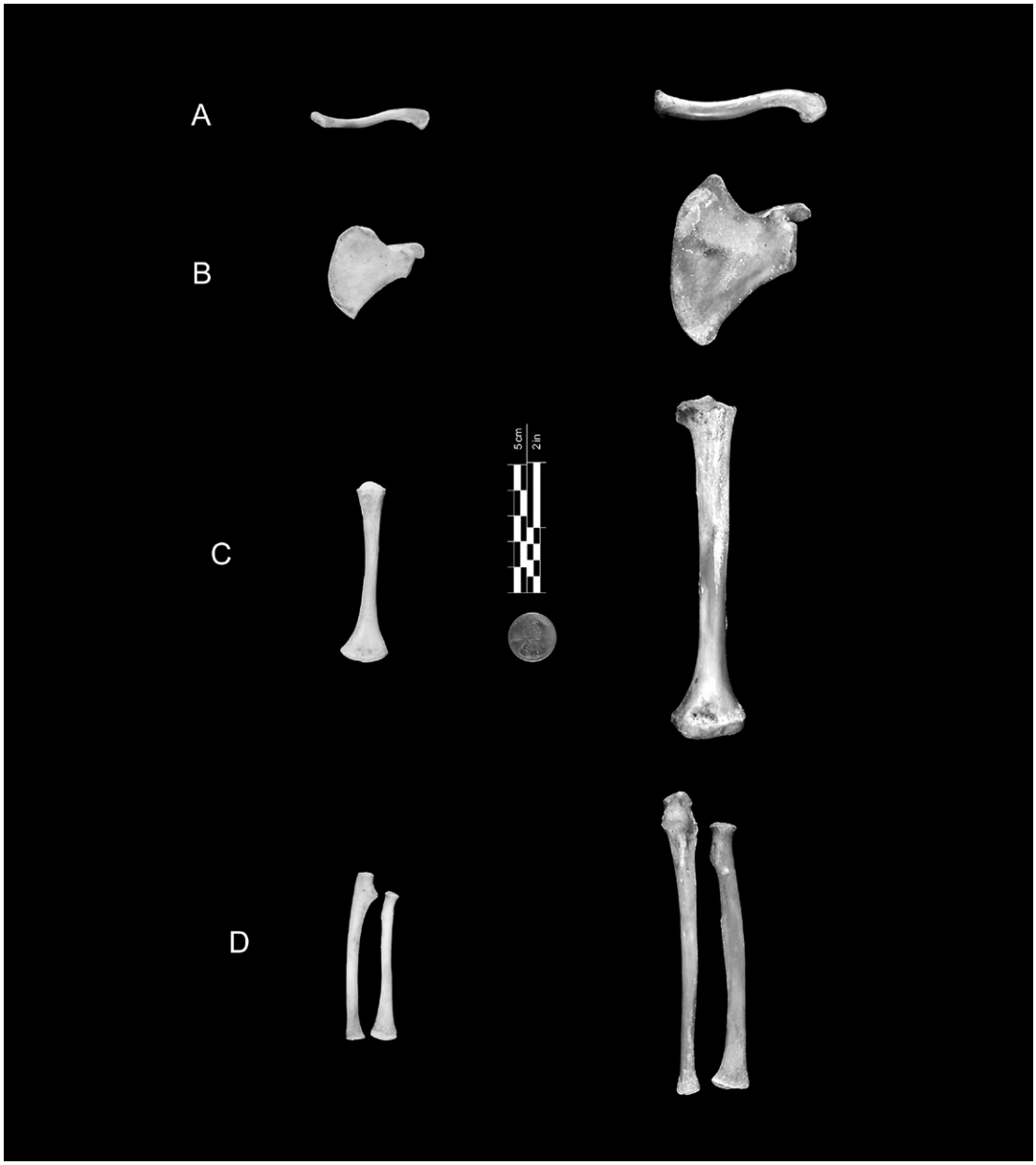

Figure 23-02: Subadult human bones of the upper extremity. The left arm and shoulder bones from a newborn infant (left) are compared to those of a 3–4-year-old child (right). The bones represented include the clavicle (A), scapula (B), humerus (C), and ulna and radius (D).

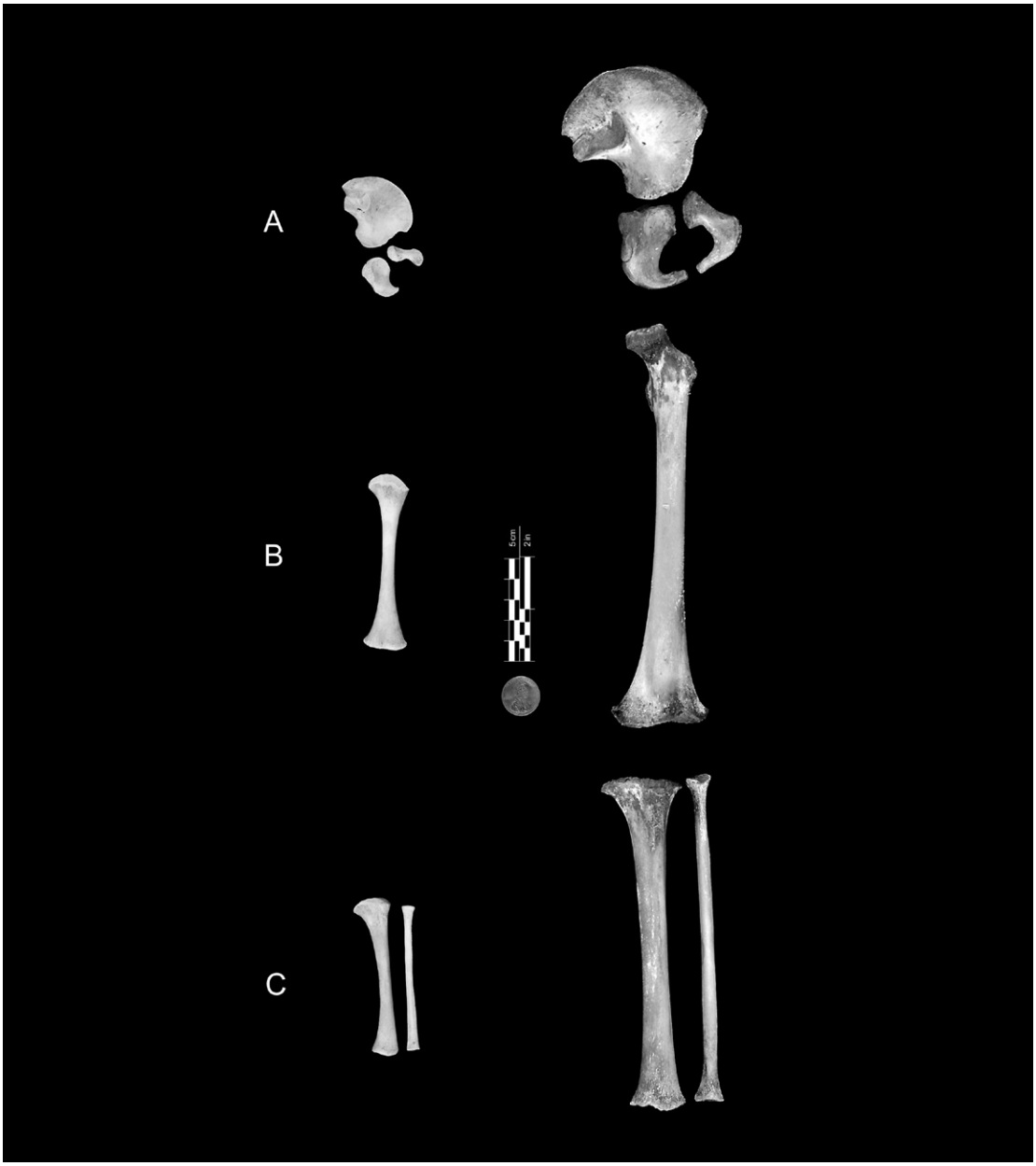

Figure 23-03: Subadult human bones of the lower extremity. The left pelvis and leg bones from a newborn infant (left) are compared to those of a 3–4-year-old child (right). The bones represented include the innominate (A), femur (B), and tibia/fibula (C).

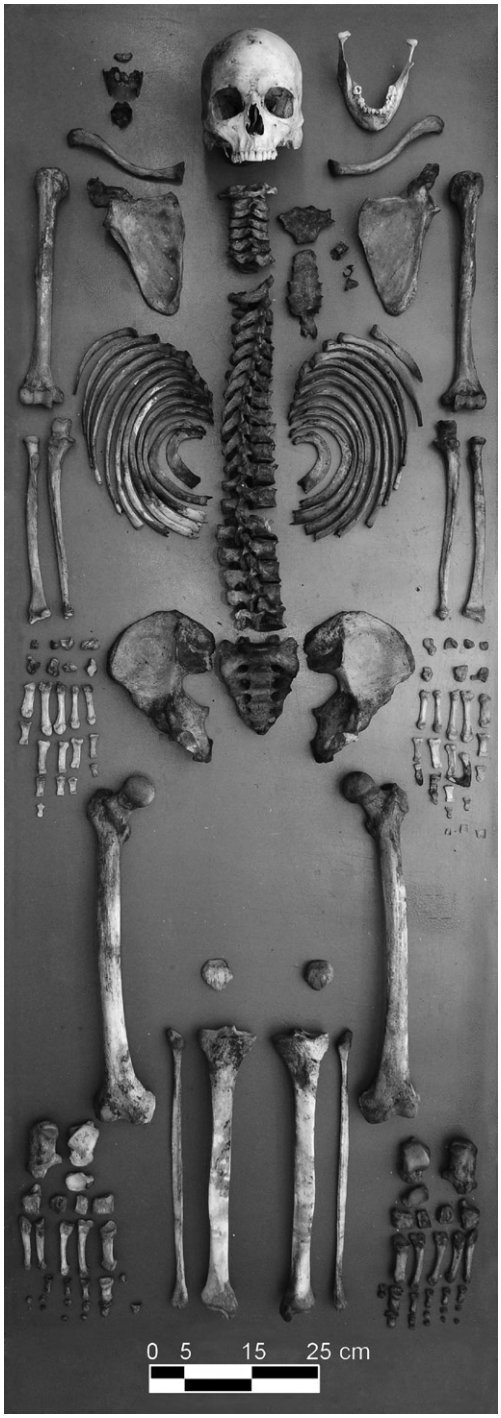

Figure 23-04: Adult human skeleton positioned in anatomical order (i.e., anterior view with hands at the side and palms forward).

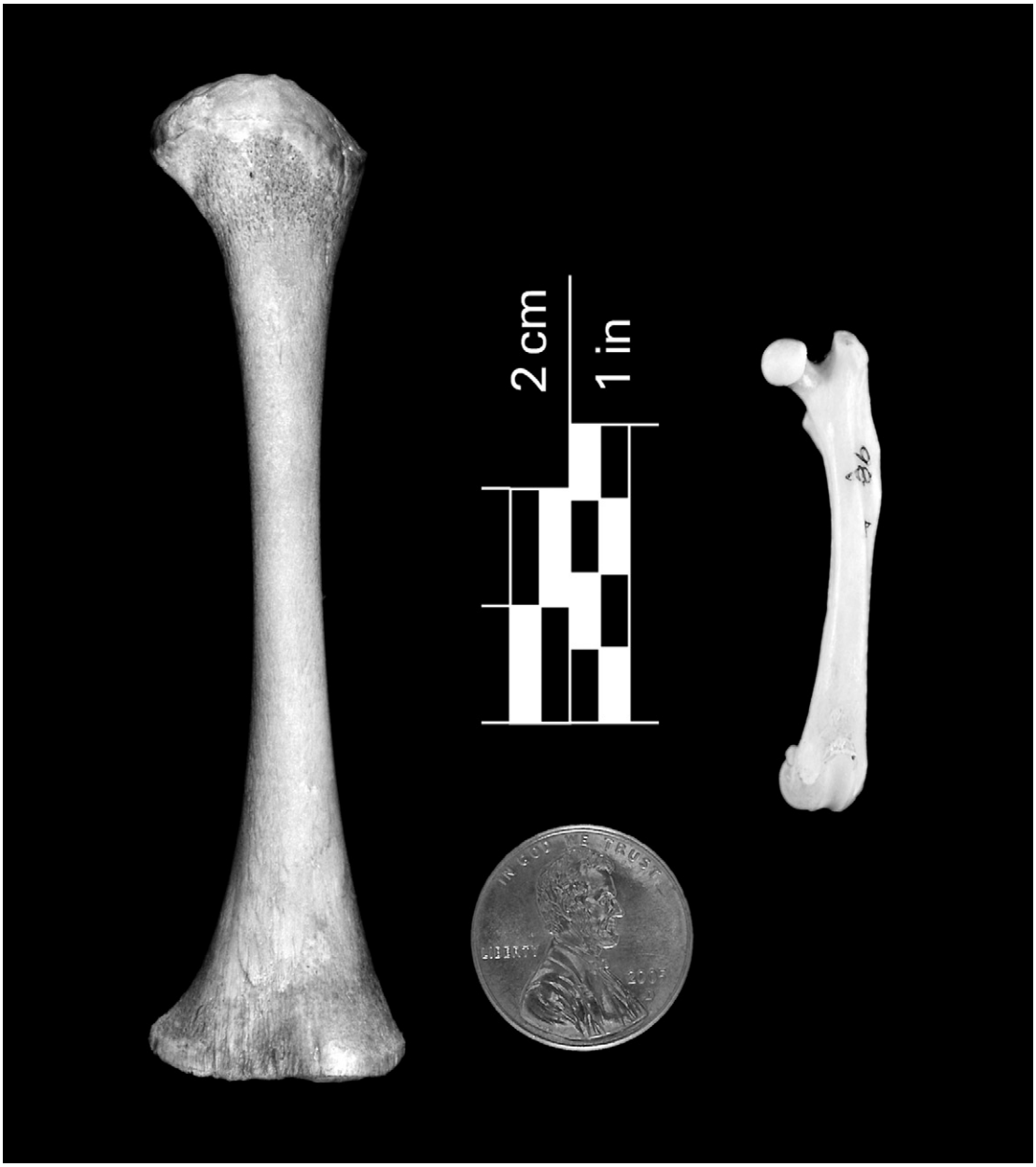

Figure 23-05: A newborn human left femur (anterior view) is compared to a rat's (*Rattus norvegicus*) left femur (cranial view).

Figure 23-06: A cat's left humerus (cranial view) is compared to a juvenile bobcat's (*Lynx rufus*) left humerus (cranial view). Note the presence of the supercondylar foramen on both specimens (arrows).

Figure 23-07: A dog's left femur (cranial view) is compared to a fox's (*Vulpes vulpes*) left femur (cranial view). Note the morphological similarities between the two canid species.

Figure 23-08: A newborn human left humerus (anterior view) is compared to a snapping turtle's (*Chelydra serpentina*) left humerus (cranial view).

Figure 23-09: A newborn human left humerus (posterior view) is compared to a snapping turtle's left humerus (caudal view).

Figure 23-10: A newborn human left radius and ulna (A, anterior view) are compared to a turtle's right and left radii (B) and ulnae (C).

Figure 23-11: A newborn human left femur (anterior view) is compared to a snapping turtle's left femur (cranial view).

Figure 23-12: A newborn human left femur (posterior view) is compared to a snapping turtle's left femur (caudal view).

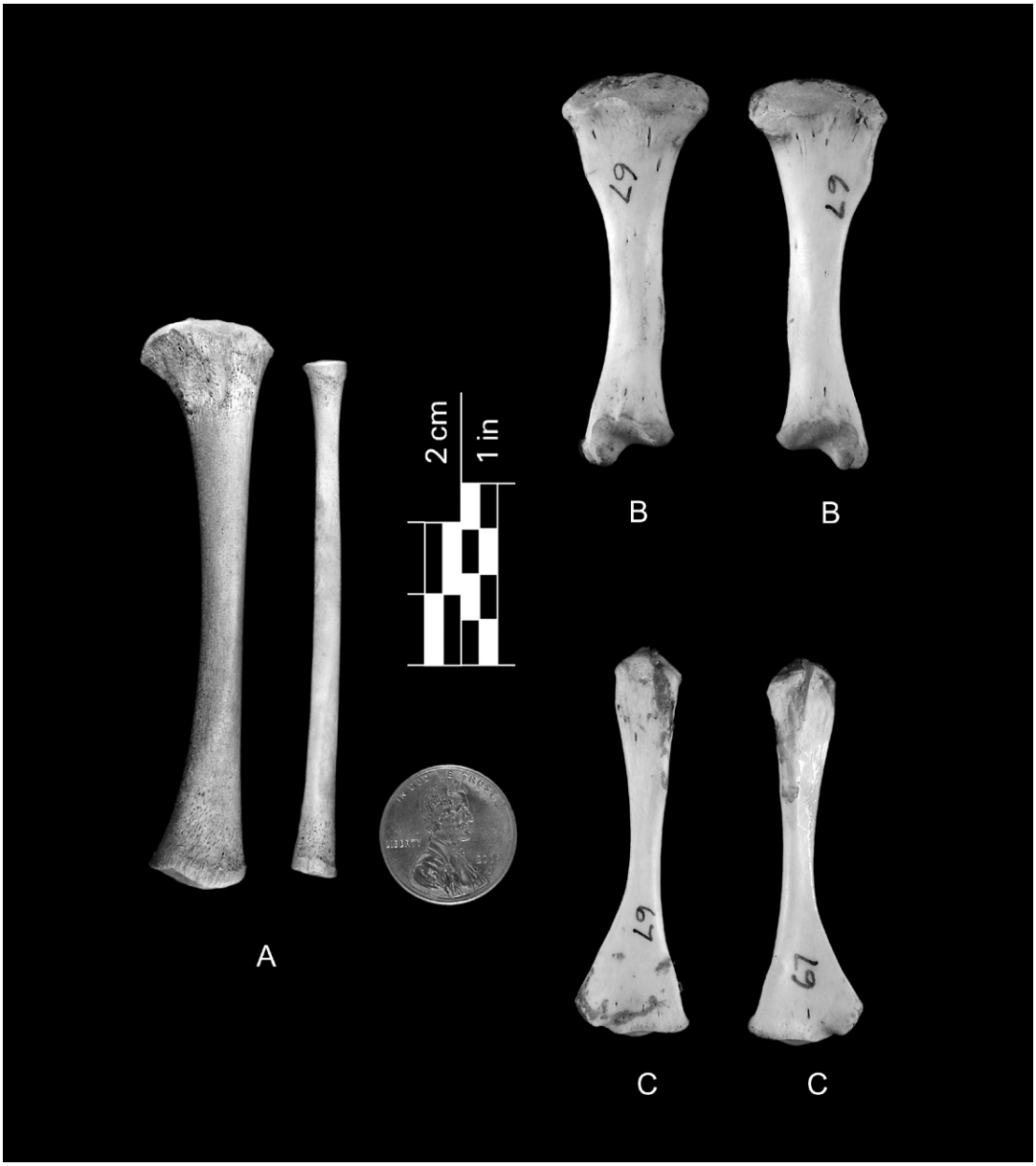

Figure 23-13: A newborn human left tibia and fibula (A, anterior views) are compared to a snapping turtle's right and left tibiae (B) and fibulae (C).

Figure 23-14: A newborn human left scapula (A) anterior view is compared to a snapping turtle's left shoulder girdle. Note that the turtle's shoulder girdle includes three elements: the scapula (C, horizontal position), the acromion (C, vertical portion), and the anterior coracoid (B). The scapula and the acromion are fused. The clavicle is fused to the plastron, or base of the shell.

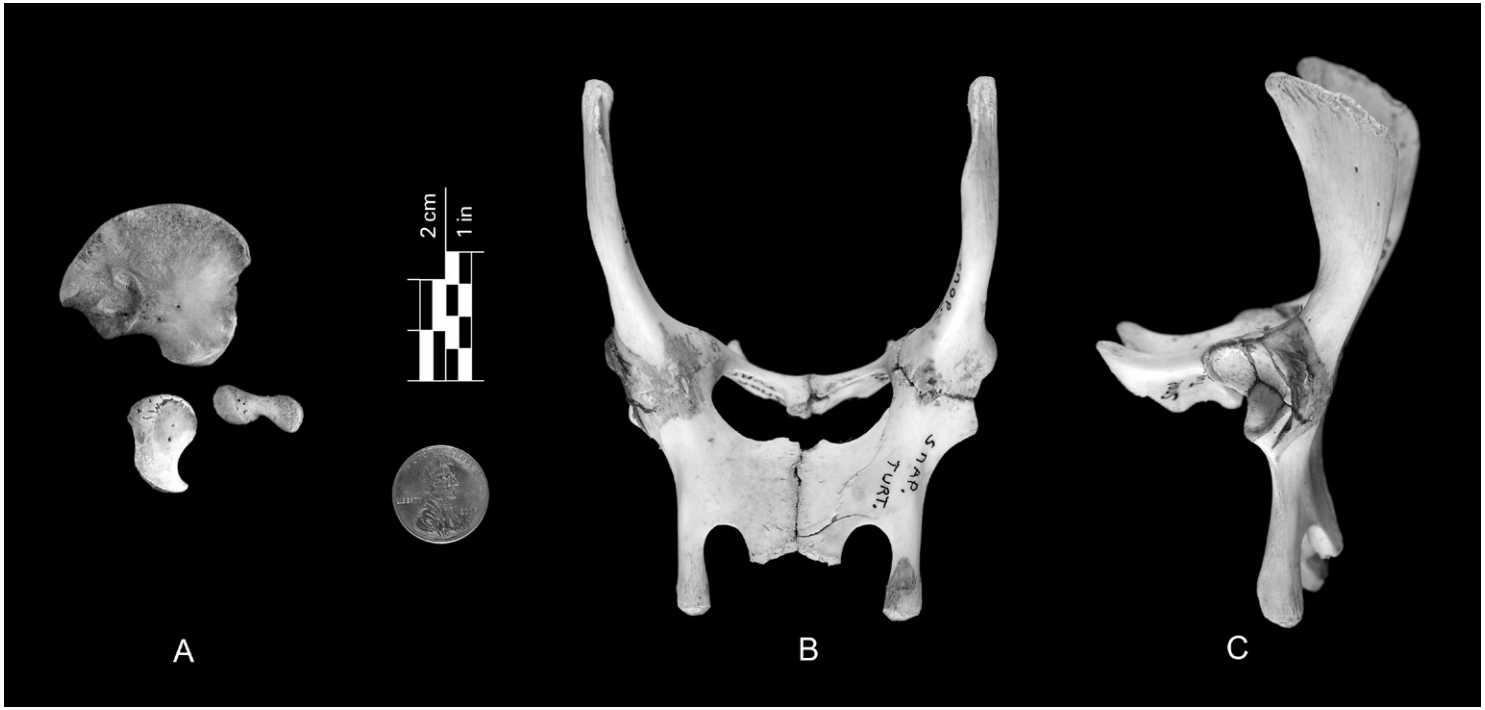

Figure 23-15: A newborn human left innominate (A, medial view) is compared to a turtle's pelvic girdle (B, ventral view; C, lateral view).

CHAPTER 24

Traces of Butchery and Bone Working

Pam Crabtree and Douglas V. Campana

Introduction

Animal bones often reveal marks of butchery associated with meat or marrow processing. Butchered bones may be recovered as important behavioral evidence from archaeological sites, or they may be collected within the forensic context and mistaken for human bones with marks of trauma. Archaeologists can use these butchery marks to study the ways in which past human populations butchered, distributed, and consumed meat. In a forensic context, tool marks on bone may be a good indication that the remains are non-human in origin, but this is not always the case. The intentional dismemberment of a human body by another individual (usually with the goal of hindering identification or facilitating transportation of the remains) may mimic the appearance of a butchered cow or pig to the untrained observer. An experienced osteologist should *always* be consulted if there is any doubt. Figure 24-01 shows several commercially butchered cow bones that were mistaken for human remains and turned over to law enforcement. Figures 24-02 and 24-03 are views of a human femur and humerus from an individual who was murdered and subsequently dismembered with a power saw.

This chapter will illustrate the types of butchery marks that are typically found on animal bones from modern-day, historic, and prehistoric contexts. Butchered remains of cattle and pigs are most commonly found on historic archaeological sites in North America, while prehistoric sites often yield substantial numbers of butchered deer bones. Cow and pig are also the most frequently encountered butchered bones from the present-day context and, based on their size, they are commonly mistaken for human bones. This chapter will also include schematic drawings of a pig, a cow, a lamb, and a deer that show the major cuts of meat. The chapter will conclude with a brief discussion of some of the ways in which bone has been used as a raw material for the manufacture of tools and other artifacts.

Comparative Osteology. DOI: 10.1016/B978-0-12-388437-4.00024-7

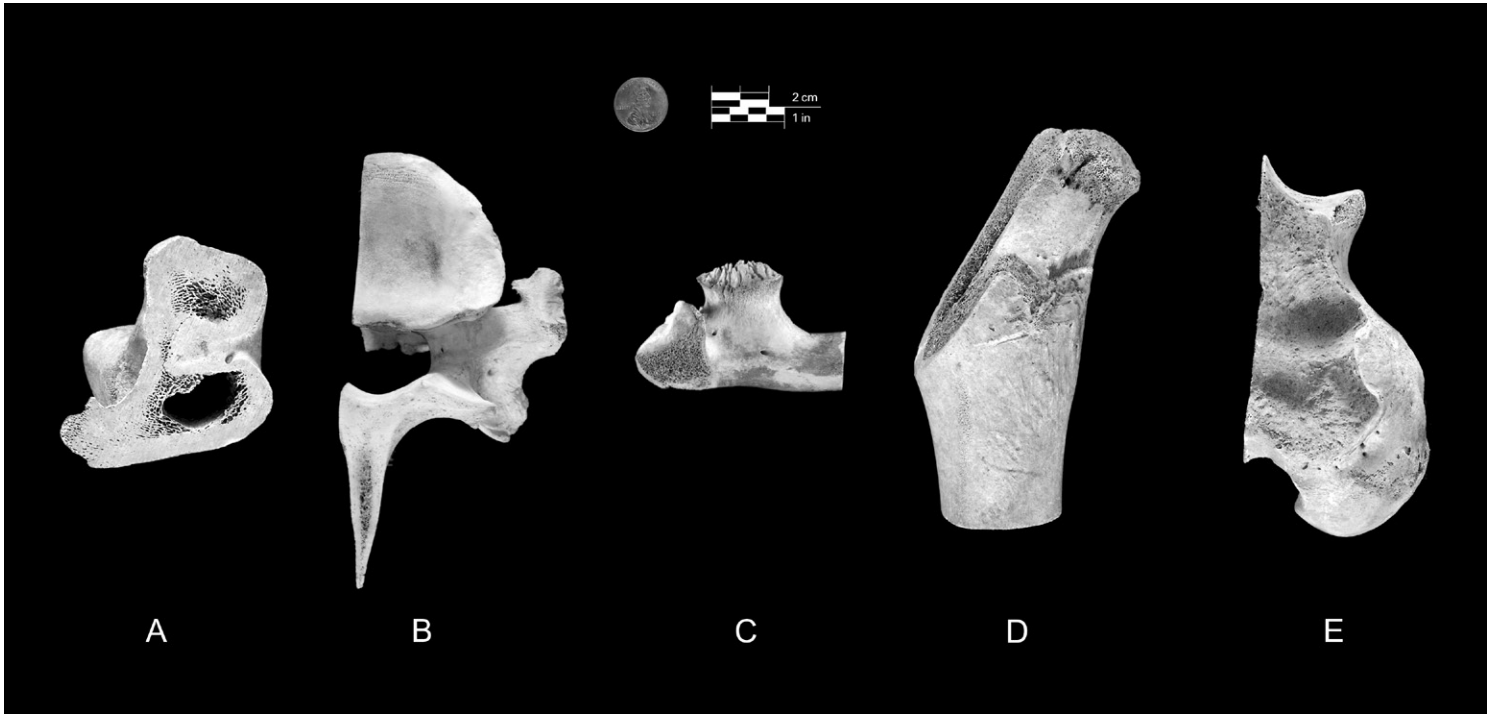

Figure 24-01: Various examples of cattle bones that were butchered with a saw. These are from the present day and were mistaken for human remains and turned over to the Medical Examiner's Office in New York City. From left to right: (A) A cattle distal humerus; the humerus has been sawn through just above the distal end. (B) A cattle thoracic vertebra (caudal view); the vertebra has been sawn in half axially and the thoracic spine has been sawn off. (C) The head of a cow's rib that has been sawn through. (D) An immature cow's femur (cranial view; note that the head of the femur is unfused); the proximal end of the femur has been sawn through, separating the greater trochanter from the rest of the bone; the shaft of the femur has been sawn through as well. (E) The epiphysis of a distal right femur that has been sawn in half.

Figure 24-02: Proximal right human femur (A) and proximal left human humerus (B), both anterior views. These bones are from an adult individual who was murdered and then dismembered with a power saw. Note the false start kerf (arrow), which is an incomplete cut with the saw blade. Measurements of the kerf width can be an indication of blade type.

Figure 24-03: Different views of the dismembered human femur and humerus in Figure 24-02 that show the sawn margins and associated striae created by the saw's teeth.

Modern Butchery: Eighteenth Century to the Present

Butchers have two main goals: they seek to divide the animal carcass into a number of smaller and more manageable pieces and, in many cases, they also seek to remove some of the meat from the animal's skeleton. The typical cuts of beef, pork, mutton, and venison are illustrated in Figures 24-04 through 24-07. Since the eighteenth century, American butchers have used saws to butcher large animals, and saw marks are some of the most common traces of butchery seen on modern animal skeletons. Hand saws were used in the eighteenth and nineteenth centuries, but modern butchery most commonly employs power saws. Sawing can be readily recognized by the characteristic kerfs, or saw marks, left behind on the sawn bone surface. Hand-sawn bone can be distinguished by the somewhat irregular sawn surface, with groups of parallel, often coarse, striations at angles to one another on the kerf walls; machine-sawn bone usually shows a flat, polished surface with fine, parallel striations on the kerf walls. The analysis of kerf features can also be very informative in the forensic context when assessing tool marks left on bone from human dismemberment cases (e.g., Symes et al. 1998, 2002). For the processing of food remains, saws are used both to split the carcass into sides and to subdivide the carcass into joints of meat.

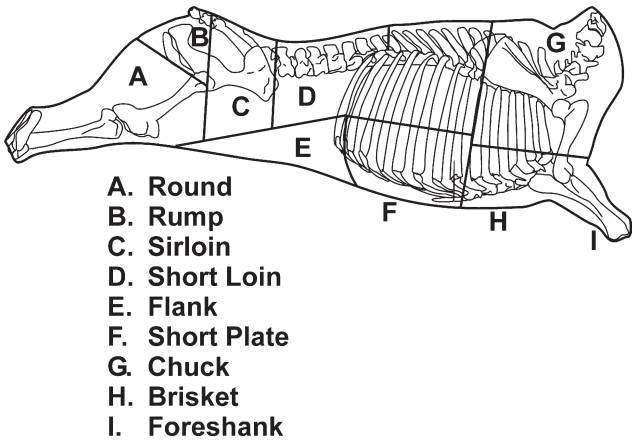

Figure 24-04: Modern beef cuts.

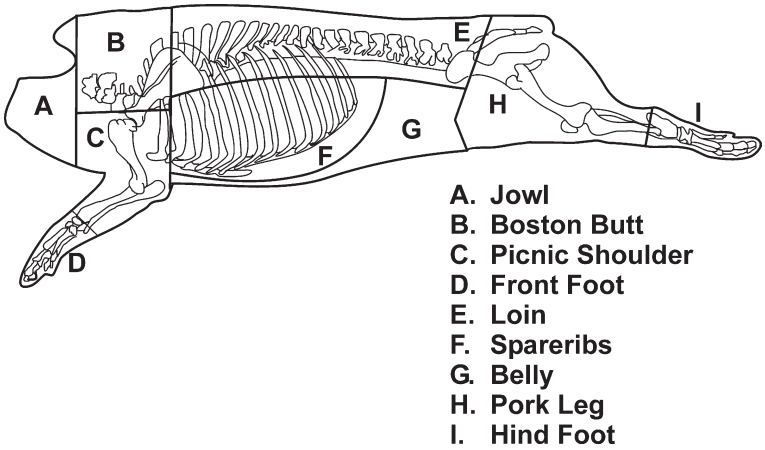

Figure 24-05: Modern pork cuts.

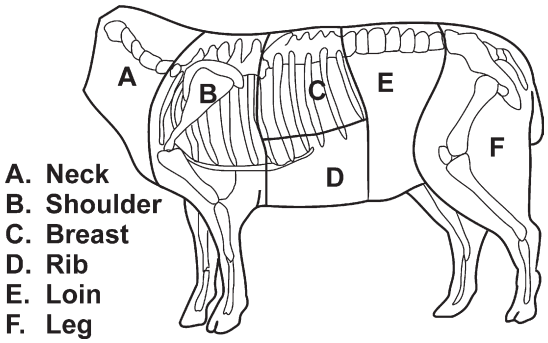

Figure 24-06: Modern lamb (mutton) cuts.

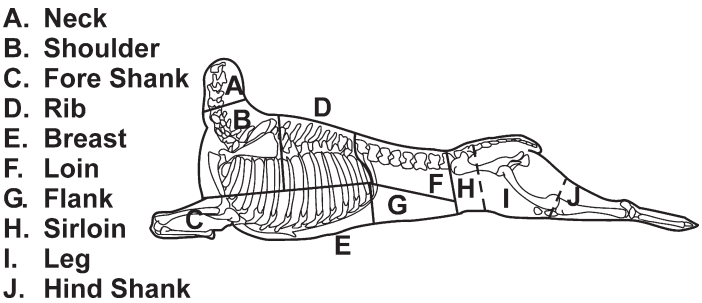

Figure 24-07: Modern deer (venison) cuts.

Figure 24-08 shows a cow scapula that has been sawn with a hand saw. This bone dates to the eighteenth century and was recovered from deposits associated with the New York City Poor House, located on the grounds of the modern City Hall. Figure 24-09 shows a cow's atlas (C1) that has been sagittally sawn. This example came from a forensic case file from New Jersey. Figures 24-10 and 24-11 are sawn bones from a late-twentieth-century pig farm in central New Jersey. In this case, a saw has been used to separate the lower limbs from the meatier portions of the upper fore- and hindlimbs. The central portion of the tibial shaft (Figure 24-10) and the distal parts of the radial and ulnar shafts (Figure 24-11) have all been sawn through.

Saws are commonly used to divide an animal's carcass into a series of joints of meat. Figure 24-12 shows a cow's humerus from a nineteenth-century deposit at the archaeological site of Fort Johns in Sussex County, New Jersey (Crabtree et al. 2002). The humerus has saw marks near the distal end and on the central portion of the shaft. A second saw mark is visible on the central portion of the shaft where the butcher's saw must have slipped early in the process. These saw marks were used to produce a chuck or arm roast.

Saws are often used to divide beef ribs into small, 4–6 inch (10–15 cm) sections. Figure 24-13 (top) shows a central portion of a cow's rib with saw marks on either end, producing a cross-rib cut. This example was also recovered from a nineteenth- or early-twentieth-century context at the Fort Johns site. A second rib section from Fort Johns (Figure 24-13, bottom) includes the articular portion of the bone (the part closest to the vertebral column).

Other typical examples of nineteenth-century butchery from the Fort Johns site include a cow's ilium (Figure 24-14a) that has been sawn into a roughly 1 inch (2.5 cm) segment, probably for a steak, and the glenoid portion of a cow's scapula (Figure 24-14b) that has been sawn through, possibly to produce a chuck roast. The Fort Johns excavations also produced a dorsal spine of a cow's thoracic vertebra (Figure 24-14c) that has been sawn through. Large, sawn sections of less meaty elements, such as tibial and radial shafts of cattle, are often used as soup bones (Milne and Crabtree 2002: 164). Figure 24-14d shows a sawn section of a cow's tibia from the Five Points site, a nineteenth-century multi-ethnic neighborhood in lower Manhattan (Milne and Crabtree 2001).

Knife cuts and other butchery traces resulting from meat removal can often be seen on modern faunal remains. For example, Figure 24-15 shows an immature pig's femur and tibia cut across each shaft. Figure 24-16 shows an immature pig's tibia that has been made into a spiral ham. The circular cut marks can be seen on the proximal shaft of the tibia.

Figure 24-08: A cow's scapula that has been sawn in half. This example is from the eighteenth-century Poor House in New York City.

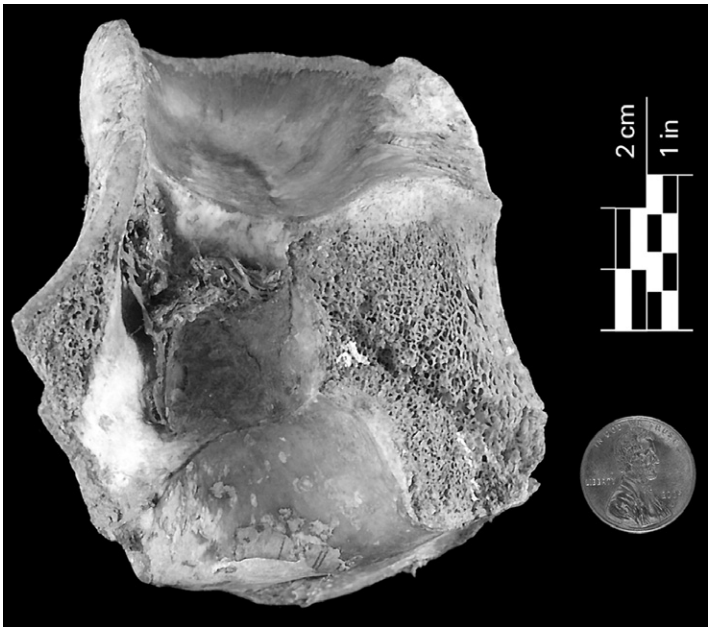

Figure 24-09: A cow's cervical vertebra on which saw marks can be seen.

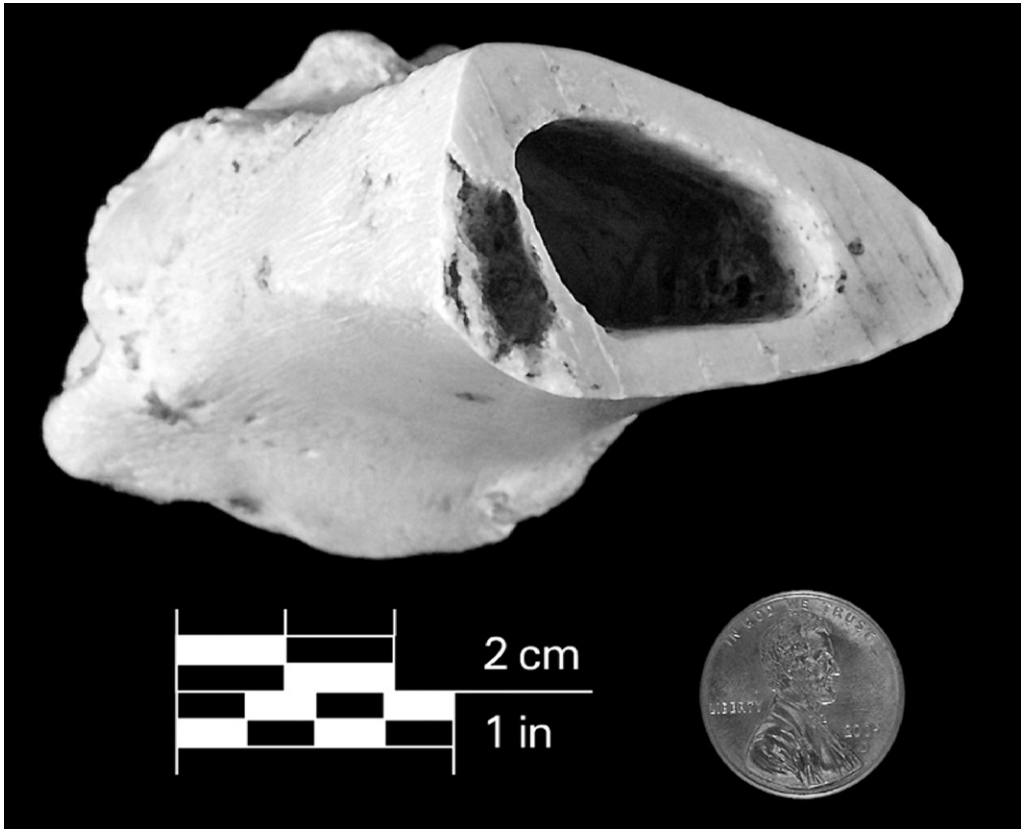

Figure 24-10: Traces of machine sawing can be seen on this shaft of a pig's tibia from a twentieth-century farm in New Jersey.

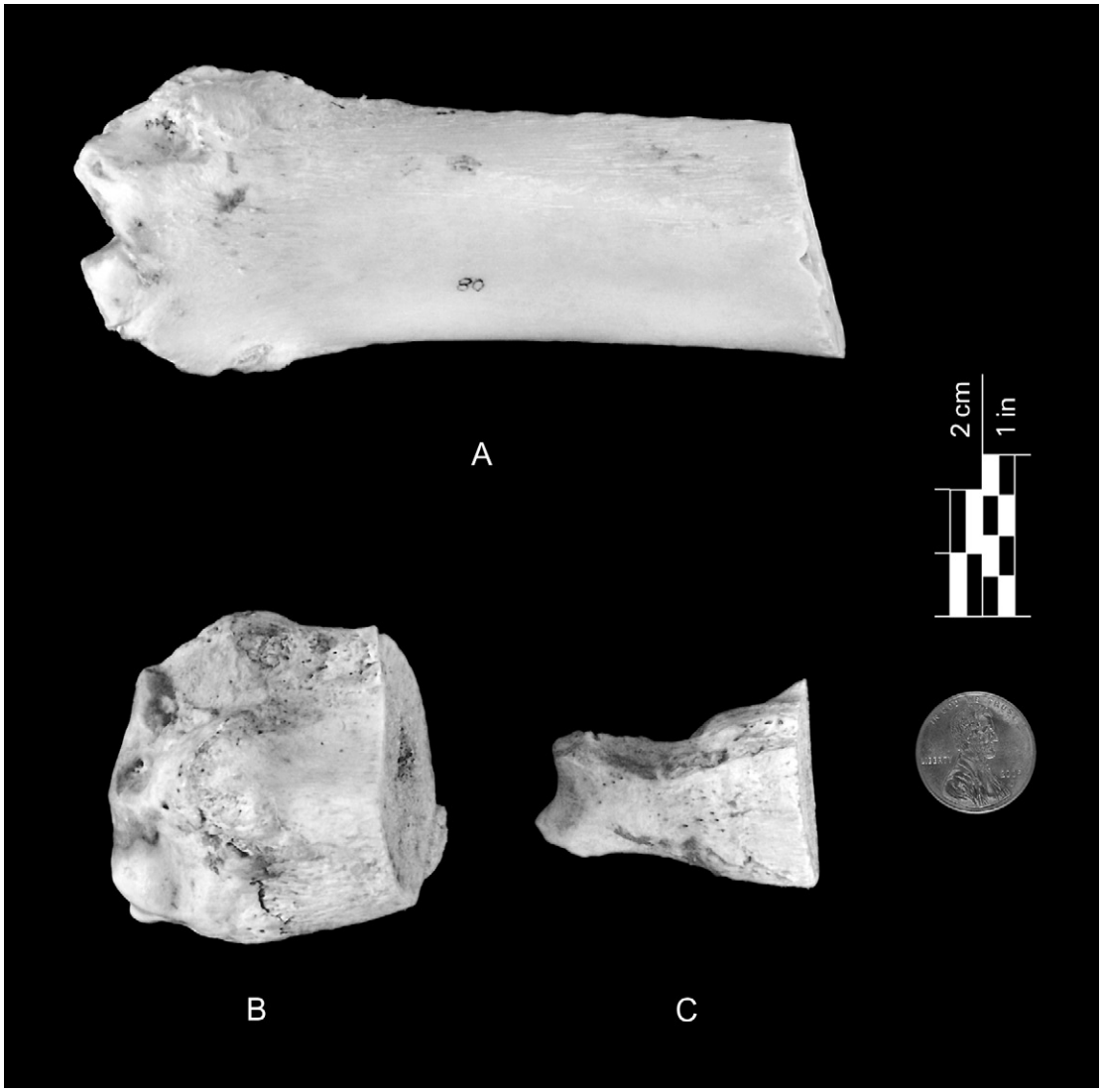

Figure 24-11: Sawn shafts of a pig's tibia (A), radius (B), and ulna (C) from a late-twentieth-century farm in New Jersey.

Figure 24-12: A sawn cow's humerus from the historic Fort Johns site in Sussex County, New Jersey. Arrows show locations of saw marks.

Figure 24-13: A sawn section of a cow's rib from the Fort Johns site (top). Also shown (bottom) is the sawn section of a cow's rib including the dorsal portion that articulates with the thoracic vertebrae.

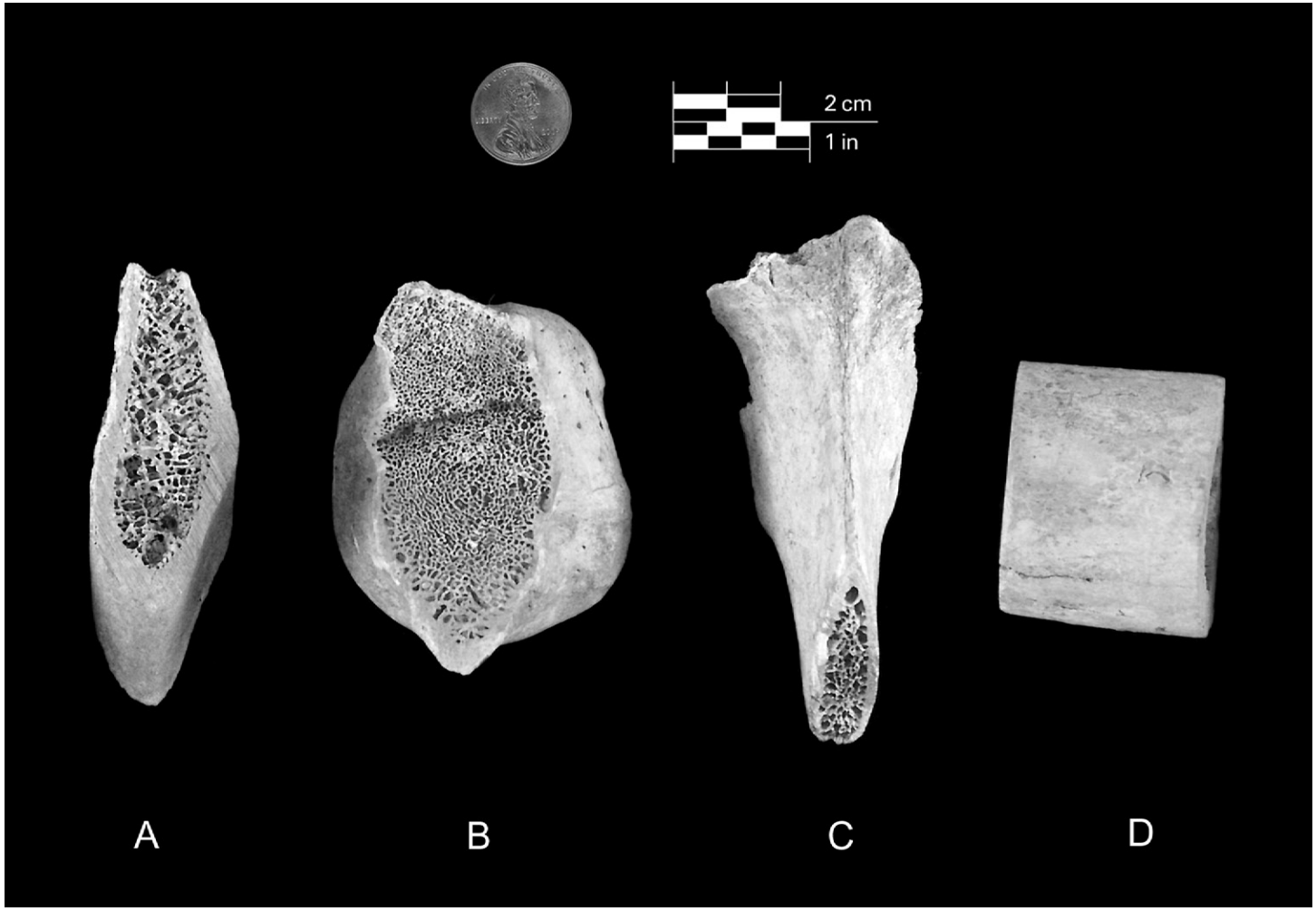

Figure 24-14: Typical examples of butchery from nineteenth-century archaeological sites in the north-eastern USA. A cow's sawn ilium (A), scapula (B), and thoracic spine from the Fort Johns site in New Jersey (C), and a section of a cow's tibia from the Five Points site in Manhattan (D).

Figure 24-15: Distal femur and proximal tibia from a juvenile pig showing cut marks through the shafts of both bones.

Figure 24-16: Proximal tibia of a modern pig showing cut marks (arrows). This bone is the remnant of a spiral-cut ham.

Figure 24-17: A butchered cow's femur from Brandon, a Middle Saxon (ca. 650–850 AD) site in eastern England that has been split with a cleaver. An initial, unsuccessful chop mark can also be seen on the proximal end near the femoral head (arrow).

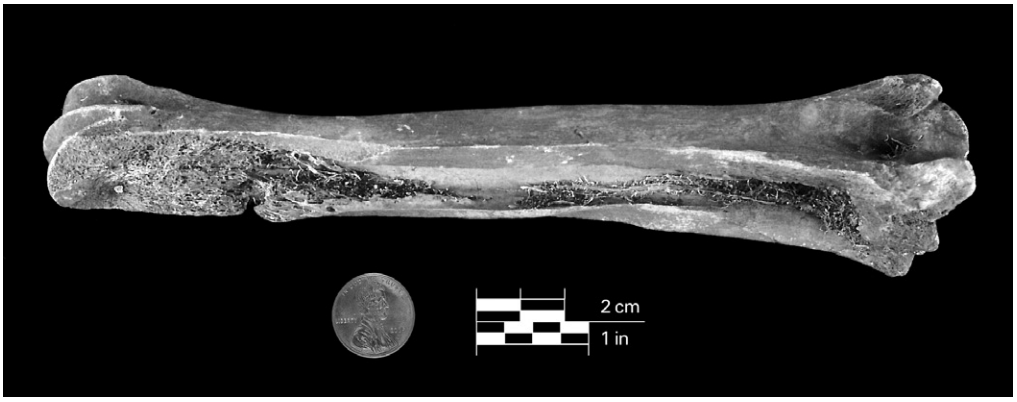

Figure 24-18: A split cattle metatarsus from the Middle Saxon site of Brandon.

Butchery Using Cleavers and Heavy Knives

Prior to about 1700 AD, most butchery was carried out using cleavers and heavy knives. These tools were also commonly used for home butchery during the eighteenth and nineteenth centuries. Figure 24-17 shows a cow's proximal femur that has been split using a cleaver. An initial, unsuccessful chop mark can also be seen on the proximal end near the femoral head. This example comes from the Middle Saxon (ca. 650–850 AD) settlement site of Brandon in eastern England (Carr et al. 1988).

Figure 24-19: Chop marks (arrows) on a cow's mandible from the second- to fourth-century Roman site of Icklingham in eastern England.

Lower limb bones, especially the metacarpals and metatarsals of the ruminant artiodactyls, are often split for the extraction of marrow. Figure 24-18 shows a cattle metatarsal that has been axially split. This example was also recovered from the Brandon site.

Professional butchers can dismember a large animal carcass skillfully using sharp cleavers. The following examples from the Roman (second- to fourth-century AD) site of Icklingham in eastern England show how Roman butchers could dismember animal carcasses using sharp iron tools. Figure 24-19 shows the types of chop marks that are typically produced by a heavy knife or cleaver. These marks appear near the gonial angle of a cow's mandible. Figure 24-20 shows similar heavy chop marks on the caudal portion of a cow's radius. Figure 24-21 shows a cow's pubis that has been chopped through using a cleaver.

Figure 24-20: Chop marks (arrows) on the caudal portion of a cow's radius from Icklingham.

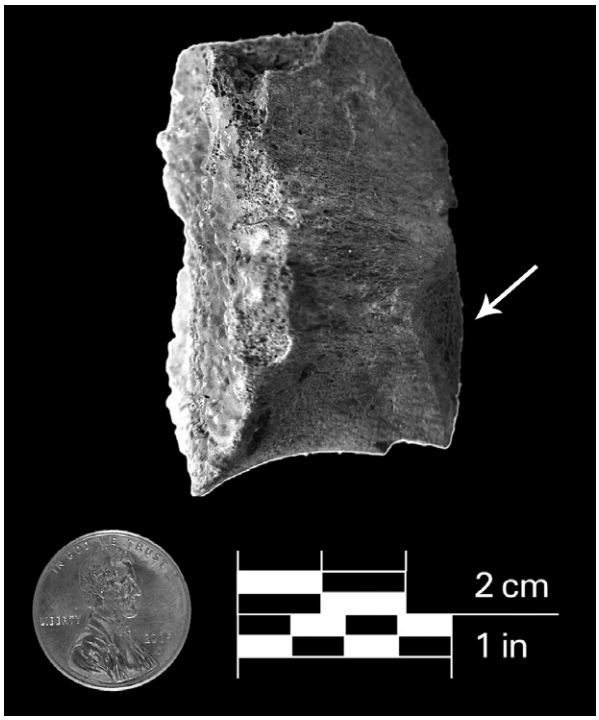

Figure 24-21: Chop marks (arrow) on a cow's pubis from Icklingham.

Figure 24-22: An astragalus fragment of a wild goat (*Capra aegagrus*) from the Middle Paleolithic levels of Shanidar Cave in Iraq showing stone tool cut marks.

Prehistoric Butchery

Before the development of high-quality metal tools, butchery was carried out using stone tools. The earliest examples of animal bones butchered with stone tools date back to about 2.6 million years ago in East Africa (Semaw 2000; Semaw et al. 2003). In North America, animal bones were butchered using stone tools until the early seventeenth century, when metal knives and other tools were introduced from Europe. For example, a well-preserved iron cleaver was recovered from the seventeenth-century site of Martin's Hundred in Virginia (Noël Hume 1979: 147). Archaeologists working on prehistoric sites in the Americas are likely to encounter animal bones that have been butchered using stone knives and flakes. When compared to the traces left by iron tools, butchery traces left by stone tools are far more subtle. For example, a butcher using iron tools will often separate the femur from the

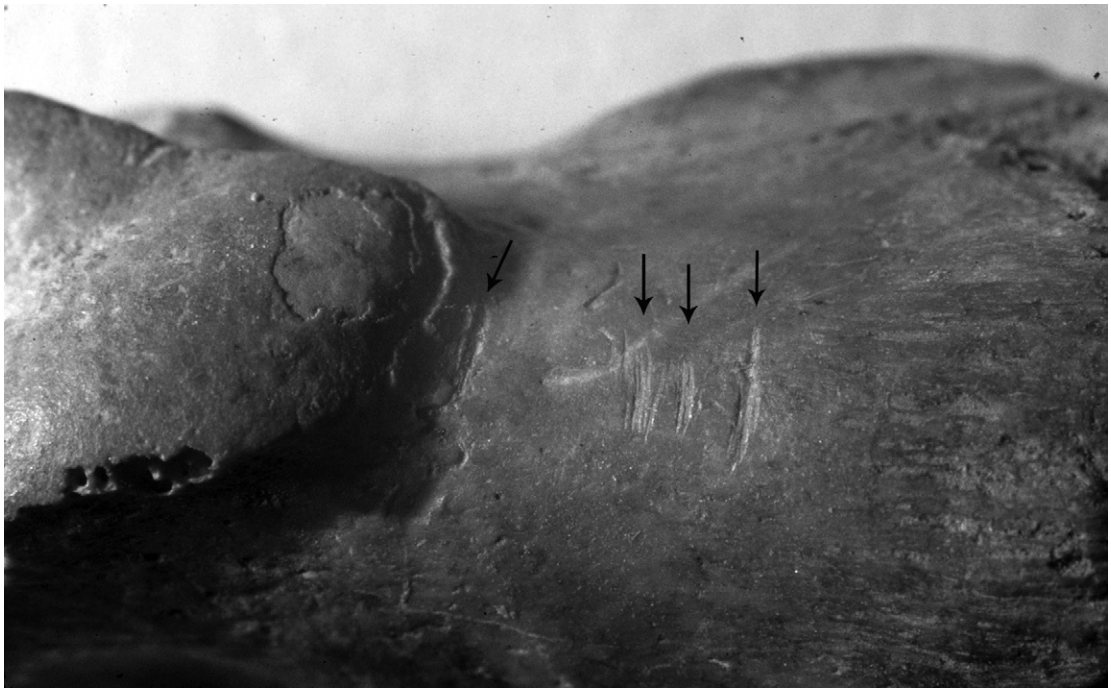

Figure 24-23: A wild goat's (*Capra aegagrus*) second phalanx from the Middle Paleolithic levels of Shanidar Cave showing cut marks (arrows) made with a stone tool.

acetabulum by chopping through the neck of the femur (see Figure 24-17). A prehistoric butcher using stone tools would cut around the outside of the acetabulum to detach, or disarticulate, the femur.

Figure 24-22 shows an astragalus of a wild goat (*Capra aegagrus*) that was butchered by the Neanderthals inhabiting Shanidar Cave in Iraq between 60,000 and 44,000 BP (Solecki 1971). The relatively deep, V-shaped cuts across the bone were left by the edge of a flint flake during the disarticulation of the animal's leg. Figure 24-23 is the phalanx of a Shanidar goat; these clear, somewhat shallower V-shaped cuts were left during the process of skinning the animal. Figure 24-24 is a phalanx of a modern white-tailed deer (*Odocoileus virginianus*) that has been experimentally skinned using flint tools similar to those found at Shanidar. The placement and appearance of these markings are very similar to those found on the archaeological specimens.

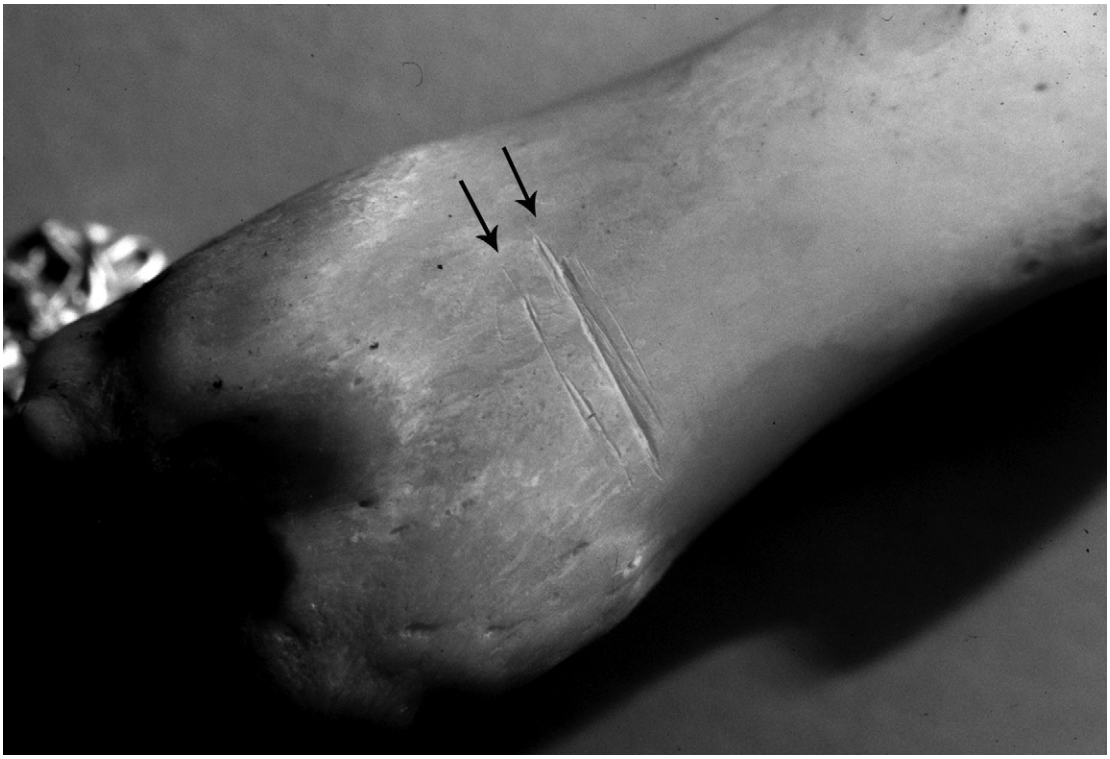

Figure 24-24: Experimental cut marks (arrows) made with a stone tool on a white-tailed deer's first phalanx.

Bone as a Raw Material

Bone has served as an important raw material throughout nearly all of human history. Bone was commonly used as a raw material for tools and other artifacts until its replacement by plastic after World War II. For example, bone toothbrushes are commonly found on nineteenth-century archaeological sites. Bone spools were used to hold thread for tatting (lace-making) as recently as the 1930s.

Not all bones are equally suitable for the manufacture of bone tools and artifacts. Prehistoric and historic craftworkers often chose to use ungulate metacarpals, metatarsals, and tibiae because these bones are characterized by a relatively long, cylindrical shaft made up of thick, compact bone. This bone is made up of a calcitic matrix deposited around a central nutrient canal, forming the osteons, or Haversian system. The osteons of long bones are oriented parallel to the shaft, splaying outwards toward the ends. The combination of thick, compact bone with parallel osteons results in a set of physical characteristics of the material in the bone shaft that is advantageous for the manufacture of bone implements. The shaft of a long bone is markedly anisotropic in strength; that is, it is much stronger when stressed along the length

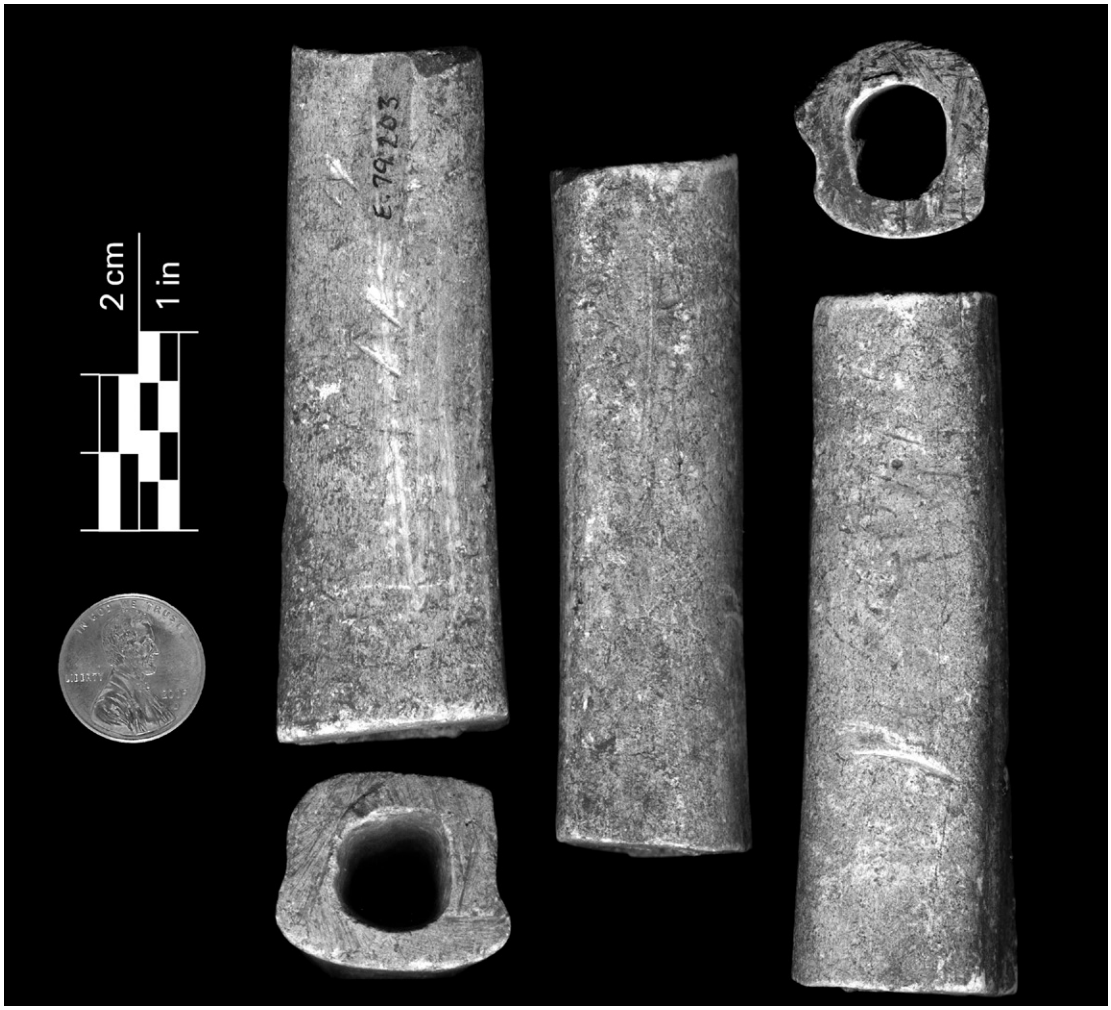

Figure 24-25: A sawn section of a cow's metatarsal from the Iron Age site of Dún Ailinne in Ireland. This appears to be a blank for bone working.

of the bone than it is around the circumference of the bone. Consequently, long bones tend to fracture in long, thin fragments that are suitable for making into tools and other artifacts.

Figure 24-25 shows a section of a cow's metatarsal that has been sawn at both the proximal and the distal ends. The metatarsus was recovered from the Iron Age (approximately 200 BC to 100 AD) site of Dún Ailinne in Ireland (Wailes 1990, 2004; Johnston and Wailes 2007). Although sawing was not used in butchery in Ireland until about 1700, saws were used in bone working from the early Iron Age onward. This bone object is the earliest known example of sawing in Ireland (Raftery 1994: 119). This bone appears to be a blank that was prepared for bone working. Figure 24-26 shows a finished bone tool made on a split gazelle

Figure 24-26: This bone tool made from a gazelle metapodial was recovered from the 11,000-year-old site of Salibiya I in the West Bank.

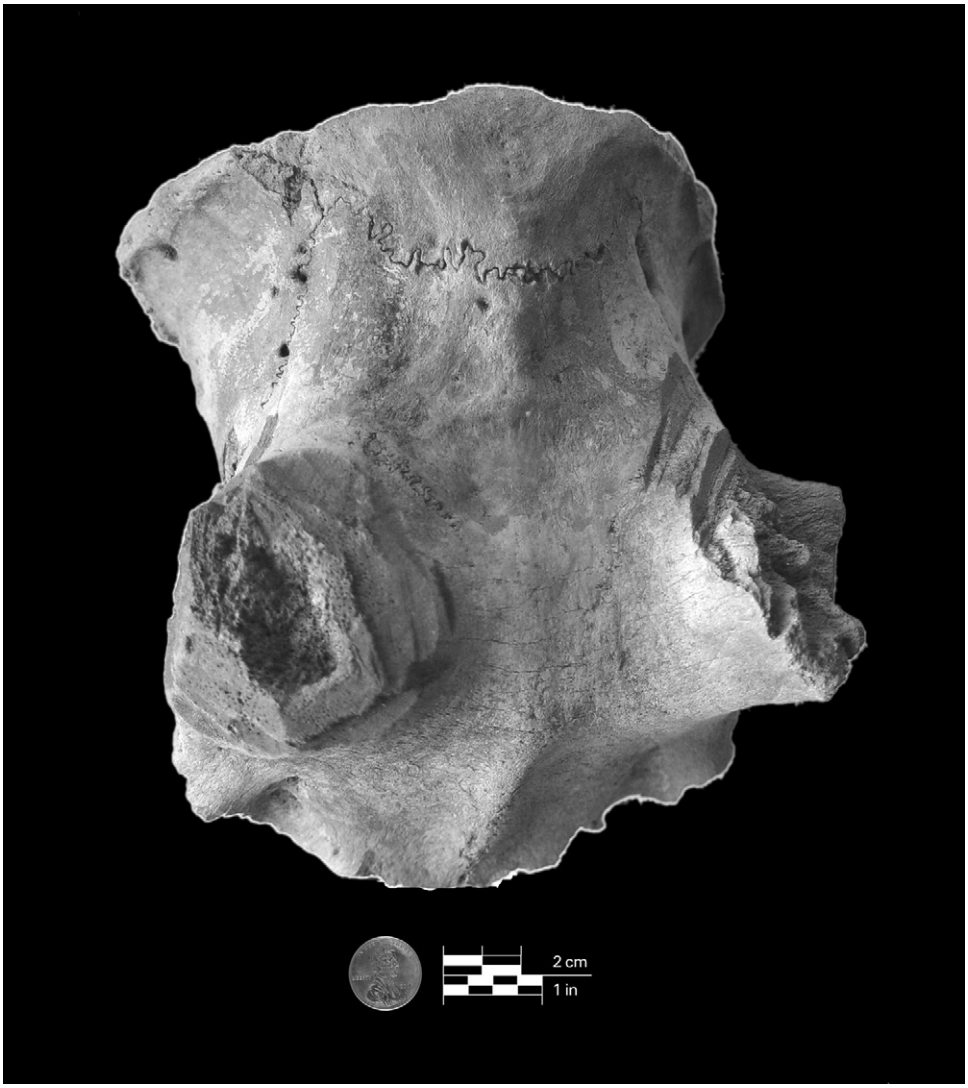

Figure 24-27: A red deer (*Cervus elaphus*) skull from the Anglo-Saxon site of Brandon in eastern England. One antler has been chopped off, while the other has been sawn off.

metapodial from the 11,000-year-old site of Salibiya I in the lower Jordan Valley, West Bank (Crabtree et al. 1991).

Deer antler was also a valuable raw material that was commonly used for handles and other artifacts. Figure 24-27 shows a red deer (*Cervus elaphus*) skull from the medieval Brandon site in eastern England. Both a saw and a heavy cleaver have been used to remove the antlers from the deer's skull. In the Middle Ages, antler was commonly used to manufacture bone combs. Figure 24-28 is an example of an early medieval antler comb from Iceland.

Figure 24-28: An antler comb from medieval Iceland.

References

Bass, W. M. (2005). *Human osteology* (5th ed.). Columbia, MO: Missouri Archaeological Society.

Boessneck, J. (1969). Osteological differences between sheep (*Ovis aries* Linne) and goat (*Capra hircus* Linne). In D. Brothwell & E. Higgs (Eds.), *Science in archaeology* (pp. 331–358). New York, NY: Praeger.

Boessneck, J., Muller, H. H. & Teichert, M. (1964). Osteologische Unterscheidungsmerkmale zwischen Schaf (*Ovis aries* Linne) und Ziege (*Capra hircus* Linne). *Kuhn-Archiv*, *78*, 1–129.

Brothwell, D. R. (1981). *Digging up bones* (3rd ed.). Ithaca, NY: Cornell University Press.

Brown, C. L. & Gustafson, C. E. (1979). *A key to postcranial skeletal remains of cattle/bison, elk, and horse*. Pullman, WA: Washington State University. Washington State University Reports of Investigations 57.

Byers, S. N. (2010). *Introduction to forensic anthropology* (4th ed.). Boston, MA: Pearson Education.

Carr, R. D., Tester, A. & Murphy, P. (1988). The Middle-Saxon settlement at Staunch Meadow, Brandon. *Antiquity*, *62*, 371–377.

Cattaneo, C., Porta, D., Gibelli, D. & Gamba, C. (2009). Historical determination of the human origin of bone fragments. *Journal of Forensic Science*, *54*(3), 531–533.

Chang, K. C. (1986). *The archaeology of ancient China* (4th ed.). New Haven, CT: Yale University Press.

Cohen, A. & Serjeantson, D. (1996). *A manual for the identification of bird bones from archaeological sites* (Revised ed.). London: Archetype Publications.

Cornwall, I. W. (1956). *Bones for the archeologist*. New York, NY: Macmillan Press.

Crabtree, P. J., Campana, D. V., Belfer-Cohen, A. & Bar-Yosef, D. (1991). First results of the excavations at Salibiya I, Lower Jordan Valley. In O. Bar-Yosef & F. Valla (Eds.), *The Natufian culture of the Levant* (pp. 161–172). Ann Arbor, MI: International Monographs in Prehistory.

Crabtree, P., Campana, D. V. & Wright, J. R. (2002). Exploring the archaeological potential of French and Indian war fortifications. *CRM*, *25*(3), 21–22.

Evans, H. E. & de Lahunta, A. (1980). *Miller's guide to the dissection of the dog*. Philadelphia, PA: W. B. Saunders.

France, D. L. (2009). *Human and Nonhuman Bone Identification*. Boca Raton: CRC Press.

Getty, R. (1975). *Sisson and Grossman's the anatomy of the domestic animals* (5th ed.). Philadelphia, PA: W. B. Saunders.

Gilbert, B. M. (1990). *Mammalian osteology* (2nd ed.). Columbia, MO: Missouri Archaeological Society.

Gilbert, B. M., Marin, L. D. & Savage, H. G. (1981). *Avian osteology*. Columbia, MO: Missouri Archaeological Society.

Halstead, P., Isaakidou, V. & Collins, P. (2002). Sorting the sheep from the goats: Morphological distinctions between the mandibles and mandibular teeth of adult *Ovis* and *Capra*. *Journal of Archaeological Science*, *29*, 545–553.

Hillier, M. L. & Bell, L. S. (2007). Differentiating human bone from animal bone: A review of histological methods. *Journal of Forensic Science*, *52*(2), 249–263.

Hillson, S. (1995). Mammal Bones and Teeth. Institute of Archaeology, London.

Johnston, S. A. & Wailes, B. (2007). *Dún Ailinne: Excavations at an Irish Royal Site, 1968–1975*. Philadelphia, PA: University of Pennsylvania Museum.

Milne, C. & Crabtree, P. J. (2001). Prostitutes, a rabbi, and a carpenter – Dinner at Five Points in the 1830s. *Historical Archaeology*, *35*(3), 31–48.

Milne, C. & Crabtree, P. J. (2002). Revealing meals: Ethnicity, economic status and diet at Five Points, 1800–1860. In R. Yamin (Ed.), *Tales of the five points: Working class life in nineteenth century New York, Volume II: An interpretive approach to working class life* (pp. 130–196). New York, NY: General Services Administration.

Mulhern, D. M. & Ubelaker, D. H. (2001). Differences in osteon banding between human and nonhuman bone. *Journal of Forensic Science*, *46*, 220–222.

Noël Hume, I. (1979). *Martin's Hundred: The discovery of a lost colonial Virginia settlement*. New York, NY: Dell.

Olsen, S. J. (1964). *Mammal remains from archaeological sites*. Cambridge, MA: Peabody Museum. Papers of the Peabody Museum of Archaeology and Ethnology, Harvard University 56-1.

Olsen, S. J. (1968). *Fish, amphibian and reptile remains from archaeological sites*. Cambridge, MA: Peabody Museum. Papers of the Peabody Museum of Archaeology and Ethnology, Harvard University 56-2.

Owsley, D. W. & Mann, R. W. (1990). Medicolegal case involving a bear paw. *Journal of the American Podiatric Medical Association*, *80*, 623–625.

Payne, S. (1985). Morphological distinctions between the mandibular teeth of sheep, *Ovis*, and goats, *Capra*. *Journal of Archaeological Science*, *12*, 139–147.

Raftery, B. (1994). *Pagan Celtic Ireland: The emigma of the Irish Iron Age*. London: Thames and Hudson.

Schaefer, M., Black, S. & Scheuer, L. (2009). *Juvenile Osteology*. San Diego: Academic Press (Elsevier).

Scheuer, L. & Black, S. (2000). *Developmental juvenile osteology*. San Diego, CA: Academic Press.

Schmid, E. (1972). *Atlas of animal bones for prehistorians, archaeologists, and quaternary geologists*. New York, NY: Elsevier.

Semaw, S. (2000). The world's oldest stone artifacts from Gona, Ethiopia: Their implications for understanding stone technology and patterns of human evolution between 2.6–1.5 million years ago. *Journal of Archaeological Science*, *27*, 1197–1214.

Semaw, S., Rogers, M. J., Quade, J., Renne, P. R., Butler, R. F., Dominguez-Rodrigo, M., et al. (2003). 2.6-million-year-old stone tools and associated bones from OGS-6 and OGS-7, Gona, Afar, Ethiopia. *Journal of Human Evolution*, *45*, 169–177.

Silver, I. A. (1969). The ageing of domestic animals. In D. Brothwell & E. Higgs (Eds.), *Science in archaeology* (pp. 283–302). New York, NY: Praeger.

Solecki, R. S. (1971). *The first flower people*. New York, NY: A. Knopf.

Steele, D. G. & Bramblett, C. A. (1988). *The anatomy and biology of the human skeleton*. College Station, TX: Texas A&M University Press.

Stewart, T. (1979). *Essentials of forensic anthropology*. Springfield, IL: Charles C. Thomas.

Symes, S. A., Berryman, H. E. & Smith, O. C. (1998). Saw marks in bone: Introduction and examination of residual kerf contour. In K. J. Reichs (Ed.), *Forensic osteology* (pp. 389–409) (2nd ed.). Springfield, IL: Charles C. Thomas.

Symes, S. A., Williams, J. A., Murray, E. A., Hoffman, J. M., Holland, T. D., Saul, J. M., et al. (2002). Taphonomic context of sharp-force trauma in suspected cases of human mutilation and dismemberment. In W. D. Haglund & M. H. Sorg (Eds.), *Advances in forensic taphonomy* (pp. 403–434). Boca Raton, FL: CRC Press.

Ubelaker, D. H. (1989). *Human skeletal remains: Excavation, analysis, interpretation*. Washington, DC: Taraxacum.

Wailes, B. (1990). Dún Ailinne: A summary excavation report. *Emania*, *7*, 10–21.

Wailes, B. (2004). Irish royal sites. Ancient Europe 8000 B.C.–A.D. 1000. In P. Bogucki & P. Crabtree (Eds.), *Encyclopedia of the barbarian world* (vol. 2, pp. 239–240). New York, NY: Scribner's.

West, S. E. (1985). *West Stow: The Anglo-Saxon village. East Anglian archaeology*. Ipswich: Suffolk County Planning Department. No. 24.

White, T. D. (2000). *Human osteology* (2nd ed.). San Diego, CA: Academic Press.

White, T. D. & Folkens, P. A. (2005). *Human bone manual*. San Diego, CA: Elsevier Academic Press.

Zeder, M. A. & Lapham, H. A. (2010). Assessing the reliability of criteria used to identify postcranial bones in sheep, *Ovis*, and goats, *Capra*. *Journal of Archaeological Science*, *37*, 2887–2905.

Zeder, M. A. & Pilaar, S. E. (2010). Assessing the reliability of criteria used to identify mandibles and mandibular teeth in sheep, *Ovis*, and goats, *Capra*. *Journal of Archaeological Science*, *37*, 225–242.

This page intentionally left blank

Index

B

C

D

G

H

S

T